Chemical tools to validate *N*-myristoyltransferase as a new target in cancer therapy

A thesis presented in partial fulfilment of the requirements for the degree of Doctor of Philosophy and the Diploma of Imperial College London

By
Emmanuelle Thinon

Department of Chemistry
Imperial College London
London SW7 2AZ

December 2013

Declaration of originality

I hereby declare that this thesis is my own work, generated as a result of my own original research. Information derived from the published and unpublished work of others has been acknowledged in the text and references are given.

Emmanuelle Thinon

December 2013

Copyright declaration

Abstract

N-myristoylation is the irreversible attachment of myristate, a C14-lipid, to the N-terminal glycine of a protein. This modification is catalysed by myristoyl CoA: protein *N*-myristoyltransferase (NMT). *N*-myristoylation has been shown to be essential for the viability and survival of many organisms, including plants, parasites and humans. In *humans*, two isoforms of NMT, HsNMT1 and HsNMT2, were identified and it was suggested that they possess overlapping substrate specificities. NMT was identified as a potential chemotherapeutic target for cancer 18 years ago and subsequent studies showed that NMT was up-regulated in several cancers. However, no study demonstrated that NMT could be a therapeutic target in cancer therapy.

In this study, chemically-tagged analogues of myristic acid were synthesised and applied to cancer cell lines to study protein *N*-myristoylation. The analogues can be incorporated on the N-terminal glycine of NMT substrates. The tag in this system enables a second extremely selective and high-yielding chemical ligation to any reporter of choice, for instance a dye label. Visualisation of the tagged proteins was carried out by in-gel fluorescence. Tagged-proteins could also be enriched and analysed by mass spectrometry-based proteomics. The combination of chemical proteomics with a potent NMT inhibitor is described in this thesis as a new method to identify with high confidence a large number of NMT substrates.

In search for novel and potent human NMT inhibitors, various compounds were tested using an *in vitro* assay and a cell cytotoxicity assay. On-target inhibition of NMT in cells was assessed by in-gel fluorescence using analogues of myristic acid.

The best inhibitors were employed as tools to study NMT inhibition in cancer cells. Western blot analysis and flow cytometry were used to assess the phenotype of NMT inhibition.

Finally, the substrate specificity of the two isoforms was studied in cells using siRNAs against HsNMT1 or HsNMT2, and *in vitro* by screening for activity libraries of peptides against NMT1 or NMT2.

Acknowledgements

I would like to thank everyone who has helped me over the past few years.

First, I would like to thank my supervisors, Ed Tate and David Mann for giving me the opportunity to work on such an interesting and varied project. I have learnt so much in their presence and they have provided me with countless encouragements, guidance, advice, availability and enthusiasm over the past four years.

I would like to thank current and past members of the Tate and Mann groups for creating such an enjoyable and productive working environment and for all their help during my PhD project. I am grateful to Will and Megan for teaching me the basics of chemical biology and Victor for all his help with the enzyme assay. I am thankful to Jenny, Victor, Will and Jone for their good advice on organic synthesis and their patience when answering my questions. I am also grateful to Neki for all his help with the peptide synthesiser, Ute for teaching me everything I know about cell culture, Antonio for his help with the ELISA assay and Chris for his help with the *E. coli* work. Special thanks go to Remi for his advice and time spent on the proteomics experiments.

I would like to thank everyone who provided with compounds, which were used in this study, or helped me run some experiments. I thank Megan, Goska and Kalesh for giving me some capture reagents and all the people from the medicinal chemistry project who provided me with inhibitors. I would also like to acknowledge Goska, Remi, James and Tom for running my samples on the Q-exactive. I am grateful to Jane Srivastava, for her kindness and patience when teaching me how to use the flow cytometer and answering all my questions. I also thank Jim Brannigan and Tony Wilkinson (University of York) for the determination of the protein crystallography and the provision of the recombinant enzymes for the assay. I would like to acknowledge Andrew Bottrill (University of Leicester) for running some of my proteomic samples.

Special thanks go to my proof-readers for their time and valuable comments: Jennie, Lisa, Mark, Megan, Remi, and Jenny.

I would like to thank current and past residents of the 5th floor office for the nice chats and their support in stressful times. Thanks to Jenny, Jennie, Megan, Yunyun, Lisa for the well-deserved lunch breaks!

I am grateful to CRUK for funding and for providing me with the opportunity to attend scientific conferences and other meetings with other CRUK students. I am also grateful to Imperial College for allowing me to go to the research summer school in Singapore and to Prof. Yao Shao Q. for giving me the chance to visit his lab for a few weeks. It was a fruitful experience and great networking opportunity.

I would like to thank my parents for their endless love, trust and support. Thank you for always letting my sisters and I choose what we wanted to do with our life and doing everything you could to make it happen.

And last but not least, Flo, thank you for all your support, especially over the past few months. Thanks for trying to keep me sane and getting me out of the lab when I needed it, especially on Friday nights when you dragged me to the Holland club or Union. Now, I promise, I will stop talking about NMT and try to relax.

Table of contents

Publications and presentations arising from this thesis

Publications

W. P. Heal, M. H. Wright, E. Thinon, E. W. Tate, "Multifunctional protein labeling via enzymatic N-terminal tagging and elaboration by click chemistry", *Nat. Protoc.* **2012**, 7, 105-117.

V. Goncalves, J. A. Brannigan, E. Thinon, T. O. Olaleye, R. Serwa, S. Lanzarone, A. J. Wilkinson, E. W. Tate, R. J. Leatherbarrow, "A fluorescence-based assay for N-myristoyltransferase activity", *Anal. Biochem.* **2012**, 421, 342-344.

D. Alibhai, D. J. Kelly, S. Warren, S. Kumar, A. Margineau, R. A. Serwa, E. Thinon, Y. Alexandrov, E. J. Murray, F. Stuhmeier, E. W. Tate, M. A. Neil, C. Dunsby, P. M. French, "Automated fluorescence lifetime imaging plate reader and its application to Förster resonant energy transfer readout of Gag protein aggregation", *J. Biophotonics*. **2013**,6(5):398-408

Conference paper: E. Thinon, D. J. Mann, E. W. Tate, "Targeting *N*-myristoyl transferase in cancer using peptide arrays*", J. pep. sc.*, **2012**: 18, S75-S75

Oral presentations

E. Thinon *et al.* "Using chemical tools to validate a new target in cancer therapy", *VIPCA Chemical Biology: Methods, Progress, Perspectives*, Vienna, Austria, February 2013.

E. Thinon *et al.* "Using chemical tools and proteomics to validate a new target in cancer therapy", *34th EORTC-PAMM-BACR Meeting, Section new cancer drug targets*, Cardiff, UK, January 2013.

E. Thinon *et al.* "Using chemical tools and proteomics to validate a new target in cancer therapy", *RSC PPSG Early Stage Researcher Meeting, London*, November 2012.

E. Thinon *et al.* "Targeting *N*-myristoyltransferase in cancer", *Imperial College Chemistry Department Postgraduate Symposium*, July 2012.

Poster presentations

E. Thinon *et al.* "Using chemical tools to validate *N*-myristoyl transferase as a new therapeutic target in cancer", *RSC Organic Division Poster Symposium*, London, UK, December 2012.

E. Thinon *et al.* "Targeting *N*-myristoyl transferase in cancer using peptide arrays", *32nd European peptide symposium*, Athens, Greece, September 2012.*

E. Thinon *et al.* "Targeting *N*-myristoyl transferase in cancer", *Cancer Research UK-Students' Meeting 2012*, London, UK, May 2012.

E. Thinon *et al.* "Targeting *N*-myristoyl transferase in cancer", *RSC-BMCS Chemical Biology for Drug Discovery*, Alderley Park, March 2012.

E. Thinon *et al.* "Targeting *N*-myristoyl transferase-1 in cancer", *RSC PPSG Early Stage Researcher Meeting*, London, November 2011.

E. Thinon *et al.* "Targeting *N*-myristoyl transferase-1 in cancer", *FASEB meeting on Protein Lipidation, Signaling and Membrane Domains*, Vermont, USA, July 2011.

E. Thinon *et al.* "Targeting *N*-myristoyl transferase-1 in cancer", *Imperial College Chemistry Department Postgraduate Symposium*, London, UK, July 2011.

E. Thinon *et al.* "Targeting *N*-myristoyl transferase-1 in cancer", *Peptide arrays as tools for study of protein interactions*, February 2010.*

* Awarded a prize for best poster based on content and delivery.

Abbreviations

°C	Degrees Celcius
AA	amnio acid
ABP	activity-based probes
Ac	acetyl
AcN	acetonitrile
AHA	azidohomoalanine
AMBIC	ammonium bicarbonate
AMC	7-amino-4-methylcoumarin
ARF	adenosine diphosphate ribosylation factor
Az	probe containing an azide functional group
AzC12	ω-azido dodecanoic acid
AzC15	ω-azido pentadecanoic acid
AzTB	azido-TAMRA-biotin capture reagent
AzKTB	azido-lysine-TAMRA-biotin capture reagent
BASP1	brain acid soluble protein 1
BPD	before pull down
Boc	*tert*-Butoxycarbonyl
BSA	bovine serum albumin
cAMP	cyclic adenosine monophosphate
*Ca*NMT	*Candida albicans N*-myristoyltransferase
c-SRC	cellular SRC
Cat. no.	catalogue number
CDI	carbonyldiimidazole
CF	cell free
CHX	cycloheximide
CP	chemical proteomics
CPM	7-diethylamino-3-(4'- maleimidylphenyl)-4- methylcoumarin)
CoA	coenzyme A
CuAAC	copper-catalysed azide-alkyne [3+2] cycloaddition
Da	Dalton
DCC	*N,N'*-dicyclohexylcarbodiimide

DCM	dichloromethane
DIC	*N*,*N*'-diisopropylcarbodiimide
DIPEA	*N,N*-diisopropylethylamine
DMAP	4-dimethylaminopyridine
DMF	*N,N*-dimethylformamide
DMEM	Dulbecco's modified eagle's medium
DMSO	dimethylsulfoxide
DNA	deoxyribonucleic acid
DTT	dithiothreitol
EC_{50}	half maximal effective concentration
EDI	Ettan Dige imager
EDTA	thylenediaminetetraacetic acid
ELISA	enzyme-linked immunosorbent assay
ER	endoplasmic reticulum
ESI	electrospray ionisation
Et	ethyl
EtOAc	ethyl acetate
FA	formic acid
FASP	filter-aided sample preparation
FBS	foetal bovine serum
FDA	food and drugs administration
FDR	false discovery rate
FTLD	frontotemporal lobar degeneration
Fmoc	9-fluorenylmethoxycarbonyl
FSC	forward scatter pulse
GDP	guanosine diphosphate
GEMM	genetically engineered mouse tumor models
GNAT	Gcn5-related *N*-acetyltransferases
GO	gene ontology
GPI	glycosylphosphatidylinositol
GTP	guanosine triphosphate
H/L	ratio heavy other light
HA	hydroxylamine
HATU	*N,N,N',N'*-Tetramethyl-*O*-(7-azabenzotriazol-1-yl)uronium hexafluorophosphate

HBTU	*N,N,N',N'*-Tetramethyl-*O*-(1*H*-benzotriazol-1-yl)uronium hexafluorophosphate
HIV	*Human immunodeficiency virus*
HMA	2-hydroxymyristic acid
HMB	4-hydroxymethylbenzoic acid
HMPA	hexamethylphosphoramide
HOAt	*N*-hydroxy-9-azabenzotriazole
HPLC	high performance liquid chromatography
HRMS	high resolution mass spectrometry
HRP	horse radish peroxidase
*Hs*NMT	*Homo sapiens N*-myristoyltransferase
Hz	Hertz
IC_{50}	concentration of inhibitor required to inhibit 50% of enzyme activity
IMP366	DDD85646, compound 4
IP	*Intellectual Property*
K_{cat}	catalytic constant or turnover number
K_M	Michaelis-Menten constant
LFQ	label-free quantification
LB media	Lauria-Bertani broth media
LC	liquid chromatography
LC-MS/MS	liquid chromatography with tandem mass spectrometry
*Lm*NMT	*Leishmania major N*-myristoyltransferase
M	Molar
[M + ...]	molecular ion plus ...
MALDI	matrix-assisted laser desorption/ionisation
MARCKS	myristoylated alanine-rich C kinase substrate
Me	methyl
MeOH	methanol
MetAP	methionine aminopeptidase
min	minute
mol	moles
MOPS	3-(*N*-morpholino)propanesulfonic acid
MP	MYR predictor
mRNA	messenger ribonucleic acid
MS	mass spectrometry

MTS 3-(4,5-Dimethylthiazol-2-yl)- 5-(3-carboxymethoxyphenyl)- 2-(4-sulfophenyl)-2H-tetrazolium, inner salt

iTRAQ isobaric tags for relative and absolute quantification

MTT (3-(4,5-Dimethylthiazol-2-yl)-2,5-diphenyltetrazolium bromide,

MW molecular weight

Myr myristic acid

MyrCoA myristoyl-coenzyme A

Myrist Myristoylator

m/z mass to charge ratio

n/a not available

Nat native

nd not determined

NMP *N*-Methyl-2-pyrrolidinone

NMR nuclear magnetic resonance

NMT *N*-Myristoyltransferase

NN non native

p p-value, inverse probability of statistically significant result

PalmCoA palmitoyl-CoA

PARP procyclic acidic repeats protein

PAT palmitoyl acyl transferase

PBS phosphate buffered saline

PD pull-down

PDB Protein Data Bank

PEG polyethyleneglycol

*Pf*NMT *Plasmodium falciparum N*-myristoyltransferase

PI propidium iodide

ppm parts per million

PMS phenazine methosulfate

PTM post-translational modification

PVDF polyvinylidene difluoride

*Pv*NMT *Plasmodium vivax N*-myristoyltransferase

R2 Coefficient of Determination

Rf retention factor

RFU relative fluorescence unit

RIA (L)	relative abundance of the light isotope.
RING finger	Really Interesting New Gene
Rt	retention time
RSMD	root-mean-square deviation
RNA	ribonucleic acid
RNAi	RNA interference
Rpm	revolutions per minute
RT	room temperature
*Sc*NMT	*Saccharomyces cerevisiae N*-myristoyltransferase
sd	standard deviation
SDS	sodium dodecyl sulfate
SDS-PAGE	Sodium dodecyl sulfate polyacrylamide gel electrophoresis
SILAC	Stable isotope labelling with amino acids in cell culture
siRNA	small interfering ribonucleic acid
SLB	sample loading buffer
SMM	small molecule microarrays
SPPS	solid phase peptide synthesis
SSC	Side-scatter pulse
STS	Staurosporine
TAMRA	carboxy-tetramethylrhodamine
*Tb*NMT	*Trypanosoma brucei N*-myristoyltransferase
TBME	*tert*-butyl methyl ether
TBS	tris buffered saline
TBS-T	TBS-Tween buffer
TBTA	Tris[(1-benzyl-1H-1,2,3- triazol-4-yl)methyl]amine
TC_{50}	tagging inhibitory concentration
TCEP	Tris(2- carboxyethyl)phosphine
TEAB	triethylammonium bicarbonate
TFA	trifluoroacetic acid
THF	tetrahydrofuran
TIRF	total internal reflection fluorescence
TIS	triisopropylsilane
TLC	Thin layer chromatography
TMB	3,3', 5,5' tetramethyl benzidine

TMS	trimethylsilyl
TRAIL	TNF-related apoptosis-inducing ligand
TUNEL	Terminal dUTP Nick End-Labeling
Tris	tris(hydroxymethyl)aminomethane
Tris DBA	Tris (dibenzylideneacetone) dipalladium
Ts	toluenesulfonyl
UV	ultraviolet
v-SRC	virus SRC
Vmax	maximum velocity
Wt	weight
Yn	probe containing an alkyne functional group
YnC12	tetradec-13-ynoic acid
YnC15	heptadec-16-ynoic acid
YnTB	alkynyl-TAMRA-biotin capture reagent

Chapter 1 Introduction

In recent years, target drug discovery has been preferred over cytotoxic chemotherapy drug discovery to generate small molecule cancer drugs.[1] This strategy was made possible by the sequencing of cancer genomes and the better understanding of abnormal biology and genetics of cancer cells. Target drug discovery, which has already proven beneficial for numerous cancer patients, is a giant step towards the establishment of a personalised medicine strategy.

However, new cancer drug targets are still needed for the development of new strategies to trigger additional cancer types.[1] Target validation is a fundamental step in the target-based drug discovery pipeline. Failure to identify effective targets has been suggested to be the main cause for failure in drug discovery campaigns.[1] In order to validate a new target, it is important to first show that the target is druggable and that the modulation of the target of interest would give the desired therapeutic effect. Additionally, the functional role of the molecular target must be clearly defined in the disease of interest.[1]

N-Myristoyltransferase (NMT) has been shown to be implicated in cancer [2] and the current study evaluates the potential of NMT as an anti-cancer drug target.

1.1 *N*-Myristoylation

Protein *N*-myristoylation is the irreversible N-terminal glycine acylation of a target protein with a C_{14} saturated fatty acid (myristate) via formation of an amide bond (Figure 1).[3-5] This protein modification is catalysed by myristoyl Coenzyme A (MyrCoA) : protein *N*-myristoyltransferase (NMT).

N-Myristoylation usually occurs co-translationally after the excision of the terminal methionine by methionine aminopeptidase (MetAP) to expose a N-terminal glycine,[6,7] when the growing protein chain is less than 100 amino acids long.[6] It can also occur post-translationally, as for instance for the protein BID implicated in the apoptotic pathway, where cleavage by caspase 8 leads to the exposure of an internal glycine residue.[8]

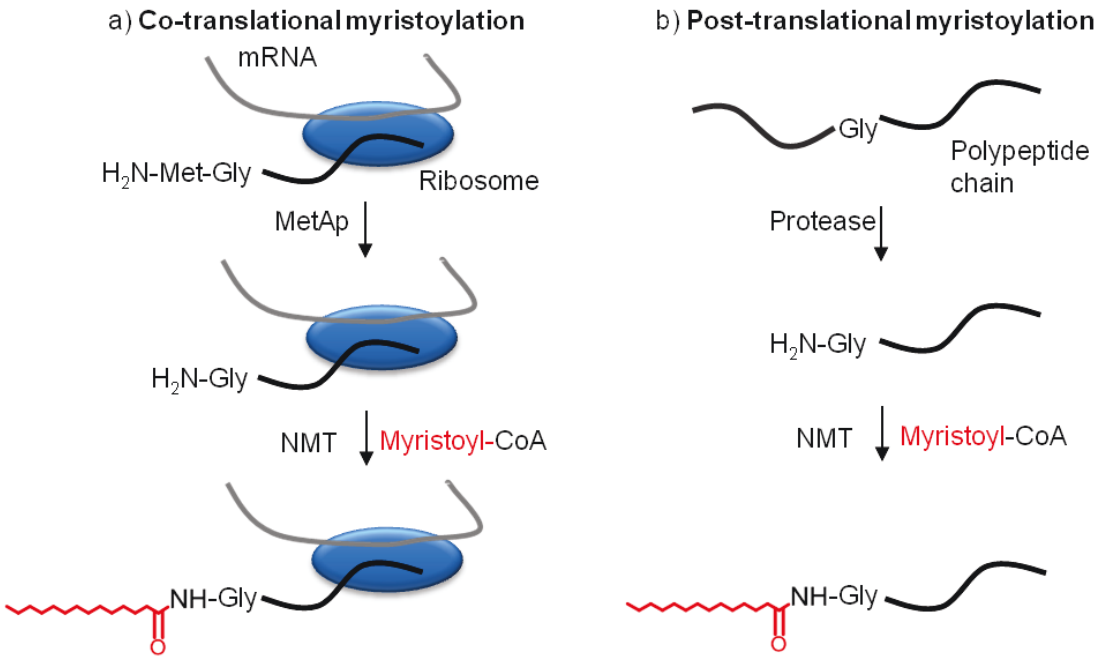

Figure 1: Co-translational (a) and post-translational (b) *N*-myristoylation.

NMT is a monomeric enzyme and a member of the Gcn5-related *N*-acetyltransferases (GNAT) superfamily of proteins.[9] It has been purified and characterised in many organisms such as plants (*Arabidopsis thaliana*),[10] fungi (*Candida albicans,*[11] *Saccharomyces cerevisiae,*[12,13] *Cryptococcus neoformans,*[11] *Aspergillus nidulans,*[14] and *Triticum aestivum* [15]), parasites,[15] protozoa (*Leishmania major,*[16] *Trypanosoma brucei,*[16] *Plasmodium falciparum* [17]), insects (*Drosophila melanogaster*),[18]and mammals (rat,[19] cow [20] and human [21]). The extensive distribution of NMT across species indicates that *N*-myristoylation is a ubiquitous protein modification.[6,22,23] NMT was shown to be essential for

cell survival and for the viability in several organisms (*Saccharomyces cerevisiae,*[24] *Candida albicans,*[25] *Cryptococcus neoformans* [26] and mouse [27]). NMT in lower eukaryotes is encoded by a single copy gene, whereas in higher organisms including plants, mice and humans, two distinct NMT genes, *NMT1* and *NMT2* have been identified.[27-29] In *Homo sapiens*, NMT1 and NMT2 diverge in the protein-binding region, and they might possess distinct but overlapping substrate specificity and function.[27,28,30-33]

N-Myristoylation of a protein can have various effects. In isolation it can direct relatively weak and reversible attachment of proteins to a lipid bilayer membrane, and plays a role in subcellular localisation and protein-protein interaction.[34] Not all *N*-myristoylated proteins have been experimentally determined but it has been suggested that 1% of eukaryotic proteins are myristoylated.[35,36] Known myristoylated proteins include the pro-apoptotic protein BID, guanosine triphosphate (GTP)-binding proteins such as Gα and ARF (ADP-Ribosylation Factor) proteins, oncogene products such as SRC family tyrosine kinases and viral proteins, such as HIV-Gag protein.[5] These proteins have diverse biological functions in signal transduction and oncogenesis.[2]

In humans, there is evidence showing the connection of mis-regulated myristoylation to several diseases including epilepsy,[31] Alzheimer's disease,[37] Noonan-like syndrome [38] and HIV infection.[39] NMT has been suggested as a new therapeutic target to treat cancer [2] (Section 1.7) inflammatory diseases [40] and viral or bacterial infection.[35] Interestingly, certain viruses and intracellular bacteria exploit host NMT to myristoylate their own proteins and to complete their life cycle. NMT is also a therapeutic target for protozoan parasites and fungi as *N*-myristoylation is essential for the viability and survival of these human pathogens.[41] By selectively targeting the pathogen NMT, it would be possible to kill the parasite and prevent any toxicity to humans.[42] Small molecule inhibitors have been developed for NMT from *Leishmania major,*[19] *Trypanosoma brucei,*[16,43] *Plasmodium falciparum,*[16,43,44] and *Candida albicans.*[45]

1.2 Human NMT: two isozymes

In the 1990s, several groups isolated and characterised a single human cDNA encoding for NMT.[21] As there was biochemical evidence of multiple distinct NMTs *in vivo*, i.e. different molecular weights and subcellular distribution, the enzyme was termed HsNMT1.[5] A second distinct NMT cDNA was later isolated by Giang and Cravatt and labelled HsNMT2.[29] HsNMT2 has been identified as a single 65 kDa protein whereas HsNMT1 appears to have several splice isoforms.[29] The biological significance of these multiple HsNMT1 isoforms remains unknown. Giang and Cravat identified four distinct forms of HsNMT1 in transfected COS-7 cells, ranging in size from 49 to 68 kDa, and they suggested that these several forms may arise from *in vivo* processing events. Later, McIlhinney *et al.* showed that several forms of HsNMT1 were likely the result from alternative splicing of the mRNA.[46]

HsNMT2 is comprised of 496 AA while HsNMT1 is comprised of 498 AA. HsNMT1 and HsNMT2 share only 76-77% sequence identity. Distinct roles have been suggested for the two isozymes *in vivo* as there is evidence of distinct substrate specificity. They may have a different role in protein *N*-myristoylation, cell proliferation and apoptosis (see Section 1.7, Relevance to cancer).[27-29,47]

1.2.1 HsNMT1 structure

No crystallographic analysis of the apo-enzyme HsNMT2 has been published to date. However, four structures of HsNMT1 with MyrCoA and /or inhibitors are deposited in the Protein Data Bank (PDB). The overall structure of HsNMT1 comprises several β-sheets and α-helices (Figure 2). The enzyme has a MyrCoA binding pocket and a deep peptide binding pocket (see Section1.4).

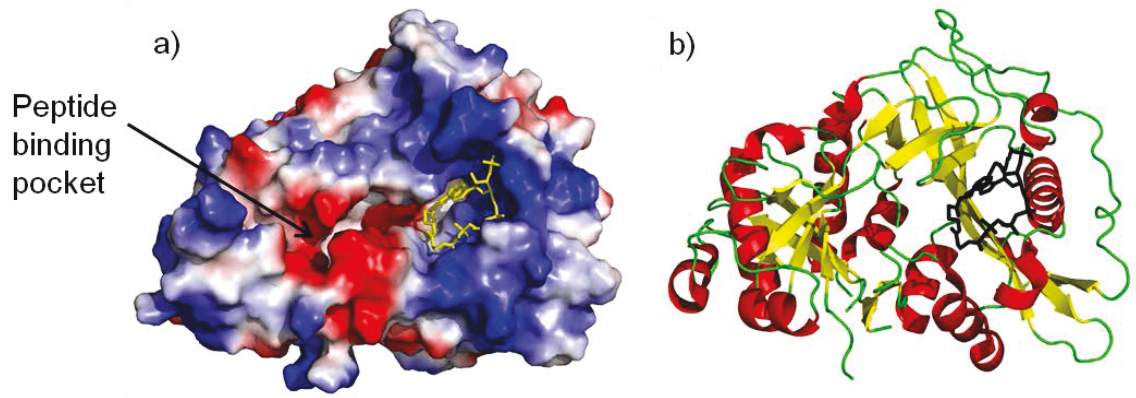

Figure 2: Crystal structure of HsNMT1 with bound MyrCoA. The figure was generated in PyMOL and using the PDB ID: 3IU1. **a)** The enzyme is shaded in white, red and blue, showing the calculated electrostatic surface (red = negative; white = neutral; blue = positive). **b)** The enzyme is shaded in red, yellow and green showing the secondary and tertiary structure of the enzyme**.**

1.2.2 Homology of HsNMT1 and HsNMT2 sequences

As previously mentioned, all mammals studied to date appear to have two NMT isozymes. Multiple sequence alignment showed that each isomer has a high degree of similarity to the same isomer of other species.[48] For instance, HsNMT1 and mouse NMT1 share 97% identity in their amino acid sequence, and HsNMT2 and mouse NMT2 share 96% identity.[29]

Comparison of the amino acid sequences of the two human NMT isozymes showed 76-77% identity (Figure 3). Sequence divergence is greatest in the N-terminal domain of the enzyme and corresponds to missing amino acids (AA), replacement of an AA by a similar one such as isoleucine (I) by valine (V), or replacement by an AA having different properties. The N-terminal domain is not important for NMT catalytic activity,[50] but these differences may influence the recognition or interactions with substrates,[22,29] by varying the geometry of the enzyme, its localisation in the cell, or modifying the substrate binding interactions (hydrogen bonds and/or the hydrophobicity of the peptide-binding site). The MyrCoA binding pocket is highly conserved across species and between isoforms.[51]

```
NMT1_HUMAN   MADESETAVKPPAPPLPQMMEGNGNGHEHCSD-CENEEDNSYNRGGLSPANDTGAKKKKK  59
NMT2_HUMAN   MAEDSESAASQQSLEL--------DDQDTCGIDGDNEEET--EHAKGSPGGYLGAKKKKK  50
             **::**:*..  :  *        : :: *.   :***:.  ::.  **.   *******

NMT1_HUMAN   KQKKKKEKG----SETDS-------AQDQPVKMNSLPAERIQEIQKAIELFSVGQGPAKT  108
NMT2_HUMAN   KQKRKKEKPNSGGTKSDSASDSQEIKIQQPSKNPSVPMQKLQDIQRAMELLSACQGPARN  110
             ***:****     :::**         :** *  *:* :::*:**:*:**:*. ****:.

NMT1_HUMAN   MEEASKRSYQFWDTQPVPKLGEVVNTHGPVEPDKDNIRQEPYTLPQGFTWDALDLGDRGV  168
NMT2_HUMAN   IDEAAKHRYQFWDTQPVPKLDEVITSHGAIEPDKDNVRQEPYSLPQGFMWDTLDLSDAEV  170
             ::**:*: ************ **:.:** :******:*****:***** **:***.*  *

NMT1_HUMAN   LKELYTLLNENYVEDDDNMFRFDYSPEFLLWALRPPGWLPQWHCGVRVVSSRKLVGFISA  228
NMT2_HUMAN   LKELYTLLNENYVEDDDNMFRFDYSPEFLLWALRPPGWLLQWHCGVRVSSNKKLVGFISA  230
             ************************************ ******** *.:********

NMT1_HUMAN   IPANIHIYDTEKKMVEINFLCVHKKLRSKRVAPVLIREITRRVHLEGIFQAVYTAGVVLP  288
NMT2_HUMAN   IPANIRIYDSVKKMVEINFLCVHKKLRSKRVAPVLIREITRRVNLEGIFQAVYTAGVVLP  290
             *****:***: ********************************.***************

NMT1_HUMAN   KPVGTCRYWHRSLNPRKLIEVKFSHLSRNMTMQRTMKLYRLPETPKTAGLRPMETKDIPV  348
NMT2_HUMAN   KPIATCRYWHRSLNPRKLVEVKFSHLSRNMTLQRTMKLYRLPDVTKTSGLRPMEPKDIKS  350
             **:.**************:************:**********:. **:****** ***

NMT1_HUMAN   VHQLLTRYLKQFHLTPVMSQEEVEHWFYPQENIIDTFVVENANGEVTDFLSFYTLPSTIM  408
NMT2_HUMAN   VRELINTYLKQFHLAPVMDEEEVAHWFLPREHIIDTFVVESPNGKLTDFLSFYTLPSTVM  410
             *::*:. *******:***.:*** *** *:*.********. **::*************:*

NMT1_HUMAN   NHPTHKSLKAAYSFYNVHTQTPLLDLMSDALVLAKMKGFDVFNALDLMENKTFLEKLKFG  468
NMT2_HUMAN   HHPAHKSLKAAYSFYNIHTETPLLDLMSDALILAKSKGFDVFNALDLMENKTFLEKLKFG  470
             .**:************:**:***********:*** ************************

NMT1_HUMAN   IGDGNLQYYLYNWKCPSMGAEKVGLVLQ496
NMT2_HUMAN   IGDGNLQYYLYNWRCPGTDSEKVGLVLQ498
             *************:**.  :********
```

Figure 3: Sequence alignments of HsNMT1 and HsNMT2 using the program ClustalOmega (http://www.ebi.ac.uk/Tools/msa/clustalo/).[49]
The consensus is the following: * identical residues; **:** conserved substitutions; **.** semi-conserved substitutions; no sign : no match. The residues Phe-258, Leu-259 are written in green (see Section 1.3, NMT catalytic reaction).

Glover *et al.* also proposed that the N-terminal domain of HsNMT1 may target the enzyme to the ribosome *in vivo,*[21] and HsNMT2 might also be localised at the ribosome. However, it was suggested that the two NMT isozymes may have different intracellular locations: one might be ribosome-based and act co-translationally while the other could be cytosol-based and operate post-translationally.[22]

Figure 4 shows the crystal structure of HsNMT1 with bound MyrCoA. The divergences in sequence with HsNMT2 are shown in red. The N-terminal part of HsNMT1 is missing in the crystal structure and many differences in the sequence are in this region.[29] At the amino acid level, there does not appear to be any divergence in the peptide-binding pocket. However, it has been suggested that the two isoforms have a different peptide affinity *in vitro* and *in vivo.*[29,52]

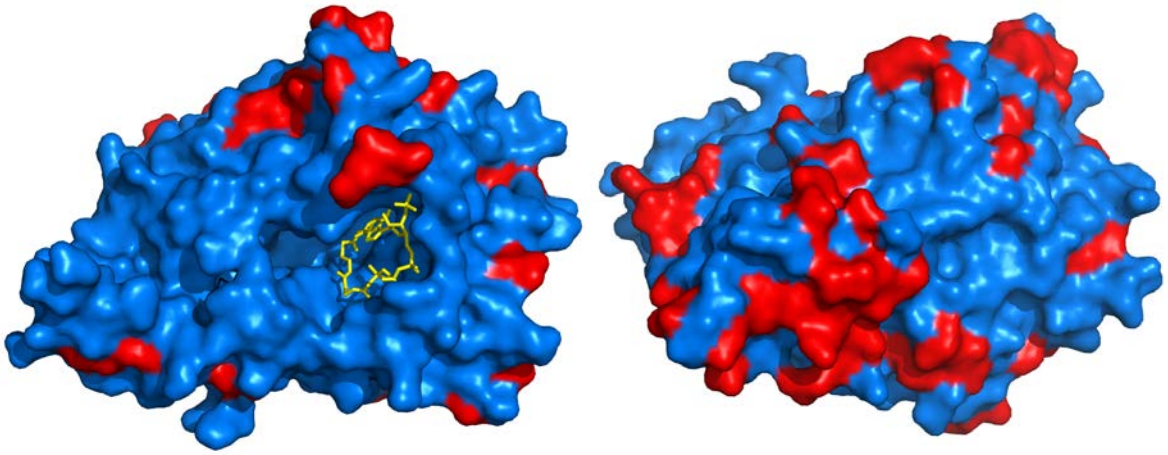

Figure 4: Co-Crystal structure of HsNMT1 with bound MyrCoA (Yellow). The figure was generated in PyMOL using the PDB ID: 3IU1. The similarities in the AA sequence with HsNMT2 are shown in blue and the divergences are shown in red. The two pictures represent the same structure but rotated by 180° about the vertical axis.

Interestingly, in the context of HIV infection, knock down of NMT1 but not NMT2 resulted in a decrease in HIV-1 production and mislocalisation of Gag, a myristoylated protein known to be essential for the progression of the virus infection.[53] However, these results contradict a previous report as they suggested that Gag mostly associates with NMT2 in cells while Nef, another *N*-myristoylated viral protein, can immunoprecipitate NMT1.[47]

Recently, Toska *et al.* also noticed that the two isoforms might have different substrate specificity *in vivo*.[54] The brain acid soluble protein 1, BASP1, is known to be myristoylated and function as a WT1 transcriptional corepressor in cells only when it is myristoylated. Interestingly, knockdown of NMT1,

but not NMT2, decreased the transcriptional repression activity compared to the wild-type cells, suggesting that BASP1 is preferentially lipidated by NMT1.

1.2.3 Sequence similarity and identity across species

NMT is a drug target against different protozoa parasites, *Leishmania major* (*Lm*), [16] the causative agent of Leishmaniasis, *Trypanosoma brucei* (*Tb*),[16] responsible for the sleeping sickness and *Plasmodium falciparum* (*Pf*),[17] the parasite causing malaria. While the MyrCoA binding pocket is usually well conserved across species, the peptide binding pocket is more diverse. Drugs inhibiting the parasite NMT should be specific for the parasite enzyme over the human isoforms to avoid undesirable toxicity. Table 1 compares NMT protein identity and similarity for the different organisms' isoforms described in this PhD thesis.

Table 1. Percentages of sequence identity (blue) and percentages of sequence similarity (grey) of the catalytic domain of NMT from different species. The values were defined by BLAST [55] between the catalytic domains of Human NMT isoforms HsNMT1 (Swiss-Prot P30419) and HsNMT2 (Swiss-Prot O60551) and NMTs from *L. donovani* (*Ld*NMT, EMBL accession number FN555136), *P. falciparum* (*Pf*NMT, Swiss-Prot Q81LW6), *T. brucei* (*Tb*NMT, EMBL FN554973). The table was adapted from Bell *et al.*[56]

%	HsNMT1	HsNMT2	*Ld*NMT	*Pf* NMT	*Tb*NMT
HsNMT1		91	63	70	58
HsNMT2	83		65	71	59
*Ld*NMT	42	44		60	72
*Pf*NMT	52	52	40		55
*Tb*NMT	41	44	54	36	

As discussed in Section 1.2.2, NMT1 and NMT2 active sites seem to be well conserved as the sequences mostly diverge in the N-terminal domain of the enzymes. Interestingly, the active site of human and Pf NMTs are relatively similar, suggesting it might be possible to use PfNMT inhibitors as tools to study NMT inhibition in human cells.

1.3 NMT catalytic reaction

The structure and the catalytic mechanism of NMT have been well studied for *Saccharomyces cerevisiae* (*Sc*).[13,22,57,58] Using kinetic studies, Rocque *et al.* have shown that the catalytic mechanism of NMT established for *Sc* was also valid for human NMT.[59] Considering that NMT (role, structure, substrate specificity) is well conserved across species from different kingdoms, it can be supposed that the mechanism is conserved across all eukaryotes.

Rudnick *et al.* have established that NMT follows an ordered Bi-Bi mechanism where two products and two substrates are involved in the reaction (Figure 5).[58]

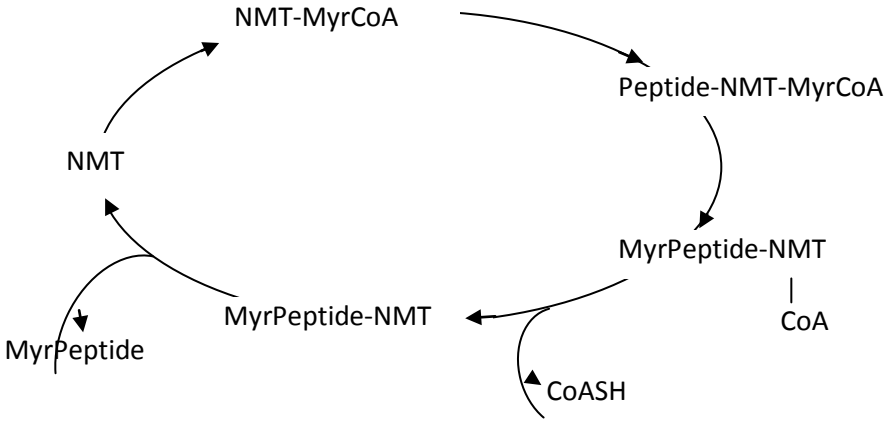

Figure 5: NMT catalytic cycle, adapted from Bhatnagar *et al.* [57]

MyrCoA binds to NMT prior to the peptide and induces a conformational change of the Ab loop (a loop connecting helix A and strand b) in the peptide-binding site. The thioester carbonyl of MyrCoA interacts with an oxyanion hole formed by two amides (Phe-170, Leu-171 for *Sc*NMT and Phe-258, Leu-259 for HsNMT) of the enzymatic backbone via hydrogen bonding. This interaction creates a partial positive charge on the carbonyl and activates it for nucleophilic substitution.[57]

Secondly, the peptide substrate binds to the enzyme in the C-terminal domain of NMT, in a deep and narrow pocket. Residues in the Ab loop contribute to peptide recognition and binding. The N-terminal Glycine of the peptide substrate, which is positively charged in the physiological environment, is deprotonated by the C-terminal carboxylate of NMT, producing a nucleophilic amine. This amine attacks the carbonyl of the thioester to form a tetrahedral intermediate, which is stabilised by interaction with the oxyanion hole. The Coenzyme A (CoA) by-product is released first, leading to a relaxed structure and elimination of the myristoylated peptide. The C-terminal

carboxylic acid is then deprotonated, most likely by solvent interactions, leaving the enzyme ready for another round of catalysis.[57,58]

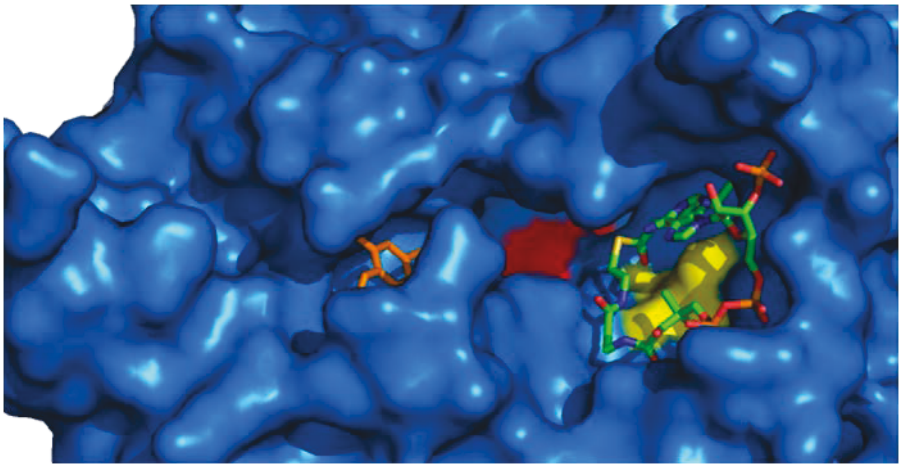

Figure 6: Co-crystal structure of HsNMT1 with bound MyrCoA (*Multicolour*) and an inhibitor (orange). ((2R)-2-(4-hydroxy-5-methoxy-2-[3-(4-methylpiperazin-1-yl)propyl]phenyl)-3-pyridin-3-yl-1,3-thiazolidin-4-one) (Orange). The figure was generated in PYMOL with the PDB ID: 3IU2. The enzyme is shaded in blue, the C-terminus of the enzyme is shown is red and the key residues Phe-258 and Leu-259 are shaded in yellow.[60]

1.4 Substrate specificity

NMT is specific to MyrCoA and to proteins or peptides bearing an N-terminal glycine.[13]

1.4.1 Myristoyl CoA

MyrCoA is a C14 fatty acid which accounts for 1-3% of the total cellular fatty acid in cells.[5,34] The synthesis of MyrCoA in cells, from free CoA and myristic acid, is catalysed by acyl CoA synthetase.[34] This enzyme is ubiquitous in prokaryotes and eukaryotes.[61] Kinetic studies of fatty acid analogues have provided some understanding of the MyrCoA specificity of NMT. In general, these experiments were carried out using *Sc*NMT, and the MyrCoA analogues investigated include fatty acids with different chain lengths and compounds with various modifications such as double bonds, sulfur or oxygen atoms or aromatic groups.[58,62-67]

NMT-Bound MyrCoA shows four bends (relative to a fully extended chain) and its conformation is similar to a question mark (Figure 7).[22] Several features are essential for MyrCoA recognition and specificity: 1) fatty acid length;[62] 2) the interaction with the oxyanion hole (see Section 1.3);[57] 3) the conformation of MyrCoA with bends at C1 and C6;[22] 4) the distance between C1 and the first bend;[68] 5) the distance between C1 and the C-terminus of the fatty acid;[64] 6) the floor of the MyrCoA binding

site. [22] Kinetic studies have also shown that the fatty acyl chain length is more important than the hydrophobicity for binding.[62]

It was suggested that the fatty acyl binding pocket acts as a measuring tool which measures and recognises the distance from the thioester carbonyl to the omega terminus of the chain.[63,64,69] This pocket also specifically recognises the steric bulk at the omega terminus. Towler and Glover showed that other available fatty acids *in vivo*, such as C10 and C12 fatty acyl CoA, are low-affinity substrates of NMT. Longer acyl chains, such as the abundant palmitoyl-CoA (PalmCoA), are not transferred to proteins.[67,70] However, PalmCoA can bind to NMT *in vitro*, but this binding is less thermodynamically favoured.[71] There is no evidence that PalmCoA compete with MyrCoA *in vivo*.

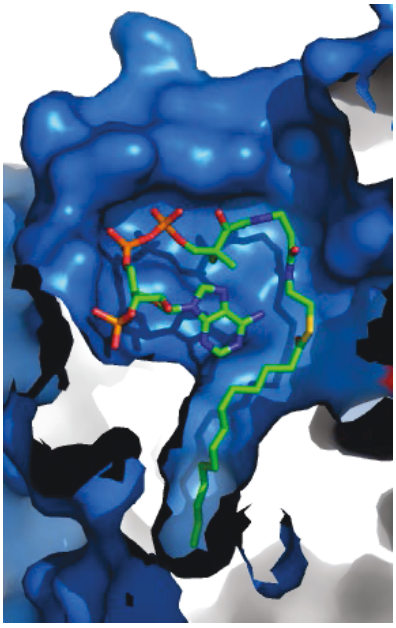

Figure 7: Zoom of a co-crystal structure of HsNMT1 with bound MyrCoA (multicolour). The figure was generated in PyMOL with the PDB ID: 3IU1.[72]

The acyl-CoA binding site is highly conserved across species studied to date (yeast,[62] plant,[73] rat,[70] human [65]). Rundle *et al.* have compared the K_M of MyrCoA in the presence of v-SRC and recombinant HsNMT1 or HsNMT2. The K_M is the substrate concentration at which the rate of reaction is half its maximum value. They found that the K_M of MyrCoA was four fold higher for HsNMT2 (6.6 µM) than for HsNMT1 (1.6 µM).[50] These results are surprising as the acyl-CoA binding pocket is well-conserved.[62,65,70] However, this difference between K_M values might not be significant and might be attributed to experimental errors.

1.4.2 Protein substrate: prediction and consensus

Not all proteins bearing an N-terminal glycine can be *N*-myristoylated [74]. Extensive studies of both peptide [67,70] and protein [75,76] substrates of *Sc*NMT established a consensus regarding the substrate sequence. The first eight residues were shown to be essential for enzyme specificity.[70,77] However, this consensus cannot be applied to HsNMT as the substrate specificity has been shown to be different.[59]

Maurer-Stroh *et al.* used a bioinformatic approach to establish a consensus for HsNMT (Figure 8). They found that, as for other organisms, an N-terminal glycine residue is critical. NMT has a preference for small polar residues at position 3, polar residues at position 4, large hydrophobic AA at position 5, small, polar residues such as serine at position 6 and finally lysine or threonine at position 7.[78] Bulky residues are not favoured at position 8, 10 and 11, basic and hydrophilic residues are preferred at position 9 and small polar residues are favoured at positions 11 and 12.

Maurer-Stroh *et al.* have also proposed that the 17 first amino acids are needed to determine whether or not a protein is myristoylated.[78] They identified three regions in the peptide substrate: in region 1 (position 2-7), the residues bind to the active site; in region 2 (position 8-12), the residues interact with the enzyme surface at the entrance of the narrow peptide binding pocket; in region 3 (position 13-18), the residues act as a hydrophilic linker.[78] The third region is mainly composed of hydrophilic residues, probably to prevent the N-terminal chain from folding and inhibiting the recognition by the enzyme.

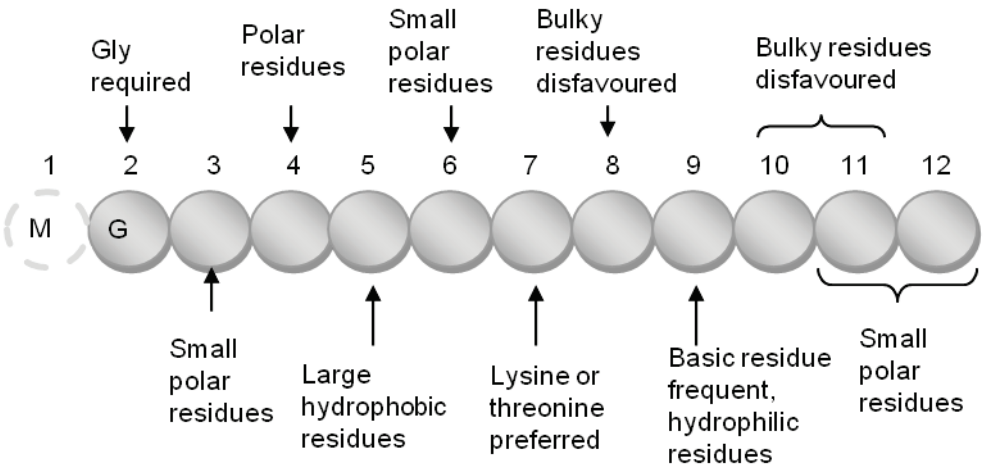

Figure 8: HsNMT peptide substrate specificity. Residue 1 is the leader methionine removed by MetAP prior to *N*-myristoylation.[78]

Based on these observations, two predictors of myristoylation are available online: the Myr predictor [79,80] and Myristoylator.[81,82] Giglione *et al.* also prepared a predictor able to predict N-terminal methionine removal, N-terminal acylation such as *N*-myristoylation, and *N*-palmitoylation in various organism and plants.[83,84] Another model of prediction was developed recently but is not accessible online.[85]

However, these predictors are not always reliable even at the peptide level, and it is unknown to what extent they apply in live cells or *in vivo*.[86,87] More work is therefore required in order to understand the protein substrate specificity of HsNMT. Proteomics studies in live cells are required to identify more NMT substrates in a native context. Furthermore, little is known about the peptide specificity of HsNMT1 and HsNMT2, although experiments to date suggest that they possess similar but distinguishable specificity with recombinant enzymes or in live cells.[29,47,52]

1.5 *N*-myristoylated proteins

1.5.1 Co-translationally myristoylated proteins

Co-translational myristoylation is more prevalent than post-translational myristoylation. Known co-translationally myristoylated proteins have diverse biological functions in signal transduction and oncogenesis.[2] Examples of myristoylated proteins include protein kinases such as the oncogenes SRC and LYN, phosphatases, G_{α} proteins, ADP ribosylation factor (ARF) GTP-binding proteins, the myristoylated alanine-rich C kinase substrate (MARCKS).[51]

Many of these co-translationally myristoylated proteins have been implicated in diseases such as cancer (Section 1.7). Interestingly, it has been shown that a genetic disease, the Noonan-like syndrome, depends on the myristoylation of the protein SHOC2.[38] SHOC2 is normally not myristoylated but the genetic disease induces a mutation of SHOC2 and introduces an *N*-myristoylation site in SHOC2. The myristoylated SHOC2 is relocated to the plasma membrane, resulting in aberrant signalling.[38]

Methods to identify and study *N*-myristoylated proteins will be discussed in Section 1.10 and co-translationally myristoylated proteins will be discussed more in detail in Chapter 4.

1.5.2 Post-translationally myristoylated proteins

Post-translational myristoylation of proteins is involved in the regulation of programmed cell death, known as apoptosis [88]. The apoptosis process involves cysteine-aspartic proteases called caspases, which cleave several proteins in the cell. One apoptotic pathway corresponds to the cleavage of the protein p22 BID by Caspase-8 (Figure 9). The p15 Bid fragment released is myristoylated post-

translationally during the apoptotic process [8] and is relocated to the mitochondrial membrane where it can trigger cytochrome c release leading to further caspase activation. Other proteins have been shown to be myristoylated post-translationally, such as the p21-activated protein kinase-2 (PAK-2) or β-actin and gelsolin (an actin-binding protein).[89]

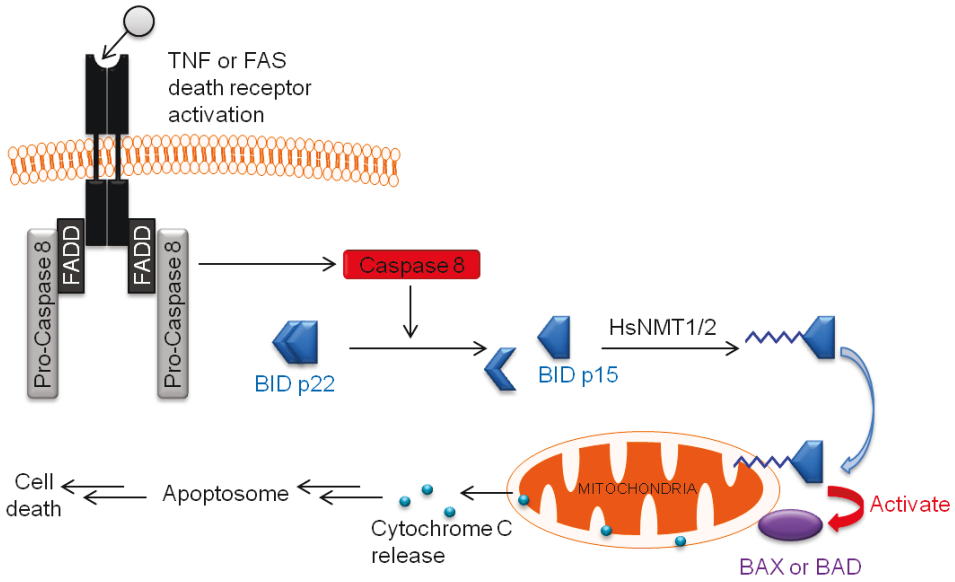

Figure 9. Post-translational myristoylation of BID upon apoptosis induction with a death receptor ligand.

Recently, Martin *et al*. developed a method to identify post-translational *N*-myristoylation proteins in the context of apoptosis.[90] They designed a caspase-cleavable tandem fluorescent reporter protein for each protein they wanted to assess and expressed the reporter protein in COS7 cells. The reporter proteins were composed of several fluorescent moieties as well as a caspase cleavage site (four amino acids: DEVD) followed by a putative *N*-myristoylation sequence of 10 amino acids. After induction of apoptosis, the reporter proteins were cleaved by caspases and revealed the new N-terminal sequence which could be tagged by myristic acid analogues and detected in fluorescence (see Section 1.10).

Five proteins were identified: cell division control protein 6 homolog (Cdc6), induced myeloid leukemia cell differentiation protein (Mcl-1), microtubule-actin cross-linking factor 1 (MACF1), YTH domain family protein 1 (YTHFD2) as well as the protein involved in Huntingtin disease (HTT).[89] The role of *N*-myristoylation of these proteins has yet to be studied. For instance, the importance of HTT *N*-myristoylation for the progression of the Huntingtin disease remains unclear. Many proteins cleaved during apoptosis have an N-terminal glycine after the protease cleavage site,[91,92] suggesting that new post translationally myristoylated proteins remain to be identified.

However, the method developed Martin *et al*.[90] presents several limitations. The caspase cleavage site of these proteins was not always known and was thus predicted. This method does not provide any strong evidence that the cleavage site is correct since the putative caspase cleavage sequence was replaced by the DEVD sequence. Additionally, the five novel substrates were not identified in the native context.

1.5.3 Biological function and regulation of myristoylation

Protein myristoylation increases the protein hydrophobicity and affinity for membranes.[93] Localisation to membranes is thought to be essential for the function and regulation of *N*-myristoylated proteins and to trigger cellular transformations. The addition of myristate can also stabilise the tertiary structure of a protein [94] or be part of a protein-protein interaction site.[95]

1.5.3.1 Two signal membrane binding model

N-Myristoylation allows localisation of a protein to the membrane. It has been estimated that 10 carbons, out of 14 of myristate, incorporate into the lipid bilayer.[96] Peitzsch and McLaughlin estimated the Gibbs free energy of binding of a myristoylated peptide to membrane lipids to be around 8 kcal/mol, corresponding to an apparent dissociation constant of 10^{-4} M. This binding energy is relatively weak and the hydrophobicity increase is not enough to provide a stable association to membranes implying that another interaction is often required to localise a protein to the membrane.[97] The membrane affinity can be increased by the addition of a second lipid such as palmitate, close to the protein N-terminus. Palmitate is a C16 fatty acid, typically added to one or several cysteine residues of a protein. This protein modification is often reversible.[98] Many *N*-myristoylated proteins are dual-lipidated, such as SRC-family tyrosine kinases FYN and LCK.[99] It has been noticed that for these proteins, myristoylation is required for palmitoylation. [100]

Membrane affinity of an *N*-myristoylated protein can also be enhanced by the presence of an electrostatic interaction at the protein N-terminus. A cluster of basic amino acids at the N-terminus of the protein can interact with membrane acidic phospholipid head groups. MARCKS [101] and HIV Gag [96] use the combination of hydrophobic (myristate) and electrostatic (basic residues) interactions to associate to membranes. Finally, Resh suggested that membrane localisation could be promoted by a protein-protein interaction with another membrane-bound protein.[93]

1.5.3.2 Molecular switches

N-Myristoylated proteins are usually partitioned between cytosolic and membrane compartments. They undergo regulated and reversible membrane binding, modulated by ‘‘switches’’ occurring in response to additional covalent or non-covalent modifications.[93,102]

Four different mechanisms have been proposed for the myristoyl-switch and are shown in Figure 10.[51,93,102] When myristate is exposed, it can trigger membrane binding. In scenario A, upon ligand binding, the protein undergoes a conformational change. Myristate is buried in a hydrophobic pocket in the *N*-myristoylated protein and cannot interact with the membrane bilayer. In B and C, membrane binding of the *N*-myristoylated protein is achieved by an electrostatic switch. Binding of a negatively charged ligand or phosphorylation, decreases the charge of the polybasic cluster reducing membrane binding (Section 1.5.3.1). Scenario D describes the myristoylated switch of ARF-GTPases. GTP is hydrolysed by Guanine nucleotide exchange factors (GEFs) into guanosine diphosphate (GDP) and contributes to regulation of ARFs. GTP-bound ARF can associate to membrane but upon hydrolysis of GTP to GDP, a conformational change occurs and, similar to scenario A, myristate is buried into the protein.

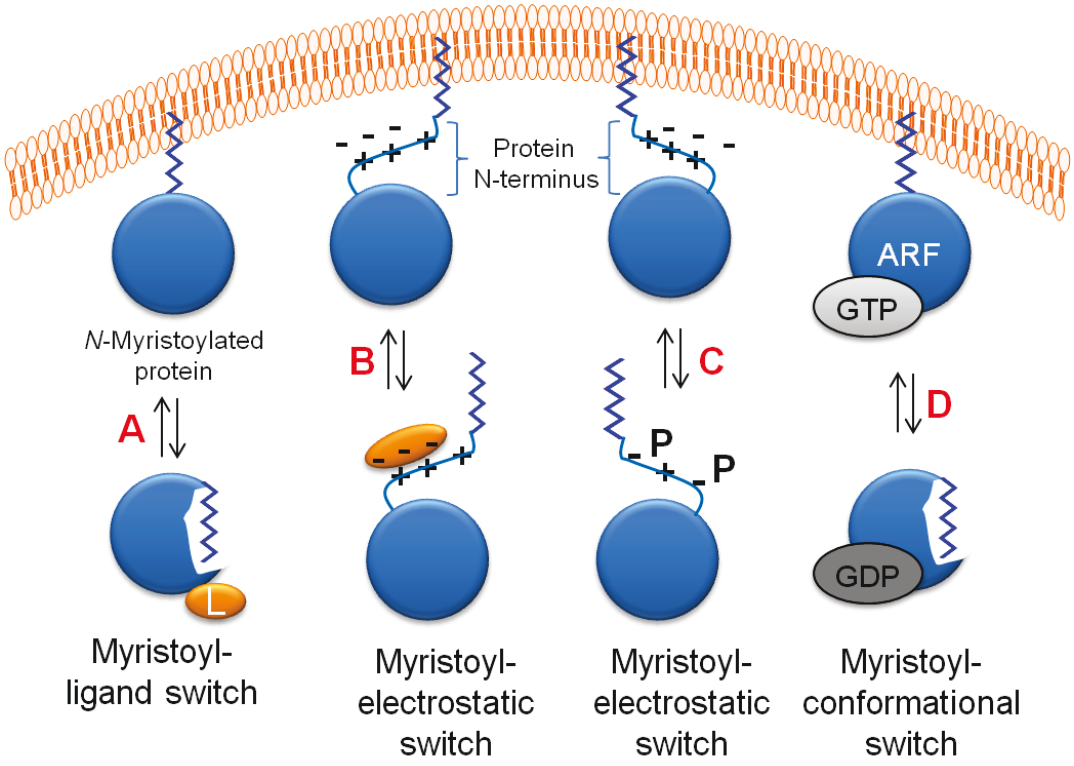

Figure 10. Reversible membrane association of *N*-myristoylated proteins. The figure was adapted from Wright *et al.* [51]

Many proteins, including HIV-Gag, the tyrosine kinase ABL, MARCKS and ARF proteins, undergo a myristoyl-switch.[93,102,103] The only exception known to date is the tyrosine kinase c-SRC.[104] Myristate is not buried in a hydrophobic pocket and as a consequence, nearly 90% of c-SRC present in cells is membrane bound.[104]

1.5.3.3 Reversible myristoylation

For a long time, *N*-myristoylation was thought to be an irreversible protein modification as there was little evidence of the presence of de-myristoylated substrates *in vivo*. The only protein reported to be de-myristoylated was MARCKS, the myristoylated alanine-rich C kinase substrate as non lipidated MARCKS was found in synaptosomes from rat and bovine brain.[105,106] The biological relevance of de-myristoylation in eukaryotic cells is unclear but it's been suggested that de-myristoylation might regulate MARCKS' membrane association.[106,107] *N*-myristoylated MARCKS associates with membranes, while non-myristoylated MARCKS is mainly found in cytosolic fractions (see Section 1.5.3.2). It's also been suggested that NMT could de-myristoylate a substrate in the absence of a CoA pool in cells but the hypothesis has yet to be validated *in vivo.*[108]

Recently, cleavage of the myristoyl moiety has been shown to be possible by a bacterial effector protein with cysteine protease activity, the *Shighella* virulence factor IpaJ, in the context of human infection.[109] This process is irreversible as the *N*-myristoylated glycine is cleaved from the protein. Several substrates, such as ARF1, c-SRC or MARCKS were shown to be cleaved by IpaJ. This process might allow *Shigella* to exploit host cell signalling pathways and is one of the events triggering bacterial infection.

1.6 Regulation of NMT activity

Regulation of NMT activity *in vivo* is not well understood. It was suggested that NMT activity in cells might be limited to the amount of available MyrCoA.[110,111] It was also proposed that levels of NMT might be optimal to myristoylate endogenous proteins but, in this context it is difficult to understand why NMT levels would be higher in many tumour tissues (Section 1.7).[48] It has also been proposed that NMT has several biological inhibitors in cells, such as the NMT inhibitor protein 71 (NIP71) isolated from bovine brain and these could play a role in NMT regulation. However, this possibility has yet to be validated *in vivo*.[48]

NMT could also be regulated via a phosphorylation/dephosphorylation mechanism and NMT localisation in cells could be an important feature for regulation of NMT activity.[112]

1.6.1 NMT phosphorylation

Sharma *et al.* suggested that NMT could be regulated by phosphorylation.[112] HsNMT1 was phosphorylated *in vitro* by non-tyrosine kinases FYN, LYN, and LCK.[113] They proposed that phosphorylated NMT could associate with other proteins and be relocated within cells. As they noticed that an NMT mutant missing the N-terminal region (149 first AA) was only poorly phosphorylated by LYN *in vitro*, they suggested that the phosphorylation site was located in the

N-terminal region of NMT. Site-directed mutagenesis experiments suggested that Tyr 100 could be the phosphorylation site.[113] Sharma *et al*. have also shown that NMT could be dephosphorylated *in vitro* by calcineurin, a Ca^{2+}/ calmodulin-dependant protein phosphatase.[112] Phosphorylation decreased NMT activity, and could possibly reduce ribosome association. Regulation of NMT by phosphorylation/dephosphorylation has yet to be validated *in vivo.*

1.6.2 NMT localisation

The N-terminus of NMT is not essential for catalytic activity but functions as a targeting signal.[114] It enables the localisation of NMTs, possibly both at the ribosome (Section 1.2.2) and it was suggested that it could provide access to myristoyl-CoA pools in cells.[114]

Subcellular fractionation of different human cancer cell lines showed that HsNMT1 was mostly present in cells as a 60 kDa protein localised to the ribosome.[21] Full length HsNMT1 and HsNMT2 possess a poly-lysine cluster at their N-terminus, often referred as the "K box motif". This region is known to be a ribosomal targeting signal.[21] As expected, NMT is mainly localised at the ribosome, where it can myristoylate proteins co-translationally.

Glover et *al.* noticed the presence of NMT in other subcellular fractions which was explained by the existence of a shorter isoform of NMT (Section 1.2). This shorter isoform might arise from proteolytic degradation and was truncated at the N-terminus, thus missing the required K box motif to bind to the ribosome. However, the function of this shorter isoform was not well understood.[21] Recently, HsNMT1 and HsNMT2 have been shown to be cleaved at the N-terminus during apoptosis, removing the K box motif and allowing the enzymes to relocate from the ribosome to the cytosol.[115]

Interestingly, Sharma *et al.* observed that NMT localisation could change in cancerous cells. In bone marrow mononuclear cells, NMT was localised in the nucleus, while it was found in the cytoplasm of control samples.[116] They proposed that abnormal NMT localisation could be used as a biomarker to detect early stage colon cancer.

1.7 Relevance to cancer

Considering that NMT is a critical cellular enzyme and that some *N*-myristoylated proteins are involved in proliferative signalling pathways, Felsted *et al.* suggested in 1995 that NMT could be a chemotherapeutic target for cancer.[2] They proposed that further investigations were necessary 1) to understand the relationship between *N*-myristoylation and cancer by establishing if *N*-myristoylation is a cause or a consequence of cancer; 2) to understand how protein *N*-myristoylation is regulated in

mammalian cells; 3) to find strategies to selectively target *N*-myristoylation in tumour cells to avoid toxicity in healthy cells.

Extensive studies by Sharma *et al.* later showed that NMT is up-regulated in colorectal cancer,[33,48,117-119] brain cancer,[30] gallbladder carcinoma,[117,120] and breast cancer,[121] and in many clinical cases increased NMT expression correlates with increased invasiveness.[122]

Furthermore, RNA interference (RNAi) experiments on a mouse xenograft model of mammary adenocarcinoma suggested that knockdown of NMT1 inhibits tumour growth, whereas knockdown of NMT2 had no effect.[28] These results provided the first direct evidence that isoform-specific inhibitors against NMT1 might be effective anti-cancer agents. If residual NMT2 activity can compensate for loss of NMT function in healthy cells, potential toxicity may also be minimised.[28] However, these experiments were poorly controlled, and the results have yet to be confirmed by other groups; work is on-going in our lab to investigate this hypothesis.

Previous studies have established that c-SRC and LCK, both tyrosine kinases of the SRC family are oncogenes that require myristoylation for activity.[104,123,124] c-SRC is activated after being autophosphorylated in trans at Tyr416 via an intermolecular mechanism.[125] Patwardhan *et al*. suggested that the tyrosine kinase activity of myristoylated c-SRC might be increased due to the optimal conformation of membrane bound *N*-myristoylated c-SRC as the proteins might be oriented and in close packing.[104] Elevated activity of c-SRC was reported in some human cancers such as colon cancer, and c-SRC was shown to be a critical regulator of several human cancers.[126] Inhibition of SRC-family tyrosine kinases is now an established therapeutic strategy for cancer therapy as a selective inhibitor, dasatinib, has recently been FDA-approved (Food and Drugs Administration-approved). Inhibition of myristoylation might have the same effect on cancer cells as non-myristoylated SRC family members have reduced activity.

Interestingly, activation of the tyrosine kinase ABL is not associated with cancer progression but has instead been shown to inhibit tumorigenesis, metastasis and invasion of breast cancer cells.[127,128] Association of the myristoyl moiety of ABL with a hydrophobic pocket in its kinase domain was shown to be essential for the formation of an autoinhibitory complex of ABL (Section 1.5.3.2). Yang *et al.* developed an inhibitor to block the myristoyl binding pocket, leading to a change in the structure of ABL and activation of ABL as seen by the phosphorylation of the two key tyrosine residues (Tyr 245 and Tyr 412).[129] However, it is unclear if NMT inhibition could have the same effect on ABL. Upon NMT inhibition ABL would not adopt an autoinhibited conformation and might thus be activated. However, it is possible that myristoylation might be needed to phosphorylate the two

tyrosine residues, as required for full activation, given that the tyrosine kinase SRC requires myristoylation to be phosphorylated and fully activated.[125]

N-Myristoylation of the tumour suppressor Fus1 is required for its proper activity in cells. A tumour-suppressor gene, or anti-oncogene, tends to enhance the apoptosis of cells that appear to be mutated, therefore preventing it becoming a cancer cell. The tumour-suppressor gene *Fus1* is located in the critical 3p21.3 chromosomal region often mutated in human cancers. When Fus1 protein is not myristoylated in human lung cancer cells, it loses its tumour suppressor activity.[130] Ji *et al.* suggested that Fus1 is not myristoylated efficiently in cancer cells but the reason is not understood. The myristoylation process might be down regulated and non-myristoylated Fus1 might be degraded by proteases in human lung cancer cells, but if this is the case the cause is nevertheless not well understood.[131] These latter results are in contradiction to the concept that inhibition of NMT could be an effective anticancer agent. However, no study has replicated these results to date.

1.8 HsNMT inhibitors

Several compounds have been reported in the literature to inhibit HsNMT activity but they are almost exclusively tested against HsNMT1 and any selectivity over HsNMT2 has not been established. HsNMT1 or HsNMT2 selective inhibitors could be valuable tools to study the isoforms substrate specificity in cells. They could also be used as chemical genetic tools to confirm the results from the RNAi experiments described in Section 1.7. Inhibitors of HsNMT1 include myristic acid analogues, non-hydrolysable MyrCoA analogues, peptidomimetic compounds and synthetic organic compounds targeting the fatty acyl or peptide-binding pocket.[48]

1.8.1 Lipidic inhibitors

Myristic acid analogues such as 2-hydroxymyristic acid (HMA) or non-hydrolysable MyrCoA analogues (e.g. S-(2-oxopentadecyl)-CoA) have been designed as alternative substrates for NMT. They showed inhibition of mouse NMT,[132,133] bovine NMT,[134] and yeast NMT [135] with IC_{50} values up to the micromolar range. Myristic acid analogues have been used to demonstrate that NMT could be a therapeutic target against HIV-1 [136] [137] and Hepatitis B.[138]

One lipidic inhibitor of particular interest is HMA. It is commercially available and was shown to decrease [^{3}H]myristate labelling in cells,[139] suggesting that it inhibits NMT activity. HMA is metabolically activated in cells to yield 2-hydroxymyristoyl-CoA, which is responsible for NMT inhibition.[133] HMA will be discussed in Section 3.2.1.

Myristic acid analogues and non-hydrolysable MyrCoA target the MyrCoA binding pocket of the enzyme. This pocket is thought to be well-conserved across isoforms and species. However, if this is the case and if an HsNMt1 or HsNMT2 selective inhibitor is required, it would be difficult to target one isoform selectively using these compounds. It has been suggested that selective inhibitors should target the peptide binding pocket, which is known to be less conserved.[65]

1.8.2 Other NMT inhibitors

Bhandarkar *et al.* found that a palladium complex generally used as a catalyst in organic synthesis, Tris (dibenzylideneacetone) dipalladium (Tris DBA), had an antitumor activity against A375 melanoma. Treating the cells with 10 µg/mL (~11 µM) of Tris DBA resulted in a 96% decrease of cell count.[140] Using Western blot and gene array analyses, they found that HsNMT1 expression decreased upon treatment with Tris DBA. However, expression of many other genes was also affected and some experiments are missing to prove that Tris DBA targets NMT in cells. The authors have not for instance shown that Tris DBA was a competitive inhibitor of the peptide substrates of NMT or that an overexpression of NMT rescues the cells from inhibition.

James *et al.* reported several selective peptidic and peptidomimetic inhibitors of *Candida albicans* NMT.[45] In their study, they also found potent HsNMT1 inhibitors *in vitro* (Figure 11). However, the potency against HsNMT1 has not been tested in live cells or *in vivo*.

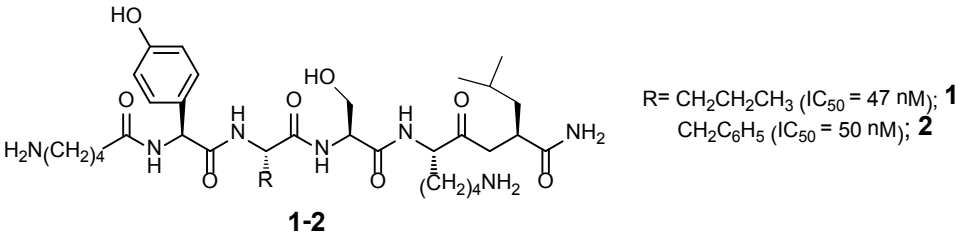

1-2

Figure 11: Peptidomimetic inhibitors of HsNMT1. 1 and **2** were the more potent inhibitors against recombinant HsNMT1identified by James *et al.* [45]

French *et al.* discovered a novel class of HsNMT inhibitors based on cyclohexyl-octahydro-pyrrolo[1,2-α]pyrazin.[141] They showed by kinetic studies that the compounds were competitive inhibitors with respect to the peptide substrate. The best inhibitor, COPP-24, is shown in Figure 12.

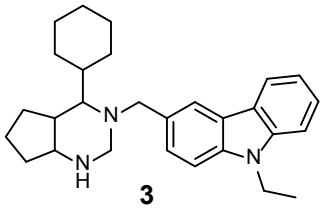

3

Figure 12: HsNMT1 inhibitor COPP-24.[141]

COPP-24 inhibited the proliferation of various tumour cell lines (DU145: prostate; HepG2: liver; HT29: colon; MCF-7: breast; MCF-10A B: breast non–transformed; MDA-MB-231: breast; Panc-1: pancreas, SKOV3: Ovary, A-498: kidney) in a concentration-dependent manner. However, the IC_{50} and EC_{50} values were in the micromolar range (0.9–14.8 μM), suggesting that these compounds have a low affinity for NMT *in vitro* and in cells.

Two analogues of L-histidine, L-histidinol and histamine, have been shown to inhibit HsNMT1 activity *in vitro* as non-competitive inhibitors. They inhibited HsNMT1 in a concentration-dependent manner with 50% inhibition at 18 and 1.5 nM respectively. These results have not been confirmed *in vivo* or in live cells.[48]

Recently, Wyatt *et al.* have identified a series of *N*-heterocyclic sulphonamide analogues that inhibit HsNMT1 with an IC_{50} in the micro- to nanomolar range.[142] The best of these inhibitors were tested in a variety of cancer cell lines (Figure 13, Table 2). The EC_{50}, which is the concentration of inhibitor that induces a response halfway between the minimum and the maximum was determined.

All inhibitors showed a high potency for recombinant HsNMT1 but the selectivity over HsNMT2 has not been reported. These inhibitors also have high potency in various cancer cell lines. The reason why the EC_{50} is significantly different in several cell lines for a given inhibitor is currently unclear. However, the cytotoxicity assay used might be misleading and will be discussed in Chapter 3.

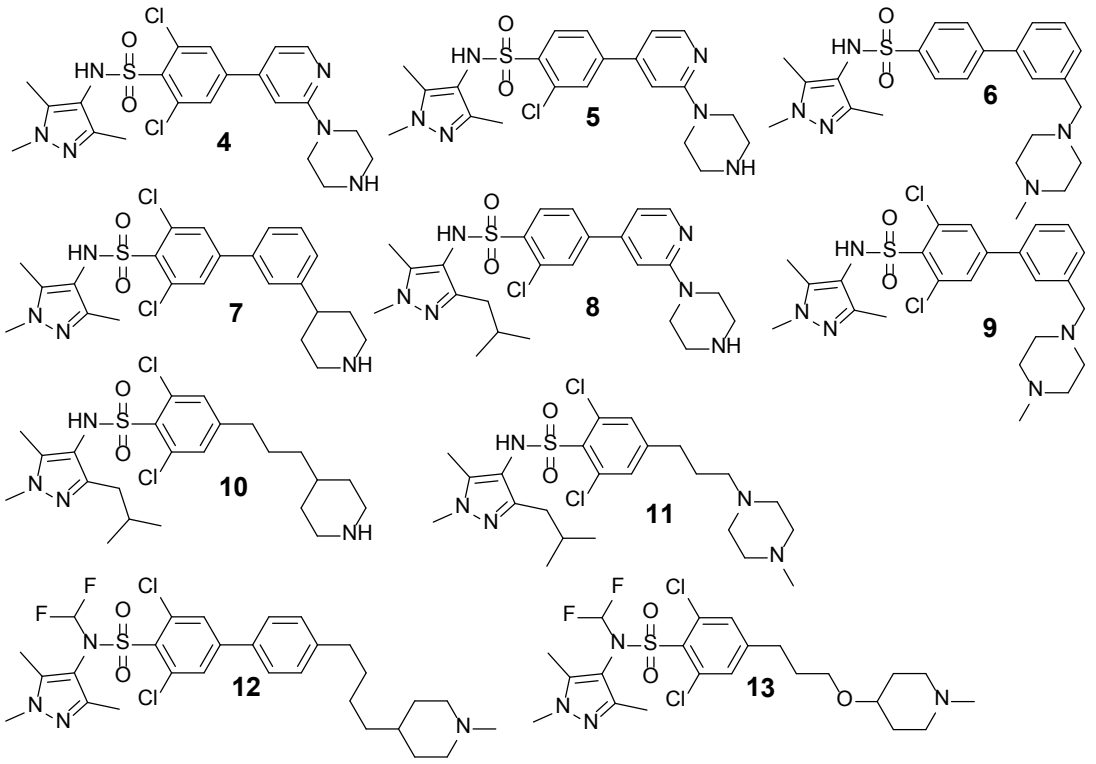

Figure 13.**HsNMT1 inhibitors.**[142]

Table 2: Activity of HsNMT1 inhibitors 4-13 determined in vitro using recombinant HsNMT1 (SPA assay) and several human cancer cell lines. HT29 : Human colon adenocarcinoma grade II cell line; HCT 116: Human colorectal carcinoma cell line; SkBr3: Human breast adenocarcinoma cell line; RT112: Human urinary bladder carcinoma (epithelial); C6: human glioma cell line; H460: Human lung carcinoma cell line; MRC5: Human lung cancer cell line; HT1080: Human connective tissue fibrosarcoma cell line; A549: adenocarcinomic human alveolar basal epithelial line; NCI-H1299 human non-small cell lung carcinoma cell line derived from the lymph node; MDA-MB-231: human breast adenocarcinoma cell line; OE19: human adenocarcinoma of gastric cardia/esophageal gastric junction cell line; OE21: human squamous carcinoma of mid oesophagus.

	IC_{50} (µM)	EC_{50} (µM)												
	SPA assay	HT29	HCT116	SkBr3	RT112	C6	H460	MRC5	HT1080	A549	NCI-H1299	MDA-MB-231	OE19	OE21
4	0.003	0.112	0.234	0.108	0.33	1.16	1.32	0.123	0.123	0.157	0.57	0.23	0.66	0.29
5	0.003	0.154	0.422	0.141	0.425	1.89	2.53	0.209	0.209	0.213				
6	0.02										1.08	0.64	4.37	1.39
7	0.008										3.71	0.89	4.57	1.20
8	0.001										0.096	0.047	0.132	0.057
9	0.006	0.176	0.629									0.448		
10	0.004	0.281	0.921									0.537		
11	0.002	>10	1.91									2.23		
12	0.006		0.282									0.218		
13	0.005		0.419									0.249		

1.8.3 NMT Assays

Several assays have been reported in the literature. A scintillation proximity assay (SPA), which uses detection based on radioactivity, has become widely used, including in our lab.[44] However, this assay is complex to implement, suffers from the inherent hazards associated with radioactive assays and the high cost of reagents, and is discontinuous. Recently, a fluorescence-based assay[143] and an ELISA assay [144] have been published to study the enzymatic activity of NMT while another has been developed in our lab using CPM (*N*-[4-(7-diethylamino-4-methyl-3-coumarinyl)phenyl]maleimide) (see Section 2.2.2 for more details). [145] This latter assay can be used for kinetic studies as well as for high-throughput screening of NMT inhibitors.

1.9 Selective HsNMT inhibitors as tools to study isoform substrate specificities

1.9.1 Possible strategies

As explained in Section 1.7, it may be possible to develop novel anticancer drugs by selectively targeting HsNMT1 over HsNMT2. A selective inhibitor could also be used as a tool to study isozyme substrate specificities in cells. The acyl-CoA pocket is thought to be well conserved and several authors have suggested that selective inhibitors of NMT should target the peptide binding pocket.[65,141] The divergence in peptide substrate specificity for the two HsNMT isoforms might therefore be exploited for drug development but this will require a better understanding of the isozyme substrate specificity.

Several methods are widely used to generate starting points for developing drug-like inhibitors, including high-throughput screening,[146] fragment based approaches,[147] *in silico* screening,[148] or a substrate mimetic approach.[149] The first method is usually expensive, while using docking studies would be problematic for designing a selective HsNMT1 inhibitor as the crystal structure of HsNMT2 has not been determined to date. The last method, using a substrate mimicking approach would be advantageous to determine the isozyme substrate specificity as large libraries of peptides can be prepared relatively easily and quickly compared to libraries of synthetic organic compounds. In order to design a peptide inhibitor or substrate, the proposed consensus of myristoylated proteins should be respected (see Section 1.4.2). Farazi *et al.* have also suggested that the selectivity and potency of an inhibitor may be improved by adding features that modify the conformation and dynamics of the Ab loop of NMT (see Section 1.3) [22].

Each isozyme could, in principle, be screened for activity using peptide libraries prepared using techniques including peptide macroarrays (also known as SPOT™ technology),[150] peptide microarrays[151], one-bead one-peptide (OBOP) libraries,[152] or phage display [153] combined with a

method to select or detect sequences that are myristoylated, for example using a chemical labelling technology developed for the detection of myristoylation.[154] The SPOT™ technology appeared advantageous as it allows rapid preparation and screening for activity a large number of peptides.[150]

1.9.2 SPOT™ synthesis

SPOT™ synthesis is a high throughput and miniaturised screening tool which was first introduced by Frank in 1992.[150] It allows highly parallel synthesis of peptides up to the microgram range.[150,155,156] On the equipment available in our lab up to 1200 peptides can be prepared at the same time (on two membranes of 600 sequences each), with purities that are expected to be sufficient for a screening assay on cellulose membrane. The cellulose-bound peptide arrays were shown to be well suited for the rapid investigation of molecular recognition events such as protein–protein interactions.[157] The membranes are constructed via optimised solid-phase synthesis methods.[157] The cellulose membrane is first functionalized with an amino moiety to allow the attachment of the growing molecules (Figure 14).

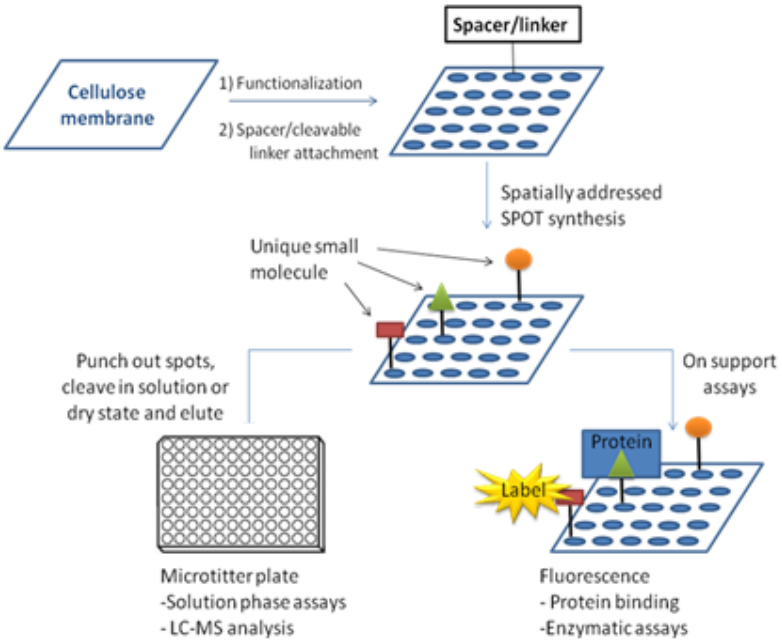

Figure 14: General schematic of SPOT™ synthesis.

A cleavable linker or a spacer can be added. A spacer, such as PEG, would enhance the accessibility of membrane-bound molecules for ensuing reactions and for on-support screening. In the next step, peptides are assembled from the C- to the N-terminus, using Fmoc/*t*Bu chemistry.[158] After side chain deprotection, peptide arrays are ready to be used for biological assays. Depending on the linker chemistry used, peptides may be cleaved from the cellulose membrane in the dry state (e.g. using

gaseous reagents or light) or in solution in order to do solution phase assays. However, on-support assays are more attractive as they require minimal peptide processing relative to off-support assays.[159] The quality of SPOT-synthesised peptides can be investigated by cleaving the peptide and analysing them by LC-MS or MALDI. The main disadvantage of this technique is that it is impossible to quantify absolutely the binding activities. Hits would need to be re-synthesised and tested using solution-phase assays.

1.10 Detection of myristoylation using bioorthogonal reactions

1.10.1 Traditional methods to study protein *N*-myristoylation

Before the democratisation of bioorthogonal reactions such as "click chemistry", several techniques have been used to demonstrate that a protein was *N*-myristoylated in cells. Radiolabelling with [^{3}H] myristate followed by detection by fluorography was one of the two main techniques used for studying protein acylation. However, the exposure time required was long (weeks to months) and to improve this, an analogue of myristate containing [^{125}I] was developed more recently. The sensitivity was greatly improved and the exposure time was much faster. However, both techniques require the use of hazardous material and unambiguous detection of the protein myristoylation often necessitates the purification or immunoprecipitation of the protein. Immunoprecipitation is a laborious technique and one antibody, often expensive or difficult to produce, is required for each protein of interest. As NMT is thought to have up to 100 targets in cells, new methods were needed to study myristoylation.

Myristate is only attached to the N-terminal glycine of NMT substrates and allows them to localise to the membrane (see Section 1.5.3). Overexpression of a G2A mutant of the protein in cells often leads to mislocalisation of the protein and can be seen by fluorescence microscopy in the presence of a fluorescent antibody for the molecule of interest. Several proteins have been shown to be myristoylated using this technique such as the neuron-specific calcium-binding protein hippocalcin, HPCA,[160] but it has several drawbacks. The proteins are not strictly shown to be *N*-myristoylated at the endogenous level as the protein is overexpressed in cells, greatly increasing the effective substrate concentration. Moreover, similarly to the radiolabelling experiments, this technique also requires expensive antibodies for each protein substrate.

Mass spectrometry can also be used to identify post-translational modifications (PTM) such as *N*-myristoylation, but this method also usually requires the enrichment or purification of the proteins of interest. The whole protein can be purified, digested with trypsin and analysed by MALDI or LC-MS/MS. The site of modification and the nature of the PTM can be identified and a few

proteins, such as BASP1,[161] were shown to be myristoylated using this technique. Alternatively, the whole cell lysate can be digested with trypsin. Recently, Bienvenut *et al.* analysed the modification of the N-terminal peptides of proteins in A2780 cells.[86] They managed to identify three N-myristoylated proteins, GNAI2, SLC44A1 and PSMC1 by identification of the N-terminal myristoylated peptide. However, such analysis of complex mixtures is extremely difficult, as suggested by the fact that only three NMT substrates were identified. This analysis is also limited by the need of a unique peptide and a tryptic site in the right place.

All this suggests that a simple, cheap and reliable method is needed to label as well as enrich *N*-myristoylated proteins.

1.10.2 Metabolic chemical tagging and bioorthogonal ligation

Chemical labelling technologies have recently been developed to detect *N*-myristoylation based on an enzymatic tagging strategy combined with bioorthogonal reactions, such as Copper-catalysed azide-alkyne cycloaddition (CuAAC).[154,163] The metabolic tagging strategy involves the incorporation of a unique functionality, a chemical reporter, into targets of interest, followed by chemical labelling with a small molecule probe (Figure 15).[162]

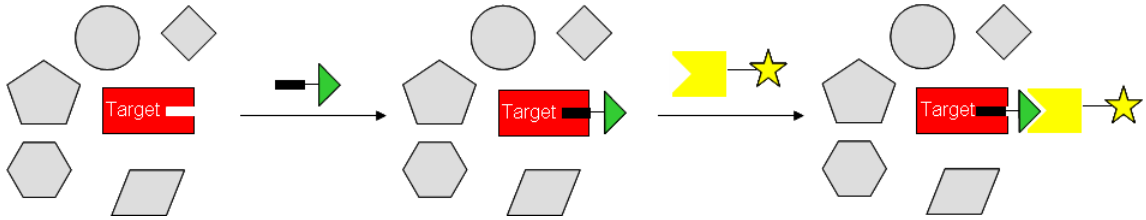

Figure 15: The metabolic tagging strategy (also referred to as the bioorthogonal chemical reporter strategy. A probe, which comprises a chemical reporter unit (black) and a reactive group or warhead (green triangle), is introduced into a target biomolecule or peptide through cellular metabolism. The probe covalently reacts with the biomolecule or peptide. In a second step, the reporter is chemically labelled with an imaging moiety (yellow). [162]

The term 'bioorthogonal ligation reaction' has been coined to encapsulate the concept of reactions that can couple two molecules bearing particular functional groups with complete specificity against the background of a complex biological system. Some authors extend this to reactions that are strictly non-toxic to cells or animals.[164] Bioorthogonal ligation is mainly used for *in vitro* and cell-free applications, although some have been used *ex vivo* and *in vivo.*[162] An ideal bioorthogonal reaction should be specific, fast and irreversible, producing no by-products (or only non-toxic by-products) and take place readily in buffers or *in vivo*. Reactions of particular interest are those with azide or alkyne as chemical reporters because of their small size and their absence in natural systems.[162]

Several bioorthogonal reactions have been studied to date including Staudinger ligation, Copper-catalysed azide-alkyne cycloaddition (CuAAC) and Strain-promoted azide-alkyne cycloaddition (SPAAC) (Scheme 1).

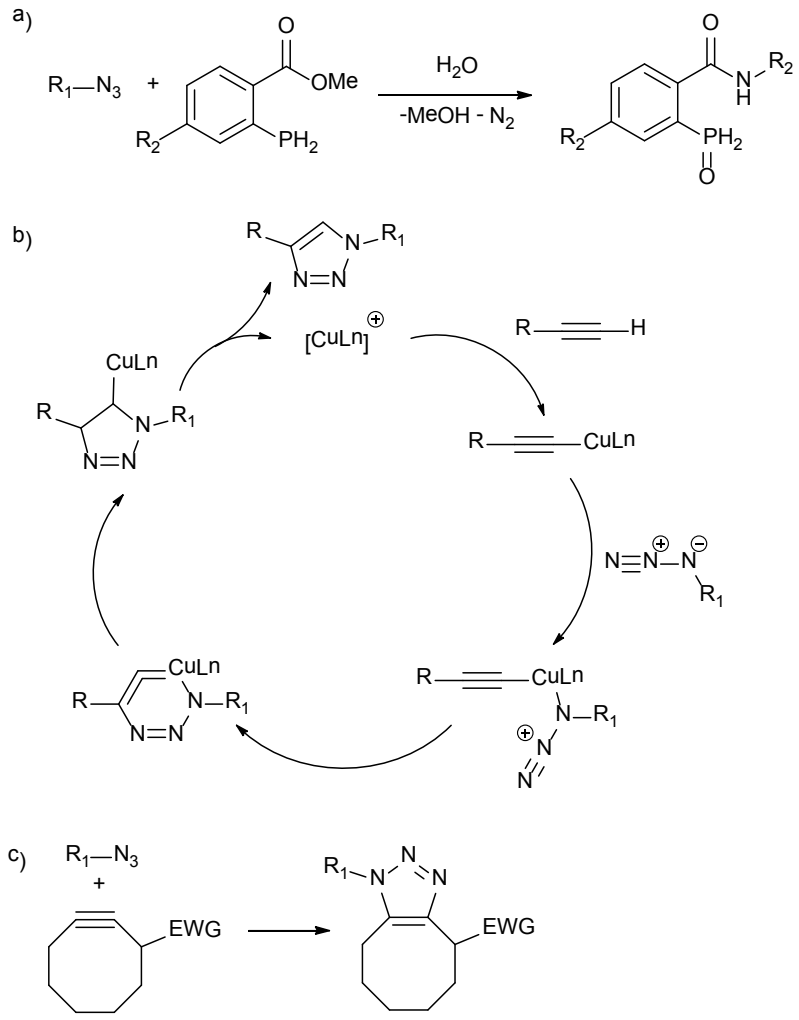

Scheme 1. Commonly used bioorthogonal reactions. a) Staudinger ligation; **b)** Copper-catalysed azide-alkyne cycloaddition (CuAAC); **c)** Copper-free cycloaddition (EWG= electron widrawing group).

1.10.2.1 The Staudinger ligation

The Staudinger ligation is a reaction between an azide and an ester-derivatised phosphine, producing an amide.[165] Although this reaction is highly specific and reagents are easily prepared, the reaction is slow and suffers from competing oxidation of the phosphine reagents.[166]

1.10.2.2 Copper-catalysed azide-alkyne cycloaddition (CuAAC)

The Cu-catalysed azide–alkyne cycloaddition (CuAAC), also known as the most widely recognised "click reaction", was first developed by Sharpless *et al.* [167] and Meldal *et al.*.[168] This reaction,

between an azide and a terminal alkyne, activated by a Cu catalyst and provides a 1,4-disubstituted triazole with a high reaction rate . The reaction is highly specific and has been used in Dr Tate's group to perform chemical labelling and tag-mediated proteomics.[154] However, this reaction requires the use of several reagents including either copper (I) or copper (II) and a reducing agent, and a ligand in addition to the azide and alkyne moieties. The reaction conditions need to be optimised for a given application.

1.10.2.3 Strain-promoted azide-alkyne cycloaddition (SPAAC)

An alternative reaction is catalyst-free [3 + 2] cycloaddition with azides activated by ring strain. This strain-promoted cycloaddition is a reaction between an azide and an alkyne affording a bicyclic triazole, and was discovered by Wittig and Krebs in 1961.[169] They noted that cyclooctyne, the smallest of the stable cyclooctynes, reacted spontaneously with phenyl azide to give a triazole. The bond angle of the acetylene in an 8-member ring is 163° ,[170] whereas the normal bond angle of acetylene is 180°. This considerable bond angle deformation of the acetylene represents 18 kcal/mol of ring strain.[170] This destabilisation of the ground state of the reaction decreases the activation energy and provides a significant rate acceleration compared to unstrained alkynes.[170] The reaction can also be promoted by appending electron-withdrawing groups (fluorine or aromatics) to the octyne ring in order to lower the energy of the LUMO of the alkyne. This allows a greater overlap with the azide HOMO and favours the reaction. A number of compounds have been developed to date, but they usually suffer from demanding synthesis (many steps, low yield), low stability and slower reaction kinetics compared to the copper catalysed reaction.[166] Several reagents have been reported in the literature that when used in cell lysates or *in vivo* suffer from high background.[171]

1.10.3 Analogues of MyrCoA used as chemical reporters

In order to study myristoylation, our group has developed two myristic acid analogues, adding an azide or alkyne at the terminal position (Figure 16). The two analogues, azido dodecanoic acid (**15**, AzC12) and tetradec-13-ynoic acid (**16**, YnC12), mimic myristic acid as they respect the chain length and flexibility. Importantly, they have been shown to be transferred with equal efficiency *in vivo.*[154] The fatty acid chain acts as the reactive group (warhead) and binds covalently to a protein or peptide substrate in the presence of NMT. The alkyne and azide moieties act as a chemical reporter, which is needed to perform bioorthogonal ligation in the second step (Figure 15).

The myristic acid analogues can be directly fed to the cells as they are converted into the CoA thioester in cells by CoA transferase.[154] However, to carry out *in vitro* experiments, the two myristic acid analogues need to be converted into the CoA thioesters: AzC12CoA (**18**) and YnC12CoA (**19**) (Figure 16).[154]

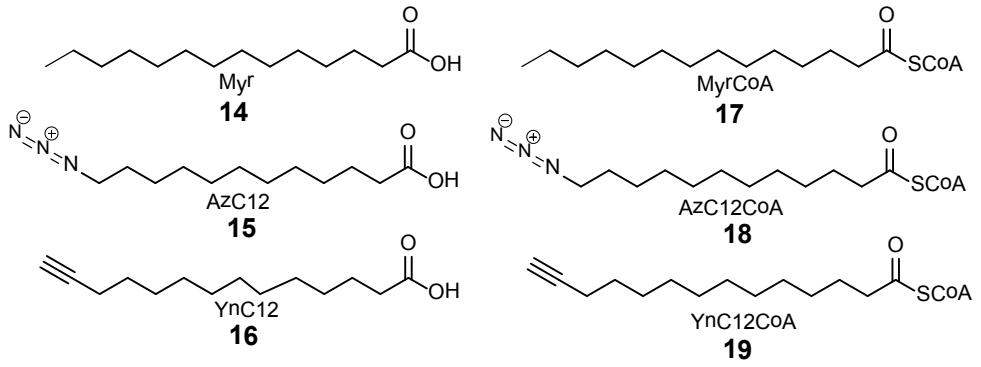

Figure 16: Myristic acid (Myr) and analogues (AzC12 and YnC12) and MyrCoA and MyrCoA analogues (AzC12CoA and YnC12CoA).

Imaging probes using click chemistry have also been developed in our lab.[163] Probes **20** (referred to as AzTB) and **21** (referred to as YnTB) comprise a fluorescent moiety (TAMRA), biotin, a linker and a chemical reporter moiety (azide and or alkyne respectively) (Figure 16). The fluorescent moiety allows direct visualisation of the myristoylated proteins by fluorescence while the biotin moiety allows enrichment of the myristoylated proteins on streptavidin beads or detection of the proteins by chemiluminescence (using a horseradish peroxidase (HRP) anti-biotin antibody conjugate) when fluorescence detection is not appropriate. Probe **22** is composed of a fluorescent moiety (fluorescein) and an alkyne tag. These probes are used to carry out tag-mediated proteomics experiments, also referred as chemical proteomics (see Section1.11). A typical workflow applied to study *N*-myristoylation in cells or in vivo is presented in Figure 18.

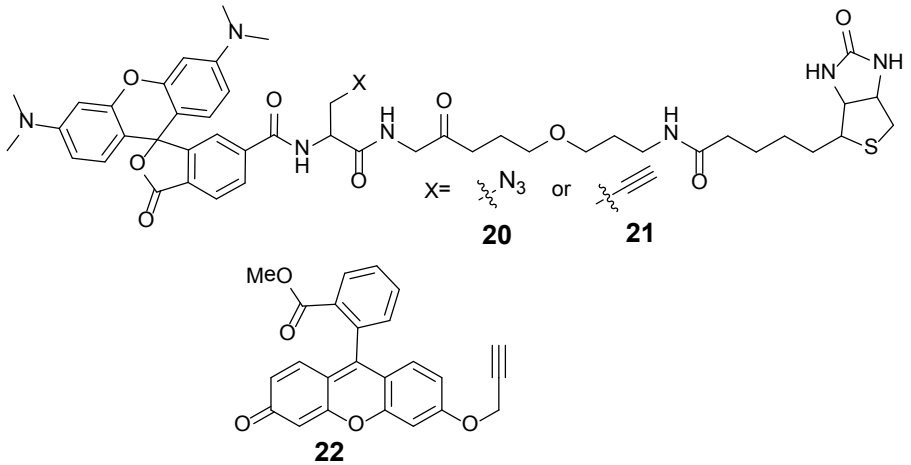

Figure 17: Imaging probes AzTB 20, YnTB 21 and fluorescein-alkyne22.

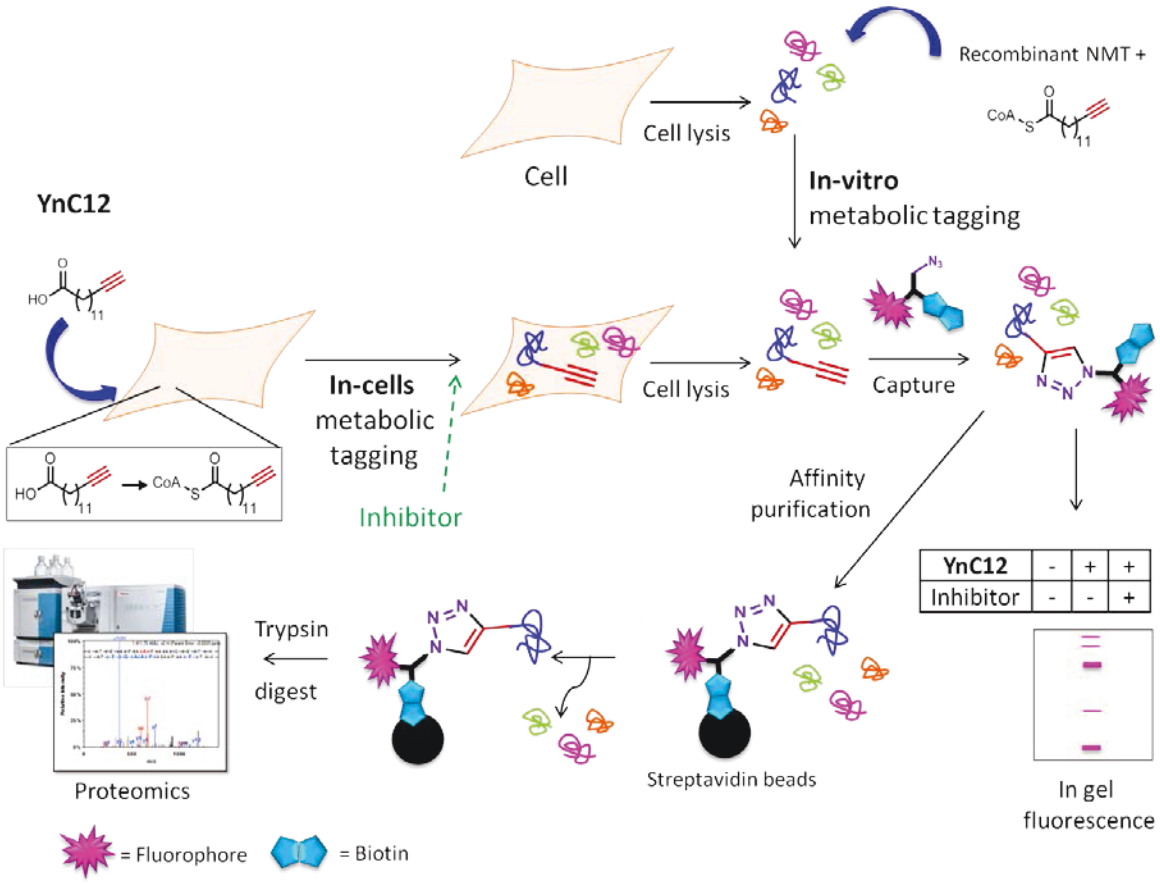

Figure 18. *In vitro* and in-cell chemical labelling of *N*-myristoylated proteins by YnC12.

It was suggested that the enzymes mediating protein palmitoylation are less specific and transfer probes of different length,[172,173] implying that YnC12 could label palmitoylated proteins.[163] Protein palmitoylation, catalysed by palmitoyl acyltransferases, predominantly corresponds to the reversible attachment of a C16-fatty acid to side-chain cysteine residues (*S*-palmitoylation), but irreversible attachments have also been reported (*N*-palmitoylation, through S-N rearrangement forming amide bond).

Alkyne-tagged probes have been reported to study protein palmitoylation, such as YnC15 (**24**) [174] and YnC16 (**25**)[172,175] (Figure 19). YnC16 (also referred to as 17-ODYA or 17-octadeynoic acid)[172,173,175], is widely used to study protein palmitoylation but it has also been shown to label *N*-myristoylated proteins, possibly in place of myristate.[175]

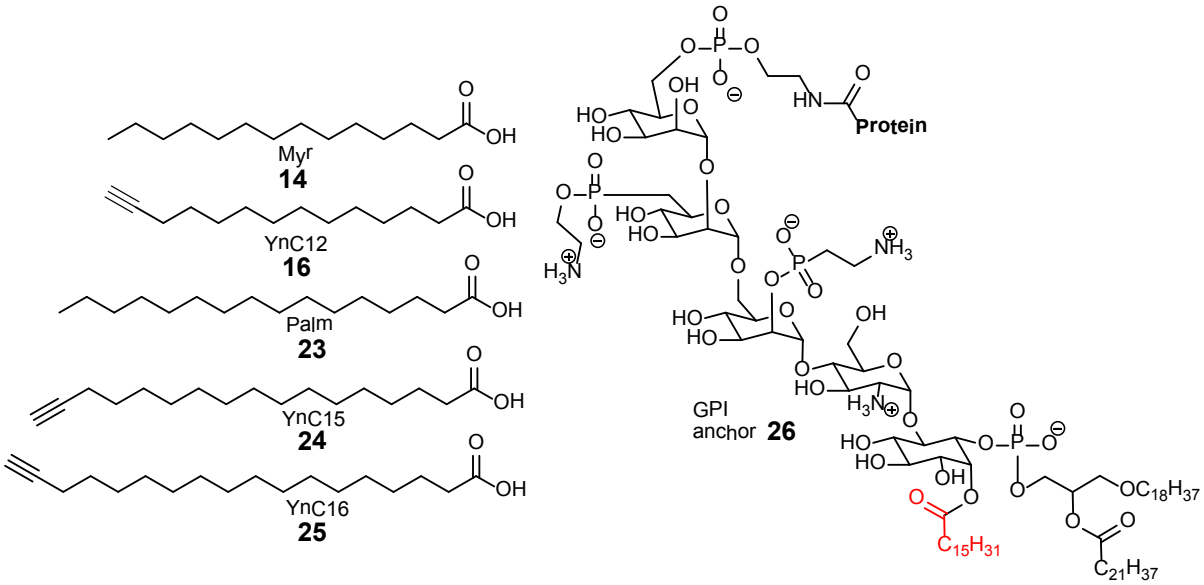

Figure 19. Structure of palmitic acid (Palm) and analogues compared to Myr and YnC12, and structure of human glycosylphosphatidylinositol (GPI) anchor. Palmitate is shown in red in the GPI-anchor.[176]

YnC12 could also incorporate into glycosylphosphatidylinositol (GPI)-anchored proteins (Figure 19). GPIs are glycolipids attached post-translationally to the C-terminus of a protein, and are composed of lipids, carbohydrates, and inositol phosphoester groups.[177] In some species, such as *Plasmodium*, GPIs incorporate myristic acid via an ester linkage and YnC12 was shown to label GPI-anchored proteins.[163] Whilst GPIs in humans are not enriched in myristate, they do incorporate palmitic acid. It is probable that YnC12 also labels GPI-anchored proteins in humans, in the same way that YnC12 can replace palmitate in *S*-palmitoylation.

1.11 Mass spectrometry for chemical proteomics

1.11.1 Introduction to mass spectrometry-based proteomics

Mass spectrometry (MS)-based proteomics is now widely used to answer biological questions.[178] It relies on the accurate measurement of the mass-to-charge ratio (m/z) of a protein or peptides originating from proteins, which can then be identified using various databases and software. Equipment and computational software are rapidly improving and many sample preparation protocols are now available for a wide-range of needs and applications. MS-based proteomics can for example allow identification of the protein composition of a cell or an interacting protein from a purified protein complex, as well identifying PTMs of proteins in a lysate.

Two approaches have been developed for sample preparation and analysis. A protein can be purified and characterised directly by analysis of its mass ("top-down proteomics"). This technique presents

many drawbacks; large proteins are sometimes difficult to identify as the mass differences between proteins with similar composition is small and complex mixtures cannot be analysed using this approach.[179]

Bottom-up proteomics relies on the analysis of peptides derived from the enzymatic cleavage of proteins.[178] The proteins can be separated prior to the digest, enriched on beads (see Section 1.10.3), separated on a SDS-PAGE gel, or complex mixtures can be digested and analysed ("Shotgun") (Figure 20). Proteins are usually cleaved into small peptides by the addition of a proteolytic enzyme, such as trypsin, which cleaves the protein backbone after each lysine and arginine residue. Peptides mixtures are analysed by liquid chromatography coupled to a tandem mass spectrometer (LC-MS/MS). Peptides are separated by liquid chromatography (LC), ionised and the mass of the peptide analysed by MS. A first MS-spectrum (MS1) shows the ion current versus the mass-to-charge ratio (m/z). The most abundant peptides are selected and fragmented by collision with an inert gas at low pressure ("collision induced dissociation"). A second MS-spectrum (MS2) presents the list of m/z ratios for different fragments, which will allow the identification of the peptide sequence by calculating the mass difference between the various fragments and correlating it to the mass of an amino acid. The whole data recorded (Retention time (Rt), MS1 and MS2) is automatically recorded and saved as a .raw file. Using software, the data is searched against genome-specific protein databases to identify proteins *via* their "peptide mass fingerprint".[180] A peptide is referred as a "unique peptide" when its sequence can only be found in one protein in the protein database. One unique peptide can be sufficient to identify a protein, but two or more peptides provide higher confidence identification.

The most widely used peptide search engines, Mascot [181] and SEQUEST [182] are commercially available but free program such as X!Tandem are also available.[183] Each MS2 is compared to model MS2 spectra of all candidate peptides in a protein database. Once the peptides have been identified, a second software, such as Scaffold, is required to identify the proteins.[184]

For quantitative proteomics, MaxQuant was used in the current study as it was available free of charge and provided with its own research engine, Andromeda.[185] A typical proteomics workflow is presented in Figure 20.

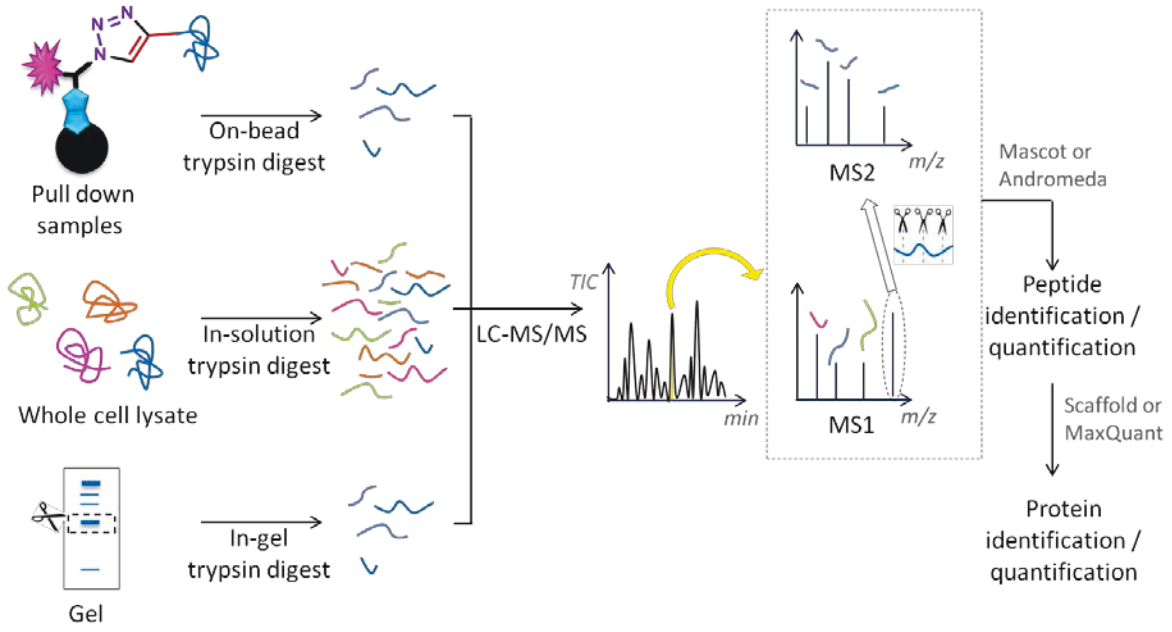

Figure 20. Typical proteomics workflow.

One of the key challenges in MS-based proteomics is to separate and detect peptides in very complex mixtures. LC methods can be optimised to allow better resolution of the peptides but sample fractionation or protein enrichment is often require to reduce complexity. Sample fractionation can be achieved by eluting proteins on a 1D or 2D SDS-PAGE gel. The gel can be cut in several portions, proteins in-gel digested and peptides extracted.[186] Alternatively, whole cell lysates can be subjected to a subcellular fractionation. A detergent such as sodium dodecyl sulphate (SDS) may be required for cell lysis but this is not always compatible with in-solution digestion of the sample and MS analysis. To overcome this problem, a new method was recently reported, filter-aided sample preparation (FASP).[187]

Another strategy to reduce sample complexity relies on digest of a complex mixture of proteins into peptides which can then be separated and fractionated according to their polarity (using a reverse phase column) or according to their charge (using a strong cation exchange column).

Finally, proteins of interest can also be tagged using activity-based probes (ABP) [188]or a metabolic chemical tagging approach (Section 1.10.2), subjected to CuAAC with a capture reagent bearing a biotin moiety and enriched on streptavidin beads, before being subjected to on-bead digestion. The latter method is highly advantageous to enrich and detect *N*-myristoylated proteins tagged with an analogue of MyrCoA and captured as described in Section 1.10.3. In theory, only tagged proteins should be enriched on beads and detected. Moreover, this approach dramatically reduces the

sample complexity and should allow the identification of a large number of *N*-myristoylated proteins, including proteins poorly abundant in cells.

1.11.2 Quantification

In the last ten years, many methods have been developed to allow relative quantification between samples. Absolute quantification is also possible by using an internal standard, but is often not required as relative quantification is often sufficient to answer biological questions.[189,190] The choice of the method depends on the cost, number of samples to be compared, simplicity of sample preparation and the accuracy required. Most techniques are based on the introduction of an isotopic label at different stages of the sample preparation, which can then be differentiated by mass spectrometry. When the isotope is introduced at the beginning of the sample preparation, the samples to be compared are mixed, prepared (digested/fractionated/enriched) and analysed together. This approach is advantageous as there is a low risk of experimental bias arising from sample loss during enrichment/fractionation, from the sample digest or with the LC-MS/MS analysis. Isotopic label can be incorporated directly in the biological sample, such as for SILAC (Stable isotope labelling with amino acids in cell culture) or can also be added just prior to the LC-MS/MS analysis as for the isobaric labelling method iTRAQ (isobaric tags for relative and absolute quantification)[191] or dimethyl labelling method.[192] Label-free quantification is also possible and has the advantage of an easy and inexpensive sample preparation.[189,193] Protein quantification is then possible using either spectral counting or ion peak intensity. However, as unlabelled samples are individually analysed, the workflow must be tightly controlled to avoid bias. An overview of the principles, advantages and disadvantages of the most commonly used methods is presented in Table 3.

Table 3. Most commonly used methods for MS-based quantitative proteomics:[189,190] label-free quantification,[193] SILAC,[194] spike-in SILAC,[195] dimethyl labelling [192] and iTRAQ.[191] n/a = not available.

Method	Example of technique	Principle	Introduction of label	Number of samples	Main advantages	Main disadvantages
Label-free quantification	n/a	No label	no label	∞	Easy sample preparation, easy and cheap sample preparation	Experimental bias, careful processing required, samples need to be processed at the same time and analyse one after the other to decrease experimental bias
Metabolic labelling	SILAC	Arginine and lysine replaced by isotopically labelled Arg and Lys in the culture media	At lysate level, before sample processing	3	No experimental bias, can compare 2 or 3 samples in one LC/MS/MS run, Heavy Lys and Arg allow most peptides to potentially be quantified. Typically a large isotope shift (> 6Da).	Requires dialysed serum or a defined media to introduce the label, heavy amino acids are expensive, labelled Arg might convert to Pro, *in vivo* labelling is difficult as proteome turnover is required for complete labelling
Spike-in SILAC	n/a	Preparation of a standard containing heavy labelled Arg and Lys. Other samples / tissue are prepared as usual	At lysate level, before sample processing	∞	No experimental bias, no limit of the number of samples, the experiment and heavy control can be in different cell lines including tissues that cannot be SILAC labelled, samples prepared at different times can still be compared if they have the same heavy standard	Overlap is required between the SILAC and the non-labelled samples.
Isotopic tags	Dimethyl labelling	Stable isotope incorporation into primary amines at the peptide level by addition of isotopically labelled formaledhyde and sodium cyanoborohydride	At peptide level, before LC-MS/MS analysis	3	Cheap reagents, quick and reliable reaction, applicable to any samples	Experimental bias due to the introduction of the label at the peptide level, small isotopic effect during the LC separation of peptides.
Isobaric tags	Isobaric tags for relative and absolute quantification (iTRAQ)	Stable incorporation of an isobaric reagent into primary amines at the peptide level	At peptide level, before LC-MS/MS analysis	8	Applicable to any samples, can compare up to 8 samples in one LC-MS/MS run	Experimental bias due to the introduction of the label at the peptide level, reagents are expensive and not highly stable. Analysis is not well suited for Orbitraps.

1.12 Project objectives

The aim of this PhD project is to validate a set of chemical tools to study the role of NMT in cancer and provide further validation of NMT (and perhaps NMT1) as a cancer drug target. As explained in Section 1.7, NMT has been suggested as a potential therapeutic target in cancer, but to date no study has shown that NMT inhibition could kill cancer cells. Several NMT inhibitors have been reported in the literature (Section 1.8), but cell toxicity has not been correlated with on-target inhibition of NMT. It was also proposed that selective inhibition of NMT1 could be sufficient to kill cancer cells and could have reduced toxicity in healthy cells.

The main objectives of this PhD thesis were to:

1) Optimise the synthesis of myristic acid analogues and demonstrate that these analogues can be applied in cancer cells to label *N*-myristoylated proteins.

2) Identify NMT substrates in a cancer cell line using a chemical proteomics approach.

3) Identify potent inhibitors of HsNMT that could be used as tools to manipulate myristoylation in cancer cell lines.

4) Study the effects of NMT inhibition in cancer cells.

5) Explore the substrate specificity of the HsNMT isoforms.

Chapter 2 Tools to study *N*-myristoylation

Previous work in the Tate group showed that myristate analogues YnC12 and AzC12 (Figure 16) can be used in combination with trifunctional capture reagents AzTB and YnTB (Figure 17) to label proteins in HeLa, a mammalian cancer cell line.[163] This chapter describes an optimised synthesis of both myristate analogues YnC12 and AzC12 and a novel synthesis of the palmitate analogue YnC15 (Figure 19). Myristate analogues might also incorporate into palmitoylated proteins (Section 1.10.3) and YnC15 would be a valuable tool to identify crosstalk between labelling of myristoylated and palmitoylated proteins.[174]

A fluorescent assay to study *N*-myristoylation, referred to here as the CPM assay, will be described. Kinetic studies were used to define kinetic parameters of MyrCoA and a peptide corresponding to the N-terminus of known NMT substrates. These parameters have been used to set up conditions for the inhibition assay; the latter was employed to screen for new HsNMT inhibitors (Chapter 3). The kinetic parameters of MyrCoA were compared to YnC12CoA and AzC12CoA in order to show that myristate analogues mimic the natural lipid substrate and are good substrates of both HsNMT isoforms.

Initial experiments with the myristate analogues in cells will be described, including optimisation of the labelling conditions and subsequent experiments that show that the probe YnC12 can be used to label and enrich NMT substrates in HeLa cells. While the main focus of the current Chapter is on co-translational myristoylation, experiments were also carried out to optimise the labelling conditions to detect post-translational NMT substrates in cells undergoing apoptosis (Section 1.5.2).

2.1 Synthesis of analogues

Synthetic routes to prepare myristate analogues as well as a palmitate analogue are reported but modification of the reported procedures was required to achieve good yields. Myristate analogues could be directly fed to the cells but could not be used for *in vitro* studies (Section 1.10.3). As a consequence, MyrCoA analogues were also synthesised to assess NMT activity in an *in vitro* assay (Section 2.2) or to carry out *in vitro* reactions (Chapter 6).

2.1.1 YnC12 16

YnC12 synthesis was initially achieved in two steps from commercially-available 12-bromododecanoic acid **27**, according to a procedure previously published by our group.[154] The first step involved displacement of the bromide by an organolithium reagent generated *in situ* using *n*-butyl lithium and TMS-acetylene (Scheme 2). Ensuing deprotection with potassium carbonate was quantitative and the product **16**, YnC12, did not require further purification.

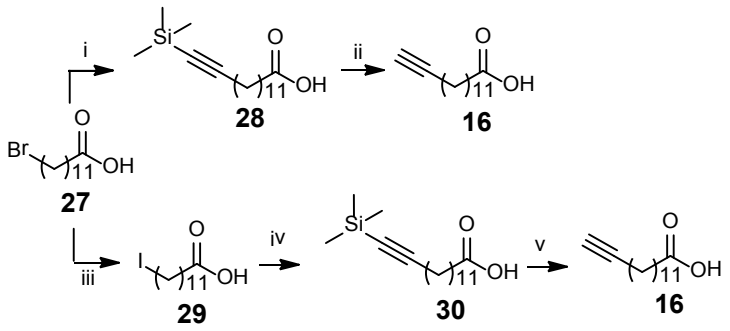

Scheme 2. Synthesis of YnC12. Reagents and conditions: i) TMS-acetylene, *n*-Buli (2.5 M in hexanes), dry THF, HMPA, -78 °C, 14%; ii) K_2CO_3, MeOH, RT, quantitative; iii) KI, dry acetone, 89%; iv) TMS-acetylene, *n*-Buli (2.5 M in hexanes), hexanes, dry THF, HMPA, -78 °C, 48%; v) 1) K_2CO_3, MeOH, RT; 2) Ethanolamine, DMSO, 120 °C; 84%.

However, the first step suffered from low yields (typically 10-20 %) due to the poor conversion of the bromo- starting material **27** to product **28** and the difficulty separating the starting material and the product by column chromatography. This yield was comparable to a previously reported yield of 25%.[154] To overcome this problem, 12-bromododecanoic acid **27** was converted to 12-iododododecanoic acid **29** (Scheme 2). The yield of the reaction to form the TMS-acetylene product **26** proved to be higher (48%) using the iodo- starting material as Iodine is a better leaving group than bromine. After this second step, the crude product **30** still contained 2 % intermediate **29** (by ^{1}H NMR) and purification was difficult. However, this impurity could easily be removed following the deprotection step by heating the product in the presence of ethanolamine in DMSO. The iodo-intermediate reacts with ethanolamine, and the polar product formed could then be removed by

washing the crude product dissolved in Et_2O with water. The product **16** did not require further purification. The overall yield of YnC12 **16** was significantly higher using this new synthetic route (36% versus 14%). The new synthesis required two additional steps, but following the last step no further purification was required. The yield of the second step could still be improved by decreasing the excess of *n*-butyl lithium used and the time of the reaction as a large excess of *n*-butyl lithium might lead to the degradation of the product. It was noticed that for similar reaction, to prepare a alkyne-tagged fatty acid of different length, using 2 eq of *n*-butyl lithium instead of 3 eq and leaving the reaction to stir at room temperature for 4 h instead of overnight, could dramatically improve the yield of the reaction up to 60-70% (observation made by Tom Charlton, Tate group, Imperial College London). This improved protocol will be used to prepare a new batch of YnC12, when required.

2.1.2 AzC12 15

AzC12 was also prepared from 12-bromododecanoic acid according to a procedure previously established in our lab.[154] However, this procedure, which involved the synthesis of AzC12 **15** in one step, via S_N2 displacement of the bromide by sodium azide, suffered from low conversion and the product was difficult to separate from the starting material.

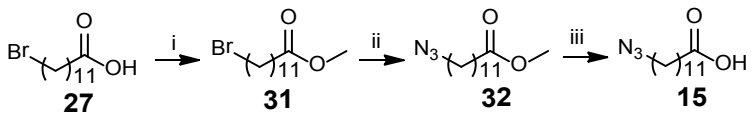

Scheme 3. Synthesis of AzC12. Reagents and conditions: i) MeOH, H_2SO_4, reflux, 93%; ii) NaN_3, DMSO, RT, 89%; iii) NaOH 2N, MeOH, 83%.

To overcome this problem, 12-bromododecanoic acid **27** was first esterified in the presence of catalytic amounts of sulphuric acid and methanol (Scheme 3). The ester **31** was then allowed to react with sodium azide to yield methyl-12-azidododecanoate in a good yield. ^{1}H NMR of the product **32** showed that there was no starting material left. Saponification of ester **32** gave 12-azidododecanoic acid **15**, AzC12, in high yield.

2.1.3 YnC15 24

YnC15 is an analogue of palmitic acid and has been used in the Tate group to study palmitoylated proteins (Section 1.5.3.1). A procedure to prepare YnC15 was previously established in our lab from the commercially available 15-bromopentadecanoic acid. However, this starting material was no longer readily available commercially and therefore another strategy was developed to prepare YnC15.

Two methods were envisaged (Scheme 4). The first method comprised the conversion of the hydroxyl group of 15-hydroxypentadecanoic acid **34** into a better leaving group such as bromine, tosylate or iodine, followed by the nucleophilic substitution of this leaving group by TMS-acetylene. Deprotection would then provide YnC15 **24**.

The second method involved the formation of a C17-fatty acid chain, bearing a terminal alcohol and an alkyne function anywhere along the chain (**36**), followed by the displacement of the triple bond to the terminal position opposite to the alcohol using to the zipper reaction (**35**).[196] The alcohol could then be oxidised to yield the expected product **24**. This strategy was applied in the literature to prepare another analogue of palmitic acid, YnC16 from the commercially available 7-hexadecyn-1-ol.[197] No suitable starting material was commercially available to prepare YnC15 using this method but **36** could be easily synthesised in one step from 11-bromoundecanol **8** and 1-hexyne **37.**

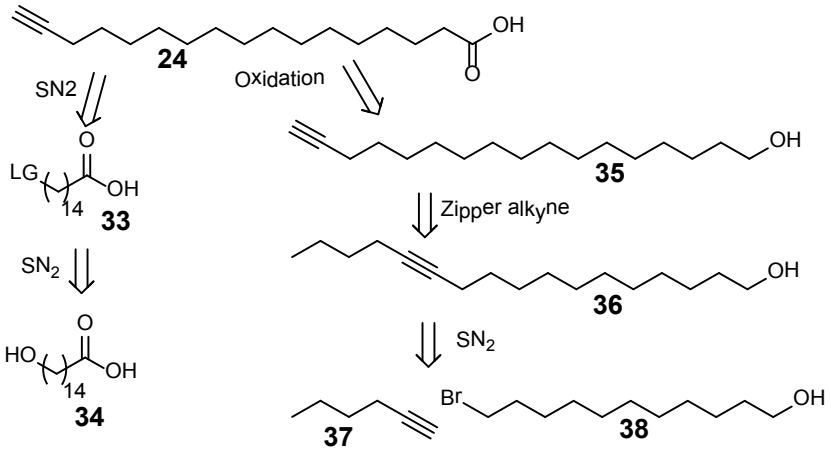

Scheme 4. Strategies to prepare YnC15 24.

2.1.3.1 First strategy

Several reactions were attempted to convert the terminal alcohol into a better leaving group (Scheme 5).

First, synthesis of 15-bromopentadecanoic acid **39** was attempted by heating a solution of 15-hydroxypentadecanoic acid **34** in HBr 33 % wt in AcOH under reflux.[198] The yield was fairly low (38%) but might have been improved by the addition of more HBr 33 % wt in AcOH. Another attempt to prepare compound **39** was carried out by adding CBr_4 and PPh_3 in acetonitrile to 15-hydroxypentadecanoic acid **34**.[199] **39** was afforded with moderate yield but an unknown impurity was present with the product and proved difficult to separate by column chromatography as the two compounds had the same retention factor (Rf) on TLC. Mass analysis did not help assign the

structure of the by-product but it appeared that an atom other than bromine was substituted at the hydroxy group as the protons adjacent to the terminal position were shifted on the NMR (Section 8.1.4). Protecting the carboxylic acid as a methyl ester and bromating the ester did not improve the reaction as a similar impurity was present.

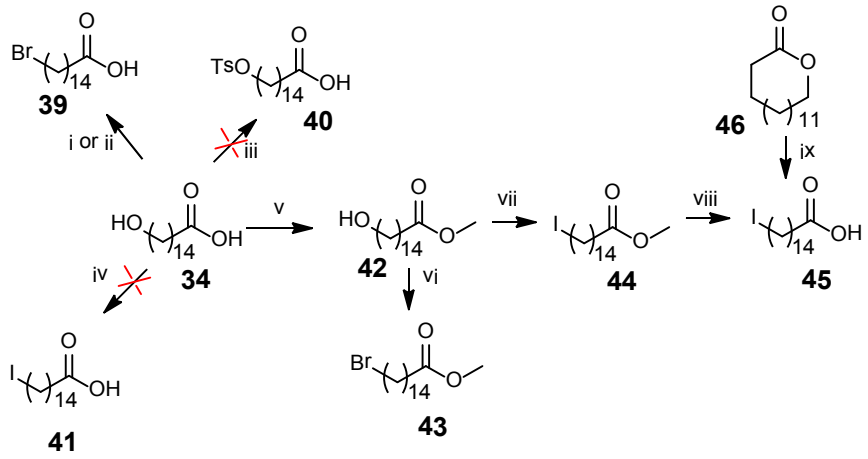

Scheme 5. Attempts to replace the hydroxyl group of 15-hydroxypentadecanoic acid 34 with a better leaving group. Reagents and conditions: i) HBr, AcOH, 80 °C, 38 %; ii) CBr_4, PPh_3, MeCN, RT, 44%; iii) TsCl, pyridine, DMAP; iv) imidazole, I_2, PPh_3, DCM; v) MeOH, H_2SO_4, Reflux, 91%; vi) CBr_4, PPh_3, AcN, RT, 44%; vii) imidazole, I_2, PPh_3, DCM, 64%; viii) 4N NaOH, THF, RT, 70 %; ix) HI, AcOH, reflux, 77 %.

Attempts to tosylate the hydroxyl group (compound **40**) or to iodinate (compound **41**) in this position were unsuccessful, and the starting material was recovered. Therefore, it was decided to protect the acid as the methyl ester. Methyl 15-hydroxypentadecanoate **42** was converted to methyl 15-iodopentadecanoate **44** in presence of imidazole, I_2, PPh_3 and DCM.[200] Ester cleavage proved difficult in aqueous solution of NaOH 2N due to the poor solubility of compound **44**. Addition of THF improved the solubility and compound **45** was afforded with good yield (70%).

Another method had been used in the literature to prepare compound **45**.[201] The commercially available pentadecanoline **46** was heated under reflux in a solution of HI in AcOH. This method afforded compound **45** in one step, with moderate yield and was preferred to prepare 15-iodopentadecanoic acid **45**. The later was then converted to YnC15 **24** in two steps, using the same method as for YnC12 (Scheme 6 and Section 2.1.1).

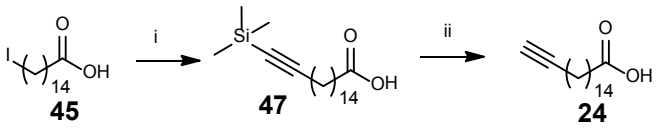

Scheme 6. Synthesis of YnC15 using the first strategy. Reagents and conditions: i) TMS-acetylene, *n*-Buli (2.5 M in hexanes), DMPU, dry THF, -78 °C then RT, 37 %; ii) K_2CO_3, MeOH, RT, 94 %.

2.1.3.2 Second strategy: zipper reaction

As described in Scheme 4, a C17 fatty alcohol bearing an alkyne in the middle of the chain could be prepared from 11-bromoundecanol **38** and 1-hexyne **37** via a S_N2 reaction and converted to a terminal alkyne using the zipper reaction. Attempts to couple these two reagents in the presence of *n*-BuLi and DMPU in THF were unsuccessful. The hydroxyl group was therefore THP-protected and the intermediate **48** was coupled to 1-hexyne **37** using the same conditions.

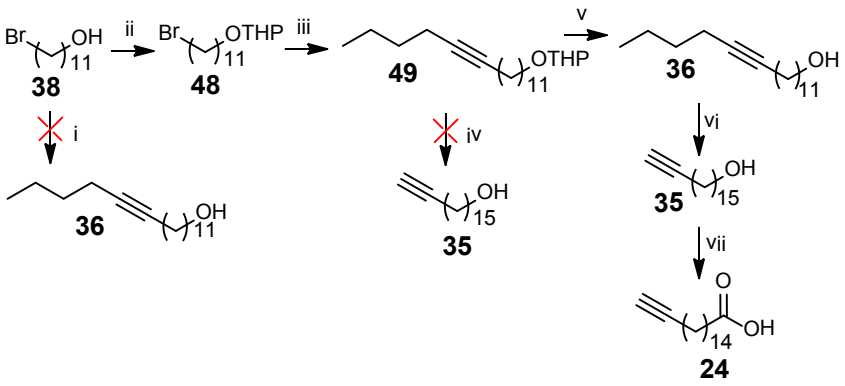

Scheme 7. Second strategy to synthesise YnC15. Regents and conditions: i) 1-hexyne **37**, *n*-BuLi, DMPU, THF; ii) DHP, *p*-TsOH, DCM, RT, 81%; iii) 1-hexyne, *n*-BuLi, DMPU, THF, -78 °C then RT; 66 %; iv) NaH, 1,3-diaminopropane; 70 °C then 50 °C, v) *p*-TsOH, MeOH, reflux, 83%; vi) NaH, 1,3-diaminopropane, 70 °C then 50 °C, 35%; vii) Jones reagent, acetone, 0 °C then RT, 67%.

The zipper reaction relies on the migration of an alkyne to the end of an alkyl chain upon exposure to strong base. The strong base is generated *in situ* by adding 1,3-diaminopropane to sodium hydride or potassium hydride, to give 1,3-diaminopropanide.[196] The reaction involves a series of alkyne/allene interconversions (Scheme 8). This process repeats itself until a stable terminal alkyne anion is formed.

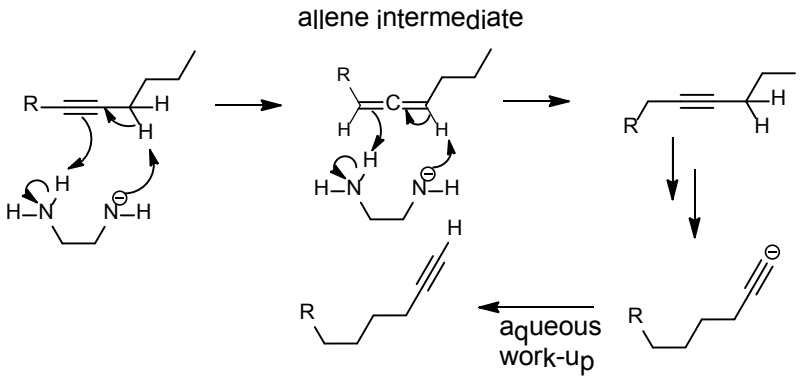

Scheme 8. Zipper reaction mechanism, adapted from Brown *et al.* [196] R represents a bulky group at one end of the alkyne chain.

Attempts to displace the alkyne of the THP-protected intermediate **49** were unsuccessful as only the starting material was recovered; the reason for this is unclear. In the literature, the reaction was carried out on the deprotected alcohol similar to **36**; thus compound **49** was deprotected.[197] The zipper reaction was carried out in anhydrous conditions and afforded **36** in low yield after purification by silica-gel chromatography.

The last step comprised the oxidation of **35** to carboxylic acid **24** using Jones reagent. Using this strategy, YnC15 **24** was synthesised in five steps, with an overall yield of 10%.

As the first strategy gave higher overall yield (27%), it is the preferred route to YnC15. However, the second strategy with the zipper reaction might be advantageous to prepare a alkyne-tagged fatty acid of different chain length if an alcohol of the correct chain length and with an internal alkyne is commercially available. The number of steps would be reduced to two and the overall yield could be improved.

2.1.4 Coenzyme A thioesters

Coenzyme A thioesters were first prepared according to *Heal et l.*.[154] The corresponding acid, AzC12 **15** or YnC12 **16**, was coupled to the commercially available but expensive Coenzyme A **50** (CoASH) via a CDI-mediated coupling (Scheme 9). The products, **18** and **19**, were isolated in low yields, 15 and 13% respectively, using preparative RP-HPLC and a gradient of methanol and 10 mM ammonium acetate buffer pH 5.2 (Table 4).

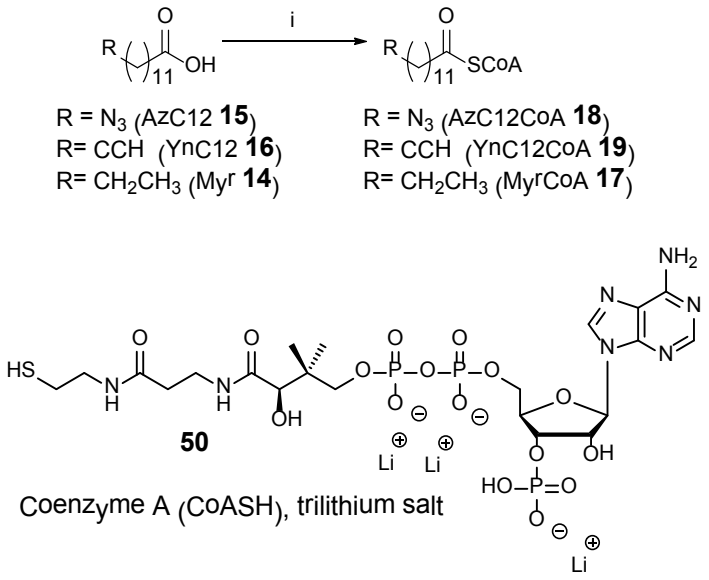

Scheme 9. Synthesis of Coenzyme A analogues and structure of the Coenzyme A trilithium salt used for the synthesis. Reagents and conditions: i) 1) CDI, THF, DCM, 2) CoASH, $NaHCO_3$ (aq) 0.5 M. Yields are reported in Table **4**.

The yields were similar to those reported in the literature.[154] The poor isolated yields were due to a low conversion and loss of product during the purification process. Some product could have been lost during the several washes with acetone and also using preparative RP-HPLC as re-suspension of the crude product in the acidic buffer for the purification was quite difficult. The crude product was easier to solubilise in weak basic buffer, such as 25 mM ammonium carbonate pH 8 and the use of this buffer should improve the yields. Importantly, no hydrolysis of the coenzyme A thioester was noticed in the basic buffer.

During this PhD project, Gaffarogullari *et al.*[202] reported a synthesis of myristoyl CoA according to *Heal et al.*[154] with modifications. The main difference was the use of 2 eq of CDI and myristic acid, instead of 1 eq, compared to the limiting reagent, CoASH. Unfortunately, no yield was reported and the fact that the product was not purified might suggest that the conversion was high or that the purification was difficult.

AzC12CoA **18**, YnC12CoA **19** and MyrCoA **17** were prepared according to these new conditions: the use of the basic buffer for the purification and 2 eq of CDI and the appropriate acid. The yields were noticeably increased, possibly due to the formation of acid anhydride as the reactive species (Table 4). AzC12CoA **18** and YnC12CoA **19** stock solutions were prepared as 20 mM stock in a 1:1 ratio 10 mM NaOAc pH 5.0:EtOH, while MyrCoA **17** was dissolved in DMSO as required for the in vitro enzyme assay (Section 2.2).

Table 4: Yields for the preparation of Coenzyme A thioesters using various conditions.

	Heal *et al.*[154]	Same conditions as Heal *et al.*[154]	After optimisation
AzC12CoA **18**	17%	13%	30%
YnC12CoA **19**	19%	15%	66%
MyrCoA **17**	n/a	n/a	32%

2.2 Kinetic studies of analogues and peptide substrates

To evaluate the specificity of NMT1 and NMT2 for MyrCoA or analogues and also for some known peptide substrate, kinetic studies were carried out.

2.2.1 Enzyme kinetics

Kinetic parameters (K_M and V_{max}) can be determined using an *in vitro* enzyme assay. The K_M is the substrate concentration at which the rate of reaction is half its maximum value and is therefore a measure of the affinity of the substrate for the binding pocket. A low K_M value indicates a tight binding of a substrate to the enzyme binding pocket. V_{max} is the maximal rate of the reaction. These two parameters can be derived according to the Michaelis Menten equations (Figure 21, Equation 1) using GraFit 7.0.

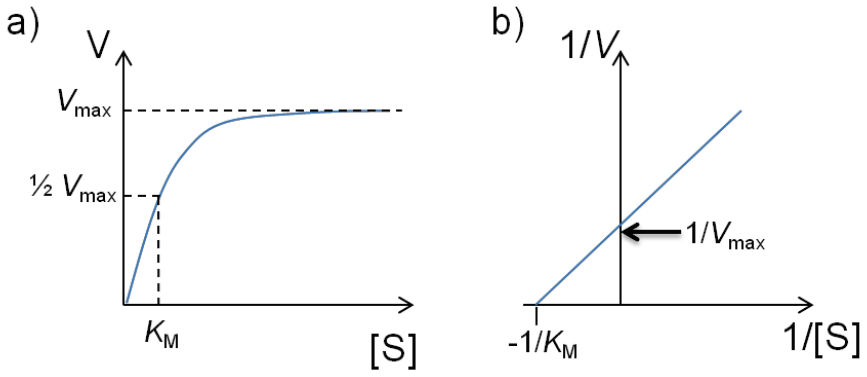

Figure 21. Graph used for the determination of the kinetic parameters, K_M and V_{max}. a) Enzyme saturation curve with plotted data of rate of reaction versus substrate concentration. [S] is the concentration of substrate and *V* is the rate of the reaction. b) Lineweaver-Burk plot from which kinetic constants can easily be determined.

a) $E + S \underset{k_{-1}}{\overset{k_1}{\rightleftharpoons}} ES \xrightarrow{k_2} E + P$ b) $V = \frac{V\max[S]}{K_M + [S]}$

c) $K_M = \frac{k_2 + k_{-1}}{k_1}$ d) $\frac{1}{V} = \frac{K_M}{V_{max}}\frac{1}{[S]} + \frac{1}{V_{max}}$

Equation 1: Michaelis Menten enzyme kinetic equation. a) Enzymatic reaction. k_1, k_{-1} and k_2 are the rate constants. **b)** Correlation between K_M, the Michaelis constant, and the rate constants. **c)** Equation connecting V (the rate of the reaction where all enzymes are unbound) with V_{max} (the maximum rate where the enzyme is completely saturated with substrate), [S] (the substrate concentration) and K_M. **d)** Correlation between $1/V$ and 1/[S] required for the (Lineweaver-Burk) plot.

2.2.2 CPM assay

A fluorescence assay was recently developed in our group to study *N*-myristoylation.[145] The assay relies on the reaction of the nucleophilic Coenzyme A **50**, by-product of the myristoylation reaction, with a Michael acceptor, 7-diethylamino-3-(4-maleimido-phenyl)-4-methylcoumarin **51** (CPM). The CPM-CoA adduct **52** is fluorescent at 490 nm, while CPM alone has no fluorescence at this wavelength (Figure 22).

The concentrations of HsNMT1 and HsNMT2 were set to 300 ng/mL in the assay. Recombinant enzymes used in the present study were prepared by Dr James Brannigan (University of York). Full length HsNMT1 and HsNMT2 (Section 1.2.2) as well as truncated HsNMT1 and HsNMT2 were used (Appendix B). The truncated proteins, referred as ΔHsNMT1 and ΔHsNMT2 correspond to the catalytic domains of both human NMT isoforms. These proteins lack the N-terminus involved in NMT subcellular localisation (Section 1.6.2).

As myristoylation operates via a Bi-Bi mechanism (Section 1.3) and two substrates are involved, the K_M of the substrate of interest cannot be determined in the absence of the other. To acknowledge the requirement for a second substrate, an apparent K_M value (K_{Mapp}) can be measured in the presence of a saturating amount of peptide, to reduce the reaction to the one-substrate situation. Once the second K_M is determined, it is necessary to check that the first K_M was measured under a saturating amount of the second substrate.

To carry out the assay, certain precautions need to be taken. The substrates, enzymes and buffers should be of high purity and stable under the conditions of the assay. Peptides or inhibitors tested should not contain any strong nucleophile such as thiols as they could react with CPM, leading to an increase of the background fluorescence.

The assay was used in this study to evaluate the kinetic parameters of peptide substrates and MyrCoA analogues, and also to study the potency of HsNMT inhibitors (Chapter 3).

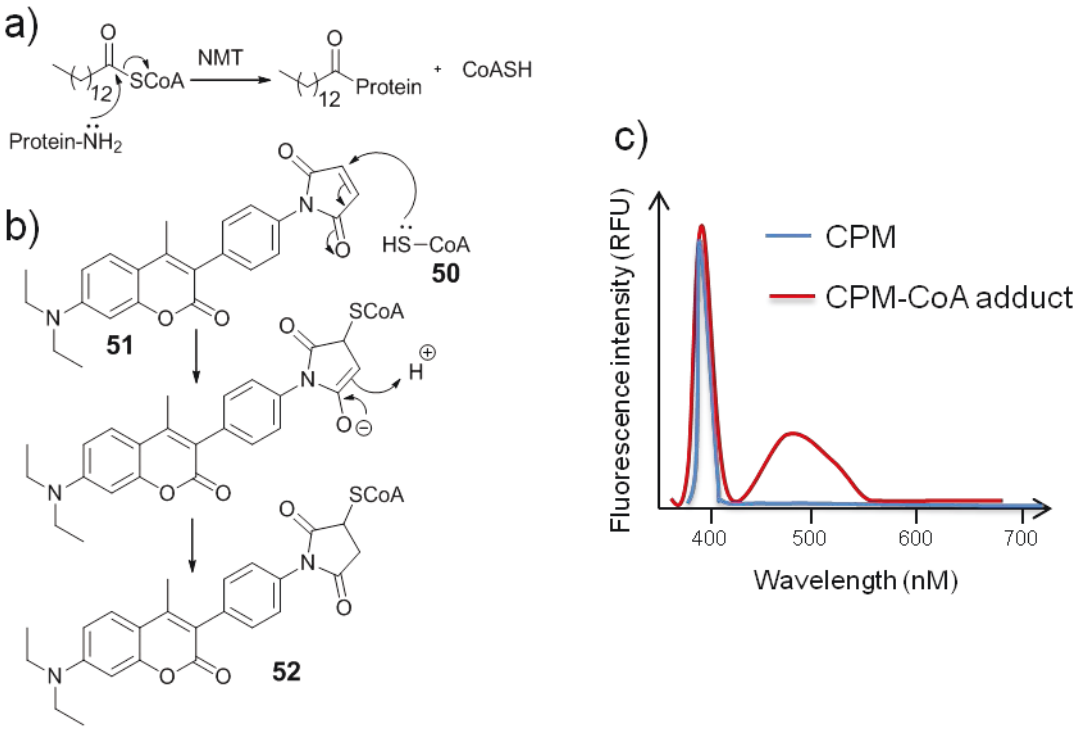

Figure 22: CPM assay. a) *N*-Myristoylation of the protein substrate releases Coenzyme A (CoASH). **b)** Nucleophilic attack of CoASH on CPM yields a stable CPM-CoA-adduct which can be seen by fluorescence. **c)** Fluorescence profile of the CPM and CPM-CoA versus the wavelength. Adapted from Goncalves *et al.*[145]

2.2.3 K_M of peptide substrates

CPM assays were carried out to evaluate the specificity of HsNMT1 and 2 for a peptide substrate in the presence of HsNMT1 or HsNMT2, CPM and MyrCoA or analogues (YnC12CoA or AzC12CoA).

As explained in Section 2.2.2, MyrCoA should be present at a concentration that saturates the enzyme binding site. By analogy with the K_M values of MyrCoA reported in the literature, the K_M was expected to be in the low micromolar range. Indeed, three values have been reported in the literature, using different assays, in the presence of the 8 amino acid (AA) v-SRC peptide (GSSKSKPKR): 15 ± 2 [65] , 2.6 [59] and 7.6[203] µM. For peptide studies the concentration of MyrCoA was set to 30 µM, and MyrCoA K_M is explored further in Section 2.2.4.

The kinetic parameters of peptide substrates were usually determined by varying the concentration of peptide from 40 µM to 0 µM or from 10 µM to 0 µM when the K_M was lower than 1 µM. Fluorescence was recorded (excitation at 390 nm, emission at 470 nm, cut-off at 435 nm) every minute. For each solution, a no-enzyme control was carried out with the peptide substrate, CPM,

and various concentrations of MyrCoA (or analogue). Initial rate of reactions were determined by calculating the initial slope of the curve plotting the fluorescence intensity versus time. The value obtained in the negative control (no peptide) was subtracted from the other values. Background signal presumably arises from spontaneous hydrolysis of CoA thioester in Coenzyme A.

K_M and V_{max} were calculated using GraFit 7.0 for each enzyme for MyrCoA, AzC12CoA and YnC12CoA (Table 5). Typical graphs obtained with GraFit are presented in Figure 23.

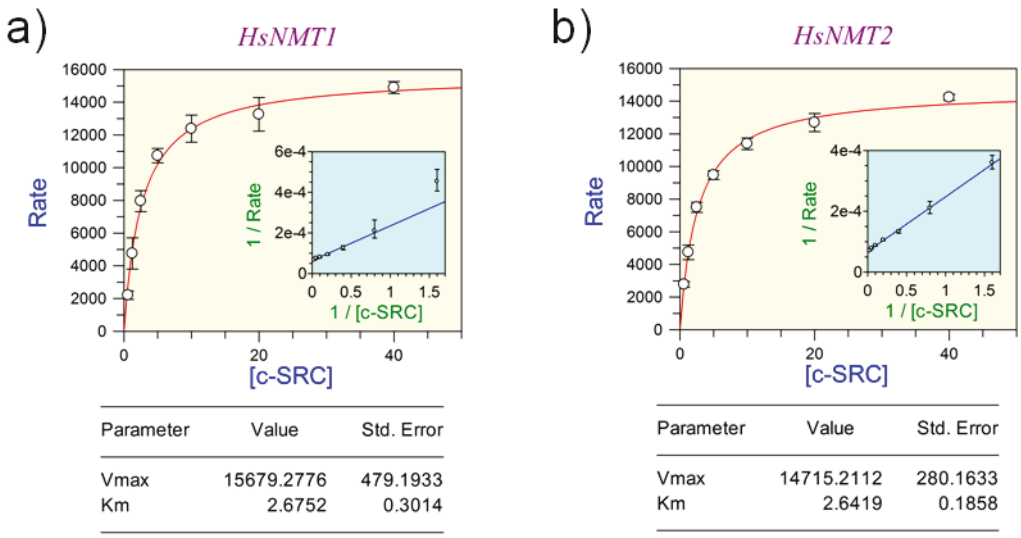

Parameter	Value	Std. Error
Vmax	15679.2776	479.1933
Km	2.6752	0.3014

Parameter	Value	Std. Error
Vmax	14715.2112	280.1633
Km	2.6419	0.1858

Figure 23: K_M determination of 8AA c-SRC using a) HsNMT1 or b) HsNMT2 and saturating amount of MyrCoA (30 µM). The figure was generated in GraFit 7.0.

The K_M values of a peptide corresponding to the 15 AA at the N-terminus of v-SRC were first determined in the presence of MyrCoA, as values had been previously reported in the literature for the 8AA peptide.[59,65,203] v-SRC is a protein found in Rous sarcoma virus, similar to the human oncogene c-SRC, which has been well studied in the literature in the context of myristoylation.[104,123,204] 15 AA v-SRC was prepared by Victor Goncalves (Tate group, Imperial College London). The values reported in the literature (44,[205] 30,[59] 44.2[203] µM) were different from the values measured using the CPM assay (Table 5), probably due to the different peptide length. It should also be noted that the conditions (enzyme concentration, concentration of MyrCoA) used for the assay in the literature were not the same as in the CPM assay and we should not expect to find exactly the same values. Interestingly, the K_M values for 15 AA c-SRC and 15 AA v-SRC, both evaluated with MyrCoA, are comparable for both HsNMT isoforms.

The K_M of 15AA c-SRC was lower than the K_M of 8 AA c-SRC (both evaluated with MyrCoA) suggesting a tighter binding to the enzyme. However, 8AA c-SRC can still be considered an NMT substrate, and 8 amino acids are enough for protein substrate recognition by the enzyme (Section 1.4.2).

Table 5: K_M and V_{max} values of various peptides in the presence of saturating amount of MyrCoA. K_M values are given in µM and V_{max} in RFU/min (RFU: relative fluorescence unit). nd indicates that the values have not been determined.

Peptide	Parameters	HsNMT1	ΔHsNMT1	HsNMT2	ΔHsNMT2
15 AA v-SRC	K_M	0.67 ±0.20	nd	1.24 ±0.27	nd
	V_{max}	14311 ±1361	nd	14817 ±1249	nd
15 AA c-SRC	K_M	0.25 ±0.05	0.84 ±0.11	0.18 ±0.04	0.18 ±0.07
	V_{max}	38496 ±1772	101442 ±3624	28952 ±1236	29421 ±2295
8 AA c-SRC	K_M	2.67 ±0.28	2.76 ±0.21	2.64 ±0.17	2.77 ±0.14
	V_{max}	15679 ±437	22895 ±487	14715 ±255	17280 ±249

Comparable K_M values were obtained in the presence of HsNMT1 and HsNMT2, suggesting that the peptide binding pocket might be well conserved between the two isoforms. Full length enzymes and truncated enzymes gave similar results for c-SRC; suggesting that in the truncated enzyme, the active site is conserved. However, when the CPM assay was used to evaluate the potency of inhibitors, the full length was preferred to ensure we would not lose any HsNMT1/HsNMT2 selectivity by removing the N-terminus of the enzymes (Section 1.2.2).

For the inhibitor assay, it was decided to use 8AA c-SRC as the peptide substrate, at a concentration close to the K_M value (4 µM). It would be difficult for an inhibitor to compete with 15AA c-SRC as it binds too tightly to the enzyme.

Another assay was performed to test if a protein or peptide substrate could still be lipidated in the presence of the MyrCoA analogues. Comparable K_M and V_{max} were obtained for 8AA c-SRC, though the K_M values were slightly higher with YnC12CoA or AzC12CoA than with MyrCoA (Table 6).

Table 6: K_M of 8AA c-SRC in the presence of saturating amount of MyrCoA analogues. K_M values are given in µM and V_{max} in RFU/min (RFU: relative fluorescence unit).

Peptide	Co-substrate	Parameters	HsNMT1	HsNMT2
8 AA c-SRC	YnC12CoA	K_M	9.8 ± 1.6	2.0 ± 0.6
		V_{max}	22953 ± 1480	17586 ± 1319
	AzC12CoA	K_M	5.9 ± 0.6	1.5 ± 0.2
		V_{max}	17405 ± 1320	13927± 351

During the work described in this thesis, different batches of enzymes or substrates were used. Every time a new batch was used, the K_M of c-SRC 8 AA and MyrCoA were compared with the original values to check the quality of the new batch.

2.2.4 K_M determination of MyrCoA and analogues

Similar experiments were carried out by varying the concentration of MyrCoA or analogue and keeping the concentration of peptide substrate constant. The parameters K_M and V_{max} were determined using GraFit 7.0 in order to characterise the specificity of HsNMT1 and 2 for MyrCoA and analogues (Figure 24). The concentration of c-SRC was set to 30 µM (~ 10x K_M).

K_M values of MyrCoA were first determined in the presence of a peptide corresponding to the N-terminus of v-SRC, as these values had been reported in the literature for the 8AA peptide.[59,65,203] The values shown in Figure 24 were similar to the reported values: 15 ± 2,[65] 2.6,[59] 7.6,[203] even though the peptide length was different.

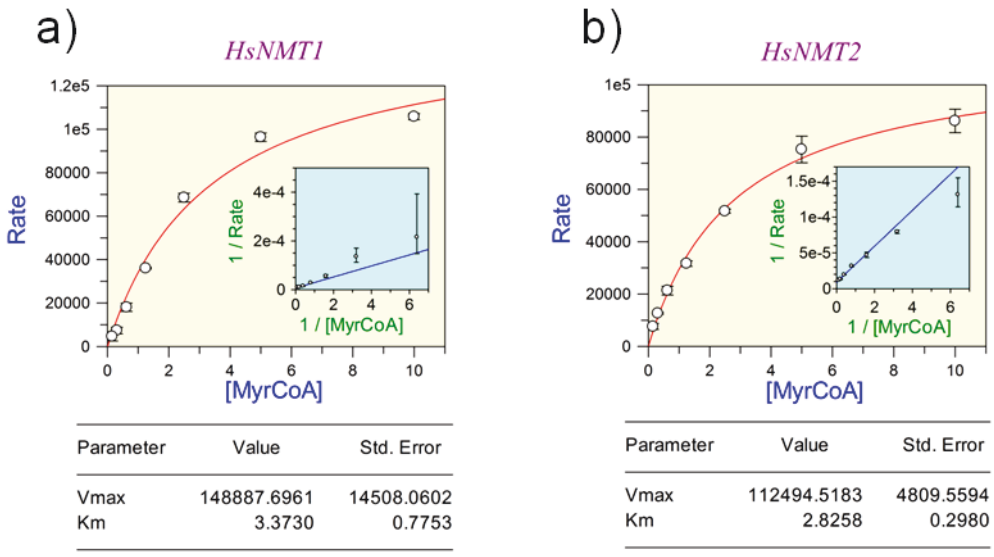

Parameter	Value	Std. Error
Vmax	148887.6961	14508.0602
Km	3.3730	0.7753

Parameter	Value	Std. Error
Vmax	112494.5183	4809.5594
Km	2.8258	0.2980

Figure 24 K_M determination of MyrCoA using a) HsNMT1 or b) HsNMT2 and saturating amount of v-SRC (30 µM). The rate is the initial rate of the reaction measured for a given concentration of substrate. The figure was generated from GraFit (7.0.).

Different studies were carried out in the presence of peptide of various lengths corresponding to the N-terminal sequence of the known NMT substrate c-SRC (Table 7).[204]

Table 7: K_M and V_{max} values of MyrCoA and analogues using 15AA v-SRC, 8 AA c-SRC or 15AA c-SRC. K_M values are given in µM and V_{max} in RFU/min (RFU: relative fluorescence unit).

		HsNMT1		HsNMT2	
Peptide	Co-substrate	K_M	V_{max}	K_M	V_{max}
15 AA v-SRC	MyrCoA	3.37 ± 0.8	148887 ± 14508	2.83 ± 0.30	112495 ± 4810
15 AA c-SRC	MyrCoA	4.43 ± 0.62	76696 ± 3593	4.70 ± 0.60	58596 ± 2524
	YnC12CoA	0.14 ± 0.05	6400 ± 243	0.48 ± 0.11	12640 ± 509
	AzC12CoA	0.76 ± 0.30	9970 ± 828	0.51 ± 0.23	13016 ± 7629
8 AA c-SRC	MyrCoA	4.07 ± 1.09	30795 ± 2537	2.86 ± 0.90	19487± 1735
	YnC12CoA	0.65 ± 0.26	17383 ± 1210	1.19 ± 0.13	15888 ± 373

Importantly, the K_M values of the MyrCoA and analogues were in the low micromolar range and 30 µM should be sufficient to saturate the MyrCoA binding pocket of the enzyme during the K_M determination of peptides (Section 2.2.3).

Surprisingly, the K_M values obtained for MyrCoA were higher than the values obtained for the analogues. However, V_{max} appeared to be an important characteristic. The V_{max} obtained with both analogues were lower than the V_{max} obtained with MyrCoA. This result suggests that the enzyme adopts a less efficient catalytic conformation with the analogues. K_M values between the two HsNMT isomers, for a given co-substrate, were similar. These results verify that the myristoylation reaction is not strongly affected by these small structural modifications of MyrCoA and that the analogues could be transferred to the N-terminal glycine of substrate equally by both NMT isoforms. The kinetic parameters were similar for YnC12CoA and AzC12CoA in the presence of 15AA c-SRC, suggesting that both analogues would be suitable to study *N*-myristoylation.

Importantly, K_M values of MyrCoA determined in the presence of a saturating amount of various peptide lengths gave similar results, suggesting that the peptide binding pocket was saturated and the K_M of MyrCoA was thus independent of the peptide substrate.

For the inhibitor assay, it was decided to use MyrCoA at a concentration similar to the K_M value (4 µM).

2.3 Validation of YnC12 as a tool to study *N*-myristoylated proteins in cells

In this study, the cervical cancer HeLa cell line was used as a model system in view of the potential of NMT as a target for cancer therapy (Section 1.7). HeLa cells are rapidly dividing, easy to work with, and have been well studied in the literature. The HeLa genome, transcriptome [206] and proteome [207] have recently been characterised.

Previous work in the Tate group has shown that YnC12 can be used as a tool to analyse *N*-myristoylated proteins in HeLa cells using in-gel fluorescence or chemical proteomics.[163] Optimisation work established that sufficient labelling could be achieved after treating the cells for 6 h with 20 µM YnC12. Preliminary proteomics experiments allowed the identification of eight known NMT substrates as well as 9 putative NMT substrates. The labelling experiments were repeated a few times to ensure a similar labelling pattern could be observed by in-gel fluorescence. A higher labelling efficiency could increase the number of NMT substrates identified by chemical proteomics.

2.3.1 Lysis buffer

Previous work in the group to identify *N*-myristoylated proteins consisted in treating the cells for 6 h with 20 µM YnC12, washing the plates with PBS (2x) to remove any excess of culture media and YnC12, followed by cell lysis.[163] A Tris-based lysis buffer was added to the plate and the cells were scraped off the plate (Table 8). Lysates were kept on ice, the insoluble materials were removed by centrifugation and the protein concentration was determined. Capture of the *N*-myristoylated proteins with AzTB (Figure 17) allowed visualisation of the proteins using in-gel fluorescence (Section 1.10). The experiment was repeated using the two analogues of myristic acid (Myr), YnC12 and AzC12, prepared in Section 2.1 (Figure 25a).

Table 8: The table shows the components of the two lysis buffer used for the labelling experiments in HeLa.

Lysis Buffer	Components
Tris	50 mM Tris pH 7.4, 1 % NP40, 1 % sodium deoxycholate, 0.1 % SDS, 150 mM NaCl, EDTA-free protease inhibitor
PBS	PBS pH 7.4, 1% Triton, 0.1 % SDS, EDTA-free protease inhibitor

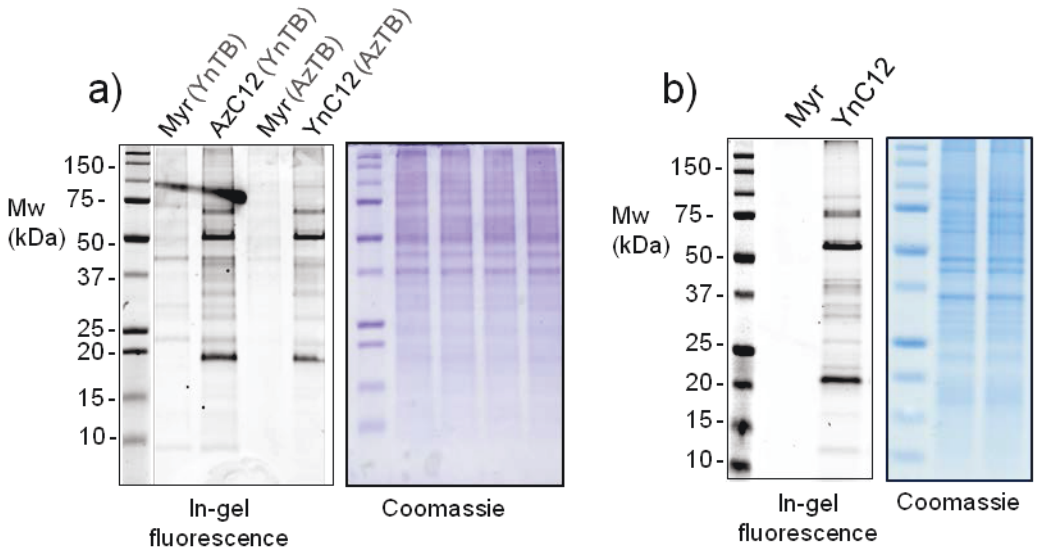

Figure 25: YnC12 and AzC12 labelling in HeLa cells using different lysis buffer. HeLa cells were treated for 24 h with YnC12 (20 µM), AzC12 (20 µM) or Myr (20 µM). After cell lysis with **a)** a Tris-based buffer or **b)** a PBS-based buffer; samples were captured (**a)** The capture reagent is indicated in brackets; **b)** AzTB was used) and analysed by in-gel fluorescence (left). Colloidal coomassie (right) staining shows equal protein loading across all lanes. Proteins molecular weight (Mw) markers were loaded on the gel (first lane).

As previously observed, YnC12 and AzC12 give similar labelling in HeLa cells (Figure 25a).[163] However, the background in fluorescence, as seen when the cells were treated with Myr, is higher when the lysate was captured with YnTB instead of AzTB. Similar observations have been made by Charron *et al.* using similar capture reagents.[172] They noticed that an alkyne-capture reagent (to detect azide-tagged proteins) often produces higher background than the use of an azido-capture reagent (to detect alkyne-tagged proteins). The decision was made to only use YnC12 for the in-cell study of *N*-myristoylated proteins, although AzC12 and AzC12CoA were used later for the *in vitro* study of *N*-myristoylated proteins (Chapter 6).

As the background fluorescence seen with lysate treated with Myr and AzTB was sometimes high, depending on the experiment (data not shown), another lysis buffer was tested. A PBS-based lysis buffer was used by other members of the group and did not seem to raise any background issues (Table 8). This lysis buffer still contained 0.1 % SDS, a detergent that breaks the plasma membrane for cell lysis, but the other detergents were modified. Detergents are also required in order to solubilise proteins, especially membrane-bound proteins such as *N*-myristoylated proteins. As shown in Figure 25b, a very similar labelling pattern was obtained with this new lysis buffer but no band could be seen in fluorescence in the Myr control. This PBS lysis buffer was thus used in all the further experiments described in the present study, except where otherwise indicated.

2.3.2 Optimisation of labelling concentration and time

In order to determine the optimal conditions for metabolic incorporation of YnC12 in HeLa cells, a concentration and time course study was performed (Figure 26). In-gel fluorescence analysis showed that maximum labelling was obtained after treating the cells for 24 h with 20 µM of YnC12.

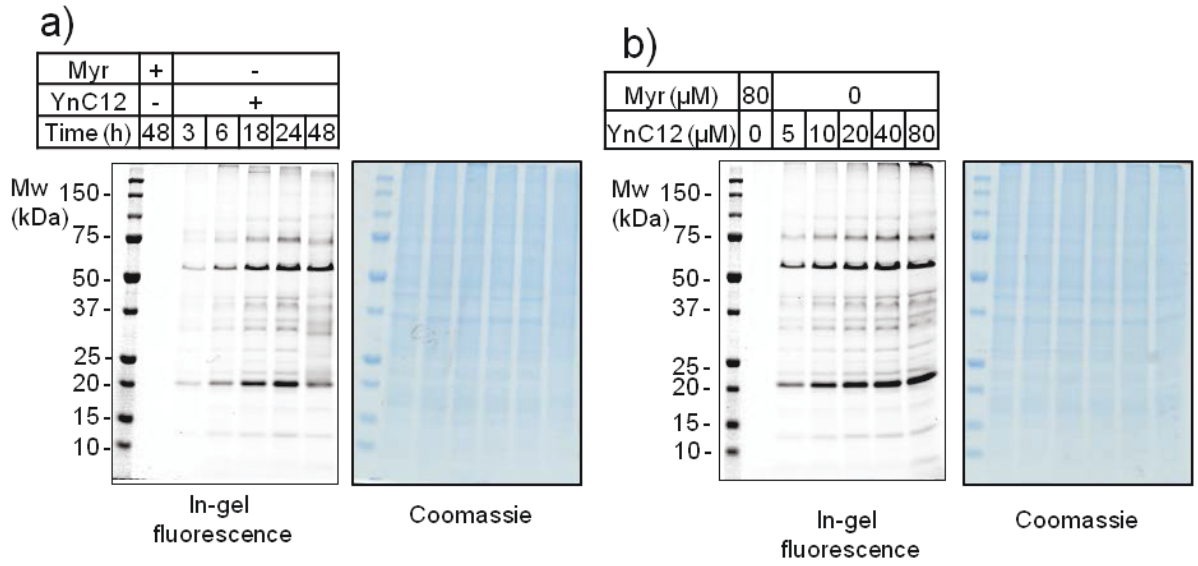

Figure 26: Optimisation of the YnC12 labelling in HeLa cells. a) Time course labelling with YnC12 (20 µM). **b)** Concentration series of YnC12. HeLa cells were labelled for 24 h.

By increasing the labelling time from 6 h to 24 h, poorly abundant NMT substrates, and those with slower turnover in cells should be more enriched and may be easier to detect by proteomics.

2.3.3 Competition experiment

A competition experiment was performed to confirm that YnC12 mimics Myr in cells in which HeLa cells were treated with YnC12 (20 µM) in combination with increasing concentration of Myr. As expected, the natural substrate outcompeted YnC12 labelling; a concentration of Myr as low as 10 µM leads to a significant decrease in YnC12 labelling, as evidenced by the reduction in fluorescent signal (Figure 27). If both substrates had equal affinity for the enzyme, the fluorescence signal would decrease by half compared to the positive control (0 µM Myr) when the cells are treated with the same concentration of Myr and YnC12 (20 µM). It is possible that YnC12 concentration might be lower than expected in cells as YnC12 could have a lower uptake, stability, or conversion to the coenzyme A thioester.

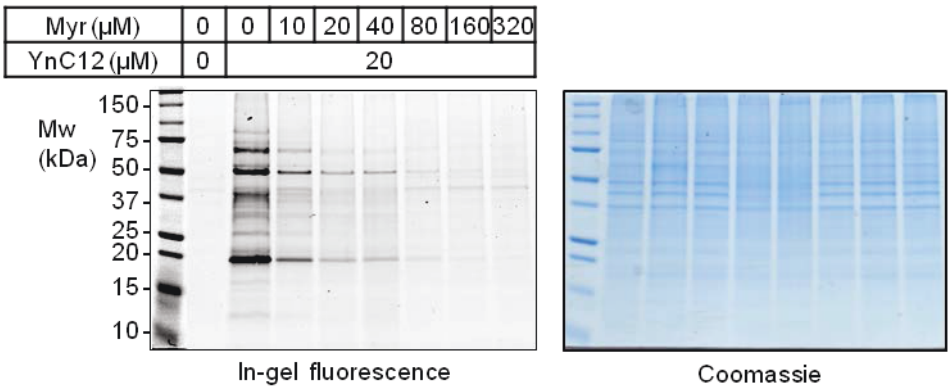

Figure 27: Competition experiment showing that YnC12 can compete with the natural lipid substrate (Myr).

2.3.4 Enrichment of known NMT substrates

An experiment was carried out to assess whether *N*-myristoylated proteins could be tagged by YnC12, captured with AzTB (bearing a fluorescent moiety and a biotin moiety, (Figure 17) and enriched on streptavidin beads (Figure 28). Western blot analysis of three known NMT substrates, MARCKS,[105] PSMC1 [208] and PRKACA [209] was performed for the samples before pull down (BPD, total lysate), the supernatant from the pull down (S) and the pull down sample (PD). In-gel fluorescence analysis showed a similar labelling pattern for both YnC12 labelled samples BPD and PD. Importantly, no signal in the supernatant was observed, indicating that alkyne-tagged proteins were immobilised quantitatively on streptavidin beads. Western blot analysis showed that the three known substrates could be tagged with YnC12 and enriched, and the proteins were still present in the supernatant suggesting they are not 100% tagged with YnC12 after 24 h treatment in HeLa cells. The equivalent of 4-fold more protein was loaded in the PD samples compared to the BDP and S to be able to detect a band by western blot analysis. Quantification of bands BPD and of the supernatant using ImageJ allowed quantification of the relative incorporation of YnC12 for MARCKS, PSMC1, and PRKACA, giving 66%, 35% and 18%, respectively. This percentage may depend strongly on the protein turnover rate, since proteins with a higher turnover rate will be more quickly degraded and synthesised in cells and will thus incorporate more YnC12. Turnover of *N*-myristoylated proteins is discussed in Chapter 5.

The incorporation of YnC12 is relatively low for PRKACA (18% of the protein was tagged). However, from earlier optimisation of labelling concentration and time (Section 1.3.2) there is no suggestion that this incorporation can be improved (Figure 26). Moreover, it has been observed by Dr. Remi Serwa (Tate group, Imperial College London) that incubating the cells with YnC12 for 7 days does not significantly improve labelling by in-gel fluorescence (data not shown).

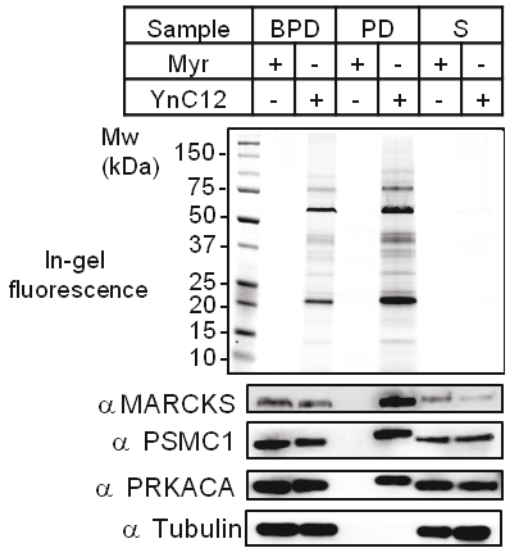

Figure 28: Enrichment of known NMT substrates. HeLa cells were treated for 24 h with YnC12 (20 µM) or Myr (20 µM). After cell lysis, samples were captured with AzTB and enriched on streptavidin beads. Samples were analyzed by in-gel fluorescence (top) and Western blotting (bottom). The samples before pull-down (BPD), pull-down samples (PD) and the supernatants from the pull-down (S) were analysed. MARCKS, PSMC1 and PRKACA are enriched in the pull-down samples. The small MW band shift of the proteins in the PD can be explained by the presence of the capture reagent. Tubulin was used as the loading control. The equivalent of 4-fold more protein was loaded in the PD samples compared to the BPD and S.

It is important to note that no study has investigated the stability of YnC12 in cells over prolonged time-periods. Other alkyne lipids analogues can be metabolised in cells or used for the synthesis of longer fatty acid chains or fatty acid analogues.[210] If YnC12 is in fact metabolised after a long incubation time, it could label other proteins than *N*-myristoylated proteins, and lead to aberrant signal for the gel-based analysis or false identification of NMT substrates by proteomics. It could also reduce the competition against Myr, resulting in a lower YnC12 incorporation. It is unclear how incorporation of YnC12 could be further increased, however the enrichment level was expected to be sufficient to carry out proteomics experiments.

2.3.5 Assessment of the toxicity of YnC12 and Myr in HeLa

A cell cytotoxicity assay was carried out to confirm that Myr and YnC12 were not toxic to HeLa cells. As these compounds were later used in combination with NMT inhibitors in cells (Chapter 3), it was important to ensure that they do not add to the toxicity of NMT inhibition.

2.3.5.1 Cell viability assay: MTS assay

A large variety of assays are available to assess cytotoxicity or cell viability in a 96-well plate format. They rely on the measure of:

- ✓ The activity of esterase substrates present in living cells. Typically, the reagent added to the cells penetrates the cell membrane and is cleaved by cytoplasmic esterase enzymes. A fluorophore is released, and the fluorescent signal is proportional to the amount of living cells.
- ✓ The amount of nucleic acid released from dead cells using a non-cell permeable nucleic acid stain. The reagent can intercalate into nucleic acids present outside the cells which leads to a large fluorescence enhancement. As living cells have an intact cell membrane, the assay only measures the amount of dead cells. This type of assay is often used in combination with the first type to concurrently measure the amount of living and dead cells.
- ✓ Oxidation or reduction occurring in metabolically active cells. A redox dye is added to the cells and converted to a fluorescent or coloured product after oxidation or reduction by viable cells. The absorbance or fluorescence is proportional to the amount of viable or metabolically active cells. Dead cells lose their membrane integrity and the metabolic processes are inactivated. Commonly used reagents are resazurin, and (3-(4,5-Dimethylthiazol-2-yl)-2,5-diphenyltetrazolium bromide (MTT).

It was decided to use a cell viability assay based on a redox reagent: 3-(4,5-dimethylthiazol-2-yl)-5-(3-carboxymethoxyphenyl)-2-(4-sulfophenyl)-2H-tetrazolium **53** (MTS). The MTS assay (Promega) is similar to the MTT assay but the procedure requires fewer steps as the reagent is water soluble (Figure 29). MTS **53** is added in combination with an electron coupling reagent, phenazine methosulfate (PMS). The MTS reagent is reduced by metabolically active cells, presumably by NADPH or NADH released by dehydrogenase enzymes.[211] The product **54** is coloured and can be detected by measuring absorbance at 490 nm. The absorbance is proportional to the amount of formazan **52** produced and consequently to the number of living cells in the well. A negative control (cells not treated with compound) and a positive control (cells treated with puromycin, a compound toxic to eukaryotic cells) are required (Figure 29). The protocol from the supplier (Promega) was slightly modified (Optimisation work performed by Dr. Will Heal, Tate group, Imperial College London). The culture media was not aspirated before adding the cytotoxic compound to be tested as it seems to perturb the cells and high error bars were obtained, even with six replicates per concentration. The cells were seeded using a smaller volume of media (50 µL) and the solution of cytotoxic compound (50 µL) was added directly to the well to give a final volume of 100 µL, as required for the assay.

This assay was also used later to assess the toxicity of NMT inhibitors in HeLa cells (Chapter 3).

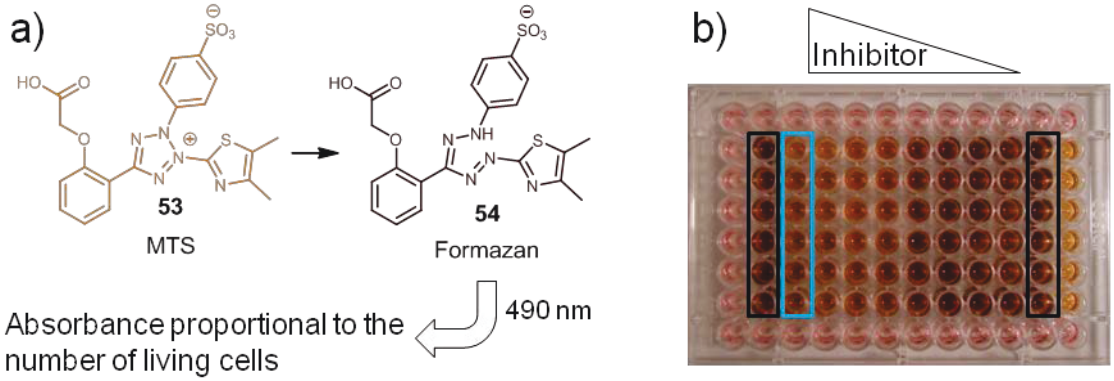

Figure 29: MTS assay. a) In living cells, MTS **53** is converted to formazan **54**. The change in absorbance can be detected at 490 nM and is proportional to the number of living cell in the plate. **b)** Picture of the 96-well plate after the MTS assay. The outer wells contain only the culture media. Cells are treated with various concentrations of compound (6 replicates; 1 concentration per column). The wells circled in black are used as a negative control (no inhibitor) and the one in blue are the positive control, where the cells have been treated with puromycin.

2.3.5.2 YnC12 and Myr are not toxic to HeLa cells

It has been suggested that fatty acids might be toxic to cells at high concentrations by activating c-SRC and altering its membrane distribution.[212] A cell cytotoxicity assay was thus carried out in HeLa cells for 3 days to check that the addition of YnC12 up to 160 µM (8 x the maximal concentration used in cells) was not toxic (Figure 30). No apparent toxicity could be seen after 1 day for Myr and up to 3 days for YnC12.

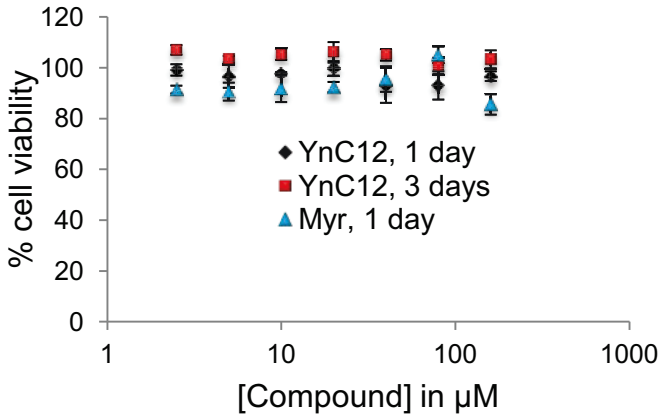

Figure 30: Non-toxicity of YnC12 and Myr in HeLa cells determined using the MTS assay (Promega). Each point corresponded to the average value of a triplicate experiment and the error bars show the standard deviation between replicates.

2.4 YnC12 as a tool to study post-translational myristoylation

As explained in Section 1.5.2, proteins have also been shown to be post-translationally *N*-myristoylated, in the context of apoptosis.[89]

As described in Section 2.3 for co-translational NMT substrates, YnC12 labelling followed by capture by AzTB and enrichment, could be used to identify the *N*-myristoylated proteins in apoptotic cells. Post-translationally myristoylated proteins have been successfully labelled with AzC12 [213] or YnC12 [115] in Jurkat T-cells. However, induction of apoptosis was always used in combination with cycloheximide, an inhibitor of protein synthesis. To date, no mass spectrometry-based proteomics experiments have been reported in the literature to identify post-translationally *N*-myristoylated proteins.

Further optimisations were required to ensure that sufficient labelling could be obtained after brief treatment with YnC12. Low abundance proteins are sometimes difficult to detect by proteomics, and it was decided not to use cycloheximide as it could possibly have other effects in cells and lead to more rapid cell death as cycloheximide is toxic.[214] However, apoptosis rapidly stops protein synthesis [39] and cycloheximide should not be needed to stop co-translational labelling.

Staurosporine (STS) was employed to induce apoptosis in HeLa cells (see Section 5.2.2.1 for more details and control for the induction of apoptosis). A preliminary experiment (data not shown) showed that the YnC12 labelling was weak after 4 h in HeLa cells treated with STS (1 μM), and so cells were therefore pre-treated for 1 h with YnC12 before the induction of apoptosis with STS (Figure 31). Cells were lysed after 4 and 8 h after the induction of apoptosis. Cells were treated with 20 μM of YnC12 as usual, or with a higher concentration, 50 μM, to determine whether labelling intensity could be improved by increasing the concentration of YnC12.

After induction of apoptosis and 8 h labelling with YnC12, with or without pre-feeding for 1 h with YnC12 (lanes 5, 8, 10, 12), several new bands appeared on the gel compared to the lane showing the co-translational labelling (lane 2). The labelling intensity was similar with 20 or 50 μM YnC12. However, labelling for 8 h significantly improved the labelling.

Pre-feeding the cells with YnC12 seemed to enhance the co-translational labelling over post-translational labelling of myristoylated proteins. For example, the labelling patterns in lanes 3 (1 h YnC12 tagging) and 4 (1 h YnC12 tagging followed by 4h YnC12 tagging in the presence of STS) were highly similar.

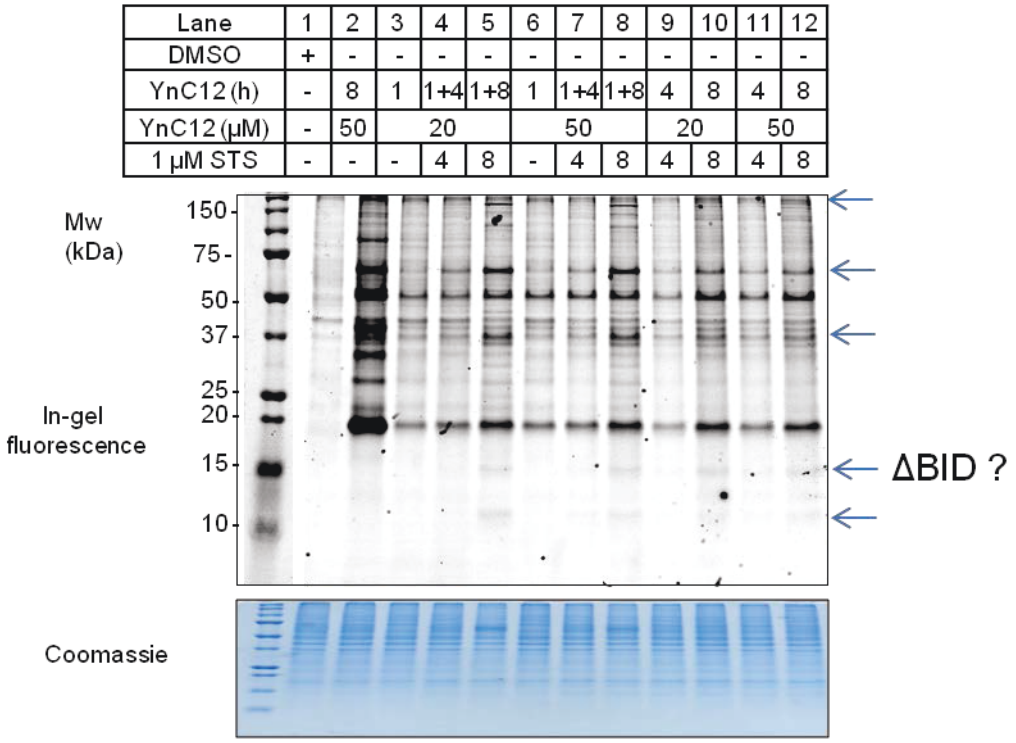

Figure 31. Post-translational *N*-myristoylation. HeLa cells were treated with DMSO (lane 1), or YnC12 (lane 2) as a control. Co-translationally myristoylated proteins are seen in lane 2. Cells in lanes 3-8 were pre-treated with YnC12 for 1 h and treated with STS (1 µM) + YnC12 for 0, 4 or 8 h. Two concentrations or YnC12 were used (20 and 50 µM). In lanes 9-12, cells were treated at the same time with STS (1 µM) + YnC12 (20 and 50 µM), and lysed after 4 or 8 h. Post translationally *N*-myristoylated proteins, as seen with the appearance of new bands by in-gel fluorescence, are indicated with a blue arrow.

Another experiment was carried out to confirm that pre-feeding with YnC12 was not required. Another time point, 16 h, was added to see if the labelling intensity could be further improved (Figure 32a). However, extensive cell death started to occur after 8 h and cells were mostly dead by 16 h, and so even if labelling intensity is slightly improved from 8 to 16 h, it would be preferable to run the experiment for the shorter period. As observed in Figure 31, pre-feeding the cells for 1 h increased co-translational labelling.

Finally, we envisaged that pre-treating the cells with STS for 1 h should decrease the contribution of co-translational labelling even further (Figure 32b). As the optimal labelling time appeared to be 8 h (Figure 32a), HeLa cells were treated for 8 h with YnC12 and STS. They were pre-treated with YnC12, STS or not pre-treated. Bands that can be attributed to co-translational myristoylated proteins are indicated with a blue arrow; pre-treatment with STS for 1 h seemed to be optimal in order to decrease co-translational labelling.

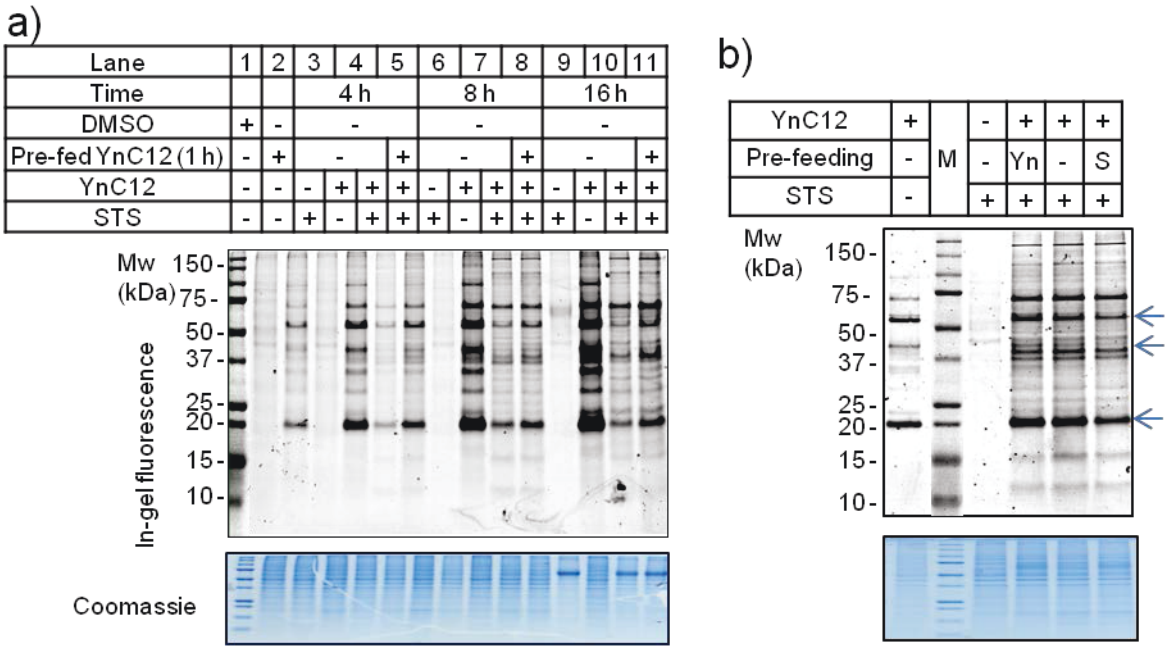

Figure 32. Optimisation of the labelling of post-translationally *N*-myristoylated proteins. a) HeLa cells were treated with DMSO (lane 1), or YnC12 (lane 2) as a control. Co-translationally myristoylated proteins should be seen in lane 2. Samples in lanes 3-5 were treated with STS for 4 ; samples in lanes 6-8 were treated with STS for 8 h and samples in lanes 9-11 were treated with STS for 16 h. Samples in lanes 3-11 were not treated with YnC12 or were treated with YnC12 at the same time as STS (with or without pre-feeding for 1 h). **b)** Cells were treated with only YnC12 (first lane) or with STS and YnC12 for 1 h. Samples were pre-fed with STS (1 µM, 1 h) or YnC12 (1 h). Bands which can be attributed to co-translationally *N*-myristoylated proteins are indicated with a blue arrow.

A band around 15 kDa could be seen by in-gel fluorescence that might correspond to the p15 BID fragment known to be post-translationally myristoylated.[8] As a relatively low amount of BID is present in cells, it would be difficult to capture BID with AzTB, enrich it and detect it by Western Blot analysis (Section 2.3.4). BID was therefore immuno-precipitated from whole cell lysate with Sepharose A beads using BID antibody, captured by AzTB on beads, released from the beads and analysed by in-gel fluorescence and Western blotting.[215] As expected, a band corresponding to BID could be seen at 15 kDa when the cells where tagged with YnC12. This method could potentially be used to validate other substrates, and proteomics experiments are currently carried out within the Tate group to identify novel post-translational NMT substrates.

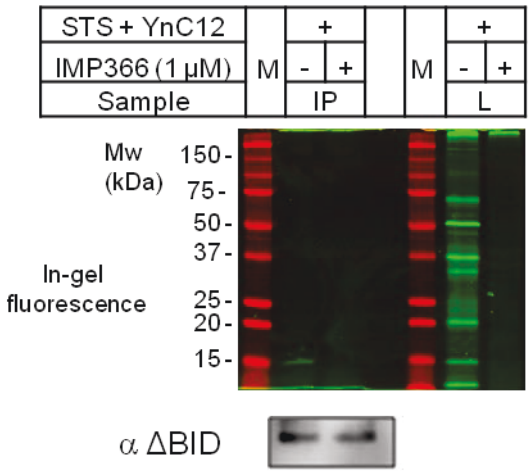

Figure 33. BID post-translational *N*-myristoylation. M = MW markers, IP = immunoprecipitation and L = whole lysate. HeLa cells were treated with STS (1 µM) and YnC12 (20 µM) for 8 h. Cells were pre-treated for 30 min with NMT inhibitor IMP366 (1 µM) (see Chapter 3). Lysate were either immunoprecipitated using BID antibody, and captured with AzTB on beads or lysates were directly captured with AzTB. The samples were analysed by in-gel fluorescence (top) and by Western blot (bottom). On the in-gel fluorescence, molecular weight (Mw) can be seen in red while the TAMRA-captured N-myristoylated proteins can be seen in green.

2.5 Conclusions

This chapter has introduced the chemical tools and assays used to study protein *N*-myristoylation in the work described in Chapters 3, 4 and 6.

Issues with the synthesis of the probes YnC12, AzC12 and YnC15 were addressed, and the probes can now be prepared reliably and in good yields (Section 2.1). The synthesis of the MyrCoA analogues was also optimised as they originally suffered from low yields.

Kinetic studies using the CPM assay developed in our group showed that tagged analogues of MyrCoA could be transferred to the N-terminal glycine of substrate proteins with similar efficiency to the natural substrate. The kinetic parameters of a peptide substrate, c-SRC, and of MyrCoA were determined and were used to set up the conditions for the inhibitor assay (Chapter 3). This inhibitor assay is based on the increase of the fluorescent signal upon release of CoA during myristoylation of the peptide substrate by NMT. The concentrations of enzyme, CPM, peptide, MyrCoA are held constant while the concentration of inhibitor varies, and this inhibitor assay will be used in Chapter 3 to study the potency of known and novel inhibitors of HsNMT1/2.

Chemically-tagged analogues of myristic acid were then applied to cancer cells to demonstrate that NMT substrates could be labelled by these probes. The tag introduced to NMT substrates enabled a second extremely selective and high-yielding chemical ligation to a capture reagent, AzTB or YnTB. These reagents are multifunctional and possess a dye label and a biotin moiety. The dye label can be used to visualise the tagged proteins by in-gel fluorescence while the biotin moiety allows the enrichment of the tagged proteins on streptavidin beads and their further analysis by mass spectrometry-based proteomics. The labelling conditions were optimised and the lysis buffer was modified to ensure that NMT substrates were tagged without increasing the background labelling. YnC12 was preferred to AzC12 as it gave no detectable background by in-gel fluorescence. Western blot analysis showed that YnC12 was a useful probe to selectively enrich known NMT substrates and a cell metabolic assay demonstrated that this probe was not toxic to the cells up to three days.

Taken together, these experiments confirmed that YnC12 could be used to study *N*-myristoylation in cancer cells and to identify novel *N*-myristoylated proteins.

Chapter 3 HsNMT inhibitors

This chapter describes the search for HsNMT inhibitors. The best inhibitors are used as tools to study the phenotype of NMT inhibition in cancer cells. The selectivity of the inhibitors for the two HsNMT isoforms is also studied, but not prioritised.

Several features will be discussed for inhibitors, including enzyme affinity and cell cytotoxicity. On-target activity of the inhibitors was assessed using YnC12 tagging in cells. YnC12 was shown to label NMT substrates (Chapter 2) and YnC12-tagged proteins can subsequently be captured by AzTB and analysed by in-gel fluorescence. Upon NMT inhibition, NMT substrates are not tagged by YnC12 in cells, hence decreasing the fluorescence on the gel.

Compounds reported as HsNMT inhibitors in the literature before the beginning of this study (Section 1.8.2) were evaluated. NMT is also under investigation as a potential therapeutic target in diseases caused by various protozoan parasites, such African sleeping sickness (*T. brucei*), malaria (*Plasmodium falciparum* and *Plasmodium vivax*) or leishmaniasis (*Leishmania* spp.). Recently, potent inhibitors of *T-brucei* (*Tb*) NMT were reported and also shown to inhibit HsNMT *ex vivo* (Section 1.8.2). The potential of these inhibitors to target recombinant NMT and NMT in cancer cells will be assessed. Additionally, inhibitors developed in-house by co-workers as part of a medicinal chemistry program at Imperial College London will also be tested. These compounds were predominantly designed as *Plasmodium falciparum (Pf*) NMT and *Plasmodium vivax* (*Pv*) NMT, but some of these compounds also had a high affinity for HsNMT *ex vivo*.

At the beginning of this project, there was no strong evidence that NMT inhibition would have a cytotoxic effect on cancer cells. Several inhibitors had been tested (Section 1.8) and shown to kill cancer cells but the correlation between NMT inhibition and cell death was never demonstrated. The cytotoxicity could only arise from off-target effects and this possibility will be discussed in this Chapter.

3.1 Inhibitor evaluation

In this Chapter, several inhibitors are evaluated. Their potential to be used as tools to study the phenotype of NMT inhibition in cells will be discussed. A good HsNMT inhibitor has to fulfil several criteria. It should:

- ✓ Have a **high enzyme affinity** (IC_{50} <1 μM). The CPM assay, described in Section 2.2.2, will be used to assess the affinity of the compounds against both recombinant HsNMT1 and HsNMT2. For an accurate IC_{50} (half maximal inhibitory concentration) determination, it is preferable to use a minimum of 10 inhibitor concentrations, equally spaced (typically 3-fold dilutions were used).[216] Half the data points on the dose dependent response should be higher than the IC50 value and half should be below the IC50 value. As discussed in Section 2.2, 8AA c-SRC peptide will be used to evaluate the potency of the inhibitors as this peptide was a modest substrate for the enzyme (K_M~ 3 μM) (Chapter 2). If the peptide binds too tightly to the enzyme, such as the 15AA c-SRC peptide, a weak competitive inhibitor would not be able to displace the peptide and no IC50 value would be determined. The lower limit for the assay corresponds to half of the enzyme concentration (~5 nM).
- ✓ **Selectively toxic to cancer cells.** Cytotoxicity of anticancer reagents is typically measured after 1-3 days in cells. Toxicity of the compounds tested is assessed here in HeLa cells treated for 3 days with a concentration range of the inhibitor using the MTS assay described in Section 2.3.5.1. The concentration that gives half maximal response (EC_{50}) is determined.
- ✓ **Act on-target through inhibition of NMT in cells.** The ability of compounds to inhibit HsNMT in cells will be assessed using the metabolic labelling technology described in Sections 1.10.2 and 2.3. If a compound inhibits NMT in live cells, the efficiency of YnC12 transfer to the N-terminal glycine of substrate proteins will be impaired, resulting in an observable decrease in the fluorescence signal on the gel

3.2 HsNMT inhibitors previously reported in the literature

Before starting this PhD project, many inhibitors of HsNMT had been described in the literature.[217] However, only two inhibitors had been employed in cancer cells to inhibit NMT (Section 1.8.2). We thus decided to evaluate these inhibitors as described in Section 3.1.

3.2.1 2-Hydroxymyristic acid

2-Hydroxymyristic acid (HMA) was first reported as a selective inhibitor of myristoylation in 1990 [133] and has been since widely used.[218-220] However, this compound is poorly soluble in the cell media at the concentration required to inhibit HsNMT in cells (typically between 0.5 mM and 1 mM). When this compound was tested in MDA-MD-231 cells, a precipitate was formed as soon as the compound (from a stock solution in DMSO) was added to the culture media and no decrease of labelling was observed by in-gel fluorescence when the cells were treated at the same time with YnC12 (data not shown). To increase the solubility, a protocol described in the literature was tested.[220] HMA was saponified using potassium hydroxide and the fatty acid salt was dissolved in warm serum-free culture media containing 20% fatty acid-free BSA before being added to the cells. The solubility improved but the fatty acid still precipitated in the culture media and no decrease of labelling was observed by in-gel fluorescence (data not shown).

All these experiments suggested that a more reliable, soluble and potent HsNMT inhibitor was needed to study NMT inhibition in cancer cells. It should be noted that even though this compound had several issues, it was shown to dose-dependently decrease [^{3}H]myristate labelling in cells.[139] Furthermore, it was successfully used to show that NMT inhibition could be a new therapeutic strategy in the context of viral infections such as varicella-zoster virus[139] and HIV.[138,221]

3.2.2 Tris DBA

The second inhibitor reported in the literature before the beginning of this PhD project was Tris DBA, an organometallic complex used as a palladium-based catalyst in organic chemistry.[140,144] The activity of this compound is quite surprising and by inspection of the chemical structure, was predicted to be poorly soluble in aqueous media such as the cell culture media.

It was reported that this compound could inhibit HsNMT1 activity *in vitro* and in cells.[140] More recently, Tris DBA was suggested to be more selective for HsNMT1 than HsNMT2 [144] with IC_{50} values of 0.5 ± 0.1 µM and 1.3 ± 0.1 µM respectively. A CPM assay was carried out to confirm these results. The IC_{50} values for HsNMT1 and HsNMT2 were in the same order of magnitude as previously reported but we found that the IC_{50} values were very similar for both HsNMT isoforms (Figure 34).

We then evaluated the cytotoxicity of this compound in HeLa using a MTS assay. No metabolically active cells remained in wells treated with a concentration of Tris DBA higher than 1 µM. Bhandarkar et *al*. similarly found that Tris DBA had a cytotoxic effect against B16 murine and A375 human melanoma after one day treatment with a concentration of 1 µM.[140] However, we noticed that Tris DBA precipitated in the media containing the cells treated with the highest concentrations of inhibitor (>1 µM). In these wells, cells seemed dead after only a few hours, as suggested by the rounded up shape.

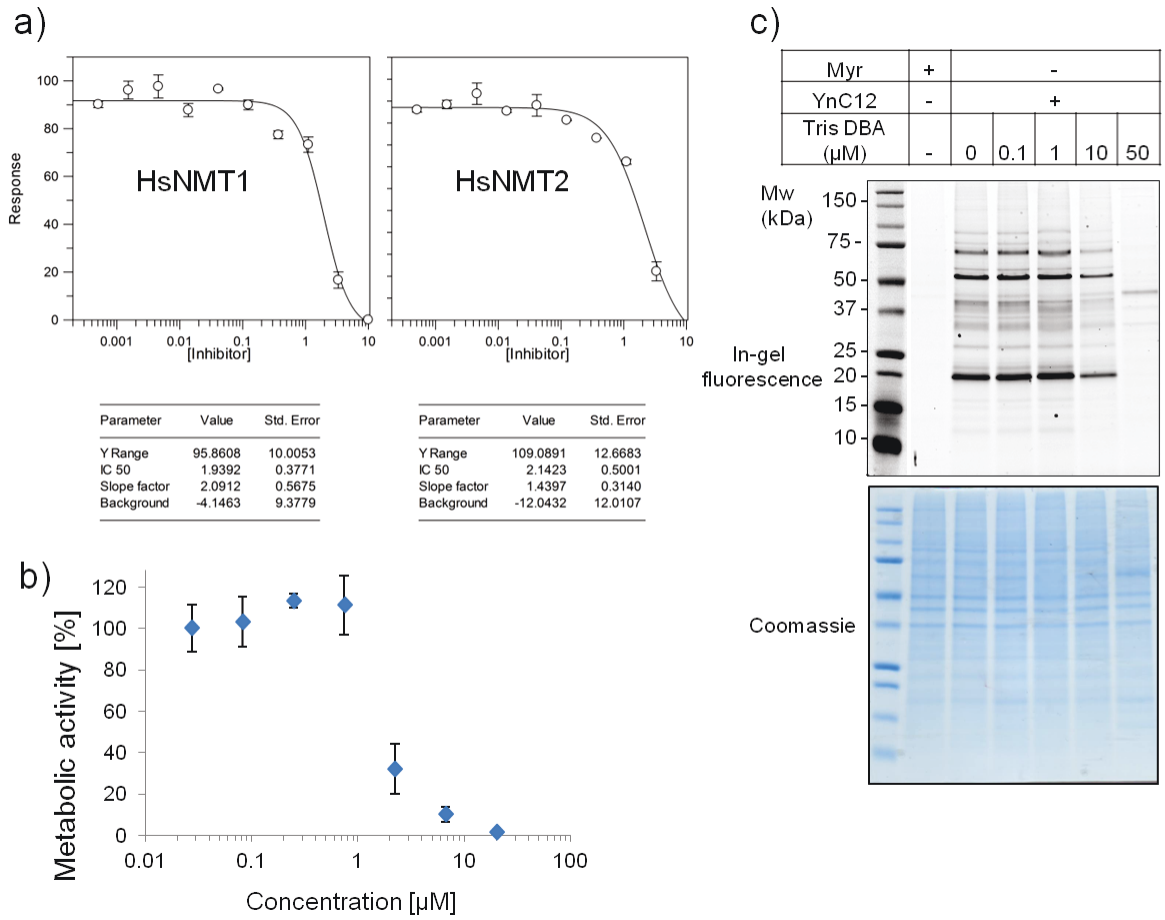

Figure 34.Evaluation of Tris DBA as an NMT inhibitor *in vitro* and in cells. a) Dose dependant response of the inhibitor determined using the CPM assay. **b)** Cell metabolic assay (MTS assay) carried out for 3 days in HeLa. c) In-gel fluorescence showing the YnC12 labelling in HeLa cells treated with various concentrations of Tris DBA. Cells were dead after 7 h treatment at 50 µM.

A YnC12 tagging experiment was carried out to see if the toxicity could be credited to NMT inhibition. If NMT is inhibited in cells, YnC12 labelling should drop dose-dependently with an increasing amount of inhibitor. At 50 µM, only one band could be seen using in-gel fluorescence and the cells seemed to be rapidly killed by the inhibitor. The proteins in this remaining band, which are still apparently labelled by NMT, are unknown but proteomics experiments could be carried out to

identify the nature of the proteins. This result could suggest that NMT is inhibited and hence the inhibitor is acting on target. However, at 10 µM cells were almost killed after three days (Figure 34b) while NMT substrates were still being tagged with YnC12 (Figure 34c), suggesting the enzyme is not completely inhibited. Tris DBA is thus not toxic due to NMT inhibition but probably due to an off-target effect. It is unclear if the loss of labelling at 10 µM could be credited to NMT inhibition or is just an artefact of the off-target effect of Tris DBA. If the compound partly inhibits protein synthesis or kills the cells, it could result in a decrease of YnC12 labelling. Bhandarkar et *al*. suggested that NMT is not inhibited by Tris DBA in cells; they proposed that Tris DBA could decrease HsNMT1 expression in cells.[140] Indeed, gene array analysis revealed that HsNMT1 gene was highly down-regulated upon inhibition with Tris DBA. However, other genes were also down-regulated, suggesting that toxicity was not only the result of a decrease of NMT activity.

A competition experiment was carried out to confirm whether Tris DBA was a competitive inhibitor of the peptide substrate. As expected, the compound is not a competitive inhibitor of the peptide binding pocket as the V_{max} values were different when the K_M of c-SRC was determined in the presence of different amount of Tris DBA (Figure 35a). If Tris DBA was a competitive inhibitor, the curves in Figure 35a should reach the same maximum at the highest concentration of peptide substrate and the linear fits in Figure 35b should cross the y axis at the same position.[222]

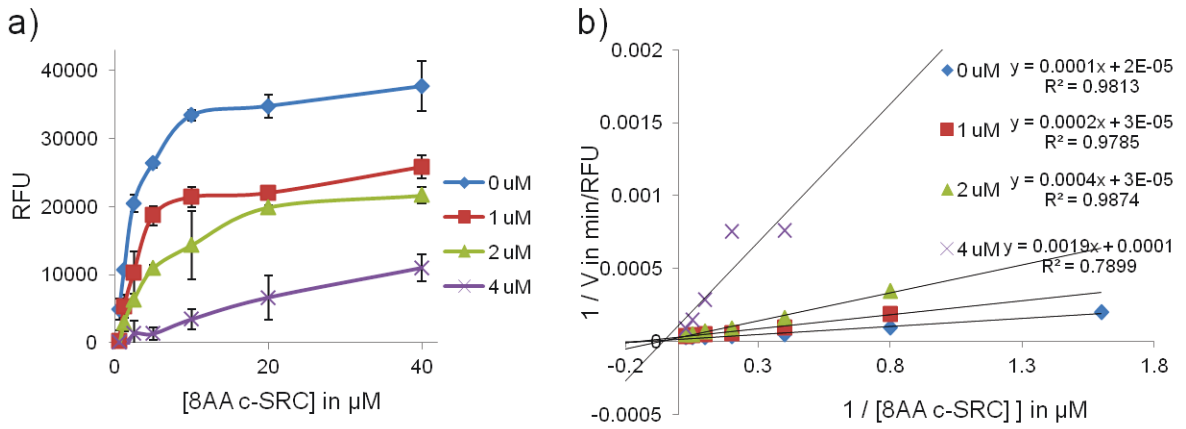

Figure 35. Competition experiment: Tris DBA does not compete with the peptide substrate. a) Shows the relative fluorescent intensity (RFU) versus the concentration of peptide substrate, 8AA c-SRC. Increasing the amount of substrate cannot overcome the inhibition, and V_{max} are different, suggesting that Tris DBA is a non-competitive inhibitor. **b)** Shows the *1/V* value versus the reverse value of the peptide concentration. The *y*-intercept is equivalent to the inverse of V_{max} and this plot confirms that the V_{max} values are different. The data were linearly fitted in Excel. The R-squared value and equation are indicated.

These results showed that Tris DBA was not a competitive inhibitor of NMT but most probably NMT activity was reduced due to enzyme aggregation. While the compound was toxic to HeLa, the toxicity could not be correlated to NMT inhibition. This compound was thus not used to study NMT inhibition in cancer cells in this work, and these results suggested that a better inhibitor was needed.

3.3 Characterisation of IMP366 (DDU85646, compound 4) and analogues:

Recently, potent inhibitors of *Trypanosoma brucei* NMT (*Tb*NMT) have been reported.[43,142,223] The protein binding pocket of the enzyme is highly conserved across species and *Tb*NMT share 83% identity and 90% similarity with human NMT1 and NMT2.

3.3.1 Evaluation of IMP366 (DDU85646, compound 4) as an HsNMT inhibitor

Inhibitor DDU85646, referred to here as IMP366, was synthesised (kind gift from Dr. Remi Serwa and Dr. Will Heal, Tate group, Imperial College London) and its potency was assessed against recombinant HsNMT1 and HsNMT2 by determining the IC_{50} values (Figure 36). Compound IMP366 was a potent inhibitor of both HsNMT isoforms with an IC_{50} in the low nM range (17 and 22 nM respectively). A comparable IC_{50} was found in the original paper against HsNMT1 (3 nM) using a different assay.[142] The slope factors were close to 1, suggesting that the inhibitor might be a competitive inhibitor. Several experiments were carried out by Dr. Victor Goncalves (Tate group, Imperial College London) to confirm that the inhibitor was a competitive inhibitor of the protein binding pocket of HsNMT1.

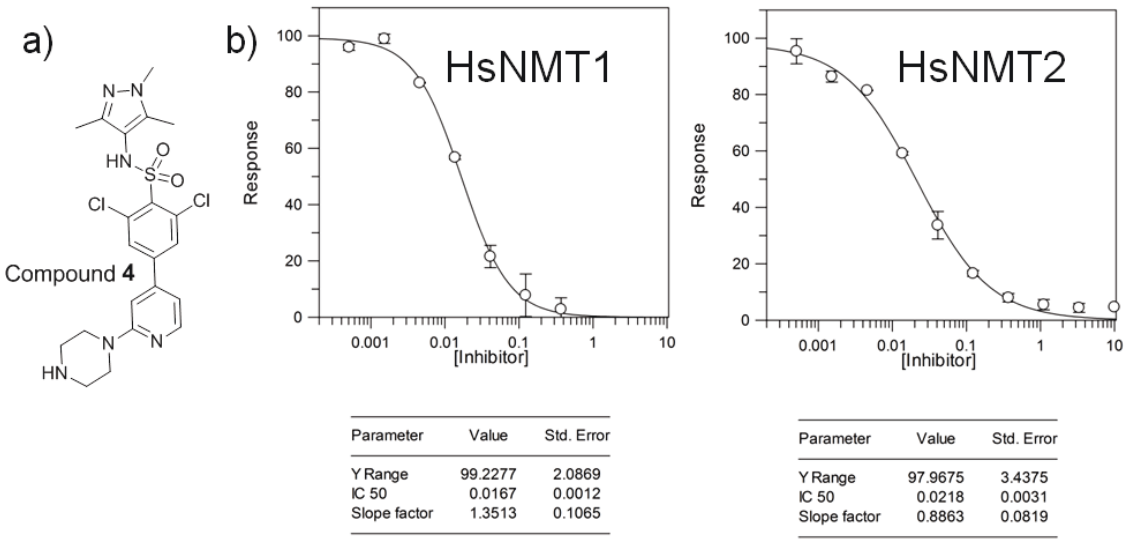

Figure 36. Enzyme affinity of IMP366. a) Structure of IMP366. **b)** Inhibition profile of IMP366 against HsNMT1 and HsNMT2. The response is the% remaining activity. The figure was generated from GraFit using the background corrected IC_{50} function.

The inhibition of HsNMT in HeLa cells was assessed. HeLa cells were treated with a concentration range of inhibitor IMP366, starting from 10 µM and using 3-fold dilutions, in the presence of YnC12 for 24 h. We envisioned that pre-feeding the cells for 1 h with the inhibitor would be sufficient to allow the compound to penetrate inside the cells and inhibit NMT. The pre-feeding time was optimised later (Section 3.3.3.3). Following cell lysis, proteins were captured with AzTB, separated on a SDS-PAGE gel and the captured proteins visualised by fluorescence (Figure 37a). The fluorescence signal decreases with increasing concentration of inhibitor in a dose dependant manner. The disappearance of the fluorescence signal at the highest concentration of inhibitor suggests that NMT is fully inhibited at this concentration.

The fluorescence of individual bands on the gel was quantified using ImageJ and plotted against the concentration of inhibitor. The error in quantification was determined through two biological replicates. The fluorescence of individual bands was normalised to the protein loading using the coomassie-stained gel, which could be quantified. The fluorescence could also have been normalised according to the relative amount of HsNMT1 and HsNMT2 in the samples. However, this quantification was subject to experimental bias (protein transfer on the membrane for example) and this method was thought to be less reliable than the coomassie stain.

The concentration, at which metabolic tagging is inhibited by 50%, referred here as the TC_{50}, was calculated for the three major bands (Figure 37b), by fitting the data to an IC_{50} function in GraFit. The slope factor of the dose-dependent response ranged from 0.96 to 1.32, similar to values observed for the determination of the IC_{50} values using the in-vitro assay. The TC_{50} values ranged from 90 nM to 253 nM, with an average value of 160 nM. These differences between bands probably reflect the specificity for NMT for each individual protein at the enzyme level. Assessing the TC_{50} on only the three major bands might not reflect perfectly the enzyme inhibition in cells. Many bands observed in fluorescence cannot be quantified, especially bands between 25 kDa and 37 kDa. Protein *N*-myristoylation on these bands might be differently affected by the concentration range of inhibitor IMP366. The fluorescence of the whole band was thus quantified using ImageJ and fitted as before to an IC_{50} function in GraFit (Figure 37c). The new TC_{50} value, 169 nM, was similar to the average TC_{50} value of the three major bands. However, this second method was more efficient, and was preferred to measure the TC_{50} values of other NMT inhibitors.

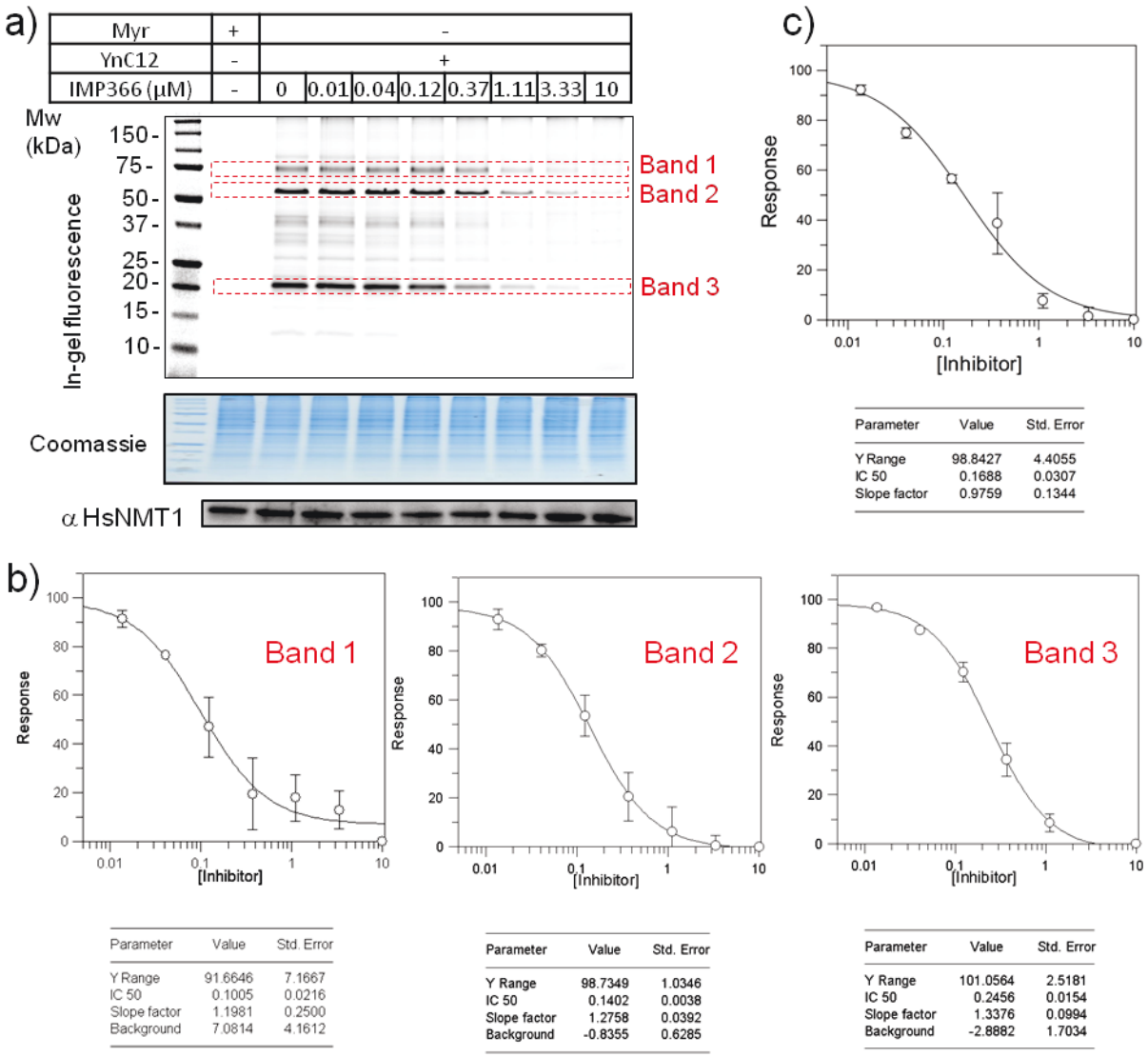

Figure 37. Effect of inhibitor IMP366 on YnC12 labelling. a) In-gel fluorescence showing that the fluorescence intensity in bands 1-3 decreases dose dependently with increasing amounts of inhibitor IMP366. Protein loading on the gel was checked by coomassie and with the Western blot against HsNMT1. **b)** Tagging IC_{50} (referred as TC_{50}) determination for the 3 major fluorescent bands. The fluorescent signal of bands 1-3 was quantified (ImageJ) and the average dose-dependent response of two biological replicates was plotted in GraFit. The error bars correspond to the standard deviation between replicates. **c)** Similar to b), the fluorescent signal for each whole lane was quantified and used to determine the tagging IC_{50} (TC_{50}).

The toxicity of the inhibitor IMP366 was then assessed in HeLa cells using the MTS assay (Figure 38). The percentage of metabolic activity for cells treated with various concentrations of the inhibitor compared to the control (no inhibitor) was measured. This response gives an indication of the relative amount of viable cells in culture compared to the control. It is interesting to notice that IMP366 has an atypical dose-dependent response in HeLa after 3 days (Figure 38a). The cells have no remaining metabolic activity at the highest concentrations of inhibitor (100 µM), and are thus

probably killed. However, the response (percentage residual metabolic activity) seems to show a plateau at 20%.

This result was correlated to the YnC12 labelling experiment (Figure 37a). As seen by in-gel fluorescence, NMT seems to be nearly completely inhibited (<10% remaining fluorescence) from concentrations higher than 1 µM, which correspond to the start of the plateau observed on the MTS assay curve. In other words, NMT inhibition for 3 days does not kill HeLa cells but leaves ca. 20% residual metabolism compared to the control (no inhibitor). We hypothesised that the cells either stop dividing or it is also possible that only a portion of the cells is sensitive to NMT inhibition, due to the presence of different colonies of HeLa cells. These hypotheses will be studied in Chapter 5. However, these experiments showed for the first time that on-target inhibition of NMT in cells could decrease the metabolic activity and thus cell viability of cancer cells.

When HeLa cells were treated with an excessive concentration of inhibitor (100 µM), no metabolic activity was observed and we hypothesised that cells were probably killed due to off-target effect (Figure 38a). At 10 µM, NMT seems completely inhibited in cells, but the metabolic activity was the same as at 1 µM.

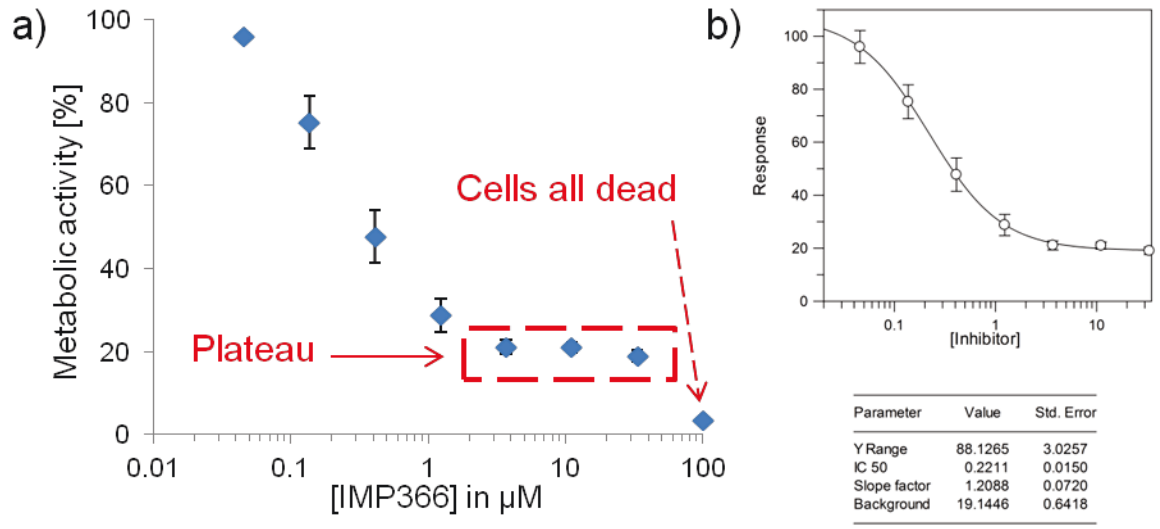

Figure 38. Evaluation of the cytotoxicity of IMP366 using the MTS assay. The assay was carried out for 3 days in HeLa cells. The error bars display the standard deviation between six biological replicates. **a)** Dose-dependent response showing the% of remaining activity versus the concentration of inhibitor. Seven concentrations of inhibitor were tested, starting from 100 µM, and using 3-fold dilutions. **b)** The dose-dependent response was plotted in GraFit. The highest concentration of inhibitor (100 µM) was discarded to allow the data points to fit the IC_{50} function in GraFit.

The EC_{50} value of this inhibitor was evaluated by fitting the data to the IC_{50} function in GraFit. The highest concentration of inhibitor was discarded as it probably does not correspond to on-target NMT inhibition and could prevent the data from fitting to the dose-dependent function in GraFit (Figure 38b).The EC_{50} value correlated well with the TC_{50} values, suggesting that the cell toxicity is predominantly, if not exclusively, due to NMT inhibition and that there is no significant off-target effect. However, to confirm this correlation, inhibitors from the same series were evaluated later (see Section 3.3.2).

IMP366 was crystallised in the presence of MyrCoA with HsNMT1 by Dr. Jim Brannigan (University of York). As expected, the inhibitor binds to the protein binding pocket of HsNMT1 (Figure 39a). It has some key interactions with the enzyme, including a salt bridge with the C-terminal carboxylate of the enzyme, a hydrogen-bonding interaction with Ser405 and a π-π interaction with Tyr 296.

The electron density map of the inhibitor IMP366 is presented in Figure 39b-c. HsNMT1 crystal structure with bound-inhibitor was superimposed with the crystal structures of the inhibitor-free HsNMT1 and inhibitor-free HsNMT2 (in each case the enzyme was bound to MyrCoA or a non-hydrolysable analogue). These structures show a very similar arrangement of key residues in the human HsNMT1 and HsNMT2 active sites. The two inhibitor-free enzymes superimpose well to the inhibitor-bound HsNMT1 structure and this feature can be characterised by the measure of the root-mean-square deviation (RMSD). The RSMD corresponds to the average distance between the backbone atoms of superimposed proteins. The RMSD value between inhibitor-free NMT1 and inhibitor-free NMT2 was 0.390 (325 to 325 atoms) and between inhibitor-bound NMT1 with inhibitor-free NMT1 was 0.117 (290 to 290 atoms).Regarding this last number, it seems that the enzyme undergoes limited rearrangement upon inhibitor binding. It suggests that the inhibitor binds tightly to a pocket that is probably pre-organized by binding of MyrCoA.[58]

The crystal structure of inhibitor-bound HsNMT1 was also superimposed with a structure of *Lm*NMT bound with the same inhibitor as this structure had been previously published and well-described.[223]

Several interactions are conserved, including the salt bridge to the NMT1 C-terminus and a hydrogen bond to Ser405, although an additional hydrogen interaction can be observed in the *Lm*NMT structure between the oxygen of the sulfonamide moiety and several surrounding amino acids.

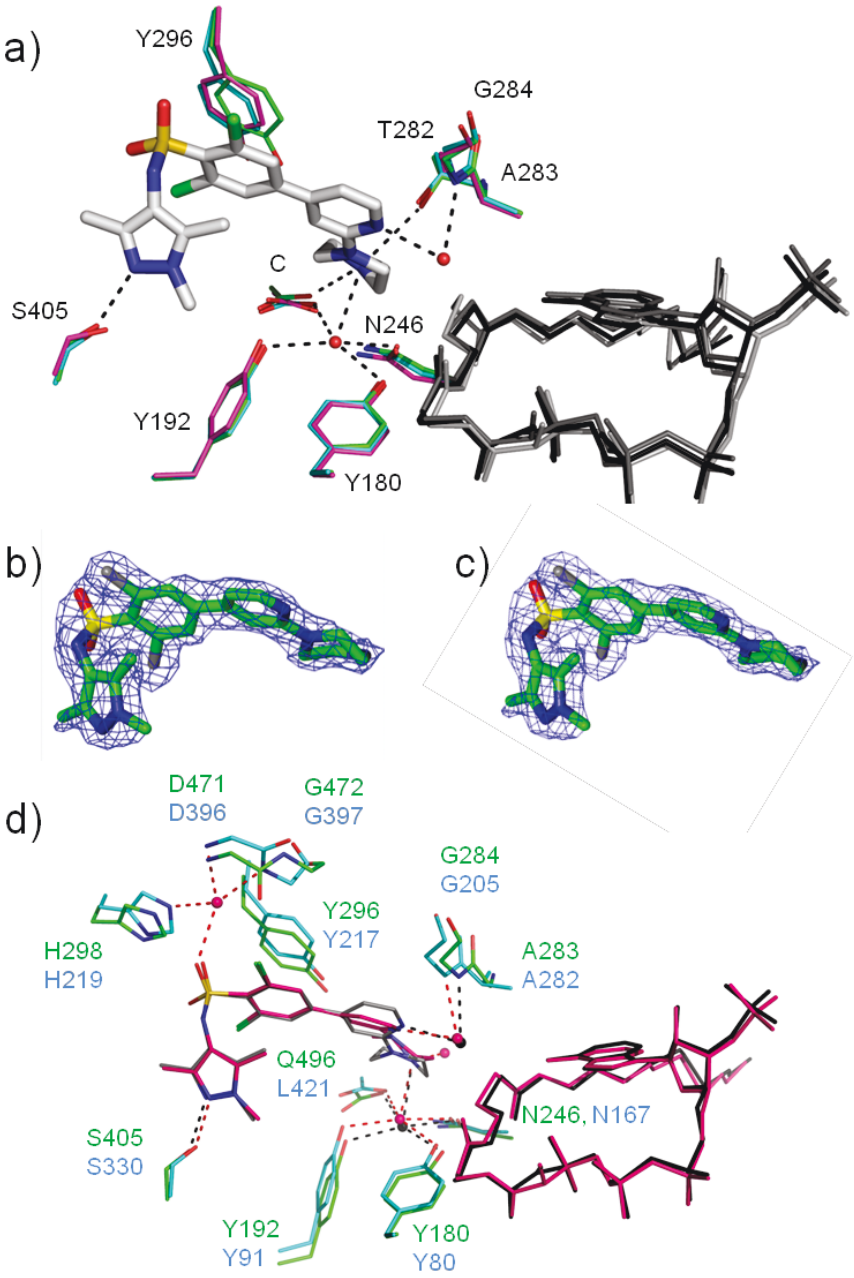

Figure 39. Crystal structure of IMP366. a) Crystal structure of IMP366 (grey) bound to NMT1 in the presence of MyrCoA. Key water molecules are shown as red spheres. Polar interactions are shown as black dashes. NMT1 key residues are shown is green and non-hydrolysable MyrCoA in black. The C-terminus is labelled C (Q496). The structure was overlayed with the apo forms of NMT1 (blue) and NMT2 (pink) bound with MyrCoA (dark grey) and non–hydrolysable MyrCoA (light grey) respectively. The figure was generated in PyMOL using PDB ID: 4C2Z (NMT1 bound to IMP366 and MyrCoA), PDB ID 4C2Y (apo NMT1) and PDB ID 4C2X (apo NMT2). **b)** and **c)** Electron density of IMP366 bound to HsNMT1 (PDB 4C2Z). **d)** Overlay of HsNMT1 and LmNMT, both bound with IMP366. Key water molecules are shown as grey spheres for HsNMT1 and pink spheres for LmNMT. Key residues are shown in green for HsNMT1 and blue for *Lm*NMT. IMP366, MyrCoA, polar interaction and key molecules are shown in grey for HsNMT1 and in pink for *Lm*NMT. Key amino acids are labelled for clarity in green for HsNMT1 and blue for LmNMT. The figure was generated in PyMOL using PDB ID 4C2Z. (NMT1 bound to IMP366 and Myr CoA), PDB ID 2WSA (*Lm*NMT).

3.3.2 Analogues within a series: correlations of IC_{50}, TC_{50} and EC_{50}.

Three analogues of IMP366 were prepared by Dr. William Heal (Tate group, Imperial College London) (Figure 40a), and their enzyme affinity assessed using the CPM assay. Compounds IMPP366, IMP653 and IMP655 had similar enzyme affinities. However, compound IMP654 was a much less potent inhibitor of HsNMT1 and HsNMT2 with an IC_{50} in the low micromolar range (1684 and 2096 nM respectively).

These similarities and differences in potency could be rationalised using the crystal structure of HsNMT1 bound to IMP366. For the less potent inhibitor IMP654, the N-O bond might disrupt the hydrogen bond between the nitrogen and the carboxyl group of Ser405, which could explain the low affinity for the enzyme. Surprisingly, an extra methyl group in position R_3 (inhibitor IMP653) did not disrupt the salt bridge interaction with the C-terminal carboxylate of the enzyme. The presence of a difluoromethyl moiety also did not dramatically change the affinity for the enzyme, as there is probably sufficient space to accommodate it in the enzyme binding pocket.

EC_{50} values were determined using the MTS assay (Figure 40b). Inhibitor IMP654 was not toxic to the cells up to 10 µM. The other two compounds, IMP653 and IMP655 showed a similar response as IMP366, with a plateau of residual activity between 3.3 and 10 µM.

Enzyme inhibition in HeLa cells was assessed using YnC12 tagging (Figure 40c). For compounds IMP653 and IMP655, as previously seen with 366 (Figure 37a), the fluorescence labelling was dose-dependently affected by the increasing amount of inhibitor, but the fluorescent signal at 0.2 and 1 uM was greater than for IMP366, confirming that the IC_{50} and EC_{50} values are higher for these compounds than for IMP366. The TC_{50} values were evaluated by quantifying the fluorescence intensity of the whole lane and normalising to the protein loading using ImageJ (Figure 40b). For a more accurate evaluation of the TC_{50} values, another inhibition experiment was carried out with a larger concentration range (7 concentrations starting from 10 µM, tripling dilutions). The gels are presented in Appendix C and the TC_{50} values in Figure 40b.

a)

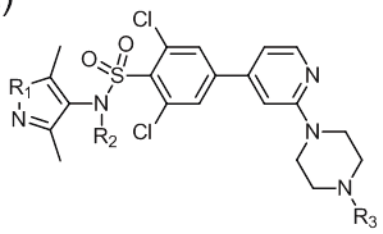

IMP-366: R_1 = NMe; R_2 = H; R_3 = H
653: R_1 = NMe; R_2 = H; R_3 = Me
655: R_1 = NMe; R_2 = CHF_2; R_3 = H
654: R_1 = O; R_2 = H; R_3 = H

c)

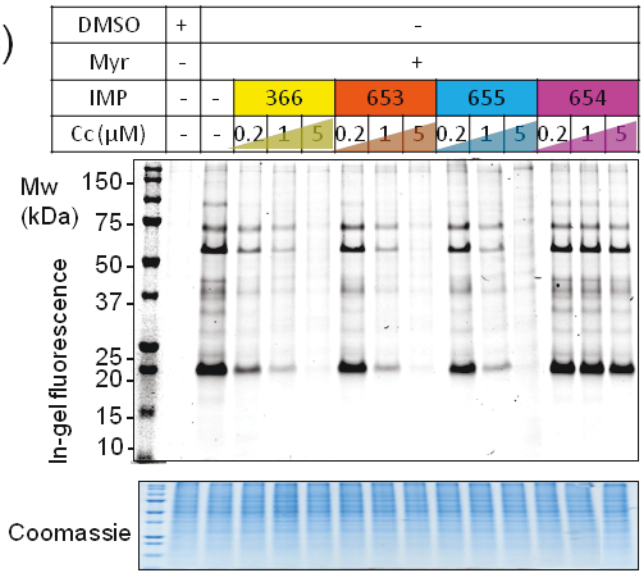

b)

Inhibitor IMP	IC_{50} (nM)		TC_{50} (nM)	EC_{50} (nM)
	HsNMT1	HsNMT2		
366	17	22	169	221
653	39	45	222	466
655	51	74	418	1060
654	1684	2096	>10000	>10000

d)

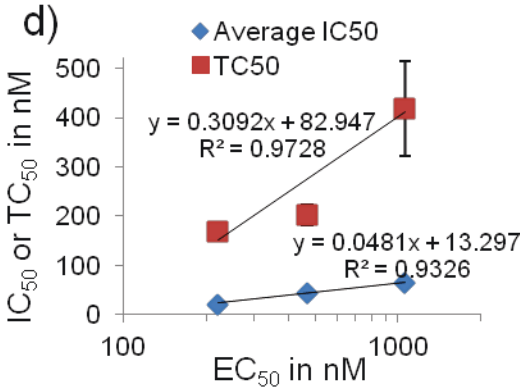

Figure 40. Assessment of IMP366/653/654/655 for on-target activity using YnC12 tagging. **a)** Structures of the four inhibitors. **b)** Enzyme and cellular data for the four inhibitors. The EC_{50} is the average value of three replicates and the TC_{50} value was calculated from in-gel fluorescence of two biological replicates **c)** In-gel fluorescence analysis. The cells were pre-treated with the inhibitor for 1 h and were tagged with YnC12 in the presence of the inhibitor for 24 h. d) Correlation between IC_{50} or TC_{50} with EC_{50}. The IC_{50} value shown here is the average value of IC_{50} against HsNMT1 and the IC_{50} against HsNMT2.

Compound IMP654 was not potent against the recombinant enzyme and the labelling experiment in cells showed no dose-dependent response. The structure of IMP654 is highly similar to IMP366 but did not show any toxicity in HeLa cells up to 10 µM. This result strongly supports the hypothesis that 366 does not have any off-target effect leading to toxicity in cells (at least up to 10 µM).

For these four analogues, there is an excellent correlation between IC_{50}, EC_{50} and NMT inhibition in HeLa cells (Figure 40d). The TC_{50} was measured based on a 24 h labelling experiment while the EC_{50} values were measured after 3 days. The TC_{50} values are slightly lower than the EC_{50} values, probably due to an experimental error that shifts everything equally.

All these results give us high confidence that IMP366 is acting on target and does not have any relevant off-targets up to 10 μM.

3.3.3 Further validation of IMP366 as a tool inhibitor

IMP366 is the first potent, specific and soluble compound targeting NMT in cells. However, before using it as a tool to study NMT inhibition in cancer cells, the compound required further investigation. The compound will be used in Chapter 4 in proteomics experiments for periods up to 24 hours, and so the toxicity of the compound up to 1 day needed to be addressed, as well as its stability, translation in HeLa and ability to inhibit *N*-myristoylation of known NMT substrates.

3.3.3.1 IMP366 is not toxic to HeLa cells after 1 day

N-Myristoylation is a co-translational process and any inhibitors of protein synthesis or any excessive cell death due to inhibitor toxicity could impair YnC12 labelling. An experiment was carried out to confirm protein synthesis was not stopped upon NMT inhibition with IMP366 for 24 h (Figure 41). An azido-homoalanine (AHA) labelling experiment was performed in HeLa cells treated with different concentration of IMP366 (Figure 41 a, b, c, d).[224] Protein synthesis was not affected at all the concentrations tested after 1 day of inhibition. A MTS assay was also carried out to check that the inhibitor was not toxic to the cells after 1 day treatment (Figure 41e).

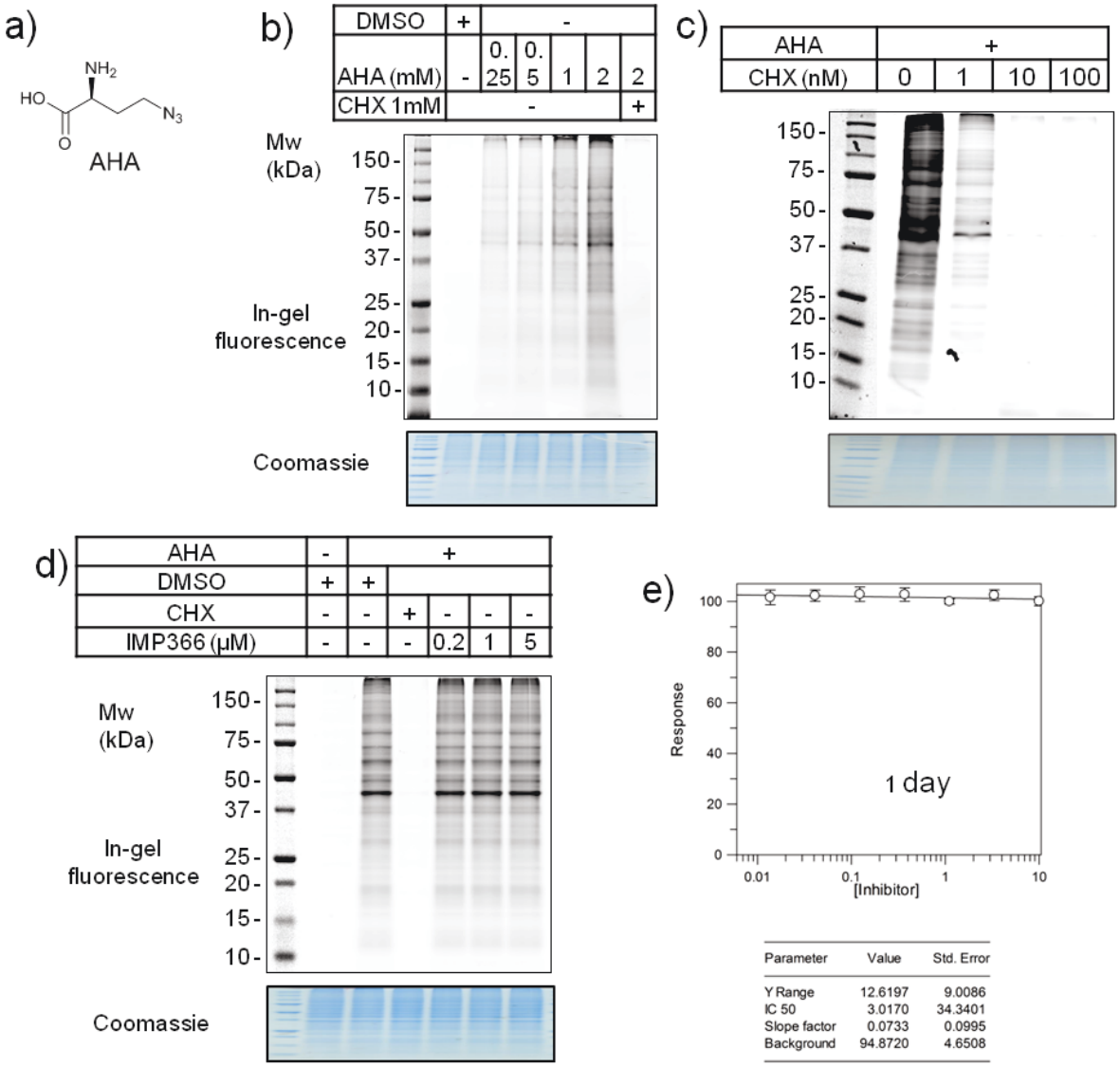

Figure 41. Inhibitor IMP366 does not inhibit protein synthesis and is not toxic to cells after 24 h treatment. **a)** Structure of L-azidohomoalaine (AHA). **b)** Dose-dependent labelling with AHA in HeLa. Cells were also treated with the highest concentration of AHA with cycloheximide (CHX), an inhibitor of protein synthesis, showing that AHA only labels newly synthesised proteins. **c)** AHA labelling with increasing amount of CHX. **d)** Cells were treated with AHA and DMSO or CHX or inhibitor IMP366. **e)** Metabolic activity in HeLa cells treated with inhibitor IMP366 for 24 h. The response corresponds to the% of metabolic activity compared to the control (cells treated with DMSO). The inhibitor concentration is in µM. The data was fitted to a dose-response curve using GraFit 7.0 (IC_{50} replicate function).

3.3.3.2 Use of the inhibitor in combination with YnC12

In the next Chapters (Chapter 4 and 5), IMP366 will be used in combination with YnC12 to carry various experiment, such as proteomics experiments to identify novel NMT substrates, or experiments to study the phenotype of NMT inhibition in cancer cells. YnC12 was shown to be not toxic to HeLa cells up to 3 days (Section 2.3.5.2) but an additional experiment was carried out to demonstrate YnC12 would not increase the toxicity of the inhibitor after 3 day treatment (Table 9).

As expected, the EC_{50} value of IMP366 in the presence of Myr or Ync12 was similar to the value obtained without any probe. The small differences may be attributed to experimental errors.

Table 9. Cell cytotoxicity of IMP366 in the presence of Myr or YnC12

IMP366	-	+ Myr (20 µM)	+ YnC12 (20 µM)
EC_{50} (µM)	0.29 ± 0.03	0.34 ± 0.03	0.21 ± 0.03

It would be right to compare IC_{50} and TC_{50} values only if IMP366 had the same binding affinity for the enzyme in the presence of MyrCoA and YnMyrCoA. A CPM assay was carried out, and as expected, the binding affinity of IMP366 was similar for HsNMT1 and HsNMT2 in the presence of MyrCoA and its alkyne-tagged analogue (Table 10).

Table 10. IC_{50} values of IMP366 against HsNMT1 and HsNMT2 measured in the presence of MyrCoA (4 µM ~ K_M) or YnMyrCoA (1 µM ~ K_M)

IC_{50} of IMP366 (nM)	HsNMT1	HsNMT2
With MyrCoA	17 ± 1	21 ± 1
With YnMyrCoA	15 ± 1	15 ± 1

3.3.3.3 Optimisation of the pre-incubation time

In all the experiments described above, the cells were pre-fed for 1 h with the inhibitor before being labelled for 24 h with YnC12 in the presence of the inhibitor. An experiment was carried out to check that 1 h pre-feeding was sufficient (Figure 42).

Interestingly, the same labelling pattern was observed for all the samples pre-fed with the inhibitor for 0-18 h. The background seems quite high on the gel, probably due to the use of only 1 µM of IMP366 and also to the use of a Tris-based buffer for cell lysis (Section 2.3.1). This result suggests that the inhibitor penetrates cells rapidly and that no pre-incubation time would be necessary. However, for the next experiments, 1 h pre-feeding was retained to ensure that all NMT was inhibited before the addition of YnC12 to the cells.

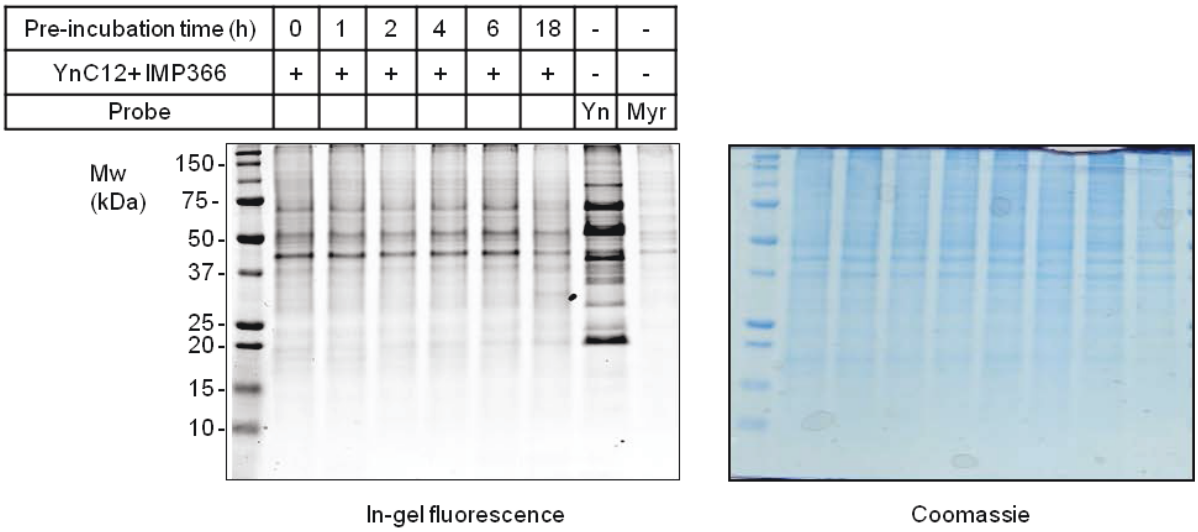

Figure 42. Results from bioorthogonal ligation experiment to optimise the pre-incubation time for inhibitor IMP366 HeLa cells. Cells were pre-fed with the inhibitor (1 µM) for 0-18h and labelled for a further 6 h with YnC12 (20 µM) in the presence of the inhibitor (20 µM).

3.3.3.4 Inhibition of *N*-myristoylation of NMT substrates

The decrease in tagging of three known *N*-myristoylated proteins, PSMC1, PRKACA, and c-SRC was also quantified, to assess if *N*-myristoylation of NMT substrates were dose-dependently affected by the inhibitor IMP366. HeLa cells were treated with several concentrations of inhibitor IMP366 and proteins were tagged with YnC12. After cell lysis and capture of the tagged proteins with AzTB, NMT substrates were enriched on streptavidin beads. Western blot analysis showed that PSMC1, PRKACA and c-SRC are dose-dependently less enriched when the inhibitor was added to the cells (Figure 43a).

The band intensities were quantified and plotted against the concentration of inhibitor (Figure 43b). The dose-dependent response of PRKACA is considerably different than the dose-dependent response of c-SRC and PSMC1. Estimation of the IC_{50} showed that half of PRKACA present in cells is not *N*-myristoylated with a concentration of inhibitor as little as 27 nM. However, to draw strong conclusions, the experiment would need to be repeated several times to take into account the error of the experiment. It would be better to use proteomics experiments to quantify accurately the decrease of enrichment of these proteins. This possibility will be discussed in Chapter 4.

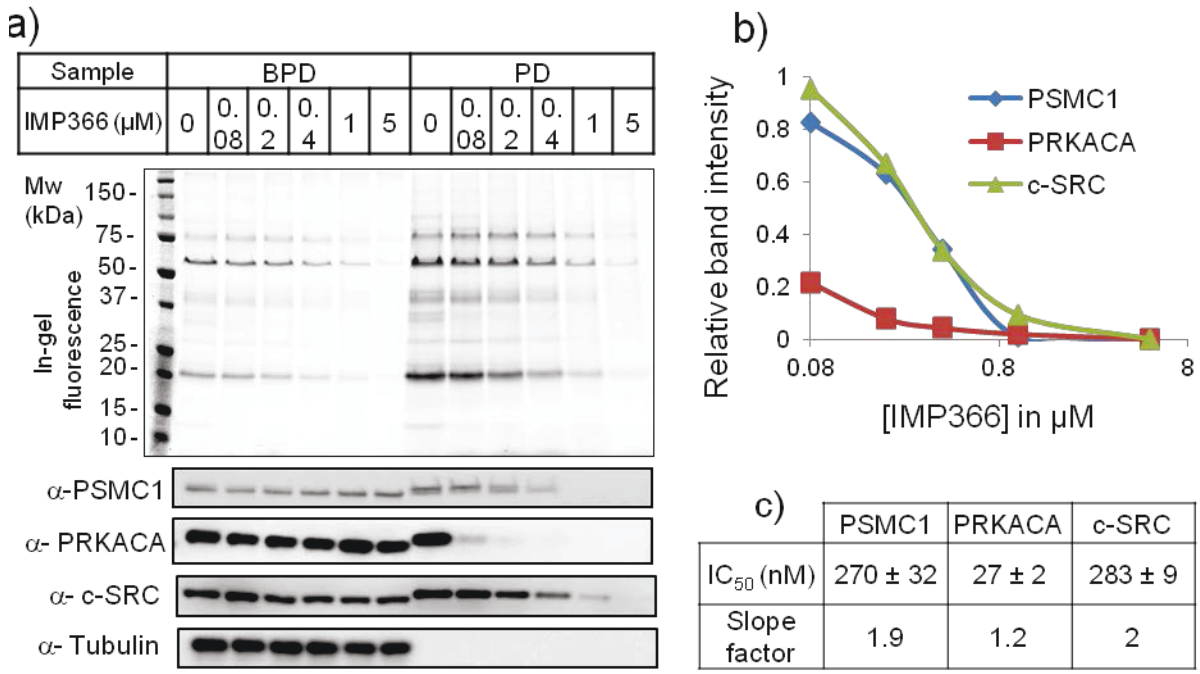

c)

	PSMC1	PRKACA	c-SRC
IC_{50} (nM)	270 ± 32	27 ± 2	283 ± 9
Slope factor	1.9	1.2	2

Figure 43. Inhibition of *N*-myristoylation of PSMC1, PRKACA and c-SRC. a) In-gel fluorescence and Western blot (Western blot, bottom) analysis showing the decrease in tagging of PSMC1, PRKACA, c-SRC after enrichment. BPD = before pull-down and PD = pull down. Tubulin was used as a loading control. The equivalent of 4-fold more protein was loaded for the PD samples. **b)** Quantification of the bands observed in the PD samples for the 3 known substrates with ImageJ. The intensities of the bands was normalised to the intensity of the band in the sample without inhibitor for each protein. The abscissa is in log scale. **c)** IC_{50} values and slope factors determined by fitting the relative band intensities to an IC_{50} function in GraFit.

This experiment confirms the observation made in Section 3.3.1. We observed earlier that the TC_{50} was different for the three major fluorescence bands, suggesting that NMT substrates will be differentially affected by an NMT inhibitor. The reason for this is currently not fully understood but will be discussed in Chapter 4.

3.3.3.5 Translation in HeLa cells

We observed that IMP366 has a relatively low translation from *in vitro* enzyme assay to *in vitro* cellular assays in HeLa cells, with an EC_{50} value approximately 10-fold higher than the IC_{50}. This 10-fold translation value was consistent with the inhibitors from the same series (Section 3.3.2). As the compound was shown to highly bind to plasma,[43] we suspected that the inhibitor might highly bind to serum in the culture media hence preventing the compounds getting into cells.

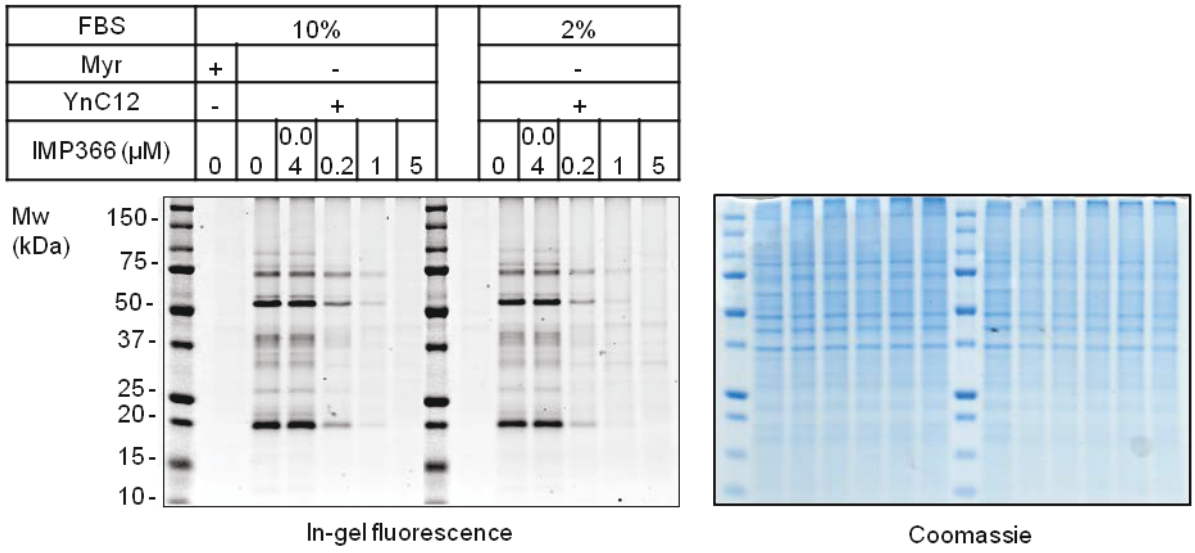

Figure 44. Effect of the serum concentration in the culture media on the uptake of IMP366 into HeLa cells. An YnC12-tagging experiment with cells treated with IMP366 in HeLa was carried out for 6 h. Cells were pre-treated for 1 h with the inhibitor. The culture media contained either 10% of Fetal Bovine Serum (FBS) or 2% of FBS.

HeLa cells are normally grown in a culture media containing 10% of fetal bovine serum (FBS) but this amount can be decrease to 2% for a few hours without impairing the cell viability. A tagging experiment was carried out for 6 h with 10% or 2% or FBS (Figure 44). No difference in fluorescence labelling was observed, suggesting that the translation cannot be increased by changing the concentration of serum in the culture media. The translation of inhibitors is known to be highly dependent on the properties of the compounds, such as lipophilicity or pKa. Thus, it may not be possible to improve translation without changing the structure of the inhibitor IMP366.

3.3.3.6 Stability of IMP366

The stability of IMP366 in aqueous solution and at 37°C was assessed using an MTS assay. Dilutions of the inhibitors were prepared in the culture media, and half of each solution was incubated for 3 days at 37°C. MTS assays were carried out in HeLa cells using these dilutions (pre-incubation and no pre-incubation) (Figure 45). The metabolic activity was highly similar between the two conditions, suggesting that the compounds would be stable for several days in the cell culture media at neutral pH.

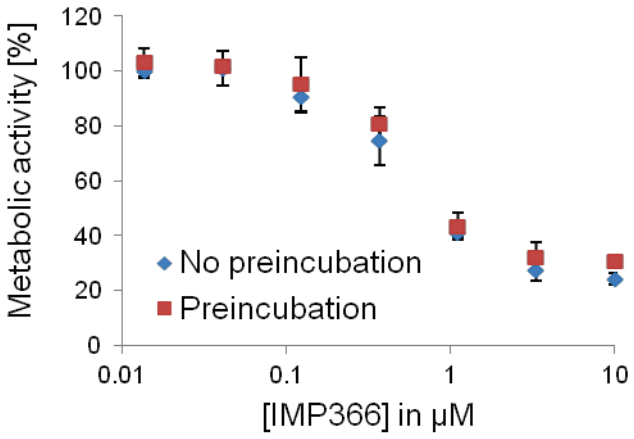

Figure 45. Stability of IMP366 incubated at 37°C in the culture media. Inhibitor dilutions were incubated for 0 day (No preincubation) or 3 days (Preincubation) in the warm culture media (37°C) and added to HeLa cells to carry out a 3-day MTS assay. The figure shows the remaining metabolic activity versus the concentration of inhibitor.

3.4 Screening of in-house NMT inhibitors

The inhibitor described above (IMP366) is a good HsNMT inhibitor. However, alternate scaffolds are needed to improve target validation and provide multiple options for drug development. Several compounds prepared in-house were thus screened.

In this Section, all the compounds assessed i*n vitro* against recombinant HsNMT1 and HsNMT2 or in HeLa cells arose from a medicinal chemistry project carried out at Imperial College London. All the compounds tested were designed, synthesised and kindly donated by Dr. Jennie Hickin, Dr. Tayo Olaleye, Dr. Mark Rackham, Dr. Victor Goncalves, Dr. Zhiyong Yu and Andy Bell. These compounds were designed to inhibit parasite NMTs, including *Pf*NMT, *Pv*NMT, *Lm*NMT (see Section 1.2.3). *In vitro* potency of the inhibitors was usually assessed by the medicinal chemistry group members against recombinant parasite NMTs and HsNMT1. The best compounds were then tested in parasites and in a human liver cancer cell line, HepG2, in order to assess the ability of the compound to kill parasites without toxicity against human host cells. Potent inhibitors of HsNMT1 were assessed as potential inhibitor tools to study NMT inhibition in cancer cells. HsNMT isoforms and parasite NMTs have a relatively high sequence identity (Section 1.2.3) and any good parasite NMT inhibitor could potentially inhibit HsNMT as well.

As discussed in Section 3.1, the IC_{50}s against both HsNMT isoforms, the cell toxicity, and the ability of the compounds to inhibit NMT in cells were all important features which were used to assess the quality of an inhibitor.

IMP366 was used as a reference compound and any future HsNMT inhibitor should have similar or improved properties. HsNMT inhibitor should have relatively **low IC_{50}** (<200 nM) and **low EC_{50}** (<10 µM); if the IC_{50} is too high, high concentrations of inhibitor would be required to treat the cells to inhibit HsNMT and some off-target effects might come into play. Additionally, HsNMT inhibitors should **inhibit NMT in cells** (assessed with YnC12 labelling). For the cell viability assay, a dose-dependent decrease of the response and a plateau of residual metabolic activity at the highest concentrations should be observed when the concentration of inhibitor increases, as seen for IMP366.

Design and synthesis of the inhibitors was not undertaken by the author of this thesis, and for intellectual property (IP) reasons inhibitor structures cannot be presented in this thesis. Compounds from the same series were sometimes tested for comparison, but the structure activity relationship will not be discussed. Inhibitors were separated in three groups. The first group corresponds to weak HsNMT inhibitors, and most unfortunately showed an off-target effect in cells and little on-target effect. The second group describes some weak inhibitors with a small selectivity for HsNMT1 over HsNMT2. The third group corresponds to some potent HsNMT inhibitors showing little off-target effect in cells. These compounds were tested in the last few months of the PhD project. Within each group, compounds are not ordered according to their respective series or structures similarity, but are ordered instead according to the order tested during this work.

3.4.1 Non selective

Many of inhibitors tested were found to have several issues that made them unsuitable as tools. First, some inhibitors had a low affinity for HsNMT1 and HsNMT2 (IMP164/253/256/261/163/266/267, coloured in orange) and were not tested in cells. Secondly, some inhibitors were relatively potent against HsNMT1 and HsNMT2 but the cell cytotoxicity assay showed that the compounds had an off-target effect in cells (compounds IMP162/168, coloured in yellow). The slope factor was high (>4 for both inhibitors) and no plateau of metabolic activity was observed. A typical EC_{50} curve is presented in Figure 46. A YnC12 labelling experiment was carried out for IMP162 (Appendix D). However, even if IMP162 led to a decrease of the fluorescence on the gel, it was not appropriate to measure a TC_{50} value without confirming that these inhibitors do not inhibit protein synthesis or are not toxic to the cells after a few hours treatment.

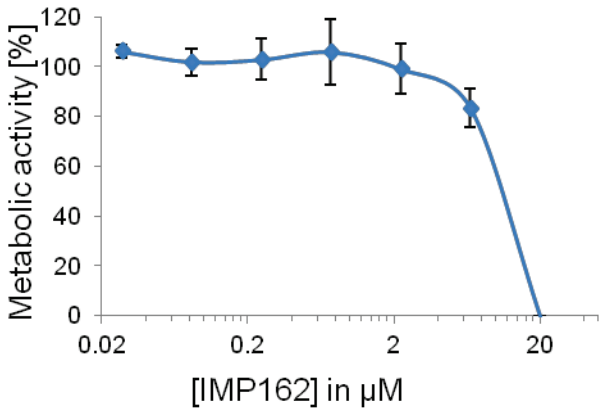

Figure 46. Typical EC_{50} plot obtained with off-target inhibitors. The curve was obtained by measuring the metabolic activity of HeLa cells treated for 3 days with a concentration range of IMP162 (n= 3 biological replicates).

The inhibitors shaded in green in Table 11 were more promising. The slope factor of the EC_{50} curve was closer to 1 and they inhibited NMT in cells dose-dependently (Appendix D). However, no plateau of metabolic activity was observed, suggesting that the inhibitors have an off-target effect in addition to NMT inhibition at the highest concentrations of inhibitor tested. Compound IMP329 was more interesting as it did not kill the cells even at 100 µM (Figure 47a and b). The translation was poor (>300) compared to IMP366 (translation~10). The TC_{50} value was determined and found to be 4.9 µM ± 1 (Figure 47c and d). This value, determined with an YnC12 tagging experiment for 6 h, was lower than the EC_{50} value, suggesting that the compound might degrade over time. However, a similar experiment, as performed on compound IMP366 (Figure 45) was carried out to study the compound stability (Figure 48a). The compound appeared to be stable when incubated at 37°C for several days in the culture media. It is unclear why the TC_{50} is much lower than the $EC_{50,}$ but the same feature was observed for IMP366 and analogues (Section 3.3.2). An AHA labelling experiment was carried out to check that the inhibitor did not inhibit protein synthesis (Figure 48b).

Table 11. Evaluation of HsNMT inhibitors. nd = not determined; n/a = not applicable. The IC_{50} was determined. When only an end-point assay was carried out, the residual activity is indicated at the concentration tested. The EC_{50} were determined and several features of the dose-dependent response are indicated. The translation was calculated by dividing the EC_{50} value by the average IC_{50} value. The "YnC12 tagging" column indicates if NMT inhibition in cells was assessed by YnC12 tagging (the gels can be seen in Appendix D or in Figure 47). IMP366 was added to the table for reference.

	IC_{50} (nM)							
IMP	NMT1	NMT2	Selectivity NMT2/ NMT1	EC_{50} (μM)	Slope factor EC_{50}	Residual % viability	Translation	YnC12 tagging
366	**17 ± 1**	**22 ± 3**	**1.3**	**221 ± 15**	**1.2**	**Plateau (19% at 10 μM)**	**n/a**	**TC_{50} = 169 ±31 μM**
164	>10	>10	n/a	nd	n/a	n/a	n/a	nd
253	73% at 5 μM	78% at 5 μM	n/a	nd	n/a	n/a	n/a	nd
256	49% at 5 μM	53% at 5 μM	n/a	nd	n/a	n/a	n/a	nd
261	87% at 5 μM	86% at 5 μM	n/a	nd	n/a	n/a	n/a	nd
263	86% at 5 μM	64% at 5 μM	n/a	nd	n/a	n/a	n/a	nd
266	76% at 5 μM	80% at 5 μM	n/a	nd	n/a	n/a	n/a	nd
267	40% at 5 μM	46% at 5 μM	n/a	nd	n/a	n/a	n/a	nd
162	68 ± 5	131 ± 20	1.9	8 ± 1.4	7.8	0% at 20 μM	53	Yes
168	57 ± 20	91 ± 80	1.6	13 ± 2	4.7	4% at 100 μM	178	nd
320	111 ± 8	162 ±13	1.5	31±13	1.2	0% at 20 μM	228	Yes
918	82 ± 9	153 ±31	1.8	35±6	1.6	0% at 20 μM	299	Yes
329	57 ± 6	86 ± 9	1.5	23.9 ±5	1.2	8.3% at 100 μM	336	Yes
ETIII032	141 ± 16	183 ± 18	1.3	>100	1	41% at 100 μM	n/a	Yes
BK14	31 ± 2	48 ± 3	1.5	22.9 ± 4.5	1	0% at 200 μM	587	nd
BK16	91 ± 13	118 ± 18	1.3	>100	3.4	8% at 200 μM	N/A	nd
BK17	73 ± 4	83 ± 4	1.1	33.5 ± 3.4	1.4	0% at 200 μM	429	nd
BK19	2367 ± 653	6891 ± 7141	2.9	n/a	n/a	n/a	n/a	nd
BK20	196 ± 17	276 ± 34	1.4	n/a	n/a	n/a	n/a	nd

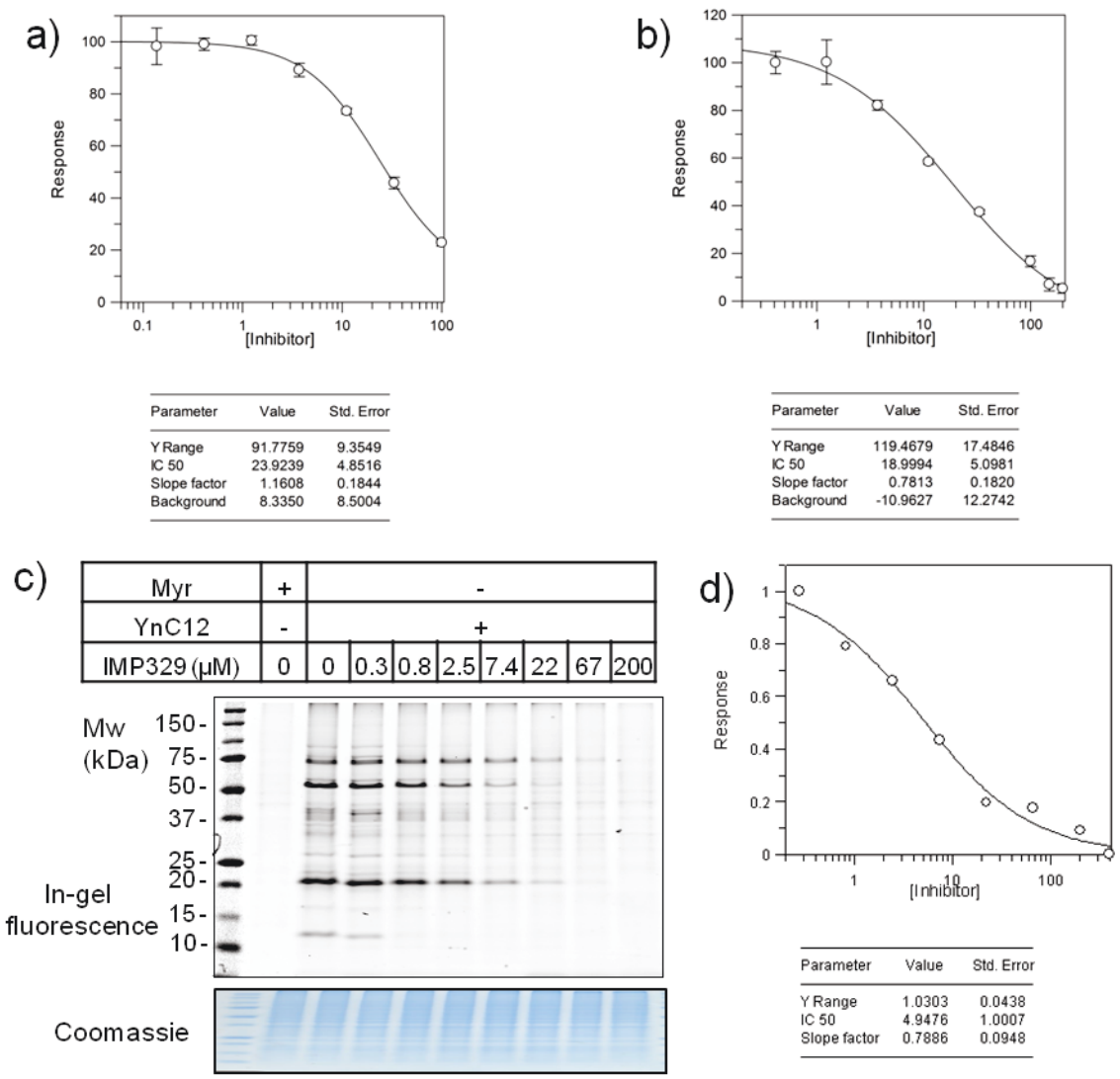

Figure 47. Evaluation of compound IMP329 in HeLa cells. A MTS assay was carried out starting from **a)** 100 µM or **b)** 200 µM (3-fold dilutions, n= 3 biological replicates, 72 h**). c)** YnC12 tagging experiment: 1 h pre-feeding with IMP329, followed by 6 h labelling with YnC12 in the presence of the inhibitor. **d)** TC_{50} plotted in GraFit.

Several analogues of this compound were produced by in collaboration with Boon Lee (BSc student, Tate group, Imperial College London) (Table 11, compounds coloured in grey). Compound BK14 had similar enzyme affinity and cell toxicity than IMP329. All the other compounds tested had a lower enzyme affinity. Compound IMP329 was thus found to be the best HsNMT inhibitor tested.

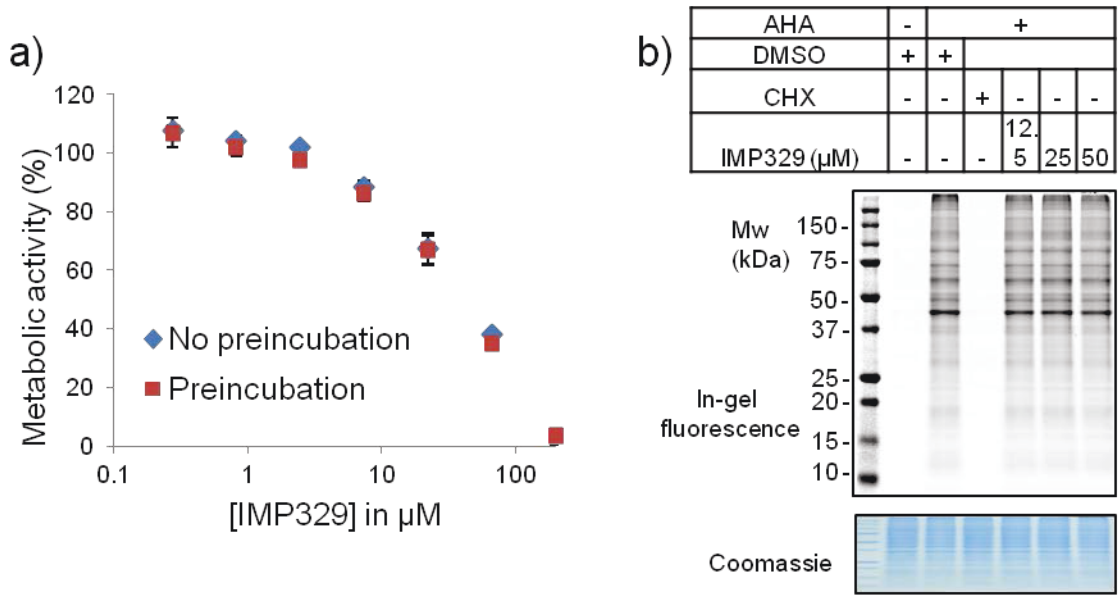

Figure 48. Further evaluation of IMP329 as an HsNMT inhibitor. a) Stability of IMP329 incubated at 37°C in the culture media. Inhibitor dilutions were incubated for 0 day (No preincubation) or 3 days (preincubation) in the warm culture media (37°C) and added to HeLa cells to carry out a 3-day MTS assay. The figure shows the remaining metabolic activity versus the concentration of inhibitor. **b)** AHA labelling experiment carried out for 24 h to check that the compound was not inhibiting protein synthesis.

3.4.2 Selective compound

As in Section 3.4.1, several inhibitors discovered during the medicinal chemistry project were tested. Compounds presented in Table 12 had > 2 fold selectivity for HsNMT1 over HsNMT2. The best compound could be used as a tool to study HsNMT1/HsNMT2 substrate selectivity in cells.

Most of the compounds tested had a moderate affinity for the enzyme, and seem to have a substantial off-target effect in cells as observed with the high slope factors (>2) of the EC_{50} curves. One of the first compound tested, IMP475 (Table 12), was further examined. This inhibitor had been prepared by Dr. Tayo Olaleye (Tate group, Imperial College London), and has a relatively high affinity for the enzyme. However, when tested in cells, this compound did not inhibit NMT and was not toxic to the cells up to 100 µM. The compound is a peptidomimetic inhibitor and has two primary amines (Scheme 10). These amines would be charged in aqueous solution, and the hydrophilic compound is unlikely to penetrate the lipid cell membrane.

Table 12. Enzyme affinity, cell cytotoxicity, tagging EC_{50s} of several HsNMT1 selective inhibitors. Compounds difficult to dissolve at a concentration higher than 20 µM are indicated by #. They might have precipitated during the MTS assay and could result in a relatively low IC_{50}. nd = not determined; N/A = not applicable. The IC_{50} and EC_{50} values were determined. Several features of the EC_{50} dose-dependent response are indicated. The translation was calculated by dividing the EC_{50} value by the average IC_{50} value. The "YnC12 tagging" column indicates if NMT inhibition in cells was assessed by YnC12 tagging (the gels can be seen in Appendix D). IMP366 was added to the table for reference.

	IC_{50} (µM)							
IMP	NMT1	NMT2	Selectivity NMT2/NMT1	EC_{50} (µM)	Slope factor EC_{50}	Residual % viability	Translation	YnC12 tagging
366	**17 ± 1**	**22 ± 3**	**1.3**	**221 ± 15**	**1.2**	**Plateau (19% at 10 µM)**	**n/a**	**TC_{50} = 169 ±31 µM**
475	52 ±5	149 ±24	2.9	>100	n/a	n/a	n/a	Yes
135	116 ±9	371 ± 35	3.2	nd	n/a	n/a	n/a	nd
476	701 ± 0.07	1815 ± 0.07	2.6	nd	n/a	n/a	n/a	nd
485	1517 ±28	4351 ± 410	2.9	nd	n/a	n/a	n/a	nd
489	697 ± 72	1604 ± 61	2.3	nd	n/a	n/a	n/a	nd
514	604 ± 47	1480 ± 76	2.5	nd	n/a	n/a	n/a	nd
166	496 ± 71	1930± 290	3.9	25 ± 1	4.4	0	21	nd
621	87 ± 9	430 ± 69	4.9	61 ± 3	2.6	21 at 50 µM	238	Yes
058 #	393 ± 67	1764 ± 622	4.5	19 ± 0.8	2.1	0	18	nd
624	103 ±8	411 ± 68	4	75 ±114	2.9	17	286	Yes
625	125 ± 12	692 ± 83	5.5	49 ± 25	3	3	120	Yes
626	74 ± 7	365 ± 56	4.9	42 ± 11	5.2	0	103	Yes
623	25 ± 2	100 ± 7	4	56 ± 34	4.6	2	900	Yes

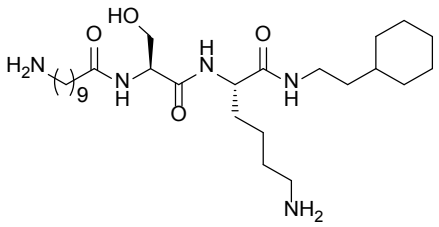

Scheme 10. Structure of IMP475.

It was envisioned that we could temporarily mask these charged amines by preparing a prodrug of this inhibitor.[225] A prodrug is an analogue of a drug molecule that is enzymatically and/or chemically transformed in cells to release the active drug. Several strategies have been developed and are reviewed here.[225] A prodrug based on a isobutanoyloxyethoxy carbamate protecting group appeared to be advantageous, since this group is cleaved in cells by esterases (Scheme 11). The reagent for the prodrug is prepared in two steps (Scheme 12), and this strategy has been successfully used to prepare a prodrug of gabapentin (Prodrug name Gabapentin enacarbil or XP13512), a drug used to treat restless leg syndrome and neuropathic pain).[225]

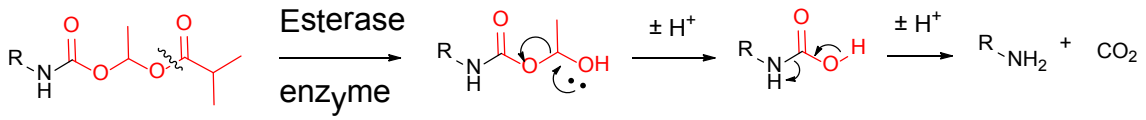

Scheme 11. Mechanism of prodrug cleavage in cells by esterase enzymes.

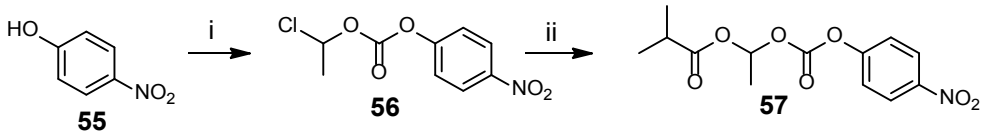

Scheme 12. Synthesis of the prodrug reagent. i) Bu_3N, 1-chloroethylchloroformate, Toluene. ii) isobutyric acid, KI, ZnO, Toluene. [226]

The prodrug of IMP475 was prepared in four steps using standard solid phase peptide synthesis (Scheme 13).[227] The prodrug reagent **57** was then coupled in one step to both primary amines of IMP475. Compound **62** was obtained in low yields.

The prodrug **62** was then tested in HeLa cells. Unfortunately, compound **62** appeared to be toxic to HeLa cells. After 7 h treatment with 10 µM, cells started to have an abnormal shape and detached from the plate (Figure 49a). The toxicity at this concentration was confirmed by the MTS assay carried out for 3 days (Figure 49b). No plateau of residual activity could be observed and the slope factor was much higher than 1. The YnC12 tagging experiment showed a decrease in labelling when cells where treated with 5 and 10 µM of the prodrug **62** (Figure 49c). However, this decrease could be attributed to cell death and not NMT inhibition (Figure 49a).

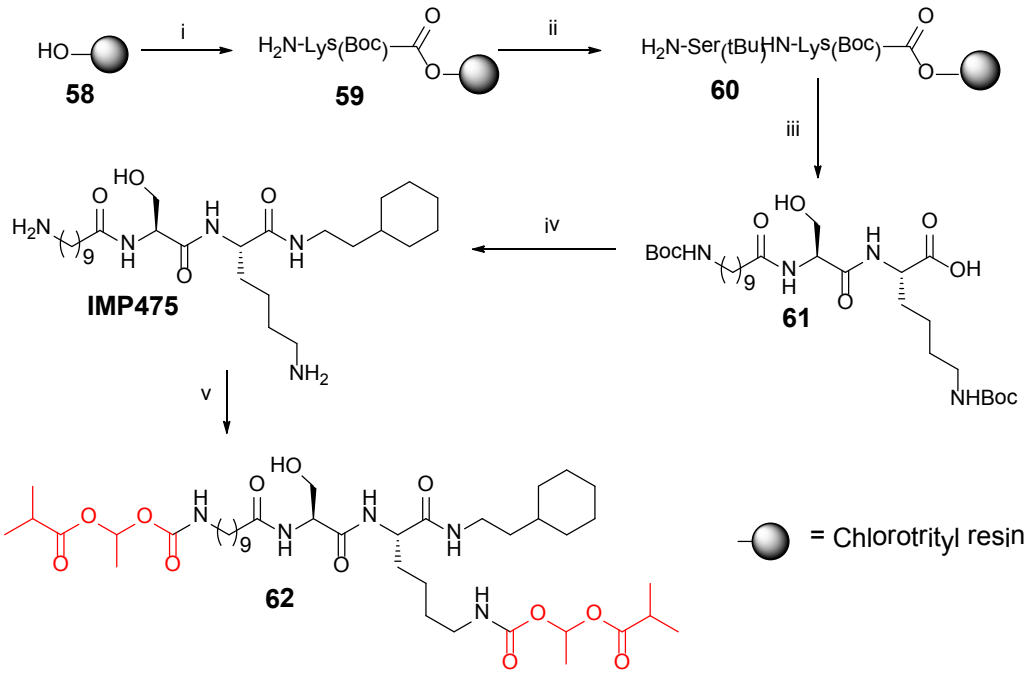

Scheme 13. Synthesis of 61. i) a) Fmoc-Lys(Boc)-OH, DIPEA, DCM; b) Fmoc deprotection. ii) a) Fmoc-Ser(*t*Bu)-OH, DIPEA, HBTU; DMF b) Fmoc deprotection. iii) a) 9-(*tert*-butoxycarbonyl)aminodecanoic acid, DIPEA, HATU; DMF; b) 0.5% TFA, DCM. iv) a) 2-cyclohexylethanaminium acetate, HATU, DIPEA, DMF; b) 95% TFA, 2.5% TIS, 2.5% H_2O; v) **57**, Tributylamine, dry THF. The synthesis route was adapted from Oaleye.[227].

All these findings showed that the prodrug **62** appeared to be cell permeable, in contrast to IMP475. However, there is no strong evidence that the compound is inhibiting NMT in cells. The results in Figure 49 suggest that this compound has off-target effects, leading to rapid cell death at approximately 10 µM.

It is also possible that the by-product of prodrug cleavage might be toxic in cells. However, this would be unexpected as this prodrug functionality is currently used for an FDA-approved drug (Gabapentin enacarbil).[225]

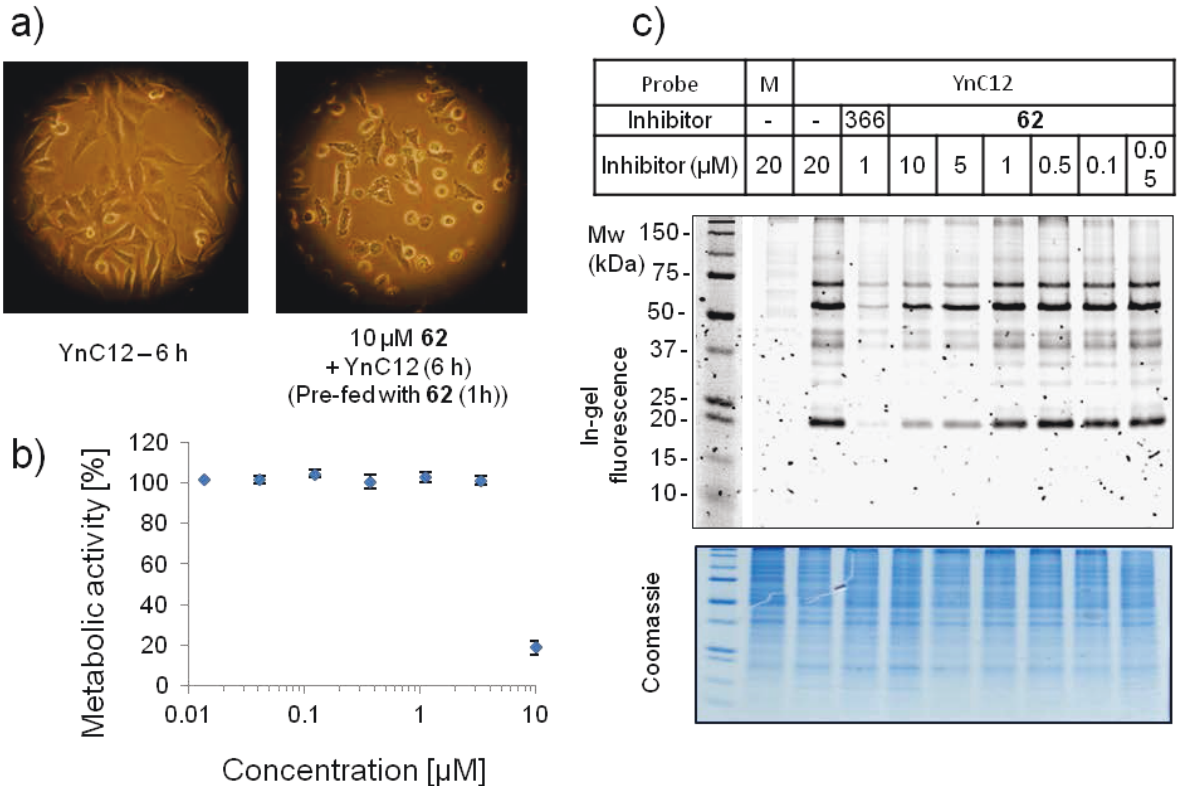

Figure 49. 62 inhibition in HeLa cells. M = Myr. **a)** Pictures of HeLa treated with YnC12 and cells treated with inhibitor **62**. **b)** MTS assay after 72 h in HeLa treated with **62**. **c)** YnC12 tagging experiment with cells treated with IMP366 or **62**.

3.4.3 Promising inhibitors with no off-target effect

In the last few months of this PhD project, four novel inhibitors were tested and were found to be promising (Table 13). The CPM and MTS assay results as well as the YnC12 tagging results are displayed in Appendix E. Compound IMP122/180/898 had a low affinity for the enzyme, relatively low EC_{50}, and all showed a plateau of residual metabolic activity between 20-40%. The TC_{50} values were evaluated and were lower than the EC_{50} values, as observed before for other on-target inhibitors.

Table 13. Enzyme affinity, cell cytotoxicity, TC_{50}s for inhibitors IMP122, IMP180, IMP898 and IMP917. IMP366 was added for reference.

	IC_{50} (μM)							
IMP	NMT1	NMT2	EC_{50} (μM)	Slope factor EC_{50}	Plateau-Residual activity (%)	Translation	TC_{50} (μM)	Comments
366	**17 ± 1**	**22 ± 3**	**221 ± 15**	**1.2**	**19% at 10 μM**	**11**	**TC_{50} = 169 ±31 μM**	
122	0.034 ±0.003	0.040 ±0.002	3.3 ± 0.6	1.3	27% at 33 μM	89	1.01	No remaining activity at 100 μM
180	0.038 ±0.009	0.098 ±0.011	5.8 ± 0.3	1.5	35% at 100 μM	85	1.97	
898	0.030 ±0.006	0.064 ±0.007	9.8 ± 1.7	1.2	21% at 100 μM	209	1.44	
917	0.017± 0.001	0.016 ±0.001	0.78 ±0.03	2.1	34% at 11 μM	47	0.62	No remaining activity at 100 μM

Interestingly, IMP917 had a binding affinity to both HsNMT isoforms comparable to the best inhibitor tested so far, IMP366, in the low nM range. While the translation (47) is not as good as for IMP366 (~10), this compound has the best translation of all the in-house inhibitors tested, leading to an EC_{50} value lower than 1 μM). The TC_{50} value was is good correlation with the EC_{50}. There was a plateau of residual activity, demonstrating that the compound did not have any off-target effect up to 10 μM. However, the slope factor of the EC_{50} curve is slightly high and further investigations would be required to understand why the slope factor is greater than 1.

It would be interesting to further validate this compound as a tool to study NMT inhibition in cancer cells. This compound could also be used as a starting point to prepare more potent HsNMT inhibitors.

3.5 Conclusions

This chapter described the search for an HsNMT1/2 inhibitor which could be used as a tool to study NMT inhibition in cancer cells. Two previously reported HsNMT inhibitors were evaluated and found to be poor HsNMT inhibitors. HMA was poorly soluble while Tris DBA was shown to be a non-competitive inhibitor of NMT. In cell experiments demonstrated Tris DBA was toxic to cells but the toxicity was most likely not related to inhibition of HsNMT.

A recently reported TbNMT inhibitor, referred to here as IMP366, was characterised. It was shown to be a potent inhibitor of both HsNMT isoforms. For the first time, specific NMT inhibition in cells was shown to lead to cell toxicity. Enzyme inhibition in cells was evaluated using a YnC12 tagging experiment and cytotoxicity was measured using the MTS assay after 3 days. Interestingly, cells were not all dead when treated at a concentration sufficient to inhibit >90% NMT in cells. Instead, a plateau of residual metabolic activity at 20-30% was observed. There could be several reasons for this phenomenon. First, the cells could stop dividing after a few hours or days. The second possible explanation is that only a population of the cells could be killed in the presence of the NMT inhibitor. These hypotheses will be addressed in Chapter 5.

Interestingly, there was a good correlation between IC_{50s}, EC_{50s} and NMT inhibition from analogues of IMP366. This observation confirms that these compounds have no or little side-effect in cells. The translation of these compounds into HeLa cells was average (~10). However, it is important to note that when an excessive concentration of inhibitor IMP366 was used in cells (100 μM), the compound was toxic and cells were all dead after 3 days. This was attributed to off-target (non-mechanism based) effects.

This compound allowed us to define the criteria for a good HsNMT inhibitor:

- ✓ High enzyme affinity (< 200 nM).
- ✓ Good translation giving a relatively low EC_{50} (< 20 μM). The slope of the EC_{50} curve should be close to 1 and if the compound does not have any off-target effect a plateau of residual metabolic activity should be observed, as shown in Figure 38.
- ✓ Dose-dependent inhibition of NMT in cells. The TC_{50} value, the concentration of inhibitor required to inhibit half the myristoylation in cells, should correlate with the EC_{50} value. This underlines the importance of probes to validate a novel drug target or inhibitor. Without the YnC12 probe, it would be difficult to rapidly evaluate the on-target effect of an inhibitor. This

could only then be done by looking at the down-regulation of pathways where NMT targets are involved, which is also difficult given the many pathways affected.

- ✓ Good correlation between IC_{50}, EC_{50} and NMT inhibition from inhibitors in the same series. Poor inhibitors of HsNMT *in vitro* should not be toxic to the cells if they do not inhibit NMT in cells.

A next logical step would be to carry out studies in mouse models of cancer, to determine whether these compounds could inhibit tumour growth *in vivo*. However, the focus in this thesis is on fully characterising the effect of NMT inhibition in cells, and this will be discussed further in Chapter 5.

Several compounds issued from an in-house medicinal chemistry project were tested. The majority of the compounds showed significant off-target effects in cells. These off-target effects were mostly observed using the MTS cytotoxicity assay. The slope factors of the EC_{50} curves were generally very high and there was not a plateau of metabolic activity as expected for an inhibitor acting on-target. YnC12 experiments were carried out for key compounds. In some cases labelling was decreased, indicating that NMT was inhibited. However, in most cases, the loss of labelling did not correlate with cell toxicity and the TC_{50} values could not be measured accurately for these compounds. The loss of labelling might be caused by significant cell death at the highest concentration of these inhibitors. Inhibitor IMP329 emerged as one of the most promising inhibitor tested. The slope factor of the EC_{50} was close to 1 and there was a good correlation between the TC_{50} value and the EC_{50}. Unfortunately, no plateau of metabolic activity was observed, potentially because off-target effects cause a phenotype before NMT is completely inhibited. This compound is currently used in the Tate group as an additional NMT inhibitor to study the phenotype of NMT inhibition in cells.

In the last few months of this PhD, four inhibitors were tested and found to be good HsNMT inhibitors with no or little off-target effects. They had all the key characteristics of a good HsNMT inhibitor as describe above. The only issue is the translation which is still relatively high, however these compounds could be further optimised to improve their translation.

Selectivity of the inhibitors for HsNMT1 or HsNMT2 was also considered as an interesting feature. One inhibitor was investigated but unfortunately showed an important off-target effect and could not be used as a tool to study HsNMT1/HsNMT2 selectivity in cells. Several inhibitors were tested towards the end of this PhD work, such as IMP621, and could be promising. Some of these inhibitors are currently under further investigation within the Tate group.

Chapter 4 Detection of co-translational NMT substrates by mass spectrometry-based proteomics

Target validation is a fundamental step in the target-based drug discovery pipeline. Failure to identify effective targets has been suggested to be the main cause for failure in drug discovery campaigns.[1] The functional role of the molecular target must be clearly defined in the disease of interest, and to evaluate the potential of NMT as an anti-cancer drug target, chemical proteomic profiling of *N*-myristoylation is an important fundamental component.

Previous work in the Tate group showed that myristate analogue YnC12 can be used in combination with the trifunctional capture reagent AzTB to detect known and putative NMT substrates in HeLa cells (Section 2.3).[163] However, the number of known and putative substrates identified was low (<20) and some known substrates, such as the proto-oncogene tyrosine kinase c-SRC, were not detected. These results suggested that more NMT substrates could be identified by optimising the proteomics experiments.

Several proteomics methods were employed in the current study to discover the myristoylated proteome in HeLa cells. Results were correlated with prediction of protein *N*-myristoylation obtained using two bioinformatic tools, MYR predictor [78] and Myristoylator.[82]

First, non quantitative proteomics experiments and label-free quantification experiments (Section 1.11) were carried out. However, these experiments had significant limitations in the confident identification of *N*-myristoylated proteins.

Secondly, double SILAC and spike-in SILAC (Section1.11) quantitative proteomics experiments were employed in combination with the highly specific HsNMT inhibitor (IMP366) characterised in Chapter 3.

The current Chapter also comments on the reliability of the YnC12 probe as a tool to identify NMT substrates in cells by chemical proteomics. YnC12 was shown to label NMT substrates (Section 2.3) but also labels other proteins such as palmitoylated proteins, in agreement with previous reports (Section 1.10.3).[173]

4.1 Previously reported NMT substrates and predictions of *N*-myristoylation

4.1.1 Previously reported co-translationally *N*-myristoylated proteins

As discussed in Section 1.5.1, many proteins have been reported to be *N*-myristoylated based on experiment evidence in the literature (see below). A non-exhaustive list of previously reported NMT substrates can be found in Appendix F. This list reports only NMT substrates expressed in HeLa cells, using the analysis of the HeLa cell proteome and transcriptome reported by Nagaraj *et al.* as a reference.[207]

Various methods are typically employed to show that proteins are *N*-myristoylated in eukaryotes, as introduced in Section 1.10.1. They are here classified in three main categories.

- ✓ **Native.** The method is referred to as "native" where an endogenous protein was shown to be *N*-myristoylated. Only six NMT substrates have been identified at a native level, typically by combining radiolabelling with [^{3}H]myristate and immunoprecipitation (Annexin XIII,[228] MARCKS,[105] c-SRC [204]). Alternatively, the protein of interest has been purified from eukaryotic cells or tissue, digested and analysed by mass spectrometry (BASP1,[161] Golgi-associated plant pathogenesis-related protein 1 (GLIPR2),[229] and cAMP dependent protein kinase alpha subunit (PRKACA) [209]).
- ✓ **Non native.** The method is referred to as "non native" where the protein of interest was overexpressed in eukaryotic cells and *N*-myristoylated using endogenous NMT. In most cases, proteins were overexpressed, labelled with [^{3}H]myristate and immunoprecipitated. 41 proteins have been previously identified as NMT substrates at a non native protein level.
- ✓ **Cell free.** The method is referred to as "cell free" where the protein of interest and NMT were expressed in a cell free system (for example AIFM2 [230] and protein Lunapark [230]) or in E. coli (for example Tescalin/CHP3) [231]. 21 proteins have been identified as NMT substrates using a cell free method.

It is important to note that the level of confidence is different for these three categories. Proteins identified as NMT substrate at a native level can be considered as high confidence substrates (and will be referred to as "known"), whilst proteins falling into the non native and cell free categories can be considered as medium and low confidence substrates respectively. Sometimes a protein has been shown to be *N*-myristoylated using several different methods. In these cases, only the method with the highest confidence is considered (native > non native > cell free). 68 proteins were experimentally shown to be *N*-myristoylated using the three methods described above and will be referred to as "previously reported" or "experimentally shown" in this Chapter.

The table shown in Appendix F also indicates whether the proteins were identified by non-quantitative chemical proteomics experiments in Jurkat T-cells in two recent studies.[173,224] These studies both used a metabolic tagging approach to label putative NMT substrates, but Wilson *et al.* used YnC12[173] while Liu *et al.* used AzC12.[224] Following capture and enrichment, tagged proteins were identified by mass spectrometry-based proteomics. Only proteins with an N-terminal MG motif, as required for NMT substrates (Section 1.4.2), will be discussed for these two studies. Wilson *et al.* [173] identified 23 putative NMT substrates, 21 of which were also expressed in HeLa cells. The two proteins not expressed in HeLa cells are HMGB1P1 and LCK. LCK has been shown to be *N*-myristoylated at a non native protein level.[232] Liu *et al.* reported 13 putative NMT substrates. The list appears to be small but unfortunately the authors only reported proteins which had been annotated as *N*-myristoylated (known, "probable" or "by similarity") in the Uniprot/KB database. 10 proteins were found in both studies and in total 27 proteins bearing an N-terminal MG motif were labelled and enriched with myristic acid analogues in Jurkat T-cells. 16 of these 27 proteins have not been validated by any other experiments. These 16 proteins were considered as putative NMT substrates as there is no strong evidence that they are *N*-myristoylated. They have been added to Appendix F for comparison.

As analogues of myristic acid are suspected also to label palmitoylated proteins, palmitoylation of proteins identified by chemical proteomics in the current study was also evaluated. The complete set of palmitoylated proteins in eukaryotes has yet to be identified. In the present study, proteins were considered to be palmitoylated when they were annotated in the UniProtKB/Swiss-Prot database or experimentally shown to be palmitoylated by mass spectrometry-based chemical proteomics.[173] However, when a protein is palmitoylated, it does not imply that the protein is not *N*-myristoylated. Indeed, some NMT substrates, such as the tyrosine protein kinase FYN or GNAI1, are known to be dually-lipidated, carrying N-terminal *N*-myristoylation and *S*-palmitoyl cysteine.

4.1.2 Prediction of *N*-myristoylation

Two bioinformatic tools were used to predict protein *N*-myristoylation, MYR predictor (MP) [78] and Myristoylator (Myrist).[82] However, these tools may not be completely reliable and may generate false positives or false negatives. These bioinformatics tools (which are based on neural network approaches) were trained on proteins annotated as *N*-myristoylated in public databases, and thus are based largely on non-native determinations of protein myristoylation, and on substrate proteins in non-mammalian systems (e.g. yeast). Furthermore, there are very few potential substrate proteins carrying an N-terminal MG motif experimentally proven to be non-myristoylated (out of the

ca. 3000 proteins with a MG motif in the human genome), presenting a very small negative control learning set for bioinformatic analysis.

The N-terminal sequences of proteins listed in Appendix F (excluding proteins only identified by chemical proteomics) were analysed by these predictors (Figure 50). As suspected, some previously reported NMT substrates were not correctly annotated by the predictors. 22% and 9% of these proteins are not correctly predicted as NMT substrates by the MYR predictor and Myristoylator respectively and the predictors disagree on more than 35% of predictions. These results demonstrate that precautions need to be taken when using these predictors as they may not always be accurate.

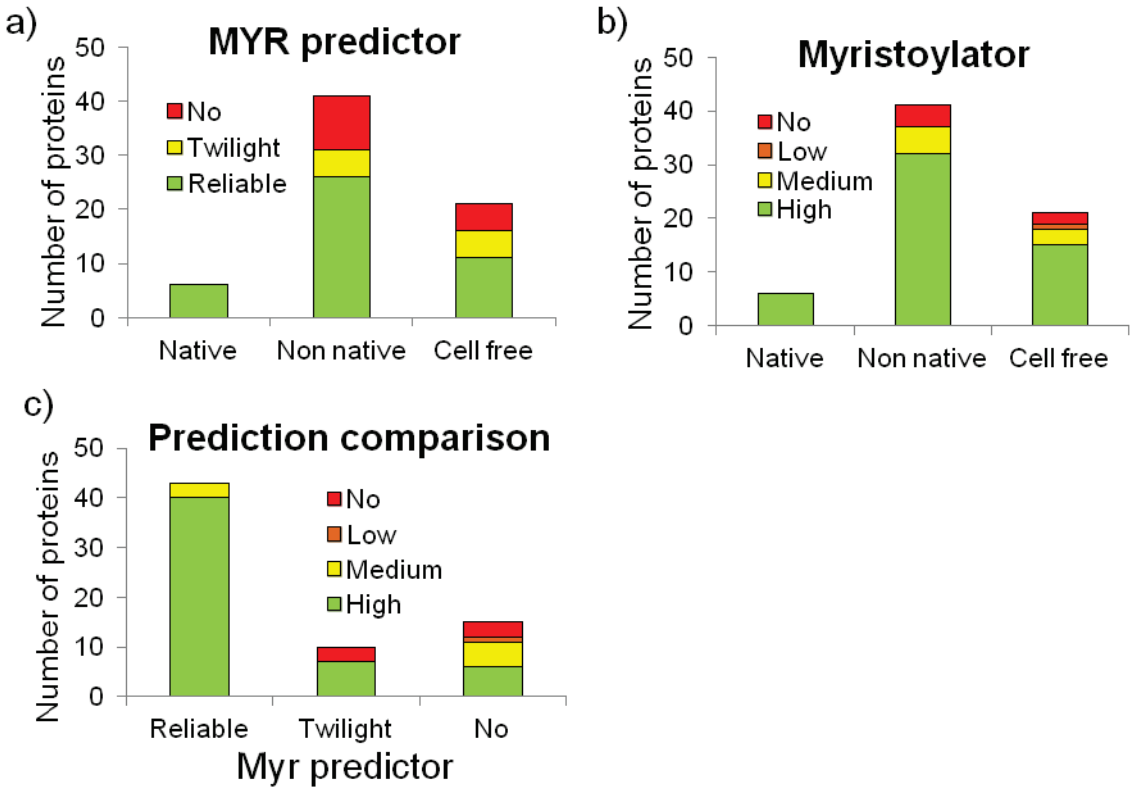

Figure 50. *N*-myristoylation prediction for the 68 proteins reported to be *N*-myristoylated (Appendix F). Predictions **a)** by Myr predictor (MP) or **b)** by Myristoylator (Myrist) are shown for proteins identified at native or non native levels or in a cell-free system. 15 and 6 proteins could not be correctly predicted as NMT substrates by the MYR predictor and Myristoylator respectively. **c)** The predictions made by Myristoylator were compared to the predictions made by MYR predictor. 40 proteins predicted as reliable by MYR predictor were also predicted with the highest confidence by Myristoylator. 3 proteins were predicted not to be *N*-myristoylated by both predictors. The predictors disagree on more than 25 predictions. Low and medium predictions made by Myristoylator were considered to be equivalent to twilight prediction by MYR predictor.

Another bioinformatic tool was tested to predict protein *N*-myristoylation: the TermiNator.[83,84] This tool can provide a prediction for N-terminal methionine cleavage of a protein and various N-terminal

post-translational modifications including *N*-myristoylation. A prediction was made using the N-terminal sequence of c-SRC and the probability that the N-terminal methionine is retained was found to be 89%. This prediction suggests that the N-terminal methionine of c-SRC is not cleaved and is in contradiction with strong evidence showing that c-SRC is *N*-myristoylated. For other previously reported *N*-myristoylated proteins such as BASP1 and MARCKS, the prediction did not give any results. This prediction tool was therefore not used as a prediction tool in this study.

4.1.3 Post-translational *N*-myristoylation

Only a few proteins have been reported to be post-translationally *N*-myristoylated (Sections 1.5.2 and 2.4). The focus of this Chapter is not on post-translationally myristoylated proteins; however, it proved useful to have a list of these proteins, to determine whether they were enriched in the proteomics experiments described in this Chapter. The list can be found in Appendix G and shows the nine post-translationally modified proteins known in eukaryotes.

4.2 First experiment: YnC12/DMSO

The low number of proteins identified as putative NMT substrates in previous studies (Section 4.1.1) suggests that in-depth coverage is lacking. A similar number of proteins were identified by Dr. Megan Wright in HeLa cells (17 previously reported and putative substrates),[163] while 68 proteins expressed in this cell line have been experimentally shown to be *N*-myristoylated (at a native/non native level or in a cell free system, see Section 4.1.1). Several explanations could explain this low coverage.

- Only a small amount of a given protein might be labelled with myristic acid analogues such as YnC12 and this level might be below the detection limit and therefore not be detected by mass spectrometry-based proteomics. *N*-myristoylation is a co-translational process and a few hours (4,[224] 6 [163] or 8 h [173]) might not be sufficient to label proteins with low turnover in cells. Low abundance proteins might also be poorly labelled and not identified with high confidence by proteomics. To overcome this problem, the labelling time could be increased to 24 h. As shown in Section 2.3.2, changing the YnC12 labelling time from 6 to 24 h dramatically improved the fluorescence labelling and the enrichment of known and putative NMT substrates.

- The scale of experiments might have been too small. This problem is related to the previous problem. Low abundance proteins could be lost during the analysis by LC-MS/MS and increasing the scale of the experiment might improve the coverage.

- Fractionation of the sample might be required to improve protein coverage.

- There might have been some issues associated with the sample preparation, such as on-bead digest with trypsin, or with the LC-MS/MS LC separation, such as the LC gradient or the sensitivity of the mass detector.

These problems needed to be addressed to improve the quality and quantity of substrates identified.

4.2.1 Experimental design

An experiment was carried out to improve the coverage and number of identifications by increasing the labelling time to 24 h and increasing the scale of the experiment compared to previous experiment carried out in the Tate group (<1 mg lysate), starting from 3 mg of lysate for capture/enrichment/digest/LC-MS/MS analysis. HeLa cells were treated with YnC12 (20 µM, as optimised in Section 2.3.2) or with DMSO as a control. Only a single sample was prepared in the first instance, as such a large scale (3 mg of lysate) might not be required. While HeLa cells are easy to culture and milligrams of protein lysate can easily be prepared, reagents used for the sample processing are relatively expensive (capture reagent, trypsin, beads for the enrichment).

While most previous proteomics experiments in the Tate group had been carried out with AzTB, a new reagent, prepared by Dr. Goska Broncel (Tate group) became available during the work described here. This reagent, referred to here as AzKTB **63** (Scheme 14) was similar to AzTB (Figure 17), as it was also composed of an azido capture group, a TAMRA fluorophore and a biotin moiety. However, AzKTB had the additional feature of a trypsin cleavage site, which should allow the modified peptide to be released upon on-bead digest of the proteins with trypsin. Moreover, the modified peptide **64** comprises a charged lysine residue which is critical for MS ionisation.

Preliminary experiments carried out by Dr. Goska Broncel showed that AzKTB performed very similarly to AzTB in experiments carried out with HeLa cell lysates labelled with YnC12. AzKTB gave a similar labelling profile by in-gel fluorescence and could also detect *N*-myristoylated proteins by mass spectrometry-based proteomics (data not shown).

Due to the increased hydrophilicity of AzKTB compared to AzTB, protein precipitation following CuAAC ligation could not be carried out as usual, and the protocol was slightly modified by Dr. Goska Broncel (Section 8.3.4.2). The reagent has a tendency to stick to proteins and several careful washes of the protein pellet with methanol were required to ensure that no capture reagent remained with the protein. Any excess of AzKTB left would impair the pull-down as the reagent could bind to the streptavidin beads and prevent AzKTB-captured proteins from being pulled down.

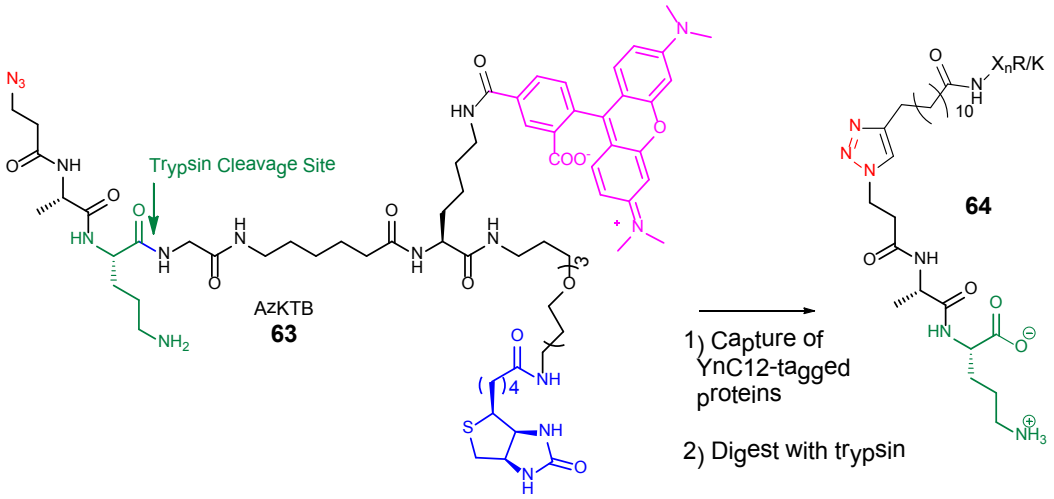

Scheme 14. Structure of AzKTB and of the modified peptide captured with AzKTB and digested with trypsin. X represents any amino acid except R and K.

A small scale capture/enrichment experiment was carried out to assess the new protocol and to test if a higher concentration of proteins could be used for the CuAAC reaction with AzKTB, as this would save some reagent, whose concentration would be kept constant (Figure 51a). A similar labelling profile was obtained by fluorescence when the proteins were captured with AzKTB at a protein lysate concentration of 1 or 2 mg/mL. This result confirms that the capture reagents (AzKTB, $CuSO_4$, TCEP and TBTA) can be used in large excess in the standard protocol and that the capture reaction could be carried out at 2 mg/mL for the large scale proteomics experiment to prevent wasting too much capture reagent.

For the proteomics experiment, Streptavidin-coated magnetic bead were switched for Neutravidin agarose beads as previous experiments carried out in the Tate group had shown that Neutravidin agarose beads were more stable during sample processing for proteomic analysis.[163] The samples were processed using the protocol described in Section 8.3. After enrichment, gel-based analysis was carried out to check that the majority of the labelled proteins had been pulled-down onto the Neutravidin agarose beads (Figure 51b). Very little fluorescence was observed in the supernatant from the pull down, indicating that most labelled proteins were bound to the beads.

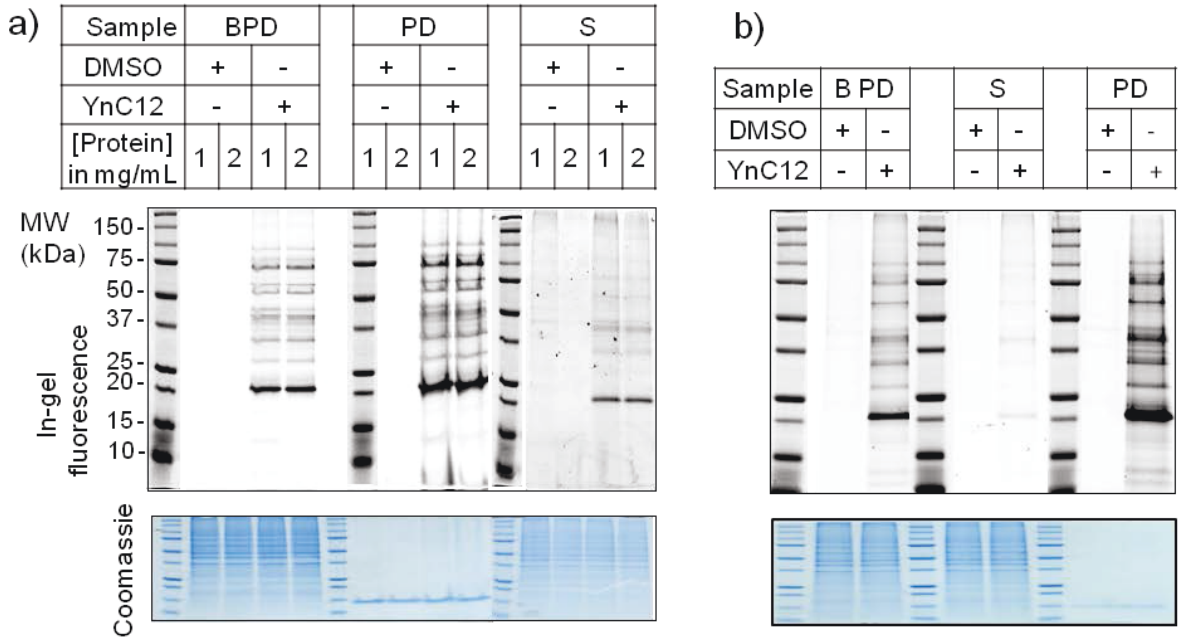

Figure 51. Capture and enrichment of YnC12-tagged proteins with AzKTB. BPB = Before pull down; PD = pull down, S = supernatant. **a)** 100 µg of lysate (HeLa treated with YnC12 for 24 h) were captured with AzKTB at a concentration of 1 or 2 mg/mL. Proteins were pulled-down onto streptavidin-coated magnetic beads. **b)** In-gel fluorescence of the DMSO and YnC12 samples processed for proteomics. The enrichment was carried out using Neutravidin agarose beads. A small amount of sample (ca. 10 µg of protein) was kept at each stage of the processing and analysed by in-gel fluorescence to ensure the pull down was efficient.

The PNACL facility at the University of Leicester provided sample analysis (on-bead digest, LC-MS/MS and database searching).The totality of the sample (enrichment from 3 mg of lysate) was run on a LTQ-Orbitrap Velos mass spectrometer (Thermo Scientific). It is difficult to evaluate the amount of protein digest injected. If 1% of the proteome is *N*-myristoylated but not all the NMT substrates are completely labelled with YnC12, the amount injected is estimated to be below 30 µg. Peptide identifications were assigned by Mascot and protein hits were provided as a Scaffold file (Appendix A). An example of sequence coverage and two assigned spectra (MS/MS) for the protein MARCKS are presented in Appendix H. More than 350 proteins with a confidence higher than 95% were identified in the YnC12 sample. Many of these proteins did not have an N-terminal glycine, as required for *N*-myristoylation. To reduce the number of false-negatives and false-positives, a first selection was made by keeping only proteins identified with the highest probability (>99.9%). Using these settings, 281 proteins were identified in total in the two samples (YnC12 and DMSO), 70 of which were common to both samples (Figure 52a and b). Proteins found in both DMSO and YnC12 samples are probably the result of non-specific binding to the Neutravidin agarose beads. Consistent with this, some of these proteins are abundant proteins such as actin and tubulin. Other proteins are endogenously biotinylated (pyruvate carboxylase, methylcrotonoyl-CoA carboxylase subunit alpha,

acetyl-CoA carboxylase 1) and are therefore likely to be pulled down onto the beads. 8 proteins were only identified in the DMSO control and mostly corresponded to keratin proteins, contaminants introduced by the operator during the sample preparation.

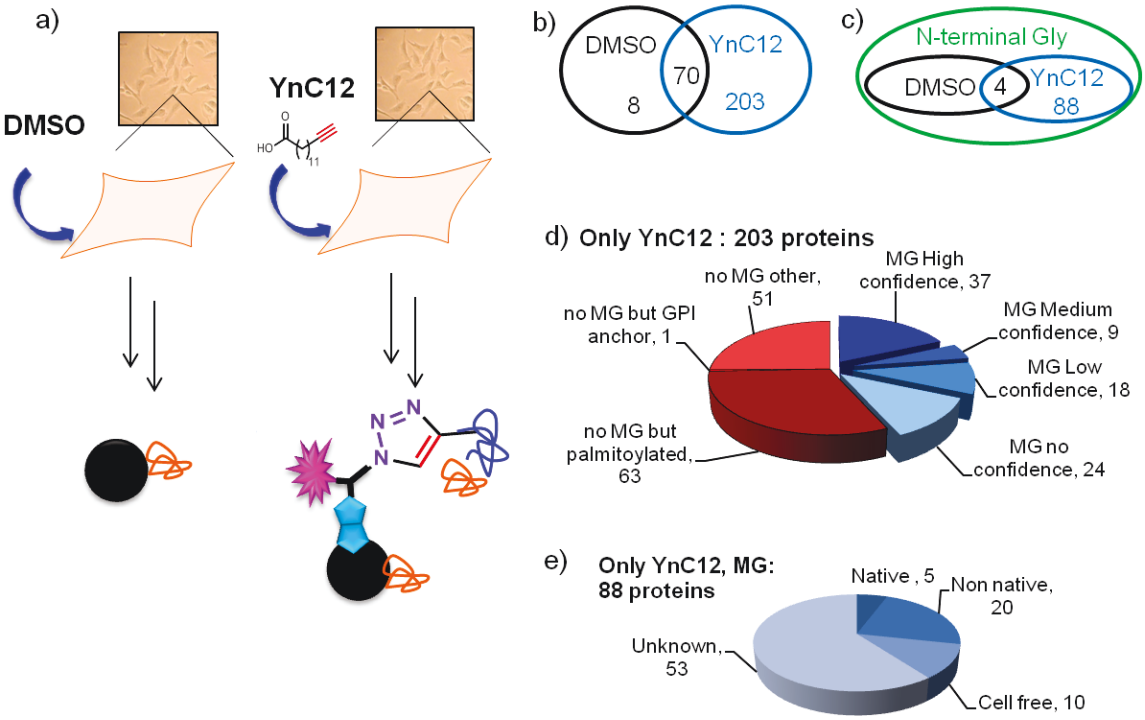

Figure 52. Non quantitative proteomics experiment (only 1 replicate). **a)** Only a few proteins were detected solely in the DMSO-treated sample; these are likely to be proteins that bound non-specifically to the beads. In the YnC12 treated sample, proteins detected correspond to YnC12 labelled proteins as well as proteins non-specifically bound to the beads. **b)** 281 proteins were identified with a protein identification probability higher than 99.9% and 70 proteins were found in both samples. **c)** 92 proteins with an N-terminal MG motif, as required for *N*-myristoylation, were identified and 88 were exclusively found in the YnC12 sample. **d)** 203 enriched proteins were identified only in the YnC12 sample. 88 of these proteins had an N-terminal MG motif. A prediction of *N*-myristoylation was performed by combining the result of the two online bioinformatic tools (Section 8.3.9). Some proteins with no N-terminal MG motif are known to be palmitoylated or incorporate a GPI anchor. **e)** 88 proteins had an N-terminal MG motif and some had been experimentally shown to be *N*-myristoylated. They are classified according to the definitions described in Section 4.1.1.

92 proteins possessed an N-terminal MG motif, which is required for transfer of myristate to a protein by NMT (Figure 52c). 88 proteins were identified exclusively in the YnC12 sample and correspond to putative NMT substrates. The N-terminal sequences of these proteins were analysed with the two predictors described in Section 4.1.2. To simplify the analysis, the results from the two predictors were combined (Section 8.3.9). 64 of these substrates were predicted to be *N*-myristoylated with low, medium or high confidence, while 24 substrates were not predicted to be *N*-myristoylated (Figure 52d). However, as discussed in Section 4.1.2., bioinformatics predictors are

not always reliable, and some of the 24 proteins not predicted might be *N*-myristoylated. Only one third of these 88 putative NMT substrates had been experimentally shown to be *N*-myristoylated (Figure 52e), implying that many NMT substrates remained to be identified. However, with the data provided by this proteomics experiment, it is difficult to identify substrates with high confidence; indeed, many of the proteins only identified in the YnC12 sample did not possess an N-terminal glycine. This suggests that some of the proteins with an N-terminal MG motif might also be the result of non-specific binding to the beads. Some of the proteins with no N-terminal MG motif are *S*-palmitoylated and they could also be labelled with YnC12, by attachment of this analogue in place of palmitate (Sections 1.10.3 and 4.1.1). One solution to decrease the number of hits could be to exclude all the *S*-palmitoylated proteins from the list of identified proteins. However, dual-lipidated proteins such as FYN would be lost. Additionally, some of the proteins with no N-terminal MG motif are glycosylphosphatidylinositol (GPI)-anchored proteins, which incorporate palmitic acid (Section 1.10.3). It is probable that YnC12 also labels GPI-anchored proteins in humans, in the same way that YnC12 can replace palmitate in *S*-palmitoylation. For the following proteomics experiments proteins hits were screened for a predicted or known GPI-anchor.

If YnC12 labels GPI-anchors and *S*-palmitoylated proteins, it would be via an ester or a thioester linkage respectively (Figure 19). As both functions are base-labile, it should be possible to remove YnC12 tagging of palmitoylated and GPI-anchored proteins by carrying out base-treatment after the CuAAC reaction. This possibility is discussed in Section 4.7.1. YnC12 could also be metabolised and incorporated into NMT non-substrate proteins. It is also possible that YnC12 might label a subset of proteins *via* other linkages. Indeed, *N*-myristate has recently been shown to be incorporated at lysine side-chains.[233]

Although the experiment with AzKTB described above had some limitations, it represented a considerable improvement compared to previous experiments carried out in the Tate group with YnC12 treated cells. The number of putative substrates was greatly improved (from 17 to 88), and previously reported NMT substrates (Appendix F), which were not previously detected, such as c-SRC, were identified. The number of unique peptides, spectral counts (referred to in Scaffold as the number of assigned spectra) and percentages of sequence coverage were high (Appendix A and Appendix H). These numbers are important features as they reflect the confidence of the identification. The spectral count is the number of spectra assigned to a given protein and the sequence coverage corresponds to the percentage of all amino acid residues in a protein sequence detected in the sample. A protein with a high number of unique peptides and thus high sequence coverage will be identified with high confidence. The number of spectral counts reflects the

enrichment of a protein in a sample. Three proteins (ARF1, the proteasome subunit 26S protease regulatory subunit 4 (PSMC1) and Niban-like protein-1) were detected in the YnC12 sample with more than 100 spectral counts, suggesting that they were highly enriched. Interestingly, Niban-like protein-1 is not known to be myristoylated; further validation would be required to confirm that it is an NMT substrate. A traditional method to validate novel NMT substrates involves labelling cells with [^{3}H]myristate or YnC12 followed by immunoprecipitation of the protein of interest (Section 1.10.1). However, it would be highly time-consuming, expensive and experimentally challenging to validate 53 putative NMT substrates by this approach (Figure 52).

4.2.2 Modified peptides

In the experiment presented in Section 4.1.1, proteins were captured with AzKTB, a reagent which allows the identification of proteins enriched with YnC12, but should also enable identification of the site of modification. N-terminal peptides of proteins which are *N*-myristoylated with YnC12 and captured with AzKTB will have a stable modification after trypsin digest (Scheme 14). The mass of this adduct was set as a stable modification of glycine and lysine residues for recognition by peptide identification software. The list of modified peptides can be found in Appendix H. An N-terminal modified peptide was identified for 25 proteins, identifying with high confidence these proteins as *N*-myristoylated. The raw data file was re-analysed with the search engine MaxQuant [185] (the previous analysis was carried out with Mascot). 34 modified peptides were identified with MaxQuant and 21 hits were common to both analyses, leading to a total of 38 modified peptides across the two analyses. Some of the proteins corresponding to these modified peptides were not identified in the original experiment; an example is ARF3. Only a few peptides are unique to ARF3 as the protein sequences of ARF1 and ARF3 are highly similar. Peptides shared by ARF1 and ARF3 had been assigned to ARF1 in the previous analysis.

Interestingly, for three proteins enriched in the YnC12 sample, a unique peptide corresponding to the protein N-terminal sequence was detected, but no modification was detected. This suggests that these N-terminal peptides have not been labelled with YnC12 and these proteins are most likely not NMT substrates. These proteins, which might be palmitoylated, are: trafficking protein particle complex 3 (TRAPPC3), surfeit locus protein 4 (SURF4) and choline transporter-like protein 2 (SLC44A2).

17 proteins for which the modified peptide was identified had previously been reported to be *N*-myristoylated. It is important to note that the experiment presented here, with the identification of the site of modification at a native protein level allows the identification of NMT substrates with higher confidence that proteins previously identified at a non native level or in a cell free system

(Section 4.1.1 and Appendix F). This novel AzKTB reagent also allowed the high confidence identification of 22 new NMT substrates (Appendix H). However, even if this reagent is a powerful tool, it will not enable a comprehensive identification of all the NMT substrates in HeLa cells as it has two main limitations:

- ✓ The N-terminal sequence requires at least 5 amino acids before the first arginine or lysine (trypsin cleavage site) to allow the identification with high confidence of the peptide and then the protein (it is difficult for example to identify one protein with a peptide composed of only a one or two amino acids as many proteins will share this peptide). Many known and putative NMT substrates, such as c-SRC (N-terminal sequence: GSNK) do not have 5 amino acids before the first cleavage site.
- ✓ The N-terminal sequence has to be unique to a protein for that protein to be identified with high confidence. This is not always the case as for the protein Guanine nucleotide-binding protein G(i) subunit alpha-1 (GNAI1) and Guanine nucleotide-binding protein G(k) subunit alpha (GNAI3). The N-terminal sequences are the same, even after a potential missed cleavage site (GCTLSAED**K**AAVE**R**).

4.2.3 Conclusions

The experiment described in Sections 4.2.1 and 4.2.2 showed much promise for the identification of the myristoylated proteome in HeLa cells. Labelling the cells for 24 h and the large scale of the experiment allowed the protein coverage to be considerably enhanced. Some of the identified proteins are known/putative NMT substrates and for others the modified peptide was detected. However, more experiments are required to validate the other protein hits. However, some of the 88 putative NMT substrates might be false positives. Therefore a label-free quantification experiment was carried out in order to help distinguish between NMT substrates and non-specifically bound proteins (Section 4.4).

A gel-based proteomic experiment was also carried out to map the NMT substrates onto an SDS-PAGE gel (Section 4.3). Some proteins have an apparent molecular weight on-gel that is different from their molecular weight but it is valuable to know the apparent band size for the purposes of Western blot analysis. This experiment would also assess if fractionation could improve the coverage and thereby allow the scale of the experiment to be decreased.

4.3 Gel-based proteomics

For this experiment, AzTB was used as the capture reagent. YnC12 treated HeLa lysates (500 µg) were captured, enriched on Neutravidin agarose beads, and beads were washed according to the

standard protocol (Section 8.3). Beads were boiled in the sample loading buffer and proteins were loaded on a SDS-PAGE gel. After the run, the gel was imaged by fluorescence and then cut into 7 portions (Figure 53). Precautions were taken to prevent keratin contamination in the samples (pre-cast gel, clean container to run the gel, freshly opened buffer and reagents, clean scalpel to cut the gel slices, etc.).

The PNACL facility at the University of Leicester provided sample analysis (in-gel digest, LC-MS/MS and database searching). Only proteins with an N-terminal MG motif and with a protein identification probability higher than 95.0% were kept and are shown Appendix H. The Scaffold file can be found in Appendix A and a summary is shown in Figure 53.

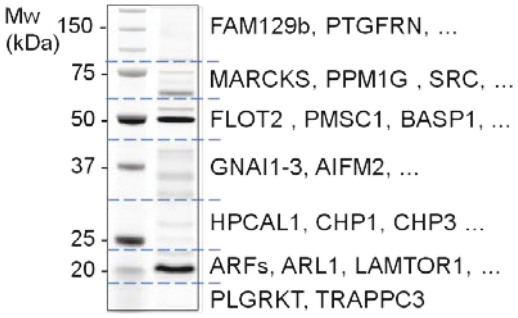

Figure 53. Gel-based proteomics analysis. YnC12-tagged proteins bearing an N-terminal MG motif were identified by gel-based proteomics. This experiment allows the localisation of YnC12-tagged proteins on a SDS-PAGE gel. The proteins were tagged with YnC12 in HeLa, captured, enriched and loaded on a SDS-PAGE gel. The picture shows the in-gel fluorescence image of the gel before it was cut in 7 portions for the gel based analysis. Blue lines show where the gel has been cut. Gene names of a few proteins identified are indicated.

The number of putative NMT substrates (N-terminal MG motif and enriched with YnC12) was lower than for the previous experiment. Most of the high molecular weight proteins (A-kinase anchor proteins, Formin-like protein 1/2, etc.) were missing, possibly due to protein aggregation or poor gel penetration.

As expected some proteins had different apparent and predicted molecular weights. For example MARCKS was found in the gel slice 60-90 kDa while its predicted molecular weight was 32 kDa. This localisation of YnC12-tagged proteins on a SDS-PAGE gel proved useful for Western blot analysis (Section 3.3.3.4).

The number of unique peptides and spectral counts were similar to the numbers found in the previous experiment (Section 4.2). However, approximately six fold less sample was analysed by LC-MS/MS. In the previous experiment, the proteins enriched from 3 mg of lysates were injected in

the LC-MS/MS while in this experiment, the equivalent of 500 µg was analysed. This result suggested, as expected, that fractionation of the sample reduced its complexity and less sample was required to obtain the same coverage.

4.4 Label-free quantification: DMSO/YnC12 (4 replicates)

4.4.1 Experimental design

A label free quantification (LFQ) experiment was carried out to assess if LFQ could be used to distinguish NMT substrates from non-specific background proteins. Due to limited availability of reagent AzKTB, the standard reagent AzTB was used, and four biological replicates were prepared for the YnC12 sample and four biological replicates for the myristic acid control sample. Samples were labelled, captured and enriched as for the first experiment (Section 4.2). However, they were digested in-house with trypsin and the peptide pellets sent to the proteomics facility at the University of Dundee for LC-MS/MS analysis. To ensure reproducibility of the samples (Section 1.11.2), samples were processed in parallel and analysed at the same time.

The data were provided as a raw file and analysed with MaxQuant (see Section 1.11.2). The mass spectral peak intensities, referred to here as LFQ intensities, were obtained for each identified protein. They were used to quantify the relative amount of a protein in the YnC12 or myristic acid samples. The reproducibility between replicates of a given sample was particularly good, as seen on the multiple scatter plots displayed in Figure 54.

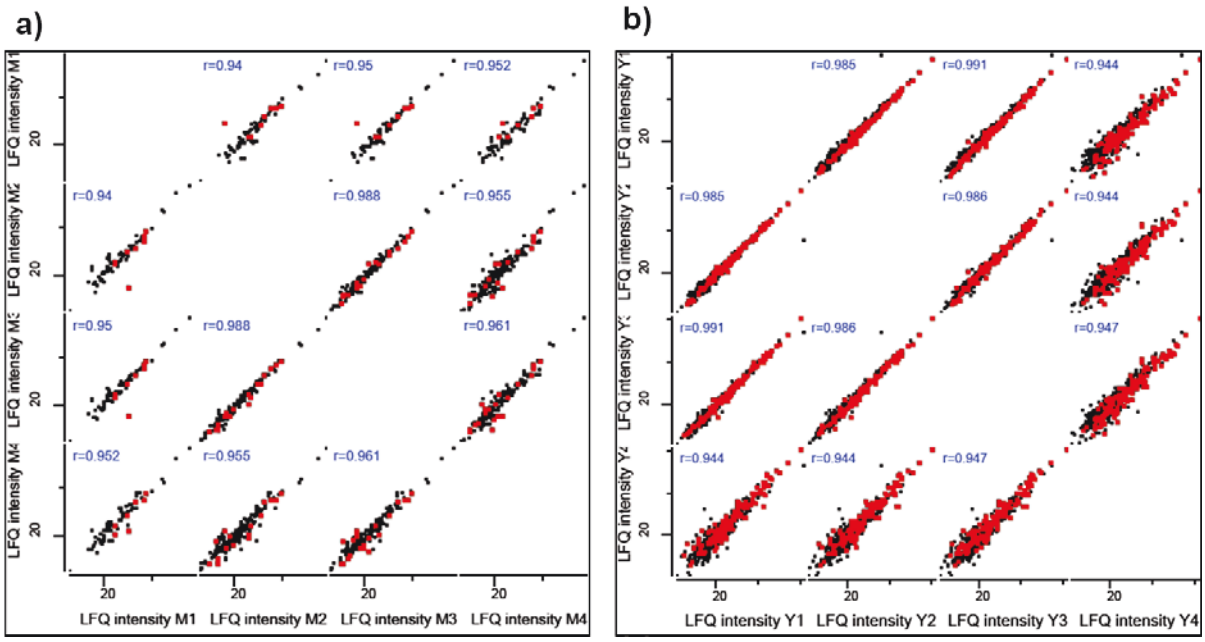

Figure 54. Multiple scatter plots showing the excellent reproducibility between replicates in the label-free quantification experiment. The label-free quantification (LFQ) intensity for one replicate is plotted against the LFQ intensity of another replicate. The logarithm values (Log_2) are indicated. The correlation coefficients are indicated. The four myristic acid biological replicates **(a)** are indicated as M1, M2, M3, M4 and the four YnC12 biological replicates **(b)** as Y1, Y2, Y3, Y4. The correlation is shown before the imputation of the missing values. The proteins with an N-terminal MG motif are highlighted in red.

4.4.2 Results and discussions

The data were further processed with Perseus,[234] and more than 800 proteins were identified in the 8 samples. To keep only the proteins identified with high confidence, the data were filtered to require at least 2 unique peptides and three (out of four) LFQ intensity values, referred to as 'valid values' across the four YnC12 replicates (Figure 55a). Proteins identified in the YnC12 sample were not always detected in the DMSO sample. However, Perseus does not permit missing values when carrying out statistical analyses and when calculating a relative enrichment between two samples. Missing values correspond to proteins not present, or present below the detection limit of LC-MS/MS. Missing values were thus imputed in Perseus with a value close to the detection limit. Log_2 values of LFQ intensities typically follow a normal distribution across a large sample (Figure 55b) and the detection limit corresponds to the left tail of this normal distribution (boxed in red in Figure 55b). Perseus was used to generate a valid value in this interval, close to the detection limit, for the missing values.

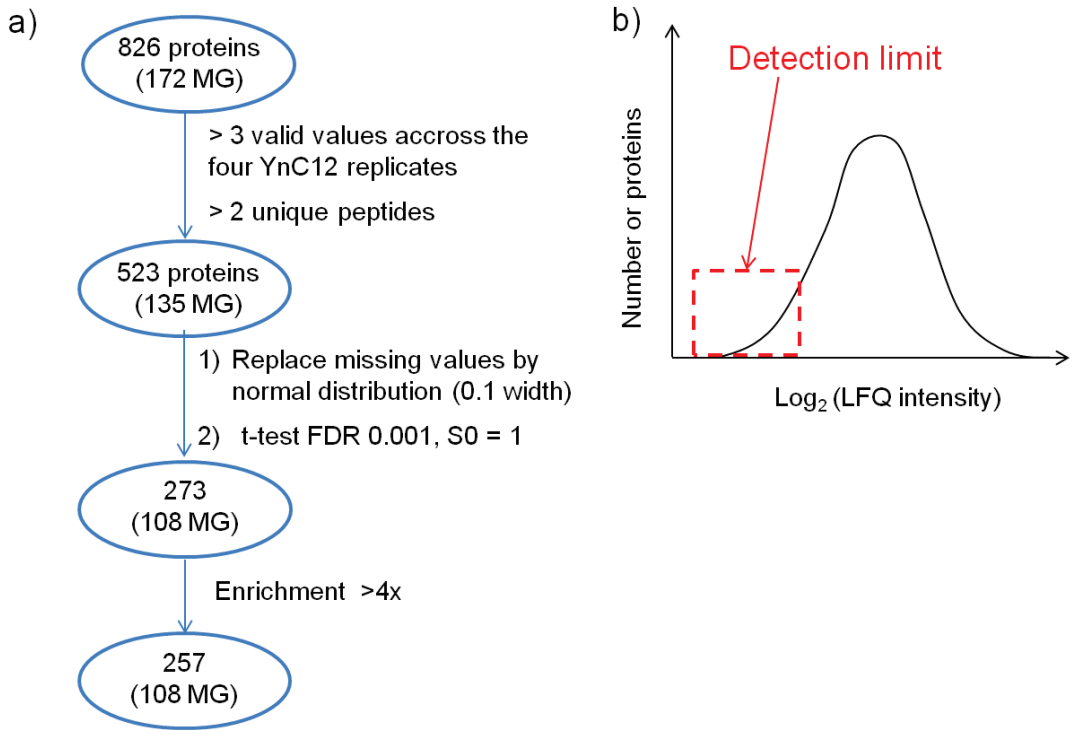

Figure 55. Data processing for the LFQ experiment. a) The scheme summarises how the proteins selectively enriched in the YnC12 sample were selected. **b)** The graph represents the normal distribution followed by the Log_2 (LFQ intensity) values. Proteins not detected in one replicate were given a value close to the detection limit after imputation by Perseus.

Proteins were then subjected to a two-sample test (Figure 56a) and only proteins at least four-fold enriched in the YnC12 samples versus the myristic acid sample were kept (Figure 55a). 257 proteins, including 108 proteins with an N-terminal MG motif, were significantly enriched in the YnC12 samples (Figure 56b, Appendix A and Appendix H). The number of proteins with a N-terminal MG motif, which correspond to putative NMT substrates, was significantly increased compared to the previous experiment (Section 4.2), probably due to the higher sensitivity of the LC-MS/MS platform and greater consistency in sample handling. Interestingly, the equivalent of only 0.2 mg of enriched protein was injected in the LC-MS/MS for each sample, which is 15 times less than for the previous experiment. This suggests that increasing the scale of the experiment might not improve protein coverage, and that the technology of the proteomics platform has a strong impact on sensitivity.

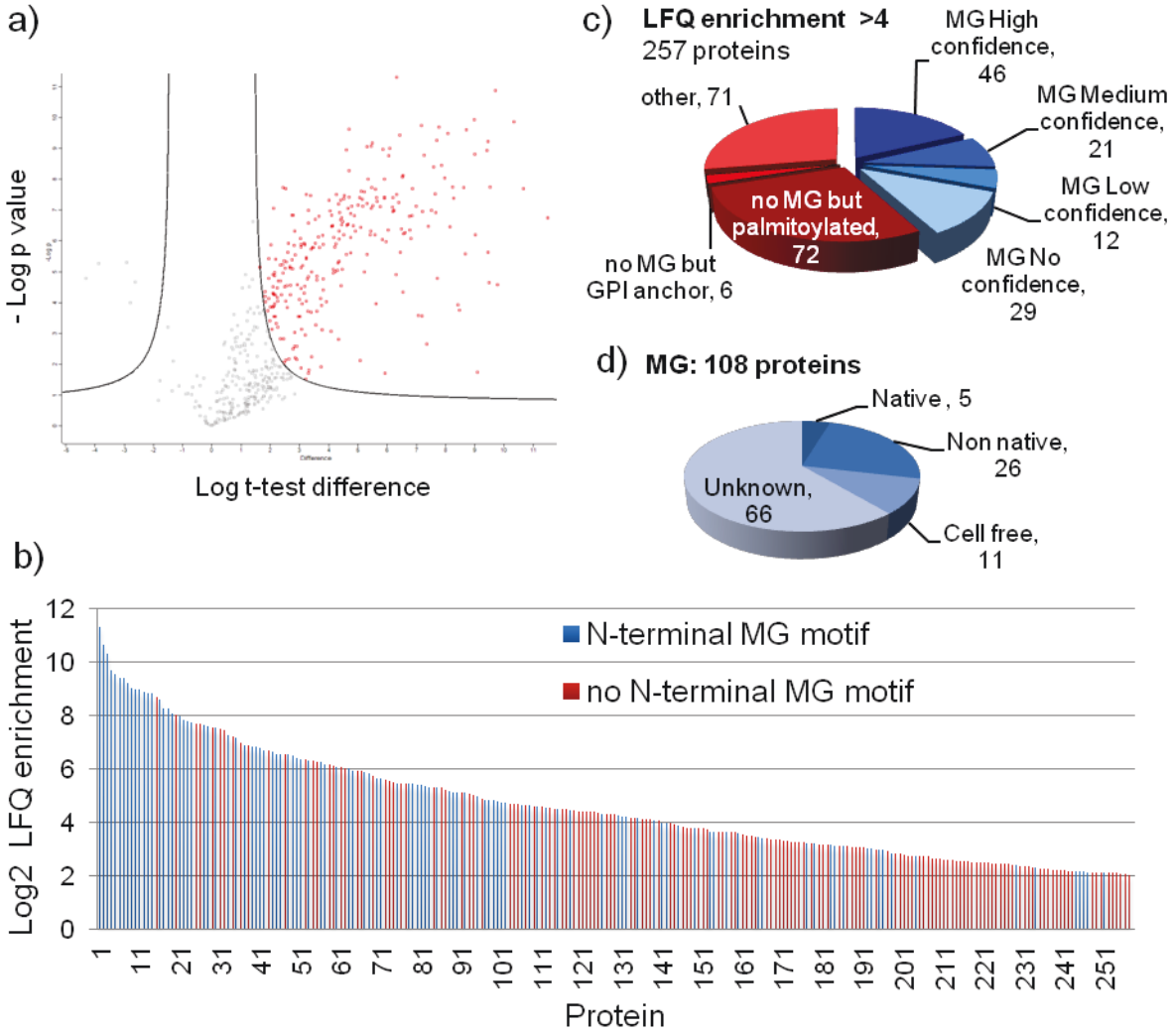

Figure 56. Label-free quantification. a) Two-sample test. To select the significantly enriched proteins in the YnC12 biological replicates, a two-sample test was carried out in Perseus (modified t-test (permutation-based FDR)) using the following criteria: 250 permutation; FDR 0.001; S0 = 1. The –log p value of the test was plotted against the difference of mean of the Myr replicates and YnC12 replicates (log_2 values). The proteins shown in red were selected as significantly enriched in the YnMyr sample. **b)** Log_2 LFQ enrichment was plotted for each protein significantly enriched in the YnMyr samples. Proteins shown in blue have an N-terminal MG motif and proteins shown in red do not have a N-terminal MG motif. **c)** 257 substrates were identified by label-free quantification (4 replicates) in HeLa cells. 108 proteins had an N-terminal MG motif, as required for myristoylation. Prediction of *N*-myristoylation was done by two online bioinformatic tools (the MYR predictor and the Myristoylator): H = high confidence; M = medium confidence; L= low confidence; N = not predicted. 78 proteins with no N-terminal MG motif are known to be palmitoylated or incorporate a GPI anchor. **d)** 108 proteins had an N-terminal MG motif and some had been experimentally shown to be *N*-myristoylated using the classification described in Section 4.1.1.

A large number of proteins with no N-terminal MG motif were significantly enriched in the YnC12 samples (Figure 56b and c), suggesting that YnC12 was incorporated into these proteins in a non NMT-mediated manner. As before, some of these other proteins (78) are palmitoylated or GPI-anchored proteins, suggesting that they might incorporate YnC12 in place of palmitate.

Predictions of *N*-myristoylation revealed that 46 of the 108 proteins with an N-terminal MG motif were predicted with high confidence to be *N*-myristoylated (although, as explained in Section 4.1.2, these predictions are not always reliable). Seven additional known/putative NMT substrates were identified compared to the non-quantitative experiment (Figure 56d).

The enrichment threshold (4 fold) could have been set to a higher value to decrease the number of proteins with no N-terminal MG motif. However, some previously reported NMT substrates (Appendix F), such as ankyrin repeat and IBR domain-containing protein 1 (ANKIB1, 4.8 fold enrichment), would have been lost as they are poorly enriched in the YnC12 samples. This might reflect the poor abundance of these proteins in HeLa cells or their slow turnover rate. Turnover of *N*-myristoylated proteins is discussed in Section 5.3.

This LFQ experiment does not enable robust distinction of NMT substrates from proteins enriched for other reasons (*S*-palmitoylated, GPI-anchored, etc.). This suggested that a further improved method was required to identify NMT substrates in HeLa cells with high confidence.

4.5 Double SILAC YnC12 +/- NMT inhibitor

4.5.1 Experimental design

Recently, two groups employed novel strategies to study protein palmitoylation in BW5147-derived mouse T-cell hybridoma cells [235] and in *Plasmodium*.[236] Both strategies were based on the use of inhibitors of biological processes combined with stable-isotope labelling with amino acids in cell culture (SILAC) (Section 1.11.2). Martin *et al.* employed a serine thioesterase-selective inhibitor to identify palmitoylated proteins which are hydrolysed by serine thioesterases in cells.[235] Jones *et al.* used 2-bromopalmitate, a non selective inhibitor of protein palmitoylation, to detect palmitoylated proteins in *Plasmodium*.[236]

In the current study, a similar approach was applied in HeLa cells by combining SILAC quantitative proteomics with the highly specific NMT inhibitor IMP366 (characterised in Chapter 3), to identify NMT substrates. This approach should solve the problems encountered with the proteomic experiments described above. The YnC12 probe appears to label NMT substrates as well as palmitoylated proteins and possibly GPI-anchored proteins, but only labelling and enrichment of NMT substrates should be sensitive to an NMT inhibitor, and for these proteins a reduction in YnC12 tagging should be observed upon NMT inhibition. This difference in YnC12 tagging can be evaluated using SILAC. The workflow of this experiment is presented in Figure 57.

Heavy isotope-labelled cells (R10K8 media, $^{13}C_6{}^{15}N_4$-Arginine and $^{13}C_6{}^{15}N_2$-Lysine) were treated with YnC12 while light isotope-labelled cells (R0K0 media, $^{12}C_6{}^{14}N_4$-Arginine and $^{12}C_6{}^{14}N_2$-Lysine) were treated with YnC12 and NMT inhibitor IMP366 at the same time. 5 µM of IMP366 was used, as this concentration was shown to be sufficient to inhibit *N*-myristoylation of most NMT substrates in cell without leading to toxicity (Chapter 3). After cell lysis, samples were mixed in a 1:1 ratio and the samples captured with AzTB, enriched on Neutravidin agarose beads and digested with trypsin as usual. For each protein, heavy/light ratios were assessed. A ratio close to 1 would indicate that the same amount of a given protein was tagged by YnC12 in both samples. A ratio significantly higher than 1 would show that tagging of a given protein was reduced in the light sample, and would strongly suggest that this protein is an NMT substrate. HeLa cells were treated with YnC12 and the inhibitor for 24 h as IMP366 was shown not to be toxic up to 24 h.

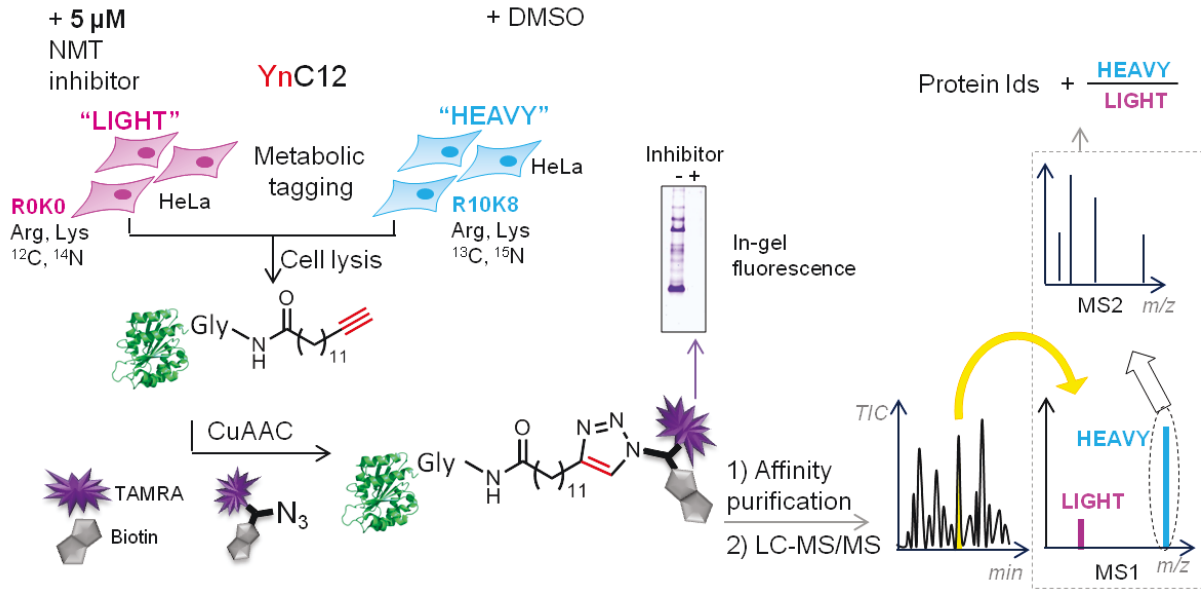

Figure 57. Double SILAC quantitative proteomics strategy to identify NMT substrates. HeLa cells cultured in the light (R0K0) cell culture media were treated with YnC12 and 5 µM IMP366. Cells cultured in the heavy (R10K8) media (with Arginine and Lysine amino acids radiolabelled with ^{14}C and ^{15}N) were treated with YnC12 and DMSO. Cells were lysed after 24 h, the lysates combined in a 1:1 ratio (heavy:light). The samples were captured with AzTB, affinity enriched, and analysed by LC-MS/MS. The data were analysed using MaxQuant and Perseus.

4.5.2 Results and discussion

Biological triplicates were prepared (4 mg total proteins (2 mg of light sample and 2 mg of heavy sample)) and the beads were sent to the PNACL facility at the University of Leicester for analysis (on-bead digest, LC-MS/MS). The data were provided as a raw file and analysed with MaxQuant. The coverage was disappointing as only 259 proteins were identified in total, including 78 proteins with

an N-terminal MG motif. When the data were filtered to require at least two quantified ratios (out of three) per protein, many proteins were lost. The remaining 174 proteins (54 MG) were analysed with Perseus (Appendix A). First, the reproducibility between the three biological replicates was assessed (Figure 58a). The correlation between the Log_2 heavy/light ratios was good between replicates. Histograms showed that most ratios (Log_2 values) followed a normal distribution centred approximately on zero (Figure 58b). Other proteins, mostly possessing an N-terminal MG motif) had a higher ratio (Log_2 value between 2 and 6). These proteins are likely to be NMT substrates as their labelling is reduced by the inhibitor.

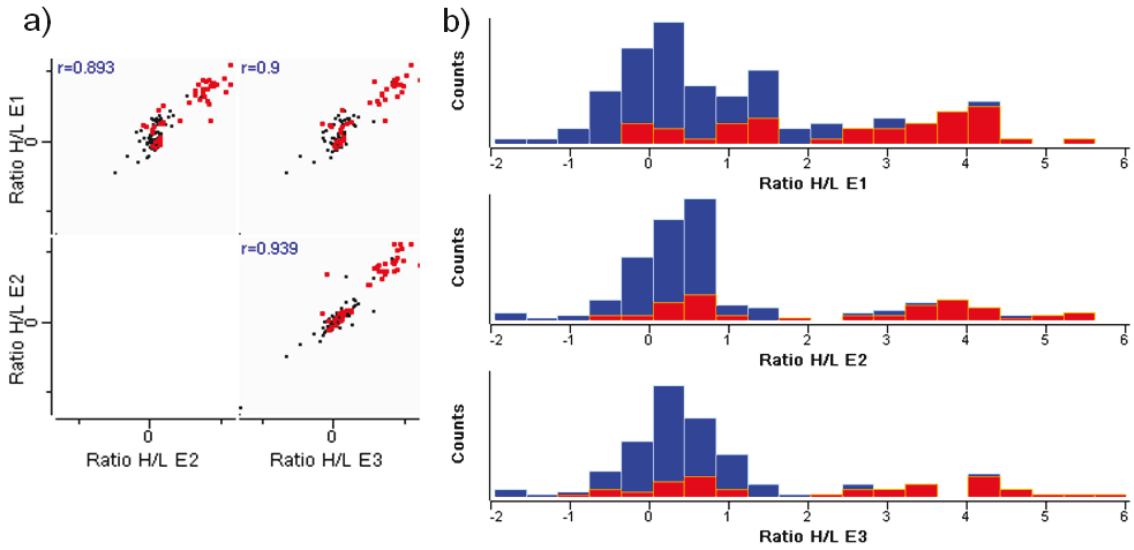

Figure 58. Distribution of the Log_2 heavy/light (H/L; not inhibited/inhibited) ratios for the 174 proteins detected in the double SILAC experiment (n= 3 biological replicates). E1, E2 and E3 correspond to the three replicates. The data were filtered to have at least two valid values (out of 3) Proteins with an N-terminal MG motif are shown in red. **a)** Scatter plot showing the good correlations of the log_2 H/L ratios between the triplicates. **b)** Histograms showing the repartition of the proteins according to their Log_2 H/L ratios. Most proteins have Log_2 H/L ratio close to 0, which means that the relative amount of the protein is the same in both samples and the protein is probably not an NMT substrate.

A modified t-test was performed (FDR 0.2, side = right) to select proteins significantly depleted in the light sample treated with the NMT inhibitor. Only proteins with a Log_2 heavy/light ratio higher than 1 were kept. The list of the 44 proteins which were significantly depleted in the heavy sample is presented in Appendix H.

33 proteins with an N-terminal glycine were significantly affected by the NMT inhibitor (Figure 59). However, 13 proteins did not have an N-terminal MG motif (Figure 59a and b). The twelfth most sensitive protein is proenkephalin-B (PDYN), a cysteine-rich protein. The N-terminal domain contains

six conserved cysteine residues thought to be involved in disulfide bonding and/or processing. Whilst this protein could potentially be *S*-palmitoylated and tagged by YnC12, it should not be sensitive to the NMT inhibitor. Other sensitive proteins with no N-terminal MG motif include bromodomain-containing protein 3 and 4 (BDR3 and BDR4), 26S protease regulatory subunit 7 (PSMC2) and Nesprin-1 (SYNE1). PSMC2 is a proteasome subunit and could have been pulled down with 26S protease regulatory subunit 7 (PSMC1), a previously reported NMT substrate, since the proteasome subunits are tightly associated. This possibility is assessed in Section 4.7.2.

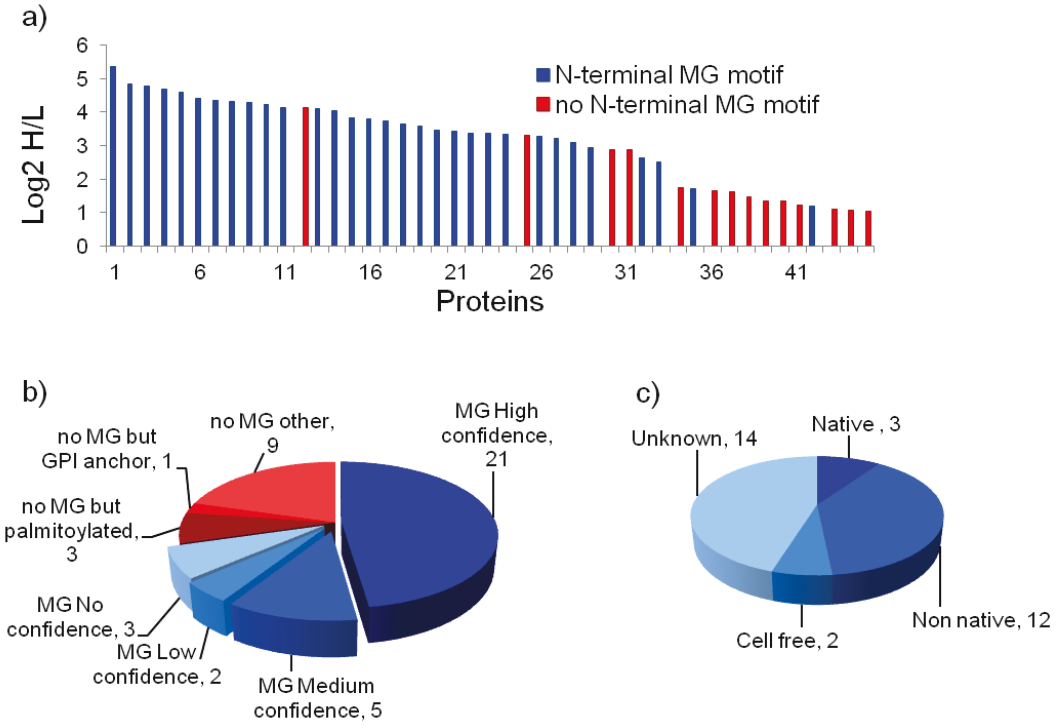

Figure 59. Double SILAC +/- NMT inhibitor (n = 3 biological replicates). 44 substrates were identified using this strategy (3 biological replicates) in HeLa cells. **a)** Log_2 ratio heavy/light (H/L) was plotted for each protein significantly depleted in the heavy sample. Proteins shown in blue have an N-terminal MG motif and proteins shown in red do not have an N-terminal MG motif. **b)** 70% of the proteins had an N-terminal MG motif, as required for protein *N*-myristoylation. Prediction of *N*-myristoylation was done by two online bioinformatic tools (the MYR predictor and the Myristoylator): H = high confidence; M = medium confidence; L= low confidence; N = not predicted. A few proteins with no N-terminal MG motif are known to be palmitoylated or incorporate a GPI anchor**. c)** 31 proteins had an N-terminal MG motif and some had been experimentally shown to be *N*-myristoylated.

4.5.3 Conclusions

Although only 33 proteins carrying an N-terminal MG motif were detected in this experiment, the number of proteins with no MG was notably reduced. In the LFQ experiment (Section 4.4.2), almost

60% of the enriched proteins did not have a MG motif, while in the SILAC experiment described in Section 4.5.2, this number had been reduced to 30%.

The low coverage suggested that there were several issues with the experiment design and the sample processing.

- ✓ The total number of proteins detected was relatively low. Without any sample filtering, only 78 proteins with an N-terminal MG motif were detected across the three replicates. This number is much lower compared to the 135 proteins detected in the LFQ experiment after filtering the data to keep at least 3 valid values across the four YnC12 samples. This observation, together with later results, strongly suggests that the LC-MS/MS used at the PNACL facility at the University of Leicester had a much lower sensitivity than the other proteomics platforms used in this study. Moreover, the SILAC experiment was carried out on a large scale. As suggested in Section 4.4, a large scale experiment might not be necessary to get good protein coverage; indeed, this excess might instead have saturated the LC column and limited protein identification.
- ✓ Log_2 ratios higher than 4 are close to the dynamic range of any LC-MS/MS apparatus.[235] Small quantities of YnC12 tagged proteins in the heavy sample might not have been detected. When cells are inhibited with 5 µM of IMP366, *N*-myristoylation should be nearly completely inhibited. MaxQuant should automatically impute a ratio value if one protein was found only in the light sample, but these ratios might not be accurate. It would be preferable to use a lower concentration of inhibitor to decrease the value of the ratios and move them away from the detection limit.

It is unclear why several proteins with no N-terminal MG motif are less enriched in the presence of the NMT inhibitor. Several hypotheses were proposed and are discussed in Section 4.7.

- ✓ Proteins might be enriched because they bind to NMT substrates. However, the interaction would need to be strong, possibly covalent, to be able to resist the highly denaturing conditions (2% SDS) during the sample processing for proteomics.
- ✓ Proteins might have an internal protease cleavage site. Proteins can sometimes be processed outside the context of apoptosis,[237] and any new N-terminal glycine could potentially be *N*-myristoylated.
- ✓ Proteins that are tagged with YnC12 in a non NMT-mediated manner could be down regulated upon NMT inhibition; however this is unlikely as NMT inhibition has little effects on the cells after 24 h (Chapter 5).

4.6 Spike-in SILAC with inhibitor

4.6.1 Experimental design

Spike-in SILAC quantitative proteomics has recently emerged as a straightforward method to quantitatively compare multiple samples.[195] A heavy isotope labelled standard (referred to as the "spike-in standard") is incorporated at the early stages of the proteomics workflow, preventing any bias due to sample processing (CuAAC, enrichment, LC-MS/MS) (Section 1.11.2). This method presents two major advantages compared to the double SILAC approach employed in Section 4.5. First, an arbitrary number of samples can be compared using this approach, while only two samples can be compared using the double SILAC approach. Secondly, for the spike-in SILAC methodology, samples to be compared can be prepared in any standard cell culture medium (DMEM and FBS for HeLa cells), while double SILAC experiments require the use of a defined media (R0K0/R10K8 labelled DMEM, dialysed FBS). Cells grown in the R0K0 and R10K8 DMEM appeared to grow more slowly than cells grown in the standard media, probably due to the removal of low molecular weight nutrients (amino acids, hormones, etc.) in the dialysed FBS. This alteration of cell growth might alter the rate of YnC12 incorporation into NMT substrates.

Heavy isotope-labelled cells (R10K8 media) were treated with YnC12 while cells grown in the standard DMEM media were treated with YnC12 and various concentrations (0, 0.08, 0.2, 0.4, 1 and 5 µM) of NMT inhibitor IMP366 at the same time (Figure 60).

The inhibitor supplemented at these concentrations to cell media was shown to give dose-dependent protein labelling by in-gel fluorescence (Section 3.3.3.4). 0.2 µM is close to the TC_{50} value while 1 µM inhibited > 90% YnC12 labelling and 5 µM almost completely inhibited YnC12-labelling in HeLa cells (Section 3.3.1). After cell lysis, the cell lysates treated with IMP366 were spiked with the heavy standard. The same ratio of proteins from "cells treated with IMP366": "spike-in standard" was used for each sample, allowing them to be compared. The proteins were then captured with AzTB, enriched on Neutravidin agarose beads and digested with trypsin as usual. For each protein and each concentration of IMP366, "inhibited"/"spike-in" ratios (also referred to as light/heavy) were assessed. For a given protein, a dose-dependent decrease of the ratios would indicate that the protein is an NMT substrate. Additionally, this method could allow the determination of in-cell IC_{50} for each NMT substrate.

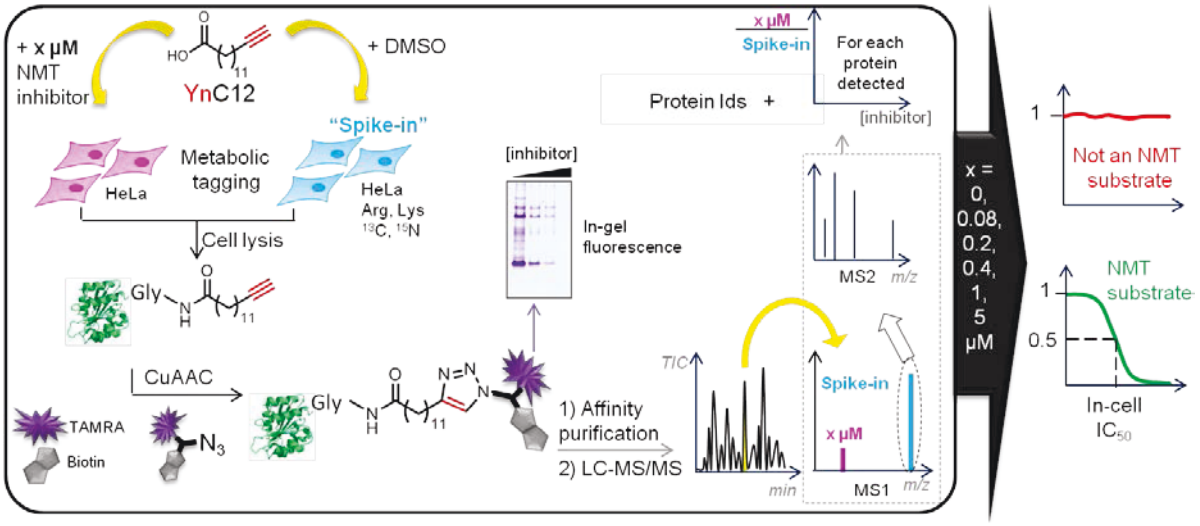

Figure 60. Quantitative proteomics strategy to identify novel NMT substrates and calculate in-cell IC_{50s}. HeLa cells cultured in the normal cell culture media were treated with YnC12 and different concentrations of inhibitors (x =0; 0.08; 0.2; 0.4; 1; 5 µM). Cells cultured in the heavy media (with Arginine and Lysine amino acids radiolabelled with ^{14}C and ^{15}N) were treated with YnC12 and DMSO. Cells were lysed after 24 h, the lysates combined in a 1:2 ratio (heavy:light). The samples were captured with AzTB, affinity enriched, and analysed by LC-MS/MS. The data were analysed using MaxQuant, Perseus and GraFit.

As explained in Section 4.5, a heavy/light ratio higher than 4 (Log2 value) is close to or within the background noise and it is possible that some ratios, especially for the 5 µM sample, would not be determined accurately due to the low abundance of the light isotope labelled proteins. Mixing samples in a 2:1 ratio "sample treated with the inhibitor": "spike-in" might overcome this problem as it would increase the relative abundance of light isotope labelled proteins.

4.6.2 Data processing

Four biological replicates and one technical replicate were prepared and analysed on a nanoLC-Q-Exactive platform at the mass spectrometry facility, Department of Chemistry, Imperial College London. The data were received as a '.raw' file and analysed with MaxQuant and Perseus. The workflow used to process the data is presented in Figure 61. The data were first filtered to require at least three valid values across the 30 samples (5 replicates of 6 concentrations of IMP366). More than 600 proteins were identified in total, including 169 proteins with an N-terminal MG motif (Appendix A). For these 169 enriched proteins (or protein groups), 17,401 unique protein-derived peptide sequences were identified and quantified with high confidence, resulting in 20,084 spike-in SILAC ratios for which the response to inhibition was analysed.

For each replicate, the ratios were normalised to the sample with 0 µM IMP366. For each protein, the ratio in the 0 µM IMP366 sample was taken as 1 whilst the ratios for all the other samples (0.08;

0.2, 0.4; 1 and 5 µM) were between 0 and 1. The closer the ratio to zero for a particular protein, the more depleted is *N*-myristoylation of that protein.

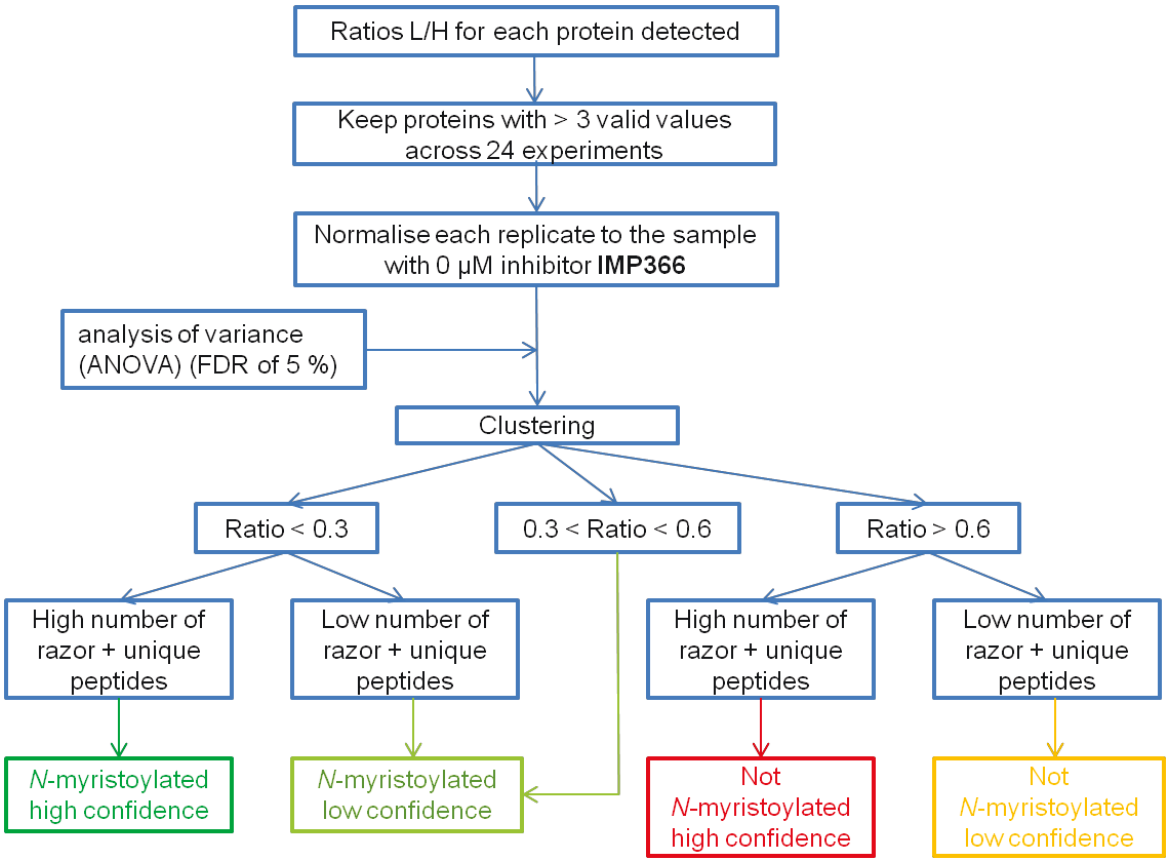

Figure 61. Analysis of the spike-in SILAC experiment. Low number of razor+unique peptides refers to proteins having 0 or 1 razor+unique peptides in the highest concentrations of inhibited samples.

Proteins were clustered to allow the rapid selection of NMT substrates versus non-substrates of NMT. The data were then manually inspected and divided up into four categories:

- ✓ ***N*-myristoylated high confidence:** This group corresponds to proteins showing a dose-dependent response to the NMT inhibitor with ratios reaching values lower than 0.3.
- ✓ ***N*-myristoylated low confidence:** This group corresponds to proteins fulfilling the previous criteria but which had a low number of unique peptide (0 or 1 unique peptides in the highest concentrations of inhibited samples) or to proteins with a minimum ratio value between 0.3 and 0.6.
- ✓ **Not *N*-myristoylated high confidence:** This group corresponds to proteins for which the ratios do not drop below 0.6.

- ✓ **Not *N*-myristoylated low confidence:** This group corresponds to proteins fulfilling the criteria for non-substrates of NMT but which had a low number of unique peptide (0 or 1 unique peptides in the highest concentrations of inhibited samples).

4.6.3 Results: proteins with a N-terminal MG motif

4.6.3.1 Identified proteins: sensitive or insensitive to inhibition

70 proteins showed a robust dose-dependent response to increasing concentration of IMP366, and could thus be assigned with confidence as NMT substrates. Figure 62a shows the response for three previously reported NMT substrates, PSMC1, c-SRC and PRKACA. The experiment also allowed the identification of 54 non NMT substrates, as for example GOLIM4, CD81 and PTGFRN, displayed in Figure 62b. Interestingly, GOLIM4 was predicted to be *N*-myristoylated (Section 4.1.2) whilst CD81 and PTGFRN were highly enriched in the LFQ experiment (Section 4.4). CD81 was detected in a non-quantitative chemical proteomics experiment by Wilson *et al*. (Appendix F).[173]

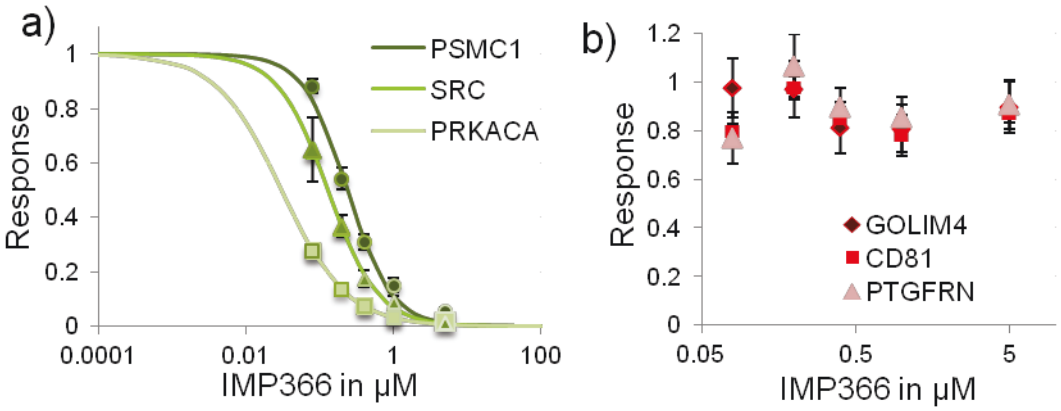

Figure 62. Identification of co-translational NMT substrates in HeLa cells. The response correspond to the ratios (spike-in SILAC ratios versus the concentration of IMP366) normalised to the 0 µM IMP366 sample (n= 4; error bars display the standard deviations). **a)** Shows the response obtained for three known/putative NMT substrates, PSMC1, SRC and PRKACA. **b)** Shows the response for three non NMT substrates, GOLIM4, CD81, PTGFRN.

Most of the 54 non substrates were enriched in the LFQ experiment. Interestingly, one previously reported substrate, identified with a cell free method, serine incorporator 1 (SERINC1) was not sensitive to the NMT inhibitor.

4.6.3.2 Proteins with N-terminal MG motif and sensitive to NMT inhibition: in-cell IC_{50}

An IC_{50} value could be determined for the 70 proteins for which enrichment is dose-dependently sensitive to NMT inhibition. Figure 63 displays the IC_{50} profiles of six NMT substrates plotted with GraFit 7.0. For most substrates, the error for the IC_{50} value was small and the slope factor was between 0.5 and 2, suggesting that sigmoidal curve fitting was excellent. While a wide range of IC_{50}

values (from 2 to 762 nM) was obtained, the average IC_{50} value (168 ± 38 nM) correlated well with the TC_{50} value (169 ± 31 nM, Section 3.3.1). Plots showing the IC_{50} profiles of the 70 NMT substrates were generated by non-linear regression of IC_{50} values and slope factors to a standard dose-response equation (GraFit 7.0) (Figure 64).

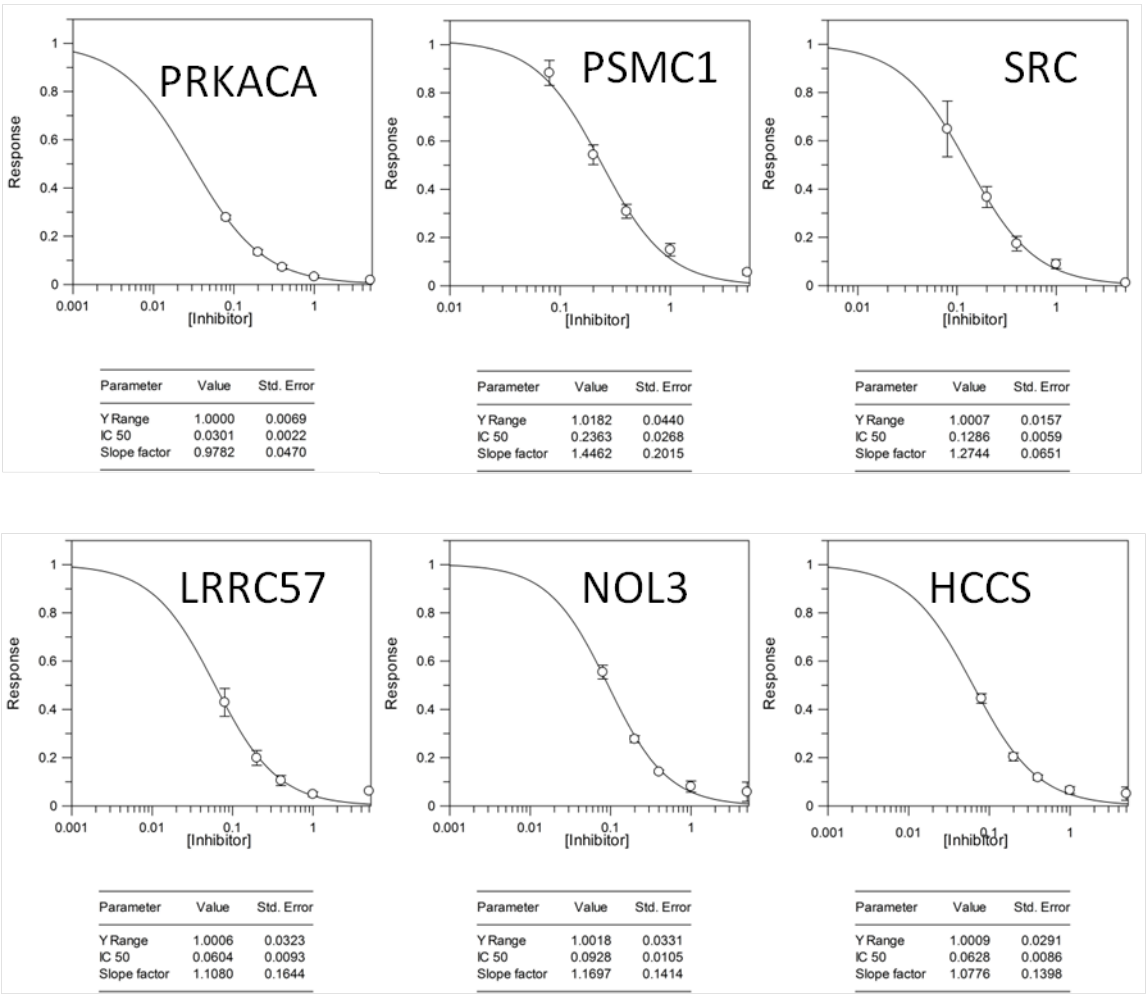

Figure 63. Examples of IC_{50} profiles obtained with GraFit 7.0. The protein gene names are indicated. PRKACA, PSMC1, SRC were known/putative NMT substrates. LRRC57 and NOL3 were not known and poorly predicted to be *N*-myristoylated while HCCS was not known but predicted with high confidence to be *N*-myristoylated.

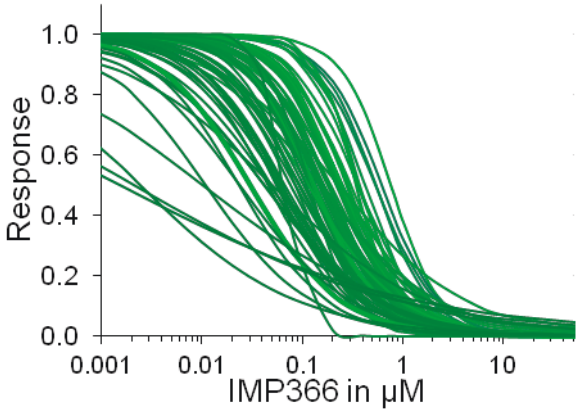

Figure 64. Dose-response for the 70 NMT substrates identified by quantitative chemical proteomics. The plot was generated by fitting the IC_{50} values and slope factors to the IC_{50} dose-response equation.

The diversity of in-cell IC_{50} values might reflect the affinity of a protein for HsNMT1/2. Indeed, a protein with a low affinity for HsNMT1/2 might be more sensitive to low concentrations of NMT inhibitor.

4.6.3.3 *N*-myristoylated low confidence

Using the spike-in SILAC approach described in this chapter, 27 proteins were defined as 'low confidence' NMT substrates as they were quantified from a smaller set of unique peptides or had an ambiguous dose response. Previous reports suggest that several of these 'low confidence' NMT substrates are likely to be *N*-myristoylated.

- ✓ **Low number of unique peptides: 7 proteins:** RING finger protein 11 (RNF11) has been shown to be *N*-myristoylated in a cell free system (Appendix F). Intriguingly, ADP-ribosylation factor-like protein 2 (ARL2) followed a nice dose-dependent response but had been previously reported not to be *N*-myristoylated.[238]

- ✓ **Ambiguous dose-response (do not drop below 0.3):** Mitochondrial peptide methionine sulfoxide reductase (MSRA) had previously been shown to be *N*-myristoylated in a non-native context (Appendix F) whilst three other proteins had been shown to be *N*-myristoylated in a cell free system. YnC12-modified N-terminal protein sequence was identified with AzKTB for Opioid growth factor receptor-like protein 1 (OGFRL1) (Section 4.2.2). Interestingly, platelet-activating factor acetylhydrolase 2, cytoplasmic (PAFAH2) had been labelled with an alkyne palmitate analogue and shown to be not sensitive to base-treatment, suggesting that it may be *N*-myristoylated (see Section 4.7 for cross-talk between *N*-myristoylation and *S*-palmitoylation).[175]

4.6.4 Conclusions

This spike-in SILAC approach allowed the identification with high confidence of a large number of co-translational NMT substrates as well as non-substrates. Seven newly identified NMT substrates were poorly predicted to be *N*-myristoylated whilst some proteins not sensitive to the NMT inhibitor had been predicted to be substrates (Figure 65). These results confirmed once again that the predictors are not always accurate.

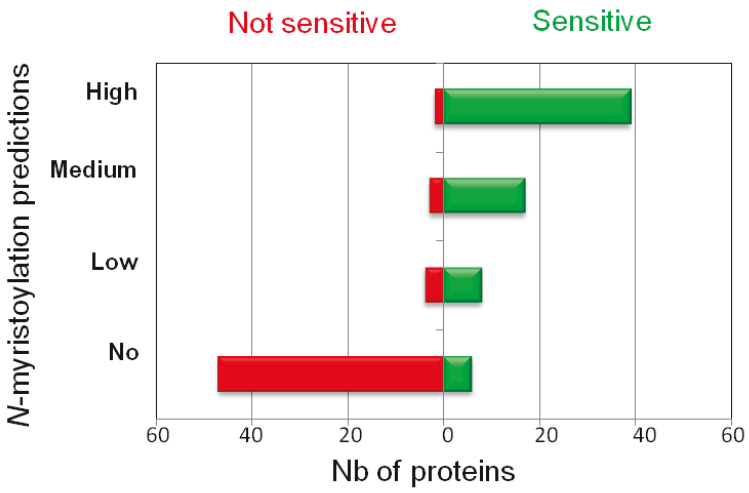

Figure 65. Identification of 70 NMT substrates in HeLa cells. Repartition of the alkyne-tagged proteins with a N-terminal MG motif : the proteins identified were either sensitive (NMT substrates) or not sensitive (not NMT substrates) to the NMT inhibitor. Proteins were predicted to be *N*-myristoylated with high confidence (H), medium confidence (M), low confidence (L) or not predicted (N) by the online predictors, the Myristoylator and the Myr predictor.

When proteins with no N-terminal MG motif were subjected to the same analysis (Figure 61), twelve proteins were found to be dose-dependently sensitive to NMT inhibition. Eleven were enriched in LFQ experiments (Section 4.4) and possible explanations are discussed in Section 4.7.2.

4.7 Proteins tagged with YnC12 but not NMT substrates

4.7.1 *S*-Palmitoylated proteins and GPI-anchored proteins

In the current study, a substantial number of non-substrates of NMT were labelled with YnC12 and highly enriched in the YnC12-treated sample over the control (myristic acid or DMSO). As discussed in Section 4.2, a large majority of these proteins do not have an N-terminal MG motif and might incorporate YnC12 in place of palmitate in *S*-palmitoylated proteins or GPI-anchored proteins.

YnC12 is attached to the N-terminal glycine of NMT substrates *via* an amide linkage. If the YnC12 probe labels *S*-palmitoylated proteins or GPI-anchored proteins, it would be *via* a thioester linkage (on side-chain of cysteine residues) or via an ester linkage to an inositol, respectively (Figure 19). It is possible to distinguish thioester and ester bonds from amide linkages by treating samples with hydroxylamine or base. Esters or thioesters would be hydrolysed by these reagents, and thus should no longer be enriched by pull-down, whilst amide bonds would be left untouched (Figure 66).

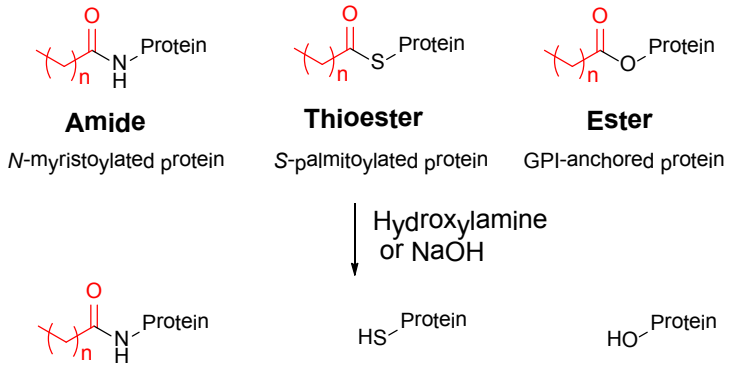

Figure 66. Effect of hydroxylamine (NH_2OH) or NaOH treatment on acylated proteins. Amide, thioester and ester linkages are typical of *N*-myristoylated, *S*-palmitoylated or GPI-anchored proteins respectively. Only amides are stable to hydroxylamine or base treatment.

Proteomics experiments carried out by Dr. Megan Wright (Tate group, Imperial College London) demonstrated that base-treatment of *Plasmodium Falciparum* lysates (labelled with YnC12) prior to the enrichment step could hydrolyse the YnC12-ester linkage within GPI-anchors, and result in a substantial decrease in enrichment of parasite GPI-anchored proteins.[163]

A few examples have been reported in the literature showing that palmitate could be hydrolysed by treating the sample with sodium hydroxide.[239,240] However, hydroxylamine-treatment of lysate has been preferred to hydrolyse thioester linkages as this method is chemically more efficient to hydrolyse thioester bonds and also milder.

Hydroxylamine treatment has been widely employed to study the loss of enrichment of YnC16-tagged *S*-palmitoylated proteins by Western blot analyses, but it has rarely been used in combination with MS-based proteomics. However, Martin *et al*. treated human Jurkat T-cells with 17-ODYA and noticed, using quantitative proteomics, the loss of enrichment upon treatment of the samples with hydroxylamine.[175] After the CuAAC reaction, they boiled the samples for 5 min in the presence of neutralized hydroxylamine (2.5% final concentration) and diluted with PBS before being enriched on Streptavidin beads. However, this treatment resulted in visible smeared bands on the

gel, suggesting that proteins had been degraded. As protein degradation could falsify the identification of hits in the MS-based proteomics experiment, it was decided not to use the same protocol as Martin et *al.* [175]

4.7.1.1 Experimental design

Hydroxylamine and base-treatments of HeLa cell lysates and *Plasmodium* samples had been previously optimised by Dr. Megan Wright (Tate group, Imperial College London). Treatment was typically carried out for 1 h, before the enrichment step; however, base/hydroxylamine cleavage of thioesters might not be complete after one hour and it might be preferable to use a quantitative approach to identify a set of proteins which were sensitive to the base-treatment. A spike-in SILAC approach appeared advantageous as it was shown in Section 4.6 to be highly reliable to quantify changes between samples. However, samples would preferably be base/hydroxylamine treated before the CuAAC reaction as it is preferable to mix the spike-in standard with the samples as early as possible in the proteomics workflow (Section 1.11.2). A fraction of YnC12-treated cell lysate was base/hydroxylamine treated and another fraction was treated with PBS buffer (to control for the salts added in the other samples). The two samples were then spiked with the same heavy standard employed in Section 4.6 (ratio 1:1).

Experiments were required to optimise the base/hydroxylamine treatment before the CuAAC reaction. As it might be difficult to observe a reduction of YnC12 labelling following base/hydroxylamine treatment of the samples, optimisations were carried out using HeLa lysates labelled with YnC15, an alkyne analogue of palmitic acid prepared as described in Chapter 2. This analogue was used in the Tate group to study protein palmitoylation,[163,174] and 50 µM YnC15 seemed optimal to label proteins in HeLa cells (Figure 67). Samples labelled with YnC12 were subjected to the same base/hydroxylamine treatment as the YnC15-labelled samples, to ensure fluorescence labelling was not completely lost and that proteins were not degraded.

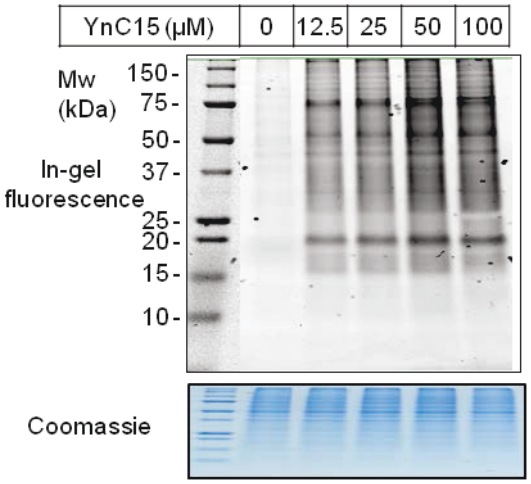

Figure 67. Optimisation of the YnC15 labelling in HeLa cells. Cells were labelled for 18 h with an increasing concentration of YnC15 or treated with DMSO (vehicle).

As it was shown that hydroxylamine could inhibit the CuAAC reaction,[163] proteins were precipitated directly after the base/hydroxylamine treatment (and thus before the CuAAC reaction) to remove excess hydroxylamine (Figure 68). As a control, samples were not precipitated before the CuAAC reaction. As expected, fluorescence signal was lost for the hydroxylamine treated samples without protein precipitation. When the samples were precipitated, a smear appeared on Coomassie, probably due to poor protein resuspension or protein degradation. Additionally, for the YnC12 labelled proteins treated with hydroxylamine, the bands seen in fluorescence at 75 kDa and 20 kDa seemed weaker and all the sharp bands between 25 and 50 kDa were shifted and smeared (Figure 68b).

The sodium hydroxide treatment seemed to give better results, even if YnC15 labelling was not completely depleted. The YnC12 labelling pattern was similar in the treated and non-treated samples. Interestingly, protein molecular weight decreased upon prolonged treatment (proteins around 55 kDa boxed in red in Figure 68b), probably due to the conversion of Asn and Gln into Asp and Glu, known to occur upon base treatment. [241] These changes modify the charges of proteins and therefore might modify their motility on the gel.

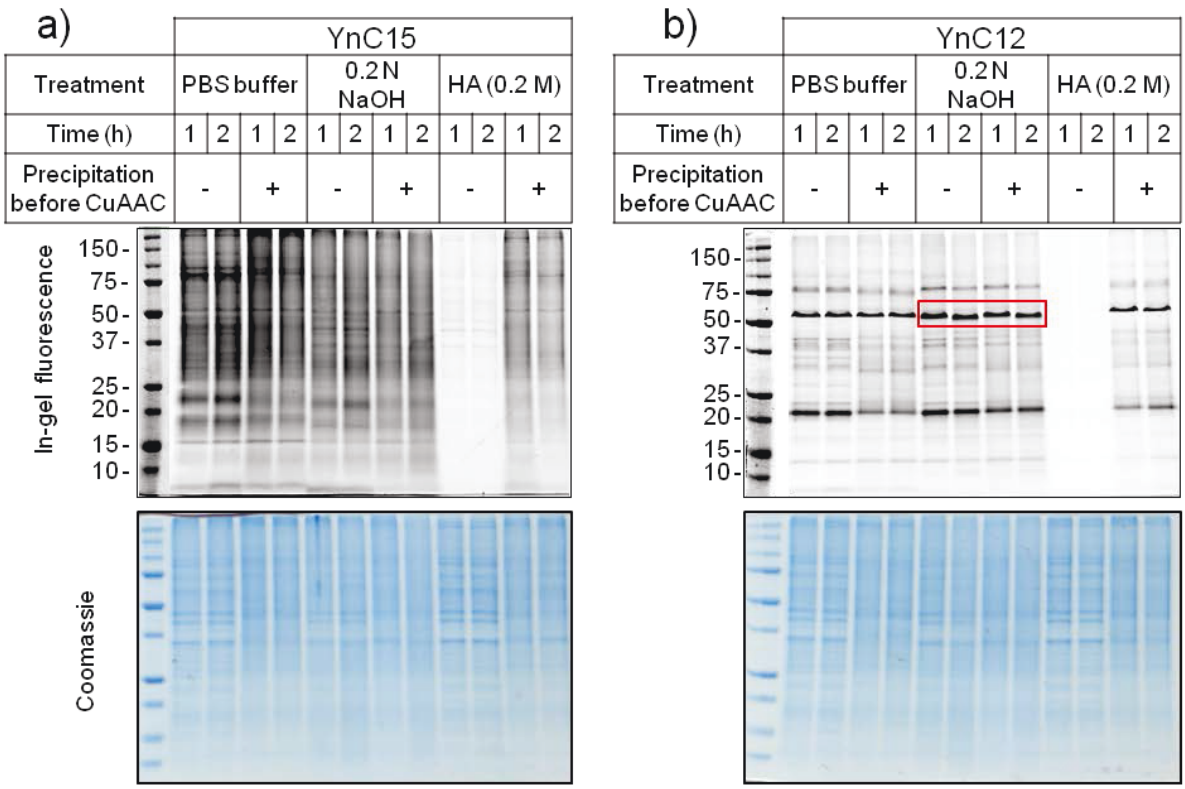

Figure 68. Base and hydroxylamine treatment optimisation in HeLa cells. HeLa cells were treated with **a)** YnC15 (18 h, 50 µM) or **b)** YnC12 (18 h, 50 µM). Samples were treated for 1 or 2 h with PBS, 0.2 N NaOH, or 0.2M freshly neutralised hydroxylamine. Samples were precipitated or not before CuAAC. Proteins shifted on the gel after the base-treatment boxed in red.

Base-mediated hydrolysis/removal of YnC15 labelling is incomplete after 2 hours as seen on the YnC15 gel. Increasing the base-treatment to 4 h helped to decrease the YnC15 labelling but at the same time, it also gave more protein degradation (smear on coomassie and smear of the proteins tagged with YnC12 observed in Figure 69). For the spike-in experiment, it was decided to treat the lysate with 0.2 M sodium hydroxide for 2 h and samples were not precipitated before the CuAAC reaction. Even if the ester and thioester bonds were not completely hydrolysed after 2 h treatment, quantitative proteomics should still identify the base/hydroxylamine sensitive proteins.

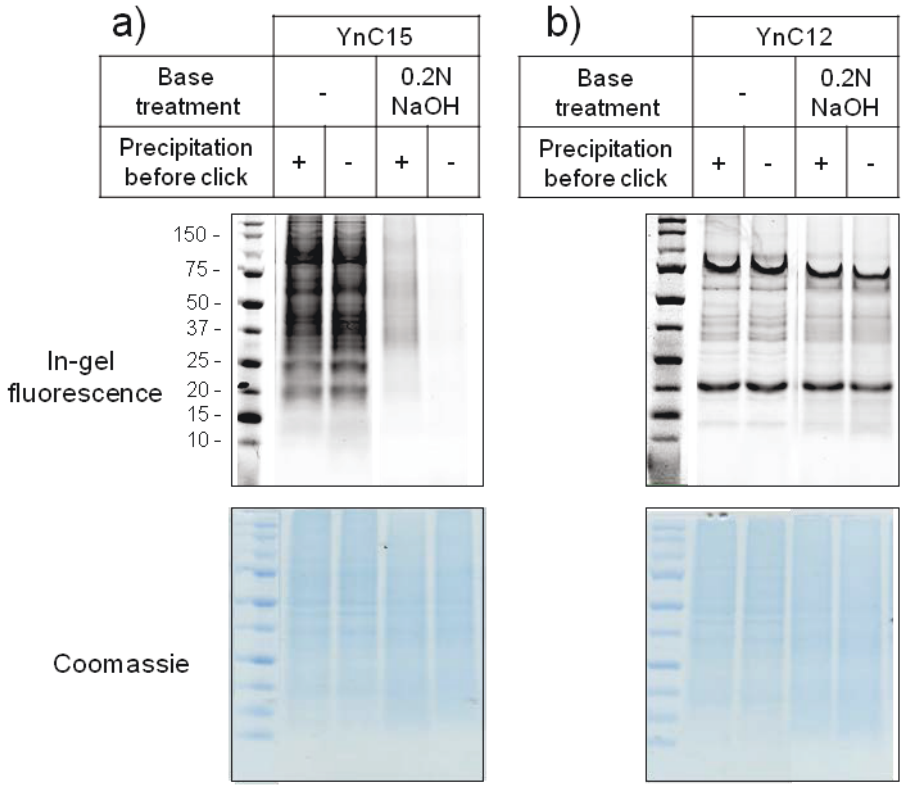

Figure 69. 4 h base-treatment (0.2N NaOH). a) YnC15 and **b)** YnC12 labelling were compared. Samples were precipitated or not before CuAAC (after the base-treatment).

4.7.1.2 Base-treatment

HeLa cells were labelled with YnC12 and four samples were prepared:

- ✓ Untreated sample + heavy spike-in (1:1 ratio) (biological duplicates)
- ✓ 2 h base-treated sample + heavy spike-in (1:1 ratio) (biological duplicates).

Samples were analysed by the mass spectrometry facility, Department of Chemistry, Imperial College London. The data were provided as raw files and analysed with MaxQuant. The data were filtered to keep only proteins with at least two valid values (out of four), resulting in a list of 421 proteins (including 122 with an N-terminal MG motif). The reproducibility between duplicates of the non-base-treated sample was particularly good, as seen on the multiple scatter plots displayed in Figure 70a. However, the reproducibility between the base-treated samples was poor, and the reason is currently unclear (Figure 70b).

Proteins were then subjected to a two-sample test (FDR 0.01, 250 permutations, S2) and only proteins with a t-test difference higher than 1 (Log2 scale) were kept (Figure 70c, Appendix A and Appendix H). 58 proteins, including 14 proteins with an N-terminal MG motif, were significantly

depleted in the base-treated samples, suggesting that they incorporate YnC12 *via* an ester or thioester bond (Figure 70d). 50 of these proteins were enriched in the YnC12 samples in the LFQ experiment (Section 4.4).

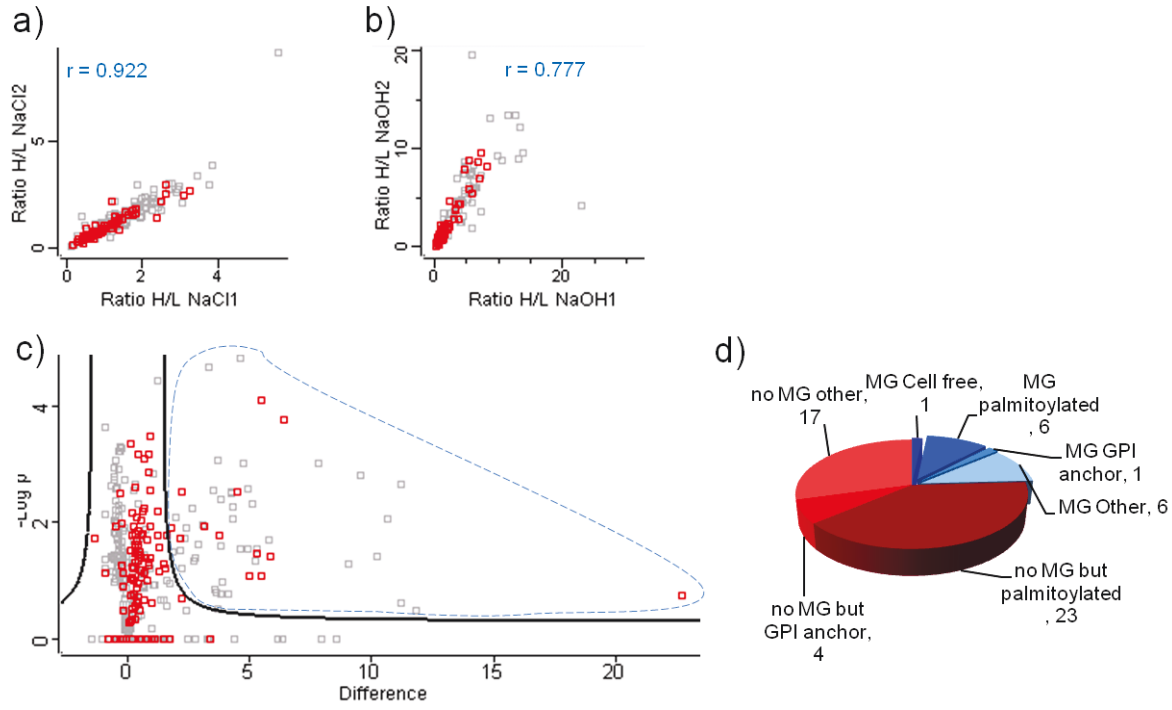

Figure 70. Base-treatment. Correlation between the two biological replicates of the samples. a) Not base-treated or **b)** base-treated. Proteins with an N-terminal MG motif are shown in red. **c)** A two sample test was used to select the proteins significantly affected by base-treatment. Proteins with an N-terminal MG motif are shown in red. **d**) Partition of the base-sensitive proteins. 14 proteins had an N-terminal glycine but only one protein was previously shown to be *N*-myristoylated.

Some known *S*-palmitoylated proteins (as reported in the Uniprot/KB database), Calnexin and CKAP4, as well as two known GPI-anchored protein BST2 and CD59 were sensitive to the base-treatment. The three proteins carrying an N-terminal MG motif and not sensitive to the inhibitor shown in Figure 62b were base-sensitive. This result confirms that they are not NMT substrates but probably *S*-palmitoylated or GPI-anchored.

Interestingly, a protein previously reported as NMT substrate,[230] SERINC1, was highly sensitive to base-treatment. This protein was not dose-dependently affected by the increasing amount of NMT inhibitor (Section 4.6.3). The fact that no dual-lipidated protein was significantly sensitive to base-treatment suggested that SERINC1 is not *N*-myristoylated.

4.7.1.3 Conclusions

The experiment described in Section 4.7.1.2 showed much promise and explained why many proteins are tagged with YnC12 but are not NMT substrates; however, this experiment should be repeated to obtain a more comprehensive dataset. Probably more than 56 proteins labelled with YnC12 are *S*-palmitoylated or GPI-anchored. In particular, the number of replicates should be increased to increase the power of the statistical analysis and the conditions used for the base-treatment could be further optimised by varying the concentration of base.

The specificity of YnC12 for palmitoylated proteins is currently unknown and YnC12 might be incorporated only into the most abundant palmitoylated proteins

4.7.2 Proteins with no N-terminal MG motif but dose-dependently sensitive to NMT inhibition

Twelve proteins with no N-terminal MG motif appeared to be sensitive to NMT inhibition (Section 1.6 and Appendix H). Eleven (all but Histone H2A.x) were significantly enriched in the YnC12 sample in the LFQ experiment (Section 4.4). Six proteins are subunits of the 26S proteasome. The proteasome is a protein complex involved in the ATP-dependent degradation of ubiquitinated proteins. 26S proteasome regulatory subunit 4 (PSMC1) is a previously reported NMT substrate [208] identified with high confidence in Section 4.6.3, and the six other subunits might be pulled down with PSMC1. It is also possible that these proteins are not specifically enriched and that their relative abundance decreases upon NMT inhibition.

Experiments were carried out to verify these hypotheses. First, relative abundance of 26S protease regulatory subunit 7 (PSMC2), the most enriched protein in the LFQ experiment was studied. Western blot analysis showed that treatment of HeLa cells with an increasing amount of IMP366 did not decrease PSMC2 levels (Figure 71a). Secondly, PSMC1 and PSMC2 were immunoprecipitated from YnC12 or myristic acid treated lysates. Both samples were captured with AzTB to label alkyne-tagged proteins, and proteins were run on an SDS-PAGE gel (Figure 71b). For PSMC1, in-gel fluorescence revealed one band in the YnC12-treated sample, corresponding to PSMC1. Western blot analysis showed a non-specific band below 50 kDa, probably corresponding to the antibody heavy chains. For PSMC2, in gel fluorescence analysis showed several bands. The band observed at ca. 60 kDa (boxed in blue in Figure 71b) corresponded to a YnC12-tagged protein as it was present only in the YnC12 treated sample (and not in the myristic acid control). The molecular weight (MW) of this band did not match the apparent MW of PSMC2 (49 kDa) (Figure 71b). However, Western blot analysis in Figure 71b, could not confirm whether the band was PSMC2 due to the presence of non-specific bands on the Western blot at the same MW as that expected for PSMC2. The

non-specific bands below 50 kDa most likely corresponded to the antibody heavy chains. PSMC2 antibody heavy and light chains probably corresponded to the extra bands observed by in-gel fluorescence. The capture reagent AzTB might bind non-specifically to the antibody released from the beads at the same time as the protein PSMC2. Attempts to decrease this background by precipitating the proteins before running the SDS-Page gel or by using milder conditions to elute the proteins from the beads were unsuccessful. More experiments are required to confirm that PSMC2 is pulled down with PSMC1 in YnC12-labelled samples.

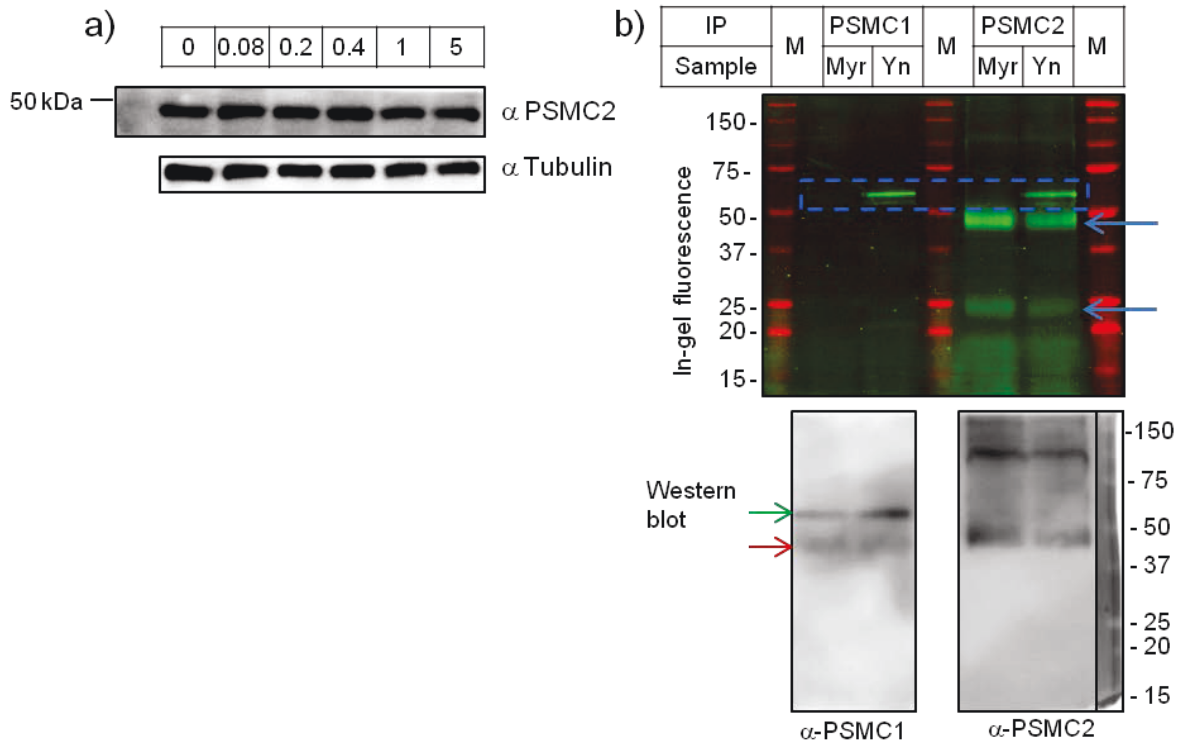

Figure 71. Possible explanation for the enrichment of PSMC2 in the YnC12 samples. a) PSMC2 levels do not decrease in HeLa cells treated with IMP3666 (μM) for 24 h. Tubulin was used as a loading control. **b)** Immunoprecipitation of PSMC1 or PSMC2 using Sepharose A beads, followed by capture on beads by AzTB. Proteins were released from the beads by boiling and the samples were run on a SDS-PAGE gel, analysed by in-gel fluorescence and Western blot. A band is common to both YnC12 (Yn) treated samples (boxed in blue). Blue arrows indicate the heavy and light chains of the antibody seen by in-gel fluorescence. A green arrow indicates the band corresponding to PSMC1 on the Western blot and a red arrow indicates a band, probably corresponding to the antibody heavy chain.

Over the last decade, the structure of the 26S proteasome and the interactions between the different subunits have been well studied.[242] The six regulatory subunits (PSMC1-6) have been shown to tightly interact *via* a coiled-coil domain present in the N-terminal region of these subunits (Figure 72).[242,243] The N-terminal region of PSMD2 has also been shown to interact with PSMC1 and PSMC2. [242]

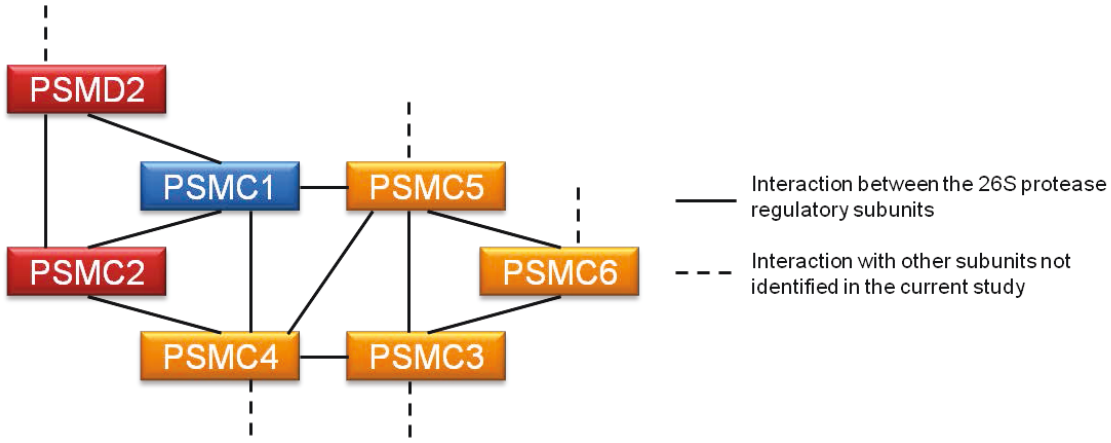

Figure 72. Interaction map between the seven subunits of the 26S proteasome detected in the current study. PSMC1, the putative NMT substrate is shown in blue. Highly enriched proteins (LFQ ratio > 10) are shown in red and other subunits are shown in orange (6 <LFQ ratio ≤ 9). Adapted from Fu *et al.* [243].

None of the interactions between the 26S proteasome subunits are thought to be covalent, but they appeared to be highly stable as they were able to resist the highly denaturing conditions (2% SDS) during the sample processing for proteomics.

Similarly, other proteins with no N-terminal MG motif form protein complexes with NMT substrates. Flotilin-1 (FLOT1, no MG motif) interacts with flotilin-2 (FLOT2, NMT substrate) [244] whilst serine/threonine-protein phosphatase 2B catalytic subunit alpha and beta isoforms also referred to as calcineurin A (PPP3CA and PPP3CB, no MG motif) interacts with calcineurin subunit B type 1 (PPP3R1, NMT substrates) as they are tightly associated subunits of calcineurin.[245]

No analogous interactions are known for the four other proteins without an N-terminal MG motif sensitive to NMT inhibition (BAG5, LANCL1, H2AFX; SERPINB6). These proteins might be post-translationally cleaved/processed and a new N-terminal glycine could be revealed and *N*-myristoylated. However, none is known to be post-translationally myristoylated (Appendix G) and none has been reported to have a cleavage site revealing an N-terminal glycine, in a proteolysis database (DegraBase).[237] Immunoprecipitation experiments could be carried out to verify that these proteins are not tagged by YnC12 but instead pulled-down with another NMT substrate.

4.7.3 Lysine side-chain myristoylation

A few examples showing that myristate was not exclusively added to the N-terminal glycine of proteins have been described in the literature. Two proteins, tumour necrosis factor alpha (TNF-alpha) [246] and interleukin 1 alpha[247] were suggested to be side-chain myristoylated on a lysine residue. Recently, the function of this post-translational modification has been explored and was

found to be involved in the regulation of protein secretion.[233] Jiang et *al.* showed that SIRT6, a sirtuin nicotinamide adenine dinucleotide (NAD)-dependent deacetylase enzyme, could hydrolyse the myristoyl moiety on Lys 19 and Lys 20 of TNF-alpha, which regulates the secretion of TNF-alpha from the cell membrane to the intracellular domain.[233] However, little is known about the incorporation of myristate on lysine side-chain residues of proteins. As NMT is thought to transfer myristate to N-terminal glycine of proteins, it is probable that another enzyme is involved in this process.

Any protein labelled with YnC12 but which is neither sensitive to NMT inhibition nor to base/hydroxylamine treatment might potentially incorporate myristate on a side-chain lysine residue. Work is on-going in the Tate group to identify these proteins.

4.8 74 *N*-myristoylated proteins identified with high confidence in HeLa

4.8.1 30 newly identified *N*-myristoylated proteins

The spike-in SILAC inhibitor experiment (Section 4.6) allowed the identification with high confidence of 70 NMT substrates in HeLa cells. An additional four proteins had been identified in Section 4.2.2 thanks to the identification of the YnC12-modified N-terminal peptide with AzKTB: coiled-coil-helix-coiled-coil-helix domain-containing protein 6, mitochondrial (CHCHD6), opioid growth factor receptor-like protein 1 (OGFRL1), plasminogen receptor (KT) (PLGRKT) and the mitochondrial import receptor subunit TOM40B (TOMM40L).

Out of these 74 proteins identified as NMT substrates in the current study, only five had been previously shown to be *N*-myristoylated in their native context in eukaryotes (no overexpression), 26 in a non-native context in eukaryotes and 13 in non-eukaryotic cells (Figure 73). Interestingly, the current study allowed the identification of 30 novel substrates. Out of these 30 substrates, only 7 had been identified previously in chemical proteomics experiments (Appendix F)[173,224]. However, in these previously reported proteomics experiments, the proteins were not directly proven to be either *N*-myristoylated or substrates of NMT.

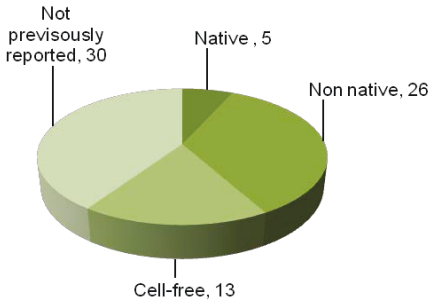

Figure 73. Upper limit of prior evidence for the 74 NMT substrates identified in this study.

4.8.2 *N*-myristoylated proteins function and localisation

NMT substrates have various functions and localisation in-cells, and may eventually lead to cell death or dysfunction when not *N*-myristoylated (Figure 74). Many of these proteins are involved in protein transport (ARFs proteins, CHP, etc.), in redox processes (CYB5R3, NDUFB7, etc.) or are kinases (SRC, LYN, etc.). Several NMT substrates, previously reported as *N*-myristoylated, are involved in protein degradation through the ubiquitin pathway: a subunit of the 26S proteasome (PSMC1), and two E3 ubiquitin ligases (MGRN1 and ZNRF2) are *N*-myristoylated (Appendix H).

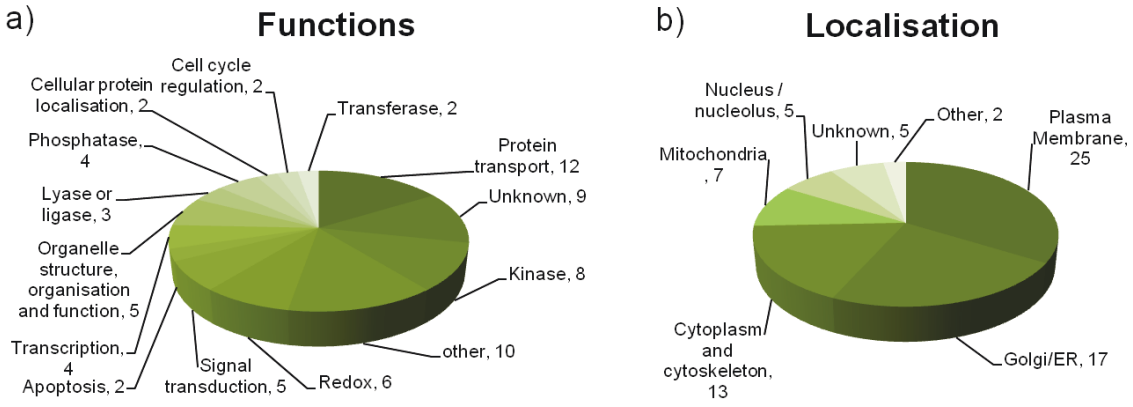

Figure 74. Biological functions (a) and localisation (b) for the 74 NMT substrates identified in this study (GO annotations).

4.8.3 Consensus

Figure 75 displays the consensus sequence for *N*-myristoylation obtained from N-terminus of the 74 proteins identified with high confidence in the current study. This consensus was compared to the consensus described in Section 1.4.2. The latter stated that uncharged residues are preferred in position 3, any residues are allowed in positions 4 and 5, serine is preferred in position 6, but other

small uncharged residues are permitted, and residue is position 7 cannot be proline. The two consensuses are thus highly consistent.

As expected, residues 9-20 were less conserved across the identified NMT substrates and no consensus could be generated. These residues do not bind to the enzyme active site. Residues 8-12 are thought to interact with the enzyme surface while residues in positions 13-18 might act as a hydrophilic linker (Section 1.4.2).

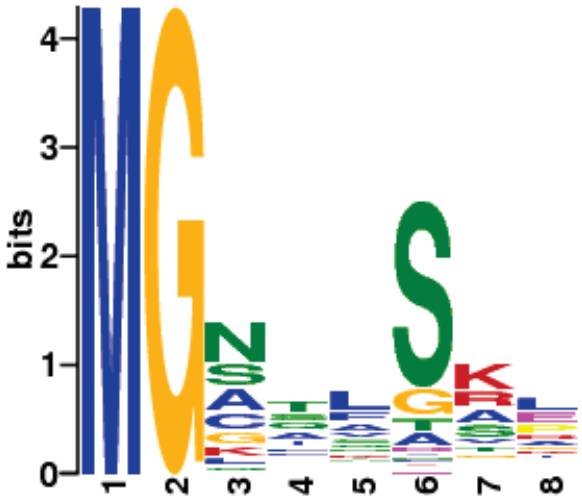

Figure 75. Sequence logo displaying the consensus for *N*-myristoylation. A consensus was generated from the N-terminal 20 amino acids of the NMT substrates identified with high confidence in the current study using MEME.[248] The size of each letter is related to the probability of finding the particular amino acid in that position and the colours correspond to the type of amino acid (hydrophobic (blue), polar (green), acidic (magenta), positively charged (red), His (pink), Gly (orange), Pro (yellow), Tyr (turquoise)).

4.8.4 Significance of the newly identified NMT substrates

In this Section, only newly identified NMT substrates (proteins not previously shown to be *N*-myristoylated in a native, non native of cell free context, Appendix F)) will be discussed.

4.8.4.1 Interaction with membranes

Several new NMT substrates are of particular interest as they were previously shown to interact with membranes but the mechanism for this interaction had not been identified.

Cytochrome c-type heme lyase (**HCCS)** is responsible for the attachment of heme to the apo-cytochrome C and is known to localise in the mitochondrial intermembrane space.[93,249,250] However, the association with the membrane is not well understood and was suggested to be peripheral. [251] In this study, HCCS was found to be *N*-myristoylated and myristate could therefore anchor the protein to the mitochondrial intermembrane.

The mitochondrial amidoxime-reducing component 1, **MARC1**, is responsible for the reduction and activation of *N*-hydroxylated pro-drugs and also takes part in regulation of nitric oxide synthesis.[252] The N-terminus has recently been shown to target MARC1 into the outer mitochondrial membrane.[253] The N-terminus is composed of two domains: a hydrophobic transmembrane helix domain (residues 21-40) and weak N-terminal mitochondrial targeting signal (1-20). The latter was shown to interact weakly with the mitochondria, and this weak interaction could be attributed to myristate, since this protein was detected as *N*-myristoylated in the present study (Section 4.6.3). **MARC2**, the second isoform of the mitochondrial amidoxime-reducing component, is another newly identified NMT substrate. It is also known to target outer mitochondrial membranes, and has similar functions in the cell [253] but its interaction with membranes has been less studied.

LAMTOR1 is a subunit of the Ragulator complex, which is responsible with Rag GTPases for recruiting mTORC1 to lysosomes, where it can be activated. mTORC1 is a signalling complex involved in the MAPK pathway and which triggers cell growth in response to various stimuli.[254] LAMTOR1 has been shown to be responsible for the association of the Ragulator complex to membrane in organelle like vesicles, a process essential for mTORC1 activation.[255] The protein has putative *N*-myristoylation and palmitoylation sites but no experiment had been carried out to show that the protein was *N*-myristoylated. In the present study, LAMTOR1 was shown to be *N*-myristoylated and myristate could direct palmitoylation and attachment to membranes (Section 1.5.3).

Disrupted in renal carcinoma 2 (**DIRC2**) is a lysosomal membrane protein that functions as an electrogenic metabolite transporter.[256] DIRC2 has several transmembrane domains and an N-terminal dileucine motif mediates its lysosomal targeting. It was suggested that *N*-myristoylation might also be involved in lysosomal targeting, but the protein had not been experimentally shown to be *N*-myristoylated.

4.8.4.2 Proteins linked to diseases

Some newly identified substrates are implicated in the progression of diseases.

Battenin (CLN3), when mutated, is a protein responsible for Batten disease, a rare and fatal neurodegenerative disorder.[257] The function of Battenin is not known but the protein has been suggested to be involved in transmembrane transport, lipid homeostasis and neuronal excitability and it was suggested that it could interact with ARF proteins.[258]

Transmembrane protein 106B (**TMEM106B**) has been linked to frontotemporal lobar degeneration (FTLD), a fatal neurodegenerative disease causing presenile dementia.[259] TMEM106B is localised to

late endosomes or lysosomes. In neurons from affected patients, TMEM106B is overexpressed and disrupts the endosomal–lysosomal pathway, resulting in an increased risk of developing FLTD.

It would be interesting to study the role of *N*-myristoylation for these two proteins involved in neurodegenerative disorders.

4.8.4.3 Proteins implicated in cancer

Some proteins have been linked to cancer. While some proteins have an anti-apoptotic effect, others have a tumour suppressor role. Previously reported NMT substrates linked to cancer are discussed in Section 5.4.

Nucleolar protein 3 (NOL3), also known as the apoptosis repressor with CARD or ARC, is an anti-apoptotic protein, [260] has a cardio-protective effect [261] and also plays a key role in pulmonary hypertension.[262] ARC is expressed in many cancer cell lines,[263] and its overexpression is often associated with cancer cell resistance to apoptosis and cancer cell survival. [260,263,264] In clinical cases, low levels of ARC are usually associated with higher patient survival rates in acute myeloid leukemia.[265] ARC inhibits the extrinsic apoptotic pathway in cancer cells via the inhibition of caspase 8,[266] and was also shown to inhibit the intrinsic pathway in p53 deficient human colon cancer cells in the context of hypoxia.[267] Regulation of ARC is not well understood but it has been proposed to be regulated by Ras, a protein which plays a critical role in the development and progression of many cancers.[268] Overexpression of activated N-Ras or H-Ras induced the transcription of ARC in epithelial cancer and ARC degradation was also decreased.

Flotilin-2 (FLOT2) is part of lipid rafts, microdomains of the plasma membrane that have high concentrations of cholesterol and glycosphingolipids.[269] Flotilin-2 was overexpressed in various breast cancer cell lines and breast cancer tissues from several patients.[270] High levels of flotilin-2 were associated with low survival rates. Depletion of flotilin-2 in a mouse breast cancer model resulted in decreased lung metastases.[271]

Plasminogen receptor (KT), **Plg-RKT**, (PLGRKT) has been well studied in macrophages, where it has been shown to regulate cell surface plasminogen activation, cell migration and inflammatory responses.[272] Plasminogen is a protein that can bind to blood clots and is converted to plasmin, a serine-protease capable of dissolving fibrin blood clots. Plg-RKT is a trans-membrane protein and the N-terminus and C-terminus are exposed on the cell surface. It is unclear what could be the role of myristoylation for this protein, but it has been shown to be expressed in a wide range of tissues, including cancerous tissues, where it may have a different function.[272] Plg-RKT has been suggested to have an anti-apoptotic function and inhibit TNFα-induced apoptosis.[272]

Protein **Niban** (FAM129A) positively regulates translation via the modulation of phosphorylation of several proteins involved in translation, including EIF2A, EIF4EBP1 and RPS6KB1.[273] Interestingly, knockdown of Niban increased apoptosis in HeLa cells.[273] Additionally, Niban modulates the ER stress response and Niban overexpression appears to protect cancer cells from genotoxic stress-induced apoptosis via degradation of p53, a protein involved in the regulation of the cell cycle and induction of apoptosis.[274] Niban is expressed in a wide range of cancer tissues.[274]

Niban-like protein 1 (FAM129B), also known as Minerva, was identified using a phosphoproteomic approach as a downstream target/downstream effector of the MAP kinase (Erk1/2) signalling cascade in melanoma cells.[275] Niban-like protein 1 enhances melanoma cell invasion upon its phosphorylation by B-Raf, a protein kinase often mutated in human melanomas. Mutations in B-Raf result in an elevated kinase activity and activation of the MAP kinase pathway. Interestingly, it was proposed that Niban-like protein 1 could enhance cell invasion by suppressing apoptosis.[276] Indeed, repression of apoptosis is crucial to allow cancer cells to replicate and spread. Knockdown of Niban-like protein 1 promoted apoptosis upon apoptosis induction by various reagents. Additionally, the protein was quickly degraded upon apoptosis induction, and its degradation might have an anti-apoptotic function.[275] Niban-like protein 1 has variable localisation in cells: in growing and spreading cells it is mostly cytoplasmic, while in confluent cells it is localised at cell junctions.[276] The mechanism of translocation is unknown but *N*-myristoylation could play a role. It has also been suggested that association of this protein to the plasma membrane might be modulated by C-terminal phosphorylation.[275] Interestingly, Niban-like 1 was also shown to have an effect on cell motility and wound repair.[277]

Coiled-coil-helix-coiled-coil-helix domain-containing protein 6, mitochondrial (CHCHD6) also referred as coiled coil helix cristae morphology 1 or **CHCM1**, is essential for cristae formation in the mitochondria.[278] These cristae are responsible for the inner mitochondrial membrane organisation and are thus vital for the proper function of mitochondria. CHCM1 localises to the mitochondrial inner membrane, and has been suggested to be an oncogene as its overexpression in cancer cells enhances resistance while its down-regulation increased sensitivity to anti-cancer drugs. It has thus been proposed to be a new target for cancer therapeutics.[278] CHCM1 has also been shown to interact with a putative *N*-myristoylated protein (see Appendix F), coiled-coil-helix-coiled-coil-helix domain-containing protein 3, mitochondrial (CHCHD3).[279]

Cytospin-B (gene name SPECC1), also known as NSP5 3a3, is expressed in cancer cells originating from various tissues.[280] It has been proposed as a new target for cancer therapeutics in head and

neck carcinoma, however, agonists of NSP5a3a are required to induce toxicity [280] as its overexpression triggers apoptosis through the TNFR-1 signalling pathway.

4.8.4.4 Other newly identified NMT substrates less studied

NADH dehydrogenase [ubiquinone] 1 alpha subcomplex assembly factor 4 (**NDUFAF4**), is part of a protein complex involved in NADH dehydrogenation and localised at the mitochondria.[281] Another NMT substrate, NADH dehydrogenase [ubiquinone] 1 beta subcomplex subunit 7 (**NDUFB7**), is part of the same protein complex.

Leucine-rich repeat-containing protein 57 (**LRRC57**) is a leucine rich protein with unknown function. Leucine rich domains are usually implicated in protein-protein interactions.[282]

Cell division cycle-associated protein 3, (**CDAC3**) is a F-box-like protein which regulates the cell cycle and especially the entry into mitosis.[283] CDAC3 is involved in E3 ligase complexes that regulate the ubiquitination and degradation of Wee1-like protein kinase (WEE1) at G2/M checkpoint.

RING finger protein 141 (**RNF141**) has a RING finger motif, capable of binding two zinc cations.[284] The function of RNF141 is not known but most RING finger proteins are involved in protein-DNA or protein-protein interactions, or ubiquitin ligases.[284,285]

Golgi reassembly-stacking protein 2 (**GRASP2**) is essential for the structure of the Golgi apparatus.[286] Protein phosphatase 1G (**PPM1G**) has not been well studied in the literature.

Protein-L-isoaspartate O-methyltransferase domain-containing protein 1 (**PCMTD1**), protein FAM49B (**FAM49B**), mitochondrial import receptor subunit TOM40B (**TOMM40L**) and Opioid growth factor receptor-like protein 1 (**OGFRL1**) have unknown functions.

MARCKS-related protein (**MARCKSL1**), cAMP-dependent protein kinase catalytic subunit beta (**PRKACB**) and **ARF3**, **ARF4**, **ARF5** were thought to be *N*-myristoylated but no strong evidence could be found in the literature. These two proteins have been well studied in the literature. MARCKSL1 is involved in various signalling events, for instance cell migration and adhesion [287] while ARF3 plays a role in protein transport.[288]

4.8.5 Comments on previously known and putative NMT substrates not identified in the present study

68 proteins expressed in HeLa cells had previously been experimentally shown to be *N*-myristoylated with varying levels of confidence (Section 4.6.2 and Appendix F)). 18 of these proteins were detected with high confidence in the spike-in SILAC experiment (Section 4.6.3.2) or thanks to the identification of the YnC12-modified N-terminal peptide with AzKTB (Section 4.2.2).

There could be several explanations:

- ✓ Proteins could have been mis-assigned as NMT substrates, as for example serine incorporator-1 (SERINC1) (Section 4.7.1).
- ✓ Some proteins were identified with low confidence in the spike-in SILAC inhibitor experiment: mitochondrial peptide methionine sulfoxide reductase (MSRA), Formin-like protein 3 (FMNL3), RING finger protein 11 (RNF11) and Zinc finger ZZ-type and EF-hand domain-containing protein 1 (ZZEF1).
- ✓ Finally, some previously reported *N*-myristoylated proteins might be below the detection limit of the methods discussed in the current Chapter as they might be poorly abundant in HeLa cells.

4.9 Conclusions

This Chapter has discussed the use of the YnC12 probe combined with several chemical proteomics approaches to identify previously reported and novel *N*-myristoylated proteins in HeLa cells at their native abundance (i.e. without the need for non-native overexpression). Non quantitative (gel-free and gel-based approaches) and label free quantification proteomics experiments were found to be less reliable than quantitative approaches as they gave more false-positive protein hits.

A spike-in SILAC approach combining the YnC12 probe and a highly specific NMT inhibitor characterised in Chapter 3 (IMP366) was developed and found to be a powerful method to identify known/putative and novel NMT substrates. This method greatly improved the accuracy and sensitivity of YnC12–based proteomics, resulting in the detection of 70 NMT substrates in one experiment. Four additional substrates were identified with the capture reagent AzKTB.

Only co-translational NMT substrates have been studied in this Chapter. It would be interesting to apply the same spike-in SILAC approach to identify post-translationally myristoylated proteins in the context of apoptosis (Sections 1.5.2 and 2.4).

Mass spectrometry-based proteomics is a valuable tool to study *N*-myristoylated protein, but experiments can sometimes fail. During the process of identification of the 74 NMT substrates in HeLa cells, several proteomics experiments (not reported here) failed to identify a similar number of proteins. For example, one problem encountered was due to an issue during trypsin digest. A triethylammonium bicarbonate solution (pH 8.5), prepared from a concentrated stock solution, was used for washing the beads after the enrichment. However, an extremely low number of proteins were identified in this experiment, probably due to the change in pH of the triethylammonium bicarbonate stock solution on storage, resulting in an ineffective digest. The optimal pH of trypsin is pH8.[289] Triethylammonium bicarbonate solution was thus replaced by freshly prepared ammonium bicarbonate pH 7.8. Quality of the data obtained for a proteomics experiment greatly depends on the protocol used for the sample preparation and the proteomics platform. Indeed, optimisation of the LC-gradient and sensitivity of the mass detector can have a massive impact on protein coverage.

Chapter 5 NMT inhibition: mode of action studies

In Chapter 4, 74 NMT substrates were identified with high confidence by chemical proteomics. These substrates have various functions in cells and *N*-myristoylation has been shown to be essential for the localisation and function of some, such as c-SRC.[104] These results suggested that *N*-myristoylation is critical for cells and NMT inhibition might cause toxicity.

In Chapter 3, a potent HsNMT inhibitor was characterised, referred to in the current study as IMP366. This compound was shown to cause dose-dependent inhibition of NMT in HeLa cells. The compound acted exclusively on-target up to 10 μM and was shown to be toxic to HeLa cells after 3 days. Interestingly, the cells were not completely killed after 3 days. A plateau of residual metabolic activity of 20-30% could be observed.

In the current Chapter, experiments are described that shed light on the consequences of NMT inhibition in HeLa cells. Longer inhibition experiments (up to 7 days) were carried out in cells to show that cancer cells can be killed completely with this strategy. The mode of action of NMT inhibitor IMP366 is also addressed in HeLa cells.

5.1 Cell cycle arrest and cell death

5.1.1 HeLa cells

5.1.1.1 Cell cytotoxicity assays

Cell metabolic assays carried out in Chapter 3 showed that IMP366 was not toxic to HeLa cells after 1 day but showed a reduction of metabolic activity after 3 days. Assays were also performed after 2 and 7 days to evaluate the toxicity of the inhibitor after different time points (Figure 76a and b).

a)

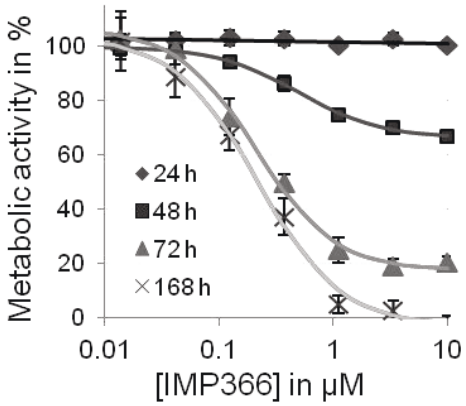

b)

	EC_{50} (nM)	Slope EC_{50}	Residual metabolic activity at 10 µM (%)
1 day	>10 ±	N/A	95
2 days	498 ±32	1.2	66
3 days	211 ±30	1.3	18
7 days	217 ±34	1	0

c)

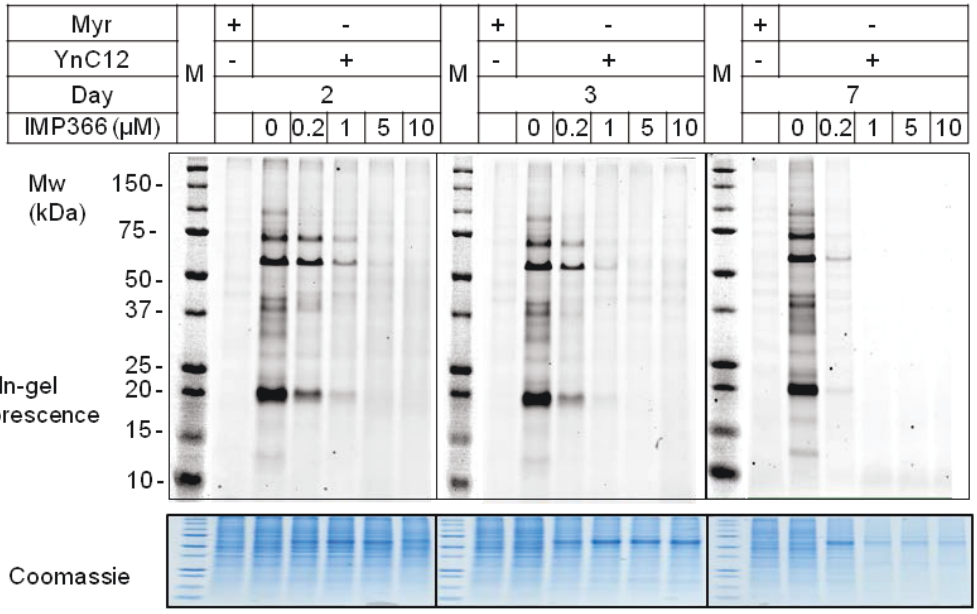

Figure 76. IMP366 inhibition in HeLa cells. For the 7 day experiment, the culture media was replaced after 3 days with fresh media containing the inhibitor. **a)** Cell cytotoxicity assay (MTS) carried out for 1, 2, 3 and 7 days. The error bars correspond to the standard deviation between replicates (n= 6 replicates). **b)** EC_{50} values and parameters of the EC_{50} curves determined with GraFit. **c)** YnC12 labelling experiment to assess NMT inhibition after 2, 3, 7, days. YnC12 was added to the cells 6 h before the end of the experiment. Loading on the gel was normalised to the protein concentration and the gel was stained with Coomassie as a loading control.

After 2 days of inhibition, a decrease of metabolic activity could be observed for cells treated with >0.1 µM IMP366. As seen after 3 days of treatment, a plateau of metabolic activity was observed, but the remaining metabolic activity was higher (66%). Interestingly, the EC_{50} values were comparable between 2, 3, and 7 days. The EC_{50} value after 2 days was slightly higher but the accuracy of this measurement was limited by the small range of the assay. The assays carried out for 7 days showed for the first time that selective NMT inhibition could completely kill HeLa cells.

The inhibitor was shown to be stable in aqueous media for 3 days (Section 3.3.3.6) and NMT should thus still be inhibited after several days. To check that the inhibitor was not metabolically hydrolysed in cells, an YnC12-tagging experiment was carried out during the final 6 hours of the viability assay (Figure 76c). This experiment confirmed that HsNMT was still inhibited dose-dependently in cells after 2, 3, and 7 days. The Coomassie had a different pattern for the cells treated with the highest concentrations of inhibitor, probably due to increasing levels of cell death. Upon NMT inhibition with >1 µM of IMP366, cells started to detach from the plate after 2 days. However, it is important to note that cells in suspension where always recovered and included in all the following experiments described in this Chapter.

We hypothesised that the cells might stop dividing and then start to die after 2 days, paralleling the decrease in metabolic activity (Figure 76a and b).

A simple experiment was performed to compare the number of cells in a plate treated with IMP366 (1 µM) for 1, 2, 3 days or with DMSO as a control (Figure 77). Cells were counted with a hemocytometer. After 1 day of treatment, the same number of cells was present in both samples (control and inhibited cells), but after 2 and 3 days there was a noticeable decrease of the number of cells compared to control, suggesting that the cells stopped dividing and/or died. A cell cycle analysis was required to understand if the hypothesis was correct; observation of cell viability with trypan blue proved difficult due to limited colour differentiation between viable and non-viable cells, and therefore alternative methods were employed to assess cell viability after several days of treatment with the NMT inhibitor (Section 5.1.1.2.2 and Section 5.2.2.2).

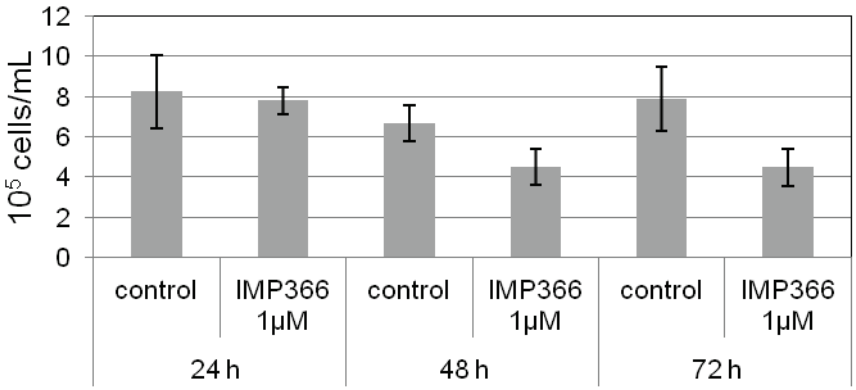

Figure 77. Cell counts. HeLa cells were treated with inhibitor IMP366 for 24, 48, 72 h or with DMSO as a control. Cells were harvested and counted using a hemocytometer. The errors bars correspond to the standard deviation of three biological replicates. Different amount of cells were seeded for the 24, 48, 72 h, aiming to reach 80-90% confluence in the control. The number of cells can thus not be compared between different time points.

Pictures of the cells were taken after 0, 1, 3, 7 days (Figure 78). After 1 day, cells treated with 1 µM of the inhibitor looked the same as at the beginning of the experiment. After 3 days, many rounded-up cells were present. After 7 days, cells were mostly rounded-up and appeared to be dead.

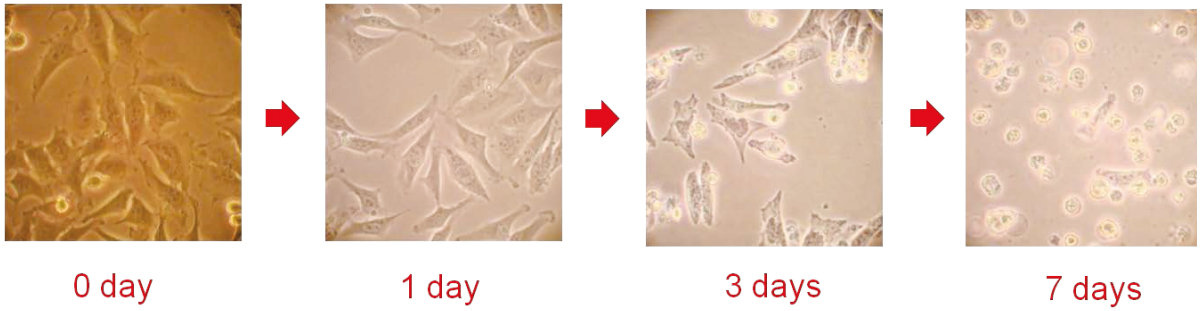

Figure 78. Pictures of the cells after 0, 1, 3, or 7 day treatment with IMP366 (1 µM).

5.1.1.2 Cell cycle analysis

5.1.1.2.1 Introduction to flow cytometry and cell cycle analysis

Flow cytometry is a process for simultaneously measuring and then analysing several physical characteristics of single particles, such as cells, as they flow through a beam of light in a fluid stream. Multiple properties can be measured thanks to the use of several lasers: the relative fluorescence intensity, the particle's relative size, granularity or internal complexity.[290]

Flow cytometry can be used to carry out cell cycle analysis experiments.[290] Cells are first fixed, killing the cell but leaving their shape and structure intact; however, the cellular membrane becomes permeable and reagents can be added to stain specific cell components. Propidium iodide (PI), a fluorescent compound which can intercalate into DNA, is commonly used to study the cell cycle (Figure 79a). Samples are usually supplemented with RNAse to digest RNA and ensure that only DNA is stained; the fluorescence intensity observed for a single cell is thus proportional to the amount of DNA. During the cell cycle, cells go through phases known as G1, S, G2 and M (mitosis) (Figure 79b). The amount of DNA is indicative of the cell cycle phase: in G1, cells have 2 copies of DNA, in S phase between 2 and 4 copies and in G2, just before mitosis, 4 copies. When cells are stained with PI, the fluorescence intensity of each individual cell can be measured by flow cytometry and the number of cells plotted against the relative fluorescence intensity (Figure 79c, non-treated HeLa cells). Two peaks are observed in Figure 79c, and the relative fluorescence intensity of the second peak (ca. 100K RFU) is 2-fold higher than the fluorescence of the first peak (ca. 50K). The second peak corresponds to cells with 4 copies of their DNA (G2 phase, coloured in blue) while the first peak corresponds to cells with only 2 copies of their DNA (G1 phase, coloured in green), and between these peaks are cells in S phase (coloured in yellow). If cells have relative fluorescence intensity lower than cells in G1, they would correspond to a so-called subG0/G1 phase, and would be the apoptotic or dead cells present in the sample. The area under the curve can be integrated using FlowJo software to determine the relative proportion of cells in each state.

For cell cycle analysis it is essential to measure the fluorescence intensity of single cells only, and thus samples are usually filtered prior to analysis to remove aggregates; however, this is often insufficient to generate a homogenous sample of single cells. The different physical characteristics of particles are therefore used to create cut off limits (gates) and define single particles: two voltage pulses are measured, the side-scatter pulse (SSC) which is related to the internal complexity of the particle, such as the shape of the nucleus, and the forward-scatter pulse (FSC), which depends on the cell volume. Each pulse has three characteristics: the height which measures the maximum fluorescence intensity, the width which corresponds to the transit time and the area which relates to the total fluorescence of the particle. Single cells have similar physical properties and gates can be created to select these cells for the cell cycle analysis (Section 5.1.1.2.2).

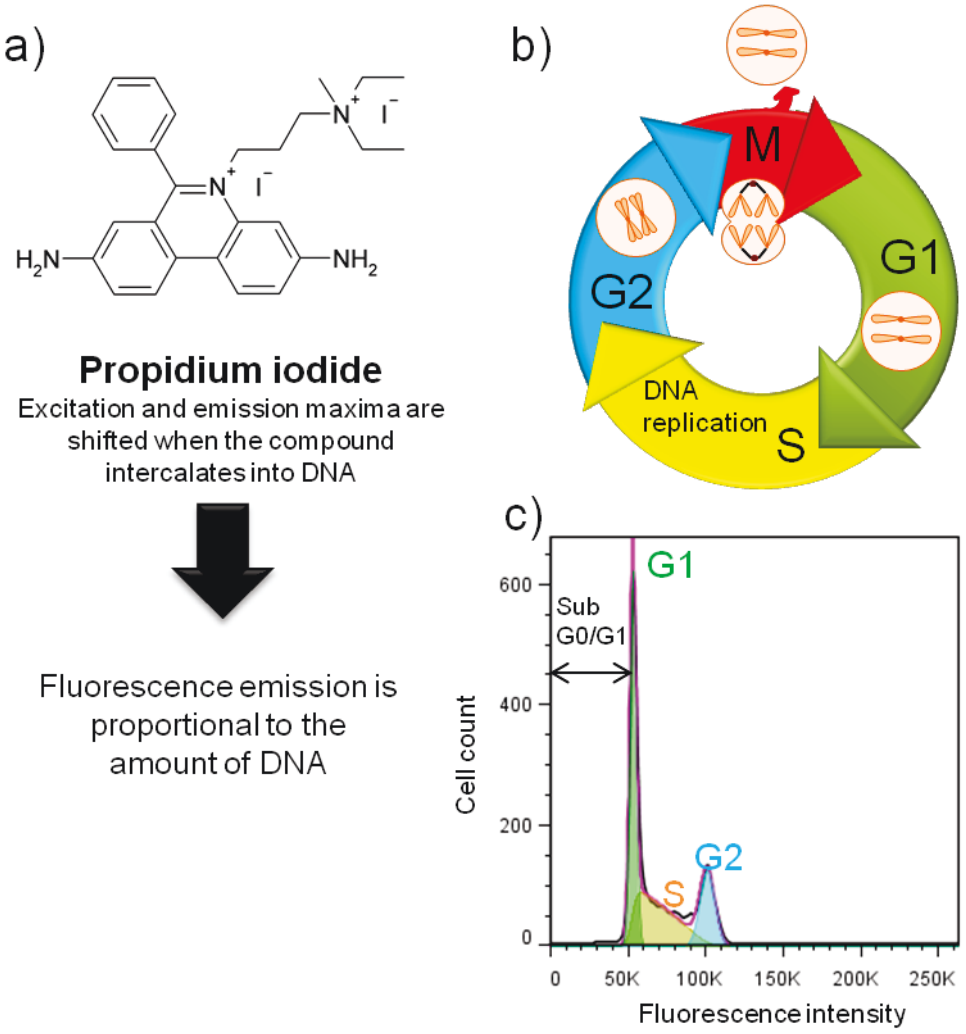

Figure 79. Principle of the cell cycle analysis using propidium Iodide (PI) and flow cytometry. a) Structure of PI. **b)** Scheme of the cell cycle showing the different phases. **c)** Typical plot obtained with FlowJo for a cell cycle analysis experiment, obtained with non-treated HeLa cells. The number of cells is plotted against the fluorescence intensity (RFU). The area under the curve corresponding to each phase of the cell cycle and can be integrated using FlowJo.

5.1.1.2.2 Cell cycle analysis after NMT inhibition

HeLa cells were treated with various concentrations of inhibitor IMP366 and with DMSO as a control for 1, 3 or 7 days and subjected to cell cycle analysis; Figure 80 shows examples of the plots obtained at 1 µM IMP366. Single cells were selected by creating gates as mentioned above (Figure 80 a and b and Section 5.1.1.2.1) and the number of single cells plotted against fluorescence intensity for different treatment conditions (Figure 80 c-f). After 3 days of treatment with 1 µM IMP366, a "shoulder" (boxed in red) can be observed on the G1 peak, characteristic of apoptotic cells. After a 7 day treatment, a substantial population of dead cells (boxed in red) can be observed. These dead and apoptotic cells correspond to the subG0/G1 phase.

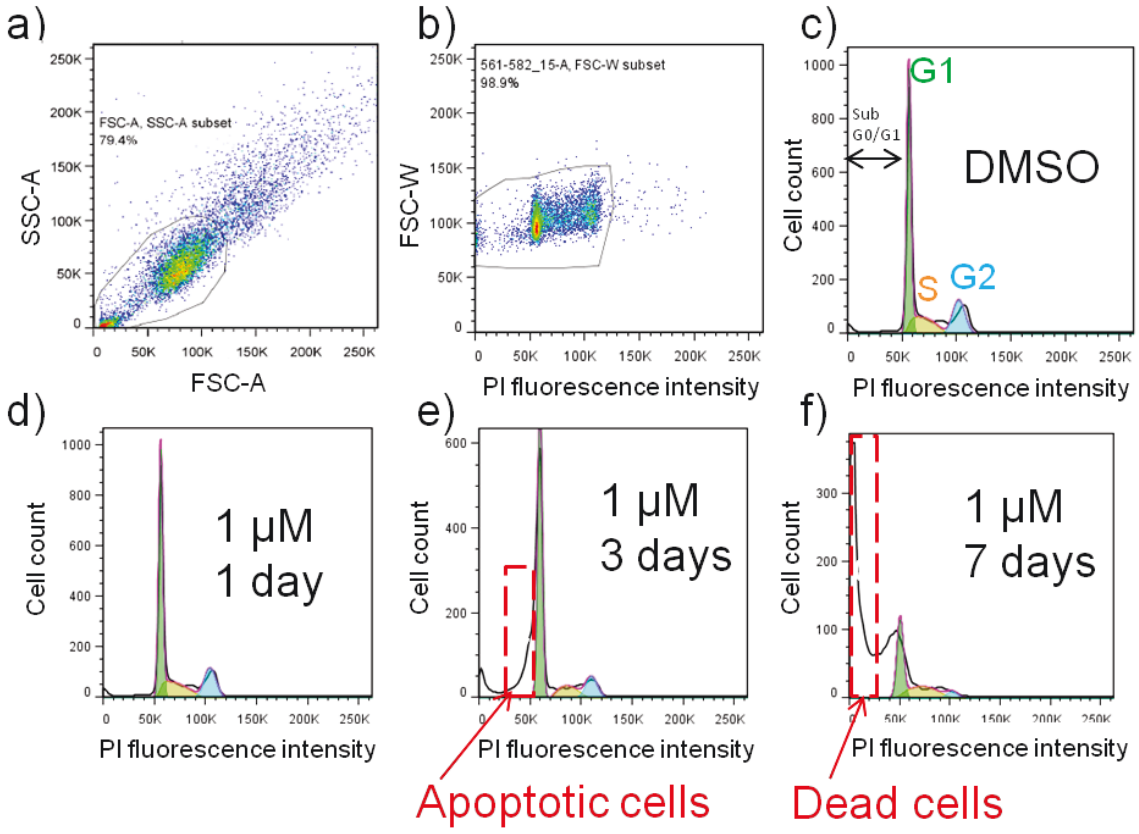

Figure 80. Typical plots obtained for a cell cycle analysis experiment. a-c) were obtained from the same sample (cells treated with DMSO as a control). **a)** and **b)** show how the data were gated using different parameters (FSC-A, FSC-A, FSC-W and PI fluorescence intensity) to select single cells. Particles (single cells and cell aggregates) are shown as dots. The colour indicates the density of particles on the scatter plots (red = high density, blue = low density). Single cell population can be selected (as circled in black) in **a)** and plotted in **b)**. **b)** Allows to further discriminate cell doublets. **c)** Shows the plot obtained after gating and doublet discrimination. **d-f)** Typical plots obtained after gating (the same gates as shown in a) and b) were used across all the samples). Cells were treated for **d)** 1 day, **e)** 3 days or **f)** 7 days with IMP366 (1 µM). The number of cells was plotted against the fluorescence intensity. Apoptotic cells can be seen after 3 days (circled in red) and an significant population of dead cells can be observed after 7 days (boxed in red). Cell cycle analysis was carried out on a BD LSRFortessa analyser and the data were analysed with FlowJo. SSC-A, FSC-A, FSC-W and PI fluorescence intensity are in RFU.

Area under the curve was integrated using FlowJo (Figure 81a). 0.2 µM corresponds to the EC_{50} value measured by MTS assay, whilst 1, 5 and 10 µM correspond to concentrations that inhibit >90% NMT in cells (Section 3.3.1), and lead to the plateau of residual MTS signal observed after 3 days (Figure 76). At 5 and 10 µM, NMT is completely inhibited in cells (Figure 76 and Section 3.3.1).

After 1 day, there were no more dead cells in samples treated with IMP366 than in the control (DMSO) (Figure 81). However, in samples treated with 1, 5, or 10 µM of the inhibitor, there is a small G1 accumulation. After 3 days, there is a substantial population of dead/apoptotic cells in the samples treated with >1 µM of inhibitor. In theory, the same partition of cells through the cell cycle

should be observed for samples treated with 5 and 10 µM inhibitor, as NMT is completely inhibited in both samples. However, it appears that more dead cells are present in the 10 µM sample, suggesting that there might be off-target effects of the inhibitor at this concentration or that the in-gel fluorescence assay is not sensitive enough. These results correlate well with the cell metabolic data (Figure 76).

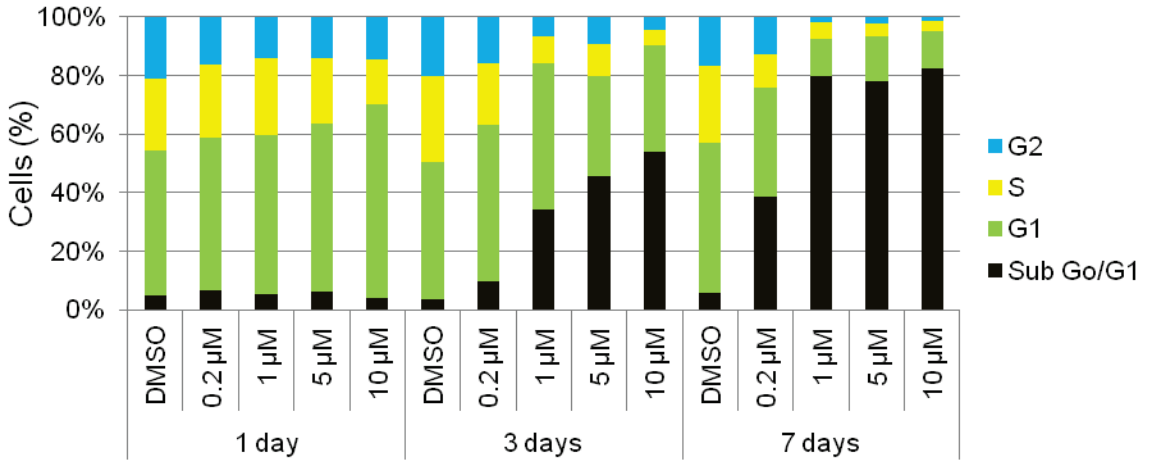

Figure 81. HeLa cells treated with IMP366 for 1, 3, 7 days. For the 7 day experiment, the culture media was replaced after 3 days with fresh media containing the inhibitor. Cell cycle analysis showing the distribution of cells across subG0/G1 (dead + apoptotic cells), G1, S and G2 phases. Standard deviation (SD, n= 3 biological replicates) was <10%. The data were processed using the Dean-Jett-Fox integration option in FlowJo.

After 7 days of inhibition, cells were mostly dead/apoptotic (subG0/G1) in the samples treated with >1 µM of inhibitor. However, the integration of the curve obtained when the number of cells is plotted against relative fluorescence intensity is prone to error during high levels of cell death due to the overlap with G1 cells, (Figure 80f) and cells dead for more than 4 days are likely to be degraded into small particles that lie outside the gates used for the experiment (Figure 80 a and b). The number of dead/apoptotic cells is therefore likely to be significantly higher than measured here, as shown by the MTS assay since there was no viable cells left after 7 days in samples treated with >5 µM of inhibitor (Figure 76). Cells treated with 0.2 µM of inhibitor are not all dead after 7 days and this result correlates well with the MTS assay after 7 days (Figure 76). These findings suggest that upon NMT inhibition cells undergo a G1 arrest followed by cell death, possibly through apoptosis (Section 5.2). NMT inhibition also appears to have a relatively slow onset of cytotoxicity, and this may be due to the time required to turn over existing *N*-myristoylated proteins in cells. The turnover of NMT substrates is studied further in Section 5.3.

5.1.1.3 Regeneration of *N*-myristoylated proteins following NMT inhibition

After 1 day inhibition, no dead cells were observed in the samples treated with a concentration sufficient to fully inhibit NMT in cells (Section 5.1.1.2.2). To test whether cells can regenerate their complement of *N*-myristoylated proteins, cells were treated with inhibitor IMP366 (1 µM) or with DMSO as a control for 24 h (Figure 82a). Cells were then washed three times with PBS buffer and fresh media containing YnC12 was added to label NMT substrates. Interestingly, cells previously treated with the inhibitor or DMSO had similar labelling patterns and intensities, across all recovery time points. After 24 h inhibition, cells appeared to recover from inhibition and this result correlates well with the apparent lack of cytotoxicity after 1 day (Figure 76).

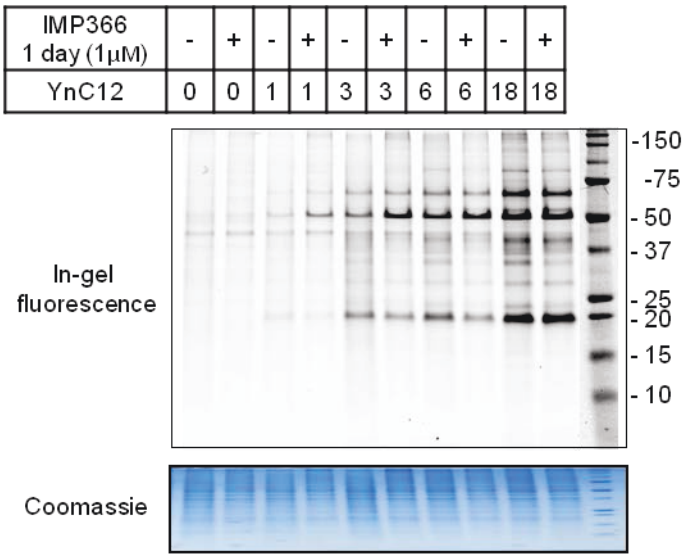

Figure 82. Recovery from inhibition. Cells were treated for 1 day with IMP366 (1 µM) or DMSO, washed with PBS (3x) and allowed to recover in fresh culture media supplemented with YnC12 (20 µM) for several hours.

5.1.2 Other cell lines

Similar experiments as described in Section 5.1.1 were performed in cancer cell lines originating from different tissues.

5.1.2.1 Cell cytotoxicity assays

MTS assays were carried out to study cytotoxicity of IMP366 in various cancer cell lines: MDA-MB-231 (breast cancer), HCT-116 (colon), MCF-7 (Breast), HepG2 (liver). Hek293, an immortalised human embryonic kidney cell line was also studied (Figure 83).

a)

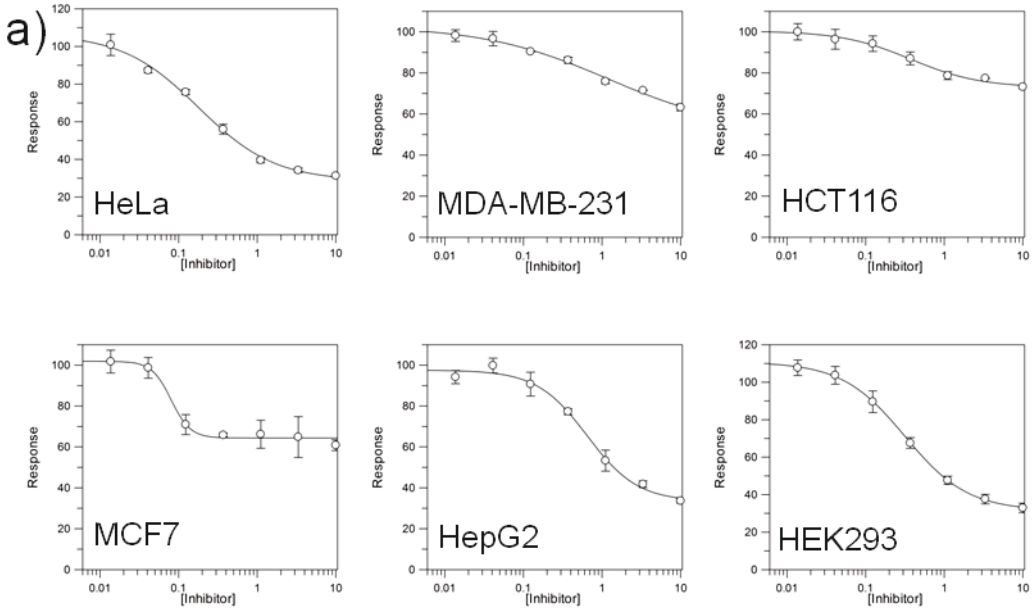

b)

	EC_{50} (nM)	Slope EC_{50}	Residual metabolic activity at 10 µM (%)
HeLa	178 ±37	0.89	29
MDA-MB-231	1200 ±1026	0.54	51
HCT116	376 ±108	0.98	73
MCF-7	80 ±13	3.5	64
HepG2	647 ± 113	1.4	33
Hek293	316 ± 11	1.09	31

Figure 83. Cytotoxicity (MTS assay) in various cell lines treated with IMP366. a) Response (% metabolic activity) was plotted against inhibitor concentration for the 6 cell lines tested. Data were fitted to an IC_{50} function in GraFit, error bars represent standard deviation (n = 3 biological replicates). **b)** EC_{50} values and parameters of the EC_{50} fit are indicated for the 6 cell lines tested. SD = standard deviation.

A similar pattern was obtained for HeLa, HepG2 and Hek293 cells. MDA-MB-231 and HCT-116 were not as strongly affected by NMT inhibition, and had residual metabolic activities of 51% and 73% respectively. MCF-7 also had a different pattern with a low EC_{50} value and a plateau of metabolic activity at 64%. It was decided to use MDA-MB-231, MCF-7 and HCT-116 for further investigations.

Cells were counted after 3 days on inhibition with IMP366 (1 µM) (Figure 84). A decrease in the number of cells was observed compared to the control for the three cell lines tested, suggesting that the cells, like HeLa cells (Figure 77), stopped dividing or died upon IMP366 treatment.

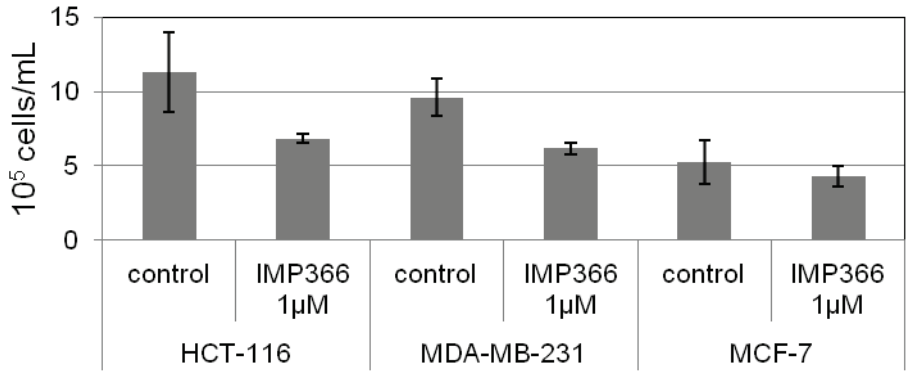

Figure 84. Cell counts after 3 day treatment with IMP366. HCT-116, MDA-MB-231 and MCF-7 were treated with inhibitor IMP366 for 72 h or with DMSO as a control. Cells were harvested and counted using a hemocytometer. The errors bars correspond to the standard deviation of three biological replicates.

5.1.2.2 Flow cytometry

Cell cycle analysis experiments were carried out in MDA-MB-231 to establish if a G1 accumulation could also be observed (Figure 86a). The cell cycle analysis was carried out after 1 and 3 day inhibition with various concentrations of IMP366.

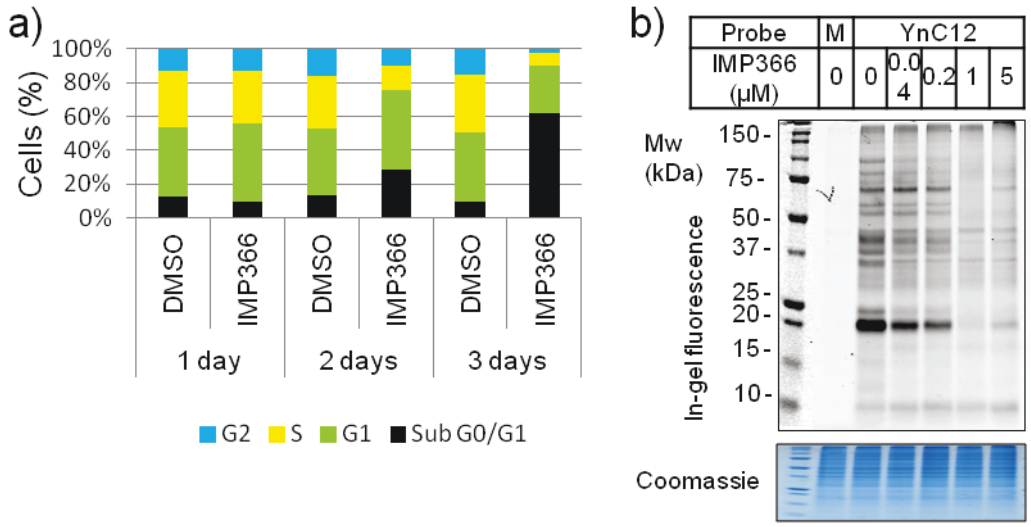

Figure 85. Effects of NMT inhibition on MDA-MB-231 cells. Cells were treated for 1 or 3 days with IMP366 or treated with DMSO as a control. M = Myr**. a)** Cell cycle analysis. SD <10%. **b)** YnC12 tagging experiment. Cells were inhibited for 24 h and Ync12 was added 6 h before the end of the experiment. The background on the gel was relatively high and samples were base-treated (0.2 M NaOH, 1 h) to determine whether the background corresponded to the incorporation of YnC12 into *S*-palmitoylated proteins**. c)** Pictures of the cells treated with DMSO or IMP366 (1 µM) after 3 days.

NMT inhibition in MDA-MB-231 resulted in a similar partition of the cells through the cell cycle as HeLa cells, and cells appeared to accumulate in G1 before dying. A YnC12-tagging experiment was also carried out after 3 days to check that the concentrations required to inhibit NMT in MDA-MB-231 were similar to the ones required in HeLa (Figure 85b).

Interestingly, MDA-MB-231 cells seemed to round and detached from the plate after 72 h treatment with 1 μM of inhibitor (data not shown). These cells were at first thought to be dead, but the cell cycle analysis showed that less than 30% of cells where in subG0/G1 in the sample, suggesting that the cells in suspension were not dead. Some NMT substrates, such as ARF6, are known to be necessary for cell adhesion and NMT inhibition might lead to a detachment of the cells when these substrates are not *N*-myristoylated.[288] However, it has been suggested that some cells can undergo apoptosis when they are in suspension[291,291] and there is clearly not a simple relationship between NMT inhibition and cell death in this cell line. The detachment of cells would make studies of NMT inhibition more difficult in MDA-MB-231.

Similar experiments were carried out with HCT-116 and MCF-7 cells (Figure 86). Cells were treated for 1, 2 or 3 days with only one concentration of IMP366 (1 μM). Similarly to HeLa and MDA-MB-231, cells underwent a G1 accumulation after 1-2 days, followed by an increase in the number of dead cells after 3 days. The appearance of the cells changed after 2 days of treatment. Cells seemed to spread less on the plate but were instead growing in clusters (data not shown). YnC12 tagging experiments confirmed NMT inhibition was maintain from up to 3 days (data not shown).

These results suggest that NMT inhibition might have a similar effect (G1 accumulation and increasing cell death over time) in a range of cancer cell lines. However, some cells appeared to be more sensitive than others to NMT inhibition (Figure 83). The sensitivity might be dependent on the NMT substrates expressed in these cell lines, the balance between NMT levels/activity, NMT substrate levels, and the particular importance of certain substrates to the specific cell line.

For the four cancer cell lines studied, all the cell cycle plots after 3 day inhibition had a characteristic shoulder on the G1 peak as observed in Figure 80e, suggesting cell death by apoptosis. Experiments are described in Section 5.2 to assess this observation.

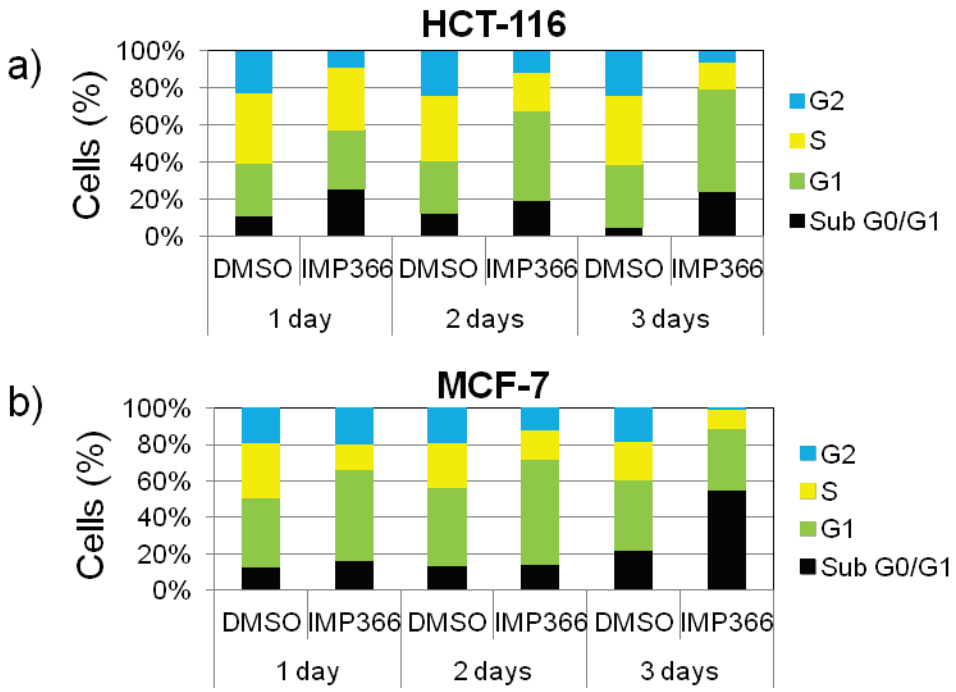

Figure 86. Cell cycle analysis of HCT-116 (a) and MCF-7 (b) treated with IMP366. The error bars represent the standard deviation from 3 biological replicates. The data were processed using the Dean-Jett-Fox integration option in FlowJo.

5.2 Apoptosis

5.2.1 Introduction to apoptosis

Apoptosis, also known as programmed cell death, corresponds to a cascade of events in cells leading to cell death.[292] Apoptosis plays key roles in the early development of an organism, cellular responses to nutrient deprivation and diseases. Healthy cells can commit suicide when they are no longer needed by activating the apoptosis pathway, and apoptosis can also be triggered in cancer cells by many therapeutically relevant agents.[292]

Although the detailed mechanisms of apoptosis can be extremely complex and is not fully understood, programmed cell death is generally triggered through two main pathways:[292] the intrinsic pathway, also referred as the mitochondrial pathway, and the extrinsic pathway, also known as the death receptor pathway; there is some crosstalk between these pathways. The extrinsic pathway usually involves the interaction of a ligand, such as TRAIL (TNF-related apoptosis-inducing ligand), with death receptors, that causes activation of initiator caspase 8, followed by the activation of the execution pathway. The intrinsic pathway can be activated by several reagents or conditions such as radiation, hypoxia or DNA damaging agents. A cascade of signalling events results

in the activation of initiator caspase 9, followed by initiation of the execution pathway. A third pathway, known as the perforin/granzyme pathway, is triggered by T-cells.[292]

Apoptotic pathways are complex and can differ from one cell line to another. Each of the three pathways mentioned above result in the initiation of the executive pathway, which is mediated through cleavage and activation of caspase 3. This has several consequences in the cell, including degradation of cellular proteins, DNA fragmentation, development of apoptotic bodies and expression of proteins and lipids on the outer cellular membrane allowing phagocytes to recognise and degrade the apoptotic cell.

Several characteristics of apoptotic cells allow their detection by analytical methods.[292]

- ✓ Detection of caspase activation or cleaved substrates can be observed by fluorescence assays or Western Blot analysis.
- ✓ Mitochondrial alterations have multiple effects, such as the release of cytochrome C from mitochondria. This change is observed only when the intrinsic pathway has been activated. Cytochrome C release can be visualised by several techniques, including western blot analysis.
- ✓ Membrane alterations result in the redistribution of ligands such as phosphatidylserine to the outer surface of cell membranes. This ligand can be detected with fluorescently labelled Annexin-V by fluorescent microscopy or flow cytometry.
- ✓ DNA fragmentation can be studied using the TUNEL (Terminal dUTP Nick End-Labelling) assay or DNA separation techniques.
- ✓ Morphological changes characteristic of apopotosis (membrane blebbing, electron dense nucleus, etc.) can be observed for late-stage apoptotic cells using microscopy.

It is important to note that cell death can also occur via other mechanisms, including necrosis [293] and autophagy.[293] Necrosis is usually caused by unexpected and accidental cell damage, but many characteristics of apoptosis and necrosis overlap and multiple analyses must be carried out to distinguish between them.[292] Autophagy has been suggested as another mechanism of programmed cell death, and involves degradation of cellular components through lysosomes.[293] Low levels of autophagy are vital in cells to regulate protein and organelle turnover (Section 5.3.1), but high levels lead to cell death. Other mechanisms of cell death, such as mitotic catastrophe, have been reported but are controversial.[294]

5.2.2 Detection of caspase activation or cleaved substrates by Western blotting

5.2.2.1 HeLa cells treated with staurosporine

As explained in Section 5.2.1, apoptosis can be detected by observing the cleavage of caspases by Western blot analysis. Cleaved caspases become activated and allow the progression of apoptosis to the next step of the cascade pathway. Activated caspases can cleave proteins, such as BID or PARP.

To establish a positive control for apoptosis, staurosporine (STS) was employed (Section 2.4). STS binds to the ATP-binding site of many kinases in cells, blocking phosphate transfer and inducing apoptosis, probably through caspase 3 activation.[295] 4 h and 8 h after the addition of STS (1 μM) to HeLa cells, caspases 3 and 8 were cleaved (Figure 87). BID, a protein involved in the intrinsic pathway, and PARP, a late marker of apoptosis, were both cleaved.

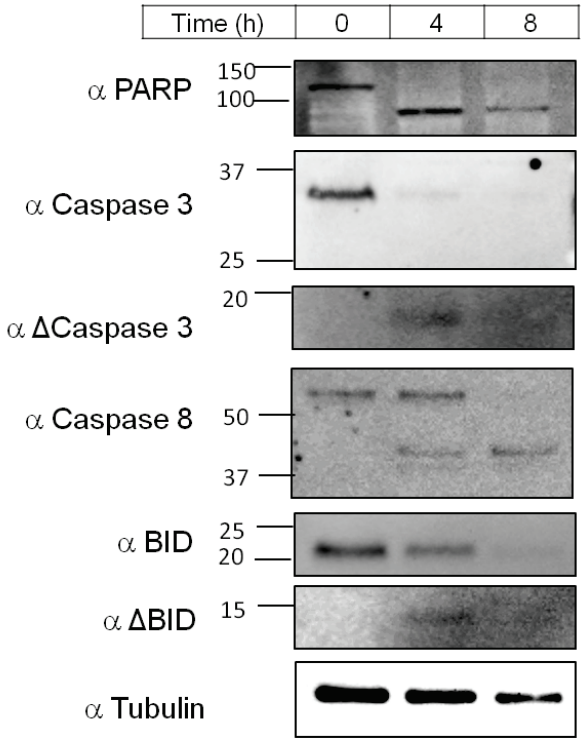

Figure 87. Western blot analysis showing the induction of apoptosis in HeLa via STS treatment. Cells were treated with STS (1μM) for 0, 4 or 8 h. Protein loading on the gel was normalised to the protein concentration and Tubulin was used as a loading control.

Tubulin was used as a loading control but the levels of tubulin decreased after 8 h. The protein loading on the Western blot was based on the total protein concentration, as determined with the DC™ protein assay (Bio-Rad). Since proteins are progressively degraded it is difficult to find a suitable loading control to study apoptotic cells.

HsNMT1 and HsNMT2 were previously shown to be cleaved during apoptosis in an extensive study of proteolysis in the apoptotic proteome by mass-spectrometry based proteomics in Jurkat T-cells.[91] Here it was found that HsNMT1 was unambiguously cleaved in HeLa cells after 4 h and a 50 kDa fragment was released (Figure 88). HsNMT2 was also cleaved upon apoptosis induction, but Western blot analysis proved to be difficult with the HsNMT2 antibody available during this PhD project. Several antibodies were tested by Ute Brassat (Tate group, Imperial College London), but none gave a selective and strong signal in chemiluminescence.

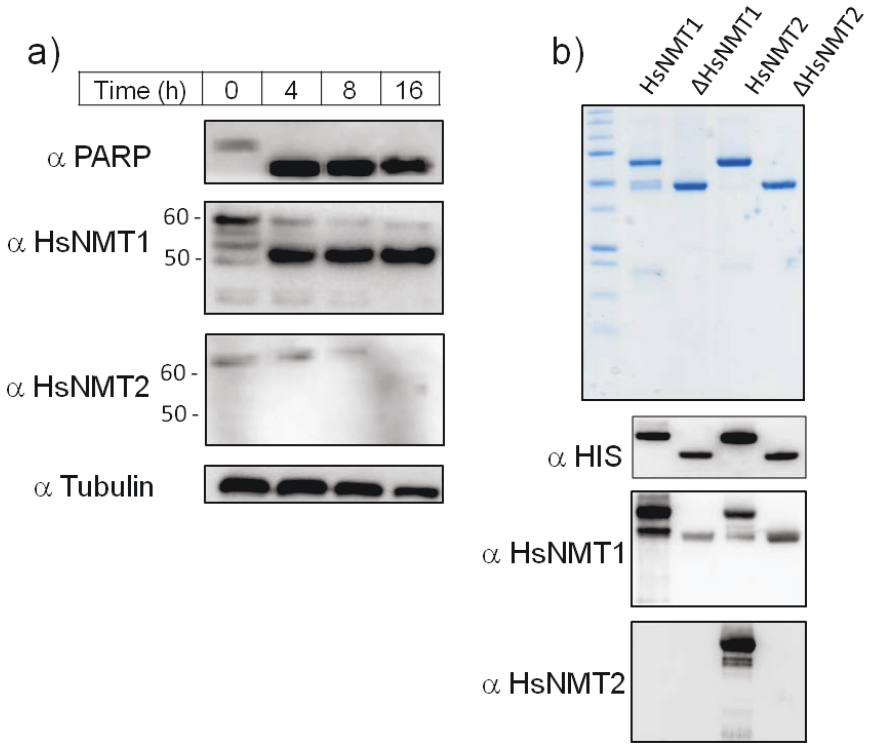

Figure 88. NMT cleavage during apoptosis. a) HeLa cells were treated with STS for 0, 4, 8 or 16 h and a Western Blot analysis was carried out. PARP was used as a control for induction of apoptosis. Loading on the gel was normalised to the protein concentration and tubulin was used as a loading control. **b)** Western blot analysis of the recombinant HsNMT enzymes: full length HsNMT1 and HsNMT2 and amino-terminal truncated HsNMT1 and HsNMT2 (ΔHsNMT). An anti-His_6 western blot was used to confirm that the enzyme had a His-tag at the C-terminus.

The HsNMT1 and HsNMT2 antibodies were tested against the four recombinant HsNMT enzymes available: the full length HsNMT1/2 and the HsNMT1/2 truncated at the N-terminus (Section 2.2.2). The HsNMT1 antibody recognised full and short length HsNMT1 as well as HsNMT2. The HsNMT2 antibody could only detect full length HsNMT2. This result was expected as the epitope of this antibody is based on the N-terminus of HsNMT2.

Recently, Perinpanayagam *et al.* identified the cleavages site of both HsNMT isoforms.[115] HsNMT1 was shown to be cleaved at Asp-72 by caspase 3 and 8 while HsNMT2 was cleaved after Asp-25 by caspase 3. The activities of cleaved and full length HsNMTs were highly similar, suggesting that cleaved enzymes are still functional and can myristoylate NMT substrates post-translationally such as BID (see Sections 1.5.2 and 2.4). This is consistent with a previous observation. Rundle *et al.* suggested that the N-terminus of HsNMT was not essential for the catalytic activity.[50]

Cleavage of HsNMT1 at Asp-73 results in the removal of the "K box motif", known to be essential for ribosomal targeting of the enzyme (Section 1.6.2). As expected, Perinpanayagam *et al.* showed that NMT moved to the cytosol upon apoptosis induction. Interestingly, HsNMT2 was cleaved just before the "K box motif" and it was shown to shift from the cytosol to the membrane fraction upon apoptosis induction. It is unclear why full length HsNMT1 and HsNMT2 have different localisation in cells; although their sequences diverge mainly in the N-terminal region (Section 1.2.2), they both carry a polybasic region ("K box motif") known to target proteins to the ribosome,[21] and this phenomenon may merit further investigation due to its apparent role in apoptosis.

5.2.2.2 HeLa cells treated with IMP366

After confirming that we could detect apoptosis in HeLa using a selection of antibodies, we studied the potential induction of apoptosis in cells treated with IMP366 for 1, 3 or 7 days. STS was used as a control for apoptosis (Figure 89). Markers of apoptosis did not changed after 1 day inhibition, suggesting that the compound does not trigger apoptosis or induce toxicity after 1 day as previously indicated (Figure 76). However, at 3 days inhibition, PARP, BID, Caspase 3 and HsNMT1 were all cleaved to a substantial extent. Tubulin was used as a loading control. After 7 days inhibition, it proved difficult to detect full length or cleaved PARP, HsNMT1 and Caspase 3; it may be supposed that these proteins have been fully degraded in these cells.

Interestingly, BID seemed to accumulate in cells after 7 days. It is possible that when BID is not *N*-myristoylated, it may be more resistant to proteolytic degradation, and may accumulate in the cytosol since it cannot relocate to the mitochondria.[8]

These results suggested that HeLa cells were dying at least in part through apoptosis. However, as explained in Section 5.2.1, it can be difficult to distinguish between apoptosis and necrosis. It is thus necessary to perform several assays, based on different principles, to confirm apoptosis.

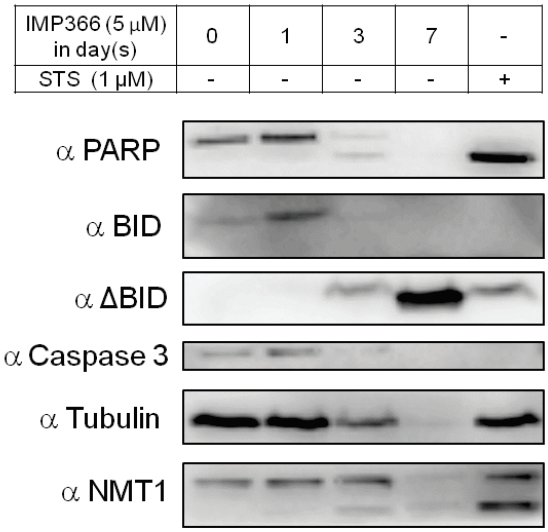

Figure 89. Evaluation of IMP366 in HeLa cells. Western blot analysis after 1, 3, or 7 days of treatment with IMP366. Cells were treated with STS (1μM) for 4 h as a control for apoptosis. Loading on the gel was normalised to the protein concentration and tubulin was used as a loading control.

5.2.3 Flow cytometry (Annexin V/PI)

An assay based on the detection of phosphatidylserine relocalised to the outer membrane of the cells by flow cytometry is a simple and reliable method for detecting dying cells [296,296] since phosphatidylserine can be detected by fluorescently-labelled Annexin V.[296] However, Annexin V cannot distinguish necrotic and dead cells from apoptotic cells as phosphatidylserine moves to the outer surface of the cell membrane in all cases; Annexin V is therefore used in combination with PI (Section 5.1.1.2.1), which only stains the nucleus of cells that have a permeable cell membrane, such as necrotic cells, late apoptotic cells or dead cells. Early/mid apoptotic cells will only be labelled by Annexin V (Figure 90a).

Treatment of the cells with 1 or 5 μM IMP366 gave consistent results, and DMSO treatment was included as a negative control (PI negative, Annexin V negative) (Figure 90b). Early apoptotic cells appeared after 24 h treatment and a substantial population of dead cells could be observed after 3 day treatment. The percentages of apoptotic cells (subG0/G1) differ from the cell cycle analysis; entry into subG1 phase is a later event than phosphatidylserine relocation, and it is therefore unsurprising that after 1 day treatment, around 14% of the cells are labelled with Annexin V whereas only 5% subG0/G1 cells were detected by cell cycle analysis. After 3 days, the percentage of cells undergoing early apoptosis plus dead cells correlates well with the number of cells in SubG0/G1 detected by cell cycle analysis, and the percentage of cells in subG0/G1 was lower for cells treated with 1 μM than with 5 μM (ca. 35% and 50% respectively).

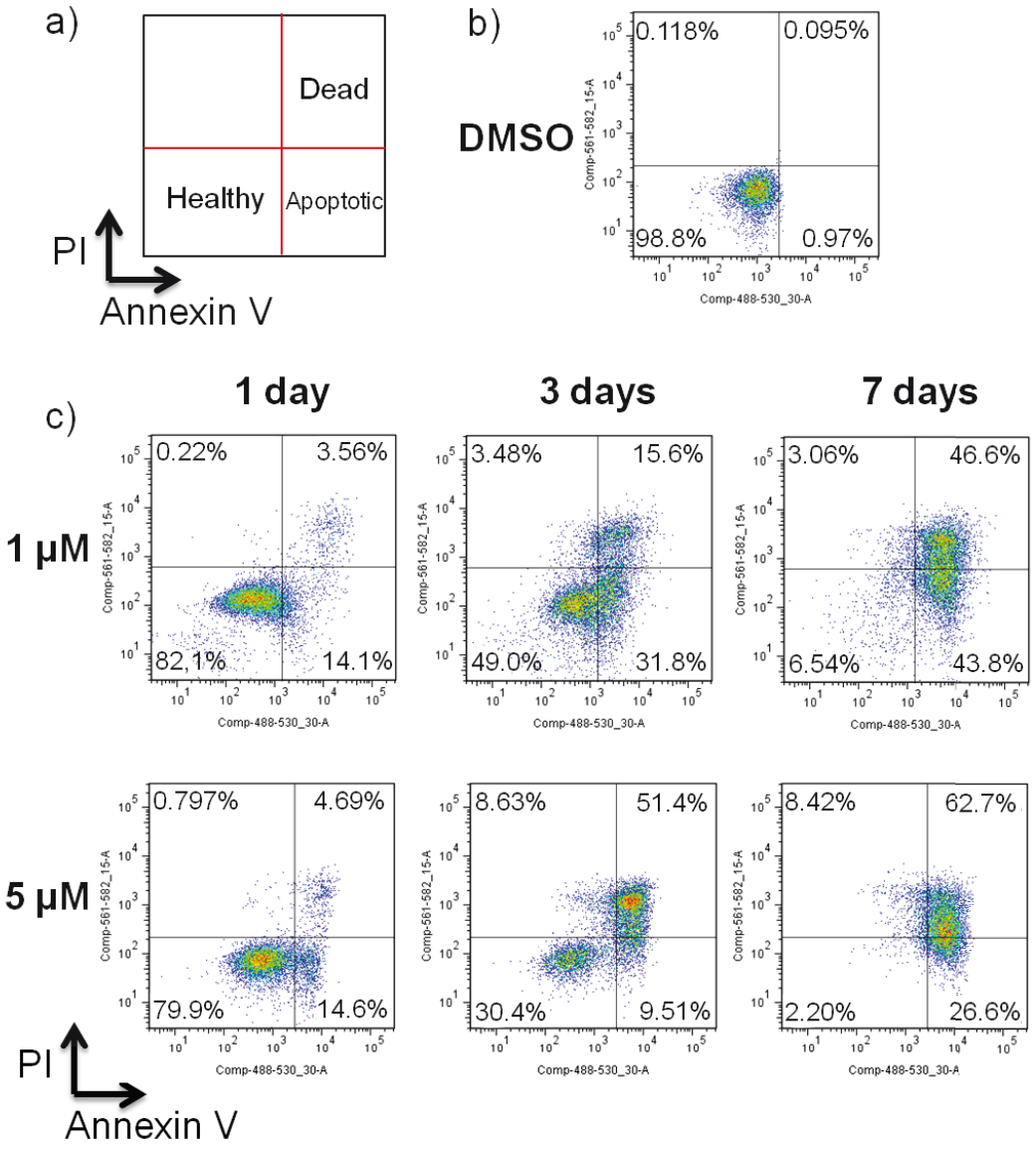

Figure 90. Annexin V/PI experiment to confirm that HeLa cells dies through apoptosis upon NMT inhibition. **a)** Scheme explaining where healthy, apoptotic and dead (as well as necrotic and late apoptotic) cells should appear when the PI-fluorescence is plotted against the Annexin V-fluorescence. **b** and **c)** HeLa cells were treated with DMSO or IMP366 (1 or 5 µM) for 1, 3 or 7 days and labelled with Annexin V/PI before being analysed by flow cytometry. Samples were analysed with FlowJo.

Cells all undergo apoptosis or are dead/necrotic after 7 days. The number of dead cells after 7 days can be underestimated as degraded cells can produce particles that fall outside the set gates (Section 5.1.1.2.2). This result is consistent with the cell cycle analysis (Figure 81) and with the MTS assay (Figure 76).

5.2.4 Comments on other possible mechanisms

The Western blot analysis and the Annexin V/PI experiment confirmed that cells were dying through apoptosis, probably via a caspase-dependent pathway. However, this mechanism might not be exclusive. First, a caspase-independent pathway can also be involved in cell death.[297] Secondly, other modes of cell death, such as autophagy can occur at the same time as apoptosis;[298] cells in the top left corner of each analysis in Figure 90 may indicate the presence of autophagic cells.[299] Moreover, different concentrations of a single reagent can also induce distinct mechanisms of cell death.[300]

Apoptosis-resistant cell lines may be resistant to NMT inhibition if the mode of cell death is exclusively apoptotic.[301] A better understanding of the mode of cell death could shed light on which (cancer) cell types are likely to be most sensitive to NMT inhibition.

Several questions remain to be answered:

- ✓ Is the mechanism of cell death only apoptotic? The evidence suggests a mix of necrosis and apoptosis.
- ✓ Is the mechanism of apoptosis via the intrinsic or extrinsic pathways? Presumably, the intrinsic pathway is involved as the NMT inhibitor does not target the death receptors. However, as BID is usually cleaved upon activation of the extrinsic pathway, suggesting that there is some crosstalk between these pathways.
- ✓ Would NMT inhibition delay apoptosis as some effectors proteins, such as BID,[8] require *N*-myristoylation to induce the next step of the apoptotic cascade? This question is discussed in Section5.2.5.
- ✓ Is only a caspase-dependent pathway involved?
- ✓ How is apoptosis initiated, and what are the key NMT substrates that lead to cell death when they are not myristoylated? This question is discussed in Section 5.4.1.
- ✓ Which tissues/cancer cell types are more sensitive to NMT inhibition?

5.2.5 Does NMT inhibition delay apoptosis?

Cytochrome C release from the mitochondria is a key characteristic of the intrinsic apoptosis pathway.[292] One of the requirements for cytochrome C release is the binding of BID to mitochondria. In early stages of apoptosis, BID is cleaved by caspase 8 and is *N*-myristoylated. *N*-myristoylation is known to be essential for cytochrome C release;[8] when BID could not be *N*-myristoylated in Fas-activated (apoptotic) MCF-7 cells, cell viability significantly increased.[8]

It was hypothesised that cytochrome C might not be released upon induction of apoptosis with the NMT inhibitor IMP366. A positive control was first carried out with STS treatment followed by cell fractionation (Figure 91a), and calnexin was used as a control for the membrane fraction. While a small percentage of tubulin is associated with the mitochondria,[302] most is cytoplasmic and hence serves as a good marker for this compartment.

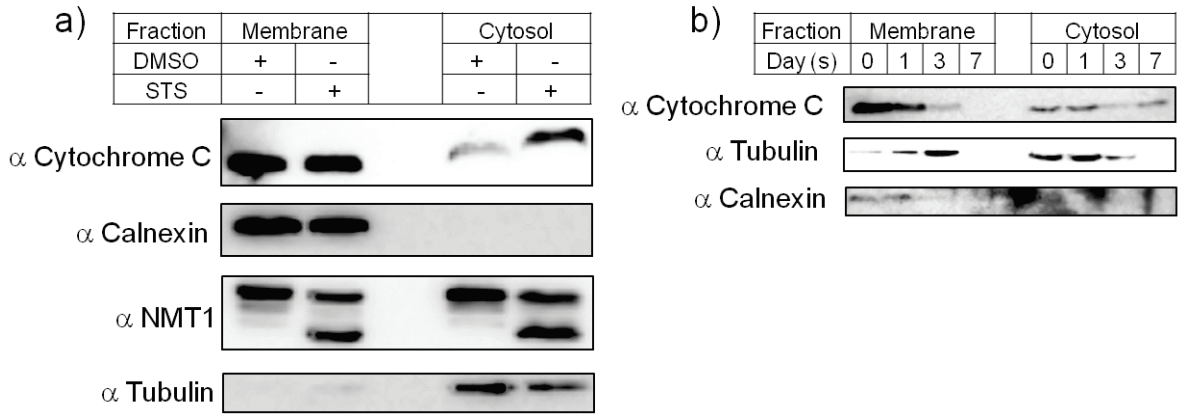

Figure 91. Cell fractionation experiments to study localisation of proteins upon apoptosis induction with STS or IMP366. a) HeLa cells were treated with DMSO or STS (1 μM) for 4 h. Cells were fractionated and the membrane and cytosolic fraction were analysed by Western blotting. **b)** HeLa cells were treated with IMP366 (5 μM) for 0, 1, 3 or 7 days. Cells were fractionated and the membrane and cytosolic fractions were analysed by Western blotting.

HeLa cells were then treated with NMT inhibitor for several days and changes in the subcellular localisation of cytochrome C were determined by Western blotting of fractionated cell lysates. Levels of cytochrome C appeared to decrease in the membrane fraction after 3 days, suggesting that cytochrome C was released from the mitochondria. However, the levels of cytochrome C in the cytosol did not increase. After 3 days, the control for the cell fractionation (tubulin and calnexin), were unreliable. Tubulin, the control for the cytosolic fraction relocated to the membrane fraction after 3 days. This relocation is probably an artefact due to the high number of apoptotic or dead cells. In the control experiment, few dead cells were observed and tubulin was cystoplasmic (Figure 91a). Calnexin could not be detected in the membrane fraction after 3 days.

From this experiment, it is difficult to conclude that cytochrome C is released from the mitochondria. The apparent decrease of cytochrome C in the membrane fraction might be caused by its degradation. An NMT substrate, HCCS, is required for the proper maturation of cytochrome C via the transfer of heme to cytochrome C (Section 4.8.4.1).[93,249] Recently, it was also demonstrated that HCCS regulates the import of cytochrome C into mitochondria.[303] It is possible that upon NMT

inhibition, HCCS might not be able to import cytochrome C to the mitochondria and cytochrome C might be degraded.

To determine if NMT inhibition could prevent or delay apoptosis, HeLa cells with treated with DMSO (8 h), STS (8 h), STS in the presence of IMP366 (8 h) and IMP366 (3 days) (Figure 92). Cleavage of caspase and effector proteins occurred in both STS-treated samples. These samples appeared morphologically similar, suggesting that IMP366 does not stop or delay apoptosis. However, STS is a non-selective kinase inhibitor and might induce apoptosis through several pathways simultaneously.[295,304]

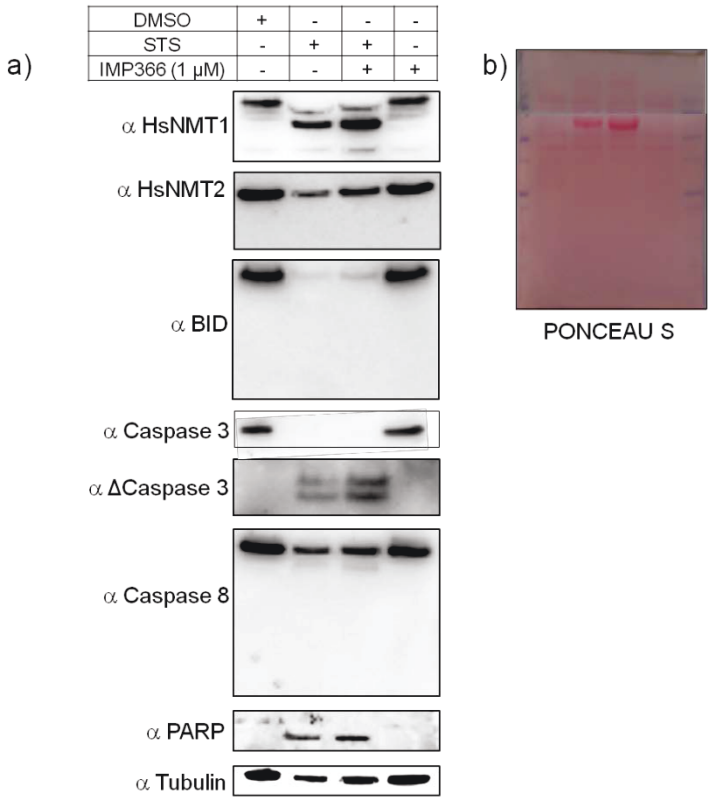

Figure 92. NMT inhibition does not delay apoptosis in HeLa. a) Western blot analysis of cells treated for 8 h with DMSO, or STS (1 µM) or STS (1 µM) in the presence of IMP366 (1 µM). after 1, 3, or 7 days of treatment with IMP366. Cells were treated with STS (1µM) for 4 h as a control for apoptosis. Loading on the gel was normalised to the protein concentration and tubulin was used as a loading control. In the last lane, the sample was treated with IMP366 (1 µM) for 2 days. **b)** Picture of a Western blot membrane stained with Ponceau S to control protein loading.

To test the hypothesis that NMT inhibition might delay apoptosis it would be advantageous to analyse a cell line highly dependent on the BID pathway or an apoptosis inducing agent triggering

only the BID pathway. In preliminary experiments, Western blotting showed that MDA-MB-231 cells and HCT-116 were not highly dependent on BID cleavage as BID was not cleaved while PARP and some caspases were cleaved (data not shown). Two other apoptosis inducing agents (TRAIL[305] and Oxaliplatin [306]) have also been tested as they have been suggested to induce apoptosis through a BID-dependent pathway. However, these reagents did not induce BID cleavage even though apoptosis was triggered (data not shown).

5.3 *N*-myristoylated proteins turnover

NMT inhibition showed a slow apoptotic response in HeLa cells and as suggested in Section 5.1.1.2.2, this might be due to the turnover rate of *N*-myristoylated proteins.

5.3.1 Introduction to protein turnover

The levels of individual proteins in cells do not only depend on the rate of synthesis, but also on rate of degradation.[307] Proteins are constantly degraded and synthesised to maintain cellular homeostasis, even when cells are not dividing. This dynamic state can be studied by evaluating the protein turnover rates, which are linked to protein half-lives. The turnover rates vary across each type of protein in a cell, between cell lines, and under different conditions. Proteins are degraded for two main reasons :[307]

- ✓ Quality control: proteins which are damaged, denatured or misfolded can be degraded.
- ✓ Regulation of biological pathways: some proteins can for example be degraded to allow the cells to enter the next phase of the cell cycle. Proteins degradation is also required for apoptosis or receptor mediated endocytosis.

They are two known mechanisms for intracellular proteolysis.[307] In lysosome-dependent degradation, lysosomes degrade extracellular proteins or intracellular components by autophagy. The other degradation mechanism is based on the ubiquitin-proteasome pathway in which proteins to be degraded are tagged with ubiquitin and digested by the proteasome, a proteolytic protein complex. Ubiquitin is covalently attached to the condemned protein by the successive action of three enzymes: E1 (ubiquitin-activating enzyme), E2 (ubiquitin-conjugating enzyme) and E3 (ubiquitin-protein ligase). It has also been suggested that some proteins might be degraded by proteasomes without ubiquitination.[308]

5.3.2 Is it possible to predict protein turnover?

It has been suggested that protein turnover could be highly dependent on the protein N-terminal sequence[309,310] and some online predictors, such as ProtParam, [311] are available to predict protein turnover rates based on this hypothesis. It was also proposed that protein stability might depend on the protein molecular weight,[312] isoelectric point,[313] protein abundance[314], or frequency of PEST motifs.[314] However, all these results are controversial.[314,315] Recently, it was suggested that proteins which are part of the same protein complex, such as the 26S proteasome, have similar turnover rates.[315]

It was also shown that phosphorylation can control protein ubiquitylation [316] and thus regulates the protein turnover. Phosphorylated proteins have been shown to have a higher turnover rate, on average, than non-phosphorylated proteins.[315]

5.3.3 Methods to study protein turnover

The development of MS-based proteomics and the use of radiolabelled isotopes have made possible the high-throughput study of protein turnover. Protein half-life in HeLa cells was reported in two recent studies,[314,315] however, they used two different methods, and they produced different results.

In the first study (published by Cambridge *et al.* in 2011)[315] protein turnover was studied in non-dividing cells. Cells were grown in a SILAC media (Section 4.5) containing a mixture of heavy and light isotopes (1:1 heavy : light (R10K8: R0K0)) for several passages. Cells were then kept highly confluent for more than 24 h and the media was replaced by heavy media (R10K8 DMEM) supplemented with only 2% FBS just before the beginning of the experiment.

This method presents several advantages and drawbacks. Studying protein turnover in non-dividing cells would avoid labelled protein dilution arising from cell division.[317,318] They assumed that the amount of each protein was kept constant, but the conditions used would also be expected to affect the turnover rate of specific proteins. Presumably, in non-dividing cells, the cell cycle is arrested and proteins required to be degraded for cell cycle progression such as cyclins might not be degraded, and thus have a lower turnover rate.[319] However, they showed that some cyclin proteins still had a high turnover rate. The other advantage of their method is that they labelled the cells with a 1:1 light : heavy isotope ratio., which allowed relative quantification of turnover of low abundance proteins even at time 0. However, the ratio of H/L might differ from one protein to the other at time 0 and might not be 0.5.

Protein half-life was determined for 43 out of the 74 NMT substrates identified in Section 4.8. The average half-life was 34.6 h, and ranged from 12.2 (for TMEM106B) to 56.1 h (for BASP1). More

recently, Boisvert *et al*. also studied the turnover of proteins in HeLa cells, incorporating fractionation of protein samples into cytoplasm, nucleus and nucleolus.[314] A complex experiment was carried out to assess protein synthesis, degradation, and turnover rates within the same sample. Cells were labelled with medium isotopes (R6K4) and the media was replaced by a heavy media (R10K8) at time 0. Samples were chased for 0.5, 4, 7, 11, 27, and 48 h. To estimate the dilution effect, they estimated the doubling time of HeLa cells by counting them at different time points using a Cell Countess (Invitrogen). The cell counts were then fitted to an exponential growth curve (see below for more details). After cell lysis, the same amounts of lysate originating from cell grown in the light media (R0K0) were added and this light sample was used as an internal reference (similar to a "Spike-in" experiment, see Section 4.6). Protein half-lives were determined for 40 out of the 74 NMT substrates identified in Section 4.8. The average half-life was 17.5 h, and ranged from 8.8 (for DEGS1; value from Cambridge *et al*.[315]: 24 h) to 32.7 h (for CHCHD3; value from Cambridge *et al* [315]: 54.9 h). These results are dramatically different from the analysis made by Cambridge *et al*. (Figure 93), and this divergence in protein half lives could be attributed to the different conditions (non-dividing or dividing cells, etc) used for the experiment.

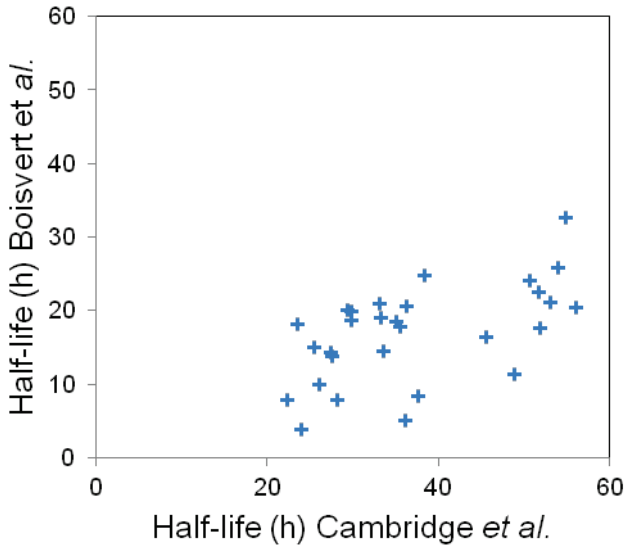

Figure 93. Scatter plot showing the correlation between the protein half-life values determined by Boisvert *et al.* [314] and Cambridge *et al.* [315] Only 30 NMT substrates are common to both analysis and are shown here.

Thus, more experiments are required to accurately determine the half-lives of NMT substrates in dividing HeLa cells. Additionally, it would be interesting to evaluate protein turnover rates in the presence of NMT inhibition. NMT inhibition might lead to a new equilibrium in cells and proteins might be degraded more or less rapidly than they have been synthesised.

5.3.4 Experimental design and results

For the purpose of determining which NMT substrate turnovers correlate with the apoptosis induced by NMT inhibition, it would be advantageous to focus specifically on the turnover of enriched *N*-myristoylated proteins as this is likely to enhance coverage. All the proteomics experiments to study protein turnover reported in the literature have been carried out on the whole cell lysate. Cell fractionation was often required to increase coverage. However, in most cases, the low abundance proteins were lost during the analysis. For example, the turnover rate of c-SRC could not be quantified from the analyses of Cambridge *et al.*[315] or Boisvert *et al.* [314].

Two methods were tested to study the turnover rate of *N*-myristoylated proteins (Figure 94). First, as in the method used by Boisvert et *al.*,[314] cells were labelled with the light isotope (R0K0), and the media replaced by heavy media (R10K8) at time 0 (Figure 94a). The light isotope was chased for 0, 2, 6, 10 and 24 h. Cells were pre-tagged with YnC12 24 h before the beginning of the experiment and YnC12 was added to the heavy media during the chasing time. After cell lysis, *N*-myristoylated proteins could be enriched as described in Section 4.2 and the ratio H/L was measured by LC-MS/MS. The decrease of the light isotope should follow an exponential decay, and the relative isotope abundance (RIA) was measured for the light isotope (RIA (L)) with the following Equation 2.[317,318]

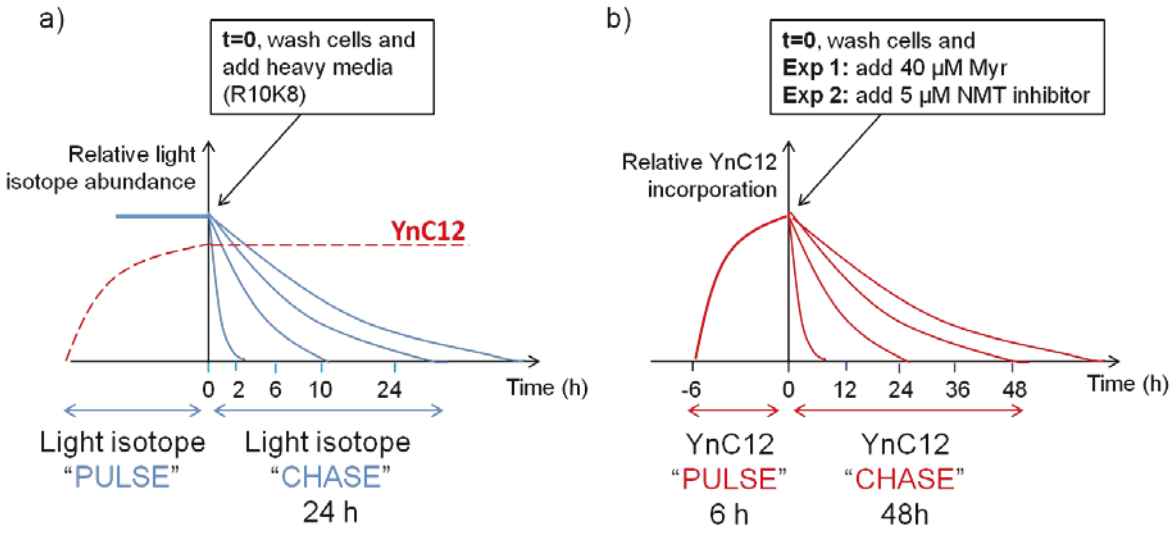

Figure 94. Strategies to study NMT substrates turnover.

Equation 2. The relative isotope abundance (RIA (L)) was measured for the light isotope for each time point. L and H represent the peak intensities detected for the light and heavy peptides respectively, for a given protein. The ratio L/H can directly be obtained from MaxQuant.

$$RIA\ (L) = \frac{L}{L+H} = \frac{1}{1+\frac{L}{H}}$$

The ratios L/H were directly obtained from the proteomics analysis using MaxQuant (see Section 4.5). A dilution rate was calculated by fitting the cell number in the sample to an exponential decay curve (Figure 95). The dilution rate (k_{dil} = 0.0277) correlated well with the dilution rate calculated based on the protein concentration in each sample (k_{dil} = 0.0296).

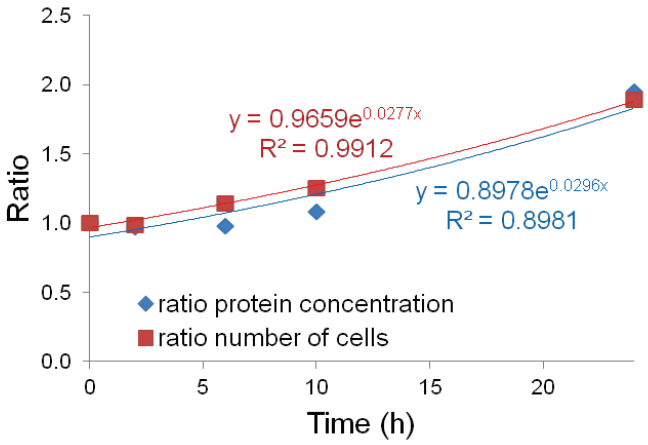

Figure 95. Determination of the dilution rate based on the number of cells or the protein concentration in the samples. Both were normalised to time 0. Cells were counted (n=6) with a Hemocytometer and protein concentration was determined with the Bio-Rad *DC* protein assay (samples were lysed using the same volume of lysis buffer to be able to compare the concentrations).

Missing values at time 0 were imputed with the median values of other NMT substrates (0.938). Many missing values were present at time 0 as no protein was labelled with the heavy isotope, but MaxQuant can often automatically determine a ratio close to the detection limit if the protein is found only in the light isotope; however, this was not the case for all the proteins. The data were fitted for each protein to an exponential curve fitting in Origin 8.0 (Equation 3) and a constant k_{loss} was obtained. The real rate of degradation (k_{deg}) was determined by subtracting k_{dil} to k_{loss}.[317] The protein half-lives were then determined according to Equation 4.

Equation 3. The *RIA (L)* was fitted to an exponential fitting curve in Origin 8.0 with the following equation. Y_0 is the RIA (L) at time 0, t is the time in h and k_{loss} is the rate of loss of the light isotope in h.

$$RIA\ (L) = Y_0 \times e^{-t \times k_{loss}}$$

Equation 4. Determination of the protein half-lives ($t_{1/2}$). RIA (L) $_{t1/2}$ is equal to 0.5 as 50% of the light isotope should be lost at the protein half-life.

$$\boldsymbol{t_{1/2} = \frac{-Ln(RIA\ (L)_{t1/2})}{k_{deg}}}$$

An average half-life of 38.3 h was found over 72 protein groups of NMT substrates (Figure 96 and Appendix I). This half-life value is highly comparable to the value obtained by Cambridge *et al.* (34.6 h).[315] Only mitochondrial import receptor subunit TOM40B (TOMM40L) and tyrosine-protein kinase ABL1 were not detected in this experiment, and Battenin (gene name CLN3) could not be quantified.

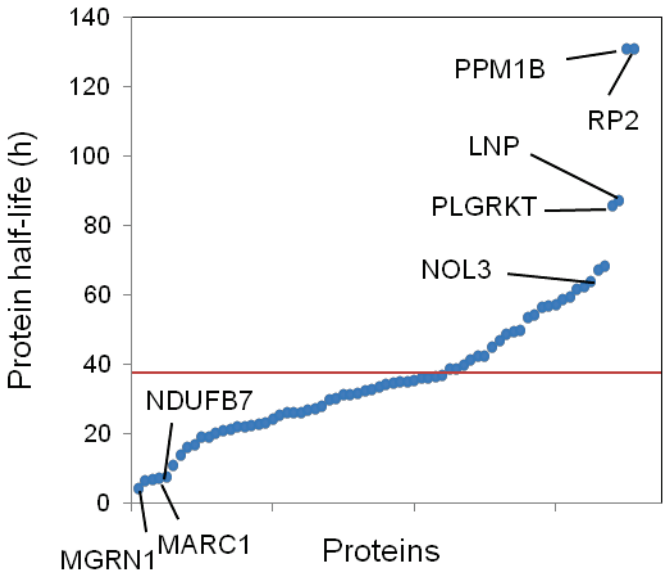

Figure 96. *N*-myristoylated proteins half-lives (h). Proteins with high and low turnover rates have been labelled. The average half-life is indicated in red.

This method presents several potential issues.[307] First, it was assumed that the protein synthesis and degradation follows a kinetic trend. To be valid, protein turnover needs to be independent of the protein concentration and follow a zero order rate law. Secondly, amino acids can be recycled, complicating later time points. In their study, Cambridge *et al.* showed that the incorporation of

internal amino acids (recycled amino acids) was negligible compared to the incorporation of external amino acids (from the media).[315] They demonstrated that in the conditions they used, newly synthesised proteins preferentially incorporate heavy amino acids rather than recycled light amino acids. It would be important to check that this is the case in the experiment described above. Finally, there might be a delay in amino acid incorporation, and this delay, if not negligible, might also lengthen the apparent rate of degradation.

To complement this half-life data, a second method was employed (Figure 94b). Proteins were pulsed with YnC12 for 6 h and chased for several days in the presence of myristic acid or inhibitor IMP366 (5 µM). Since *N*-myristoylation is believed to be mostly irreversible (Section 1.1), the amount of YnC12 label should decay as fast as proteins are degraded in cells. Each sample was then spiked-in after cell lysis with a heavy standard labelled together with YnC12 (Section 4.6), and following capture, enrichment and trypsin digest, samples were analysed by LC-MS/MS and processed with MaxQuant. As the same amount of heavy spike-in standard was added to each sample, L/H ratios directly reflected the relative incorporation of the light isotope (RIA (L)). As for the first strategy, L/H ratios were fitted to an exponential decay curve (Equation 3), and k_{deg} were determined by subtracting k_{dil} to k_{loss}. The NMT substrates turnover rates were found to be much higher than in the first approach, with an average half-life of 126 h and 263 h when YnC12 was chased with myristic acid or NMT inhibitor respectively (Appendix A and I). However, these values were determined on a smaller subset of proteins: the half-life could only be quantified for 44 proteins (myristic acid chase) or 33 proteins (inhibitor chase).

5.3.5 Conclusions

The results from the three experiments (light isotope chase experiment and both YnC12 chase experiments) were compared for each protein (Appendix I). Interestingly, some proteins, such as AIFM2 and Cytospin B (SPECC1), had highly similar half-lives. However, for most proteins, the half-life values were much higher for the YnC12 pulse-chase experiment. Strikingly, some proteins, such as BASP1, CYB5R3, FAM49B, had extremely high half-life. The difference in protein half-life between the three experiments suggests that they are flaws in the experiment design. The YnC12 pulse-chase experiment would need further refinement and validation to generate meaningful data. It is possible that the 6 h YnC12 pulse does not reflect the turnover of the whole pool of NMT substrates in cells and that the strong condition changes during the YnC12 chase do not reveal the real protein turnover. Moreover, proteins with a low turnover rate and low abundance might be labelled poorly. Only half as many substrates were identified in the YnC12 pulse-chase experiment compared to the light isotope chase experiment.

However, the light isotope chase experiment is more promising, as half-life was determined for most NMT substrates identified in the current study and the values were consistent with a previous report.[315] Interestingly, some proteins, such as MGRN1 had a very short half-life while some others, such as RP2 or PPM1B, were more resistant to proteolytic degradation (Figure 96). The relatively long half-life of NMT substrates is consistent with the slow phenotype observed upon NMT inhibition. These values might provide a key to understand which proteins are responsible for cell death upon NMT inhibition. However, there is unlikely to be a simple correlation between any one protein half-life and cytotoxicity.

All these experiments were carried out on acylated NMT substrates. It might also be interesting to study what happens to the newly synthesised but not *N*-myristoylated NMT substrates. It has been suggested that turnover rates are different when protein are not myristoylated, for instance, non myristoylated LCK and c-SRC seem to be more stable.[104,218] Padwardhan *et al*. hypothesised that membrane bound myristoylated c-SRC might have a different conformation than the non myristoylated protein, and might thus be more accessible to the ubiquitination machinery (Cbl and other E3 ubiquitin ligases).

5.4 Effect of NMT inhibition on NMT substrates

5.4.1 Hypothesis on key targets

In Chapter 4, proteomics experiments allowed the identification of 74 NMT substrates in HeLa cells. Any of these substrates might be essential to cells and it is highly unlikely that a single critical substrates would be identified that leads to cell death when not *N*-myristoylated. Many substrate proteins are involved in protein transport (ARF proteins...) or are kinases or oncogenes. Several NMT substrates are involved in protein degradation through the ubiquitin pathway. PSMC1 is a proteasome subunit, and four E3 ubiquitin ligases are *N*-myristoylated: MGRN1, RNF125, ZNRF1 and ZNRF2 in Eukaryotes (see Appendix H). It is thus possible that NMT inhibition could result in a down regulation of protein degradation.

Recently, loss of myristoylation of the 26S protease regulatory subunit 4 (PSMC1) was shown to result in a considerable growth defect in yeast.[320] Proteasome assembly and peptidase activity were not affected by the loss of myristoylation but there was a localisation defect and major problems with protein aggregation and accumulation of poly-ubiquitinated proteins. A Western blot analysis was carried out to understand if NMT inhibition could result in the accumulation of poly-ubiquitinated proteins (Figure 97a). Epoxomicin, a selective proteasome inhibitor, was use as a control. Inhibition of HeLa cells with Epoxomicin led to a rapid accumulation of poly-ubiquitinated

proteins. NMT inhibition also resulted in an accumulation of poly-ubiquitinated proteins after 1 day but levels of poly-ubiquitinated proteins decreased after 3 days. This result is not surprising since several E3 Ubiquitin ligases are also NMT substrates and loss of *N*-myristoylation might impair their ability to transfer Ubiquitin to proteins, which could explain why the signal decreases again after 3 days. However, cells have many ubiquitin ligases which could potentially compensate loss of activity of the ubiquitin ligases that are NMT substrates. It may be interesting in future to use a fluorometric assay based for example on an AMC (7-amino-4-methylcoumarin)-tagged peptide substrate which releases free, highly fluorescent AMC when the proteasome is functional, to study proteasome activity upon NMT inhibition.

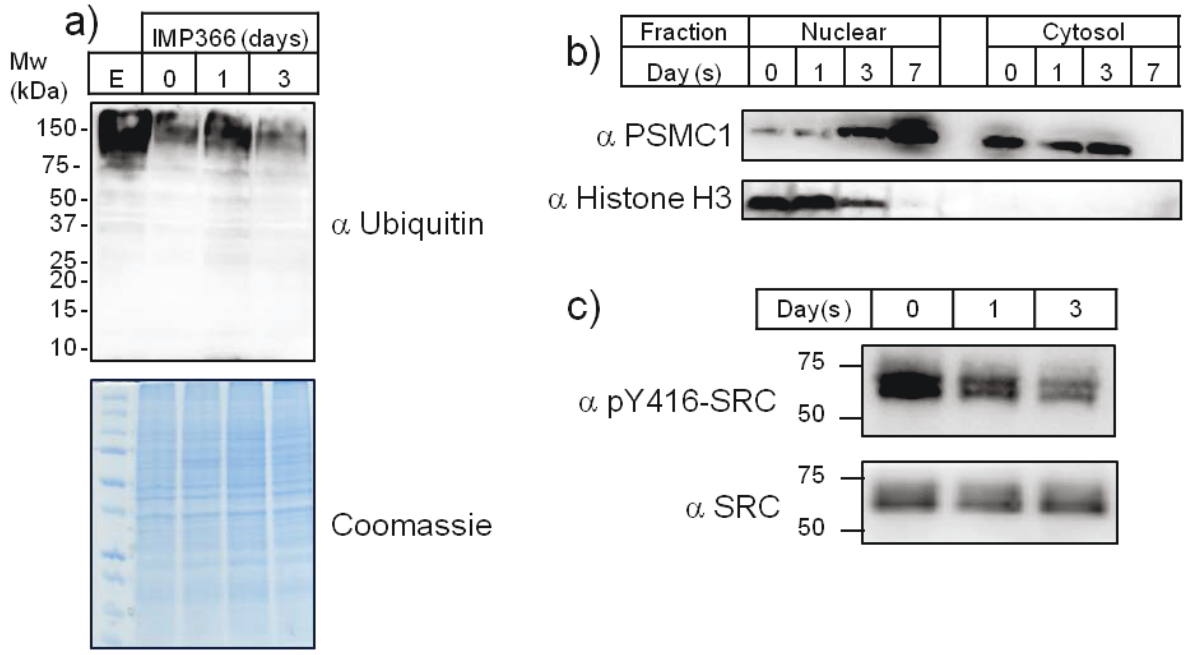

Figure 97. Possible key targets leading to cell death when they are not *N*-myristoylated. a) E= Epoxomycin. HeLa cells were treated with IMP366 (5 µM) for 0, 1 or 3 days, or with a proteasome inhibitor, Epoxomicin, for 2 h (10 µM) as a control. **b)** HeLa cells were treated with IMP366 (5 µM) for 0, 1, 3 or 7 days. Cells were fractionated and the cytosolic and nuclear fractions were analysed by Western blot. **c)** Immunoprecipitation experiment and Western Blot analysis showing that c-SRC phosphorylation decreases upon NMT inhibition in HeLa cells. Cells were treated with IMP366 (5 µM) for 0, 1 or 3 days.

Myristoylation of PSMC1 was also shown to control proteasome localisation.[320] The proteasome is mostly localised in the nucleus in yeast, but when PSMC1 was not *N*-myristoylated, the proteasome was mostly found in the cystoplasm. A similar experiment was carried out by Western blot analysis (Figure 97b). In HeLa cells, PSMC1 was localised in the cytosol in healthy cells and we observed that PSMC1 was re-localised to the nucleus upon NMT inhibition after 3 and 7 days. The proteasome localisation has been shown to be more complex in mammalian cells than in yeast, as it is distributed

between the cytoplasm and nucleus.[321,322] These results need to be replicated in a future study to be considered robust. Histone H3 (the control for the nuclear fraction) decreased after 3 and 7 days, probably due to cytotoxicity (Section 5.1.1).

The proteasome subunit is a particularly interesting target as the proteasome is a known therapeutic target in cancer. One compound, bortezomib, was recently FDA-approved for the treatment of several cancers including multiple myeloma.[323] Inhibition of the proteasome activity was shown to have varied effect in different cell lines;[324,325] treatment of HeLa cells with MG132, a proteasome inhibitor, did not result in a G1 accumulation after 1 day.[324] However, inhibition of the proteasome in MDA-MB-231 induced a G1 cell cycle arrest and caspase 3 independent apoptosis.[326] Further experiments would be required to understand the importance of PSMC1 and E3 ubiquitin ligases in inducing cell toxicity upon NMT inhibition.

c-SRC has been suggested to be a key target in cancer cells and is a known target for cancer therapy.[327] High levels of c-SRC tyrosine kinase activity have been associated with cancer progression as they promote cell survival, proliferation and metastasis,[328] and *N*-myristoylation is required for the autophosphorylation of c-SRC and, as a consequence, for its tyrosine kinase activity.[104] Upon NMT inhibition with IMP366, we observed a decrease of phosphorylated c-SRC after 1 day and 3 days, suggesting that c-SRC had a reduced protein kinase activity, while levels of total c-SRC remained constant (Figure 97).

Interestingly, inhibition of MDA-MB-231 cells with Dasatinib, a FDA-approved SRC kinase inhibitor used for the treatment of chronic myelogenous leukemia, had some similarity with IMP366.[329] Inhibition with Dasatinib resulted in a decrease of cell growth, a G1 arrest but no apoptotic cells were present after 2 days. It would be interesting to study if IMP366 and Dasatinib have a synergic effect in cancer cells. No synergic effect would suggest that they both act mainly through inhibition of SRC (indirectly or directly).

Another NMT substrate of interest is ARC (NOL3), the apoptosis repressor with caspase recruitment domain. ARC is an anti-apoptotic protein identified in the current study and discussed in Section 4.8.4.3. Interestingly, HeLa cells are resistant to Doxorubicin-mediated apoptosis, but it was shown that a knockdown of ARC promoted apoptosis. It would be interesting to study the effect of Doxorubicin combined with a NMT inhibitor in HeLa cells. Preliminary experiments (Section 5.3.4) suggested that the turnover rate of the protein is low in HeLa cells (around 60 h), compared to other NMT substrates. However, it could still play a role in apoptosis induction upon NMT inhibition.

A substantial number of other novel NMT substrates have an anti-apoptotic activity or have been associated with cancer progression (Section 4.8.4.3). It would be interesting to evaluate their role for the phenotype observed in cancer cells upon NMT inhibition.

5.4.2 Tumour suppressors

There is evidence that some NMT substrates are tumour suppressors, and inhibition of *N*-myristoylation of these substrates might lead to an unwanted effect; these include:

- ✓ Guanine nucleotide-binding protein G(i) subunit alpha-1 (GNAI1), which can repress tumour cell migration.[330]
- ✓ Protein phosphatase 1A (PPM1A) is a protein phosphatase which dephosphorylates RelA. Phosphorylated RelA has oncogenic activities.[331]
- ✓ PPM1G is a protein phosphatase. Upon DNA damage, PPM1G is activated and dephosphorylates ubiquitin protease USP7S.[332] USP7S, which is known to regulate the level of p53 in cells, then undergoes proteasomal degradation. As a consequence, levels of p53 decrease in cells, and there is an accumulation of unrepaired DNA damage as well as a p53-independent cell-cycle arrest in G1.
- ✓ Calcineurin subunit B type 1 (PPP3R1) is a regulatory subunit of calcineurin, a protein phosphatase involved in the apoptosis pathway. When levels of calcium increase in the cytoplasm, calcineurin is activated by binding a regulatory subunit, PPP3R1 and calmodulin. As a consequence, Bad is released from 14-3-3 leading to Bax activation in the mitochondria and apoptosis.[245]
- ✓ Brain acid soluble protein 1 (BASP1) is a transcriptional co-repressor which can interact with WT1, Wilms' tumour 1 protein (Section 1.2.2).[54] WT1 is a transcriptional activator which is associated with cell growth and differentiation. Upon binding of WT1 with BASP1, WT1 is covered to a transcriptional repressor. Non N-myristoylated BASP1 cannot associate with WT1 and WT1 cannot repress cell growth and differentiation.
- ✓ Cytospin B (SPECC1) and Coiled-coil-helix-coiled-coil-helix domain-containing protein 6, mitochondrial (CHCHD6), both discussed is Section 4.8.4, are also tumour suppressors.

More experiments would be required to understand the potential effect of NMT inhibition on these tumour suppressors, particularly in healthy tissues.

5.5 Conclusions

This Chapter addressed one of the main questions of this PhD thesis: could NMT be a therapeutic target for cancer therapy? The phenotype of NMT inhibition in cancer cells was described and the difficulties faced in determining the mode of action of an NMT inhibitor were outlined.

NMT inhibition was not toxic to cells after 1 day, probably due to the slow turnover of NMT substrates, and cell could recover from inhibition (Section 5.1.1.3). It would be interesting to determine whether cells could recover after a longer inhibition time.

Turnover experiments would need to be repeated to confirm the half life-values using the light isotope pulse-chase experiment (Section 5.3). It would be interesting to see if similar values could be obtained by a heavy isotope pulse-chase experiment. It might also be advantageous to start the experiment with cells grown in 50 % heavy and 50 % light, as performed by Cambridge *et al.*[315] as it would solve the issue of the missing values at time 0.

Considering that many NMT substrates seem to be essential to the cells and that many have been linked with cancer progression, NMT inhibition would most likely have pleiotropic effects resulting in cancer cell death. Several data need to be combined to understand the mode of action of the NMT inhibitor in cancer cells:

- ✓ In-cell IC_{50} values of the 74 NMT substrates (Chapter 4)
- ✓ Half-lives of these substrates
- ✓ Information (e.g. from other published studies) showing the importance of a substrate in cancer cells
- ✓ Information on highly sensitive cells lines: if a particular pathway is upregulated in different cell lines sensitive to NMT inhibition, it would give clues as to the mode of action of the inhibitor.

It would be interesting to study the effect of IMP366 on a normal cell line, to assess if NMT inhibition would lead to unwanted toxicity to patients. Interestingly, experiments showed that this inhibitor was well tolerated in mice in the context of parasite infection, suggesting the presence of a potential therapeutic window.[43]

Chapter 6 HsNMT1 and HsNMT2 selectivity

Several methods were employed to study HsNMT isoform substrate specificity, both of recombinant enzymes and in cells.

For *in vitro* studies, tagged MyrCoA substrate analogues were incorporated in the presence of recombinant NMT to the N-terminal glycine of peptide or protein substrates. The tag in this system enables a second extremely selective and high-yielding chemical ligation to any reporter of choice, for instance a dye label (Section 1.10.3 and Figure 18).

First, *in vitro* myristoylation was tested in lysates from *E. coli* cells overexpressing *Plasmodium falciparum* ARF (PfARF). PfARF was shown to be a HsNMT substrate at the peptide level using the CPM assay (Dr. Victor Goncalves, Tate group Imperial College, London).[145] Conditions required to label and detect NMT substrates were optimised and then applied to HeLa lysates obtained from cells subjected to NMT inhibition for a few hours.

This Chapter also describes a method to prepare and screen peptide libraries in order to identify chemical differences in the protein binding pocket of HsNMT1 and HsNMT2. In this approach, libraries of peptides corresponding to the N-terminal sequences of known or putative NMT substrates were prepared on a cellulose membrane using the SPOT™ technology.[150] Incubation of the library with either recombinant HsNMT1 or HsNMT2 would allow the identification of isoform substrate specificities. If peptide substrates specific to a NMT isoform could be identified, they may provide a basis for peptidomimetic inhibitors to assist in validating a specific NMT as a new therapeutic target for cancer.

In-cell substrate specificity was also studied. HsNMT1 or HsNMT2 was knocked down using specific siRNA and YnC12 labelling could be used to identify the substrates of the remaining isoform.

6.1 *In vitro* studies using recombinant HsNMT1/2

6.1.1 *In vitro* myristoylation in cell lysate

6.1.1.1 Optimisation using PfARF overexpressed in *E. coli*

To test if it was possible to *N*-myristoylate protein substrates *in vitro,* experiments were carried out in *E. coli* cells overexpressing *Plasmodium falciparum* ARF (PfARF) according to Heal *et al.*[333] After cell lysis, lysates were subjected to *in vitro* myristoylation and capture reaction with YnTB or AzTB (Figure 17, Figure 98a). CaNMT was used as a positive control as it was employed by Heal *et al.* to myristoylate PfARF.[333]

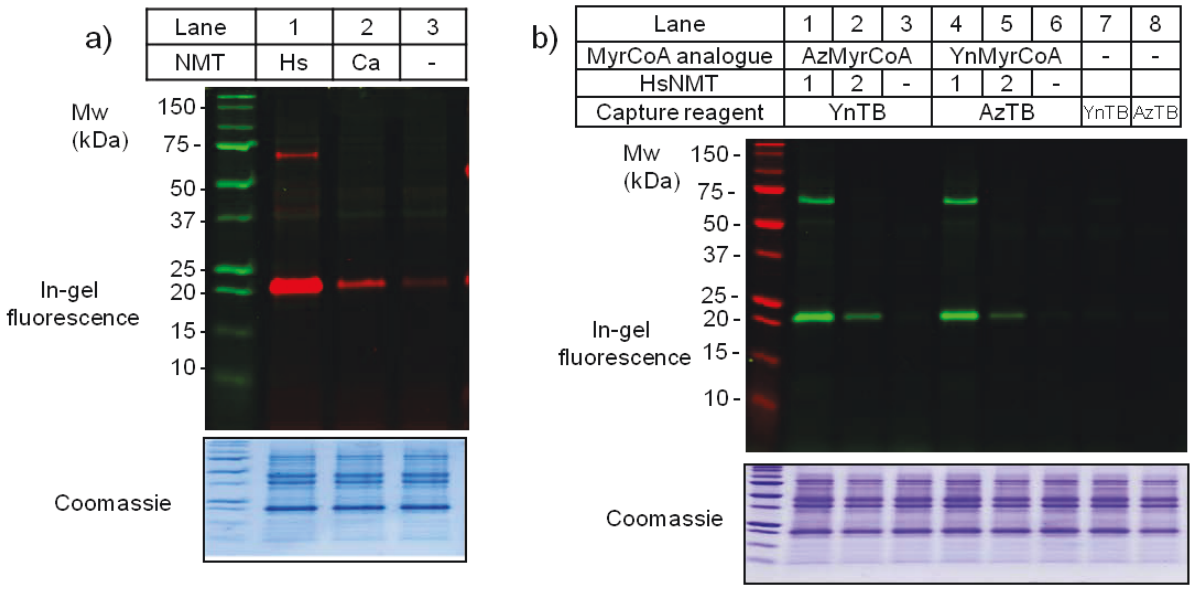

Figure 98. *In vitro* myristoylation of PfARF overexpressed in *E. coli* lysates. Tagged-analogue of MyrCoA was incubated with HsNMT for 10 min and added to the cell lysate (1mg/mL, final concetration of enzyme of 5 µg/mL and final concentration of MyrCoA analogues of 10 µM). The mixtures were incubated for 2 h at 37°C with constant agitation. Samples were then subjected to CuAAC (capture reaction) with AzTB or YnTB as described in Section 2.3 and analysed by in-gel fluorescence. Coomassie was used as a loading control. **a)** *In vitro* myristoylation was carried out in the presence of AzC12CoA and HsNMT1 (Hs) or CaNMT (Ca) or no enzyme. Azido-tagged proteins were captured with YnTB. **b)** *In vitro* myristoylation was carried out in the presence of AzC12CoA or YnC12CoA and HsNMT1 or HsNMT2 or no enzyme. Tagged proteins were captured with AzTB or YnTB. Lanes 3, 6, 7 and 8 correspond to negative controls.

PfARF can be seen by in-gel fluorescence with a band at 20 kDa in lanes 1 and 2 (Figure 98a). PfARF appeared to be a better substrate of HsNMT1 than CaNMT. In Lane 3, a band was also observed by fluorescence and corresponds to background labelling probably due to high abundance of PfARF in the lysate. An extra band was observed in lane 1 at 60-70 kDa. This band might correspond to HsNMT1. A similar experiment was carried out to compare the i*n vitro* myristoylation performed with HsNMT1 or HsNMT2 and also with YnC12CoA or AzC12CoA (Figure 98b). No labelling was

observed in the four negative controls (lane 3, 6, 7, 8), where no enzyme was used for the *in vitro* myristoylation step, suggesting that the experiment gave low background. A highly similar labelling pattern was obtained by using AzC12CoA or YnC12CoA, suggesting that both reagents could be used to carry out *in vitro* studies. The same extra band at 60-70 kDa was observed as in lane 1 in Figure 98a in the presence of HsNMT1, but this band was not observed with HsNMT2. Fluorescence labelling of PfARF appeared to be stronger in the presence of HsNMT1 than HsNMT2. Several explanations are possible. PfARF might be a better substrate of one of the NMT isoforms, or HsNMT2 might be less stable or the final concentration of HsNMT might have been inaccurate for the *in vitro* myristoylation step.

To check if the concentrations of HsNMT1 and HsNMT2 are the same, various concentrations were added to the *E. coli* lysate with overexpressed PfARF. The poly-His-tag present on both isoforms of recombinant HsNMT and PfARF was detected by chemiluminescence using enzyme coupled Neutravidin, Neutravidin-HRP (Horse Radish Peroxidase). Neutravidin is a deglycosylated form of avidin that has a high affinity for biotin with low non-specific binding. [334] The enzyme on Neutravidin is then detected selectively by a chemiluminescent substrate.

The signal was highly similar for HsNMT1 and HsNMT2 at the different concentrations used, suggesting that the concentrations were similar.

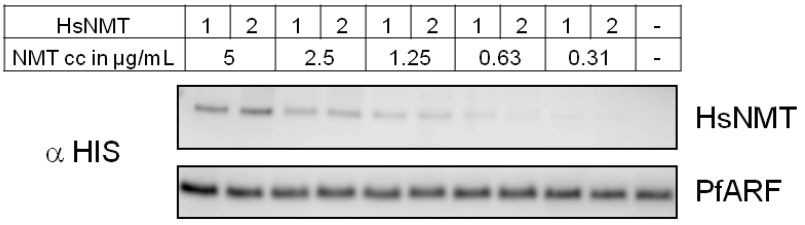

Figure 99. Verification of the enzyme concentration used for the *in vitro* myristoylation. HsNMT1/2 were added to *E. coli* lysate with overexpressed PfARF. Samples were separated on a SDS-Page gel. HsNMT1 and 2 are both HIS-tagged at the N-terminus and the tag can be detected by Neutravidin HRP and revealed in chemiluminescence. PfARF is also HIS-tagged and was used as a loading control.

A time course experiment was carried out to optimise the *in vitro* myristoylation reaction time (Figure 100a). *N*-myristoylation seemed to be complete after 1h with HsNMT1 and was slower with HsNMT2. The experiment was repeated for HsNMT2 with the *in vitro* myristoylation time increased up to 4 h (Figure 100b). The reaction was complete after 2 h with HsNMT2. For the following experiments, the *in vitro* myristoylation step was carried out for 2 h.

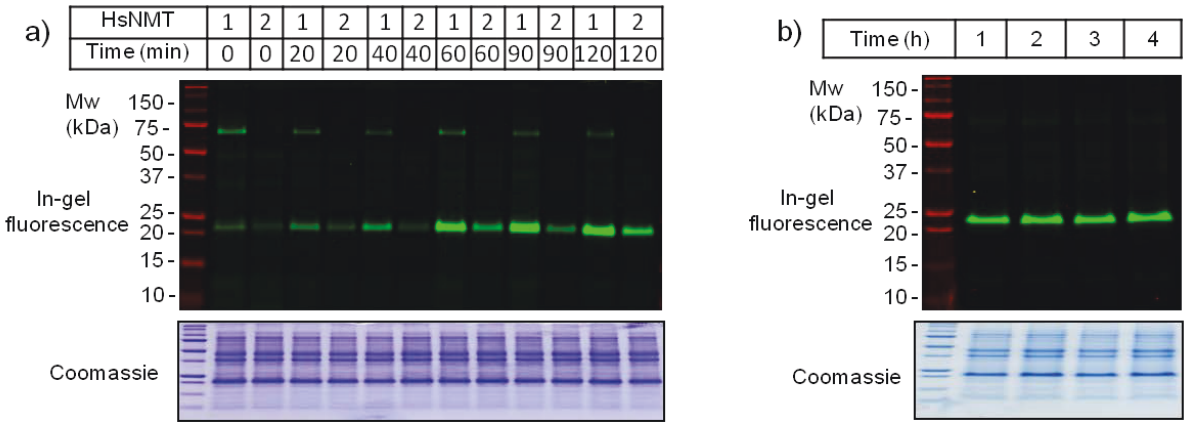

Figure 100. Optimisation of *in vitro* myristoylation time. A similar protocol as for Figure 98 was used. *In vitro* myristoylation was performed in the presence of AzC12CoA and **a)** HsNMT1/2 **b)** HsNMT2. CuAAC was carried out with YnTB. Coomassie was used as a loading control.

It would be interesting to understand why the reaction stopped after 1-2 h. It could be because all PfARF was consumed, or due to a low stability of the enzyme or the reagent. It is also possible that the concentration of the analogue of MyrCoA was too low, therefore this reagent was the limiting reagent. To check if all PfARF was myristoylated, a pull down experiment was carried out (Figure 101).

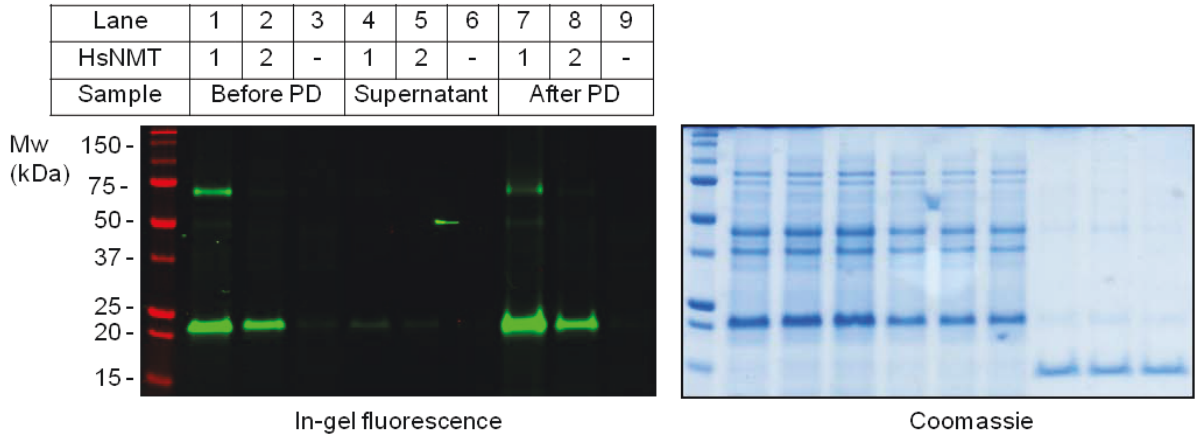

Figure 101. Pull down experiment to check if all PfARF was *N*-myristoylated *in vitro*. Lysates were subjected to *in vitro* myristoylation with AzC12CoA in the presence of HsNMT1, HsNMT2 or no enzyme for 2 h. The capture reaction was performed in the presence of YnTB and the samples were enriched as described in Section 2.3.4. 2 fold less protein was loaded for the supernatant samples compared to the samples before pull down (before PD) and pull down (PD). The strong band at 20 kDa seen by Coomassie corresponds to PfARF (overexpressed in *E. coli* lysate) and the band at 15 kDa in the PD samples corresponds to streptavidin released from the beads.

Not all PfARF was pulled down using these conditions, suggesting that not all PfARF was labelled and captured. It is probable that AzC12CoA was the limiting reagent of *in vitro* myristoylation.

The extra band at 60-70 kDa was also pulled down, suggesting that AzC12 is covalently attached to this protein, which is presumably HsNMT1. AzC12 could have been transferred to a cysteine residue or it is also possible that HIS-tagged HsNMT1 might *N*-myristoylate itself. The N-terminal sequence of His-tagged HsNMT1 (GSSHHHHHH) was prepared and tested in the CPM assay but showed no activity against both recombinant HsNMT1 and HsNMT2. It is unclear why this extra band is observed with HsNMT1 but not with HsNMT2.

To conclude, NMT substrates can be *N*-myristoylated *in vitro* in the presence of analogues of MyrCoA. Alkyne and azide analogues of MyrCoA gave similar results. The reaction seemed to be complete with both HsNMT isoforms after 2 h. *N*-myristoylated proteins can be detected by in-gel fluorescence, as previously described in Section 2.3 for HeLa cells labelled with YnC12. This method could be used to determine HsNMT1 and HsNMT2 substrate specificity *in vitro* in HeLa lysate.

6.1.1.2 Test *in vitro* myristoylation in HeLa cells lysate

In vitro myristoylation would be carried out in lysis buffer. It was preferable not to use detergent to lyse the cells as it could denature the enzyme and prevent *in vitro* myristoylation. A HEPES-based lysis buffer had been previously used in the group to perform *in vitro* enzymatic reactions and appeared suitable.[335] An experiment was carried out to ensure that *in vitro* myristoylation could occur in these conditions. PfARF was purified from *E. coli* lysates (Figure 102a). HeLa cells were treated with IMP366 for 6 h, lysed in HEPES lysis buffer and purified PfARF was added to the lysate (Figure 102b). As seen in lane 7, PfARF could be *N*-myristoylated in HEPES buffer. However, the background was relatively high as seen with some extra bands in lanes 5 and 6.

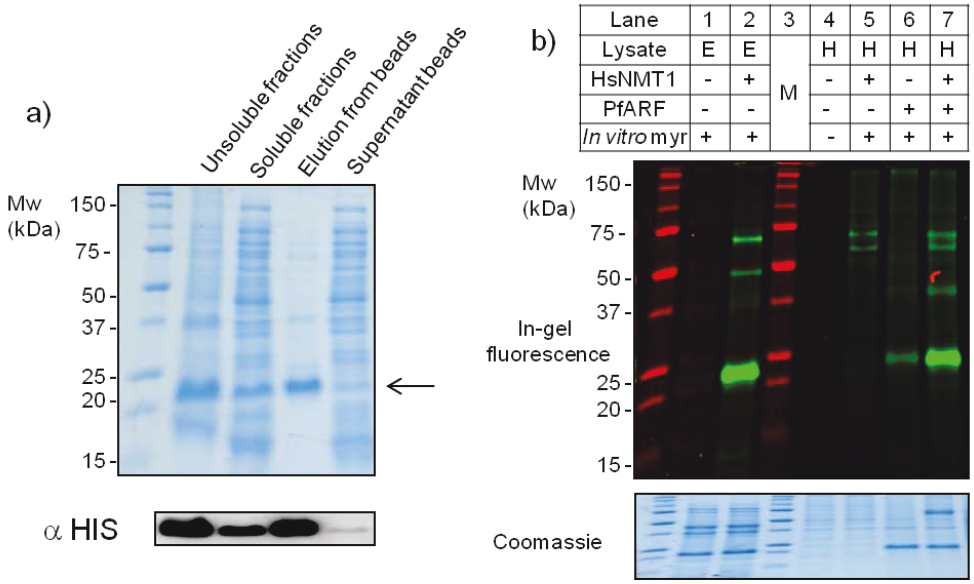

Figure 102. *In vitro* myristoylation of PfARF in HEPES lysis buffer. a) PfARF was purified from E. coli lysates. Top: Coomassie and Bottom: Western blot. An arrow indicates PfARF on the gel. **b)** M: Markers. E: *E. coli* lysate with overexpressed PfARF. H: HeLa cells lysate in HEPES lysis buffer. Cells were treated with IMP366 (1 µM) for 6 h. Purified PfARF was added to some samples (final concentration 0.2 mg/mL) and in vitro myristoylation was performed for samples in lanes 1, 2, 5, 6, 7, with HsNMT1 or no enzyme. All samples were subjected to CuAAC with AzTB.

In vitro myristoylation was tested again, without adding purified PfARF (Figure 103). The labelling obtained with HsNMT1 and YnC12CoA was compared to the labelling obtained with cells treated with YnC12 before lysis. Similar labelling patterns were observed for HeLa cells treated with YnC12 (lane 2) and *in vitro* myristoylation in the presence of YnC12CoA and recombinant HsNMT1 (lane 4). However, the strong fluorescent band seen in lane 2 at 20 kDa, and probably corresponding to ARF proteins (Chapter 4), was weak in lane 4. Moreover, the background in lane 4 was relatively high, possibly due to the labelling of cysteine residues with YnC12. A highly similar labelling pattern was obtained by replacing HsNMT1 with HsNMT2 (data not shown). Preliminary optimisation experiments (data not shown) showed that decreasing the amount of DTT (1 mM in the HEPES lysis buffer) increased the background. However, a high quantity of DTT might also inhibit the CuAAC reaction (data not shown). More optimisation would be required to decrease the background labelling and to understand why the proteins at 20 kDa cannot be efficiently *N*-myristoylated *in vitro*. However, it appeared more accurate to carry out in-cell studies of the isoform substrate specificities (Section 6.1.4) as this would reflect the *in vivo* substrate specificity of the two isoforms.

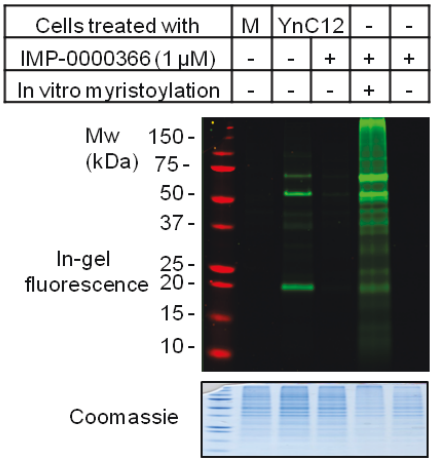

Figure 103. *In vitro* myristoylation in HeLa lysates. HeLa cells were labelled with myristic acid or YnC12 for 6 h and/or treated with IMP366 for 6 h. *In vitro* myristoylation was carried out on one sample in the presence of YnC12CoA and HsNMT1. All lanes were subjected to CuAAC with AzTB. In-gel fluorescence allowed the visualisation of tagged proteins and Coomassie was used as a loading control.

6.1.2 Spot synthesis

6.1.2.1 Assay principle

Several peptide libraries were prepared on cellulose membranes using an automated ResPep peptide synthesiser (Intavis). The membranes, purchased from Intavis, already contained a spacer (PEG linker, 10 PEG units) and were amino-functionalised. A cleavable linker was sometimes added before the peptide synthesis in order to perform post-synthesis cleavage of peptides. Two membranes of 600 individual peptides could be prepared simultaneously on the equipment available in the Tate group. After the synthesis, membranes were dried in a desiccator overnight to remove any residual solvent and cut into several units. After side-chain deprotection according to Intavis' protocol, the membrane units were ready to be used for on-support assay or cleavage of the spots for further analysis (Figure 104).

No assay had previously been developed to detect *N*-myristoylation on a solid support such as a cellulose membrane, therefore the assay conditions (concentration of reagents, time of the assay, method of detection, etc) required optimisation. The assay comprised three steps (Figure 104). First, the peptides were deprotected with a TFA mixture. The second step, later referred to as the *N*-myristoylation step, involved the incorporation of a myristic acid analogue to peptide substrates of HsNMT, using YnC12CoA or AzC12CoA. This step was carried out for 2 h in the presence of recombinant HsNMT1/2, as the analogous experiment in *E. coli* lysate (Section 6.1.1.1) showed that the reaction was complete after 2 h. The concentration of enzyme was set to 500 ng/mL as this concentration was used in early optimisation experiments for the CPM assay. Analogues of MyrCoA

were used at a concentration higher than K_M (around 1 µM). After incubation for 2 h, the unbound tagged MyrCoA analogues could be washed away.

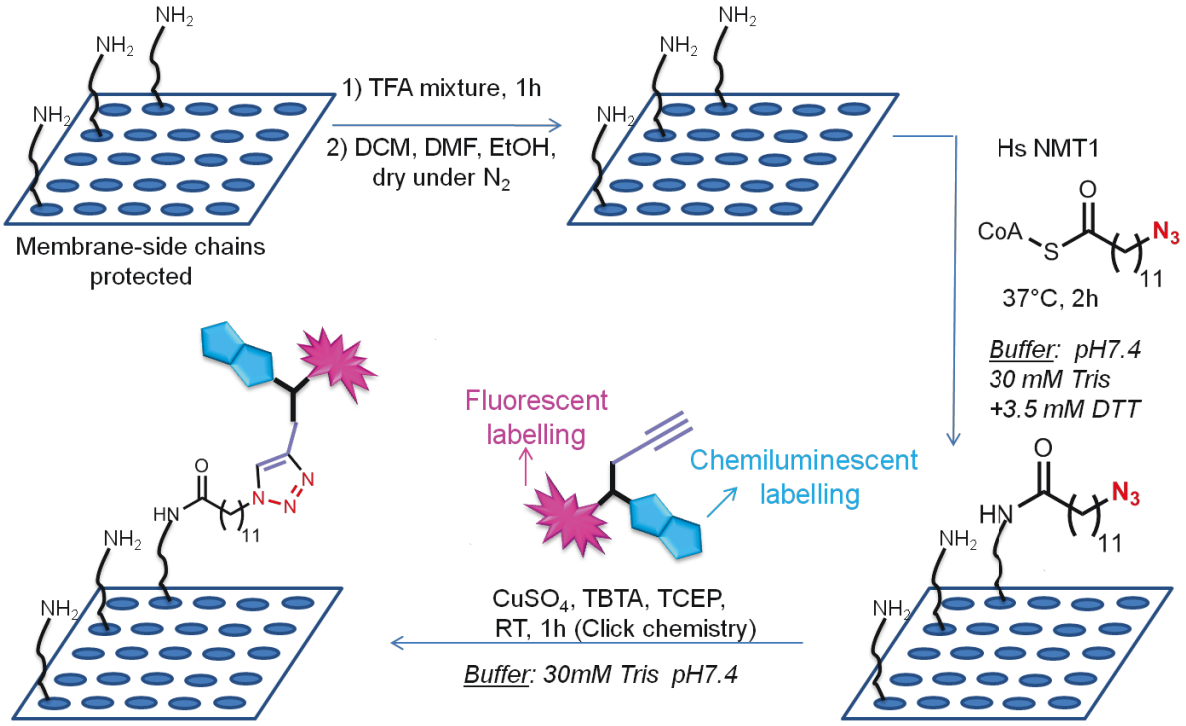

Figure 104. Typical myristoylation assay on membrane. First step: peptide side-chains deprotection. Second step: *in vitro* myristoylation. Third step: capture reaction (CuAAC, "click" reaction) which allows to detect the tagged peptides in fluorescence or chemiluminescence.

The third step corresponds to the capture reaction, where the tag (shown as an azido moiety in Figure 104) reacts selectively with a chemical reporter (the alkyne moiety in Figure 104) via bioorthogonal ligation. The chemical reporter carries an imaging probe, such as a fluorescent dye. Click chemistry was used as the bioorthogonal ligation in the assays. The reaction requires several reagents and the conditions were chosen according to conditions established previously for capture of YnC12-tagged proteins in HeLa cell lysate (0.1 mM capture reagent, 1 mM $CuSO_4$, 1 mM TCEP and 0.1 mM TBTA) (Section 2.3). By considering the amount of amino acid added per spot and assuming 100% yield, the amount of peptide was estimated at 0.1 µmol per spot. 30 mM Tris Buffer, 3.5 mM DTT pH 7.4 was chosen as the assay buffer as a similar buffer had been used in our group to study *N*-myristoylation *in vitro.*[154] For the capture reaction, DTT was not needed as the click ligation already requires the use of a reducing agent (TCEP).

Several membranes were prepared in order to check the reliability of peptide synthesis on a cellulose membrane and the reliability of the detection method. Typically one membrane made of

several repeating units was prepared. The membrane was then cut to separate all the repeating units which were analysed separately to optimise the detection methods. The peptide sequences of the membranes prepared during this study, referred to here as membrane A-F, can be found in Appendix J.

8 or 15 amino acid peptides corresponding to the N-terminus of putative *N*-myristoylated proteins (Section 1.4.2) were synthesised on the membrane and several controls were included:

✓ Positive controls:

-Known myristoylated proteins

-CuAAC controls: an azido or alkyne moiety was added at the N-terminus of peptides synthesised on the membrane to control the efficiency of the CuAAC reaction. In early experiments, 5-hexynoic acid and AzC12 were coupled at the peptides N-terminus. Later, AzC12 was replaced by 4-azidobutyric acid 67 (Figure 105). This compound was prepared in two steps from the commercially available ethyl 4-azidobutyrate 65, according to the procedure employed to prepare AzC12 **15** (Section 2.1.2).

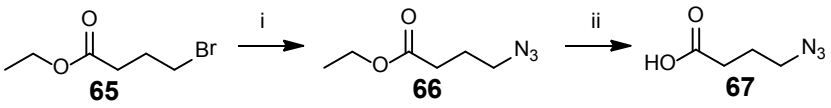

65 **66** **67**

Figure 105. Preparation of 4-azidobutyric acid. Reagents and conditions: i) NaN_3, DMSO, RT, 91%; ii) NaOH 2N, MeOH, quantitative.

✓ Negative controls:

-Non *N*-myristoylated proteins

-G2A controls: known myristoylated protein where the N-terminal glycine was replaced by alanine.

-Known myristoylated proteins acetylated at the N-terminus.

-Cysteine and tryptophan rich sequences were added as controls, as these amino acids were suspected to give non-specific background in fluorescence.

Furthermore, a few spots were low-loaded using a mixture of Fmoc:Boc 1:10 amino acid as the first coupled residue, and some peptides were only 8 amino acids long (instead of 15 amino acids).

6.1.2.2 Optimisation of the synthesis

6.1.2.2.1 Check membrane quality

To check the membrane quality, a cleavable linker was added at the C-terminus of some peptides. This allowed these peptides to be cleaved from the membrane for analysis by MALDI or LC-MS.

Membrane A (Appendix J) was prepared by first coupling a cleavable linker, 4-hydroxymethylbenzoic acid (HMB) **69**, onto the membrane **68** (Figure 106). A similar experiment was described in the literature and comprised the use of TBTU (1.1 eq) and DIPEA (2 eq).[336] TBTU was replaced by HBTU in the present work, which is a similar reagent. The coupling of the first amino acid, Fmoc-Gly-OH, via an esterification reaction is known to be difficult on cellulose membrane. Ay *et al.* improved this reaction by using 3 eq of CDI as activator in the reaction.[337] 15 amino acids were subsequently coupled by standard solid-phase peptide synthesis (SPPS).

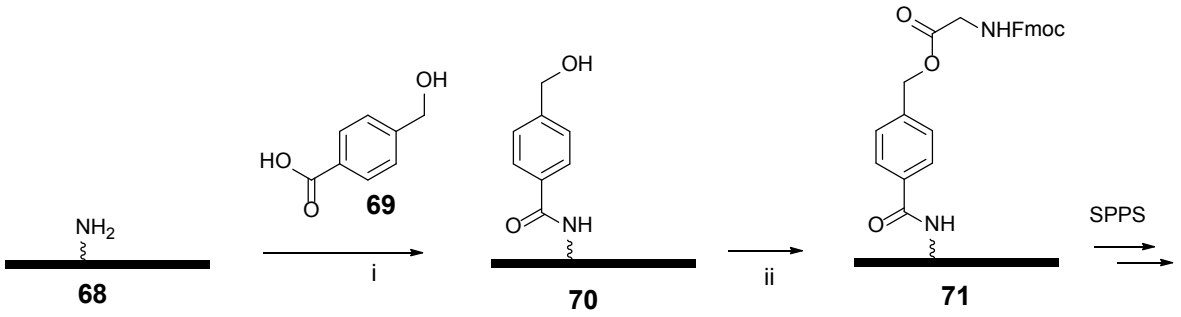

Figure 106. Attachment of the HMB linker to the cellulose membrane before SPPS. Reagents: i) HBTU, DIPEA, NMP; ii) Fmoc-Gly-OH, CDI, NMP.

HMB is labile to nucleophilic attack. Several cleavage procedures were proposed in the literature including ammonia vapour to give the carboxamide,[338] high pressure ammonia/THF vapour using a Schlenk line,[339] 1N NaOH,[340] or methanolic ammonia.[341] The two methods using ammonia vapour appeared to be less convenient and less safe than the other methods, and the use of 1N NaOH could be problematic for the analysis of the sample by LC-MS, due to high salt concentration in the sample. A mixture of ammonia in methanol was thus preferred.

The spots were punched out in different wells of a 96-well plate and the peptides were cleaved overnight using 7N ammonia in MeOH. The mixture was allowed to evaporate and the peptides were dissolved in a mixture of H_2O/MeOH. The amount of peptide for one spot was small (<1 μmol) and a pellet was usually not observed, thus it was difficult to check if the cleavage method was efficient. Attempts to analyse few cleaved peptides by LCMS were unsuccessful, as the amount of analyte was likely too small to be detected. MALDI analysis was more efficient as a few masses were detected;

however, the masses corresponding to the full length peptides were not detected. It was proposed that the problem was due to an inefficient esterification reaction between the HMB linker and the first amino acid. To solve this problem, a linker composed of Fmoc-Gly-OH and HMB **69**, was prepared in solution, prior to attachment to membranes (Compound **74**, Figure 107). Two methods were proposed to prepare this cleavable linker from the commercially available HMB **69**. The first one relies on the orthogonal protection of the acid **69,** by a phenacyl protecting group, to prevent trans-esterification in the next step (Figure 107).[342] Compound **72** was then coupled to Fmoc-Gly-OH via an esterification reaction mediated by DCC and DMAP. Subsequent removal of the phenacyl protecting group using zinc powder and AcOH gave the crude Fmoc-Gly-HMB-OH **74**. Pure **74** was obtained after silica-gel purification with an overall yield of 71%.

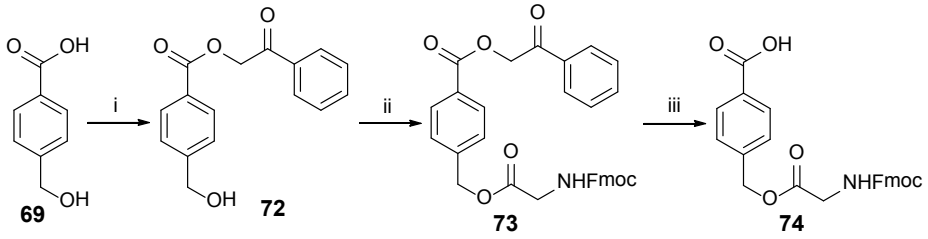

Figure 107. Synthesis of Fmoc-Gly-HMB-OH. Reagents and conditions: i) 2-Bromoacetophenone, Et_3N, EtOAc, RT, quantitative; ii) Fmoc-Gly-OH, DCC, DMAP, DCM, 91%; iii) Zn, AcOH, H_2O, EtOAc, 78%

The second method proposed to prepare the linker **74** relies on the direct coupling of the carboxylic acid **69** with Fmoc-Gly-OH **75**, following the procedure of Ay *et al*.[337] An excess of Fmoc-Gly-OH **75**(2 eq) was necessary to prevent trans-esterification of compound **69**. Purification of the crude product by silica gel column chromatography gave **74** in relatively low yield (26%), thus the former method was preferred (71% overall yield), despite the longer reaction sequence.

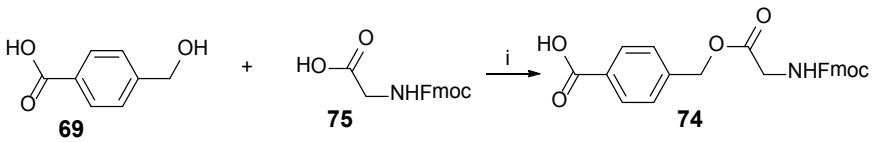

Figure 108. Synthesis of Fmoc-Gly-HMB-OH in one step. Reagents and conditions: CDI, DMF, RT, 26%

Membrane B was prepared using two different cleavable linkers (see Appendix J). The membrane was composed of 12 repeated units of 24 peptides. 6 units were prepared without any cleavable linker, 3 with the Fmoc-Gly-HMB-OH linker **74** and 3 with a rink amide linker **75** (Figure 109). The two linkers were coupled using HBTU/DIPEA, as normal amino acids in the sequence.

Rink amide linker is acid labile and can be cleaved by TFA during side chain deprotection. This linker is widely used in SPOT™ synthesis to check synthesis quality [159] and would be an additional control. However, it would not be possible to use the membrane unit bearing the rink linker to perform on-membrane assays as side-chain deprotection with TFA is required prior to the assay.

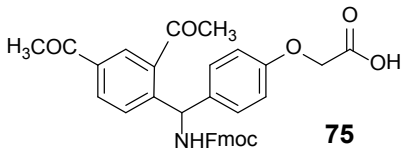

75

Figure 109. Rink amide linker

After the synthesis, peptides synthesised on a HMB linker-unit or on a rink amide linker-unit were cleaved in solution. The peptides on the HMB unit were cleaved after side-chain deprotection with TFA using 7N ammonia in MeOH as described above. Peptides on the rink amide unit were cleaved with a mixture of TFA:TIS:H_2O:EDT 94:1:2.5:2.5.

Most compounds characterised by MALDI were shown to be of the correct molecular weight and sufficient purity (only few other masses detected) to do on-support assays. Most of the spots contained contaminating shorter sequences but they should not be a problem for the assay since they are acetylated at the end and therefore cannot be myristoylated to give a signal in chemiluminescence. For a few peptides, such as low loading peptides or peptides with shorter sequence (8 amino acids), the expected molecular weight was not detected by MALDI. This may be due to a problem during analysis or isolation/synthesis.

6.1.2.2.2 Check the relative amount of peptides

Peptide synthesis on the membrane could be checked by staining the membrane with bromophenol blue or Ponceau S (Figure 110). However, the spot intensity varied with the sequences. The staining depends on the number of free amino groups since the reagents are acid/base indicators. For example, it was expected to see no spot on position A1, A2, D5 and E1 in Figure 110 c and d as the peptides have a no free amino group. Ponceau S and bromophenol blue gave similar results (Figure 110 c and d). However, some spots have a weaker intensity and this might be due to a problem during the synthesis. Fmoc fluorescence might be a more efficient method of determining coupling efficiency. Before Fmoc-deprotection, the intensity of the spots should be identical if the synthesis was efficient.

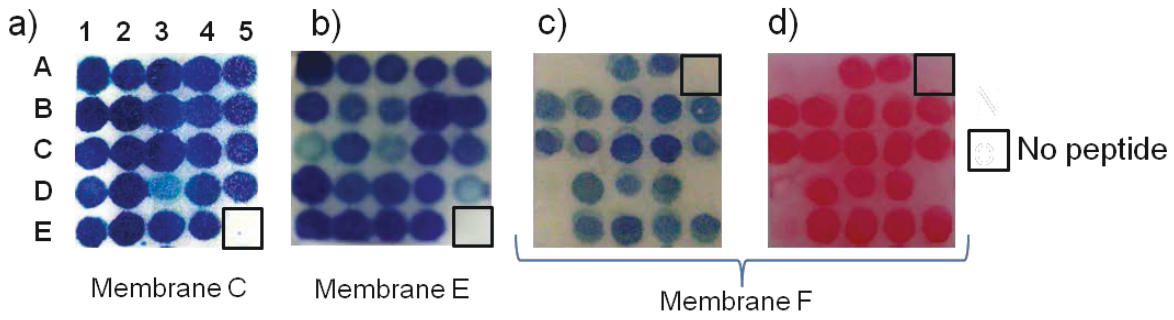

Figure 110. Membrane staining with bromophenol blue (a-c) or Ponceau S (d). The position with no peptide on the membrane is indicated by a black box. a) Membrane C. b) Membrane E. Membrane F is shown in c) and d).

6.1.2.3 Detection method

6.1.2.3.1 Fluorescence:

Various fluorescent reagents were tested on the membrane: AzTB, Yn-fluorescein, Yn-BODIPY. Only the CuAAC reaction was carried out and thus only the CuAAC controls should have given a signal in fluorescence. However, all these reagents gave high background in the negative controls, due to the auto-fluorescence of some peptides and probably because the capture reagent stuck unspecifically to the membrane and the peptides (data not shown). Copper used for the CuAAC reaction was suspected to give high background. However, the use of a strain promoted azide alkyne cycloaddition reagent (DABCO-TAMRA) **75** (Figure 111), available in the Tate group, did not reduce the background. Stringent washes for 1 h with NaOH 0.1 N or blocking the membrane for 1 h before the CuAAC did not decrease the background. Finally, membranes were captured with a DABCO-biotin **76** reagent, blocked in 5% milk before being incubated with Streptavidin Alexa Fluor 647 (1/10 000) in 5% milk and image in chemiluminescence. Using this method, a high background was also obtained. All these results suggested that fluorescence could not be used as a reliable detection method on cellulose membrane. This was confirmed by Mahrenholz *et al.*[343] as they also showed that fluorescence gave high background on cellulose membranes. It seemed preferable to use chemiluminescence as a detection method.

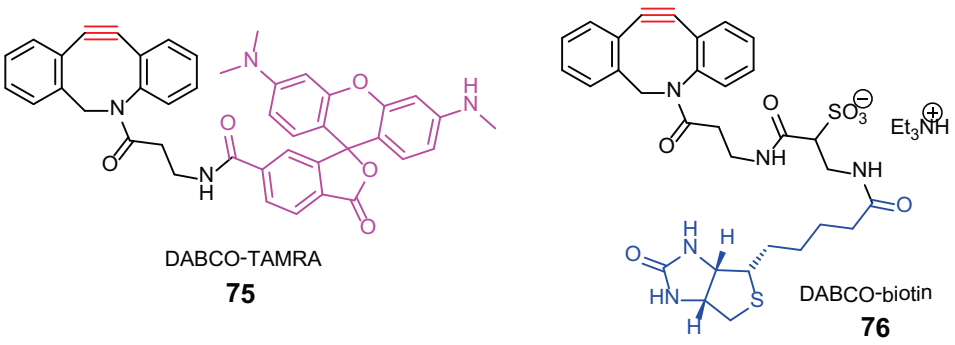

Figure 111. Structure of DABCO-TAMRA 75 and DABCO-biotin 76.

6.1.2.3.2 Chemiluminescence

The procedure using chemiluminescence was slightly different to the procedure using fluorescence. After the capture reaction using a biotinylated probe, the membrane was blocked with Bovine Serum Albumin (BSA) to prevent non-specific protein interactions. The bound capture reagent was probed with Neutravidin-HRP, and a series of controls were performed to determine whether chemiluminescence gave less background than fluorescence.

✓ **Control 1:** no *N*-myristoylation - no capture reaction

The membrane was probed in chemiluminescence directly after side chain deprotection of the peptides. The membrane was blocked, probed with Neutravidin-HRP and with the chemiluminescent reagent. Figure 112 demonstrates that there was no high non-specific background using this method. However, it should be noted that spot A4 (Figure 112a) appeared to have a small signal in chemiluminescence, probably due to low-level non-specific interaction.

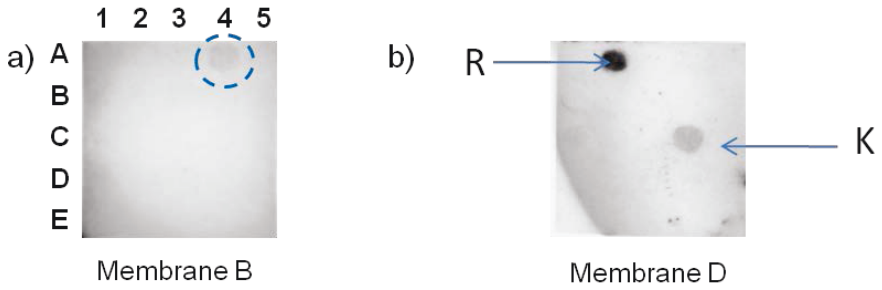

Figure 112. Background in chemiluminescence. Membranes B (a) and D (b) were probed in chemiluminescence, without prior *N*-myristoylation or CuAAC. a) Spot A4 (peptide sequence: azido-GSNKSKPKDASQRRR, showed a small signal (exposure time 2 min). b) All peptides on the membrane have the following sequence: $GGGX_5GGG$, where X_5 represents a 5-fold repeat of any amino acid. Peptides showed a signal in chemiluminescence when X was R and K.

Mahrenholz *et al.* suggested that some amino acids could also give high background in chemiluminescence.[343] A membrane comprising peptides made of 5 repeating units of each amino acid was prepared. As suggested by Mahrenholz et al., Arg and Lys gave relatively high background.

✓ **Control 2:** Only the capture reaction

A second control on membrane B was performed to check that the capture reaction was possible on the solid support and to verify that it was specific. The capture reaction was performed after side-chain deprotection of the peptides and the membrane unit was probed in chemiluminescence. More spots than expected were detected, as can be seen in Figure 113. Only four spots, corresponding to the click controls, should be detected. These click controls have an azido moiety at the end of the peptide chain and should specifically react with YnTB when subjected to the CuAAC reaction.

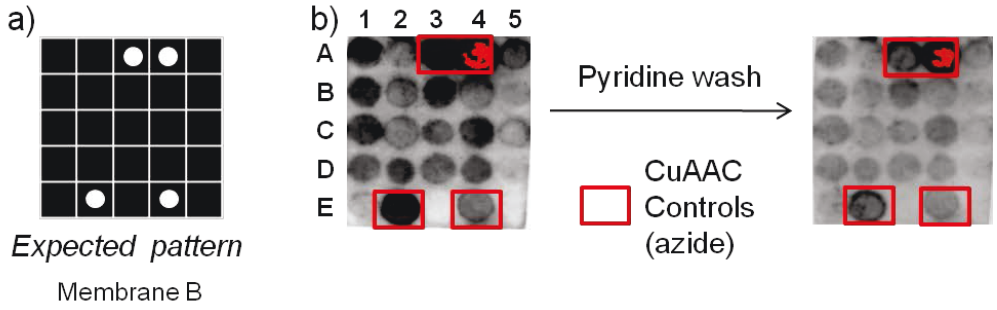

Figure 113: Image in chemiluminescence of membrane B after only the capture reaction (with YnTB). Subsequent wash with pyridine gave a different pattern. The click controls (azide) are outlined in red.

It was then proposed that this unexpected pattern could be caused by the non-specific interaction of copper with some peptides. As pyridine is known to be a good ligand for copper, the membrane was stripped and washed for 1 hour with pyridine. The membrane was then washed several times with DMF, DCM and EtOH to remove pyridine and probed again. Washing the membrane with a solution of EDTA gave similar results. Only three spots were unaffected by the washes, all corresponding to the click controls. One click control (E4,Figure 113) could not be detected, perhaps due to a problem during the synthesis.

✓ **Assay:** membrane B

A normal assay was then performed (Figure 114). As observed in Figure 113 , the background was high and the membrane was washed with pyridine. Interestingly, the same click controls as in Figure 113 were detected, with three other spots corresponding to known myristoylated peptides. The peptide sequences of spots B1, C1, D1 are based on the N-terminal sequence of c-SRC. D1 has only 8 amino acids while B1 and C1 are composed of 15 amino acids. The C1 SRC peptide has a low loading (10%) compared to B1. Chemiluminescence signal was highly similar for spots B1, C1, D1, suggesting that 8 amino acids are enough for enzyme recognition and that a smaller amount of peptide is required to obtain a maximum signal in chemiluminescence. Spots B2, C2, D2, based on the N-terminal sequence of ARF were expected to be myristoylated as well. The reason why they are not myristoylated is not yet clear, and tryptophan or cysteine rich sequences were not prone to high background. These results were promising but required further experimental validation.

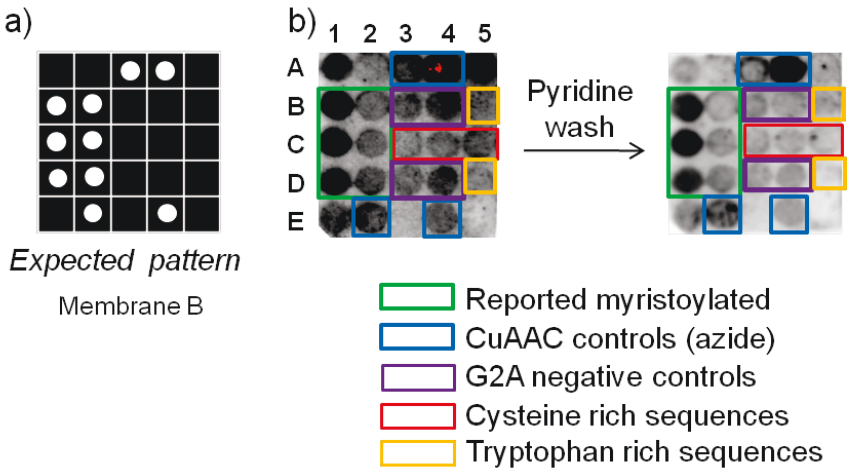

Figure 114: Image in chemiluminescence of membrane B after *N*-myristoylation (with HsNMT1 and AzC12CoA) and capture reaction (with YnTB). a) Expected pattern**. b)** Subsequent wash with pyridine gave a different pattern. The CuAAC controls (azide) are outlined in red. The known myristoylated peptides are outlined in green.

✓ **Assay:** reproducibility of the syntheses

Membrane C was synthesised twice, at different time, to control for the reproducibility of the synthesis (Figure 115). A similar pattern was obtained in Figure 115 b and c, suggesting that the peptide synthesis and the assay were reproducible.

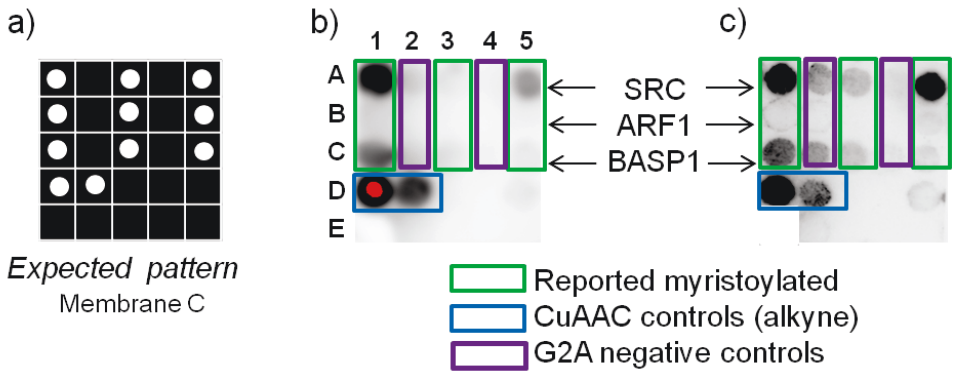

Figure 115. Reproducibility of the synthesis and the assay. Units of membrane C (b and c) were synthesised and subjected to in vitro myristoylation (YnC12CoA and HsNMT1) and CuAAC (with AzTB) for comparison. The expected pattern is shown in a).

✓ **Assay: test different capture reagents**

The previous assays were all carried out with AzTB or YnTB via a CuAAC reaction and gave similar patterns. It appeared advantageous to use a copper free/strain promoted azide-alkyne cycloaddition (SPAAC) reagent, as this would not require a subsequent washing step with pyridine or EDTA. The strain promoted reagent **76** (Figure 111), was compared to AzTB (Figure 116).

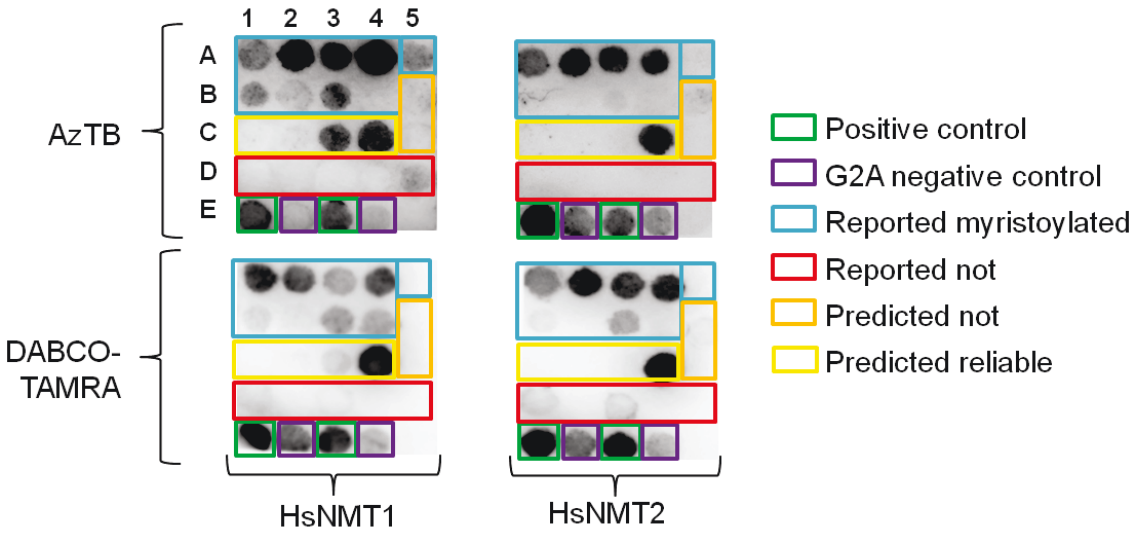

Figure 116. Comparison of two capture reagents. Units of membrane E were subjected to *in vitro* myristoylation followed by CuAAC reaction with AzTB (1 µM) or SPAAC with DABCO-TAMRA (0.2 µM). Peptide sequences can be seen in Appendix J.

Interestingly, the two reagents, AzTB (CuAAC) and DABCO-TAMRA (SPAAC), gave similar results for both HsNMT isoforms. As expected, no signal was obtained for peptides reported or predicted not to

be *N*-myristoylated. A weak signal was obtained for the G2A controls. It is possible that G2A peptides might be low affinity substrates of HsNMT, even if an N-terminal glycine is known to be optimal for *N*-myristoylation (Chapter 1). Interestingly, a few peptides, such as peptide C3, seem to have a different pattern when a different HsNMT isoform was used.

For validation of these results, a few of the labelled peptides were synthesised using standard SPPS techniques and tested with the CPM assay (Table 14). Interestingly, peptide C3 had a lower K_M value with HsNMT1, which suggests (as seen in Figure 116) that it is a better substrate of HsNMT1. Further experimental analysis is required to validate these results.

The ratio K_{cat}/K_M , also referred as to the specificity constant, [344] can also be used to compared the enzyme-catalysed reaction efficiencies. K_{cat} is the catalytic constant, also referred to as the turnover number. It can be calculated by dividing V_{max} by the enzyme concentration. The ratios K_{cat}/K_M were different for HsNMT1 and HsNMT2 for all the peptides shown in Table 14. It is unclear if this ratio is a good indication of the isoforms substrate specificity as this ratio has been suggested to have some limitations.[345]

Table 14. Kinetic parameters of peptides presented in Figure 116 evaluated with the CPM assay in the presence of a saturating amount of MyrCoA. Error < 10%.

	HsNMT1			HsNMT2		
Peptide	K_M (μM)	*V*max (RFU/min)	K_{cat}/K_M (x10^5 RFU/min/μM)	K_M (μM)	*V*max (RFU/min)	K_{cat}/K_M (x10^5 RFU/min/μM)
A2	21.61	101388	9.3	9.01	21434	4.7
A3	0.54	47774	174.7	0.51	11662	45.3
C3	7.08	23653	6.6	63.3	15678	0.5
C4	10.93	79674	14.4	9.74	17384	3.5

6.1.2.4 Screening of a small peptide library

A small peptide library (141 peptides) was prepared on a cellulose membrane (2 repeating units, one for each HsNMT isoform, membrane G, Appendix J). The membrane units were screened against HsNMT1 and HsNMT2 using DABCO-biotin (Figure 117). The membrane was quite large, and difficult to fit in a dish without wasting reagents; this may have resulted in a problem during incubation of the membrane with HsNMT1, as no spots can be seen from positions 1 to 9. Future studies should consider screening a smaller membrane.

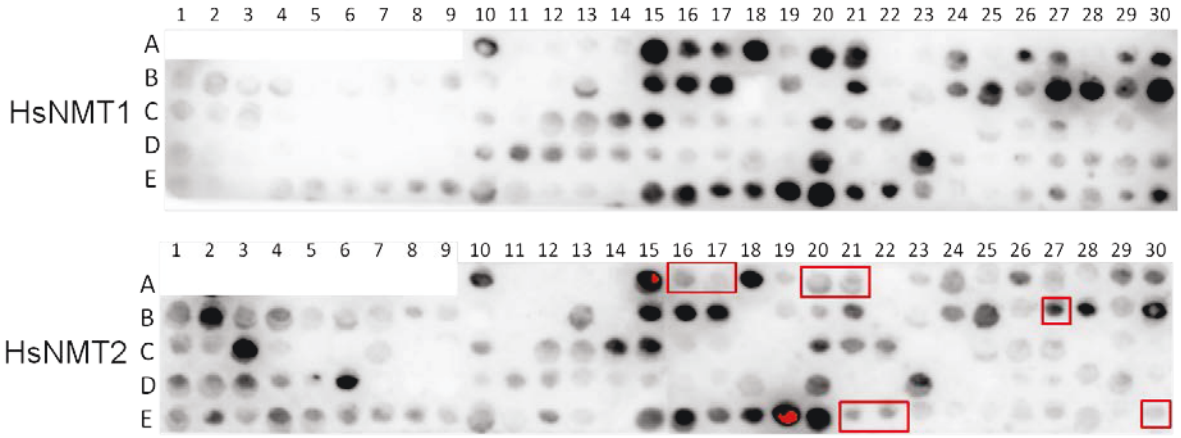

Figure 117. Assessment of 141 putative HsNMT substrates. Sequences can be found in Appendix J (Membrane G). Peptides circled in red seem to be better substrates of HsNMT1 over HsNMT2.

As expected, c-SRC (E20) was detected on both membranes. However, N-terminal sequences of proteins identified as substrates in Chapter 4, were not myristoylated, such as tescalin (A11) or NDUFB7 (A14). It is possible that these peptides have a lower affinity for the enzyme and that they require a higher concentration of YnC12CoA or enzyme to be *in vitro* myristoylated.

Some differences could be observed between both membranes. Peptides outlined in red seemed to be better substrates of HsNMT1. Alignment of these peptide sequences did reveal a consensus, however, for potentially selective peptides (Figure 118). Only Gly in position 1 and Ser in position 5 were common to the 8 peptides, and these two amino acids are often observed for NMT substrates (Section 1.4.2).

```
MARCKS (A16)                    GAQFSKT--AAKGEAAA-
Cytochrome B5 reductase (A17)   GAQLSTLGHMVLFPV---
Adenylate kinase 1 (A20)        GCCSSS---DPRREDDLR
XRP2 (A21)                      GCFFSKR---RKADKESR
Hippocalcin 2                   GKQNSKLRPEMLQDL---
Dymeclin                        GSNSSRIGDLPKNEY---
MARCKS like 1                   GSQSSK---APRGDVTAE
Cyclin dependant kinase 5       GTVLSL---SPASSAKGR
                                *   *
```

Figure 118. Sequence alignment of peptides outlined in red on Figure 117.The alignment was performed with Cluster omega.

6.1.2.5 Conclusions SPOT synthesis and introduction to microarrays

The peptide screening results are promising but require validation as the number of NMT substrates seems relatively low (30-40 out of the 141 peptides). It would be interesting to prepare a new membrane with only the NMT substrates identified with high confidence in Chapter 4. The main

disadvantages of SPOT synthesis are that the peptides might be of variable quality, fluorescence cannot be used as a detection method, and it is impossible to determine a K_M value for the peptides. These problems could be solved using small molecule microarrays (SMM).[346] A SMM is a miniaturized tool that allows screening many different compounds at once and is mainly used to discover protein-small molecule interactions.[346,347] A library of chemically synthesised compounds is printed on a glass plate. The compounds bind covalently or via a strong interaction (biotin-avidin, thiol-alkene...) to the glass plate. Using this technique, it is possible to quantify the binding activities by printing different amount of compounds on the plate.[151] Several groups have carried out SMM-based enzyme assays and fingerprinting studies.[347-349] The spots are smaller than the spots obtained with arrays on cellulose membrane, also referred to macroarrays (0.1-0.5 mm). The signal-to-background ratio is usually high as the peptides are more accessible to be screened at planar surfaces and fluorescence can be used [350]. However, this technique needs certain equipment and is also time consuming and expensive as all the compounds need to be prepared in solution or using SPPS before being printed on the glass plate.

A small library of peptides bearing a PEG-biotin moiety at the C-terminus were prepared and spotted on a streptavidin functionalised microscope slide [151] by an OmniGrid Micro microarrayer (Digilab, UK) using 946MP2 pins (ArrayIt, USA) Microarrayer (in collaboration with Dr. Ali Salehi-Reyhani, Professor Paul French and Dr Mark Neil research groups, Imperial College London).

As a control, AzTB was spotted on the glass plate but after several washes with PBS, no fluorescent signal could be detected using the Ettan Dige Imager (EDI, GE Healthcare) equipment generally used to image in-gel fluorescence, probably due to the low amount of fluorophore attached to the plate and the sensitivity limit of the EDI. Fluorescence was thus detected with a TIRF (total internal reflection fluorescence) microscope. The sensitivity was much higher than the EDI. However, the glass plate functionalisation was not perfect as small dust particles were stuck to the plate and some scratches could be observed with the microscope. Another procedure could have been used to improve functionalisation.[351] However, the spotting on the glass plate was extremely laborious as the needle used to spot the solution had to be manually removed and washed each time the solution was changed. The software was not user friendly as each spot had to be set up manually with the coordinates on the plate. Moreover, for detection spots would need to be analysed one by one. It appeared extremely time consuming to optimise and screen a small library of peptides (around 100) using these equipments. However, this method holds promise if efficient automation and detection platforms were available.

6.1.3 ELISA assay

A few peptides could not be characterised using the CPM assay for several reasons. Some peptides corresponding to the N-terminal sequences of NMT substrates, such as FYN and XRP2, contained a cysteine residue. This amino acid is not compatible with the CPM assay as it leads to high background (Section 2.2.2). Other peptides, such as HCCS were highly insoluble in the CPM assay buffer. Preparing different lengths of HCCS (from 8 AA to 22 AA) did not improve the solubility.

During the project described in this thesis, an ELISA assay was being developed in parallel by Dr. Antonio Konitsiotis (Tate group, Imperial College London) for an unrelated acyl transferase, and appeared attractive to solve the problems listed above. The peptides were synthesised with a biotin moiety at the C-terminus and bound to a streptavidin-coated 96-well plate (Figure 119). The peptides were incubated with recombinant HsNMT1/2 in the presence of YnC12CoA. After 1 h, the plate-bound peptides were washed and captured with an azido-FLAG peptide. After several washes, FLAG could be specifically recognised by a HRP-coupled FLAG antibody. The HRP substrate was revealed using a TMB (3,3', 5,5' tetramethyl benzidine) substrate (BD Biosciences) which allowed the detection of the antibody by absorbance. Absorbance should be proportional to the amount of alkyne-tagged peptides in the plates, and the assay differs from the CPM assay since it can only operate as an end-point assay (the CPM assay can be end-point or continuous).

ELISA experiments were carried out with 15AA c-SRC biotinylated at the C-terminus. Conditions used in the assay (buffers, concentrations of reagents, incubation time) were optimised by Antonio Konitsiotis (Tate group, Imperial College London). All the other experiments described here have been carried out by the author.

For the first experiment, 1 µM of peptide, 4 µM YnC12CoA and 500 ng/mL of enzyme were used. An acetylated c-SRC biotinylated peptide was prepared as a negative control (Figure 120). MyrCoA and no enzyme were also used as negative control. A similar absorbance signal was obtained for HsNMT1 and HsNMT2 in the presence of YnC12CoA. A low signal was observed in all the controls and the Z factor was close to 1, suggesting that the background is relatively low for this assay.

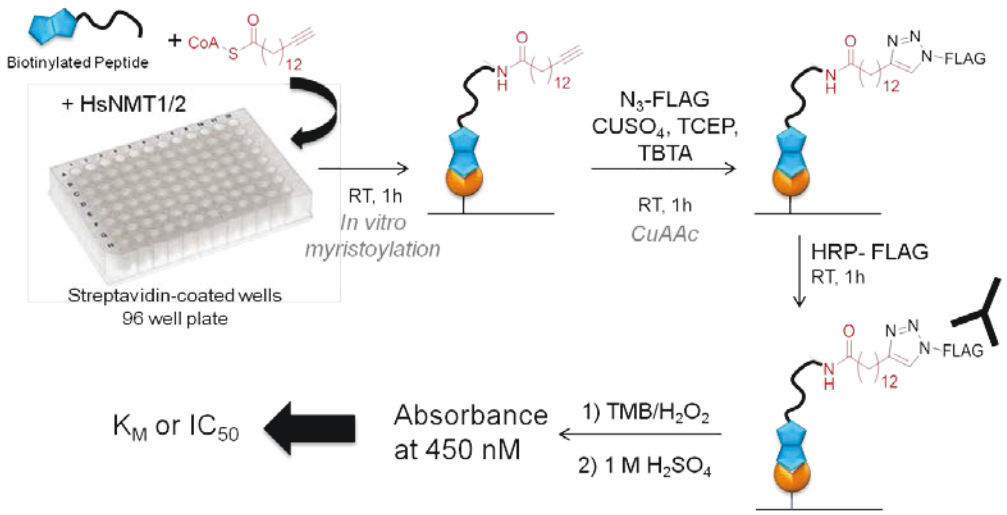

Figure 119 ELISA **NMT assay**

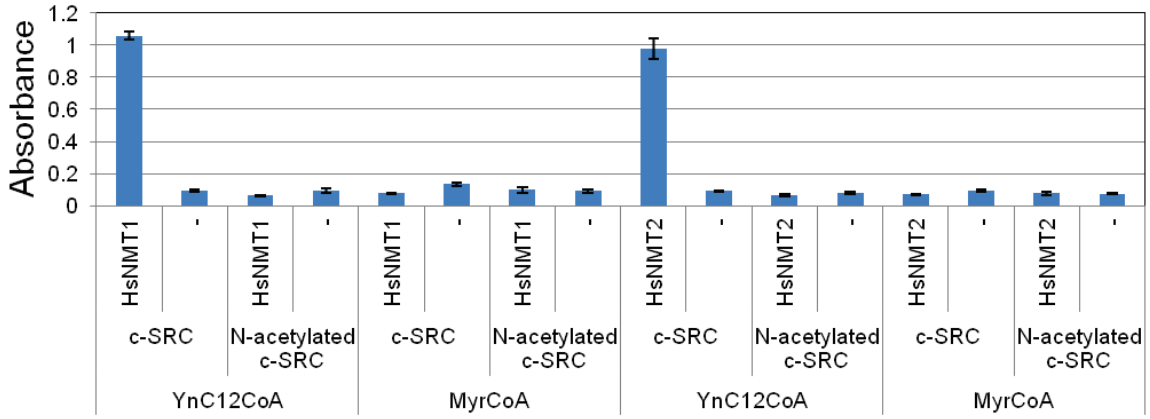

Figure 120. ELISA assay with 15AA biotinylated c-SRC. The error bars represent the standard deviation of two replicates. 15AA c-SRC and N-acetylated 15AA c-SRC (both biotinylated at the C-terminus) were incubated in the presence of YnC12CoA or MyrCoA (4 µM) and recombinant HsNMT1 or HsNMT2 (500 ng/mL) for 1 h in the streptavidin coated plate. After several washes, the plate-bound peptide was captured with Az-FLAG, and revealed using the TMB substrate reagent set (BD Biosciences). The Z factor of the assay was estimated for HsNMT1 (0.99) and HsNMT2 (0.98) in the presence of YnC12CoA and c-SRC (the background was the sample with the same conditions but no enzyme).

The concentration of enzyme used in this ELISA assay was optimised across a range of several concentrations of HsNMT1/2 (0.16–2500 ng/mL) with 1 µM YnC12CoA and 4 µM peptide (Figure 121a). The absorbance signal was obtained by subtracting the signal from the no enzyme control. From 10 to 1000 ng/mL there is acceptable correlation between absorbance and concentration of enzyme. It was decided to use 300 ng/mL, the same concentration as in the CPM assay, to compare results between assays.

The K_M of YnC12CoA and the K_M of 15AA c-SRC were determined (Figure 121b). The values were similar to the values obtained with the CPM assay, confirming that the ELISA assay could be used to determine the kinetic parameters of peptides.

a)

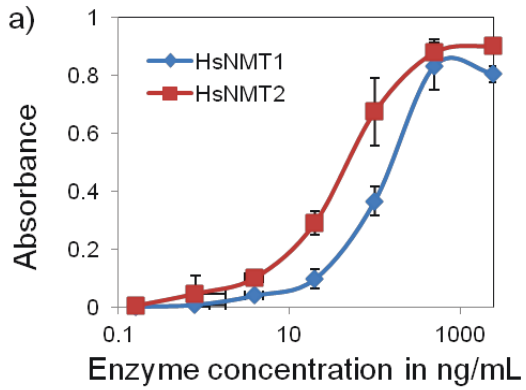

b)

		K_M in µM	
		HsNMT1	HsNMT2
YnC12CoA	CPM	0.13 ±0.04	0.28 ±0.09
	ELISA	0.15 ±0.02	0.14 ± 0.02
c-SRC	CPM	0.25 ±0.05	0.18 ±0.04
	ELISA	0.17 ±0.03	0.08 ±0.01

Figure 121. Optimisation and validation of the ELISA NMT assay. a) The enzyme concentration was optimised by varying the concentration of HsNMT1 or HsNMT2 from 0.16 to 2500 ng/mL in the presence of 1 µM YnC12CoA and 4 µM biotinylated 15AA c-SRC. The background (absorbance value with no enzyme) was subtracted from each absorbance value. The error bars represent the standard deviation of two replicates. **b)** The K_M of YnC12CoA or biotinylated 15AA c-SRC were determined in the presence of saturating amounts of biotinylated 15AA c-SRC (30 µM) or YnC12CoA (2 µM) respectively. The enzyme concentration was set to 300 ng/mL. The values were compared to values obtained with the CPM assay. The error represents the standard deviation of two replicates.

The assay was then used to study the 15aa peptide derived from the N-terminus of HCCS, a highly insoluble peptide difficult to study with the CPM assay; addition of a PEG-biotin moiety coupled to the C-terminus greatly improved solubility in buffer. The background was slightly higher than with c-SRC (Figure 122a). A K_M value was determined with NMT1 and NMT2 and HCCS was found to have a good affinity for both isoforms, with K_M values lower than 1 µM. The protein HCCS was identified with high confidence as a novel NMT substrate in Chapter 4 and these kinetic studies confirmed that the protein is an NMT substrate for the recombinant enzymes.

a)

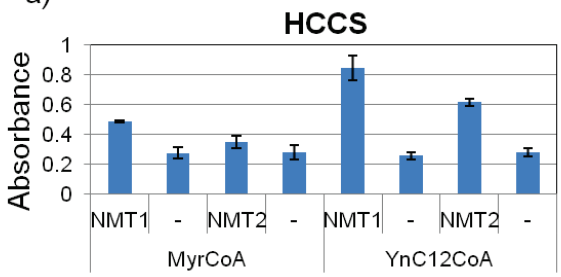

b)

	K_M HCCS (µM)
HsNMT1	0.27 ± 0.08
HsNMT2	0.40 ± 0.08

Figure 122. ELISA NMT assay with HCCS. The error represents the standard deviation of two replicates. a) Absorbance values obtained for the assay carried out using various conditions. HsNMT1, HsNMT2 or no enzyme was added to the well in the presence of YnC12CoA or MyrCoA and biotinylated 15AA HCCS peptide (10 µM). b) The K_M values of HCCS were determined in the presence of HsNMT1 or HsNMT2.

An assay was then carried out with two cysteine-containing peptides, FYN and XRP2 (Figure 123 a and b). MyrCoA and no enzyme samples were used as negative controls. The background was relatively high for these peptides, and the assay buffer contained 1 mM DTT, which should be sufficient to prevent oxidation of cysteine residues. Optimisation experiments were carried out to decrease the background, including more stringent washes with a high salt buffer (1x PBS supplemented with 0.2% SDS and 0.5 M NaCl) after the first step of the assay (myristoylation reaction) (Figure 123c). However, the absorbance signal was lost using these conditions, probably because the CuAAC reaction was inhibited.

Washing peptides with hydroxylamine after the *in vitro* myristoylation step significantly decreased the background. However, it also decreased the window of the assay making it difficult to measure K_M values accurately using these conditions. Further optimisation would be required to measure the affinity of cysteine containing peptides. The buffer used for in vitro myristoylation and for washes could be varied.

In conclusion, this ELISA assay could be employed to assess the affinity of hydrophobic peptides poorly soluble in the CPM assay buffer but further optimisation would be required for cysteine containing peptides. The assay could also be used in the future as an inhibitor assay to test inhibitors containing an electrophilic moiety or atom such as oxygen or sulphur that would be incompatible with the CPM assay.

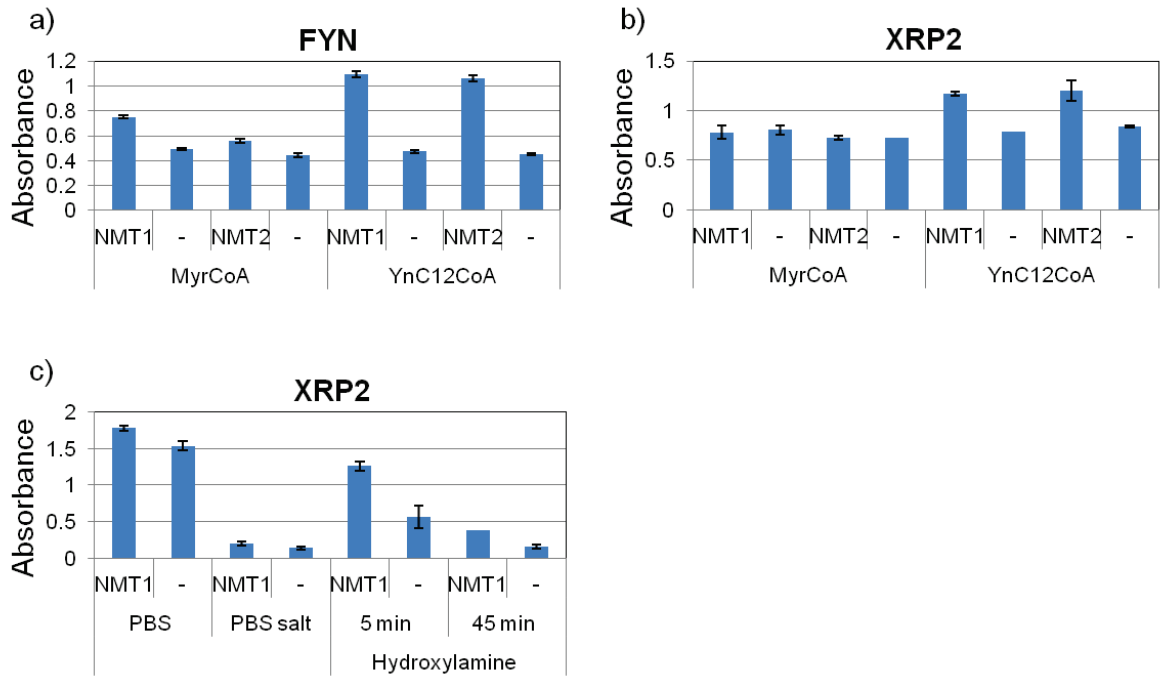

Figure 123. ELISA NMT assay with cysteine containing peptides. The error bars represent the standard deviation of two replicates. **a)** and **b)** Absorbance values obtained for the assay carried out using different conditions. NMT1, NMT2 or no enzyme was added to the well in the presence of YnC12CoA or MyrCoA and a) biotinylated 15AA FYN or b) biotinylated 15AA XRP2. **c)** An ELISA assay was carried out in the presence of HsNMT1, YnC12CoA and biotinylated 15 AA XRP2. Different washing conditions were used to try decreasing the background. After the in vitro myristoylation step, the plate-bound peptides were washed with PBS, a PBS buffer supplemented with 0.2% SDS 0.5 M NaCl (PBS high salt), or 0.3 M Hydroxylamine in PBS for 5 or 45 min.

6.1.4 Conclusions on *in vitro* HsNMT1/2 selectivity

Studies of the HsNMT isoform substrate specificities *in vitro* had not shed much light on whether the two isoforms have different substrate specificities *in vivo*. Additional studies were carried out with two peptides which were previously proposed to have a different selectivity *in vivo*: HIV-GAG and HIV-NEF. Kinetic studies using the CPM assay did not show any selectivity in vitro between these two peptides (Appendix K). If the peptide binding pockets of the two isoforms are highly similar, it would be difficult to design a selective HsNMT1 over HsNMT2 inhibitor.

These concerns were confirmed when the crystal structure of HsNMT2 was obtained (Figure 39). Key residues in the active site superimpose remarkably well with the key residues in the HsNMT1 crystal structures (apo enzyme and enzyme bound to inhibitor IMP366). Moreover, when NMT inhibitors were tested (Chapter 3), no more than 3 to 4-fold selectivity could be achieved between the two isoforms. Recent high throughput screening of a diverse subset of the Pfizer corporate collection (ca. 150,000 compounds) showed that no more than 3-fold selectivity could be achieved between the recombinant isoforms, which is likely to be insufficient in a physiological context.[352]

However, siRNA experiments showed that selective knockdown of one isoform resulted in different substrate patterns, suggesting that selectivity could be achieved *in vivo*.[28] The two isoform sequences mainly differ at the N-terminus, a region that has been shown to be essential for localisation of the enzymes in cells (Section 1.6.2), and recently the two isoforms were suggested to have different localisation.[115] It is possible that isoform substrate specificity could arise from this different localisation and not from divergence in the isozyme active sites. As a consequence, It appeared more relevant to study the isoforms substrate specificity in cells by combining siRNA, YnC12 labelling and Proteomics.

6.2 In-cell studies using siRNA

To study HsNMT isoform substrate specificity in cells, expression of HsNMT1 or HsNMT2 was knocked down using specific siRNAs.[28] HeLa cells were treated with HsNMT1 siRNA or HsNMT2 siRNA, and a YnC12 labelling strategy combined with proteomics allowed detection of substrates of the isoform which was not knocked down. As it was unlikely that complete knockdown could be achieved, quantitative proteomics appeared to be an attractive method. In their study of the protein turnover in HeLa (Section 5.3), Cambridge *et al.* determined that the half lives of HsNMT1 and HsNMT2 was 50 and 58.8 h respectively,[315] suggesting that at least a 2 day knockdown experiment would be required to decrease the level of one isoform by about 50%.

The toxicity of several transfection reagents was assessed: Lipofectamine (Invitrogen), Lipofectamine 2000 (Invitrogen) and RNAiMAX (Invitrogen). HeLa cells were seeded in a 6-well plate 24 h before treatment (50 000 or 100 000 cells per well). The transfection reagents were added (2 or 4 µL of Lipofectamine or RNAiMax, or 2.5 pr 5 µL of Lipofectamine 2000) according to the supplier's protocol. 6 h after the beginning of the treatment, the media was replaced with fresh media. The cells were mostly dead after 48 h in wells where only 50 000 HeLa cells were seeded. In the other wells, less toxicity was obtained with Lipofectamine 2000 (2.5 or 5 µL).

A siRNA knockdown experiment was carried out for 2 days using Lipofectamine 2000 (5 µL) and siRNA (2 µL of a 50 mM stock solution) (Figure 124a). The knockdown efficiency of a siRNAi experiment can be evaluated by Western Blotting, with a reduction in protein level. Unfortunately, no signal could be detected for HsNMT2 due to the poor quality of the antibody. The level of HsNMT1 decreased in the samples transfected with the siRNA against HsNMT1 and a combination of siRNA against both HsNMT isoforms.

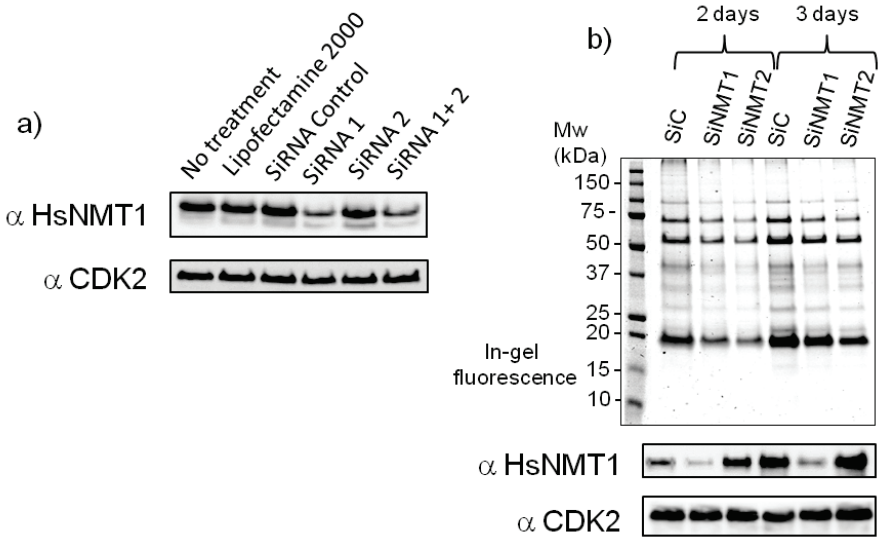

Figure 124. Optimisation of the siRNA transfection in HeLa. 100 000 HeLa cells were seeded (in a 6-well plate) in growth media containing 10% FBS (no antibiotic) 24 h before treatment. A complex of siRNA (2 µL of a 50 mM stocksolution; control siRNA, siRNA against HsNMT1 or HsNMT2, or mix of siRNA against HsNMT1 and HsNMT2) with Lipofectamine 2000 (5 µL) was prepared in Opti-MEM media (Invitrogen), according to the supplier's protocol. The mixture was added to the cells and incubated for 6 h. After this time, the growth media was changed (DMEM + 10%FBS) and the cells were allowed to grow for several hours. **a)** Cells were lysed 2 days post-treatment. Several controls were used: no treatment, cells only treated with Lipofeactimne 2000 or cells treated with a non-targeting siRNA as a control. These controls checked that the conditions used for the cells were not toxic and determined the abundance of HsNMT1 in cells with no knockdown of HsNMT1 by Western blotting. CDK2 was used as a loading control. **b)** Cells were lysed 2 or 3 days post-treatment. 6 h before cell lysis, cells were treated with YnC12. Myrsistoylated proteins were captured with AzTB and visualised by in-gel fluorescence. Western Blot analysis was performed to check the levels of HsNMT1 in cells and CDK2 was used as loading control. HsNMT2 antibody did not give a sufficient signal in chemiluinescnce.

A similar experiment was carried out to compare the efficiency of the knock down after 2 or 3 days. Cells were labelled with YnC12 6 h before cell lysis (Figure 124b). YnC12 labelling significantly decreased in the samples treated with siRNA against HsNMT1 or HsNMT2 but not in the samples treated with the control siRNA. Western blotting confirmed that HsNMT1 levels decreased in cells transfected with the siRNA against HsNMT1. Knockdown was similar after 2 or 3 days but it was decided to perform 3 day transfections for the next experiments.

HsNMT1 knockdown was not complete after 3 days and it seemed more reliable to use quantitative proteomics to identify HsNMT1 or HsNMT2 substrates. Cell lysates were prepared by Dr. Ute Brassat (Tate group, Imperial College London) in view to perform iTRAQ quantitative proteomics experiments (Section 1.11.2). The isotopic label would be introduced just before the analysis by LC-MS/MS. This method would compare four samples: cells treated with the siRNA control, siRNA against HsNMT1, HsNMT2 or combination of HsNMT1 and HsNMT2 siRNA. Samples were captured and enriched as described in Chapter 4 (Figure 125). Interestingly, there is a noticeable difference in

the YnC12 labelling of HeLa cells treated with siRNA against HsNMT1 or HsNMT2. Unfortunately, technical issues prevented analysis of these samples within the timeframe of this thesis, but analysis of these samples by the optimised quantitative chemical proteomic workflow described in Chapter 4 should be a priority for future work.

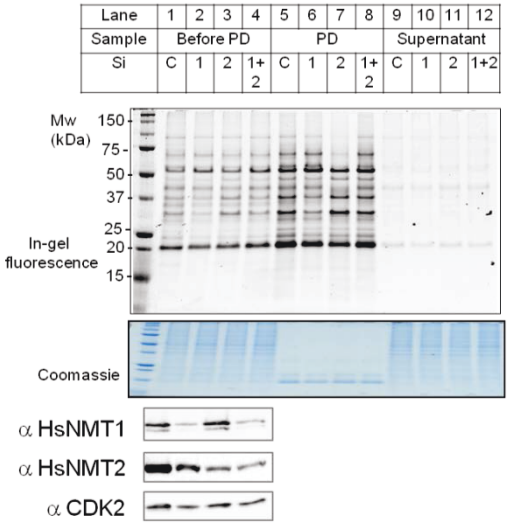

Figure 125. siRNA treated samples for quantitative proteomics (ITRAQ). HeLa cells were treated for 3 days with siRNA (control, HsNMT1, HsNMT2 or HsNMT1+HsNMT2). Lysates were prepared by Dr. Ute Brassat (Tate group, Imperial College London). Samples were captured with AzTB and enriched on Neutravidin agarose beads. Sample before pull down (Before PD), pull down (PD) and the supernatant were loaded on the gel. The levels of HsNMT1 and HsNMT2 were checked by Western Blotting. Coomassie and CDK2 were used as loading controls for the gel and Western Blotting respectively.

6.3 Conclusions

In this Chapter, different methods were assessed to identify HsNMT1 or HsNMT2 substrates *in vitro* or in cell.

First, experiments carried out in *E. coli* lysates with overexpressed PfARF showed that an HsNMT substrate could be *in vitro* myristoylated in lysate, in the presence of analogues of MyrCoA and recombinant HsNMT1/2. The newly *N*-myristoylated PfARF could be captured by AzTB or YnTB and detected by in-gel fluorescence. This method was applied to HeLa lysates obtained from cells treated with an NMT inhibitor. Many HsNMT substrates could potentially be myristoylated *in vitro*. However, the labelling pattern seen by in-gel fluorescence was different from the labelling typically obtained with cells treated with only YnC12. Moreover, the background labelling was higher, suggesting that this experiment would require further optimisation.

Secondly, small libraries of peptides were prepared on cellulose membrane and screened for activity against HsNMT1 and HsNMT2. If some of these peptides were selective for HsNMT1 over HsNMT2 (or HsNMT2 over HsNMT1), they could be developed as peptidomimetic inhibitors and then employed in cells to study HsNMT1/2 protein substrates. Several experiments were carried out and showed that it was possible to myristoylate and detect HsNMT1/2 peptide substrates on a cellulose membrane. However, the use of cellulose membranes presented some limitations. Fluorescence, which provides a rapid readout, could not be used to detect the substrates on a cellulose membrane due to background problems. Moreover, peptides which were previously reported to be myristoylated were not always detected using this method, perhaps due to their lower affinity for the isoforms or synthesis issues on the membrane.

Affinity of the peptides for HsNMT1 or HsNMT2 could be confirmed using the CPM assay for a few peptides. However, due to solubility issues or the presence of a nucleophile (a cysteine residue for example), kinetic parameters of some peptides could not be determined using the CPM assay. An ELISA end-point assay was developed. This assay was shown to be suitable to measure the K_M of c-SRC peptide as similar values were obtained with the CPM and ELISA assays. The K_M values of a peptide poorly soluble in the CPM assay buffer could also be determined. However, further optimisation would be required to measure the kinetic parameters of peptides bearing a nucleophile as a high background was observed.

To date, there is no strong evidence that the two HsNMT isoforms have different substrate specificities *in vitro* and it might be more reliable to carry out in-cell studies with specific siRNA against one isoform. The conditions of HsNMT1/2 knock down were optimised. Several proteomics

experiments were performed, using ITRAQ or triple SILAC, but were unsuccessful. Proteomics experiments will be repeated using the Spike-in SILAC method.

In the last few years, a novel method has been developed to stably knock out a gene. A stop codon could be selectively introduced in the HsNMT1 and also in the HsNMT2 gene to stop expression of one of these two isoforms.[353] Cas9 and a suitable RNA would need to be co-expressed in cells. Colonies could then be selected and sequenced to check that a hetero modification was obtained. By repeating the whole process, a homo modification could be achieved.[353] It would be advantageous to study HsNMT1/2 substrate specificity in these engineered cell lines as a stable and complete knockdown of one of the isoform could potentially be obtained.

Chapter 7 Conclusions and future work

This Chapter discusses the implications of this work for our understanding of protein *N*-myristoylation and for NMT as a cancer drug target and proposes future directions for this project.

7.1 Conclusions

7.1.1 Chemical tools to study *N*-myristoylation

In the current study, several chemical tools were employed to study *N*-myristoylation *in vitro* and in cells. The synthesis of several chemical probes, YnC12, AzC12, YnC15, YnC12CoA, AzC12CoA and MyrCoA, was optimised (Chapter 2). These probes can now be prepared reliably in moderate yields.

The work described in Chapter 2 confirmed that YnC12, an alkyne-tagged analogue of myristic acid is a useful probe to study *N*-myristoylation. YnC12 can be transferred, in place of the natural lipid substrate (Myr), co- or post- translationally to the N-terminal glycine of NMT protein substrates. The YnC12 probe first allowed assessment of the on-target activity of NMT inhibitors (Chapter 3) and was then successfully applied to identify co-translational NMT substrates by chemical proteomics in HeLa cells, a cervical cancer cell line (Chapter 4). YnC12 labelling was optimised in HeLa cells, by increasing the labelling time form 6 to 24 h, leading to an enhanced labelling of NMT substrates and the detection of low abundance substrates by chemical proteomics. It is important to note that YnC12 does not only label NMT substrates but can also label *S*-palmitoylated proteins, GPI-anchored proteins and possibly other proteins, as described in Section 4.7.

A novel approach, based on the combination of three assays (Chapter 3), was developed for the rapid evaluation (potency and on-target activity in cancer cells) of HsNMT inhibitors. Traditional methods to validate on-target activity of an inhibitor involve analysing the effect on downstream targets using biological assays or Western blotting. These methods can be laborious and do not always allow the rapid evaluation of potential off-target effects. In the current study, an *in vitro* enzyme assay, based on fluorogenic CPM readout, was employed to evaluate the potency of inhibitors against both HsNMT isoforms (IC_{50}). Secondly, YnC12 labelling was used to assess on-target NMT inhibition in cells. A dose-dependent decrease of the fluorescence signal could be observed for compounds inhibiting NMT activity in cells and the in-cell tagging EC_{50s} (TC_{50s}) were determined. The third assay, the MTS metabolic activity assay, allowed the determination of EC_{50s}. A good correlation between EC_{50} and TC_{50} indicated that the inhibitor was acting on-target and showed that the inhibitor had little or no side-effects in cells. HsNMT inhibitor IMP366 was

characterised and used as a chemical tool to identify new *N*-myristoylated proteins in HeLa cells (Chapter 4) and to study the phenotype of NMT inhibition (Chapter 5).

7.1.2 Identification of *N*-myristoylated proteins in HeLa cells

In Chapter 4, several chemical proteomics methods were studied for the identification of *N*-myristoylated proteins in HeLa cells, the cervical cancer cell line used in this study.

Acylated proteins, such as *N*-myristoylated proteins and *S*-palmitoylated proteins, are typically identified using alkyne-tagged analogues of the fatty acid of interest combined with non-quantitative proteomics experiments (Section 4.2). Another approach, based on the use of double SILAC quantitative proteomics combined with an inhibitor (Section 4.5), has also recently been employed to study *S*-palmitoylated proteins.

In the current study, these two approaches were applied to study protein *N*-myristoylation in HeLa cells and many putative NMT substrates were identified. However, both methods showed drawbacks as many proteins with no N-terminal MG motif were also detected. These proteins are most likely tagged with YnC12 in a non NMT-mediated manner, probably because these proteins are S-palmitoylated or GPI-anchored proteins.

In the current study, a novel approach was developed to identify simultaneously and with high confidence a large number of *N*-myristoylated proteins (70 proteins) in HeLa cells. This method combined the spike-in SILAC approach, the YnC12 probe and the chemical genetic tool IMP366. This novel approach also allowed for the first time the evaluation of inhibition sensitivity (in-cell IC_{50s}) for 70 NMT substrates, demonstrating the specific in-cell on-target activity of IMP366. The significance of these in-cell IC_{50} values is discussed in the next session.

An additional four substrates were identified using the AzKTB capture reagent which allowed the detection of the YnC12-modified peptide. 74 *N*-myristoylated proteins were identified with high confidence in HeLa cells; this is a huge improvement compared to previous proteomics experiments carried out to identify NMT substrates (typically around 20 proteins were detected).[163,173,224]

7.1.3 NMT inhibition in cancer cells

On-target inhibition of NMT in HeLa cells had a well-defined phenotype, arising from potential loss of function in >74 specific NMT substrates proteins. While NMT inhibition was not toxic to the cells after 1 day treatment, apoptosis and cell death were induced after 3 days and resulted in almost complete cell death after 7 days.

NMT substrates have key biological functions in cells, are all potentially essential and could lead to cell death when they are not *N*-myristoylated. Western blots and chemical proteomics experiments were carried out to assess the potential mode of action of NMT inhibitor IMP366. Loss of function of c-SRC and PSMC1 was evaluated by Western blot analysis. However, NMT inhibition is most likely to have a pleiotropic effect.

The NMT inhibition/spike-in SILAC method described in Section 4.6, allowed the determination of inhibition sensitivity (in-cell IC_{50s}) for 70 NMT substrates. In-cell IC_{50} values might reflect the affinity of a protein for HsNMT1/2, and to date, it is unclear how in-cell IC_{50} could be used to identify the key NMT targets leading to cell death. These values might need to be correlated with protein function, importance of the protein for the cells, turnover rate and possibly abundance in cells.

In-cell IC_{50} values were plotted against the protein half-lives determined in Chapter 5 (Figure 126) and with the protein abundance, determined using the sum of peptide intensities from the proteome analysis of HeLa cells.[207] However, there was no obvious correlation between in-cell IC_{50s} and protein half-life or protein abundance.

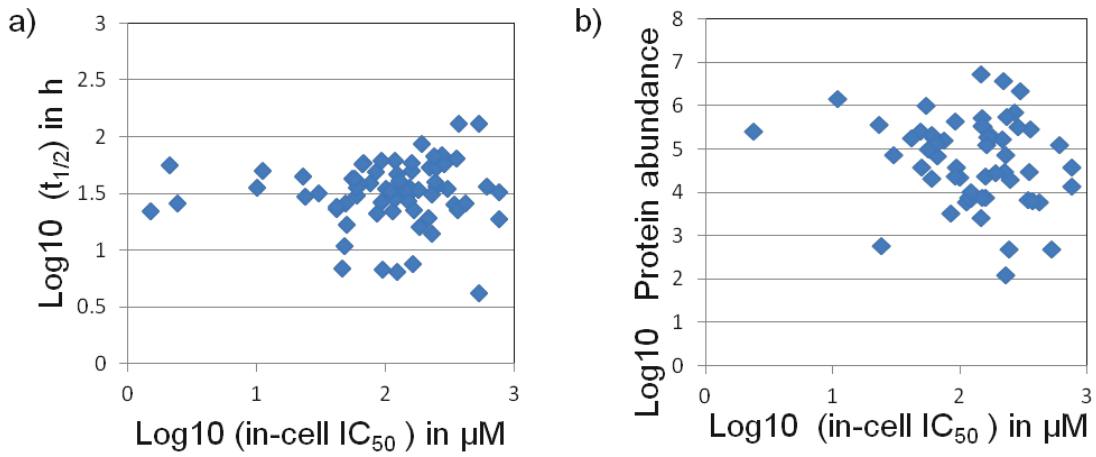

Figure 126. Plot of in-cell IC_{50} values with a) proteins half lives ($t_{1/2}$) or protein abundance. Protein abundance corresponds to the protein copies per cell as reported by Nagaraj et al. [207]

The start of the phenotype could correlate with the depletion of *N*-myristoylation of NMT substrates. If toxicity starts after 2 days, key NMT substrates might have a half-life around 1.5 or 2 days.

Taken together, these results suggest that the relationship between NMT inhibition and cell death is likely to be complex, and that more experiments are required to understand the mode of action of NMT inhibitor IMP366 in HeLa cells.

7.2 Future work

7.2.1 *N*-myristoylation

- **NMT substrates in HeLa.** While 74 NMT substrates were identified in HeLa cells in the current study, it is possible that a few substrates are missing. Indeed, more experiments need to be carried out to understand whether the NMT substrates identified with low confidence in Section 4.6.3 (27 proteins), are or not NMT substrates. It is difficult to predict how many substrates were missed in the current study. As it is thought that ca. 1% of the proteome in *N*-myristoylated (Section 1.1), ca. 100 proteins might be *N*-myristoylated in HeLa cells since Nagaraj *et al.* identified ca. 10 000 proteins in their study of HeLa cells proteome.[207]

- **NMT substrates in other cell lines or organisms or *in vivo*.** The NMT inhibition/spike-in SILAC method developed in the current study (Section 4.6), could be applied to other cancer cell lines. As different cell lines express a different subset of proteins, the NMT substrates might differ from one cell line to another.

- **Post-translational NMT substrates in HeLa.** While the main focus of the current work was on co-translational myristoylation, the NMT inhibition/spike-in SILAC approach could be applied to detect post-translationally *N*-myristoylated proteins in the context of apoptosis. HeLa cells could be treated using the conditions optimised in Section 2.4.

- **NMT1/2 localisation.** The NMT isoforms are thought to be localised at the ribosome, but recently, Perinpanayagam *et al.* suggested that HsNMT2 was localised in the cytosol (Section 5.2.2.1.). More experiment need to be carried out to understand the localisation of the isoforms in cells and to understand the interaction of HsNMT1 (and HsNMT2) with the ribosome.

- **HsNMT1 and HsNMT2 selectivity.** Experiments carried out in Chapter 6 have not confirmed that HsNMT isoforms have a different substrate specificity (Section 1.2). It is thus unclear whether HsNMT1-specific inhibitors might be effective anti-cancer agents, as suggested by Ducker *et al.*[28] Quantitative chemical proteomics experiments, combining HsNMT1 or HsNMT2 siRNA treatment and YnC12 labelling in HeLa cells, will need to be repeated to identify isoform substrate specificities (Section 6.2). If there is a different substrate specificity between the two isoforms, it would be interesting to correlate it with localisation and level of expression of the isoforms in a given cancer cell line.

- **Methionine aminopeptidase** (MetAP). MetAP removes the terminal methionine and exposes the N-terminal glycine, as required for *N*-myristoylation. Two isoforms have been identified in *humans* and specific inhibitors of HsMetAP1 [354] and HsMetAP2 [355] are available. YnC12 labelling experiments in cells could be performed to understand the impact of MetAP on myristoylation and to shed light on MetAP substrate specificity. These experiments will consist in feeding the cells first with MetAP1 and/or MetAP2 inhibitors and YnC12. Capture of the myristoylated proteins would allow visualisation by in-gel fluorescence and identification by proteomics.

7.2.2 NMT as an anti-cancer drug target

The work detailed here shows that NMT is essential in cancer cells and that its inhibition leads to cell death. However, several questions remain to be answered in order to validate NMT as an anti-cancer drug target.

- **NMT inhibitors.** Four on-target NMT inhibitors, based on different scaffolds, were identified in Section 3.4.3 and could be further optimised into lead series for the future development of an anti-cancer drug candidate. Novel inhibitors can be characterised using the CPM assay, MTS assay and YnC12 labelling assay.

- **Identify tissues highly sensitive to NMT inhibition.** The identification of cancer tissues highly sensitive to NMT inhibition could shed light on the mode of action of NMT inhibitors. One or several NMT inhibitors could be screened against a selection of cancer cell lines representing tissue type and genetic diversity of human cancers, such as the National Cancer Institute (NCI) NCI-60 cell lines. This selection comprises 59 cancer cell lines,[356] all well characterised at the proteome and transcriptome levels. This selection has recently been used to study the mode of action of a drug,[357] and could be employed to study NMT inhibition.

- **Identify the molecular pathways that lead to cell death using MS-based proteomics.** Several methods can be used to identify the mechanism of action of a drug,[358] such as transcriptome studies. Recently, mass spectrometry-based proteomics has emerged as a valuable tool for drug discovery and development,[358-360] as allows one to study the global effects of an inhibitor on the proteome.[361] Proteome studies are complementary (and potentially preferable) to transcriptome studies as they can take post-translational events or protein degradation into account.[361] Recently, Sharma *et al*. used a SILAC-based approach to identify the molecular targets of Hsp90 and the proteins that were up/down-regulated upon Hsp90 inhibition. A similar approach could be applied to NMT inhibition to decipher the mode of action of NMT inhibitors.

- **Identify *N*-myristoylated proteins in cancer cell lines highly sensitive to NMT inhibition.** To understand the mode of action of an NMT inhibitor, it would be essential to identify all the *N*-myristoylated proteins in the cell line of interest. Correlation of the list of NMT substrates with sensitivity of the cell line to NMT inhibition could help to understand the role of some NMT substrates and help to identify the mode of action of NMT inhibitors.

- **Show that NMT inhibition is not toxic to non-cancerous cells and could reduce cancer growth in mouse models, such as human tumour xenografts.** To validate NMT as a new cancer drug target, it would be important to show that NMT inhibition could decrease tumour growth in mouse models without increasing toxicity to healthy cells/tissues. NMT inhibition-mediated toxicity should be highly dependent on protein turnover, implying that slowly dividing cells (non cancerous cells) might be less sensitive to NMT inhibition.

  It is important to note that human tumour xenografts poorly predict the response of human cancers, and therefore, success of mouse-model experiments do not imply that a compound will be a safe clinical candidate able to decrease tumour growth in cancer patients.[1] Recently, genetically engineered mouse tumour models (GEMM) have emerged as a more clinically relevant model to study human cancers.[362] The tumours are initiated in a more natural environment (contrary to xenografts where human tumours are injected into mice) *via* the mutations of specific genes leading to the overexpression of oncogenes or depletion of tumour suppressors. However, it can be challenging to produce a GEMM to study the target of interest.[1]

Chapter 8 Materials and methods

8.1 Chemical synthesis

8.1.1 General methods

All reagents and solvents were purchased from Sigma-Aldrich, NovaBiochem UK or National Diagnostics UK and used without further purification. Ultrapure water was obtained from MilliQ® Millipore water purification system. Moisture sensitive reactions were performed under nitrogen atmosphere using dried glassware and standard syringe/septa techniques.

Thin Layer Chromatography was performed on Merck pre-coated Silica plates (Aluminum oxide 60 F254, Merck). Spots were visualized by UV light (operating at 254 nm), and using the appropriate stain (iodine, potassium permanganate, ninhydrin or *p*-anisaldehyde stain). Silica gel column chromatography was carried either by hand-made columns with Merck Silica 60Å, or using an Isolera (Biotage, Uk) automated apparatus with fractions collector equipped with SNAP cartridges columns (Biotage, Uk). The freeze drying was carried out using a freeze dryer Alpha 2-4 LD plus, Christ (Germany).

NMR spectra were recorded on 400MHz Bruker instruments and were referenced to TMS or residual solvent signals. Data are presented as follows: chemical shift, multiplicity (s = singlet, d = doublet, t = triplet, q = quartet, m = multiplet), coupling constant(s) in Hz and integration. NMR spectrometry was carried out at room temperature, except were indicated otherwise.

Mass spectrometry characterisation was obtained from the Mass Spectrometry Service of Department of Chemistry, Imperial College London.

Analytical and semi-preparative RP-HPLC were carried out on a Waters 2767 system equipped with a photodiode array, a mass spectrometer and an X-Bridge C18 column (5 µM, 4.6 mM × 100 mM).The following elution methods were used: ***Method A*** :(gradient of 25 mM ammonium carbonate pH 8 and MeOH): 0 min 50% MeOH, 0-10 min up to 98% MeOH, 10-15 min 98% MeOH, 15-16 min 98 to 5% MeOH, 16-20 min 5% MeOH; ***Method B*** (gradient of H_2O and MeOH, supplemented with 0.1% formic acid): 0-10 min 5-98% MeOH, 10-12 min 98% MeOH, 12-13 min 98 to 5% MeOH, 13-17 min 5% MeOH; ***Method C*** (gradient of H_2O and MeOH, supplemented with 0.1% formic acid): 0-10 min 50-98% MeOH, 10-12 min 98% MeOH, 12-13 min 98 to 50% MeOH, 13-17 min 50% MeOH; ***Method D***: (gradient of 25 mM ammonium carbonate pH 8 and MeOH), 0 min 2 % MeOH, 0-10 min 2-98%

MeOH, 10-15 min 98% MeOH, 15-16 min 98 to 5% MeOH, 16-20 min 5% MeOH;. The flow rate of 1.2 mL/min was used for the analytical mode and 20 mL/min were used for the preparative mode.

All peptide synthesis reagents and solvents were purchased from Sigma-Aldrich, Merck Chemicals or National Diagnostics and used without further purification. Peptides were synthesised manually or by automated solid phase peptide synthesis with a ResPep SL apparatus (Intavis, Germany)

The following general methods were used for the manual peptide synthesis on resin:

- ✓ **Method 1: Fmoc deprotection.** The resin was swelled in DMF for 1 h and Fmoc deprotected by treating it with 20% piperidine/DMF (3 × 3 mL) for 10 min per treatment. After the third treatment, the resin was washed with DMF (3 × 3 mL), DCM (3 × 3 mL) and swelled in DMF (3 × 3 mL) for subsequent steps.
- ✓ **Method 2: General procedure for the manual coupling of amino acids or special acids to peptides on resins.** The resin (typically 20 μmol) was swelled by addition of 1 mL DMF followed by shaking at room temperature for 1 h. DMF was removed by filtration. A mixture of the appropriate acid (5 eq of amino acid or 3 eq of special acid or amino acid) was pre-activated by the addition of the appropriate coupling reagent (5 eq HBTU for an amino acid or 3 eq of HATU for a special acid or amino acid) and DIPEA (10 eq if HBTU was used or 6 eq if HATU was used). After 5 min, the mixture was added to the resin bound peptide and shaken at room temperature for 2 h. The reagent mixture was removed by filtration and the coupling step was repeated. The reagent mixture was removed by filtration peptides washed with DMF (5 × 2 mL), DCM (3 × 2 mL), MeOH (3 × 2 mL) and Et_2O (3 × 2 mL) and left to dry in a desiccator. If another coupling was required, the resin was Fmoc-deprotected as explained in Method 1 before starting the second coupling.

8.1.2 YnC12 synthesis

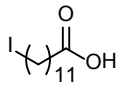

12-Iodododecanoic acid (29)

To a solution of 12-Bromododecanoic acid (1.00 g, 3.58 mmols, 1 eq) in dry acetone (20 mL) was added NaI (1.61 g, 10.74 mmols, 3eq) in one portion. The mixture was stirred at room temperature overnight. Completion of the reaction was checked by ^{1}H NMR. Water (200 mL) and DCM (100 mL) were added. The layers were separated and the aqueous layer was extracted with DCM (2 x 70 mL). The combined organic layers were washed with saturated aqueous sodium thiosulphate (100 mL), Brine (100 mL), dried over $MgSO_4$ and concentrated under reduced pressure to yield a white solid

(1.05 g, 90 %). The crude product was used without further purification for the next reaction. **^{1}H NMR** (400 MHz, $CDCl_3$) δ = 3.17 (t, *J*=7.1, 2H), 2.33 (t, *J*=7.5, 2H), 1.84 – 1.75 (m, 2H), 1.64 – 1.56 (m, 2H), 1.27 (m, 14H).

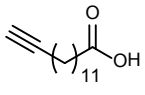

Tetradec-13-ynoic acid (YnC12, 16) [154]

Under nitrogen atmosphere, a solution of TMS-acetylene (1.12 mL, 7.82 mmol, 2.5 eq) in dry THF (8 mL) was cooled down to -78 °C using a bath of acetone and dry ice. A solution of *n*-BuLi in hexanes (3.8 mL, 2.5 M solution, 9.39 mmol, 3.0 eq) was added dropwise. The clear reaction mixture was allowed to warm to room temperature for 10 minutes and then cooled to -78 °C. DMPU (7.9 mL, 21 eq) and a solution of 12-iododododecanoic acid **29** (1.02 g, 3.13 mmol, 1.0 eq) in dry THF (8 mL) were added dropwise. The yellow reaction mixture was allowed to warm to room temperature and stirred overnight. The reaction mixture was cooled to -78 °C and quenched by the dropwise addition of saturated NH_4Cl (240mL). Et_2O (100 mL) and water (50 mL) were added to the brown solution. The layers were separated and the aqueous layer was extracted with Et_2O (2 x 50 mL). The combined organic layers were washed with water (100 mL), brine (100 mL), dried over sodium sulphate, filtered and concentrated under reduced pressure. The brown residue was purified by silica-gel chromatography (gradient chex: EtOAc: AcOH 99:0:1 to 95:4:1) to yield a white solid (500 mg, 54 %). NMR analysis of the product showed that the product contained < 2 % of 12-Iododododecanoic acid.

To a suspension of TMS-protected alkyne (490 mg, 1 eq, 1.65 mmol) in MeOH (10 mL) was added K_2CO_3 (457 mg, 3.31 mmol, 2 eq). The reaction mixture was stirred at room temperature overnight to give a clear reaction mixture. The mixture was concentrated under reduced pressure. The residue was taken up in 2N HCl (50 mL) and Et_2O (50 mL). The layers were separated and the aqueous layer was extracted with Et_2O (2 x 50 mL). The combined organic layers were washed with water (50 mL), brine (50 mL), dried over sodium sulphate, filtered and concentrated under reduced pressure to yield an off-white solid (359 mg, 96 %). NMR analysis of the product showed that the product contained < 2 % of 12-Iododododecanoic acid.

The white solid (YnMyr + < 2 % Iododododecanoic acid **29**; 340 mg, 1.52 mmol) was dissolved in DMSO (500 µL) and ethanolamine (25 eq regarding 2 % impurity, 0.76 mmol, 46 µL) was added in one portion. The reaction mixture was heated to 120 °C for 2 h and then allowed to cool down to room temperature. Et_2O (100 mL) and 2N HCl (100mL) were added. The layers were separated and the aqueous layer was extracted with Et_2O (50 mL). The combined organic layers were washed with 0.5N

HCl (50 mL), Brine (50mL), dried over $MgSO_4$ and concentrated under reduced pressure to yield **16** as a white solid (296 mg, 74%; overall yield = 37 %). **^{1}H NMR** (400 MHz, $CDCl_3$) δ 2.33 (t, *J* = 7.5, 2H, C*H*$_2$CO$_2$H), 2.16 (dt, *J* = 7.1, 2.6, 2H, C*H*$_2$C≡CH), 1.92 (t, *J* = 2.7, 1H, C≡C*H*), 1.65 – 1.55 (m, *J* = 7.3, 14.8, 2H, C*H*$_2$CH$_2$CO$_2$H), 1.54 – 1.45 (m, 2H, C*H*$_2$CH$_2$C≡CH), 1.41 – 1.19 (m, 14H, 7xC*H*$_2$); **^{13}C NMR** (101 MHz, $CDCl_3$) δ 179.69 (C=O), 85.03(*C*≡CH), 68.02 (C≡*C*H), 34.14, 29.49, 29.45, 29.40, 29.20, 29.11, 29.00, 28.71, 28.50, 24.87, 18.60; **HRMS** (ESI, negative mode) found 223.1698 ([M - H]$^-$ requires 223.1699). The analysis was consistent with the NMR and MS analysis reported in the literature.[154]

8.1.3 AzC12 synthesis

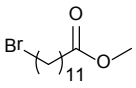

Methyl 12-bromododecanoate (31)

To a solution of 12-bromododecanoic acid **27** (2.00 g, 7.16 mmol, 1 eq) in MeOH (20 mL) were added 214 µL (30 µL/mmol) of concentrated H_2SO_4. The mixture was heated under reflux for 2 hours. The reaction mixture was allowed to cool down to room temperature and concentrated under reduced pressure. The residue was diluted in Et_2O and washed with $NaHCO_3$ sat. (1x), brine (1x). The organic layer was dried with sodium sulphate and concentrated under reduced pressure to yield **31** as a clear oil (1.96 g, 93%). The product was used without further purification for the next reaction. **^{1}H NMR** (400 MHz, $CDCl_3$) δ 3.64 (3H, s, -CH_3), 3.38 (t, 2H, J=7.0 Hz, *CH*$_2$Br), 2.28 (t, 2H, *CH*$_2$CO$_2$Me), 1.87 – 1.77 (m, 2H), 1.66 – 1.54 (m, 2H), 1.38 (d, J = 7.4, 2H), 1.25 (m, 12H); **^{13}C NMR** (101 MHz, $CDCl_3$) δ 174.53 (-COOMe), 51.64, 34.31, 34.24, 33.03, 29.64, 29.59(2C), 29.43, 29.33, 28.94, 28.37, 25.14; **HRMS** (ESI, positive mode) found 293.1114 ([M + H]$^+$, requires 293.1116)

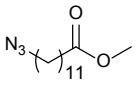

Methyl 12-azidododecanoate (32)

To a solution of methyl 12-bromododecanoate **31** (1.95 g, 6.65 mmol, 1 eq) in DMSO (80 mL) was added dropwise sodium azide (520 mg, 7.98 mmol, 1.2 eq) and the clear reaction mixture stirred overnight at room temperature. The reaction mixture was then diluted with water (20 mL) and quenched with 1 N HCl (~15 mL) cautiously. Once cool, the mixture was extracted with ethyl acetate (3x) and the combined organic layers washed with water (3 x) then brine (2 x 50 mL), dried over sodium sulphate, filtered and concentrated under reduced pressure. A yellow oil was obtained and purified by silica gel column chromatography (hexanes: Et_2O 9:1) to yield **32** as a clear oil (1.64 g, 88%). **Rf** (hex: Et_2O 9:1) = 0.2; **^{1}H NMR** (400 MHz, $CDCl_3$) δ 3.64 (3H, s, CO_2CH_3), 3.23 (2H, t, J= 7.0Hz, *CH*$_2$N$_3$), 2.27 (2H, t, J= 7.5Hz, *CH*$_2$CO$_2$Me), 1.52-1.63 (4H, m, *CH*$_2$CH$_2$CO$_2$H and *CH*$_2$CH$_2$N$_3$), 1.37 –

1.21 (14H, m, $(CH_2)_6$); **^{13}C NMR** (101 MHz, $CDCl_3$) δ 174.51 (-COOMe), 51.66, 51.62, 34.28, 29.62(2C), 29.56, 29.41, 29.31 (2C), 29.02, 26.89, 25.12; **HRMS** (ESI, positive mode) found 228.2001 ($[M + H - N_2]^+$ requires 228.1947).

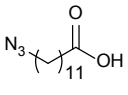

12-azido-dodecanoic acid (AzC12, 15) [154]

Methyl 12-azidododecanoate **32** (1.5 g, 5.88 mmol, 1 eq) was suspended in 2N NaOH solution (5.9 mL, 11.76 mmol, 2.0 eq). 3ml of MeOH were added slowly to obtain a homogeneous solution. The mixture was stirred at room temperature for 24 hours, then MeOH was removed under reduced pressure. EtOAc (20mL) was added. The aqueous layer was acidified with 2N HCl. The two layers were separated and the aqueous layer was extracted with EtOAc (2 x 50 mL). The product was extracted with Et_2O (4 x 100 ml), and the combined organic layers were dried over anhydrous sodium sulphate, filtered, and concentrated under reduced pressure to give the expected compound **15** as a white solid (1.32 g, 93%). The product did not require further purification. **^{1}H NMR** (400 MHz, $CDCl_3$) δ 3.23 (2H, t, J = 7.0 Hz, -CH_2N_3), 2.33 (2H, t, J = 7.5 Hz, CH_2CO_2H), 1.55–1.72 (4H, m, $CH_2CH_2CO_2H$ and $CH_2CH_2N_3$), 1.24–1.43 (14H, m, $(CH_2)_6$); **^{13}C NMR** (101 MHz, $CDCl_3$) δ 179.71 (C=O), 51.70, 34.14, 29.64 (2C), 29.57, 29.41, 29.34, 29.24, 29.04, 26.91, 24.87; **HRMS** (ESI, negative mode) found 240.1719 ($[M - H]^-$ requires 240.1712). The analysis was consistent with the NMR and MS analysis reported in the literature.[154]

8.1.4 YnC15 synthesis

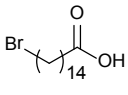

15-bromopentadecanoic acid (39)

<u>-1st method:</u>[198] 15-hydroxypentadecanoic acid **34** (300 mg, 1.16 mmol, 1 eq) was dissolved in HBr 33 % wt in AcOH (5 mL). The mixture was heated to 80 °C for 3h, allowed to cool down and partitioned between water (20 mL) and DCM (20 mL). The layers were separated and the aqueous layer was extracted with DCM (20 mL). The combined organic layers were washed with$NaHCO_3$ saturated aqueous solution (10 mL), brine (10 mL), dried over sodium sulphate and concentrated under reduced pressure. The crude product was purified by silica gel column chromatography (hex: Et_2O: AcOH 9:1:0.1) to yield **39** as a white solid (142 mg, 38%). **Rf** (hex: Et_2O: AcOH 9:1:0.1) = 0.33; **^{1}H NMR** (400 MHz, $CDCl_3$) δ 3.39 (t, *J* = 6.9, 2H), 2.33 (t, *J* = 7.5, 2H), 1.88 – 1.78 (m, 2H), 1.67 – 1.56 (m, 2H), 1.46 – 1.35 (m, 2H), 1.24 (m, 18H). The analysis was consistent with the NMR analysis reported in the literature.[363]

-2nd method:[199] To a suspension of 15-hydroxypentadecanoic acid **34** (150 mg, 0.58 mmol, 1 eq) was added PPh_3 and CBr_4 at 0°C. The mixture was stirred at room temperature overnight. The reaction mixture was filtered and the filtrate was concentrated under reduced pressure before being partitioned between water (20 mL) and DCM (20 mL). The layers were separated and the aqueous layer was extracted with DCM (20 mL). The combined organic layers were washed with $NaHCO_3$ saturated aqueous solution (10 mL), brine (10 mL), dried over sodium sulphate and concentrated under reduced pressure to give a yellow residue. The crude product was purified by silica gel column chromatography (hex: Et_2O: AcOH 9:1:0.1) to yield **39** as a white solid (82 mg, 44%). The product was seen as one spot on TLC (hex: Et_2O: AcOH 9:1:0.1, Rf=0.33) but according to the ^1H NMR analysis, this product contained 40 % impurity seen with the following chemical shifts:**^{1}H NMR** (400 MHz, $CDCl_3$) δ 3.50 (t, J = 6.8, 2H), 2.33 (t, J = 7.5, 2H), 1.78 – 1.70 (m, 2H), 1.61 (m, 2H), 1.40 (m, 2H), 1.24 (s, 18H).

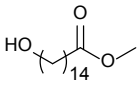

Methyl 15-hydroxypentadecanoate (42)

Same procedure as methyl 12-bromododecanoate **31** with slight modifications and starting from 15-hydroxypentadecanioc acid (300 mg, 1.16 mmol, 1 eq). The reaction mixture was heated under reflux for 3 h, allowed to cool down and quenched by the addition of a saturated solution of NH_4Cl (20 mL). The product was extracted with Et_2O (3 x 20 mL). The combined organic layers were washed with brine, dried over sodium sulphate and concentrated under reduced pressure to give **42** as a white crystalline solid (480 mg, 91%). **^{1}H NMR** (400 MHz, $CDCl_3$) δ 3.64 (s, 3H, C*H*$_3$ -), 3.62 (br s, 2H, HO-C*H*$_2$-), 2.28 (t, *J* = 7.6, 2H, -C*H*$_2$-COOMe), 1.64 – 1.55 (m, 4H), 1.30-1.20 (m, 20H); **HRMS** (ESI, positive mode) found 273.2421 ($[M - H + HCOO^-]^+$ requires 273.2424).

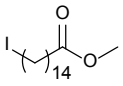

Methyl 15-iodopentadecanoate (44) [200]

To a solution of imidazole (318 mg, 4.68 mmol, 2.2 eq) and PPh_3 (671 mg, 2.56 mmol, 1.2 eq) in DCM (10 mL) was added I_2 dropwise at 0 °C. An orange/yellow solution was obtained and a solution of methyl 15-hydroxypentadecanoate **42** (580 mg, 2.12 mmol, 1eq) in DCM (5 mL) was added dropwise. The reaction mixture was stirred at room temperature (RT) for 3h and partitioned between DCM (50 mL) and H_2O (50 mL). The layers were separated and the aqueous layer was extracted with DCM (2 x 50 mL). The combined organic layers were washed with brine (50 mL), dried over sodium sulphate and concentrated under reduced pressure to give a dark brown residue. The crude product was purified by silica gel column chromatography (gradient hex: EtOAc; %EtOAC 1 to

4%) to yield **44** as a yellow solid (518 mg, 64%). **Rf** (chex: EtOAc 9.5:0.5) = 0.22; **^{1}H NMR** (400 MHz, $CDCl_3$) δ 3.65 (s, 3H, C*H*$_3$ -), 3.17 (t, *J* = 7.1, 2H, I-C*H*$_2$-), 2.28 (t, *J* = 7.6, 2H, -C*H*$_2$-COOMe), 1.79 (dd, *J* = 7.2, 14.5, 2H), 1.60 (s, 2H), 1.41 – 1.32 (m, 2H), 1.32 – 1.19 (m, 18H).

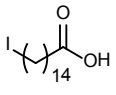

15-Iodopentadecanoic acid (45)

-1st method: Ester hydrolysis. To a solution of methyl 15-iodopentadecanoate **44** (500 mg, 1.3 mmol) in THF (15 mL) was added NaOH 4N (610 µL). The suspension was stirred at room temperature for 2 days. The reaction mixture was concentrated under reduced pressure and the residue was partitioned between Et_2O (50 mL) and 2N HCl (20 mL). The layers were separated and the aqueous layer was extracted with Et_2O (2 x 50 mL). The combined organic layers were washed with brine (50 mL), dried over sodium sulphate and concentrated under reduced pressure to give a white solid. The crude product was purified by silica gel column chromatography (gradient hex: EtOAc : AcOH; 9:1:0.1 to 7:3:0.1) to yield **45** as a yellow solid (337 mg, 70%).

-2nd method: Pentadecanoline **46** (2.2 mL, 8.3 mmol, 1 eq) was added to a mixture of hydrogen iodide (57 % in H_2O, 8 mL) and AcOH (4 mL). The reaction mixture was heated under reflux for 3 hours. The brown reaction mixture was allowed to cool down to room temperature. A brown precipitate was obtained. The reaction mixture was quenched with a saturated solution of Na_2SO_7 (50 mL) and DCM (50 mL) was added to dissolve the precipitate. The layers were separated. The aqueous layer was extracted with DCM (2 x 100 mL). The combined organic layers were washed with brine (1 x 100 mL), dried over sodium sulphate, filtered and concentrated under reduced pressure. The yellow residue was purified by silica-gel chromatography (gradient chex: EtOAc:AcOH 94:5:1 to 74:25:1) to yield **45** as white crystals (2.28 mg, 75%).

Rf (chex: EtOAc:AcOH 8:2:0.1) = 0.22; **^{1}H NMR** (400 MHz, $CDCl_3$) δ 3.17 (t, J = 7.1, 2H, CH_2CH_2I), 2.33 (t, J = 7.5, 2H, CH_2CO_2H), 1.80 (dt, J = 14.5, 7.1, 2H, CH_2CH_2I), 1.66 – 1.56 (m, 2H, , $CH_2CH_2CO_2H$), 1.41 – 1.21 (m, 20H, 10 x C*H*$_2$); **^{13}C NMR** (101 MHz, $CDCl_3$) δ 179.42 (C=O), 34.10, 33.79, 30.73, 29.80 (3C), 29.75 (2C), 29.63 (2C), 29.45, 29.27, 28.76, 24.89, 7.60 (TMS); **HRMS** (ESI, negative mode) found 413.1188 ($[M - H + HCOO^-]^-$ requires 413.1189). The analysis was consistent with the NMR and MS analysis reported in the literature.[201]

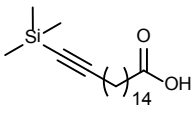

TMS-protected Heptadec-16-ynoic acid (47)

Under nitrogen atmosphere, a solution of TMS-acetylene (920 µL, 2.58 mmol, 2.5 eq) in dry THF (6 mL) was cooled down to -78 °C using a bath of acetone and dry ice. A solution of *n*-BuLi in hexanes (3.1 mL, 2.5 M solution, 3.0 eq) was added dropwise. The clear reaction mixture was allowed to warm to room temperature for 10 minutes and then cooled to -78 °C. DMPU (6.5 mL, 54 mmol, 21 eq) and a solution of 15-iodopentadecanoic acid **45** (950 mg, 2.58 mmol, 1.0 eq) in dry THF (6 mL) were added dropwise. The yellow reaction mixture was allowed to warm to room temperature and stirred overnight. The reaction mixture was cooled to -78 °C and quenched by the dropwise addition of saturated NH_4Cl (20 mL). Et_2O (50 mL) and water (20 mL) were added to the brown solution. The layers were separated and the aqueous layer was extracted with Et_2O (2 x 50 mL). The combined organic layers were washed with water (3 x 20 mL), brine (2 x 20 mL), dried over sodium sulphate, filtered and concentrated under reduced pressure. The brown residue was purified by silica-gel chromatography (gradient chex: EtOAc: AcOH 99:0:1 to 74:25:1) to yield **47** as a white solid (320 mg, 37%). **Rf** (chex: EtOAc: AcOH 8:2:0.1) = 0.3; ^{1}H NMR (400 MHz, $CDCl_3$) δ 2.33 (t, J = 7.5, 2H, C*H*$_2$CO$_2$H), 2.19 (t, J = 7.2, 2H, -C*H*$_2$-CC-TMS), 1.61 (dt, J = 14.9, 7.4, 2H, $CH_2CH_2CO_2H$), 1.49 (m, 2H, C*H*$_2$CH$_2$-CC-TMS), 1.27 (d, J = 28.4, 20H), 0.13 (m, 9H, TMS); HRMS (ESI, negative mode) found 265.2156 ([M – H –TMS) requires 265.2173

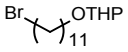

2-(11-Bromoundecoxy)tetrahydro-2*H*-pyran (48)

To a solution of 11-bromoundecanol **38** (500 mg, 2.0 mmol, 1 eq) and p-TsOH (38 mg, 0.2 mmol, 0.1 eq) in DCM (10 mL) was added DHP (266 mg, 3.0 mmol, 1.5 eq) at RT and the reaction mixture was stirred for 2h. The mixture was concentrated under reduced pressure and the crude product was purified by silica-gel chromatography (gradient chex: EtOAc 9:0.1 to 9:1) to yield **48** as a clear oil (410 mg, 62%). **Rf** (chex: EtOAc 20:1) = 0.28; **^{1}H NMR** (400 MHz, $CDCl_3$) δ 4.57 – 4.52 (m, 1H, -O-C*H*-O-), 3.89 – 3.80 (m, 1H, THP), 3.74 – 3.66 (m, 1H, -C*H*$_2$-OTHP), 3.52 – 3.43 (m, 1H, THP), 3.38 (t, *J* = 6.9, 2H, -C*H*$_2$-Br), 3.36 – 3.31 (m, 1H, -C*H*$_2$-OTHP), 1.87 – 1.76 (m, 3H, -C*H*$_2$-CH$_2$-OTHP+1H THP), 1.74 – 1.63 (m, 1H, THP), 1.61 – 1.45 (m, 6H, 4H THP + 2H Br-CH$_2$-C*H*$_2$-), 1.32 (d, *J* = 55.9, 14H); **^{13}C NMR** (101 MHz, CDCl3) δ 99.08, 67.92, 62.58, 34.27, 33.05, 31.00, 29.96, 29.74, 29.67 (2C),, 29.62 , 28.97, 28.39, 27.12, 26.44, 25.72.

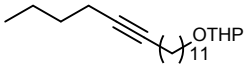

17-(tetrahydro-2H-pyran-2-yloxy)-heptadeca-5-yne (49) [197,364]

To a solution of 1-hexyne (151 µL, 1.3 mmol, 1.1 eq) in THF (3 mL) was added *n*-Buli dropwise at 78 °C. The reaction mixture was allowed to warm to RT for 10 min. A solution of compound **48** (400 mg, 1.2 mmol, 1 eq) in DMPU (3 mL) and dry THF (3 mL) was added dropwise at -78°C. The yellow solution was stirred at RT overnight. The reaction mixture was cooled to -78 °C and quenched by the dropwise addition of saturated NH_4Cl (10 mL). Et_2O (20 mL) and water (10 mL) were added The layers were separated and the aqueous layer was extracted with Et_2O (2 x 10 mL). The combined organic layers were washed with brine (2 x 10 mL), dried over sodium sulphate, filtered and concentrated under reduced pressure. The yellow oil was purified by silica-gel chromatography (gradient chex: EtOAc 99:1 to 97:3) to yield **49** as a clear oil (252 mg, 63%). **Rf** (chex: EtOAc 9:1) = 0.5; **^{1}H NMR** (400 MHz, $CDCl_3$) δ 4.57 – 4.53 (m, 1H, -O-C*H*-O-), 3.90 – 3.80 (m, 1H, THP), 3.71 (dt, *J* = 9.6, 6.9, 1H, -C*H*$_2$-OTHP), 3.53 – 3.43 (m, 1H, THP), 3.36 (dt, *J* = 9.6, 6.9, 1H, -C*H*$_2$-OTHP), 2.16 – 2.07 (m, 4H, -C*H*$_2$-C-C-C*H*$_2$-), 1.86 – 1.75 (m, 1H), 1.74 – 1.64 (m,1H), 1.61 – 1.22 (m, 26H), 0.88 (t, *J* = 7.2, 3H); **^{13}C NMR** (101 MHz, $CDCl_3$) δ 99.06 (-O-*C*H-O-), 80.44 (-CH_2-*C*-C-CH_2-), 80.38 (-CH_2-C-*C*-CH_2-), 67.92, 62.56, 31.49, 31.01, 29.98, 29.80, 29.77, 29.75, 29.71, 29.38, 29.08, 26.46, 25.73, 22.14, 19.92, 18.97, 18.66; **HRMS** (ESI, positive mode) found 337.3097 [M + H]$^+$ requires 337.3107.

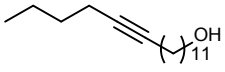

Heptadec-12-ynol (36)

To a solution of compound **49** (100 mg, 0.3 mmol, 1 eq) in MeOH was added p-TsOH and the reaction mixture was heated under reflux overnight. The reaction mixture was concentrated under reduced pressure. The clear oil was taken up in Et_2O (10 mL) and a saturated solution of $NaHCO_3$ (10 mL was added. The layers were separated and the aqueous layer was extracted with Et_2O (10 mL). The combined organic layers were washed with brine, dried over sodium sulphate, filtered and concentrated under reduced pressure. The yellow oil was purified by silica-gel chromatography (gradient chex: EtOAc 9:1 to 6:4) to yield **36** as a white solid (60 mg, 78 %). **Rf** (chex: EtOAc 1:1) = 0.5; **^{1}H NMR** (400 MHz, CDCl3) δ 3.62 (t, *J* = 6.6, 2H, -C*H*$_2$-OH), 2.16 – 2.08 (m, 4H, -C*H*$_2$-C-C-C*H*$_2$-), 1.61 – 1.50 (m, 2H), 1.49 – 1.19 (m, 20H), 0.88 (t, *J* = 7.2, 3H); **^{13}C NMR** (101 MHz, $CDCl_3$) δ 80.43 (-CH_2-*C*-C-CH_2-), 80.39 (-CH_2-C-*C*-CH_2-), 63.32, 33.03, 31.49, 29.81, 29.74, 29.64, 29.37, 29.07, 25.95, 22.14, 18.97, 18.66, 13.85.

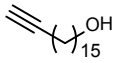

Heptadec-16-ynol (35)

NaH (150 mg, 6.2 mmol, 8eq) was washed with n-hexanes and added to 1.3-diaminopropane (4 mL). The suspension was stirred at 70 °C for 30 min under N_2 atmosphere. The brown reaction mixture was allowed to cool down to RT and a solution of compound **36** (200 mg, 0.8 mmol, 1 eq) in 1.3-diaminopropane (1 mL) was added dropwise at 70 °C . The reaction mixture was stirred overnight at 50 °C and allowed to cool down and then cool down to 0 °C. Water (20 mL) was added slowly followed by the addition of HCl 2N (20 mL). The product was extracted with Et_2O (3x30 mL). The combined organic layers were washed with washed with brine, dried over sodium sulphate, filtered and concentrated under reduced pressure. The yellow residue was purified by silica-gel chromatography (gradient chex: EtOAc 9:1 to 6:4) to yield **35** as a yellowish solid (71mg, 36 %). **^{1}H NMR** (400 MHz, $CDCl_3$) δ 3.62 (t, *J* = 6.6, 2H, -C*H*$_2$-OH), 2.16 (td, *J* = 7.1, 2.6, 2H, C*H*$_2$C≡CH), 1.92 (t, *J* = 2.6, 1H, CH_2C≡C*H*), 1.53 (m, 2H, -C*H*$_2$-CH_2-OH), 1.23 (m, 22H); **^{13}C NMR** (101 MHz, $CDCl_3$) δ 68.04, 63.14, 32.84, 29.66 (2C), 29.63 (2C), 29.52, 29.45, 29.13 (2C), 28.79, 28.52, 25.76, 18.42; **HRMS** (ammonia CI, positive mode) found 270.2798 ($[M+NH4]^+$ requires 270.2791).

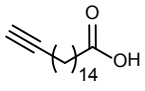

Heptadec-16-ynoic acid (24) [174]

-1st method: To a suspension of TMS-protected alkyne **47** (310 mg, 1 eq, 0.92 mmol) in MeOH (15 mL) was added K_2CO_3 (253 mg, 1.83 mmol, 2 eq). The reaction mixture was stirred at room temperature overnight to give a clear reaction mixture. The mixture was concentrated under reduced pressure. The residue was taken up in 2N HCl (20 mL) and Et_2O (30 mL). The layers were separated and the aqueous layer was extracted with Et_2O (2 x 30 mL). The combined organic layers were washed with water (20 mL), brine (20 mL), dried over sodium sulphate, filtered and concentrated under reduced pressure to yield **24** as an off-white solid (230 mg, 94%). The product did not require further purification.

-2nd method: Jones reagent (2, 90 mL) was added dropwise to a solution of heptadec-16-ynol **35** (70 mg, 0.28 mol) in acetone (10 mL) at 0 °C. The reaction mixture was stirred for 15 min at 0 °C and 15 min at room temperature. The solution became orange and a precipitate started to form in the reaction mixture (Cr salt). The mixture was cooled down to 0 °C and isopropanol (20 mL) was added dropwise to quench the excess of Jones reagent. The reaction mixture was filtered to remove the chromium salt and concentrated under reduced pressure. The residue was taken up in EtOAC and

washed with 0.1N HCl (4 x 25 mL), brine, dried over sodium sulphate and concentrated under reduced pressure to yield **24** as a white solid (50 mg, 67%).

^{1}H NMR (400 MHz, $CDCl_3$) δ 2.33 (t, J = 7.5, 2H, C*H*$_2$CO$_2$H), 2.16 (td, J = 7.1, 2.6, 2H, C*H*$_2$C≡CH), 1.92 (t, J = 2.6, 1H, C≡C*H*), 1.60 (dd, J = 7.3, 14.8, 2H, C*H*$_2$CH$_2$CO$_2$H), 1.55 – 1.45 (m, 2H, C*H*$_2$CH$_2$C≡CH), 1.30 (m, 20H, 10 x CH_2); **^{13}C NMR** (101 MHz, CDCl3) δ 178.90 (C=O), 84.86 (C≡CH), 68.04 (C≡CH), 33.84, 29.63 (4C), 29.52, 29.44, 29.25, 29.13, 29.07, 28.79, 28.52, 24.70, 18.42; **HRMS** (ESI, negative mode) found 265.2170 ([M - H]$^-$ requires 265.2168). The analysis was consistent with the NMR and MS analysis reported in the literature.[174]

8.1.5 YnC12CoA synthesis (19)

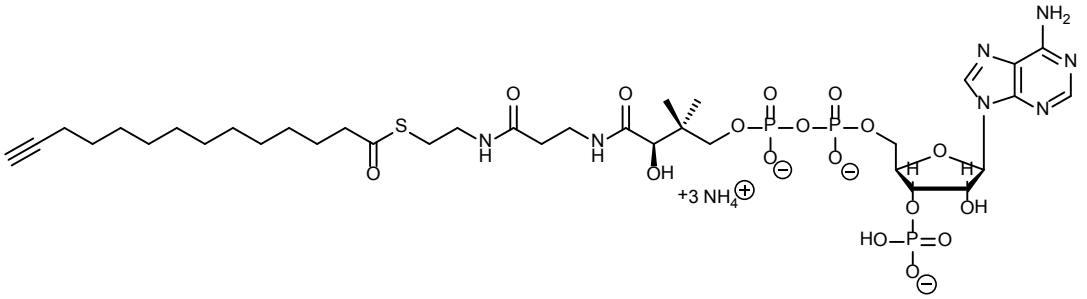

To a suspension of tetradec-13-ynoic acid (**16**, 14.8 mg, 65 µmol, 2 eq) in dry THF (1.0 mL) was added a solution of 1,1'-carbonyl-diimidazole (12.7 mg, 78 µmol, 2.4 eq) in DCM (1.0 mL), under nitrogen atmosphere. The clear reaction mixture was stirred for 45 minutes at room temperature. The reaction mixture was concentrated under reduced pressure. The yellow residue was dissolved in dry THF (1.0 mL). Co-enzyme A hydrate from yeast (25 mg, 32.6 µmol, 1 eq) was dissolved in an aqueous solution of $NaHCO_3$ (0.5 M, 3.4 mL) and added to the solution of activated acid. The reaction mixture was stirred at room temperature for 3 hours under nitrogen atmosphere. The THF was removed under reduced pressure. The product was precipitated by adding 20% perchloric acid dropwise (1 mL). The white solid was pelleted by centrifugation and washed with 1 % perchloric acid. The product was purified by preparative RP-HPLC over a gradient of 25 mM ammonium carbonate pH 8 in MeOH (Method A). YnC12CoA **19** was obtained as a white lyophilised solid (22.2 mg, 66% yield). **LC-MS:** R_T=10.04 min (Absorption wavelength = 258 nm; Method A), m/z (positive mode) = 974.94, m/z (negative mode) = 486.28 and 972.8, Purity > 98%; **^{1}H NMR** (400 MHz, D_2O) δ 8.54 (s, 1H, Ar-H), 8.24 (s, 1H, Ar-H), 6.14 (d, J = 6.6, 1H, C*H*(Pur)), 4.59 – 4.53 (m, 2H, 2 × Rib-C*H*), 4.23 – 4.18 (m, 3H, O-C*H*$_2$ and Rib-C*H*), 4.01 (bs, 1H, C(O)C*H*OH), 3.84-3.79 (m, 1H, C*H*$_2$C(CH$_3$)$_2$), 3.55-3.50 (m, 1H, C*H*$_2$C(CH$_3$)$_2$), 3.42 (t, J = 6.6, 2H, SCH$_2$C*H*$_2$), 3.33 – 3.28 (m, 2H, C(O)CH$_2$C*H*$_2$NH), 2.99 – 2.94 (m, 2H, C(O)C*H*$_2$CH$_2$NH), 2.58-2.52 (t, J = 7.3, 2H, (CH$_2$)$_2$C*H*$_2$C(O)NH), 2.40 (t, J = 6.7, 2H, SC*H*$_2$), 2.30 (t, J = 2.6, 1H, C≡C*H*), 2.15 (td, J = 2.6, 7.1, 2H, C*H*$_2$C≡CH), 1.57-1.52 (m, 2H, CH$_2$C*H*$_2$CH$_2$C(O)NH), 1.47 –

1.40 (m, 2H, CH_2CH$_2$C≡CH), 1.30 (bs, 2H, CH_2), 1.18 (bs, 12H, 6xCH_2), 0.86 (s, 3H, -CH_3), 0.72 (s, 3H, -CH_3). The analysis was consistent with the NMR analysis reported in the literature.[154]

8.1.6 MyrCoA synthesis (17)

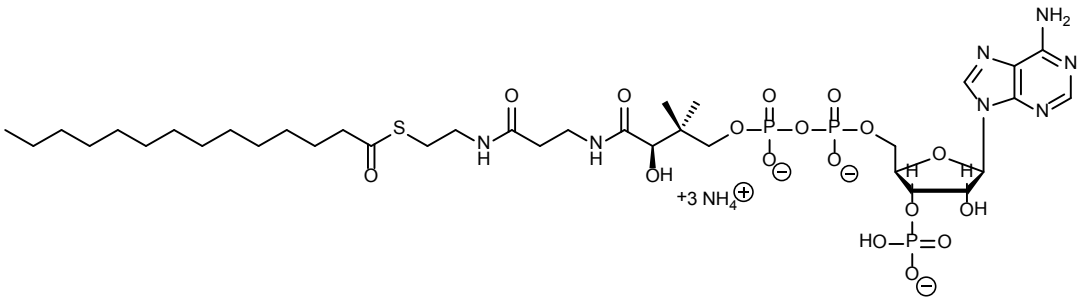

A similar procedure as YnC12CoA **19** was used to prepare MyrCoA **17**, replacing YnC12 **16** by myristic acid **14** (65 µmol) (10.1 mg, 32 %). **LC-MS:** R_T=12.80 min (Absorption wavelength = 258 nm; method A), m/z (positive mode) = 974.4, Purity > 98%; **^{1}H NMR** (400 MHz, D_2O) δ 8.56 (s, 1H, Ar-H), 8.26 (s, 1H, Ar-H), 6.17 (d, J = 6.4, 1H, Rib-C*H*), 4.60-4.57 (m, 2H, 2 × Rib-C*H*), 4.26-4.22 (m, 3H, O-CH_2 and Rib-C*H*), 4.04 (bs, 1H, C(O)C*H*OH), 3.87-3.82 (m, 1H, CH_2C (CH_3)$_2$), 3.58-3.53 (m, 1H, CH_2C(CH_3)$_2$), 3.45 (t, J = 6.7, 2H, SCH$_2$CH_2), 3.36-3.32 (m, 2H, C(O)CH$_2$CH_2NH), 2.99 (t, *J* = 6.3, 2H, C(O)CH_2CH$_2$NH), 2.60-2.55 (m, J = 7.3, 2H, (CH$_2$)$_2$CH_2C(O)NH), 2.42 (t, J = 6.7, 2H, SCH_2), 1.60-1.55 (m, 2H, CH$_2$CH_2CH$_2$C(O)NH), 1.1 (bs, 24H, 12 x CH_2), 0.89 (s, 3H, -CH_3), 0.84 (t, *J* = 6.9, 3H, CH_3-(CH$_2$)$_{12}$-), 0.75 (s, 3H, -CH_3).

8.1.7 AzC12CoA (18)

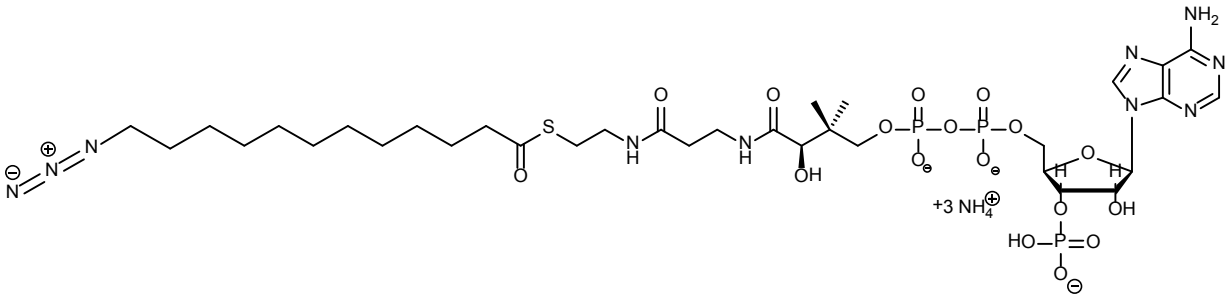

The same procedure as for YnC12CoA **19** was used (except using 12-azido-dodecanoic acid **15** (15.7 mg, 65 µmol), and afforded AzC12CoA **18** as a white solid (10 mg, 30 % yield). **LCMS:** R_T=10.54 min (Absorption wavelength = 258 nm; Method A), m/z (positive mode) = 991.4, Purity > 98%; **^{1}H NMR** (400 MHz, D_2O) δ 8.43 (s, 1H, Ar-H), 8.24 (s, 1H, Ar-*H*), 6.14 (d, *J* = 7.0, 1H, Rib-C*H*), 4.75-4.70 (m, 2H, 2×Rib-C*H*), 4.54 (bs, 1H, Rib-C*H*), 4.20 (bs, 2H, Rib-CH_2), 4.00 (bs, 1H, C(O)C*H*OH), 3.83-3.78 (m, 1H, CH_2C(CH_3)$_2$), 3.54-3.49 (m, 1H, CH_2C(CH_3)$_2$), 3.42 (t, *J* = 6.6, 2H, SCH$_2$CH_2), 3.33-3.24 (m, 4H, CH_2N$_3$ and C(O)CH$_2$CH_2NH), 2.96 (t, *J* = 6.3, 2H, C(O)CH_2CH$_2$NH), 2.57-2.53 (m, *J* = 7.3, 2H, (CH$_2$)$_2$CH_2C(O)S), 2.39 (t, *J* = 6.6, 2H, SCH_2), 1.60-1.50 (m, 4H, CH$_2$CH_2CH$_2$C(O)S

and C*H*$_2$CH$_2$N$_3$), 1.34 – 1.14 (m, 14H, 7 × C*H*$_2$), 0.85 (s, 3H, -C*H*$_3$), 0.71 (s, 3H, -C*H*$_3$). The analysis was consistent with the NMR analysis reported in the literature.[154]

8.1.8 Prodrug synthesis

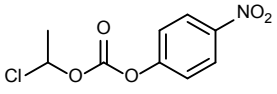

(1-chloroethyl)-(4-nitrophenyl)carbonate (56) [226]

To a suspension of 4-nitrophenol (**55)** in toluene (8 mL, 1 eq, 1.43 mmol) was added dropwise 1-chloroethylchloroformate (200 µL, 1.3 eq, 1.85 mmol) and tributyl amine (442 µL, 1.3 eq, 1.85 mmols). After few minutes, a clear brown solution was obtained. The reaction mixture was stirred at room temperature for 90 min. Completion of the reaction was followed by TLC (hex: EtOAc 1:1 Rf product = 0.71; Rf 4- nitrophenol = 0.54.). The reaction mixture was washed with 1N HCl (40 mL), water (2 x 20 mL), brine (20 mL), dried over $MgSO_4$ and filtered. The crude product **56** was directly used for the next step. **^{1}H NMR** (400 MHz, $CDCl_3$) δ 8.32 – 8.25 (m, 2H, aromatic), 7.45 – 7.36 (m, 2H, aromatic), 6.48 (q, *J* = 5.8, 1H, -C*H*-), 1.91 (d, *J* = 5.8, 3H, C*H*$_3$); **^{13}C NMR** (101 MHz, $CDCl_3$) δ 155.15 (C=O), 150.66 (C-NO_2), 145.92 ($C_{aromatic}$-O), 125.65 (*C*H-C-NO_2), 121.90 (*C*H-CH-C-NO_2), 85.44 (C*H*-CH_3), 25.33 (C*H*$_3$).

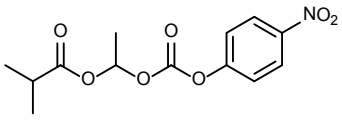

1-(((4-nitrophenoxy)carbonyl)oxy)ethyl 2-methyl propanoate (57) [226]

Zinc oxide, potassium iodide and isobutyric acid were added to **56** in one portion. The suspension was heated to 75 ^{o}C for 2 h. Toluene was removed under reduced pressure to yield a brown oil. The oil was taken up in EtOAc, washed with a saturated solution of $NaHCO_3$ (50 mL), brine (20 mL), dried over $MgSO_4$ and concentrated under reduced pressure to give a brown oil. The crude product was purified by silica gel chromatography using hex: EtOAc 9:1 as eluent. (Rf product = 0.15). A yellow oil was obtained (420 mg). NMR showed that the product contained around 20 % of the intermediate. 50 mg of the product was purified with a Sepak column (gradient 100% H_2O-to 100% AcN). 12 mg of **57** was obtained (9%). **^{1}H NMR** (400 MHz, $CDCl_3$) δ 8.32 – 8.20 (m, 2H, aromatic), 7.43 – 7.32 (m, 2H, aromatic), 6.82 (q, *J* = 5.4, 1H, -O-C*H*Me-O-), 2.66 – 2.52 (m, 1H, -C*H*$(CH_3)_2$), 1.60 (d, *J* = 5.4, 3H), 1.19 (dd, *J* = 7.0, 0.6, 6H); **^{13}C NMR** (101 MHz, $CDCl_3$) δ 175.25 (CH-C(O)-O), 155.39 (O-C(O)-O), 150.73 (C-NO_2), 145.77 ($C_{aromatic}$-O), 125.55 (*C*H-C-NO_2), 121.96 (*C*H-CH-C-NO_2), 92.55 (CH), , 34.01 (CH), 19.62 (O-CH-*C*H_3), 18.85(*C*H3-CH-CH3). 18.79 (*C*H_3-CH-CH_3).

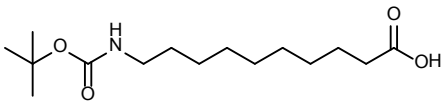

9-(*tert*-butoxycarbonyl)aminodecanoic acid 77

NH_4OH (160 mL, 25% in H_2O) was added to bromododecanoic acid (5.0 g, 20 mmol, 1 eq) and the brown suspension was stirred at RT for 24h. The mixture was concentrated under reduced pressure to give a brown solid, 8-aminooctanoic acid. To the crude product was added sodium hydroxide (840 mg, 21 mmol, 1.05 eq), H_2O (18mL) and tert-butanol (9 mL). The solution was stirred at RT overnight. The solution was partitioned between Et_2O (40 mL) and 1N HCl (30 mL). The layers were separated and the aqueous layer was extracted with Et_2O (2 x 10 mL). The combined organic layers were concentrated under reduced pressure to give **77** as a brown solid (5.1 g, 88 %). **^{1}H NMR** (400 MHz, $CDCl_3$) δ 4.50 (br s, 1H, -N*H*Boc), 3.08 (apparent q, *J* = 6.3, 2H, -CH_2-NHBoc), 2.32 (t, *J* = 7.5, 2H, -CH_2-COOH), 1.61 (m, 2H, -CH_2-CH_2-NHBoc), 1.44 (m, 12H), 1.24 (apparent dd, *J* = 12.4, 5.7, 9H, Boc).

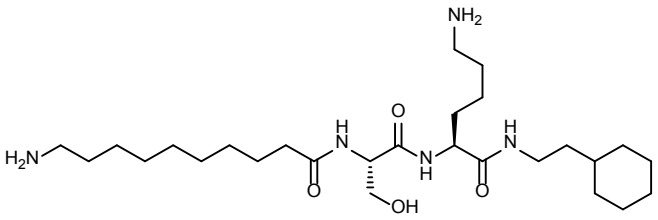

(9-aminodecanoyl)-Ser-Lys-2-cyclohexylethylamide (IMP475)

Chlorotrityl resin was swelled in DCM for 1 h. Fmoc-Lys(Boc)-OH (514 mg, 1.10 mmol, 1.2 eq) and DIPEA (0.765mL, 4.4 mmol, 4.8 eq) were dissolved in dry DCM (7 mL) and added to the resin (750 mg, Loading: 1.22 mmol/g). The mixture was shaken for 2 h. The resin was drained and washed with DCM/MeOH/DIPEA (3 × 17:2:1) and with DMF (3x), DCM (3x), MeOH (3x), Et_2O (3x) before being dried in a desiccator overnight. The resin was swelled in DMF for 1 h and Fmoc deprotected using method 1. Fmoc-Ser(t-Bu)-OH and 9-(*tert*-butoxycarbonyl)aminodecanoic acid **77** were coupled on the resin as explained in method 2 (HBTU and HATU were used as coupling reagents respectively). The peptide was cleaved off the resin by adding a mixture of triisopropylsilane (TIS, 0.5%) and Trifluoroacetic acid (TFA, 0.5%) in DCM. The mixture was shaken for 2 h at RT and filtered. All volatiles were evaporated by flushing the mixture with N_2. The brown oily residue was purified by preparative LC-MS (Method C). 80 mg of yellowish oil were obtained (yield 13 %) and directly used for the next step. To a solution of the product (0.13 mmol, 1 eq) in DMF (4 mL) was added HATU(144 mg, 0.38 mmol, 3eq), DIPEA (219 µL, 1.3 mmol, 10 eq) and 2-cyclohexylethanaminium acetate (49 mg, 0.38 mmol, 3eq, kindly donated by Tayo Olaleye, Imperial College London). The yellow solution was stirred at RT overnight. DCM (40 mL) was added and the organic layer was

washed with 1N HCl (100 mL), H_2O (50 mL) and Brine (50 mL). The organic layer was concentrated under reduced pressure to give a brown oil. A mixture of TFA:TIS:H_2O 95:2.5:2.5 (2 mL) was added to the residue and stirred at room temperature for 3 h. Completion of the deprotection (Boc and tBu) was checked by LC-MS (Method C). The mixture was flushed with N_2 and dried in the desiccator overnight. The crude product was purified by preparative LC-MS (Method C) to give **IMP475** as a yellowish oil (54 mg, overall yield 11%). **^{1}H NMR** (500 MHz, MeOD) δ ppm 8.52 (1H, s), 4.46 (t, *J* = 6.0, 1H), 4.36-4.31 (m, 1H), 3.96 – 3.86 (m, 2H), 3.35-3.25 (m, 2H), 3.10 – 3.02 (4H, m), 2.40 (t, *J* = 7.4, 2H), 1.99 – 1.87 (m, 1H), 1.76 – 1.60 (11H, m), 1.55 – 1.20 (19H, m), 1.03 – 0.91 (2H, m); **Rt**: 6.65 min (Method C); **HRMS** (ESI, positive mode) found 512.4167 ([M + H]$^+$ requires 512.4131).

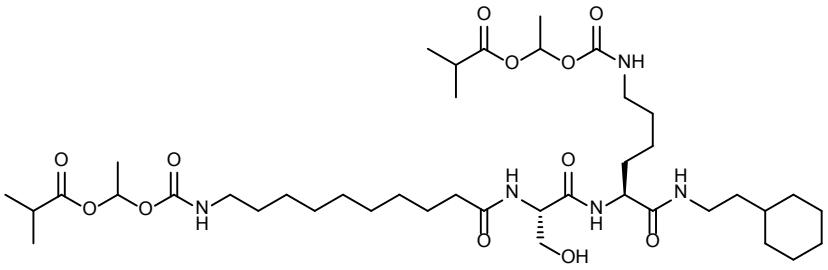

Compound 62

To a solution of (9-aminodecanoyl)-Ser-Lys-2-cyclohexylethylamide **61** (5 mg, 9.8 µmol, 1 eq) in dry THF (0.5 mL) was added 1-(((4-nitrophenoxy)carbonyl)oxy)ethyl-2-methyl propanoate **61** (6.6 mg, 19.5 µmol, 2eq) and tributylamine (10.6 µL, 39 µmol, 4eq). The mixture was stirred at RT for 6 h and concentrated under reduce pressure. The crude product was purified by preparative LC-MS (Method C) to give **62** as a white solid (1.5 mg, 18%). **Rt**: 12.38 min (Method C). **^{1}H NMR** (500 MHz, DMSO) δ 7.95 (d, *J* = 8.2, 1H), 7.91 (d, *J* = 6.9, 1H), 7.87-7.82 (m, 1H), 7.72 (t, *J* = 5.4, 1H), 7.41-7.35 (m, 2H), 6.63 (q, *J* = 5.4, 2H,2 x -O-C*H*Me-O-), 4.87 (t, *J* = 5.5, 1H), 4.14--4.05 (m, 1H), 3.55-3.50 (m, 2H), 3.10-2.98 (m, 2H), 2.96-2.86 (m, 4H), 2.63-2.61 (m, 1H), 2.37-2.34 (m, 1H), 2.13 (t, *J* = 7.4, 2H), 2.02-1.96 (m, 1H), 1.68-1.59 (m, 6H, 2x C*H*$_3$CH -prodrug), 1.50-1.42 (m, 4H), 1.40-1.33 (m, 8H), 1.3-1.1 (m, 18H), 1.05 (dd, *J* = 7.0, 2.5, 12H, 2 x CH(C*H*$_3$)$_2$), 0.84 (m, 2H). **HRMS** (ES-ToF, positive mode) 828.5347 expected 828.5328.

8.1.9 4-azidobutyric acid

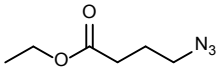

Ethyl 4-azidobutyrate (66)

Same procedure as methyl 12-azidodecanoate, starting from Ethyl 4-bromobutyrate (2 g, 10.3 mmols, 1 eq). A clear oil was obtained (1.27 g, 81 % yield).**^{1}H NMR** (400 MHz, $CDCl_3$) δ 4.12 (q, *J* = 7.1, 2H, -C*H*$_2$-CH$_3$), 3.33 (t, *J* = 6.7, 2H, -C*H*$_2$-N$_3$), 2.38 (t, *J* = 7.3, 2H, -C*H*$_2$-COOEt), 1.89 (p, *J* = 7.0,

2H, -CH_2-C*H*$_2$-CH_2-), 1.27 – 1.21 (t, *J* = 7.1, 3H, -C*H*$_3$); **^{13}C NMR** (101 MHz, $CDCl_3$) δ 172.91 (CO), 60.78 (CH_3-*C*H_2-), 50.86 (-*C*H_2-COOH), 31.39 (-*C*H_2-N_3), 24.47 (-CH_2-*C*H_2-CH_2-), 14.41 (*C*H_3).

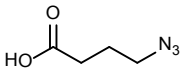

4-azidobutyric acid (67)

Same procedure as 12-azidodecanoic acid, starting from ethyl 4-azidobutyrate **66** (1.2 g, 7.6 mmols, 1 eq). A clear oil was obtained (1.0 g, quantitative).**^{1}H NMR** (400 MHz, $CDCl_3$) δ 3.36 (t, *J* = 6.7, 2H, -C*H*$_2$-N_3), 2.46 (t, *J* = 7.2, 2H, -C*H*$_2$-COOH), 1.90 (p, *J* = 7.0, 2H, -CH_2-C*H*$_2$-CH_2-); **^{13}C NMR** (101 MHz, $CDCl_3$) δ 179.07 (CO), 50.66 (-*C*H_2-COOH), 31.07 (-*C*H_2-N_3), 24.14 (-CH_2-*C*H_2-CH_2-); **HRMS** (CI, positive mode) found 147.0883 ($[M + NH4]^+$ requires 147.0877).

8.1.10 Linker for the spot synthesis

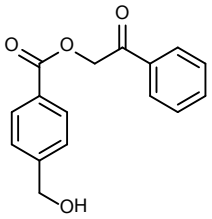

Phenacyl-4-(hydroxymethyl)benzoate(72) [342]

To a suspension of 4-(hydroxymethyl)benzoic acid **69** (500 mg, 3.3 mmol, 1 eq) in EtOAc (30mL) was added 2-bromoacetophenone (726 mg, 3.63 mmol, 1.1 eq) and triethylamine (460 µL, 3.3 mmol, 1 eq). The reaction mixture was stirred at room temperature overnight and concentrated under reduced pressure. The residue was purified by silica gel column chromatography (Hex:EtOAc 2:1) to yield **72** as a white powder (900 mg, quantitative). **Rf** (hex:EtOAc 1:1)= 0.45; **^{1}H NMR** (400 MHz, DMSO) δ 8.04 – 7.98 (m, 4H, -C_6H_4-CH_2-OH), 7.74 – 7.69 (m, 1H, CH_2-CO-C_6H_5), 7.59 (t, *J* = 7.7, 2H, CH_2-CO-C_6H_5), 7.51 (d, *J* = 8.4, 2H, CH_2-CO-C_6H_5), 5.75 (s, 2H, C*H*$_2$-CO-C_6H_5), 5.42 (t, *J* = 5.7, 1H, -C_6H_4-CH_2-O*H*), 4.61 (d, *J* = 5.7, 2H, C_6H_4-C*H*$_2$-OH); **^{13}C NMR** (101 MHz, DMSO) δ 193.30 (CH_2-*C*O-C_6H_5), 165.72 (-*C*O-C_6H_4-CH_2-OH), 149.20 (-CH_2-CO-*C*$_6$$H_5$), 134.52 (*C*$_6$$H_4$-$CH_2$-OH), 134.36 ($CH_2$-CO-*C*$_6$$H_5$), 129.78 (Ar), 129.45 (Ar), 128.29 (Ar), 127.93 (Quaternary C, CH_2-CO-*C*$_6$$H_5$), 126.87 (Ar), 67.53 (-*C*H_2-CO-C_6H_5), 62.84 (C_6H_4-*C*H_2-OH). The analysis was consistent with the NMR and MS analysis reported in the literature.[342]

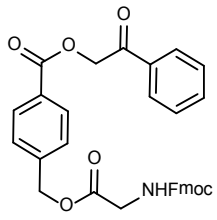

Phenacyl-4-1-[[N-(9-fluorenylmethoxycarbonyl)-L-glycyl]oxy]- methyllbenzoate (73)

To a solution of **73** (890 mg, 3.3 mmol, 1 eq), Fmoc-Gly-OH (921 mg, 3.3 mmol, 1 eq) and DMAP (60.5 mg, 3.3 mmol, 1 eq) in DCM (15 mL) was added at 0 °C a solution of DCC (680.9 mg, 3.3 mmol, 1 eq) in DCM (5 mL). The suspension was stirred at 0 °C for 2 h and at room temperature overnight. The reaction mixture was filtered and concentrated under reduced pressure. The white residue was diluted in DCM and washed with NH_4Cl (aq) 1N, brine, water, dried over sodium sulphate and concentrated under reduced pressure. The residue was purified by silica gel column chromatography (gradient: hex:EtOAc 3:1 to hex:EtOAc 1:1) to yield **73** as a white powder (1.65 g, 91%). **Rf** (hex:EtOAc 3:1)= 0.25; **^{1}H NMR** (400 MHz, DMSO) δ 8.03 – 7.98 (m, 4H, -C_6H_4-CH_2-OH), 7.89 (d, *J* = 7.5, 2H, Fmoc), 7.83 (t, *J* = 6.1, 1H, Fmoc), 7.74-7.67 (m, 3H, 1H of CH_2-CO-C_6H_5+ 2H of Fmoc), 7.61 – 7.57 (m, 2H, CH_2-CO-C_6H_5), 7.57-7.51 (m, 2H, CH_2-CO-C_6H_5), 7.41 (t, *J* = 7.4, 2H, Fmoc), 7.31 (td, *J* = 6.5, 7.4, 2H, Fmoc), 5.74-5.76 (m, 2H, CH_2-CO-C_6H_5), 5.19-5.26 (m, 2H, -C_6H_4-CH_2-OCO-CH_2-NH-), 4.25-4.34 (m, *J* = 7.0, 2H, -NH-COO-CH_2-), 4.12-4.25 (m, 1H, CH_2-N*H*-Fmoc), 3.78-3.90 (m, 2H, -C_6H_4-CH_2-OCO-CH_2-NH-); **^{13}C NMR** (101 MHz, DMSO) δ 192.71 (CH_2-*C*O-C_6H_5), 170.10 (-*C*(O)-CH_2-NHFmoc), 164.99 (-*C*O-C_6H_4-CH_2-), 156.59, 143.80, 141.77, 140.76, 134.07, 133.88, 129.52, 128.99, 128.69, 127.86, 127.79, 127.66, 127.09, 125.18, 125.18, 120.16, 67.23, 65.82, 65.17, 46.58, 42.26; **HRMS** (ESI, positive mode) found 550.2004 ($[M + H]^+$ requires 550.1866).

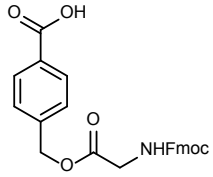

4-[N-(9-fluorenylmethoxycarbonyl)-L-glycyl]oxy]methyl]benzoic acid (74)

-1st method: To as suspension of **73** (1.5 g, 2.73 mmol, 1 eq) in EtOAc (5.5 mL) and water (5.5 mL) were added AcOH (13.5 mL, 5 mL / mmol) and zinc powder (1.25 g, 19.11 mmol, 7 eq). The mixture was stirred at room temperature overnight. The mixture was filtered and the precipitate washed with DCM (5 mL) and MeOH (5 mL). The organic layer was concentrated under reduced pressure and the residue was taken up in DCM (20 mL). The organic layer was washed with $NaHCO_3$ (aq) sat., brine, water, dried over sodium sulphate and concentrated under reduced pressure. The residue was purified by silica gel column chromatography (hex:EtOAc:AcOH 1:1:0.01) to afford **74** as a white powder (920 mg, 78%).

-2nd method: direct coupling. To a solution of Fmoc-Gly-OH **75** (977 mg, 3.29 mmol, 2 eq) in DMF was added CDI (533 mg, 3.29 mmol, 2 eq) in one portion. After stirring at room temperature for 30 min, a solution of 4-(hydroxymethyl)benzoic acid **69** (250 mg, 1.64 mmol, 1 eq) was added dropwise. The reaction mixture was stirred at room temperature for 3 h and concentrated under reduced pressure. The residue was purified by silica gel column chromatography (gradient DCM:EtOAc 9:5 to DCM:EtOAc:AcOH 9:5:0.01) to yield **74** as a white powder (220 mg, 26%). **Rf** (hex:EtOAc:AcOH 1:1:0.01)= 0.5; **^{1}H NMR** (400 MHz, DMSO) δ 7.87-7.94 (m, 4H, HOOC-C_6H_4-CH_2-), 7.83 (t, *J* = 6.1, 1H, Fmoc), 7.70 (d, *J* = 7.5, 2H, Fmoc), 7.47 (d, *J* = 8.2, 2H, Fmoc), 7.41 (t, *J* = 7.5, 2H, Fmoc), 7.32 (t, *J* = 7.0, 2H, Fmoc), 5.16-5.22 (m, 2H, C_6H_4-CH_2-OCO-CH_2-NH-), 4.25-4.34 (m, 2H, -NH-COO-CH_2), 4.23 (t, *J* = 6.9, 1H CH_2-N*H*-Fmoc), 3.78-3.88 (m, 2H, C_6H_4-CH_2-OCO-CH_2-NH-); **^{1}H NMR** (500 MHz, DMSO, **50°C**) δ 7.90-7.93 (m, 2H, HOOC-C_6H_4-CH_2-), 7.87 (d, *J* = 7.6, 2H, HOOC-C_6H_4-CH_2-), 7.67-7.70 (m, 1H, Fmoc), 7.46 (d, *J* = 8.2, 2H, Fmoc), 7.41 (t, *J* = 7.5, 2H, Fmoc), 7.32 (d, *J* = 7.4, 2H, Fmoc), 5.21 (s, 2H, C_6H_4-CH_2-OCO-CH_2-NH-), 4.33 (d, *J* = 6.9, 2H, -NH-COO-CH_2-), 4.23 (s, 1H, CH_2-N*H*-Fmoc), 3.86 (s, 2H, -C_6H_4-CH_2-OCO-CH_2-NH-); **^{13C} NMR** (101 MHz, DMSO) δ 170.10 (-*C*(O)-CH_2-NHFmoc), 156.56 (-*C*OOH), 143.79, 140.83, 140.75, 129.42, 127.65, 127.60, 127.09, 125.18, 120.16, 65.79, 65.24, 46.58, 42.23; **HRMS** (ESI, negative mode) found 430.1291 ($[M - H]^-$ requires 430.1291).

8.1.11 Peptide synthesis

8.1.11.1 Peptides on cellulose membranes (SPOT™ synthesis)

The peptides were either pre-activated before the synthesis or pre-activated by the apparatus before each coupling. The peptides were synthesized either without any linker or with a cleavable linker (HMB, Fmoc-Gly-HMB-OH, or rink amide linker). The cleavable linker was coupled as a normal amino acid. 600 peptides were prepared on the same membrane (20 x 30 peptides).

8.1.11.1.1 Pre-activated in the apparatus before each coupling

Solutions of amino acids or linkers (0.5 M in NMP), HOBt (1.1 M in NMP), DIC (1.1 M in NMP) were prepared and placed in the apparatus. The membrane was swelled for 30 min in DMF and placed in the apparatus. The membrane was washed with EtOH (2 x 15 s) and dried by extraction (900 s). The reagents needed for the 1st step were automatically taken (2 coupling x number of peptide having this derivative in the sequence x (0.1 µL of derivative+0.05 µL of HOBt solution +0.5 µL DIC solution + 0.001 µL NMP) and mixed in smaller vials. 0.22 µL of the pre-activated solution were added to each spot on the membrane and allowed to react for 10 minutes. The coupling step was repeated twice. Then, the membrane was extracted for 30 s and capped for 10 minutes with a 2% (v/v) Ac_2O solution in NMP. The membrane was extracted (30 s), washed with DMF (8 x 5 s), EtOH (2 x 5 s) and extracted for 90 s. The N-terminal Fmoc group was cleaved using 20% piperidine (v/v) in DMF (2 x 5 min). The

membrane was extracted (30 s), washed with DMF (8 x 10 s), EtOH (2 x 10 s) and extracted for 900 s. The cycle of pre-activation, couplings, capping, washes, deprotection and washes was repeated for each amino acid in the peptide sequence. After the final amino acid coupling, the membrane was removed and dried in a vacuum desiccator overnight.

8.1.11.1.2 Pre-activated before the synthesis

Solutions comprising amino acids or linkers (0.5 M), HOBt (1.1 M), DIC (1.1 M) in NMP were prepared and mixed for 20 min at room temperature before being placed in the apparatus. Fresh solutions were prepared every 6 cycles (~24 h). The membrane was swelled for 30 min in DMF and placed in the apparatus. The membrane was washed with EtOH (2 x 15 s) and dried by extraction for 900 s. 0.22 µL of the activated solutions were automatically taken, spotted on the membrane and allowed to react for 10 min (repeated twice). Then, the membrane was extracted, capped, washed, deprotected and washed as described for the previous method. The cycle of couplings, capping, washes, deprotection and washes was repeated for each amino acid in the peptide sequence. After the final amino acid coupling, the membrane was removed and dried overnight in the desiccator. The membrane was then cut in several units which were kept at -18 °C.

8.1.11.1.3 Side chain deprotection:

To a membrane, placed in a 15 mL Falcon tube, was added a solution of TFA 94%, water 2.5%, EDT 2.5%, TIS 1%. The mixture was stirred at room temperature for one hour. The membrane was then washed with DCM (4 x 2 min), DMF (4 x 2 min) and EtOH (2 x 2 min) and dried under N_2. The membrane was then ready to perform assays or to be cleaved in solution for subsequent analysis.

8.1.11.1.4 Peptide cleavage in solution

✓ HMB linker

The spots were cut out and placed in different vials of a 96-well plate. A solution of ammonia 7 N in MeOH (100 µL) was added to each spot and the plate was shaken overnight at room temperature. The spot paper was removed and the solutions were heated at 60 °C for 2 hours to evaporate the solvent. Then, the residue was dissolved in MeOH: H_2O (1:1) (20 µL) and analysed by MALDI.

✓ Rink amide linker

The spots were cut out and shaded with a pencil to give a much more visible grey pellet. The spots were cleaved using a solution of TFA 94%, H_2O 2.5%, EDT 2.5%, TIS 1% (200 µL for each spot). After 3 h, the spot paper was removed and the peptides were precipitated with *tert*-butylmethylether (TBME). The grey solid was pelleted by centrifugation and washed with TBME (2x). TBME was

removed and the peptides were allowed to dry for 2 hours at room temperature. The pellet was dissolved in MeOH: H_2O (1:1) (20 µL) and analysed by MALDI.

8.1.11.2 Solid Phase Peptide Synthesis (SPPS)

Peptides bearing a C-teminal amino group were synthesised using Tentagel S RAM resin (substitution: 0.3 mmol/g). FLAG peptides (with an acid at the C-terminus were synthesised on a Wang resin pre-loaded with Lysine. Peptides bearing a biotin moiety at the C-terminus were synthesised using a Biotin-PEG NovaTag resin (Merck)

The resin (20 µmol per well) was swelled in DMF for 30 min before deprotection of the N-terminal Fmoc protecting group with 20% piperidine (v/v) in DMF for 10 min (400 µL; 3 repeats). 4.38 equivalents of the incoming *N*-Fmoc protected amino acid (as a 0.5 M solution in DMF; 87.5 µmol) was activated in a separate vial with HBTU (0.5 M solution in DMF; 85 µmol, 4.25 eq), *N*-methyl pyrrolidinone (NMP) (5 µL) and *N*-methyl-morpholine (4 M; 52 µL; 208 µmol, 10.4 eq). The activated amino acid was added to the resin and allowed to couple for 35 min (repeated twice). The peptide was capped using a solution of 5% (v/v) acetic anhydride in NMP (400 µL). The resin was washed with DCM (2x) and DMF (6x) and the cycle of deprotection, DMF wash, amino acid couplings, capping and DMF wash was repeated for each amino acid in the peptide sequence. After the final amino acid coupling, the N-terminal Fmoc was cleaved using 20% piperidine (v/v*)* in DMF (400 µL, 3× 10 min). The resin was placed in a 10 mL syringe equipped with a polyethylene frit and a syringe cap. The resin bound peptide was then washed with DMF (3×), DCM (3×), MeOH (3×) and Et_2O (3×) before being dried in a vacuum desiccator overnight. The peptide was deprotected and cleaved from the resin using a deprotection/cleavage mixture of 95% TFA, 2.5% water, 2.5% TIS. 6 mL of this mixture was added to the resin-bound peptide and it was shaken at room temperature for 3 h. For cysteine containing peptides, a different deprotection/cleavage mixture was used (88% TFA, 5% water, 2% TIS, 5% DTT).The liquid was filtered, and the resin washed with 2 mL of deprotection mixture. To the solution was added 10 mL cold tert-butylmethyl-ether (TBME) to precipitate the peptide. The mixture was centrifuged (4000 rpm, 4 °C, 15 min) and the solid washed with 10 mL TBME two more times. The peptide was then placed in a vacuum desiccator overnight before being purified by semi-preparative HPLC and freeze-dried. Characterisation data for these peptides is shown in Table 15.

8.1.11.3 Manual coupling at the peptide N-terminus

When an acid instead of an amino acid (myristic acid, YnC12, 5-pentynoic acid or azido-butyric acid) was coupled at the N-terminus of the peptide, the coupling was done manually to ensure a better yield. Following standard SPPS the peptide was transferred to a 5 mL syringe equipped with a

polyethylene frit and the coupling was carried out as described in Method 2. The peptide was deprotected as described in Section 8.1.11.2. Characterisation data for these peptides is shown in Table 15.

8.1.12 Manual acetylation at the peptide N-terminus

Following standard SPPS the peptide was transferred to a 5 mL syringe equipped with a polyethylene frit and the resin swelled by addition of 1 mL DMF followed by shaking at room temperature for 1 h. DMF was removed by filtration, and 1 mL acetylation mixture (10% acetic anhydride, 20% DIPEA in DMF (v/v)) added and shaken at room temperature for 1 h. The reagent mixture was removed by filtration and the peptides washed and deprotected as described in Section 8.1.11.2. Characterisation data for these peptides is shown in Table 15.

8.1.13 Peptide characterisation

The following peptides were prepared:

Table 15. Sequences, names, characterisation of the peptides prepared for the current study. Purif. = Purification method.

Peptide	Sequence	Purif.	MW (g/mol)	Exact mass (g/mol)	ES^+ peaks	R_t	Yield (%)	Solvent stock
c-SRC 15AA	GSNKSKPKDASQRRR-NH_2	B	1713.901	1712.940	858.13, 572.29, 429.57	0.98	15%	DMSO
c-SRC 8AA	GSNKSKPK-NH_2	B	843.964	843.482	844.92, 423.16	1.33	26%	H_2O
BASP1 15AA	GGKLSKKKKGYNVND-NH_2	B	1634.88	1633.916	818.67; 546.13	1.18	16%	DMSO
ARF1 15AA	GNIFEKLFKSLLGKK-NH_2	C	1721.099	1720.029	861.59, 574.54	8.94	11%	DMSO
HIV Gag	GARASVLSGGKLDAW-NH_2	D	1486.675	1485.794	744.11	9.64	18%	DMSO
HIV Nef	GKWSKSSIVGWPAV--NH_2	B	1557.796	1556.835	780.08; 1558.45	9..58	32%	DMSO
Human sphingolipid delta	GNSASRNDFEWVYTD-NH_2	D	1759.788	1758.749	881.02	10.16	26%	DMSO
MARCKS	GAQFSKTAAKGEAAA-NH_2	B	1406.543	1405.720	704.23; 1407.22	0.95	21%	DMSO
SRC like adaptor 2	GSLPSRRKSLPSPSL-NH_2	B	1580.832	1579.905	791.28	7.9	16%	DMSO
Annexin 13b	GNRHSQSYTLSEGSQ-NH_2	B	1649.678	1648.744	825.52	7.21	4%	DMSO
HIS-tag	GSSHHHHHHS-NH_2	B	1158.145	1157.486	579.99	0.88	26%	DMSO
CCHL 8AA	GLSPSAPA-NH_2	B	697.772	697.365	698.55	6.55	22%	DMSO
CCHL 12AA	GLSPSAPAVAVQ-NH_2	B	1095.246	1094.597	1095.70; 548.38	9.29	11%	DMSO
CCHL 15AA	GLSPSAPAVAVQASN-NH_2	B	1367.506	1366.709	1368.49; 684.60	10.54	8%	DMSO
CCHL 20AA	GLSPSAPAVAVQASNASASP-NH_2	B	1780.936	1779.900	891.54	9.3	6%	DMSO
c-SRC-biotin	GSNKSKPKDASQRRR-biotin	B	2144.136	2142.514	537.48; 716.04	8.31	17%	H_2O
YnC12-SRC-biotin	YnC12-GSNKSKPKDASQRRR-biotin	B	2348.88	2347.38	471.04, 588.30, 784.4	10.37	20%	H_2O
acetylated c-SRC-biotin	Ac-GSNKSKPKDASQRRR-biotin	B	2186.17	2184.524	1093; 730.13	11.56	7%	DMSO
BASP1-biotin	GGKLSKKKKGYNVND-Biotin	B	2064.25	2063.49	688.80; 517.55	1.22	24%	DMSO
acetylated BASP1-biotin	Ac-GGKLSKKKKGYNVND-Biotin	B	2106.39	2105.50	703.24; 527.69	6.98	17%	DMSO
Fyn-biotin	GCIKSKENKSPAIKY-biotin	B	2094.553	2093.141	1048.09; 699.40; 524.68	8.78	34%	H_2O
XRP2-Biotin	GCFFSKRRKADKESR-biotin	B	2243.667	2242.186	1122.65; 784.94; 562.18	0.8	26%	H_2O
CCHL_biotin	GLSPSAPAVAVQASN-biotin	B	1797.091	1795.953	899.35	10.59	7%	H_2O
Yn-FLAG	Yn-DYKDDDDK-COOH	B	1107.094	1106.517	554.27	8.11	51%	H_2O
Az-FLAG	Az-DYKDDDDK-COOH	B	1124.014	1123.437	562.82	8.77	31%	H_2O

8.2 Biological and biochemical methods

8.2.1 General methods

The capture reagents, AzTB and YnTB were prepared and kindly donated by Dr. Megan Wright (Imperial College London) as previously described.[333] The capture reagent AzKTB was synthesised by Dr. Goska Broncel (Imperial College London). DABCO-TAMRA and DABCO-biotin were available in the Tate group (unknown suppliers). Azidohomoalanine (AHA) was purchased from Iris Biotech and 3,3'-5,5' tetramethylbenzidine from Thermo scientific.

In-gel fluorescence was recorded using an ETTAN Dige Imager (GE Healthcare). Chemiluminescence was recorded using a LAS-3000 Imaging System (Fujifilm). Absorbance in 96-well plates was measured using a SpectraMax M2/M2e Microplate Reader from Molecular devices.

Culture media and reagents for HeLa cell culture were obtained from Sigma Aldrich, Gibco (Life technologies) and A&E Scientific (PAA).

Microtiter plates pre-coated with streptavidin and pre-blocked were purchased from Thermo Fisher (Streptavidin Coated Plates (HBC), 8-well strips, clear, cat. no. 15501). The FLAG-HRP antibody used for the ELISA assay was obtained from Sigma-Aldrich (A8592).

8.2.2 Enzymatic assay

Kinetic studies and IC_{50} values determinations were carried out using a 7-diethylamine-3-(4'maleimidylphenyl)-4-methylcoumarin (CPM) fluorescence assay, as described by Goncalves *et al*. [145]. The full length NMT1 and NMT2 enzymes were produced by Jim Brannigan, University of York, as described before [145]. The enzymes were stored in the following buffer: 125 mM NaCl, 10 mM Tris-HCl pH 8.5, 1mM EGTA, 1 mM EDTA, 25% glycerol. HsNMT1, HsNMT2, ΔHsNMT1 and ΔHsNMT2 were used at a final concentration of 300 ng/mL

For kinetic studies, the initial rates values are the mean value of 3 initial rate values determined with Wallac EnVison Manager software. The data was fitted to the enzyme kinetics function in GraFit 7.0 (Erithacus Software Ltd, UK). IC_{50} values are the mean value of two or more determinations and IC50 values were determined using GraFit 7.0 (Erithacus Software Ltd, UK) by non-linear regression fitting.

8.2.3 NMT ELISA assay

The following assay buffer was freshly prepared: 1 mM DTT, 0.1 % BSA, 0.05 % Tween, 1 x PBS, pH 7.4

The plate was washed with PBS-T (3 X 200 µL) and with assay buffer (3 X 200 µL). YnC12CoA (4 µM final), peptide (4 µM final) and recombinant enzyme (300 ng/mL) were added to the plate and incubated at RT for 1 h on a shaker. The plate was washed with PBS-T (3 X 200 µL) and PBS (3 X 200 µL). Click mixture (94 µL PBS, 1 µL 10 mM N_3FLAG, 2 µL 50 mM $CuSO_4$, 2 µL 50 mM TCEP, 1 µL 10 mM TBTA) was prepared and 100 µL added to each well. After 1 h incubation at RT, the plate was washed with PBS-T (3 X 200 µL) and PBS (3 X 200 µL). A solution of anti-FLAG (1:20 000) in PBS was added to each well (100 µL) and the plate incubated at RT for 1 h. The plate was washed with PBS-T (3 X 200 µL) and PBS (3 X 200 µL). A mixture of 3,3'-5,5' tetramethylbenzidine (TMB) and H_2O_2 (100 µl) was added to each well and the plate incubated at room temperature for 3 min. The reaction was stopped with addition of 50 µl of 1N H_2SO_4. The absorbance of each well was read at 450 nm.

8.2.4 Mammalian cancer cell culture

HeLa, MDA-MB-231 and MCF-7 cells were grown in DMEM supplemented with 10% FBS and 1% penicillin/streptomycin. HCT 116 cells were grown in McCoy's 5a Medium Modified supplemented with 0.22 g/L Glutamine and with 10% FBS and 1% penicillin/streptomycin. All cells were grown in a humidified 10 % CO_2 containing atmosphere at 37 ^{o}C. Cells were plated 24 h before treatments using the following cell concentrations (Table 16). 100 µL, 2 mL, 5 mL and 10 mL of culture media were used per well in 96-well plates, 6-well plates, 6-cm plates or 10-cm plates respectively.

Table 16. Number of cells plated 24 h before the beginning of an experiment

	HeLa					MDA-MB-231					HCT116					MCF7				
Treatment time (h)	6	24	48	72	168	6	24	48	72	168	6	24	48	72	168	6	24	48	72	168
10^3 cells / mL	100	50	25	16	16	160	80	45	30	30	160	80	45	30	30	120	60	30	15	15

8.2.4.1 YnC12 labelling and feeding cells with inhibitor in HeLa

A solution of culture media containing the inhibitor was prepared in a Falcon tube and incubated at 37^{o}C for 5 min (typically for a 10 cm plate, final concentration 1 µM of inhibitor: 1 µL of a 10 mM stock solution was added to 10 mL of culture media and the solution was mixed). The culture media was aspirated and replaced by the medium containing the inhibitor. The cells were incubated for 1 h. The media of each plate was then removed and replaced by a solution containing the inhibitor and YnC12 (typically 20 µM) in the culture media. Cells were incubated for several hours (typically 24 h)

before cell lysis. The total amount of DMSO was normalised to the maximum amount of DMSO used in each plate (typically 0.05 %).

8.2.4.2 Cell lysis

8.2.4.2.1 Using detergents

The culture media was aspirated and cells were washed with cold PBS (2 x). The plate was placed on ice and lysis buffer (PBS 1x, 0.1% SDS, 1% Triton X-100, 1 EDTA-free Complete protease inhibitor (Roche Diagnostics) was added to each plate (typically 0.3 mL for a 10 cm plate). To study c-SRC phosphorylation, the lysis buffer was supplemented with 1x phosphatase inhibitor cocktail set V (Millipore). Cells were scraped off the plates and the lysates transferred to microcentrifuge tubes and kept on ice for 20 min. The lysates were centrifuged at 17,000 ×g for 20 min to pellet insoluble material. Supernatants were collected and stored at -80 ^{o}C. Protein concentration was determined using the Bio-Rad *DC* Protein Assay. A calibration curve was prepared using BSA (bovine serum albumin) solutions in lysis buffer (0-4 mg/mL). The absorbance was measured using SpectraMax M2/M2e Microplate Reader from Molecular Devices.

8.2.4.2.2 Cell lysis for *in vitro* myristoylation studies (no detergents)

Cells were trypsinised and washed with PBS (2 x 1 mL). Cells were resuspended in lysis buffer (50 mM Hepes pH 7.2, 10 mM NaCl, 5 mM $MgCl_2$, 1 mM DTT, 1x 1 EDTA-free Complete protease inhibitor (Roche Diagnostics) and mechanically lysed by passing the lysate through a 25 G needle (~ 20 times) using a 1 ml syringe. The lysates were kept on ice for 15 min and centrifuged at 17,000 ×*g* for 20 min to pellet insoluble material. The protein concentration was determined as described above and the samples were flash-frozen using liquid nitrogen and kept at -80 ^{o}C prior to analysis.

8.2.4.2.3 Cell fractionation

Cells were trypsinised and washed with PBS (2 x 1 mL). Cells were resuspended in lysis buffer (250 mM Sucrose, 20 mM HEPES pH 7.4, 10 mM KCl, 1.5 mM $MgCl_2$, 1 mM EDTA, 1 mM EGTA, 1 x protease inhibitor cocktail) and mechanically lysed by passing the lysate through a 25 G needle 10 times using a 1 ml syringe. The lysates were kept on ice for 15 min and centrifuged at 720 ×*g* for 5 min to pellet insoluble material. The supernatant (membrane + cytosolic fractions) was removed. 200 µL of the lysis buffer were added to the pellet and the mixture was passed through a 25G needle (10 times), and centrifuged a 720 x g for 5 min. The supernatant was discarded and the pellet was resuspended in 2% SDS, 10 % glycerol. To help dissolving the pellet, the mixture was sonicated for 5 s and passed through a 25 G needle again to break any aggregates. The membrane + cytosolic fractions were centrifuged at 10,000 x*g* for 10 min. The supernatant (cytosolic fraction) was

removed and the pellet (membrane fractions) was washed with lysis buffer (1x). The membrane fraction was resuspended in 2 % SDS in PBS.

8.2.5 Gel electrophoresis

Bis-Tris gels used for sample separation by gel electrophoresis were prepared using the following recipe:

Table 17. Reagents to prepare 12 % Bis-Tris gels. Components of the recipe were mixed in the amounts given in Table 15 and cast in 1.0 mm glass plates (Bio-Rad).

Component	Volume (mL) for 25 mL resolving gel (12%)	Volume (mL) for 7.5 mL stacking gel (4%)
30 % acrylamide/bis-acrylamide	10	1
1.25 M Bis-tris (pH 6.7)	9	2.7
dH2O	5.8	3.8
10 % w/v ammonium persulphate	0.2	0.037
N,N,N′,N′-Tetramethylethylenediamine	0.01	0.006

8.2.6 CuAAC and in-gel fluorescence

Lysates were thawed on ice. 100 µg of proteins was taken and diluted to 1 mg / mL using the lysis buffer. A click mixture was prepared by adding reagents in the following order and by vortexing between the addition of each reagent: the capture reagent (1 µL, stock solution 10 mM in DMSO, final concentration 0.1 mM), $CuSO_4$ (2 µL, stock solution 50 mM in DMSO, final concentration 1 mM), TCEP (2 µL, stock solution 50 mM in DMSO, final concentration 1 mM), TBTA (1 µL, stock solution 10 mM in DMSO, final concentration 0.1 mM). 6 µL of the click mixture was added to each sample. The samples were vortexed at RT for 1 h. Next, 1 mL ice cold MeOH and EDTA (final concentration 10 mM) were added to each sample. The samples were quickly vortexed and kept at -80 ^{o}C overnight. The samples were centrifuged at 17,000 ×g for 30 min to pellet precipitated proteins. The pellets were washed with 1 mL ice-cold MeOH and dried. 75 µL 2 % SDS in PBS, 10 mM EDTA was added and the samples were vortexed. Once the proteins were completely dissolved, 25 µL of 4 x SLB (Sample loading buffer prepared by mixing 4 x sample loading buffer (NuPAGE LDS sample buffer): β-mercaptoeptanol 5:1) was added (final concentration of proteins 1 mg/mL). The samples were boiled for 5 min, centrifuged at 1,000 ×g for 2 min and loaded on a SDS-PAGE gel. Typically, 10 µg of proteins were loaded on the gel. After the run, the gel was washed with MilliQ (3x) and soaked in fixing solution (40 % MeOH, 10 % acetic acid, 50 % water) for 20 min, washed with

MilliQ (3x). The fluorescence on the gel was detected using an Ettan DIGE Imager, GE Healthcare, and the protein loading was checked by Coomassie. The quantification of fluorescent bands to calculate in-cell tagging IC_{50} was carried out using ImageJ. The signal was measured by integrating the area under each band of interest using the 'gel analyzer' function and normalised relative to no inhibition (YnMyr). The signal was normalised to the total protein loading by integrating the gel stained with Coomassie. In-cell tagging IC_{50s} (TC_{50s}) were determined using GraFit 7.0 (Erithacus Software Ltd, UK) by non-linear regression fitting.

8.2.7 Enrichment of myristoylated proteins

For enrichment of myristoylated proteins, 100 µL of lysate was captured by CuAAC as described above. After protein precipitation, the pellet was resuspended in 2 % SDS in PBS, 10 mM EDTA (20 µL). Once the pellet was completely dissolved, 80 µL of PBS was added (final concentration 1 mg/mL, 1 % SDS). 20 µL was reserved for the "before pull-down" sample. The remaining 80 µL was diluted to 0.2 % SDS and 0.5 mg/mL by the addition of 80 µL PBS. 15 µL Dynabeads® MyOne™ Streptavidin C1 were washed with 0.2 % SDS in PBS (3 × 250 µL). The sample was added to the beads and the beads were gently vortexed for 1h30. The supernatant was removed and the beads were washed with 0.2 % SDS (3 x 250 mL). 30 µL of 2 % SDS in PBS and 10 µL 4x SLB were added to the beads and the beads were boiled for 10 min. 7 µL SLB was added to the "before pull down" sample and 7 µL SLB was added to 20 µL of supernatant. Both samples were boiled for 5 min. Samples were centrifuged at 1,000 ×g for 2 min and loaded on a SDS-PAGE gel ("before pull down" sample: 10 µL (7.5 µg of proteins); supernatant: 10 µL (7.5 µg of proteins); pull down: 15 µL (30 µg of proteins).

8.2.8 Western blot analysis

Proteins were transferred to PVDF membranes (Millipore, Immobilon-P^{SQ} membrane, pore size 0.2 µM) or nitrocellulose membrane (GE Healthcare, Hybond ECL, pore size 0.45 µM) using a wet transfer set-up and a Tris-glycine transfer buffer supplemented with 0.1% SDS and 10 % MeOH. Membranes were washed with TBS-T (1 x TBS, 0.1 % Tween-20), blocked (5 % dried skimmed milk in TBS-T), washed with TBS-T (3x) then incubated with the appropriate primary antibody (Table 18) in blocking solution overnight, washed with TBS-T (4x 10 min), incubated with the appropriate secondary antibodies in blocking solution for 1 h (*Mouse*: HRP Goat anti Mouse, 1/20 000, BD Pharmingen, cat. no. 554002 or *Rabbit*: HRP Goat anti Rabbit, 1/5000, Invitrogen, cat. no. G-21234) washed with TBS-T (4x 10 min) and developed with Luminata Crescendo Western HRP substrate (Millipore) according to the manufacturer's instructions and on a Fujifilm LAS 3000 imager.

Table 18. Antibodies used in the present study

Protein	Supplier	Cat. no.	Dilution (Western blots)	Secondary antibody	/clonal	Immunogen	Apparent MW (if different from MW)
BASP1	Abcam	ab79349	1/1000	Rabbit	Poly	Synthetic peptide from the effector domain of Mouse BASP1	52 kDa
BID	Cell signaling technology	2002S	1/250	Rabbit	Poly	Residues surrounding the cleavage site of human BID	
Calnexin	Santa Cruz	sc-23954	1/200	Mouse	Mono	1-76 full length bovine ubiquitin	
Caspase3	Santa Cruz	sc-13156	1/1000	Rabbit	Poly	Amino acids 1-277 representing full length procaspase-3 of human origin	
Caspase 8	Cell signaling technology	9746S	1/500	Mouse	Mono	Carboxy-terminal sequence of the p18 fragment of human caspase-8	
Cdk2	Santa Cruz	sc-163	1/2000	Rabbit	Poly	C-terminus of Cdk2	
Cleaved caspase 3	Cell signaling technology	9664S	1/250	Rabbit	Mono	Amino-terminal residues adjacent to Asp175 of human caspase-3	
c-SRC	Cell signaling technology	2123	1/500	Rabbit	Mono	Residues 1-110 of human SRC protein	
Cytochrome C	Santa Cruz	sc-13156	1/250	Mouse	Mono	Amino acids 1-104 of cytochrome c of equine origin	
HCCS	Atlas	HPA002946	1/500	Rabbit	Poly	Amino acids 63-203 of HCCS of human origin	
Histone H3	Santa Cruz	Sc-10809	1/500	Rabbit	Poly	Amino acids 1-136 of Histone H3 of human origin	
HsNMT1	Sigma aldrich	HPA022963	1/500	Rabbit	Poly	Amino acids 66-135	
HsNMT2	BD Biosciences	611310	1/125	Mouse	Mono	Human NMT-2 amino acids. 10-119	
PARP	Santa Cruz	sc8007	1/250	Mouse	Mono	Amino acids 764-1014	
PKA C-α	Cell signaling technology	5842S	1/500	Rabbit	Mono	Residues surrounding Ser326 of human PKA C-α protein.	
PSMC1	Atlas	HPA000872	1/500	Rabbit	Poly	Amino acids 295-436of PSMC1 of human origin	
Phospho-Src (Tyr416)	Cell signaling technology	2101S	1/500	Rabbit	Poly	Synthetic phosphopeptide corresponding to residues surrounding Tyr416 of human SRC	
MARCKS	Cell signaling technology	D88D11	1/500	Rabbit	Mono	Residues surrounding Ala245 of human MARCKS protein.	70-90kDa
α-Tubulin	Santa Cruz	sc-53646	1/2000	Mouse	Mono	Full-length α Tubulin (human)	
Ubiquitin	Cell signaling technology	3936S	1/500	Mouse	Mono	1-76 full length bovine ubiquitin	

8.2.9 Immunoprecipitation and capture of myristoylated proteins

200 µg of protein was incubated with 10 µL primary antibody on a rotation wheel overnight at 4°C. 15 µL of Sepharose A beads (GE Healthcare, Fast Flow) pre-washed with 3 x PBS, were added and the samples were incubated at 4°C for a further 2 h on a rotation wheel. The supernatant was discarded and the beads washed with ice-cold lysis buffer (2x) and 0.1% SDS in PBS (2x), and then resuspended in 47 µL PBS for on-bead click labelling. Click reagents were premixed (TAMRA-capture reagent (0.5 µL of 10 mM stock), $CuSO_4$ (1 µL of 50 mM stock), TCEP (1 µL of 50 mM stock) and TBTA (0.5 µL of 10 mM stock)) and added to each samples. The samples were incubated on ice for 1.5 h and gently vortexed occasionally. The supernatant was removed and the beads were washed with 0.1 % SDS in PBS (3 x). Beads were boiled in 1 x SLB (5 µL SLB + 15 µL 2 % SDS), except where indicated otherwise.

8.2.10 Metabolic activity assay (MTS assay)

HeLa cells were seeded in a 96-well plate 24 h before treatments. Cell suspensions were prepared by multiplying the cell concentrations reported in Table 16 by 2. 50 µL of cell suspension were transferred to wells B-G in columns 2-11 of a 96-well plate. 100 µL of growth media were added to the outer wells. 24 h after seeding, 50 µL of growth media containing DMSO (maximum amount of DMSO used for the inhibitor dilutions, typically 0.04%) were added to wells B-G in columns 2 and 11 as a positive control. A solution of Puromycin (4 µg/mL, 50 µL, final concentration in the plate 2 µg/mL) was used as a negative control and added to wells B-G in column 3. 7 concentrations of inhibitor were prepared (same final percentage of DMSO, dilution factor = 3, typically triple dilutions starting from 20 µM (final concentration in the plate starting from 10 µM) and 50 µL were added to the wells B-G in columns 4-10 (total volume of the wells = 100 µL).

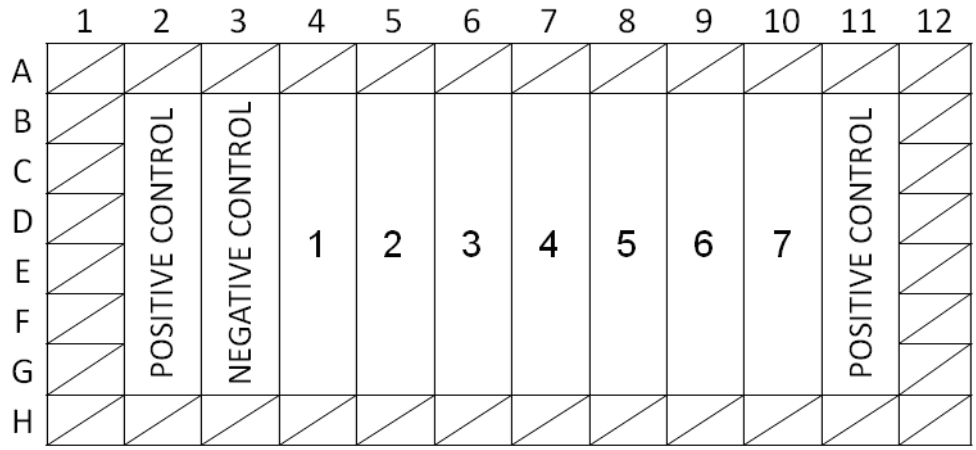

24h, 48 h, 72 h or 164 h later the MTS reagent (Promega) was prepared according to the supplier's protocol and 20 µL of this reagent were added to each well of the 96-well plate. Absorbance was measured at 490 nm after 2 h. The average of absorbance values of the negative control (cells treated with Puromycin) was subtracted from each value. The metabolic activity was calculated as a percentage relative to the positive control. EC_{50s} were calculated by fitting the data to the IC_{50} function using GraFit 7.0 (Erithacus Software Ltd, UK).

8.2.11 Cell cycle analysis

For this experiment, 6 cm plates were typically used and cells were plated as described in Section 8.2.4. After treatment with the inhibitor or DMSO, both adherent and floating cells were harvested and washed with PBS (2 x 1 mL). Cell pellets were resuspended in 70 % EtOH and fixed overnight at 4 ^{o}C or for several days at -20 ^{o}C. Fixed cells were washed with PBS (2 x 1 mL). Cell pellets were resuspended in 300 µL propidium iodide (PI) solution (50 µg/mL) and transferred to a 5 mL tube for flow cytometry analysis. 10 µL of RNAse was added to each tube. Samples were incubated at RT in the dark prior to analysis. Samples were diluted with PBS prior to analysis if necessary. Samples were processed using a BD LSRFortessa cell analyzer (BD Biosciences, UK). The distribution of cells in each phase of the cell cycle was calculated using FlowJo 7.6.5 software.

8.2.12 Annexin V / PI analysis

Dead and apoptotic cells were detected using FITC Annexin V Apoptosis Detection Kit I (BD Pharmingen™) as described by the supplier with some modifications.

For this experiment, 6 cm plates were typically used and cells were plated as described Section 8.2.4. After treatment with the inhibitor or DMSO, both adherent and floating cells were harvested and washed with PBS (2 x 1 mL). Cell pellets were resuspended in 200 µl of 1X Binding Buffer (1 x 10^6 cells / mL). 100 µl of the solution were transferred to a 5 ml tube. 5 µl of FITC Annexin V and 5 µl PI were added. The samples were vortexed and incubated for 15 min at RT in the dark. 400 µl of 1X Binding Buffer were added to each tube prior to analysis by flow cytometry. Samples were analysed within 1 h following PI and Annexin V addition. Samples were processed using a BD LSR Fortessa cell analyzer (BD Biosciences, UK). Samples were compensated automatically using: untreated cells (unstained), apoptotic cells (1 uM STS treatment for 6 h, stained with Annexin V), dead cells (2 µg/mL Puromycin for 24 h, stained with PI). The distribution of apoptotic, dead, alive cells was calculated using FlowJo 7.6.5 software.

8.2.13 SiRNA transfection

The following SiRNA sequences were used: [28]

siRNA NMT1: 5’ aatgaggaggacaacagctac 3’ mRNA

siRNA NMT2: 5’ aaaaggttggactagtactac 3’

100 000 HeLa cells/well were seeded in a 6-well plate and the growth medium (no PS) was replaced after 24 h. 5 µL of Lipofectamine 2000 (Invitrogen) was incubated at RT in DMEM without FBS and without PS (250 µL) for 5 min. 2 µL of SiRNA (50 mM) were mixed with 250 µL of DMEM media (no FBS, no PS). SiRNA mixture and Lipofectamine solution were combined and incubated at RT for 25 min before addition to the corresponding well. The plates were gently mixed and incubated at 37°C for 6 h. The media was replaced (DMEM + 10 % FBS) and the cells incubated at 37°C for 48 h or 72 h. YnC12 (1.2 µL 50mM stock in DMSO, final conc. 20 µM) was added 6 h before cell lysis.

8.2.14 Assays on cellulose membrane

8.2.14.1 Preparation of the buffers

The following buffers were prepared for the assays:

Buffer A: 30 mM Tris, 3.5 mM DTT, pH 7.4

Buffer B: 30 mM Tris, pH 7.4

8.2.14.2 Myristoylation and click chemistry

The membrane was placed in a 15 mL Falcon tube and soaked with buffer A. A mixture of MyrCoA analogue (YnC12CoA or AzC12CoA) and NMT in buffer A (3 mL) was incubated at 37°C for 5 min in another Falcon tube (Table 19). The membrane was added to this solution and the resulting mixture was incubated at 37°C for 2 h with constant shaking. The membrane was washed with buffer B (4 x 2 min). 3 mL of buffer B and the following click chemistry reagents were added to the membrane (Table 20)

Table 19.In vitro myristoylation on cellulose membranes

Compounds	Final concentration	Quantity	Stock concentration	Volume in µL
Hs NMT	500 µg/mL	1.5 µg	9.8 mg /mL	0.15
N_3-Myr-CoA	1 µM	3 nmol	10 mM	3

Table 20. Capture reaction on cellulose membranes

Compounds	Final concentration	Quantity	Stock concentration	Volume in µL
Capture reagent	10 µM	30 nmol	10 mM	3
$CuSO_4$	40 µM	120 nmol	40 mM	3
TCEP	40 µM	120 nmol	50 mM	2.4
TBTA	4 µM	12 nmol	10 mM	1.2

The membrane was stirred at room temperature for 1 h and washed with buffer B (3 x 2 min). The membrane was directly imaged using an ETTAN Dige Imager (Fluorescein: Cy2 excitation/emission: 492/520 nm; TAMRA: Cy3 excitation/emission: 550/570 nm) or probed in chemiluminescence.

8.2.14.3 Chemiluminescence assay

The membrane was washed with TBS-T (3x), blocked for 1 h (5% BSA in TBS-T) and washed with TBS-T (3x). A solution of Neutravidin HRP (Invitrogen, cat. no. A2664) (2.5 µL) in blocking solution (5 mL) was prepared and added to the membrane. The membrane was stirred for 1h at room temperature and the membranes was washed with TBS-T (3 x) and developed with Luminata Crescendo Western HRP substrate (Millipore) according to the manufacturer's instructions and imaged on a Fujifilm LAS 3000 imager. After imaging, the membrane was directly washed with TBS-T (2x) and kept in the fridge before stripping.

8.2.14.4 Membrane stripping

The membrane was washed with TBS-T (1x) and H_2O (1x). 5 mL of a 1st stripping solution (62.5 mM Tris, pH 6.8, 100 mM β-mercaptoeptanol, 2% SDS) was prepared and added to the membrane. The membrane was incubated at 50°C for 30 min. The membrane was then washed with H_2O (3x), TBS-T (3x) and H_2O (2x). 5 mL of a 2nd stripping solution (50% EtOH, 10% acetic acid glacial, 40% H_2O) was prepared and added to the membrane. The membrane was incubated at RT for 30 min with constant agitation. The membrane was then washed with H_2O:EtOH 1:1 (1x) and TBS-T (4x). The membrane was then probed again directly or kept at -20°C.

8.2.15 Protein expression in *E. coli*

All manipulations of *E. coli* were carried out in an aseptic environment (flame-sterilized area) and kanamycin stock solution was filtered-sterilised. E. coli lysate co-expressing CaNMT and PfARF, and co-fed with or without AzC12 were kindly donated by Dr. William Heal (Imperial College London).

Plasmids cloning the sequences used were the following: CaNMT1 into pET11c vector (Nde1/BamH1 restriction site, ampicillin resistance) and *P. falciparum* ADP ribosylation factor 1 (PfARF1) into pET28a (Nco1/Xho1 restriction site, kanamycin resistance).

8.2.15.1 Competent *E. Coli* transformation

Lauria-Bertani (LB) broth media (10 g/L NaCl, 10 g/L tryptone, 5 g/L yeast extract, pH 7) and LB agar (10 g/L NaCl, 10 g/L tryptone, 5 g/L yeast extract, 20 g/L agar, pH 7) were prepared and autoclaved.

An aliquot of chemically competent *E. Coli* (BL21(DE3) strain) were thawed on ice (chemically competent *E. Coli* were kindly donated by Chris Douse) 1µL of DNA (100ng) was added to 100 µL of

competent *E. Coli*. The mixture was mixed gently and left on ice. The cells were heat shocked by placing them in a water bath at 42°C for 1 min and then returned to ice for 2 min. 400 µL of warm LB media was added and the cells were incubated at 37°C for 1h with constant stirring. 100 µL of the cell suspension was plated onto LB agar plates containing the relevant antibiotics (50 µg/mL of Kanamycin), and the plates incubated at 37 °C for 18 h.

8.2.15.2 PfARF1 expression

In a 50 mL Falcon tube, 10 mL LB media containing 50 µg/mL kanamycin was inoculated with a single colony of BL21(DE3) cells containing the pET28a plasmid (including a His6-tag on the PfARF C-terminus) to form a starter culture. The mixture was incubated at 37 °C with constant oscillation overnight. 200 µL of the starter culture was added into 10 mL fresh LB media containing 50 µg/mL kanamycin, and the mixture was incubated at 37 °C with constant oscillation until optical density (OD600) measurements reached 0.5–0.6 AU (Absorbance unit). IPTG (10 µL of 1M stock solution, 1 mM final concentration) was added and the tube was incubated at 37 °C for a further 4 h with constant oscillation. The culture was centrifuged (4000 rpm, 4 °C, 15 min), the supernatant removed, the cell pellet was washed with 2 x 1 mL PBS and frozen at −80 °C.

The cell pellet was thawed on ice and 300 µL lysis buffer was added. The lysis buffer was prepared by mixing 9 mL of 50 mM Tris.HCl pH 8, 150 mM NaCl with 1 L of Bugbuster (Roche), and 1x Complete EDTA-free protease inhibitor tablet (Roche). The cells were resuspended in the lysis buffer by pipetting up and down (10 times) and transferred to an microcentrifuge tube. The cells were kept on ice for a further 20 min and centrifuged at 17,000 ×g for 30 min to pellet insoluble material. The supernatant (soluble fraction) was transferred to another microcentrifuge tube and the pellet (insoluble fraction) was retained. The protein concentration was determined using the Bio-Rad *DC* Protein Assay and the samples were kept at -80^{o}C prior to analysis or purification.

8.2.15.3 PfARF1 purification

PfARF1 was expressed as described above, but with the following modifications: 1 L instead of 10 mL of culture was grown and the reagents were adjusted as required; the cells pellet was not frozen overnight before lysis but was lysed directly after the 4 h of cell growth.

The following buffers were prepared:

- ✓ Buffer C: 20mM Tris pH8 , 0.5M NaCl
- ✓ Buffer D: 20mM Tris pH8 , 0.5M NaCl, 5mM imidazole, 6M urea
- ✓ Buffer E: 20mM Tris pH8 , 0.5M NaCl, 40mM imidazole

The pellet was resuspended in 10 mL Buffer C. The pellet was kept on ice and sonicated 2 x 1 min (power 20). The sample was spun down at 3,000 x g for 10 min at 4 ^{o}C to give the soluble fraction (supernatant) and the insoluble fraction (pellet).

The pellet was washed with 10 m buffer C and the supernatant was discarded. The pellet was resuspended in 10 ml buffer D by leaving the sample on a rotation wheel overnight at 4 ^{o}C. The sample was then spun down at 3,000 x g for 10 min and 4 ^{o}C. The supernatant was retained for in-gel analysis of the insoluble fraction.

Chelating Sepharose Fast Flow (500 µL, GE Healthcare) beads were pre-equilibrated as follows. They were washed with MilliQ (2 x 2 mL), gently vortexed for 5 min at RT with a solution of 10mM $NiSO_4$ in MilliQ, spun down, washed with MilliQ (4 x 1ml) and buffer C (3 x 1 ml). The soluble fraction was added to the beads. The mixture was incubated for 45 min on a rotation wheel at 4 ^{o}C. The supernatant was discarded and the beads were washed with buffer C (3 x 15 mL). The beads were incubated with 500ul of buffer E for 5 min on a rotation wheel at RT. The sample was spun down and the supernatant was reserved (elution 1). The elution was repeated 2 times. The three elution samples were centrifuged at 17,000 x g for 10 min. A SDS-PAGE gel was run to confirm protein purity, and the elution fractions were then dialysed overnight into storage buffer (50 mM Hepes, 10 mM NaCl, 5 mM $MgCl_2$) using a Slide-A-Lyzer 3500 MW dialysis cassette in 2 L buffer at 4 °C. Dialysis was performed twice more using the same conditions for 1 h each time. The protein concentration was determined using the Bio-Rad *DC* Protein Assay and the protein was flash frozen in liquid nitrogen.

8.2.16 *In vitro*-myristoylation

Mammalian cells were grown as described in Section 8.2.4, treated with inhibitor IMP366 for 24 h and lysed as described in Section 8.2.4.2.2. *E. coli* lysates were prepared as described in Section 8.2.15.

In vitro myristoylation was carried out by incubating 50 µg of lysate (1 mg/mL final concentration) with AzC12CoA or YnC12CoA (10 µM final concentration) and the appropriate enzyme (HsNMT1, HsNMT2 or CaNMT, final concentration 5 µg/mL) for 2h at 37 ^{o}C with constant stirring. The capture reaction and in-gel fluorescence analysis were carried out as described in Section 8.2.6.

8.3 Chemical Proteomics

8.3.1 General methods

For quantitative proteomics (SILAC), R10K8 and R0K0 DMEM media was purchased from Dundee cell products. Cell dissociation buffer (enzyme free, PBS-based) obtained from Gibco (Life Technologies) was used instead of trypsin to detach the cells before splitting them. Dialysed FBS was obtained from Sigma-Aldrich. All buffers were filtered using a 0.2 μM filter to prevent any contamination. Low binding tubes (Protein LoBind tubes, Eppendorf) were used to carry out the enrichment of NMT substrate for MS-based proteomics and to freeze-dry the digested peptides.

8.3.2 Lysate preparation

Lysates for non quantitative proteomics experiments or label-free quantification were prepared as described in Section 8.2.4.

8.3.2.1 Spike-in SILAC

To prepare the Spike-in SILAC standard,[195] cells were grown in a "heavy" growth medium. The heavy growth medium was composed of SILAC DMEM (containing ^{13}C and ^{15}N labelled arginine, and ^{13}C and ^{15}N labelled lysine (R10K8)) supplemented with 10% dialysed FBS and 1% penicillin/streptomycin. Cells were grown for >10 passages in this growth medium before starting the experiment. The incorporation of the heavy label was determined by analysing 20 μg of cell lysate (from cells grown in the heavy media) by proteomics and found to be 97.7%.

8.3.3 Base treatment of the lysate before CuAAC

Lysates from cells treated for 24 h with YnC12 (20 μM) were used. 500 μg of lysate (200 μL, 2.5 mg/mL) were base-treated with NaOH (50 μL 1 N NaOH; 0.2 M NaOH final; concentration of protein 2 mg/mL) for 2 h. The samples were then neutralised by the addition of HCl 1N. In the control sample, a neutralised mixture of NaOH and HCl was added (100 μL) to 500 μg of lysates. To both samples was added the spike-in standard (1:1 ratio sample:spike-in standard) and the samples diluted to 2 mg/mL with PBS (total amount of proteins: 1mg; volume: 500 μL).

8.3.4 Capture and enrichment for MS-based proteomics

8.3.4.1 Using AZTB

Samples were subjected to CuAAC and affinity enrichment as before with the following modifications: CuAAC reaction was carried out with 2 mg/L of proteins. For Spike-in SILAC proteomics, the spike-in standard was mixed in a 2:1 sample:spike-in standard ratio before the

CuAAC reaction. For SILAC experiments, the samples were mixed in a 1:1 ratio heavy: light before the CuAAC reaction.

For affinity enrichment, Dynabeads were replaced by NeutrAvidin agarose resin (Thermo Scientific). Typically 200 µL of bead slurry were used for 4 mg of lysate. The enrichment was carried out for 2 h and the protein concentration was 1 mg/mL (0.2 % SDS). The supernatant was removed and the beads were washed with 3x 1% SDS in PBS, 3x 4M urea in 50 mM ammonium bicarbonate (AMBIC), 5x 50mM AMBIC. For each wash, 1 mL of washing solution was added to the beads, the beads were gently vortexed for 5 min, spun at 3,000 ×g for 3 min and the supernatant was carefully removed and discarded. Beads were stored in 50 mM AMBIC at 4°C. The efficiency of the enrichment was checked by in-gel fluorescence by loading the samples before enrichment and the supernatant from the pull down.

8.3.4.2 Identification of the modified peptide with AzKTB.

Proteins were captured by CuAAC as before with the following modifications: CuAAC reaction was carried out for 2 hours and with AzKTB in place of AzTB. Proteins were precipitated following CuAAC via a modified chloroform/methanol precipitation procedure: 4 volumes of MeOH, 1 vol. $CHCl_3$, 3 vol. H_2O were added to the sample, which was centrifuged at 17,000 ×g for 5 min to pellet proteins at the interface. Both layers were then removed simultaneously, the pellet resuspended in 0.2 % SDS/PBS to the original volume and the precipitation procedure repeated. The pellet was then washed twice with MeOH. Resuspension, affinity enrichment and preparation for LC-MS/MS were performed as before with the following modifications: beads were washed with 10 % ACN in TEAB following digest and this wash was combined with the supernatant from on-bead digest to improve recovery of modified peptides. The solutions were freeze dried overnight to give a white solid. The samples were kept at 4°C prior to analysis.

8.3.5 On-bead reduction, alkylation and digest.

All reagents and buffers were freshly prepared. Beads were spun at 3000 x g for 5 min and the excess liquid discarded. For a volume of beads of ~ 150 µL: samples were reduced (7.5 µL of 100 mM dithiothreitol in 50 mM AMBIC) at 60 °C for 30 minutes and allowed to cool to room temperature. The beads were washed with 2 x 50 mM AMBIC. Cysteines were alkylated (7.5 µL of 100 mM iodoacetamide in 50 mM AMBIC) at room temperature for 30 min in the dark. The beads were washed with 2 x 50 mM AMBIC. 15 µL of acetonitrile were added (~10% of total volume). Trypsin (6 µg Sequencing Grade Modified Trypsin (Promega) dissolved in 50 mM AMBIC) was added to the beads and samples were placed on a shaker and digested overnight at 37 °C. The samples were centrifuged and the supernatant was transferred into clean tubes. The beads were washed with

2 % FA, 10 % acetonitrile in water and these washes were combined with the supernatant removed after the addition of formic acid. The solutions were freeze dried overnight to give a white solid.

The samples were kept at 4 °C prior to analysis. The solid was resuspended in 200 µL 2% acetonitrile, 0.1 % FA in water; 50 µL / mg of lysate), vortexed for 5 min, sonicated for 25 min, vortexed again for 5 min and spun down at 17000 x g for 10 min at 7 °C. The samples were transferred few hours before analysis to LC-MS vials.

8.3.6 Gel-based proteomics: sample preparation, in-gel reduction, alkylation and digest

For gel-based proteomics, 10 µL of 4x SLB (Sample loading buffer prepared by mixing 4x sample loading buffer (NuPAGE LDS sample buffer): β-mercaptoeptanol, 5:1) and 30 µL of 2 % SDS in PBS were added to the beads (~150 µL beads for 3 mg of lysate). The beads were boiled for 10 min, spun at 3,000 ×*g* for 5 min and the supernatant was loaded on a gel (NuPAGENovex 10 % Bis-Tris Gel, 1.5 mm thick). Proteins were stained with Instant Blue (Expedeon) for 30 min, and the gel was cut in 7 portions. The gel pieces were kept frozen in 50 mM TEAB before digest.

In-gel reduction, alkylation and digestion were performed by the University of Leicester Proteomics Facility, the raw data files were obtained for each LC-MS/MS acquisition.

For in-gel reduction, alkylation and digest, the following protocol was used: each slice was destained using 200 mM TEAB/20 % acetonitrile, followed by reduction (10 mM dithiothreitol) at 60 °C for 30 minutes, alkylation (100 mM iodoacetamide) at room temperature for 30 minutes in the dark and enzymatic digestion (0.1 µg sequencing grade modified porcine trypsin) overnight at 37 °C. The liquid was evaporated to dryness and resuspended using 20 µL of a 10 fmol/µL yeast alcohol dehydrogenase tryptic digest standard (Waters, UK).

8.3.7 LC-MS/MS runs.

8.3.7.1 Proteomics facility, University of Leicester

LC-MS/MS was carried out using an RSLCnano HPLC system (Dionex, UK) and an LTQ-Orbitrap-Velos mass spectrometer (Thermo Scientific). Samples were loaded at high flow rate onto a reverse-phase trap column (0.3 mm i.d. x 1 mm), containing 5 µm C18 300 Å Acclaim PepMap media (Dionex) maintained at a temperature of 37 °C. The loading buffer was 0.1 % formic acid / 0.05 % trifluoroacetic acid in water. Peptides were eluted from the trap column at a flow rate of 0.3 µl/min and through a reverse-phase capillary column (75 µm i.d. x 250 mm) containing Symmetry C18 100 Å media (Waters, UK) that was manufactured in-house using a high pressure packing device (Proxeon Biosystems, Denmark). The output from the column was sprayed directly into the nanospray ion source of an LTQ-Orbitrap-Velos mass spectrometer set to acquire a single microscan FTMS scan

event at 60000 resolution over the m/z range 350-1250 Da in positive ion mode. Accurate calibration of the FTMS scan was achieved using a background ion lock mass for polydimethylcyclosiloxane (445.120025 Da). Subsequently up to 10 data dependent HCD MS/MS were triggered from the FTMS scan and performed in the LTQ-Velos ion-trap. The isolation width was 2.0 Da, normalized collision energy 45.0, Activation time 0.1 ms. Dynamic exclusion was enabled.

8.3.7.2 Proteomics facility, Imperial College London

The analysis was performed using reverse phase Acclaim PepMap RSLC column 50 cm × 75 µm inner diameter (Thermo Fisher Scientific) using a 2 h acetonitrile gradient in 0.1 % formic acid at a flow rate of 250 nL/min. Easy nLC-1000 was coupled to a Q Exactive mass spectrometer via an easy-spray source (all Thermo Fisher Scientific). The Q Exactive was operated in data-dependent mode with survey scans acquired at a resolution of 75 000 at m/z 200 (transient time 256 ms). Up to the top 10 most abundant isotope patterns with charge +2 from the survey scan were selected with an isolation window of 3.0 m/z and fragmented by HCD with normalized collision energies of 25 W. The maximum ion injection times for the survey scan and the MS/MS scans (acquired with a resolution of 17 500 at m/z 200) were 250 and 80 ms, respectively. The ion target value for MS was set to 10^6 and for MS/MS to 10^5.

8.3.8 LC-MS/MS data analysis.

8.3.8.1 Non quantitative proteomics (gel-based analysis)

The .raw data file obtained from each LC-MS/MS acquisition was processed using the Raw2MSM application.[365] The resulting .msm files were searched using Mascot (version 2.2.04, Matrix Science Ltd.)[181] against a database containing the UniProtKB/Swissprot[10] accessions for *Homo sapiens*. The peptide tolerance was set to 5 ppm and the MS/MS tolerance was set to 0.02 Da. Fixed modifications were set as carbamidomethyl cysteine with variable modifications as oxidised methionine. The enzyme was set to Trypsin/P and up to 3 missed cleavages were allowed. A decoy database search was performed.

Data were further processed using Scaffold (version 3.6.02, Proteome Software).[184] The Mascot .data files were imported and searched using X!Tandem (version 2006.9.15.4, The Global Proteome Machine Organization).[183] PeptideProphet[366] and ProteinProphet[367] (Institute for Systems Biology) probability thresholds of 95 % were calculated from each of the Mascot and X!Tandem decoy searches and Scaffold was used to calculated an improved 95 % peptide and protein probability threshold based on the data from the two different search algorithms, resulting in a peptide false discovery rate of 0.0 %. Protein identifications were required to contain at least 2 peptides exceeding 95 % probability giving a calculated protein false discovery rate of 0.05 %.

8.3.8.2 Other proteomics data processing

The data were processed with MaxQuant version 1.3.0.5, and the peptides were identified from the MS/MS spectra searched against the database using the Andromeda search engine. Cysteine carbamidomethylation was used as a fixed modification and methionine oxidation and protein N-terminal acetylation as variable modifications. For the identification, the false discovery rate was set to 0.01 for peptides, proteins and sites, the minimum peptide length allowed was five amino acids, and the minimum number of unique peptides allowed was set to one. Other parameters were used as pre-set in the software. "Unique and razor peptides" mode was selected; this calculates ratios from unique and razor peptides (Razor peptides are non-unique peptides assigned to the protein group with the most other peptides). Data were elaborated using Microsoft Office Excel 2007, Perseus version 1.3.0.4, Origin 8.5 and GraFit 7.0.

When the capture reagent AzKTB was used, N-terminal addition of 520.3373 (corresponding to the triazole adduct) was added as variable modification for the search.

8.3.8.2.1 Label-free quantification

Label free quantification experiments in MaxQuant was performed using the built in label free quantification algorithm,[193,368] enabling the 'Match between runs' option (time window 2 minutes) and were analyzed with Perseus version 1.3.0.4. The experiment comprised 4 biological replicates treated with Myr and 4 biological replicates treated with YnC12. The label-free approach chosen was based on intensities of proteins calculated by MaxQuant from peak intensities and based on the ion currents carried by several peptides whose sequences match a specific protein to provide an approximation of abundance). [369.] The replicates were grouped together.

YnC12 protein group was filtered to require three valid values (three values out the four replicates) and in addition at least 2 peptides (unique and razor) were required. Label free intensities were logarithmised (base 2) and empty values were imputed with random numbers from a normal distribution, whose mean and standard deviation were chosen to best simulate low abundance values close to noise level (imputation criteria: width 0.1 and down shift 1.8). A modified t-test with permutation based FDR statistics (Hubner et al., 2010; Tusher et al., 2001) was applied. We performed 250 permutations and required an FDR of 0.001. The parameter s0 was set to 1 to separate outliers from the background distribution. The data was further filtered by keeping only the proteins with an LFQ enrichment higher than 4. The LFQ enrichment was determine by first calculating the mean value of the LFQ intensities (non logarithmic values) of the Myr replicates and the mean value of the LFQ intensities (non logarithmic values) of the YnC12 replicates. The mean of YnC12 intensities was then divided by the mean of Myr intensities.

8.3.8.2.2 Spike-in SILAC.

Ratios light/heavy (L/H, corresponding to amount of protein in the lysate with increasing amount of inhibitor/spike-in standard) found for each protein, each condition (concentration of inhibitor) and each replicate (four biological replicates 1 technical replicate in total) were determined by MaxQuant as explained above. The data was filtered to require three valid values per protein. For each replicate, the values were normalized to the sample with 0 µM of inhibitor, in order to normalize to the spike-in standard. The amount of protein in the 0 µM of inhibitor samples was then defined as 1. To compare the six conditions (six concentrations of inhibitor), an analysis of variance (ANOVA) was performed with Benjamini Hochberg correction at an FDR of 5 %. In addition, a hierarchical clustering was performed in Perseus. Proteins sensitive to NMT inhibition were clustered together while the insensitive proteins were in different clusters. The data was then manually inspected. In cell IC_{50} values were determined using the mean values of the ratios between the five replicates and determined using GraFit 7.0 (Erithacus Software Ltd, UK) by non-linear regression fitting (IC_{50} back corrected function).

8.3.9 Bioinformatics

Myristoylation predictions were carried out using two online predictors (Myr predictor [80] and Myristoylator [81]. The Myr predictor shows three levels of confidence: R = reliable; T = twilight, N = not myristoylated and the Myristoylator has four levels of confidence: H = high probability, M = medium probability, L = low probability, N = not myristoylated. Four levels of Myristoylation confidence were defined by combining the results of the 2 predictors: N = not myristoylated, P = probable, L= low, M = medium, H =high. For example, if one protein had the probability R (Myr predictor) and H (Myristoylator), we reported this protein with a high probability to be myristoylated (H). If one protein had the probability R (Myr predictor) and M (Myristoylator), we reported this protein with a medium probability to be myristoylated (M).

In the present study, proteins were described as palmitoylated when they were identified as palmitoylated in at least one proteomics experiments as reported by Wilson *et al.* [173](+: found in 1 study, ++: found in 2 studies; +++: found in 3 studies; ++++: found in 4 studies) [173]; or reported as palmitoylated in the UniProtKB/Swiss-Prot database (indicated as u in the dataset). GPI-anchored proteins are reported as found in the UniProtKB/Swiss-Prot database.

Chapter 9 References

(1) Hoelder, S.; Clarke, P. A.; Workman, P. *Mol. Oncol.* **2012**, *6*, 155.

(2) Felsted, R. L.; Glover, C. J.; Hartman, K. *J. Natl. Cancer Inst.* **1995**, *87*, 1571.

(3) Resh, M. D. *Subcell. Biochem.* **2004**, *37*, 217.

(4) Gordon, J. I.; Duronio, R. J.; Rudnick, D. A.; Adams, S. P.; Gokel, G. W. *J. Biol. Chem.* **1991**, *266*, 8647.

(5) Boutin, J. A. *Cell Signal.* **1997**, *9*, 15.

(6) Deichaite, I.; Casson, L. P.; Ling, H. P.; Resh, M. D. *Mol. Cell. Biol.* **1988**, *8*, 4295.

(7) Wilcox, C.; Hu, J. S.; Olson, E. N. *Science* **1987**, *238*, 1275.

(8) Zha, J.; Weiler, S.; Oh, K. J.; Wei, M. C.; Korsmeyer, S. J. *Science* **2000**, *290*, 1761.

(9) Dyda, F.; Klein, D. C.; Hickman, A. B. *Annu. Rev. Biophys. Biomol. Struct.* **2000**, *29*, 81.

(10) Boisson, B.; Giglione, C.; Meinnel, T. *J. Biol. Chem.* **2003**, *278*, 43418.

(11) Lodge, J. K.; Johnson, R. L.; Weinberg, R. A.; Gordon, J. I. *J. Biol. Chem.* **1994**, *269*, 2996.

(12) Wiegand, R. C.; Carr, C.; Minnerly, J. C.; Pauley, A. M.; Carron, C. P.; Langner, C. A.; Duronio, R. J.; Gordon, J. I. *J. Biol. Chem.* **1992**, *267*, 8591.

(13) Towler, D. A.; Adams, S. P.; Eubanks, S. R.; Towery, D. S.; Jackson-Machelski, E.; Glaser, L.; Gordon, J. I. *Proc. Natl. Acad. Sci. USA* **1987**, *84*, 2708.

(14) Shaw, B. D.; Momany, C.; Momany, M. *Eukaryot. Cell* **2002**, *1*, 241.

(15) Dumonceaux, T.; Rajala, R. V.; Sharma, R.; Selvaraj, G.; Datla, R. *Genome* **2004**, *47*, 1036.

(16) Panethymitaki, C.; Bowyer, P. W.; Price, H. P.; Leatherbarrow, R. J.; Brown, K. A.; Smith, D. F. *Biochem. J.* **2006**, *396*, 277.

(17) Gunaratne, R. S.; Sajid, M.; Ling, I. T.; Tripathi, R.; Pachebat, J. A.; Holder, A. A. *Biochem. J.* **2000**, *348*, 459.

(18) Ntwasa, M.; Aapies, S.; Schiffmann, D. A.; Gay, N. J. *Exp. Cell Res.* **2001**, *262*, 134.

(19) Rioux, V.; Beauchamp, E.; Pedrono, F.; Daval, S.; Molle, D.; Catheline, D.; Legrand, P. *Mol. Cell. Biochem.* **2006**, *286*, 161.

(20) Raju, R. V.; Kalra, J.; Sharma, R. K. *J. Biol. Chem.* **1994**, *269*, 12080.

(21) Glover, C. J.; Hartman, K. D.; Felsted, R. L. *J. Biol. Chem.* **1997**, *272*, 28680.

(22) Farazi, T. A.; Waksman, G.; Gordon, J. I. *J. Biol. Chem.* **2001**, *276*, 39501.

(23) Rajala, R. V.; Datla, R. S.; Moyana, T. N.; Kakkar, R.; Carlsen, S. A.; Sharma, R. K. *Mol. Cell Biochem.* **2000**, *204*, 135.

(24) Duronio, R. J.; Towler, D. A.; Heuckeroth, R. O.; Gordon, J. I. *Science* **1989**, *243*, 796.

(25) Weinberg, R. A.; McWherter, C. A.; Freeman, S. K.; Wood, D. C.; Gordon, J. I.; Lee, S. C. *Mol. Microbiol.* **1995**, *16*, 241.

(26) Lodge, J. K.; Jackson-Machelski, E.; Toffaletti, D. L.; Perfect, J. R.; Gordon, J. I. *Proc. Natl. Acad. Sci. USA* **1994**, *91*, 12008.

(27) Yang, S. H.; Shrivastav, A.; Kosinski, C.; Sharma, R. K.; Chen, M. H.; Berthiaume, L. G.; Peters, L. L.; Chuang, P. T.; Young, S. G.; Bergo, M. O. *J. Biol. Chem.* **2005**, *280*, 18990.

(28) Ducker, C. E.; Upson, J. J.; French, K. J.; Smith, C. D. *Mol. Cancer Res.* **2005**, *3*, 463.

(29) Giang, D. K.; Cravatt, B. F. *J. Biol. Chem.* **1998**, *273*, 6595.

(30) Lu, Y.; Selvakumar, P.; Ali, K.; Shrivastav, A.; Bajaj, G.; Resch, L.; Griebel, R.; Fourney, D.; Meguro, K.; Sharma, R. K. *Neurochem. Res.* **2005**, *30*, 9.

(31) Selvakumar, P.; Lakshmikuttyamma, A.; Charavaryamath, C.; Singh, B.; Tuchek, J.; Sharma, R. K. *Biochem. Biophys. Res. Commun.* **2005**, *335*, 1132.

(32) Selvakumar, P.; Smith-Windsor, E.; Bonham, K.; Sharma, R. K. *FEBS Lett.* **2006**, *580*, 2021.

(33) Selvakumar, P.; Sharma, R. K. *Int. J. Mol. Med.* **2007**, *19*, 823.

(34) Johnson, D. R.; Bhatnagar, R. S.; Knoll, L. J.; Gordon, J. I. *Annu. Rev. Biochem.* **1994**, *63*, 869.

(35) Maurer-Stroh, S.; Eisenhaber, F. *Trends Microbiol.* **2004**, *12*, 178.

(36) Aude, M.; José, A. T.; Benoît, V.; Myriam, F.; Christelle, E.; Geneviève, E.; Michel, Z.; Carmela, G.; Thierry, M. *Proteomics* **2008**, *8*, 2809.

(37) Su, R.; Han, Z.-Y.; Fan, J.-P.; Zhang, Y.-L. *Neurosc. Bull.* **2010**, *26*, 338.

(38) Cordeddu, V.; Di Schiavi, E.; Pennacchio, L. A.; Ma'ayan, A.; Sarkozy, A.; Fodale, V.; Cecchetti, S.; Cardinale, A.; Martin, J.; Schackwitz, W.; Lipzen, A.; Zampino, G.; Mazzanti, L.; Digilio, M. C.; Martinelli, S.; Flex, E.; Lepri, F.; Bartholdi, D.; Kutsche, K.; Ferrero, G. B.; Anichini, C.; Selicorni, A.; Rossi, C.; Tenconi, R.; Zenker, M.; Merlo, D.; Dallapiccola, B.; Iyengar, R.; Bazzicalupo, P.; Gelb, B. D.; Tartaglia, M. *Nat. Genet.* **2009**, *41*, 1022.

(39) Provitera, P.; El-Maghrabi, R.; Scarlata, S. *Biophys. Chem.* **2006**, *119*, 23.

(40) Eckert, R. E.; Neuder, L. E.; Park, J.; Adler, K. B.; Jones, S. L. *Am. J. Respir. Cell Mol. Biol.* **2010**, *42*, 586.

(41) Bowyer, P. W.; Tate, E. W.; Leatherbarrow, R. J.; Holder, A. A.; Smith, D. F.; Brown, K. A. *ChemMedChem* **2008**, *3*, 402.

(42) Tate, E. W.; Bell, A. S.; Rackham, M. D.; Wright, M. H. *Parasitology* **2013**, 1.

(43) Frearson, J. A.; Brand, S.; McElroy, S. P.; Cleghorn, L. A. T.; Smid, O.; Stojanovski, L.; Price, H. P.; Guther, M. L. S.; Torrie, L. S.; Robinson, D. A.; Hallyburton, I.; Mpamhanga, C. P.; Brannigan, J. A.; Wilkinson, A. J.; Hodgkinson, M.; Hui, R.; Qiu, W.; Raimi, O. G.; van Aalten, D. M. F.; Brenk, R.; Gilbert, I. H.; Read, K. D.; Fairlamb, A. H.; Ferguson, M. A. J.; Smith, D. F.; Wyatt, P. G. *Nature* **2010**, *464*, 728.

(44) Bowyer, P. W.; Gunaratne, R. S.; Grainger, M.; Withers-Martinez, C.; Wickramsinghe, S. R.; Tate, E. W.; Leatherbarrow, R. J.; Brown, K. A.; Holder, A. A.; Smith, D. F. *Biochem. J.* **2007**, *408*, 173.

(45) James, A. S.; Balekudru, D.; Mark, E. Z.; Sandra, K. F.; David, L. B.; Hwang-Fun, L.; Srinivasan, N.; Pramod, P. M.; Arlene, C. W.; Nandini, S. K.; Martin, L. B.; Daniel, P. G.; Charles, A. M.; Jeffrey, I. G. *J. Pept. Sci.* **1997**, *43*, 43.

(46) McIlhinney, R. A.; Young, K.; Egerton, M.; Camble, R.; White, A.; Soloviev, M. *Biochem. J.* **1998**, *333 (Pt 3)*, 491.

(47) Hill, B. T.; Skowronski, J. *J. Virol.* **2005**, *79*, 1133.

(48) Selvakumar, P.; Lakshmikuttyamma, A.; Shrivastav, A.; Das, S. B.; Dimmock, J. R.; Sharma, R. K. *Prog. Lipid Res.* **2007**, *46*, 1.

(49) Sievers, F.; Wilm, A.; Dineen, D.; Gibson, T. J.; Karplus, K.; Li, W.; Lopez, R.; McWilliam, H.; Remmert, M.; Soding, J.; Thompson, J. D.; Higgins, D. G. *Mol. Syst. Biol.* **2011**, *7*, 539.

(50) Rundle, D. R.; Rajala, R. V. S.; Anderson, R. E. *Exp. Eye Res.* **2002**, *75*, 87.

(51) Wright, M. H.; Heal, W. P.; Mann, D. J.; Tate, E. W. *J. Chem. Biol.* **2009**.

(52) Seaton, K. E.; Smith, C. D. *J. Gen. Virol.* **2008**, *89*, 288.

(53) Takamune, N.; Gota, K.; Misumi, S.; Tanaka, K.; Okinaka, S.; Shoji, S. *Microbes Infect.* **2008**, *10*, 143.

(54) Toska, E.; Campbell, H. A.; Shandilya, J.; Goodfellow, S. J.; Shore, P.; Medler, K. F.; Roberts, S. G. *Cell Reports* **2012**, *2*, 462.

(55) Mount, D. W. *CSH Protoc* **2007**, *2007*, pdb top17.

(56) Bell, A. S.; Mills, J. E.; Williams, G. P.; Brannigan, J. A.; Wilkinson, A. J.; Parkinson, T.; Leatherbarrow, R. J.; Tate, E. W.; Holder, A. A.; Smith, D. F. *PLoS Negl. Trop. Dis.* **2012**, *6*, e1625.

(57) Bhatnagar, R. S.; Futterer, K.; Waksman, G.; Gordon, J. I. *Biochim. Biophys. Acta* **1999**, *1441*, 162.

(58) Rudnick, D. A.; McWherter, C. A.; Rocque, W. J.; Lennon, P. J.; Getman, D. P.; Gordon, J. I. *J. Biol. Chem.* **1991**, *266*, 9732.

(59) Rocque, W. J.; Mcwherter, C. A.; Wood, D. C.; Gordon, J. I. *J. Biol. Chem.* **1993**, *268*, 9964.

(60) Qiu, W.; Hutchinson, A.; Wernimont, A.; Lin, Y.-H.; Kania A; Ravichandran, M.; Kozieradzki, I.; Cossar, D.; Schapira, M.; Arrowsmith, C.; Bountra, C.; Weigelt, J.; Edwards, A.; Wyatt, P.; Ferguson, M.; Frearson, J.; Brand, S.; Robinson, D.; Bochkarev, A.; Hui, R. In *Structural Genomics* 2009/8/29

(61) Starai, V. J.; Escalante-Semerena, J. C. *Cell Mol. Life Sci.* **2004**, *61*, 2020.

(62) Heuckeroth, R. O.; Glaser, L.; Gordon, J. I. *Proc. Natl. Acad. Sci. USA* **1988**, *85*, 8795.

(63) Heuckeroth, R. O.; Jackson-Machelski, E.; Adams, S. P.; Kishore, N. S.; Huhn, M.; Katoh, A.; Lu, T.; Gokel, G. W.; Gordon, J. I. *J. Lipid Res.* **1990**, *31*, 1121.

(64) Kishore, N. S.; Lu, T. B.; Knoll, L. J.; Katoh, A.; Rudnick, D. A.; Mehta, P. P.; Devadas, B.; Huhn, M.; Atwood, J. L.; Adams, S. P.; et al. *J. Biol. Chem.* **1991**, *266*, 8835.

(65) Kishore, N. S.; Wood, D. C.; Mehta, P. P.; Wade, A. C.; Lu, T.; Gokel, G. W.; Gordon, J. I. *J. Biol. Chem.* **1993**, *268*, 4889.

(66) Rudnick, D. A.; McWherter, C. A.; Adams, S. P.; Ropson, I. J.; Duronio, R. J.; Gordon, J. I. *J. Biol. Chem.* **1990**, *265*, 13370.

(67) Towler, D. A.; Eubanks, S. R.; Towery, D. S.; Adams, S. P.; Glaser, L. *J. Biol. Chem.* **1987**, *262*, 1030.

(68) Bhatnagar, R. S.; Futterer, K.; Farazi, T. A.; Korolev, S.; Murray, C. L.; Jackson-Machelski, E.; Gokel, G. W.; Gordon, J. I.; Waksman, G. *Nat. Struct. Mol. Biol.* **1998**, *5*, 1091.

(69) Lu, T.; Li, Q.; Katoh, A.; Hernandez, J.; Duffin, K.; Jackson-Machelski, E.; Knoll, L. J.; Gokel, G. W.; Gordon, J. I. *J. Biol. Chem.* **1994**, *269*, 5346.

(70) Glover, C. J.; Goddard, C.; Felsted, R. L. *Biochem. J.* **1988**, *250*, 485.

(71) Bhatnagar, R. S.; Schall, O. F.; Jackson-Machelski, E.; Sikorski, J. A.; Devadas, B.; Gokel, G. W.; Gordon, J. I. *Biochemistry* **1997**, *36*, 6700.

(72) Qiu W, H. A., Wernimont A, Lin Y-H, Kania A, Ravichandran M, Kozieradzki I, Cossar D, Schapira M, Arrowsmith CH, Bountra C, Weigelt J, Edwards AM, Wyatt PG, Ferguson MAJ, Frearson JA, Brand SY, Robinson DA, Bochkarev A, Hui R, *Structural Genomics* **2009/8/29**

(73) Qi, Q.; Rajala, R. V.; Anderson, W.; Jiang, C.; Rozwadowski, K.; Selvaraj, G.; Sharma, R.; Datla, R. *J. Biol. Chem.* **2000**, *275*, 9673.

(74) Tsunasawa, S.; Stewart, J. W.; Sherman, F. *J. Biol. Chem.* **1985**, *260*, 5382.

(75) Kaplan, J. M.; Mardon, G.; Bishop, J. M.; Varmus, H. E. *Mol. Cell Biol.* **1988**, *8*, 2435.

(76) Pellman, D.; Garber, E. A.; Cross, F. R.; Hanafusa, H. *Proc. Natl. Acad. Sci. USA* **1985**, *82*, 1623.

(77) Duronio, R. J.; Rudnick, D. A.; Adams, S. P.; Towler, D. A.; Gordon, J. I. *J. Biol. Chem.* **1991**, *266*, 10498.

(78) Maurer-Stroh, S.; Eisenhaber, B.; Eisenhaber, F. *J. Mol. Biol.* **2002**, *317*, 523.

(79) Maurer-Stroh, S.; Eisenhaber, B.; Eisenhaber, F. *J. Mol. Biol.* **2002**, *317*, 541.

(80) URL: http://mendel.imp.ac.at/myristate/SUPLpredictor.htm

(81) URL: http://web.expasy.org/myristoylator

(82) Bologna, G.; Yvon, C.; Duvaud, S.; Veuthey, A. L. *Proteomics* **2004**, *4*, 1626.

(83) Martinez, A.; Traverso, J. A.; Valot, B.; Ferro, M.; Espagne, C.; Ephritikhine, G.; Zivy, M.; Giglione, C.; Meinnel, T. *Proteomics* **2008**, *8*, 2809.

(84) Frottin, F.; Martinez, A.; Peynot, P.; Mitra, S.; Holz, R. C.; Giglione, C.; Meinnel, T. *Mol. Cell. Proteomics* **2006**, *5*, 2336.

(85) Cao, W.; Sumikoshi, K.; Nakamura, S.; Terada, T.; Shimizu, K. *Bioinformation* **2011**, *6*, 204.

(86) Bienvenut, W. V.; Sumpton, D.; Martinez, A.; Lilla, S.; Espagne, C.; Meinnel, T.; Giglione, C. *Mol. Cell. Proteomics* **2012**, *11*, M111 015131.

(87) Traverso, J. A.; Giglione, C.; Meinnel, T. *Proteomics* **2013**, *13*, 25.
(88) Mishkind, M. *Trends Cell Biol.* **2001**, *11*, 191.
(89) Martin, D. D.; Beauchamp, E.; Berthiaume, L. G. *Biochimie* **2011**, *93*, 18.
(90) Martin, D. D.; Ahpin, C. Y.; Heit, R. J.; Perinpanayagam, M. A.; Yap, M. C.; Veldhoen, R. A.; Goping, I. S.; Berthiaume, L. G. *FASEB J.* **2012**, *26*, 13.
(91) Dix, M. M.; Simon, G. M.; Cravatt, B. F. *Cell* **2008**, *134*, 679.
(92) Mahrus, S.; Trinidad, J. C.; Barkan, D. T.; Sali, A.; Burlingame, A. L.; Wells, J. A. *Cell* **2008**, *134*, 866.
(93) Resh, M. D. *Biochim. Biophys. Acta* **1999**, *1451*, 1.
(94) Zheng, J.; Knighton, D. R.; Xuong, N. H.; Taylor, S. S.; Sowadski, J. M.; Ten Eyck, L. F. *Protein Sci.* **1993**, *2*, 1559.
(95) Zheng, G. Q.; Hu, X.; Cassady, J. M.; Paige, L. A.; Geahlen, R. L. *J. Pharm. Sci.* **1994**, *83*, 233.
(96) Murray, D.; Hermida-Matsumoto, L.; Buser, C. A.; Tsang, J.; Sigal, C. T.; Ben-Tal, N.; Honig, B.; Resh, M. D.; McLaughlin, S. *Biochemistry* **1998**, *37*, 2145.
(97) Peitzsch, R. M.; McLaughlin, S. *Biochem.* **1993**, *32*, 10436.
(98) Smotrys, J. E.; Linder, M. E. *Annu. Rev. Biochem.* **2004**, *73*, 559.
(99) Koegl, M.; Zlatkine, P.; Ley, S. C.; Courtneidge, S. A.; Magee, A. I. *Biochem. J.* **1994**, *303 (Pt 3)*, 749.
(100) Alland, L.; Peseckis, S. M.; Atherton, R. E.; Berthiaume, L.; Resh, M. D. *J. Biol. Chem.* **1994**, *269*, 16701.
(101) Vergeres, G.; Ramsden, J. J. *Biochem. J.* **1998**, *330 (Pt 1)*, 5.
(102) Resh, M. D. *Nat. Chem. Biol.* **2006**, *2*, 584.
(103) McLaughlin, S.; Aderem, A. *Trends Biochem. Sci.* **1995**, *20*, 272.
(104) Patwardhan, P.; Resh, M. D. *Mol. Cell. Biol.* **2010**, *30*, 4094.
(105) McIlhinney, R. A.; McGlone, K. *Biochem. J.* **1990**, *271*, 681.
(106) Manenti, S.; Sorokine, O.; Van Dorsselaer, A.; Taniguchi, H. *J. Biol. Chem.* **1994**, *269*, 8309.
(107) Braun, T.; McIlhinney, R. A.; Vergeres, G. *Biochimie* **2000**, *82*, 705.
(108) Raju, R. V.; Sharma, R. K. *Mol. Cell. Biochem.* **1996**, *158*, 107.
(109) Burnaevskiy, N.; Fox, T. G.; Plymire, D. A.; Ertelt, J. M.; Weigele, B. A.; Selyunin, A. S.; Way, S. S.; Patrie, S. M.; Alto, N. M. *Nature* **2013**, *496*, 106.
(110) van der Vusse, G. J.; van Bilsen, M.; Glatz, J. F.; Hasselbaink, D. M.; Luiken, J. J. *Mol. Cell. Biochem.* **2002**, *239*, 9.
(111) Colombo, S.; Longhi, R.; Alcaro, S.; Ortuso, F.; Sprocati, T.; Flora, A.; Borgese, N. *J. Cell Biol.* **2005**, *168*, 735.
(112) Selvakumar, P.; Sharma, R. K. *Can. J. Physiol. Pharmacol.* **2006**, *84*, 707.
(113) Rajala, R. V.; Datla, R. S.; Carlsen, S. A.; Anderson, D. H.; Qi, Z.; Wang, J. H.; Sharma, R. K. *Biochem. Biophys. Res. Commun.* **2001**, *288*, 233.
(114) Rudnick, D. A.; Johnson, R. L.; Gordon, J. I. *J. Biol. Chem.* **1992**, *267*, 23852.
(115) Perinpanayagam, M. A.; Beauchamp, E.; Martin, D. D.; Sim, J. Y.; Yap, M. C.; Berthiaume, L. G. *FASEB J.* **2013**, *27*, 811.
(116) Kumar, S.; Dimmock, J. R.; Sharma, R. K. *Cancers* **2011**, *3*, 1372.
(117) Selvakumar, P.; Pasha, M. K.; Ashakumary, L.; Dimmock, J. R.; Sharma, R. K. *Int. J. Mol. Med.* **2002**, *10*, 493.
(118) Rajala, R. V.; Dehm, S.; Bi, X.; Bonham, K.; Sharma, R. K. *Biochem. Biophys. Res. Commun.* **2000**, *273*, 1116.
(119) Raju, R. V.; Moyana, T. N.; Sharma, R. K. *Exp. Cell Res.* **1997**, *235*, 145.
(120) Rajala, R. V.; Radhi, J. M.; Kakkar, R.; Datla, R. S.; Sharma, R. K. *Cancer* **2000**, *88*, 1992.

(121) Shrivastav, A.; Varma, S.; Senger, A.; Khandelwal, R. L.; Carlsen, S.; Sharma, R. K. *J. Pathol.* **2009**, *218*, 391.

(122) Clegg, R. A.; Gordge, P. C.; Miller, W. R. *Adv. Enzyme Regul.* **1999**, *39*, 175.

(123) Resh, M. D. *Cell* **1994**, *76*, 411.

(124) Abraham, N.; Veillette, A. *Mol. Cell. Biol.* **1990**, *10*, 5197.

(125) Cooper, J. A.; MacAuley, A. *Proc. Natl. Acad. Sci. U. S. A.* **1988**, *85*, 4232.

(126) Talamonti, M. S.; Roh, M. S.; Curley, S. A.; Gallick, G. E. *J. Clin. Invest.* **1993**, *91*, 53.

(127) Allington, T. M.; Galliher-Beckley, A. J.; Schiemann, W. P. *FASEB J.* **2009**, *23*, 4231.

(128) Noren, N. K.; Foos, G.; Hauser, C. A.; Pasquale, E. B. *Nat. Cell Biol.* **2006**, *8*, 815.

(129) Yang, J.; Campobasso, N.; Biju, M. P.; Fisher, K.; Pan, X. Q.; Cottom, J.; Galbraith, S.; Ho, T.; Zhang, H.; Hong, X.; Ward, P.; Hofmann, G.; Siegfried, B.; Zappacosta, F.; Washio, Y.; Cao, P.; Qu, J.; Bertrand, S.; Wang, D. Y.; Head, M. S.; Li, H.; Moores, S.; Lai, Z.; Johanson, K.; Burton, G.; Erickson-Miller, C.; Simpson, G.; Tummino, P.; Copeland, R. A.; Oliff, A. *Chem. Biol.* **2011**, *18*, 177.

(130) Uno, F.; Sasaki, J.; Nishizaki, M.; Carboni, G.; Xu, K.; Atkinson, E. N.; Kondo, M.; Minna, J. D.; Roth, J. A.; Ji, L. *Cancer Res.* **2004**, *64*, 2969.

(131) Ji, L.; Roth, J. A. *J. Thorac. Oncol.* **2008**, *3*, 327.

(132) Paige, L. A.; Zheng, G. Q.; DeFrees, S. A.; Cassady, J. M.; Geahlen, R. L. *J. Med. Chem.* **1989**, *32*, 1665.

(133) Paige, L. A.; Zheng, G. Q.; DeFrees, S. A.; Cassady, J. M.; Geahlen, R. L. *Biochem.* **1990**, *29*, 10566.

(134) Glover, C. J.; Tellez, M. R.; Guziec, F. S., Jr.; Felsted, R. L. *Biochem. Pharmacol.* **1991**, *41*, 1067.

(135) Wagner, A. P.; Retey, J. *Eur. J. Biochem.* **1991**, *195*, 699.

(136) Bryant, M.; McWherter, C.; Kishore, N.; Gokel, G.; Gordon, J. *Persp. Drug Disc. Design* **1993**, *1*, 193.

(137) Devadas, B.; Kishore, N. S.; Adams, S. P.; Gordon, J. I. *Bioorg. .Med. Chem. Lett.* **1993**, *3*, 779.

(138) Parang, K.; Wiebe, L. I.; Knaus, E. E.; Huang, J. S.; Tyrrell, D. L.; Csizmadia, F. *Antiviral Res.* **1997**, *34*, 75.

(139) Harper, D. R.; Gilbert, R. L.; Blunt, C.; McIlhinney, R. A. *J. Gen. Virol.* **1993**, *74 (Pt 6)*, 1181.

(140) Bhandarkar, S. S.; Bromberg, J.; Carrillo, C.; Selvakumar, P.; Sharma, R. K.; Perry, B. N.; Govindarajan, B.; Fried, L.; Sohn, A.; Reddy, K.; Arbiser, J. L. *Clin. Cancer. Res.* **2008**, *14*, 5743.

(141) French, K. J.; Zhuang, Y.; Schrecengost, R. S.; Copper, J. E.; Xia, Z.; Smith, C. D. *J. Pharmacol. Exp. Ther.* **2004**, *309*, 340.

(142) Brand, S.; Wyatt, P. G.; WO/2010/026365 ed. 11.03.2010; Vol. WO/2010/026365.

(143) Crowther, G. J.; Napuli, A. J.; Gilligan, J. H.; Gagaring, K.; Borboa, R.; Francek, C.; Chen, Z.; Dagostino, E. F.; Stockmyer, J. B.; Wang, Y.; Rodenbough, P. P.; Castaneda, L. J.; Leibly, D. J.; Bhandari, J.; Gelb, M. H.; Brinker, A.; Engels, I. H.; Taylor, J.; Chatterjee, A. K.; Fantauzzi, P.; Glynne, R. J.; Van Voorhis, W. C.; Kuhen, K. L. *Mol. Biochem. Parasitol.* **2010**.

(144) Rampoldi, F.; Sandhoff, R.; Owen, R. W.; Grone, H. J.; Porubsky, S. *J. Lipid Res.* **2012**, *53*, 2459.

(145) Goncalves, V.; Brannigan, J. A.; Thinon, E.; Olaleye, T. O.; Serwa, R.; Lanzarone, S.; Wilkinson, A. J.; Tate, E. W.; Leatherbarrow, R. J. *Anal. Biochem.* **2012**, *421*, 342.

(146) Macarron, R.; Hertzberg, R. P. *Methods Mol. Biol.* **2009**, *565*, 1.

(147) Neumann, L.; Ritscher, A.; Muller, G.; Hafenbradl, D. *J. Comput. Aided Mol. Des.* **2009**.

(148) Ekins, S.; Mestres, J.; Testa, B. *Br. J. Pharmacol.* **2007**, *152*, 9.

(149) Litman, P.; Ohne, O.; Ben-Yaakov, S.; Shemesh-Darvish, L.; Yechezkel, T.; Salitra, Y.; Rubnov, S.; Cohen, I.; Senderowitz, H.; Kidron, D.; Livnah, O.; Levitzki, A.; Livnah, N. *Biochem.* **2007**, *46*, 4716.

(150) Frank, R. *Tetrahedron* **1992**, *48*, 9217.
(151) Wu, H.; Ge, J.; Yao, S. Q. *Angew. Chem. Int. Ed.* **2010**, *49*, 6528.
(152) Lam, K. S.; Lebl, M.; Krchnak, V. *Chem. Rev.* **1997**, *97*, 411.
(153) Smith, G. P.; Petrenko, V. A. *Chem. Rev.* **1997**, *97*, 391.
(154) Heal, W. P.; Wickramasinghe, S. R.; Leatherbarrow, R. J.; Tate, E. W. *Org. Biomol. Chem.* **2008**, *6*, 2308.
(155) Ay, B.; Landgraf, K.; Streitz, M.; Fuhrmann, S.; Volkmer, R.; Boisguerin, P. *Bioorg. Med. Chem. Lett.* **2008**, *18*, 4038.
(156) Frank, R. *J. Immunol. Methods* **2002**, *267*, 13.
(157) Reineke, U.; Volkmer-Engert, R.; Schneider-Mergener, J. *Curr. Opin. Biotechnol.* **2001**, *12*, 59.
(158) Fields, G. B.; Noble, R. L. *Int. J. Pept. Protein Res.* **1990**, *35*, 161.
(159) Blackwell, H. E. *Curr. Opin. Chem. Biol.* **2006**, *10*, 203.
(160) O'Callaghan, D. W.; Ivings, L.; Weiss, J. L.; Ashby, M. C.; Tepikin, A. V.; Burgoyne, R. D. *J. Biol. Chem.* **2002**, *277*, 14227.
(161) Mosevitsky, M. I.; Capony, J. P.; Skladchikova, G. Y.; Novitskaya, V. A.; Plekhanov, A. Y.; Zakharov, V. V. *Biochimie* **1997**, *79*, 373.
(162) Prescher, J. A.; Bertozzi, C. R. *Nat. Chem. Biol.* **2005**, *1*, 13.
(163) Wright, M. H.; PhD Thesis, Imperial College London: 2013.
(164) Jewett, J. C.; Bertozzi, C. R. *Chem. Soc. Rev.* **2010**, *39*, 1272.
(165) Staudinger, H.; Meyer, J. *Helv. Chim. Acta* **1919**, *2*, 619.
(166) Lim, R. K.; Lin, Q. *Chem. Commun.* **2010**, *46*, 1589.
(167) Demko, Z. P.; Sharpless, K. B. *Angew. Chem. Int. Ed.* **2002**, *41*, 2113.
(168) Tornoe, C. W.; Christensen, C.; Meldal, M. *J. Org. Chem.* **2002**, *67*, 3057.
(169) Wittig, G.; Krebs, A. *Ber. Dtsch. Chem. Ges.* **1961**, *94*, 3260.
(170) Agard, N. J.; Prescher, J. A.; Bertozzi, C. R. *J. Am. Chem. Soc.* **2004**, *126*, 15046.
(171) van der Linden, W. A.; Li, N.; Hoogendoorn, S.; Ruben, M.; Verdoes, M.; Guo, J.; Boons, G. J.; van der Marel, G. A.; Florea, B. I.; Overkleeft, H. S. *Bioorg. Med. Chem.* **2012**, *20*, 662.
(172) Charron, G.; Zhang, M. M.; Yount, J. S.; Wilson, J.; Raghavan, A. S.; Shamir, E.; Hang, H. C. *J. Am. Chem. Soc.* **2009**, *131*, 4967.
(173) Wilson, J. P.; Raghavan, A. S.; Yang, Y.-Y.; Charron, G.; Hang, H. C. *Mol. Cell. Proteomics* **2011**, *10*.
(174) Heal, W. P.; Jovanovic, B.; Bessin, S.; Wright, M. H.; Magee, A. I.; Tate, E. W. *Chem. Commun.* **2011**, *47*, 4081.
(175) Martin, B. R.; Cravatt, B. F. *Nat. Methods* **2009**, *6*, 135.
(176) Paulick, M. G.; Forstner, M. B.; Groves, J. T.; Bertozzi, C. R. *Proc. Natl. Acad. Sci. U. S. A.* **2007**, *104*, 20332.
(177) Tsai, Y. H.; Liu, X.; Seeberger, P. H. *Angew. Chem. Int. Ed.* **2012**, *51*, 11438.
(178) Walther, T. C.; Mann, M. *J. Cell Biol.* **2010**, *190*, 491.
(179) McLafferty, F. W.; Breuker, K.; Jin, M.; Han, X.; Infusini, G.; Jiang, H.; Kong, X.; Begley, T. P. *FEBS J.* **2007**, *274*, 6256.
(180) Sadygov, R. G.; Cociorva, D.; Yates, J. R., 3rd *Nat. Methods* **2004**, *1*, 195.
(181) Perkins, D. N.; Pappin, D. J.; Creasy, D. M.; Cottrell, J. S. *Electrophoresis* **1999**, *20*, 3551.
(182) Eng, J.; McCormack, A.; Yates, J. *J. Am. Soc. Mass Spectrom.* **1994**, *5*, 976.
(183) Craig, R.; Beavis, R. C. *Bioinformatics* **2004**, *20*, 1466.
(184) Searle, B. C. *Proteomics* **2010**, *10*, 1265.
(185) Cox, J.; Mann, M. *Nat. Biotechnol.* **2008**, *26*, 1367.
(186) Shevchenko, A.; Wilm, M.; Vorm, O.; Mann, M. *Anal. Chem.* **1996**, *68*, 850.
(187) Wisniewski, J. R.; Zougman, A.; Nagaraj, N.; Mann, M. *Nat. Methods* **2009**, *6*, 359.
(188) Sadaghiani, A. M.; Verhelst, S. H.; Bogyo, M. *Curr. Opin. Chem. Biol.* **2007**, *11*, 20.

(189) Cox, J.; Mann, M. *Annu. Rev. Biochem.* **2011**, *80*, 273.
(190) Wasinger, V. C.; Zeng, M.; Yau, Y. *Int. J. Proteomics* **2013**, *2013*, 12.
(191) Zieske, L. R. *J. Exp. Bot.* **2006**, *57*, 1501.
(192) Boersema, P. J.; Raijmakers, R.; Lemeer, S.; Mohammed, S.; Heck, A. J. *Nat. Protoc.* **2009**, *4*, 484.
(193) Luber, C. A.; Cox, J.; Lauterbach, H.; Fancke, B.; Selbach, M.; Tschopp, J.; Akira, S.; Wiegand, M.; Hochrein, H.; O'Keeffe, M.; Mann, M. *Immunity* **2010**, *32*, 279.
(194) Mann, M. *Nat. Rev. Mol. Cell Biol.* **2006**, *7*, 952.
(195) Geiger, T.; Wisniewski, J. R.; Cox, J.; Zanivan, S.; Kruger, M.; Ishihama, Y.; Mann, M. *Nat. Protoc.* **2011**, *6*, 147.
(196) Brown, C. A.; Yamashita, A. *J. Am. Chem. Soc.* **1975**, *97*, 891.
(197) Hannoush, R. N.; Arenas-Ramirez, N. *ACS Chem. Biol.* **2009**, *4*, 581.
(198) Bidd, I.; Kelly, D. J.; Ottley, P. M.; Paynter, O. I.; Simmonds, D. J.; Whiting, M. C. *J. Chem. Soc., Perkin Trans. 1* **1983**, 1369.
(199) Jung, Christian M.; Kraus, W.; Leibnitz, P.; Pietzsch, H.-J.; Kropp, J.; Spies, H. *Eur. J. Inorg. Chem.* **2002**, *2002*, 1219.
(200) El Fangour, S.; Guy, A.; Vidal, J.-P.; Rossi, J.-C.; Durand, T. *Tetrahedron Lett.* **2003**, *44*, 2105.
(201) Wüst, F.; Dence, C. S.; McCarthy, T. J.; Welch, M. J. *J. Label. Compd. Radiopharm.* **2000**, *43*, 1289.
(202) Gaffarogullari, E. C.; Masterson, L. R.; Metcalfe, E. E.; Traaseth, N. J.; Balatri, E.; Musa, M. M.; Mullen, D.; Distefano, M. D.; Veglia, G. *J. Mol. Biol.* **2011**, *411*, 823.
(203) McIlhinney, R. A.; Patel, P. B.; McGlone, K. *Eur. J. Biochem.* **1994**, *222*, 137.
(204) Buss, J. E.; Sefton, B. M. *J. Virol.* **1985**, *53*, 7.
(205) Selvakumar, P.; Lakshmikuttyamma, A.; Sharma, R. K. *J. Biomed. Biotechnol.* **2009**, *2009*, 907614.
(206) Landry, J. J.; Pyl, P. T.; Rausch, T.; Zichner, T.; Tekkedil, M. M.; Stutz, A. M.; Jauch, A.; Aiyar, R. S.; Pau, G.; Delhomme, N.; Gagneur, J.; Korbel, J. O.; Huber, W.; Steinmetz, L. M. *G3 (Bethesda).* **2013**, *26*, 005777.
(207) Nagaraj, N.; Wisniewski, J. R.; Geiger, T.; Cox, J.; Kircher, M.; Kelso, J.; Paabo, S.; Mann, M. *Mol. Syst. Biol.* **2011**, *7*.
(208) Wang, X.; Chen, C. F.; Baker, P. R.; Chen, P. L.; Kaiser, P.; Huang, L. *Biochemistry* **2007**, *46*, 3553.
(209) Carr, S. A.; Biemann, K.; Shoji, S.; Parmelee, D. C.; Titani, K. *Proc. Natl. Acad. Sci. U. S. A.* **1982**, *79*, 6128.
(210) Thiele, C.; Papan, C.; Hoelper, D.; Kusserow, K.; Gaebler, A.; Schoene, M.; Piotrowitz, K.; Lohmann, D.; Spandl, J.; Stevanovic, A.; Shevchenko, A.; Kuerschner, L. *ACS Chem. Biol.* **2012**, *7*, 2004.
(211) Berridge, M. V.; Tan, A. S. *Arch. Biochem. Biophys.* **1993**, *303*, 474.
(212) Holzer, R. G.; Park, E. J.; Li, N.; Tran, H.; Chen, M.; Choi, C.; Solinas, G.; Karin, M. *Cell* **2011**, *147*, 173.
(213) Martin, D. D.; Vilas, G. L.; Prescher, J. A.; Rajaiah, G.; Falck, J. R.; Bertozzi, C. R.; Berthiaume, L. G. *FASEB J.* **2008**, *22*, 797.
(214) Tang, D.; Lahti, J. M.; Grenet, J.; Kidd, V. J. *J. Biol. Chem.* **1999**, *274*, 7245.
(215) Price, H. P.; Hodgkinson, M. R.; Wright, M. H.; Tate, E. W.; Smith, B. A.; Carrington, M.; Stark, M.; Smith, D. F. *Biochim. Biophys. Acta* **2012**, *1823*, 1178.
(216) Brooks, H. B.; Geeganage, S.; Kahl, S. D.; Montrose, C.; Sittampalam, S.; Smith, M. C.; Weidner, J. R. *Basics of Enzymatic Assays for HTS*; Assay Guidance Manual [Internet]. ed.; Bethesda (MD): Eli Lilly & Company and the National Center for Advancing Translational Sciences, 2012 May 1 [Updated 2012 Oct 1].

(217) Das, U.; Kumar, S.; Dimmock, J. R.; Sharma, R. K. *Curr. Cancer Drug Targets* **2012**, *12*, 667.

(218) Nadler, M. J.; Harrison, M. L.; Ashendel, C. L.; Cassady, J. M.; Geahlen, R. L. *Biochemistry* **1993**, *32*, 9250.

(219) Russwurm, C.; Zoidl, G.; Koesling, D.; Russwurm, M. *J. Biol. Chem.* **2009**, *284*, 25782.

(220) Yap, M. C.; Kostiuk, M. A.; Martin, D. D.; Perinpanayagam, M. A.; Hak, P. G.; Siddam, A.; Majjigapu, J. R.; Rajaiah, G.; Keller, B. O.; Prescher, J. A.; Wu, P.; Bertozzi, C. R.; Falck, J. R.; Berthiaume, L. G. *J. Lipid Res.* **2010**, *51*, 1566.

(221) Lindwasser, O. W.; Resh, M. D. *Proc. Natl. Acad. Sci. U. S. A.* **2002**, *99*, 13037.

(222) Berg, J. M.; Tymoczko, J. L.; Stryer, L. *Biochemistry, 5th edition*; W H Freeman: New York, 2002.

(223) Brand, S.; Cleghorn, L. A.; McElroy, S. P.; Robinson, D. A.; Smith, V. C.; Hallyburton, I.; Harrison, J. R.; Norcross, N. R.; Spinks, D.; Bayliss, T.; Norval, S.; Stojanovski, L.; Torrie, L. S.; Frearson, J. A.; Brenk, R.; Fairlamb, A. H.; Ferguson, M. A.; Read, K. D.; Wyatt, P. G.; Gilbert, I. H. *J. Med. Chem.* **2012**, *55*, 140.

(224) Liu, K.; Yang, P.-Y.; Na, Z.; Yao, S. Q. *Angew. Chem. Int. Ed.* **2011**, *50*, 6776.

(225) Rautio, J.; Kumpulainen, H.; Heimbach, T.; Oliyai, R.; Oh, D.; Jarvinen, T.; Savolainen, J. *Nat. Rev. Drug Discov.* **2008**, *7*, 255.

(226) Ben-Moha-Lerman, E.; Nidam, T.; Cohen, M.; Avhar-Mayden, S.; Balanov, A.; LTD, T. p. i., Ed. 2010; Vol. WO/2010/063002.

(227) Olaleye, T. O.; PhD Thesis, Imperial College London: 2012.

(228) Wice, B. M.; Gordon, J. I. *J. Cell Biol.* **1992**, *116*, 405.

(229) Eberle, H. B.; Serrano, R. L.; Füllekrug, J.; Schlosser, A.; Lehmann, W. D.; Lottspeich, F.; Kaloyanova, D.; Wieland, F. T.; Helms, J. B. *J. Cell Sci.* **2002**, *115*, 827.

(230) Suzuki, T.; Moriya, K.; Nagatoshi, K.; Ota, Y.; Ezure, T.; Ando, E.; Tsunasawa, S.; Utsumi, T. *Proteomics* **2010**, *10*, 1780.

(231) Gutierrez-Ford, C.; Levay, K.; Gomes, A. V.; Perera, E. M.; Som, T.; Kim, Y.-M.; Benovic, J. L.; Berkovitz, G. D.; Slepak, V. Z. *Biochemistry* **2003**, *42*, 14553.

(232) Yasuda, K.; Kosugi, A.; Hayashi, F.; Saitoh, S.-i.; Nagafuku, M.; Mori, Y.; Ogata, M.; Hamaoka, T. *J. Immunol.* **2000**, *165*, 3226.

(233) Jiang, H.; Khan, S.; Wang, Y.; Charron, G.; He, B.; Sebastian, C.; Du, J.; Kim, R.; Ge, E.; Mostoslavsky, R.; Hang, H. C.; Hao, Q.; Lin, H. *Nature* **2013**, *496*, 110.

(234) Geiger, T.; Velic, A.; Macek, B.; Lundberg, E.; Kampf, C.; Nagaraj, N.; Uhlen, M.; Cox, J.; Mann, M. *Mol. Cell. Proteomics* **2013**, *12*, 1709.

(235) Martin, B. R.; Wang, C.; Adibekian, A.; Tully, S. E.; Cravatt, B. F. *Nat. Methods* **2012**, *9*, 84.

(236) Jones, M. L.; Collins, M. O.; Goulding, D.; Choudhary, J. S.; Rayner, J. C. *Cell Host Microbe* **2012**, *12*, 246.

(237) Crawford, E. D.; Seaman, J. E.; Agard, N.; Hsu, G. W.; Julien, O.; Mahrus, S.; Nguyen, H.; Shimbo, K.; Yoshihara, H. A. I.; Zhuang, M.; Chalkley, R. J.; Wells, J. A. *Mol. Cell. Proteomics* **2013**, *12*, 813.

(238) Sharer, J. D.; Shern, J. F.; Van Valkenburgh, H.; Wallace, D. C.; Kahn, R. A. *Mol. Biol. Cell* **2002**, *13*, 71.

(239) Kostiuk, M. A.; Corvi, M. M.; Keller, B. O.; Plummer, G.; Prescher, J. A.; Hangauer, M. J.; Bertozzi, C. R.; Rajaiah, G.; Falck, J. R.; Berthiaume, L. G. *FASEB J.* **2008**, *22*, 721.

(240) Linder, M. E.; Middleton, P.; Hepler, J. R.; Taussig, R.; Gilman, A. G.; Mumby, S. M. *Proc. Natl. Acad. Sci. U. S. A.* **1993**, *90*, 3675.

(241) Hattori, S.; Adachi, E.; Ebihara, T.; Shirai, T.; Someki, I.; Irie, S. *J Biochem* **1999**, *125*, 676.

(242) Tomko, R. J., Jr.; Hochstrasser, M. *Annu. Rev. Biochem.* **2013**, *82*, 415.

(243) Fu, H.; Reis, N.; Lee, Y.; Glickman, M. H.; Vierstra, R. D. *EMBO J.* **2001**, *20*, 7096.

(244) Stuermer, C. A.; Lang, D. M.; Kirsch, F.; Wiechers, M.; Deininger, S. O.; Plattner, H. *Mol. Biol. Cell* **2001**, *12*, 3031.

(245) Rusnak, F.; Mertz, P. *Physiol. Rev.* **2000**, *80*, 1483.

(246) Stevenson, F. T.; Bursten, S. L.; Locksley, R. M.; Lovett, D. H. *J. Exp. Med.* **1992**, *176*, 1053.

(247) Stevenson, F. T.; Bursten, S. L.; Fanton, C.; Locksley, R. M.; Lovett, D. H. *Proc. Natl. Acad. Sci. U. S. A.* **1993**, *90*, 7245.

(248) Bailey, T. L.; Boden, M.; Buske, F. A.; Frith, M.; Grant, C. E.; Clementi, L.; Ren, J.; Li, W. W.; Noble, W. S. *Nucleic Acids Res.* **2009**, *37*, W202.

(249) Schaefer, L.; Ballabio, A.; Zoghbi, H. Y. *Genomics* **1996**, *34*, 166.

(250) Herrmann, J. M.; Riemer, J. *Antioxid. Redox Signaling* **2010**, *13*, 1341.

(251) Dumont, M. E.; Cardillo, T. S.; Hayes, M. K.; Sherman, F. *Mol. Cell. Biol.* **1991**, *11*, 5487.

(252) Gruenewald, S.; Wahl, B.; Bittner, F.; Hungeling, H.; Kanzow, S.; Kotthaus, J.; Schwering, U.; Mendel, R. R.; Clement, B. *J. Med. Chem.* **2008**, *51*, 8173.

(253) Klein, J. M.; Busch, J. D.; Potting, C.; Baker, M. J.; Langer, T.; Schwarz, G. *J. Biol. Chem.* **2012**, *287*, 42795.

(254) Soma-Nagae, T.; Nada, S.; Kitagawa, M.; Takahashi, Y.; Mori, S.; Oneyama, C.; Okada, M. *J. Cell Sci.* **2013**.

(255) Nada, S.; Hondo, A.; Kasai, A.; Koike, M.; Saito, K.; Uchiyama, Y.; Okada, M. *EMBO J.* **2009**, *28*, 477.

(256) Savalas, L. R.; Gasnier, B.; Damme, M.; Lubke, T.; Wrocklage, C.; Debacker, C.; Jezegou, A.; Reinheckel, T.; Hasilik, A.; Saftig, P.; Schroder, B. *Biochem. J.* **2011**, *439*, 113.

(257) Tuxworth, R. I.; Chen, H.; Vivancos, V.; Carvajal, N.; Huang, X.; Tear, G. *Hum. Mol. Genet.* **2011**, *20*, 2037.

(258) Scifo, E.; Szwajda, A.; Debski, J.; Uusi-Rauva, K.; Kesti, T.; Dadlez, M.; Gingras, A. C.; Tyynela, J.; Baumann, M. H.; Jalanko, A.; Lalowski, M. *J. Proteome Res.* **2013**, *12*, 2101.

(259) Chen-Plotkin, A. S.; Unger, T. L.; Gallagher, M. D.; Bill, E.; Kwong, L. K.; Volpicelli-Daley, L.; Busch, J. I.; Akle, S.; Grossman, M.; Van Deerlin, V.; Trojanowski, J. Q.; Lee, V. M. *J. Neurosci.* **2012**, *32*, 11213.

(260) Medina-Ramirez, C. M.; Goswami, S.; Smirnova, T.; Bamira, D.; Benson, B.; Ferrick, N.; Segall, J.; Pollard, J. W.; Kitsis, R. N. *Cancer Res.* **2011**, *71*, 7705.

(261) Li, Y.; Ge, X.; Liu, X. *Apoptosis* **2009**, *14*, 164.

(262) Zaiman, A. L.; Damico, R.; Thoms-Chesley, A.; Files, D. C.; Kesari, P.; Johnston, L.; Swaim, M.; Mozammel, S.; Myers, A. C.; Halushka, M.; El-Haddad, H.; Shimoda, L. A.; Peng, C. F.; Hassoun, P. M.; Champion, H. C.; Kitsis, R. N.; Crow, M. T. *Circulation* **2011**, *124*, 2533.

(263) Mercier, I.; Vuolo, M.; Madan, R.; Xue, X.; Levalley, A. J.; Ashton, A. W.; Jasmin, J. F.; Czaja, M. T.; Lin, E. Y.; Armstrong, R. C.; Pollard, J. W.; Kitsis, R. N. *Cell Death Differ.* **2005**, *12*, 682.

(264) Wang, J. X.; Li, Q.; Li, P. F. *Cancer Res.* **2009**, *69*, 492.

(265) Carter, B. Z.; Qiu, Y. H.; Zhang, N.; Coombes, K. R.; Mak, D. H.; Thomas, D. A.; Ravandi, F.; Kantarjian, H. M.; Koller, E.; Andreeff, M.; Kornblau, S. M. *Blood* **2011**, *117*, 780.

(266) Koseki, T.; Inohara, N.; Chen, S.; Nunez, G. *Proc. Natl. Acad. Sci. U. S. A.* **1998**, *95*, 5156.

(267) Ao, J. E.; Kuang, L. H.; Zhou, Y.; Zhao, R.; Yang, C. M. *Biochem. Biophys. Res. Commun.* **2012**, *420*, 913.

(268) Wu, L.; Nam, Y. J.; Kung, G.; Crow, M. T.; Kitsis, R. N. *J. Biol. Chem.* **2010**, *285*, 19235.

(269) Sasaki, Y.; Oshima, Y.; Koyama, R.; Maruyama, R.; Akashi, H.; Mita, H.; Toyota, M.; Shinomura, Y.; Imai, K.; Tokino, T. *Mol. Cancer Res.* **2008**, *6*, 395.

(270) Wang, X.; Yang, Q.; Guo, L.; Li, X. H.; Zhao, X. H.; Song, L. B.; Lin, H. X. *J. Transl. Med.* **2013**, *11*, 190.

(271) Berger, T.; Ueda, T.; Arpaia, E.; Chio, II; Shirdel, E. A.; Jurisica, I.; Hamada, K.; You-Ten, A.; Haight, J.; Wakeham, A.; Cheung, C. C.; Mak, T. W. *Oncogene* **2012**.

(272) Miles, L. A.; Lighvani, S.; Baik, N.; Andronicos, N. M.; Chen, E. I.; Parmer, C. M.; Khaldoyanidi, S.; Diggs, J. E.; Kiosses, W. B.; Kamps, M. P.; Yates, J. R., 3rd; Parmer, R. J. *J. Biomed. Biotechnol.* **2012**, *2012*, 250464.

(273) Sun, G. D.; Kobayashi, T.; Abe, M.; Tada, N.; Adachi, H.; Shiota, A.; Totsuka, Y.; Hino, O. *Biochem. Biophys. Res. Commun.* **2007**, *360*, 181.

(274) Ji, H.; Ding, Z.; Hawke, D.; Xing, D.; Jiang, B. H.; Mills, G. B.; Lu, Z. *EMBO Rep.* **2012**, *13*, 554.

(275) Old, W. M.; Shabb, J. B.; Houel, S.; Wang, H.; Couts, K. L.; Yen, C. Y.; Litman, E. S.; Croy, C. H.; Meyer-Arendt, K.; Miranda, J. G.; Brown, R. A.; Witze, E. S.; Schweppe, R. E.; Resing, K. A.; Ahn, N. G. *Mol. Cell* **2009**, *34*, 115.

(276) Chen, S.; Evans, H. G.; Evans, D. R. *J. Biol. Chem.* **2011**, *286*, 10201.

(277) Oishi, H.; Itoh, S.; Matsumoto, K.; Ishitobi, H.; Suzuki, R.; Ema, M.; Kojima, T.; Uchida, K.; Kato, M.; Miyata, T.; Takahashi, S. *J. Biochem.* **2012**, *152*, 549.

(278) An, J.; Shi, J.; He, Q.; Lui, K.; Liu, Y.; Huang, Y.; Sheikh, M. S. *J. Biol. Chem.* **2012**, *287*, 7411.

(279) Darshi, M.; Mendiola, V. L.; Mackey, M. R.; Murphy, A. N.; Koller, A.; Perkins, G. A.; Ellisman, M. H.; Taylor, S. S. *J. Biol. Chem.* **2011**, *286*, 2918.

(280) D'Agostino, L.; Giordano, A. *Oncotarget* **2010**, *1*, 423.

(281) Marcus, D.; Lichtenstein, M.; Saada, A.; Lorberboum-Galski, H. *Mol. Med.* **2013**.

(282) Kobe, B.; Kajava, A. V. *Curr. Opin. Struct. Biol.* **2001**, *11*, 725.

(283) Lim, H. H.; Surana, U. *Mol. Cell* **2003**, *11*, 845.

(284) Borden, K. L.; Freemont, P. S. *Curr. Opin. Struct. Biol.* **1996**, *6*, 395.

(285) Lipkowitz, S.; Weissman, A. M. *Nat. Rev. Cancer* **2011**, *11*, 629.

(286) Short, B.; Preisinger, C.; Korner, R.; Kopajtich, R.; Byron, O.; Barr, F. A. *J. Cell Biol.* **2001**, *155*, 877.

(287) Sundaram, M.; Cook, H. W.; Byers, D. M. *Biochem. Cell Biol.* **2004**, *82*, 191.

(288) D'Souza-Schorey, C.; Chavrier, P. *Nat. Rev. Mol. Cell Biol.* **2006**, *7*, 347.

(289) Walsh, K. A. In *Methods Enzymol.*; Gertrude E. Perlmann, L. L., Ed.; Academic Press: 1970; Vol. Volume 19, p 41.

(290) Shapiro, H. M. *Practical Flow Cytometry, 4th Edition*; Wiley-Liss, 2003.

(291) Grossmann, J. *Apoptosis* **2002**, *7*, 247.

(292) Elmore, S. *Toxicol. Pathol.* **2007**, *35*, 495.

(293) Nikoletopoulou, V.; Markaki, M.; Palikaras, K.; Tavernarakis, N. *Biochim. Biophys. Acta* **2013**.

(294) Kroemer, G.; Galluzzi, L.; Vandenabeele, P.; Abrams, J.; Alnemri, E. S.; Baehrecke, E. H.; Blagosklonny, M. V.; El-Deiry, W. S.; Golstein, P.; Green, D. R.; Hengartner, M.; Knight, R. A.; Kumar, S.; Lipton, S. A.; Malorni, W.; Nunez, G.; Peter, M. E.; Tschopp, J.; Yuan, J.; Piacentini, M.; Zhivotovsky, B.; Melino, G. *Cell Death Differ.* **2009**, *16*, 3.

(295) Chae, H.-J.; Kang, J.-S.; Byun, J.-O.; Han, K.-S.; Kim, D.-U.; Oh, S.-M.; Kim, H.-M.; Chae, S.-W.; Kim, H.-R. *Pharmacol. Res.* **2000**, *42*, 373.

(296) Vermes, I.; Haanen, C.; Steffens-Nakken, H.; Reutelingsperger, C. *J. Immunol. Methods* **1995**, *184*, 39.

(297) Kolenko, V. M.; Uzzo, R. G.; Bukowski, R.; Finke, J. H. *Apoptosis* **2000**, *5*, 17.

(298) Maiuri, M. C.; Zalckvar, E.; Kimchi, A.; Kroemer, G. *Nat. Rev. Mol. Cell Biol.* **2007**, *8*, 741.

(299) Zhang, H.; Kong, X.; Kang, J.; Su, J.; Li, Y.; Zhong, J.; Sun, L. *Toxicol. Sci.* **2009**, *110*, 376.

(300) Eom, Y. W.; Kim, M. A.; Park, S. S.; Goo, M. J.; Kwon, H. J.; Sohn, S.; Kim, W. H.; Yoon, G.; Choi, K. S. *Oncogene* **2005**, *24*, 4765.

(301) Fulda, S. *Int. J. Cancer* **2009**, *124*, 511.
(302) Carre, M.; Andre, N.; Carles, G.; Borghi, H.; Brichese, L.; Briand, C.; Braguer, D. *J. Biol. Chem.* **2002**, *277*, 33664.
(303) Indrieri, A.; Conte, I.; Chesi, G.; Romano, A.; Quartararo, J.; Tate, R.; Ghezzi, D.; Zeviani, M.; Goffrini, P.; Ferrero, I.; Bovolenta, P.; Franco, B. *EMBO Mol. Med.* **2013**, *5*, 280.
(304) Manns, J.; Daubrawa, M.; Driessen, S.; Paasch, F.; Hoffmann, N.; Loffler, A.; Lauber, K.; Dieterle, A.; Alers, S.; Iftner, T.; Schulze-Osthoff, K.; Stork, B.; Wesselborg, S. *FASEB J.* **2011**, *25*, 3250.
(305) Kantari, C.; Walczak, H. *Biochim. Biophys. Acta* **2011**, *1813*, 558.
(306) Kohler, B.; Anguissola, S.; Concannon, C. G.; Rehm, M.; Kogel, D.; Prehn, J. H. *PLoS One* **2008**, *3*, e2844.
(307) Hinkson, I. V.; Elias, J. E. *Trends Cell Biol.* **2011**, *21*, 293.
(308) Kravtsova-Ivantsiv, Y.; Ciechanover, A. *J. Cell Sci.* **2012**, *125*, 539.
(309) Varshavsky, A. *Genes Cells* **1997**, *2*, 13.
(310) Guruprasad, K.; Reddy, B. V.; Pandit, M. W. *Protein Eng.* **1990**, *4*, 155.
(311) URL: http://web.expasy.org/protparam/.
(312) Goldberg, A. L.; St John, A. C. *Annu. Rev. Biochem.* **1976**, *45*, 747.
(313) Dice, J. F.; Goldberg, A. L. *Proc. Natl. Acad. Sci. U. S. A.* **1975**, *72*, 3893.
(314) Boisvert, F. M.; Ahmad, Y.; Gierlinski, M.; Charriere, F.; Lamont, D.; Scott, M.; Barton, G.; Lamond, A. I. *Mol. Cell. Proteomics* **2012**, *11*, M111 011429.
(315) Cambridge, S. B.; Gnad, F.; Nguyen, C.; Bermejo, J. L.; Kruger, M.; Mann, M. *J. Proteome Res.* **2011**, *10*, 5275.
(316) Lecker, S. H.; Goldberg, A. L.; Mitch, W. E. *J. Am. Soc. Nephrol.* **2006**, *17*, 1807.
(317) Pratt, J. M.; Petty, J.; Riba-Garcia, I.; Robertson, D. H.; Gaskell, S. J.; Oliver, S. G.; Beynon, R. J. *Mol. Cell. Proteomics* **2002**, *1*, 579.
(318) Doherty, M. K.; Hammond, D. E.; Clague, M. J.; Gaskell, S. J.; Beynon, R. J. *J. Proteome Res.* **2009**, *8*, 104.
(319) Bloom, J.; Cross, F. R. *Nat. Rev. Mol. Cell Biol.* **2007**, *8*, 149.
(320) Kimura, A.; Kato, Y.; Hirano, H. *Biochemistry* **2012**, *51*, 8856.
(321) Brooks, P.; Fuertes, G.; Murray, R. Z.; Bose, S.; Knecht, E.; Rechsteiner, M. C.; Hendil, K. B.; Tanaka, K.; Dyson, J.; Rivett, J. *Biochem. J.* **2000**, *346 Pt 1*, 155.
(322) Wojcik, C.; DeMartino, G. N. *Int. J. Biochem. Cell Biol.* **2003**, *35*, 579.
(323) Kisselev, A. F.; van der Linden, W. A.; Overkleeft, H. S. *Chem. Biol.* **2012**, *19*, 99.
(324) Han, Y. H.; Moon, H. J.; You, B. R.; Park, W. H. *Oncol. Rep.* **2009**, *22*, 215.
(325) Rastogi, N.; Mishra, D. P. *Cell Div.* **2012**, *7*, 26.
(326) Choi, C. H.; Lee, B. H.; Ahn, S. G.; Oh, S. H. *Biochem. Biophys. Res. Commun.* **2012**, *418*, 759.
(327) Aleshin, A.; Finn, R. S. *Neoplasia* **2010**, *12*, 599.
(328) Wheeler, D. L.; Iida, M.; Dunn, E. F. *Oncologist* **2009**, *14*, 667.
(329) Pichot, C. S.; Hartig, S. M.; Xia, L.; Arvanitis, C.; Monisvais, D.; Lee, F. Y.; Frost, J. A.; Corey, S. J. *Br. J. Cancer* **2009**, *101*, 38.
(330) Yao, J.; Liang, L. H.; Zhang, Y.; Ding, J.; Tian, Q.; Li, J. J.; He, X. H. *Cancer Biol. Med.* **2012**, *9*, 234.
(331) Lu, X.; An, H.; Jin, R.; Zou, M.; Guo, Y.; Su, P. F.; Liu, D.; Shyr, Y.; Yarbrough, W. G. *Oncogene* **2013**, *1*, 246.
(332) Khoronenkova, S. V.; Dianova, II; Ternette, N.; Kessler, B. M.; Parsons, J. L.; Dianov, G. L. *Mol. Cell* **2012**, *45*, 801.
(333) Heal, W. P.; Wright, M. H.; Thinon, E.; Tate, E. W. *Nat. Protoc.* **2012**, *7*, 105.
(334) Invitrogen *Avidin and Streptavidin ConjugatesAvidin and Streptavidin Conjugates*, *URL: http://www.invitrogen.com/site/us/en/home/References/Molecular-Probes-The-*

Handbook/Antibodies-Avidins-Lectins-and-Related-Products/Avidin-Streptavidin-NeutrAvidin-and-CaptAvidin-Biotin-Binding-Proteins-and-Affinity-Matrices.html [19 September 2010].

(335) Berry, A. F.; Heal, W. P.; Tarafder, A. K.; Tolmachova, T.; Baron, R. A.; Seabra, M. C.; Tate, E. W. *ChemBioChem* **2010**, *11*, 771.

(336) Volkmer-Engert, R.; Hoffmann, B.; Schneider-Mergener, J. *Tetrahedron Lett.* **1997**, *38*, 1029.

(337) Ay, B.; Volkmer, R.; Boisguerin, P. *Tetrahedron Lett.* **2007**, *48*, 361.

(338) Bray, A. M.; Maeji, N. J.; Jhingran, A. G.; Valerio, R. M. *Tetrahedron Lett.* **1991**, *32*, 6163.

(339) Brown, J. M.; Hoffmann, W. D.; Alvey, C. M.; Wood, A. R.; Verbeck, G. F.; Petros, R. A. *Anal. Biochem.* **2010**, *398*, 7.

(340) Baleux F., C. B. a. M. J. *Int. J. Pept. Protein Res.* **1986**, *28*, 22.

(341) Atherton, E.; Gait, M. J.; Sheppard, R. C.; Williams, B. J. *Bioorg. Chem.* **1979**, *8*, 351.

(342) Bray, A. M.; Maeji, N. J.; Valerio, R. M.; Campbell, R. A.; Geysen, H. M. *J. Org.Chem.* **1991**, *56*, 6659.

(343) Mahrenholz, C. C.; Tapia, V.; Stigler, R. D.; Volkmer, R. *J. Pept. Sci.* **2010**, *16*, 297.

(344) Koshland, D. E. *Bioorg. Chem.* **2002**, *30*, 211.

(345) Eisenthal, R.; Danson, M. J.; Hough, D. W. *Trends Biotechnol.* **2007**, *25*, 247.

(346) Foong, Y. M.; Fu, J.; Yao, S. Q.; Uttamchandani, M. *Curr. Opin. Chem. Biol.* **2012**, *16*, 234.

(347) Wang, J.; Uttamchandani, M.; Sun, L. P.; Yao, S. Q. *Chem. Commun.* **2006**, 717.

(348) Sun, H.; Chattopadhaya, S.; Wang, J.; Yao, S. Q. *Anal. Bioanal. Chem.* **2006**, *386*, 416.

(349) Urbina, H. D.; Debaene, F.; Jost, B.; Bole-Feysot, C.; Mason, D. E.; Kuzmic, P.; Harris, J. L.; Winssinger, N. *ChemBioChem* **2006**, *7*, 1790.

(350) Reimer, U.; Reineke, U.; Schneider-Mergener, J. *Curr. Opin. Biotechnol.* **2002**, *13*, 315.

(351) Salehi-Reyhani, A.; Kaplinsky, J.; Burgin, E.; Novakova, M.; deMello, A. J.; Templer, R. H.; Parker, P.; Neil, M. A.; Ces, O.; French, P.; Willison, K. R.; Klug, D. *Lab Chip* **2011**, *11*, 1256.

(352) Bell, A. S.; Mills, J. E.; Williams, G. P.; Brannigan, J. A.; Wilkinson, A. J.; Parkinson, T.; Leatherbarrow, R. J.; Tate, E. W.; Holder, A. A.; Smith, D. F. *PLoS Negl. Trop. Dis.* **2012**, *6*, e1625.

(353) Mali, P.; Yang, L.; Esvelt, K. M.; Aach, J.; Guell, M.; DiCarlo, J. E.; Norville, J. E.; Church, G. M. *Science* **2013**, *339*, 823.

(354) Zhang, F.; Bhat, S.; Gabelli, S. B.; Chen, X.; Miller, M. S.; Nacev, B. A.; Cheng, Y. L.; Meyers, D. J.; Tenney, K.; Shim, J. S.; Crews, P.; Amzel, L. M.; Ma, D.; Liu, J. O. *J. Med. Chem.* **2013**, *56*, 3996.

(355) Turk, B. E.; Griffith, E. C.; Wolf, S.; Biemann, K.; Chang, Y. H.; Liu, J. O. *Chem. Biol.* **1999**, *6*, 823.

(356) Moghaddas Gholami, A.; Hahne, H.; Wu, Z.; Auer, F. J.; Meng, C.; Wilhelm, M.; Kuster, B. *Cell Rep* **2013**, *4*, 609.

(357) Hearn, J. M.; Romero-Canelon, I.; Qamar, B.; Liu, Z.; Hands-Portman, I.; Sadler, P. J. *ACS Chem. Biol.* **2013**.

(358) Schenone, M.; Dancik, V.; Wagner, B. K.; Clemons, P. A. *Nat. Chem. Biol.* **2013**, *9*, 232.

(359) Moellering, R. E.; Cravatt, B. F. *Chem. Biol.* **2012**, *19*, 11.

(360) Schirle, M.; Bantscheff, M.; Kuster, B. *Chem. Biol.* **2012**, *19*, 72.

(361) Sharma, K.; Vabulas, R. M.; Macek, B.; Pinkert, S.; Cox, J.; Mann, M.; Hartl, F. U. *Mol. Cell. Proteomics* **2012**, *11*, M111 014654.

(362) Politi, K.; Pao, W. *J. Clin. Oncol.* **2011**, *29*, 2273.

(363) Davey, T. W.; Hayman, A. R. *Aust. J. Chem.* **1998**, *51*, 581.

(364) Kimmel, T.; Becker, D. *J. Org. Chem.* **1984**, *49*, 2494.

(365) Olsen, J. V.; de Godoy, L. M.; Li, G.; Macek, B.; Mortensen, P.; Pesch, R.; Makarov, A.; Lange, O.; Horning, S.; Mann, M. *Mol. Cell. Proteomics* **2005**, *4*, 2010.

(366) Keller, A.; Nesvizhskii, A. I.; Kolker, E.; Aebersold, R. *Anal. Chem.* **2002**, *74*, 5383.

(367) Nesvizhskii, A. I.; Keller, A.; Kolker, E.; Aebersold, R. *Anal. Chem.* **2003**, *75*, 4646.

(368) Eberl, H. C.; Spruijt, C. G.; Kelstrup, C. D.; Vermeulen, M.; Mann, M. *Mol. Cell* **2013**, *49*, 368.

(369) Silva, J. C.; Gorenstein, M. V.; Li, G. Z.; Vissers, J. P.; Geromanos, S. J. *Mol. Cell. Proteomics* **2006**, *5*, 144.

(370) Jackson, P.; Baltimore, D. *EMBO J.* **1989**, *8*, 449.

(371) Streb, J. W.; Kitchen, C. M.; Gelman, I. H.; Miano, J. M. *J. Biol. Chem.* **2004**, *279*, 56014.

(372) Fraser, I. D. C.; Tavalin, S. J.; Lester, L. B.; Langeberg, L. K.; Westphal, A. M.; Dean, R. A.; Marrion, N. V.; Scott, J. D. *EMBO J.* **1998**, *17*, 2261.

(373) Kahn, R. A.; Goddard, C.; Newkirk, M. *J. Biol. Chem.* **1988**, *263*, 8282.

(374) D'Souza-Schorey, C.; Stahl, P. D. *Exp. Cell Res.* **1995**, *221*, 153.

(375) Lin, C.-Y.; Li, C.-C.; Huang, P.-H.; Lee, F.-J. S. *J. Cell Sci.* **2002**, *115*, 4433.

(376) Jiang, M.; Gao, Y.; Yang, T.; Zhu, X.; Chen, J. *FEBS Lett.* **2009**, *583*, 2171.

(377) Yorikawa, C.; Shibata, H.; Waguri, S.; Hatta, K.; Horii, M.; Katoh, K.; Kobayashi, T.; Uchiyama, Y.; Maki, M. *Biochem. J.* **2005**, *387*, 17.

(378) Stabler, S. M.; Ostrowski, L. L.; Janicki, S. M.; Monteiro, M. J. *J. Cell Biol.* **1999**, *145*, 1277.

(379) Borgese, N.; Aggujaro, D.; Carrera, P.; Pietrini, G.; Bassetti, M. *J. Cell Biol.* **1996**, *135*, 1501.

(380) Beauchamp, E.; Goenaga, D.; Le Bloc'h, J.; Catheline, D.; Legrand, P.; Rioux, V. *Biochimie* **2007**, *89*, 1553.

(381) Schwertassek, U.; Buckley, D. A.; Xu, C.-F.; Lindsay, A. J.; McCaffrey, M. W.; Neubert, T. A.; Tonks, N. K. *FEBS J.* **2010**, *277*, 2463.

(382) Han, Y.; Eppinger, E.; Schuster, I. G.; Weigand, L. U.; Liang, X.; Kremmer, E.; Peschel, C.; Krackhardt, A. M. *J. Biol. Chem.* **2009**, *284*, 33409.

(383) Xu, H.; Lee, K. W.; Goldfarb, M. *J. Biol. Chem.* **1998**, *273*, 17987.

(384) Peters, D. J.; McGrew, B. R.; Perron, D. C.; Liptak, L. M.; Laudano, A. P. *Oncogene* **1990**, *5*, 1313.

(385) Mumby, S. M.; Heukeroth, R. O.; Gordon, J. I.; Gilman, A. G. *Proc. Natl. Acad. Sci. U. S. A.* **1990**, *87*, 728.

(386) Spilker, C.; Richter, K.; Smalla, K. H.; Manahan-Vaughan, D.; Gundelfinger, E. D.; Braunewell, K. H. *Neuroscience* **2000**, *96*, 121.

(387) Landlinger, C.; Salzer, U.; Prohaska, R. *Biochim. Biophys. Acta* **2006**, *1758*, 1759.

(388) Kovářová, M.; Tolar, P.; Arudchandran, R.; Dráberová, L.; Rivera, J.; Dráber, P. *Mol. Cell. Biol.* **2001**, *21*, 8318.

(389) Kim, G.; Cole, N. B.; Lim, J. C.; Zhao, H.; Levine, R. L. *J. Biol. Chem.* **2010**, *285*, 18085.

(390) Wright, K. J.; Baye, L. M.; Olivier-Mason, A.; Mukhopadhyay, S.; Sang, L.; Kwong, M.; Wang, W.; Pretorius, P. R.; Sheffield, V. C.; Sengupta, P.; Slusarski, D. C.; Jackson, P. K. *Genes Dev.* **2011**, *25*, 2347.

(391) Chida, T.; Ando, M.; Matsuki, T.; Masu, Y.; Nagaura, Y.; Takano-Yamamoto, T.; Tamura, S.; Kobayashi, T. *Biochem. J.* **2013**, *449*, 741.

(392) Aitken, A.; Cohen, P.; Santikarn, S.; Williams, D. H.; Calder, A. G.; Smith, A.; Klee, C. B. *FEBS Lett.* **1982**, *150*, 314.

(393) Mitchelhill, K. I.; Michell, B. J.; House, C. M.; Stapleton, D.; Dyck, J.; Gamble, J.; Ullrich, C.; Witters, L. A.; Kemp, B. E. *J. Biol. Chem.* **1997**, *272*, 24475.

(394) Oakhill, J. S.; Chen, Z. P.; Scott, J. W.; Steel, R.; Castelli, L. A.; Ling, N.; Macaulay, S. L.; Kemp, B. E. *Proc. Natl. Acad. Sci. U. S. A.* **2010**, *107*, 19237.

(395) Saeki, K.; Miura, Y.; Aki, D.; Kurosaki, T.; Yoshimura, A. *EMBO J.* **2003**, *22*, 3015.

(396) Sullivan, A.; Uff, C. R.; Isacke, C. M.; Thorne, R. F. *Exp. Cell Res.* **2003**, *284*, 222.

(397) Rowe, D. C.; McGettrick, A. F.; Latz, E.; Monks, B. G.; Gay, N. J.; Yamamoto, M.; Akira, S.; O'Neill, L. A.; Fitzgerald, K. A.; Golenbock, D. T. *Proc. Natl. Acad. Sci. U. S. A.* **2006**, *103*, 6299.

(398) Martin, D. D. O.; Vilas, G. L.; Prescher, J. A.; Rajaiah, G.; Falck, J. R.; Bertozzi, C. R.; Berthiaume, L. G. *FASEB J.* **2008**, *22*, 797.

(399) Hoxhaj, G.; Najafov, A.; Toth, R.; Campbell, D. G.; Prescott, A. R.; MacKintosh, C. *J. Cell Sci.* **2012**, *125*, 4662.

(400) Lee, F.-J. S.; Huang, C.-F.; Yu, W.-L.; Buu, L.-M.; Lin, C.-Y.; Huang, M.-C.; Moss, J.; Vaughan, M. *J. Biol. Chem.* **1997**, *272*, 30998.

(401) Barroso, M. R.; Bernd, K. K.; DeWitt, N. D.; Chang, A.; Mills, K.; Sztul, E. S. *J. Biol. Chem.* **1996**, *271*, 10183.

(402) Dimitrov, A.; Paupe, V.; Gueudry, C.; Sibarita, J. B.; Raposo, G.; Vielemeyer, O.; Gilbert, T.; Csaba, Z.; Attie-Bitach, T.; Cormier-Daire, V.; Gressens, P.; Rustin, P.; Perez, F.; El Ghouzzi, V. *Hum. Mol. Genet.* **2009**, *18*, 440.

(403) Barr, F. A.; Puype, M.; Vandekerckhove, J.; Warren, G. *Cell* **1997**, *91*, 253.

(404) Walker, J. E.; Arizmendi, J. M.; Dupuis, A.; Fearnley, I. M.; Finel, M.; Medd, S. M.; Pilkington, S. J.; Runswick, M. J.; Skehel, J. M. *J. Mol. Biol.* **1992**, *226*, 1051.

(405) Panaretou, C.; Domin, J.; Cockcroft, S.; Waterfield, M. D. *J. Biol. Chem.* **1997**, *272*, 2477.

(406) Utsumi, T.; Sakurai, N.; Nakano, K.; Ishisaka, R. *FEBS Lett.* **2003**, *539*, 37.

(407) Vilas, G. L.; Corvi, M. M.; Plummer, G. J.; Seime, A. M.; Lambkin, G. R.; Berthiaume, L. G. *Proc. Natl. Acad. Sci. U. S. A.* **2006**, *103*, 6542.

Appendix A: List of electronic files

File name	File type(s)	Section	Description
Non quantitative_ AzKTB	Scaffold	4.2	HeLa metabolic labelling with YnC12 or DMSO as a control (AzKTB, no quantification).
Gel based analysis	Scaffold	4.3	HeLa metabolic labelling with YnC12 (AzTB, no quantification). The gel was cut in 7 portions.
Label free quantification	Excel	4.4	HeLa metabolic labelling with YnC12 or Myr as a control (AzTB, 4 biological replicates, label-free quantification).
Heavy label incorporation	Excel + Scaffold	4.5	Whole cell lysate from HeLa grown in the heavy media (R10K8) were analysed by LC-MS/MS to determine the average percentage of heavy label incorporation in proteins.
Double SILAC inhibitor	Excel	4.5	HeLa metabolic labelling with YnC12, in the presence or not of IMP366 (5 μM (AzTB, biological triplicate, spike-in SILAC quantification).
Spike-in inhibitor	Excel	4.6	HeLa metabolic labelling with YnC12, in the presence IMP366 (0-5 μM, 6 concentrations) (AzTB, 5 replicates, spike-in (heavy) SILAC quantification, Lysate:spike-in 2:1).
Base	Excel	4.7.1	HeLa metabolic labelling with YnC12, followed by base treatment with NaOH (AzTB, two biological replicates, spike-in SILAC quantification).
Turnover	Excel	5.3	Study of the turnover rate for the 74 NMT substrates identified with high confidence in Chapter 4.

Website address to download the Scaffold viewer to open proteomics data files: http://www.proteomesoftware.com/Proteome_software_prod_Scaffold.html

Appendix B: Sequences of ΔHsNMT1 and ΔHsNMT2

Sequence alignments of ΔHsNMT1 and ΔHsNMT2 using the program ClustalOmega (http://www.ebi.ac.uk/Tools/msa/clustalo/).
The consensus is le following: * identical residues; : conserved substitutions; . semi-conserved substitutions; no sign:no match.

ΔHsNMT1 and ΔHsNMT2 were stored in the following buffer: 125 mM NaCl, 10 mM Tris-HCl pH 8.5, 1 mM EGTA, 1 mM EDTA, 25% glycerol.

```
ΔHsNMT1          MGSSHHHHHHSSGLEVLFQGPHMEEASKRSYQFWDTQPVPKLGEVVNTHGPVEPDKDNIR
ΔHsNMT2          MGSSHHHHHHSSGLEVLFQGPHMDEAAKHRYQFWDTQPVPKLDEVITSHGAIEPDKDNVR
                 ************************:**:*: ************ **:.:** :******:*

ΔHsNMT1          QEPYTLPQGFTWDALDLGDRGVLKELYTLLNENYVEDDDNMFRFDYSPEFLLWALRPPGW
ΔHsNMT2          QEPYSLPQGFMWDTLDLSDAEVLKELYTLLNENYVEDDDNMFRFDYSPEFLLWALRPPGW
                 ****:***** **:***.*  ************************************

ΔHsNMT1          LPQWHCGVRVVSSRKLVGFISAIPANIHIYDTEKKMVEINFLCVHKKLRSKRVAPVLIRE
ΔHsNMT2          LLQWHCGVRVSSNKKLVGFISAIPANIRIYDSVKKMVEINFLCVHKKLRSKRVAPVLIRE
                 * ******** *.:**************:***: **************************

ΔHsNMT1          ITRRVHLEGIFQAVYTAGVVLPKPVGTCRYWHRSLNPRKLIEVKFSHLSRNMTMQRTMKL
ΔHsNMT2          ITRRVNLEGIFQAVYTAGVVLPKPIATCRYWHRSLNPKKLVEVKFSHLSRNMTLQRTMKL
                 *****.******************:.***********:**:************:******

ΔHsNMT1          YRLPETPKTAGLRPMETKDIPVVHQLLTRYLKQFHLTPVMSQEEVEHWFYPQENIIDTFV
ΔHsNMT2          YRLPDVTKTSGLRPMEPKDIKSVRELINTYLKQFHLAPVMDEEEVAHWFLPREHIIDTFV
                 ****:. **:****** ***  *::*:. *******:***.:*** *** *:*.******

ΔHsNMT1          VENANGEVTDFLSFYTLPSTIMNHPTHKSLKAAYSFYNVHTQTPLLDLMSDALVLAKMKG
ΔHsNMT2          VESPNGKLTDFLSFYTLPSTVMHHPAHKSLKAAYSFYNIHTETPLLDLMSDALILAKSKG
                 **. **::************:*.**:************:**:***********:*** **

ΔHsNMT1          FDVFNALDLMENKTFLEKLKFGIGDGNLQYYLYNWKCPSMGAEKVGLVLQ
ΔHsNMT2          FDVFNALDLMENKTFLEKLKFGIGDGNLQYYLYNWRCPGTDSEKVGLVLQ
                 ***********************************:**.  :********
```

Appendix C: TC_{50} inhibitor IMP-653/654/655

Figure C1: YnC12 tagging assay and TC_{50} evaluation for inhibitors IMP653/654/655 (Section 3.3.2).

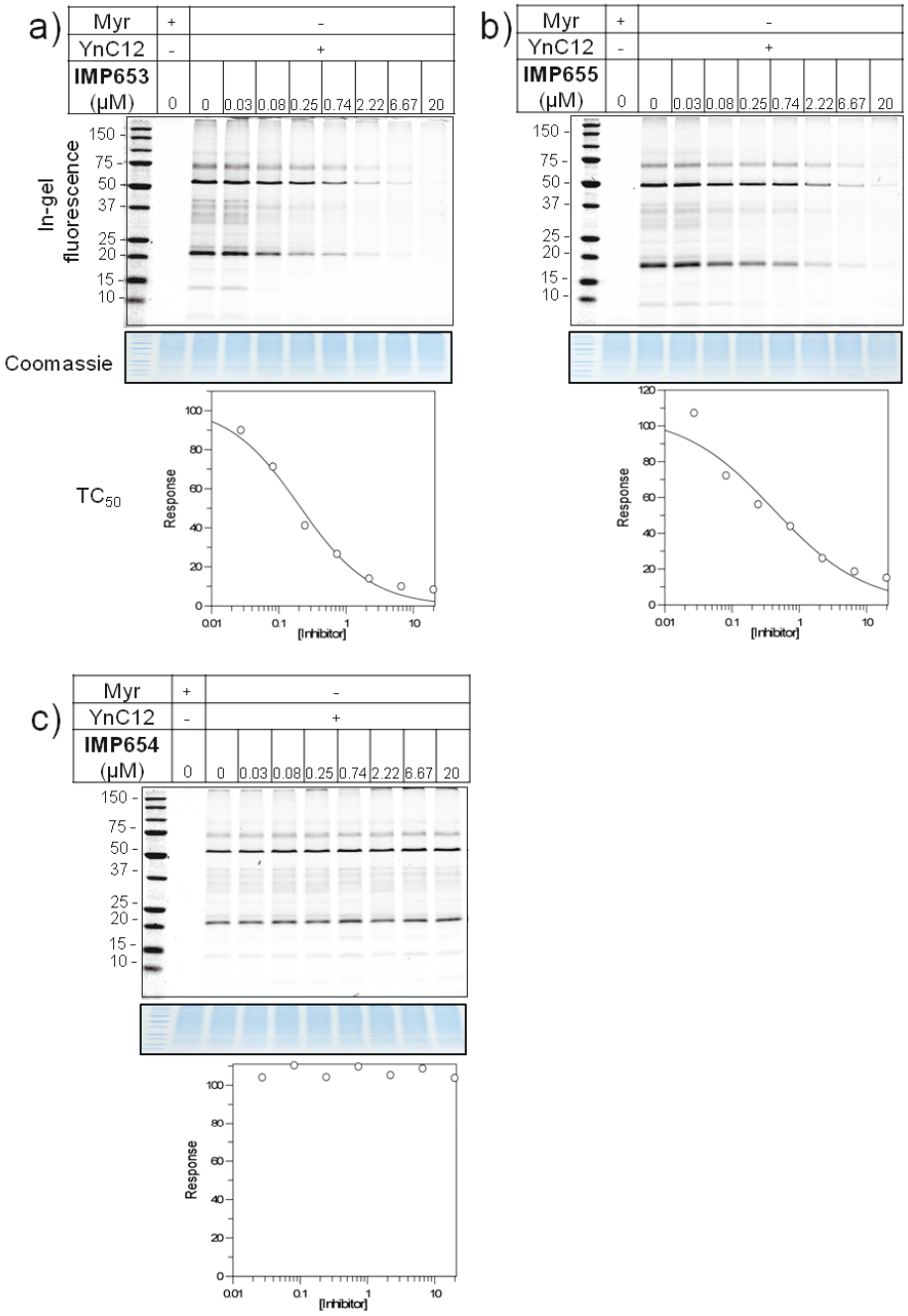

Appendix D: YnC12 labelling assay - non specific HsNMT inhibitor

- ✓ **Figure D1:** YnC12 tagging assay (Section 3.4.1).
- ✓ **Figure D2:** YnC12 tagging assay (Section 3.4.2).

Figure D1: YnC12 tagging assay (Section 3.4.1).

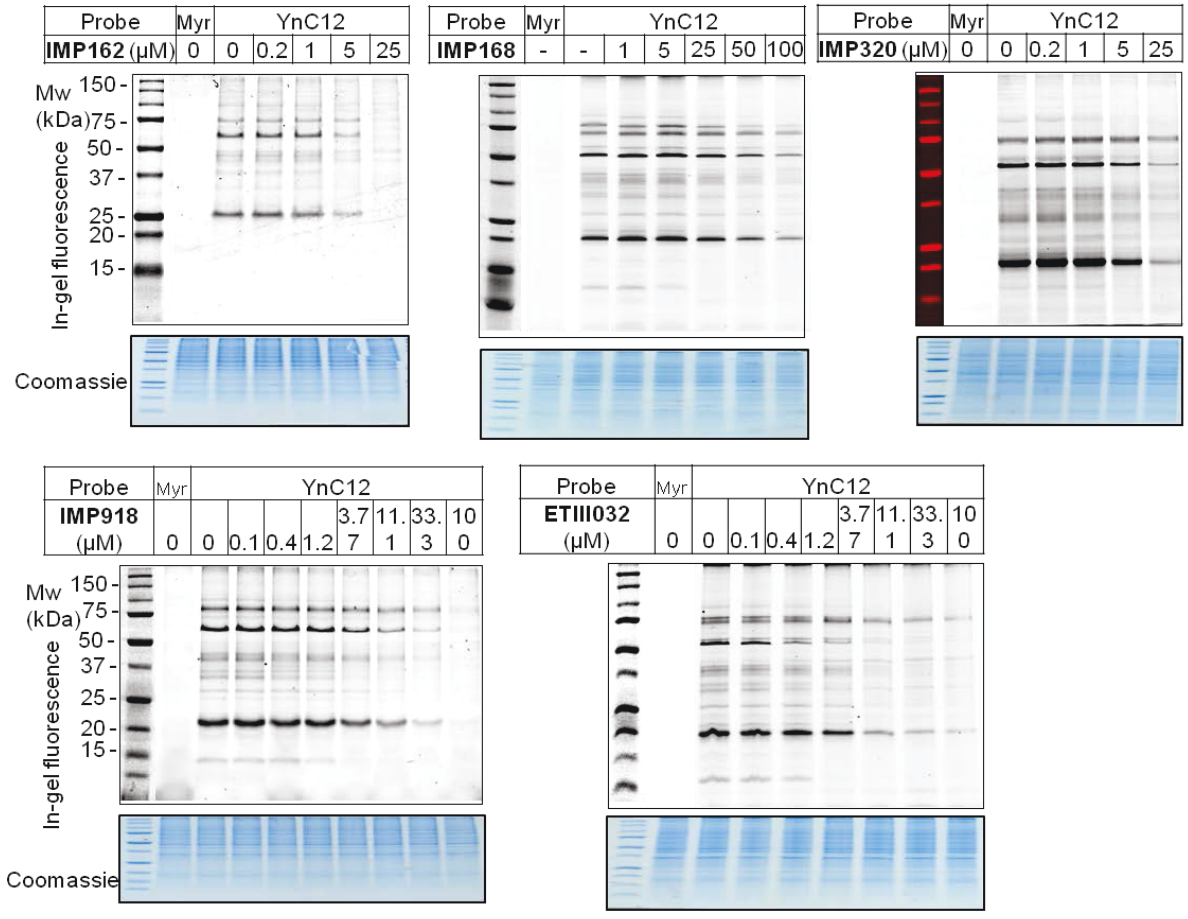

Figure D2: YnC12 tagging assay (Section 3.4.2).

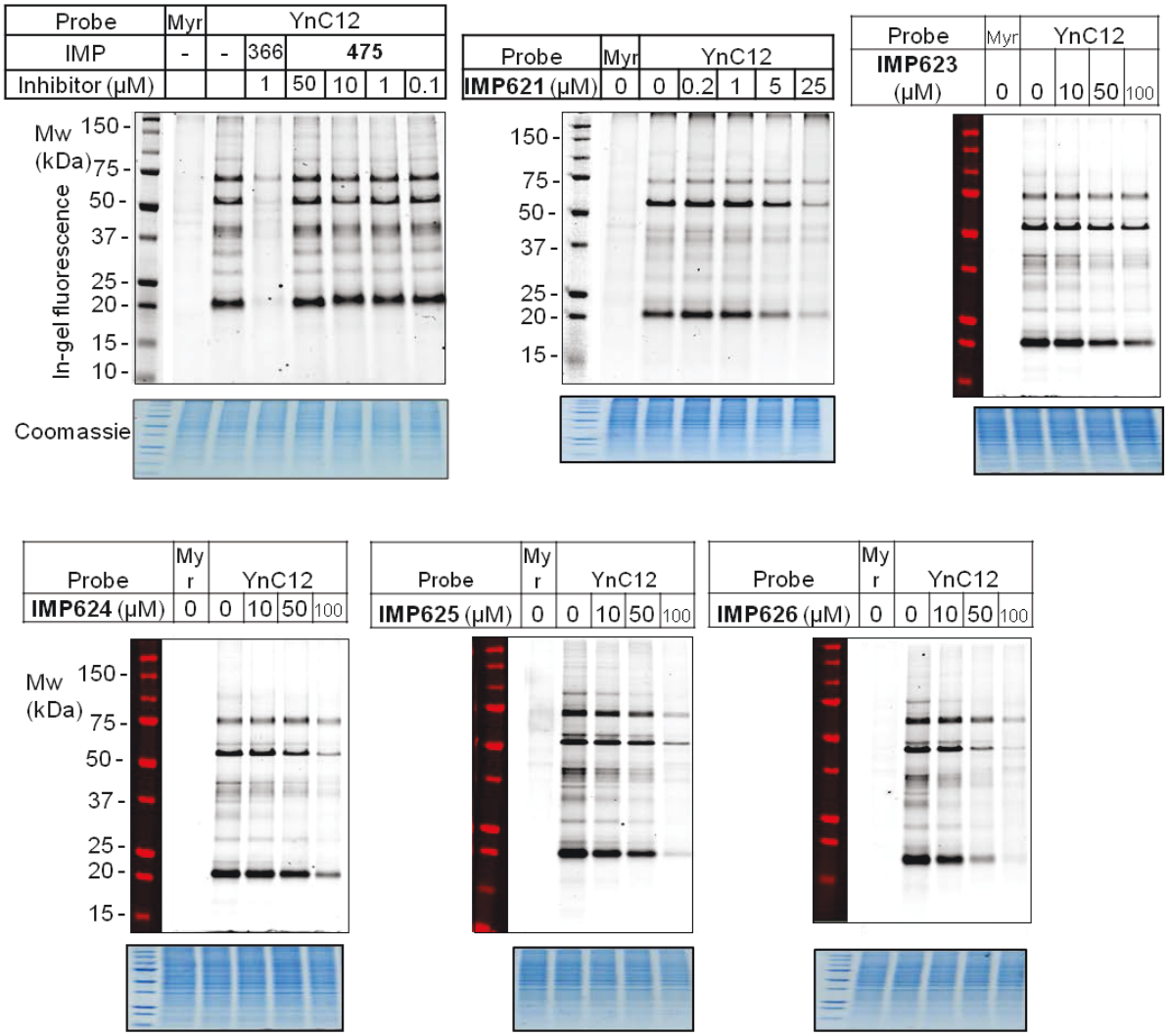

Appendix E: Best in-house HsNMT inhibitors

- ✓ **Figure E1:** CPM assay for the best in-house HsNMT inhibitors (Section 3.4.3).
- ✓ **Figure E2:** MTS assay results for the best in-house HsNMT inhibitors (Section 3.4.3).
- ✓ **Figure E3:** YnC12 tagging experiment for the best in-house HsNMT inhibitors (Section 3.4.3).

Figure E1: CPM assay for the best in-house HsNMT inhibitors.

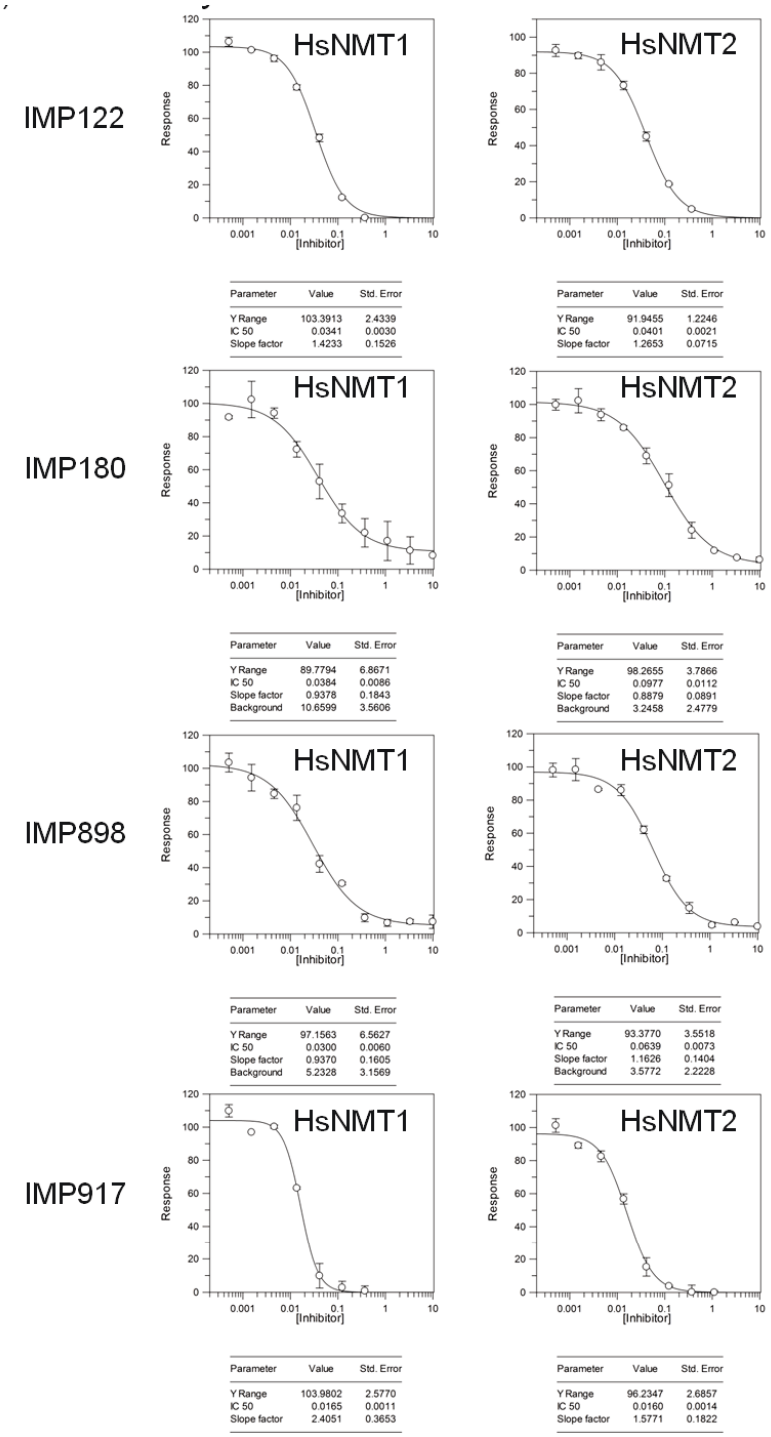

Figure E2: MTS assay results for the best in-house HsNMT inhibitors.

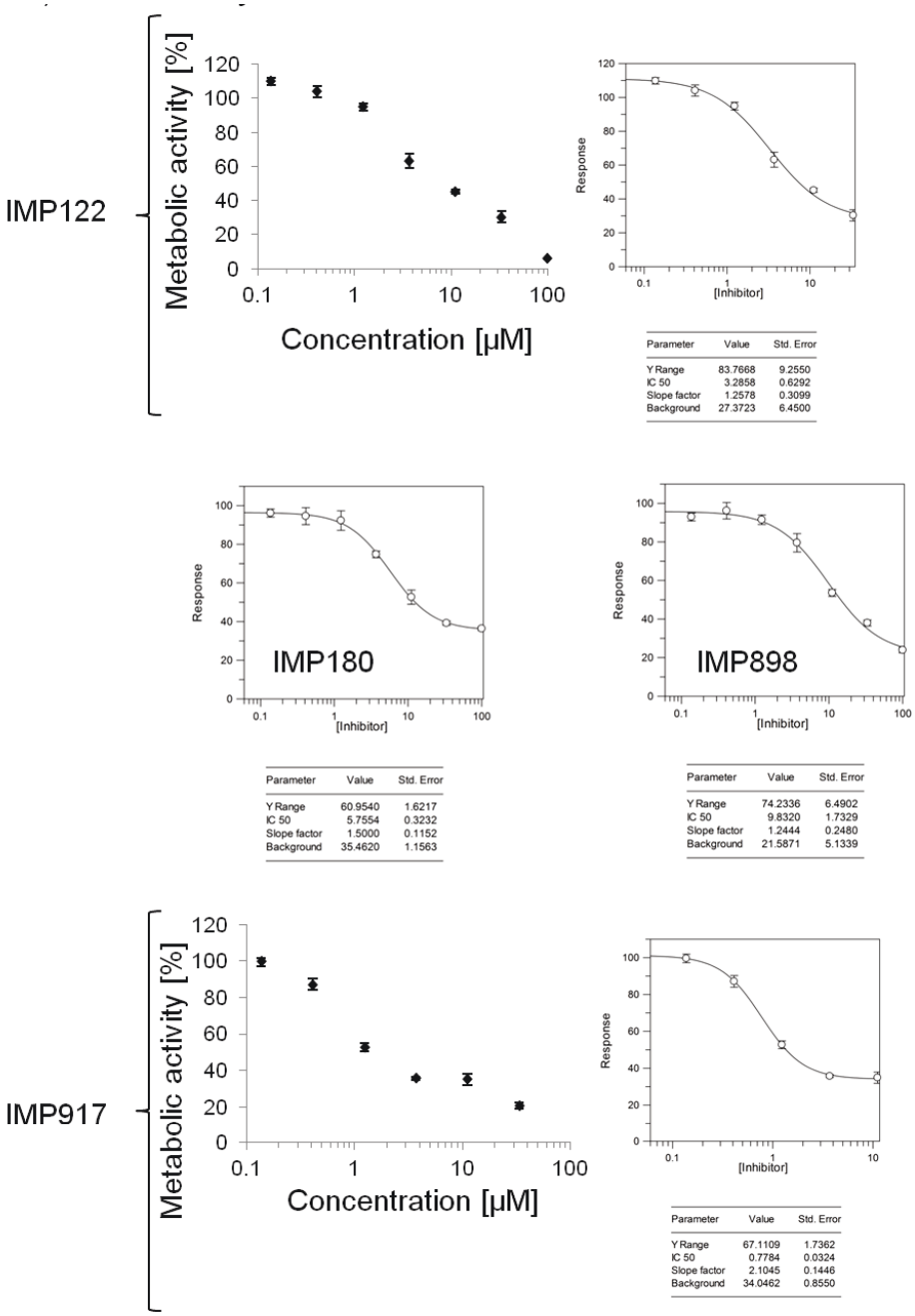

Figure E3: YnC12 tagging experiment for the best in-house HsNMT inhibitors

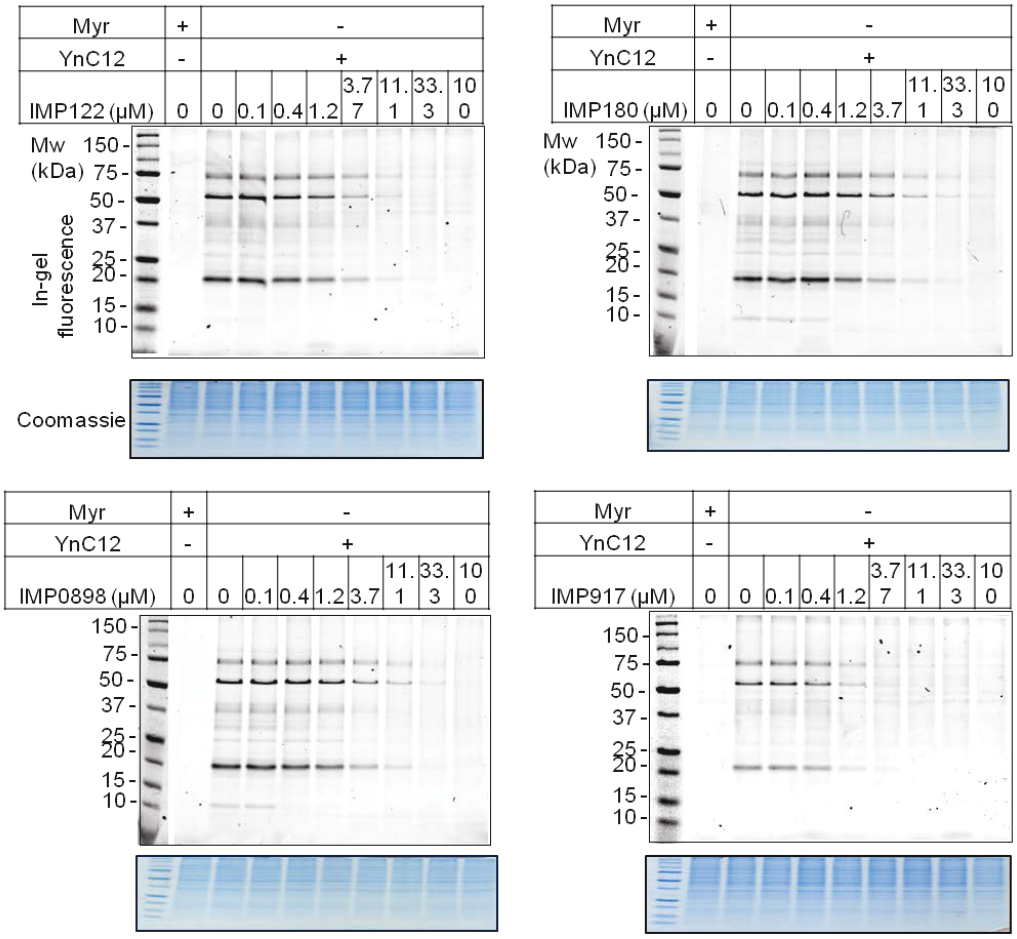

Appendix F: Previous studies of co-translationally *N*-myristoylated proteins

Table F1: Previous studies of co-translationally *N*-myristoylated proteins expressed in HeLa cells. Proteins with an N-terminal MG motif were experimentally shown to be *N*-myristoylated using a cell-free system or *E. coli* expression system (CF), a non native protein in eukaryotic cells (NN) or the native proteins in eukaryotic cells (Nat). Proteins identified by chemical proteomics (CP) are also reported.[173,224] Only proteins expressed in HeLa are reported in this table.[207] A column indicates if the proteins have been predicted to be *N*-myristoylated by online predictors (Myr predictor (MP): R= Reliable; T= twilight, N= No. Myristoylator (Myrist): H= high probability; M= medium probability; L= low probability; N= not myristoylated). A column shows if the protein is palmitoylated (+: found in 1 study, ++: found in 2 studies; +++: found in 3 studies; ++++: found in 4 studies;[173] u: reported as palmitoylated in the UniProtKB/Swiss-Prot database). A column indicates if the proteins have been detected in non quantitative proteomics experiments in Jurkat T-cell.[173,224]

Method	Protein name	Gene name	Protein IDs	Ref	Palm	MP	Myrist	CP
Nat	Annexin XIII	ANXA13	P27216	[228]		R	H	
	Brain acid soluble protein 1	BASP1	P80723	[161]		R	H	
	Golgi-associated plant pathogenesis-related protein 1	GLIPR2	Q9H4G4	[229]		R	H	
	MARCKS	MARCKS	P29966	[105]		R	H	
	cAMP dependent protein kinase alpha subunit	PRKACA	P17612	[209]		R	H	+[173]
	Tyrosine protein kinase Src	SRC	P12931	[204]	+	R	H	
NN	ABL1	ABL1	P00519	[370]		T	N	
	A-kinase anchor protein 12	AKAP12	Q02952	[371]		R	H	
	A-kinase anchor protein 7	AKAP7	O43687	[372]	u	R	H	
	ADP ribosylation factor 1	ARF1	P84077	[373]	++	T	H	+[173,224]
	ADP ribosylation factor 6	ARF6	P62330	[374]		R	H	
	ADP-ribosylation factor-like 5B	ARL5B	Q96KC2	[375]		N	M	
	Cyclin-Y	CCNY	Q8ND76	[376]	+++	R	H	
	Coiled-coil-helix-coiled-coil-helix domain-containing protein 3, mitochondrial	CHCHD3	Q9NX63	[279]	+	R	H	+[173,224]
	Charged multivesicular body protein 6	CHMP6	Q96FZ7	[377]		N	H	+[173]
	Calcium and integrin-binding protein 1	CIB1	Q99828	[378]		R	H	
	NADH cytochrome b5 reductase 3	CYB5R3	P00387	[379]	++	R	H	+[173]
	Sphingolipid delta(4)-desaturase DES1	DEGS1	O15121	[380]		T	H	
	Dual specificity protein phosphatase 22	DUSP22	Q9NRW4	[381]		N	H	
	Formin-like protein 1	FMNL1	O95466	[382]		T	N	
	Fibroblast growth factor receptor substrate 2 FRS2	FRS2	Q8WU20	[383]		R	H	
	Fibroblast growth factor receptor substrate 3 FRS3	FRS3	O43559	[383]		R	H	
	Tyrosine protein kinase Fyn	FYN	P06241	[384]	u; ++	R	H	

	Guanine nucleotide-binding protein G(i) subunit alpha-1	GNAI1	P63096	[385]	u; ++	R	H	
	Guanine nucleotide-binding protein G(i) subunit alpha-2	GNAI2	P04899	[385]	u; +++ +	R	H	+[173]
	Guanine nucleotide-binding protein G(k) subunit alpha	GNAI3	P08754	[385]	u; +++ +	R	H	+[173,224]
	Guanine nucleotide-binding protein G(o) subunit alpha	GNAO1	P09471	[385]	u; +++	R	H	+[173]
	Guanine nucleotide-binding protein G(z) subunit alpha	GNAZ	P19086	[385]	u; +	R	H	
	Neuron-specific calcium-binding protein hippocalcin	HPCA	P84074	[160]		R	H	
	Hippocalcin-like protein 1	HPCAL1	P37235	[386]		R	H	
	LanC-like protein 2	LANCL2	Q9NS86	[387]		N	H	
	Tyrosine protein kinase Lyn	LYN	P07948	[388]	u; +	R	H	
	Mitochondrial peptide methionine sulfoxide reductase	MSRA	Q9UJ68	[389]		R	H	
	Neuronal calcium sensor 1	NCS1	P62166	[160]		R	H	
	Nephrocystin-3	NPHP3	Q7Z494	[390]		T	H	
	cGMP-dependent 3',5'-cyclic phosphodiesterase	PDE2A	O00408	[219]	u	N	N	
	Protein phosphatase 1A	PPM1A	P35813	[391]		N	H	
	Protein phosphatase 1B	PPM1B	O75688	[391]		N	M	
	Calcineurin B type 1	PPP3R1	P63098	[392]		R	H	
	5'-AMP-activated protein kinase subunit beta-1	PRKAB1	Q9Y478	[393]		N	N	
	5'-AMP-activated protein kinase subunit beta-2	PRKAB2	O43741	[394]		N	M	
	26S protease regulatory subunit 4	PSMC1	P62191	[208]	++	R	H	+[173,224]
	Raftlin	RFTN1	Q14699	[395]	u	N	H	
	Protein-associating with the carboxyl-terminal domain of ezrin (PACE-1)	SCYL3	Q8IZE3	[396]		R	H	
	TIR domain-containing adapter molecule 2	TICAM2	Q86XR7	[397]		R	M	
	Tyrosine protein kinase Yes	YES1	P07946	[398]	u; ++	R	H	
	E3 ubiquitin-protein ligase ZNRF2	ZNRF2	Q8NHG8	[399]		R	M	
CF	Apoptosis-inducing factor 2	AIFM2	Q9BRQ8	[230]		R	H	
	Ankyrin repeat and IBR domain-containing protein 1	ANKIB1	Q9P2G1	[230]		R	H	
	ADP ribosylation factor-like protein 1	ARL1	P40616	[400]		R	H	
	BTB/POZ domain-containing protein 7	BTBD7	Q9P203	[230]		R	M	
	Calcineurin B homologous protein 1	CHP1	Q99653	[401]		R	H	
	Calcineurin B homologous protein 3	CHP3	Q96BS2	[231]		R	H	
	Dixin	DIXDC1	Q155Q3	[230]		T	N	
	Dymeclin	DYM	Q7RTS9	[402]		R	H	
	Formin-like protein 2	FMNL2	Q96PY5	[230]		T	H	
	Formin-like protein 3 (FMNL3)	FMNL3	Q8IVF7	[230]		N	M	
	Golgi reassembly-stacking protein 1 (GRASP65)	GORASP1	Q9BQQ3	[403]		R	H	
	Uncharacterized protein KIAA1522	KIAA1522	Q9P206	[230]		N	H	
	TLD domain-containing protein KIAA1609	KIAA1609	Q6P9B6	[230]		T	H	

	Protein Lunapark	LNP	Q9C0E8	230		T	H	
	E3 Ubiquitin-protein ligase MGRN1	MGRN1	O60291	230		R	H	
	NADH dehydrogenase [ubiquinone] 1 beta subcomplex subunit 7	NDUFB7	P17568	404		N	L	
	Phosphoinositide 3-kinase regulatory subunit 4 (PIK3R4)	PIK3R4	Q99570	405		T	H	
	RING finger protein 11	RNF11	Q9Y3C5	230		N	M	
	Serine incorporator 1	SERINC1	Q9NRX5	230		N	N	
	Tescalin	TESC	Q96BS2	231		R	H	
	Zinc finger ZZ-type and EF-hand domain-containing protein 1	ZZEF1	O43149	230		R	H	
CP	ADP ribosylation factor 4	ARF4	P18085	173,224	+	R	H	+
	ADP ribosylation factor 5	ARF5	P84085	173,224	+	R	H	+
	CD81 antigen	CD81	P60033	173	+++	N	N	+
	CD82 antigen	CD82	P27701	173	+	N	N	+
	ATP-dependent RNA helicase A	DHX9	Q08211	173	+	N	N	+
	Elongation factor 1-alpha 1	EEF1A1	P68104	173	++	N	N	+
	Protein FAM49b	FAM49B	Q9NUQ9	173,224		N	M	+
	Glyceraldehyde-3-phosphate dehydrogenase	GAPDH	P04406	173	+++	N	M	+
	Golgi reassembly-stacking protein 2	GORASP2	Q9H8Y8	224	u	R	H	+
	High mobility group protein B1	HMGB1	P09429	173	+	N	N	+
	Cation-independent mannose-6-phosphate receptor	IGF2R	P11717	173	++	N	N	+
	Ragulator complex protein LAMTOR1	LAMTOR1	Q6IAA8	173		T	H	+
	MARCKS related protein	MARCKSL1	P49006	173,224	+	R	H	+
	Protein phosphatase 1G	PPM1G	O15355	173,224	+	R	M	+
	60S ribosomal protein L10	RPL10	P27635	173	++	N	N	+
	40S ribosomal protein S8	RPS8	P62241	173	+	N	N	+

Appendix G: Previous studies of post-translationally *N*-myristoylated proteins

Table G1: Previously reported post-translationally *N*-myristoylated proteins. Proteins were shown to be post0translationally myristoylated at a native (Nat) or non native (NN) level in eukaryotic cells. A column indicates if the new N-terminal sequences have been predicted to be *N*-myristoylated by online predictors: Myr predictor: R= Reliable; T= twilight, N= No. Myristoylator: H= high probability; M= medium probability; L= low probability; N= not myristoylated). A column indicates if the protein is palmitoylated (+: found in 1 study, ++: found in 2 studies; +++: found in 3 studies; ++++: found in 4 studies;[173] u: reported as palmitoylated in the UniProtKB/Swiss-Prot database).

Method	Protein name	Gene name	Protein IDs	Reference	New N-terminal sequence	Cleavage site	MP	Myrist
Nat	BH3-interacting domain death agonist	BID	P55957	[8]	GNRSSHSRLGRIEADSESQEDIIRNIARHL	G60	R	H
NN	Actin, cytoplasmic 1 (β-actin)	ACTB	P60709	[406]	GQVITIGNERFRCPEALFQPSFLGMESCGI	G245	T	N
	Cell division control protein 6 homolog	CDC6	Q99741	[90]	GNRMTLSQEGAQDSFPLQQKILVCSLMLLI	G443	R	H
	Gelsolin	GSN	P06396	[406]	GLGLSYLSSHIANVERVPFDAATLHTSTAM	G404	R	M
	Huntingtin	HTT	P42858	[90]	GTQASSPISDSSQTTTEGPDSAVTPSDSSE	G551	R	H
	Microtubule-actin cross-linking factor 1, isoforms 1/2/3/5	MACF1	Q9UPN3	[90]	GSDASQLLHQAEVAQQEFLEVKQRVNSGCV	G5087	R	H
	Induced myeloid leukemia cell differentiation protein	MCL1	Q07820	[90]	GSLPSTPPPAEEEEDELYRQSLEIISRYLR	G158	R	H
	p21-activated protein kinase-2	PAK2	Q13177	[407]	GAAKSLDKQKKKTKMTDEEIMEKLRTIVSI	G213	T	H
	YTH domain family protein 2	YTHDF2	Q9Y5A9	[90]	GNGVGQSQAGSGSTPSEPHPVLEKLRSINN	G367	R	M

Appendix H: Proteomics data

- ✓ **Figure H1:** Example of the sequence coverage and two assigned spectra (MS/MS) for the protein MARCKS for the proteomics experiment presented in Section 4.2.
- ✓ **Table H1:** List of putative *N*-myristoylated proteins identified in Section 4.2.1. (non quantitative proteomic analysis with AzKTB).
- ✓ **Table H2:** List of modified peptides identified with AzKTB (Section 4.2.2).
- ✓ **Table H3:** Gel-based analysis. List of putative NMT substrates identified in the non-quantitative gel-based proteomics experiment. (Section 4.3).
- ✓ **Table H4:** Label-free quantification (LFQ) of proteins enriched in the YnC12 treated samples compared to sample treated with myristic acid (Section 4.4.).
- ✓ **Table H5:** Double SILAC +/- IMP366 (5 µM) (Section 4.5.).
- ✓ **Table H6:** Spike-in SILAC with inhibitor IMP366 (High confidence NMT substrates) (Section 4.6).
- ✓ **Table H7:** Spike-in SILAC with inhibitor IMP366 (Low confidence NMT substrates) (Section 4.6).
- ✓ **Table H8:** Spike-in SILAC with inhibitor IMP366 (Protein with no MG motif sensitive to the NMT inhibitor IMP366) (Section 4.6).
- ✓ **Table H9:** Base-treatment (Section 4.7).
- ✓ **Table H10:** List of NMT substrates identified with high confidence in the current study (Section 4.8).

Figure H1: Example of the sequence coverage and two assigned spectra (MS/MS) for the protein MARCKS for the proteomics experiment presented in Section 4.2. a) Example of the sequence coverage and peptides identified for MARCKS resulting from YnC12 tagging of the N-terminus of MARCKS following capture with AzKTB and enrichment by pull down, followed by on-bead digestion with trypsin. Identified peptides are highlighted in yellow. Modified residues (with AzKTB) are highlighted in green. **b)** Example of MS/MS spectrum for peptide from the sequence (K)AAEEPSKVEEK(K), with assigned peaks. **c)** Example of MS/MS spectrum of a peptide modified with AzKTB, with the sequence (M)gAQFSK(T). All figures are directly exported from Scaffold.

✓ Sequence coverage for MARCKS (59%)

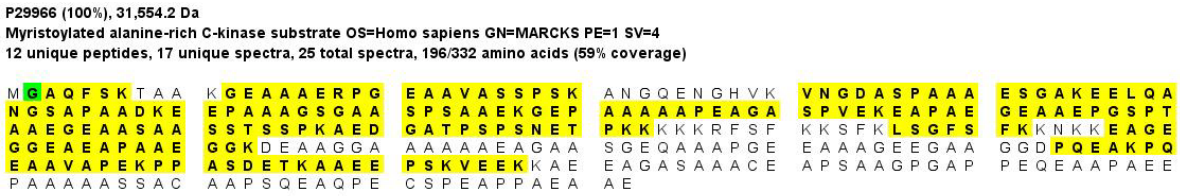

✓ Spectrum for peptide: (K)AAEEPSKVEEK(K)

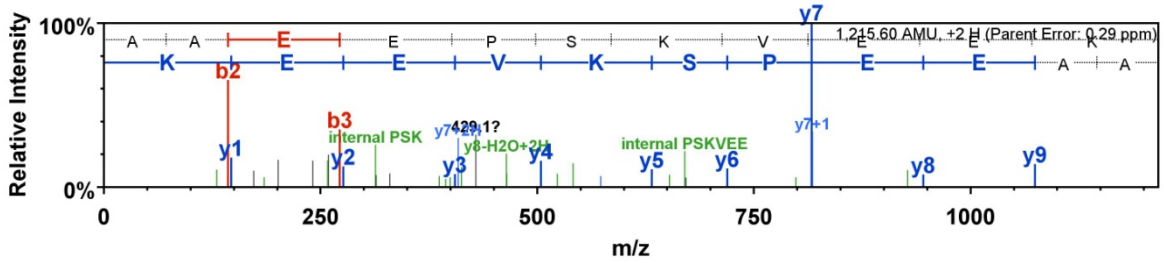

✓ Spectrum for the modified peptide: (M)gAQFSK(T)

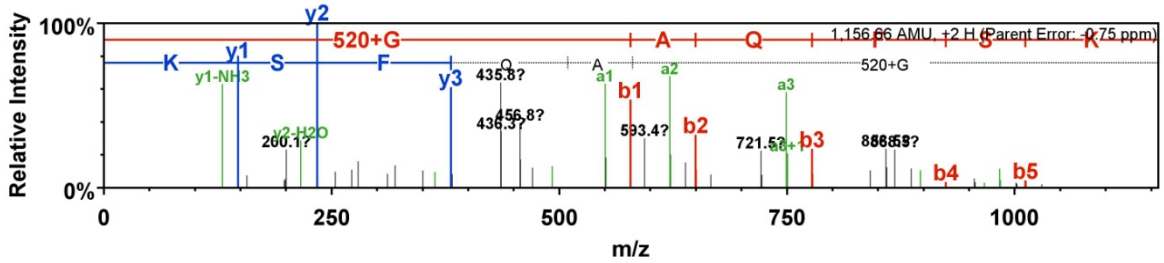

Table H1: Non quantitative proteomics to compare DMSO and YnC12 treated HeLa cells captured with AzKTB.

Spectral counts and unique peptides are given for YnC12 and DMSO samples. Only proteins bearing an N-terminal MG motif are reported in this table. The minimum protein identification probability was set to 99.9% and the minimum peptide identification probability was set to 95%. Four proteins were detected in both samples and are indicated with #. A column ("modified peptide") shows if the modified peptide was detected (see Table H2) and a column ("PR") indicates if the protein was previously reported to be *N*-myristoylated (see Table F1 in Appendix F) in a cell-free system (CF), using the native (Nat) or non native (NN) protein or using chemical proteomics experiments (CP) . For prediction of *N*-myristoylation, two online bioinformatics tools, the MYR predictor (MP) and Myristoylator (Myrist) were used. The MYR predictor shows three levels of confidence: R= reliable; T= twilight, N= not myristoylated and the Myristoylator has four levels of confidence: H= high probability, M=medium probability, L= low probability, N= not myristoylated. A column indicates if the protein is palmitoylated (+: found in 1 study, ++: found in 2 studies; +++: found in 3 studies; ++++: found in 4 studies; u: reported as palmitoylated in the UniProtKB/Swiss-Prot database) and a column shows if the protein is a GPI anchored protein (as reported in the UniProtKB/Swiss-Prot database).[173] A star indicates if an N-terminal peptide was detected with no modification from the capture reagent AzKTB.

			Spectral count		Unique peptide							
Protein name	Gene name	Protein ID	YnC12	DMSO	YnC12	DMSO	PR	MP	Myrist	GPI	Palm	Modified peptide
ADP-ribosylation factor 1	ARF1	P84077	247	0	17	0	NN	T	H	No	++	+
Niban-like protein 1	FAM129B	Q96TA1	130	0	35	0		N	H	No		+
26S protease regulatory subunit 4	PSMC1	P62191	112	0	28	0	NN	R	H	No	++	+
Protein phosphatase 1G	PPM1G	O15355	69	0	22	0	CP	R	M	No	+	+
cAMP-dependent protein kinase catalytic subunit alpha	PRKACA	P17612	69	0	20	0	N	R	H	No	-	+
NADH-cytochrome b5 reductase 3	CYB5R3	P00387	66	0	19	0	NN	R	H	No	++	+
Guanine nucleotide-binding protein G(i) subunit alpha-2	GNAI2	P04899	62	0	21	0	NN	R	H	No	++++	+
Protein FAM49B	FAM49B	Q9NUQ9	59	0	18	0	CP	N	M	No	+++	
Annexin A2 #	ANXA2	P07355	57	22	23	14		N	N	No	+	
Glyceraldehyde-3-phosphate dehydrogenase #	GAPDH	E7EUT4	49	14	12	6	CP	N	N	No	+++	
ADP-ribosylation factor 4	ARF4	P18085	49	0	7	0	CP	R	H	No	+	+
L-lactate dehydrogenase A chain #	LDHA	P00338	39	23	20	12		N	N	No	++	
Cytochrome c-type heme lyase	HCCS	P53701	38	0	16	0		R	L	No		+
ARF-like protein 1	ARL1	P40616	38	0	11	0	CF	R	H	No		
A-kinase anchor protein 12	AKAP12	Q02952	37	0	22	0	NN	R	H	No		+
Apoptosis-inducing factor 2	AIFM2	Q9BRQ8	37	0	16	0	CF	R	H	No		
Cytospin-B	SPECC1	Q5M775	36	0	24	0		T	N	No		+
Elongation factor 1-alpha 1 #	EEF1A1	P68104	35	25	14	11	CP	N	N	No	++	
Hippocalcin-like protein 1	HPCAL1	P37235	34	0	13	0	NN	R	H	No	-	

Golgi reassembly-stacking protein2	GORASP2	Q9H8Y8	33	0	15	0	CP	R	H	No	u	+
Guanine nucleotide-binding protein G(k) subunit alpha	GNAI3	P08754	29	0	8	0	NN	R	H	No	u ++++	
Flotillin-2	FLOT2	Q14254	28	0	18	0		N	N	No	+++	
ADP-ribosylation factor 6	ARF6	P62330	28	0	6	0	NN	R	H	No		
Ragulator complex protein LAMTOR1	LAMTOR1	Q6IAA8	26	0	9	0		T	H	No		
Myristoylated alanine-rich C-kinase substrate	MARCKS	P29966	25	0	12	0	N	R	H	No		+
Brain acid soluble protein 1	BASP1	P80723	23	0	11	0	N	R	H	No		
Phosphoinositide 3-kinase regulatory subunit 4	PIK3R4	Q99570	23	0	18	0	CF	T	H	No		
Tyrosine-protein kinase Yes	YES1	P07947	22	0	11	0	NN	R	H	No	u ++	
Guanine nucleotide-binding protein G(i) subunit alpha-1	GNAI1	P63096	22	0	8	0	NN	R	H	No	u ++	+
Protein phosphatase 1A	PPM1A	P35813	21	0	12	0	CF	N	H	No		+
NADH dehydrogenase [ubiquinone] 1 alpha subcomplex assembly factor 4	NDUFAF4	Q9P032	21	0	10	0		N	N	No		+
Tescalcin	TESC	Q96BS2	20	0	9	0	CF	R	H	No		+
Calcineurin B homologous protein1	CHP	Q99653	20	0	8	0		R	H	No	-	
Coiled-coil-helix-coiled-coil-helix domain-containing protein 3, mitochondrial	CHCHD3	C9JRZ6	20	0	8	0	NN	R	H	No	+	+
ADP-ribosylation factor 5	ARF5	P84085	19	0	8	0	CP	R	H	No	+	+
Prostaglandin F2 receptor negative regulator	PTGFRN	Q9P2B2	17	0	13	0		N	M	No	++	
Calcineurin subunit B type 1	PPP3R1	D3YTA9	17	0	7	0	NN	R	H	No	-	+
Choline transporter-like protein 1	SLC44A1	Q8WWI5	16	0	7	0		R	M	No	+	
Mitochondrial import receptor subunit TOM40 homolog	TOMM40	O96008	16	0	6	0		T	L	No	+	
Lysosome membrane protein 2	SCARB2	Q14108	15	0	6	0		N	N	No	++	
MOSC domain-containing protein 1, mitochondrial	MARC1	Q5VT66	14	0	9	0		N	H	No		+
Protein XRP2	RP2	O75695	14	0	7	0		R	H	No	u	+
Nucleolar protein 3	NOL3	O60936	14	0	5	0		T	L	No		+
Sphingolipid delta(4)-desaturase	DEGS1	O15121	14	0	5	0	NN	T	H	No		
Tyrosine-protein kinase Lyn	LYN	P07948	13	0	7	0	NN	R	H	No	u +	
cAMP-dependent protein kinase catalytic subunit beta	PRKACB	C9JK39	13	0	5	0		R	H	No		+

Protein phosphatase 1B	PPM1B	O75688	12	0	7	0		N	M	No		
High mobility group protein B1;Putative high mobility group protein B1-like 1	HMGB1	P09429	11	0	8	0	CP	N	N	No	+	
Leucine-rich repeat-containing protein 57	LRRC57	H3BSW0	11	0	7	0		N	N	No		+
NADH dehydrogenase [ubiquinone] 1 beta subcomplex subunit 7	NDUFB7	P17568	11	0	6	0	CF	N	L	No		+
5-AMP-activated protein kinase subunit beta-1	PRKAB1	Q9Y478	11	0	5	0	NN	N	N	No		+
Plasminogen receptor (KT)	PLGRKT	Q9HBL7	11	0	5	0		N	H	No		+
Proto-oncogene tyrosine-protein kinase Src	SRC	P12931	11	0	5	0	N	R	H	No	+	
Protein lunapark	LNP	Q9C0E8	11	0	7	0	CF	T	H	No		+
CD81 antigen	CD81	A6NMH8	10	0	3	0	CP	N	N	No	+++	
Charged multivesicular body protein 6	CHMP6	Q96FZ7	10	0	6	0	NN	R	H	No		+
Monocarboxylate transporter 4	SLC16A3	O15427	9	0	5	0		N	N	No	+	
Serine incorporator 1	SERINC1	Q9NRX5	9	0	4	0	CF	N	N	No	-	
Surfeit locus protein 4 *	SURF4	O15260	9	0	4	0		N	N	No	++	
Golgi-associated plant pathogenesis-related protein 1	GLIPR2	Q9H4G4	9	0	7	0	N	R	H	No	-	
Golgi integral membrane protein 4	GOLIM4	O00461	9	0	5	0		R	H	No	+	
Neuronal calcium sensor 1	NCS1	P62166	9	0	5	0	NN	R	H	No		
MOSC domain-containing protein 2, mitochondrial	MARC2	Q969Z3	8	0	6	0		N	N	No		+
MARCKS-related protein	MARCKSL1	P49006	8	0	4	0		R	H	No	+	+
TLD domain-containing protein KIAA1609	KIAA1609	F5GWS3	8	0	5	0	CF	T	H	No		
6-phosphogluconate dehydrogenase, decarboxylating	PGD	B4DQJ8	7	0	6	0		N	N	No	-	
Opioid growth factor receptor-like protein 1	OGFRL1	Q5TC84	7	0	5	0		N	M	No		+
Choline transporter-like protein 2 *	SLC44A2	E7ETY3	7	0	4	0		N	N	No	-	
Transforming acidic coiled-coil-containing protein 1	TACC1	G8JLK4	7	0	5	0		R	H	No		
Dymeclin	DYM	Q7RTS9	7	0	4	0		R	H	No		
Formin-like protein 2	FMNL2	Q96PY5	7	0	6	0	CF	T	H	No		
Cell surface glycoprotein MUC18	MCAM	P43121	6	0	6	0		N	N	No	+	
Scavenger receptor class B member 1	SCARB1	F8W8N0	6	0	3	0		N	N	No	+	
Serine incorporator 3	SERINC3	Q13530	6	0	3	0		N	N	No		

Guanine nucleotide-binding protein G(o) subunit alpha	GNAO1	P09471-2	6	0	3	0	NN	R	H	No	u;+++	
Transmembrane protein 106B	TMEM106B	Q9NUM4	6	0	5	0		T	H	No		
Trafficking protein particle complex subunit 3 *	TRAPPC3	A6NDN0	5	0	4	0		N	N	No	u;++	
Glucose-6-phosphate 1-dehydrogenase	G6PD	P11413-3	5	0	4	0		N	H	No		
ARF-like protein 5B	ARL5B	Q96KC2	5	0	3	0	NN	N	L	No		+
Elongation factor 1-beta	EEF1B2	P24534	5	0	3	0		N	N	No		
High affinity cationic amino acid transporter 1	SLC7A1	P30825	4	0	3	0		N	N	No	++	
Platelet-activating factor acetylhydrolase 2, cytoplasmic	PAFAH2	Q99487	4	0	3	0		N	N	No		
RING finger protein 141	RNF141	E9PLX2	4	0	3	0		N	H	No		+
E3 ubiquitin-protein ligase ZNRF2	ZNRF2	Q8NHG8	4	0	4	0		R	M	No		
Coiled-coil-helix-coiled-coil-helix domain-containing protein 6, mitochondrial	CHCHD6	Q9BRQ6	4	0	3	0		R	H	No		+
Protein Niban	FAM129A	Q9BZQ8	4	0	3	0		R	H	No		
Protein-L-isoaspartate O-methyltransferase domain-containing protein 1	PCMTD1	Q96MG8	4	0	3	0		R	H	No		+
Formin-like protein 1	FMNL1	O95466	4	0	3	0	NN	T	N	No		
Mitochondrial peptide methionine sulfoxide reductase	MSRA	Q9UJ68-5	3	0	3	0	NN	R	H	No		
Zinc transporter 1	SLC30A1	Q9Y6M5	3	0	2	0		N	N	No		
Cell division cycle-associated protein 3	CDCA3	Q99618	3	0	3	0		R	H	No		
CD151 antigen	CD151	E9PL82	2	0	2	0		N	N	No	+	

Table H2: List of modified peptides identified with AzKTB. (Peptide identification probability >95%).UP = unique peptide. The modified peptides were listed in the Scaffold file ("non quantitative_AzKTB", Appendix A) and the raw data file was re-analysed with MaxQuant. The number of unique peptides is indicated. Two unique peptides can be identified when the N-terminal peptide had a missed-cleavage site.

	Identified Proteins	Gene name	Accession Number	Scaffold UP	MaxQuant UP
1	A-kinase anchor protein 12	AKAP12	Q02952	1	1
2	ADP-ribosylation factor 1	ARF1	P84077	1	1
3	ADP-ribosylation factor 3	ARF3	P61204		1
4	ADP-ribosylation factor 4	ARF4	P18085	1	1
5	ADP-ribosylation factor 5	ARF5	P84085	1	1
6	ADP-ribosylation factor-like protein 5B	ARL5B	Q96KC2		1
7	Coiled-coil-helix-coiled-coil-helix domain-containing protein 3, mitochondrial	CHCHD3	C9JRZ6		1
8	Coiled-coil-helix-coiled-coil-helix domain-containing protein 6, mitochondrial	CHCHD6	Q9BRQ6		1
9	Charged multivesicular body protein 6	CHMP6	Q96FZ7		1
10	NADH-cytochrome b5 reductase 3	CYB5R3	P00387	1	
11	Niban-like protein 1	FAM129B	Q96TA1	2	2
12	Guanine nucleotide-binding protein G(i) subunit alpha-1	GNAI1	P63096	1	1
13	Guanine nucleotide-binding protein G(i) subunit alpha-2	GNAI2	P04899	1	
14	Golgi reassembly-stacking protein 2	GORASP2	Q9H8Y8	1	1
15	Cytochrome c-type heme lyase	HCCS	P53701	1	1
16	Protein Lunapark	LNP	B7ZLA8	1	1
17	Leucine-rich repeat-containing protein 57 (Fragment)	LRRC57	H3BSW0		1
18	MOSC domain-containing protein 1, mitochondrial	MARC1	Q5VT66		1
19	MOSC domain-containing protein 2, mitochondrial	MARC2	Q969Z3	1	1
20	Myristoylated alanine-rich C-kinase substrate	MARCKS	P29966	1	1
21	MARCKS-related protein	MARCKSL1	P49006		1
22	NADH dehydrogenase [ubiquinone] 1 alpha subcomplex assembly factor 4	NDUFAF4	Q9P032	1	1
23	NADH dehydrogenase [ubiquinone] 1 beta subcomplex subunit 7	NDUFB7	P17568	1	1
24	Nucleolar protein 3	NOL3	B4DFL0		1
25	Opioid growth factor receptor-like protein 1	OGFRL1	Q5TC84	1	1
26	Protein-L-isoaspartate O-methyltransferase domain-containing protein 1	PCMTD1	Q96MG8		1
27	Plasminogen receptor (KT)	PLGRKT	Q9HBL7	1	1
28	Protein phosphatase 1A	PPM1A	P35813	1	1
29	Protein phosphatase 1G	PPM1G	O15355	1	1
30	Calcineurin subunit B type 1	PPP3R1	D3YTA9	1	1
31	5'-AMP-activated protein kinase subunit beta-1	PRKAB1	Q9Y478		
32	cAMP-dependent protein kinase catalytic subunit alpha	PRKACA	P17612	1	1
33	cAMP-dependent protein kinase catalytic subunit beta	PRKACB	B2RB89		1
34	26S protease regulatory subunit 4	PSMC1	P62191	2	2
35	RING finger protein 141 (Fragment)	RNF141	E9PLX2	1	
36	Protein XRP2	RP2	O75695		1
37	Isoform 4 of Cytospin-B	SPECC1	Q5M775-4	1	1
38	Calcineurin B homologous protein 3	TESC	Q96BS2	1	
39	Mitochondrial import receptor subunit TOM40B	TOMM40L	Q969M		1

Table H3: Gel-based analysis. YnC12 tagged proteins were captured with AzTB, enriched and separated on a SDS-PAGE gel. The gel was cut in 7 portions. Only proteins possessing an N-terminal MG motif and identified with more than 2 unique peptides are shown in this table. The number of unique peptides and the number of assigned spectra are displayed for each protein and each gel slice. For each protein, the highest number on unique peptide or spectral count was shaded in dark blue, indicating that this protein was mainly found in this gel slice. When the same protein was also detected in other slices, it was shaded in light blue.

				Number of unique peptides							Number of assigned spectra (spectral counts)						
	Identified Proteins	Accession Number	Molecular Weight	>90 kDa	60-90 kDa	40-60 kDa	30-40 kDa	23-30 kDa	18-23 kDa	<18 kDa	>90 kDa	60-90 kDa	40-60 kDa	30-40 kDa	23-30 kDa	18-23 kDa	<18 kDa
1	Prostaglandin F2 receptor negative regulator	Q9P2B2	83 kDa	2	0	0	0	0	0	0	2	0	0	0	0	0	0
2	Niban-like protein 1	Q96TA1	84 kDa	15	18	4	0	0	0	0	31	38	4	0	0	0	0
3	Tyrosine-protein kinase Yes	P07947	61 kDa	0	9	2	0	0	0	0	0	13	2	0	0	0	0
4	Lysosome membrane protein 2	Q14108	54 kDa	0	8	0	0	0	0	0	0	15	0	0	0	0	0
5	Proto-oncogene tyrosine-protein kinase Src	P12931	60 kDa	0	5	0	0	0	0	0	0	7	0	0	0	0	0
6	Choline transporter-like protein 2	E7ETY3	80 kDa	0	3	0	0	0	0	0	0	3	0	0	0	0	0
7	Dymeclin	Q7RTS9	76 kDa	0	3	0	0	0	0	0	0	5	0	0	0	0	0
8	Polypeptide N-acetylgalactosaminyltransferase 1 soluble form #	F5GY99	57 kDa	0	3	0	0	0	0	0	0	3	0	0	0	0	0
9	Scavenger receptor class B member 1	Q8WTV0	54 kDa	0	3	0	0	0	0	0	0	4	0	0	0	0	0
10	Protein phosphatase 1G	O15355	59 kDa	0	17	4	0	0	0	0	0	56	4	0	0	0	0
11	Myristoylated alanine-rich C-kinase substrate	P29966	32 kDa	0	10	5	2	0	0	0	0	24	6	3	0	0	0
12	26S protease regulatory subunit 4	P62191	49 kDa	0	5	33	3	0	0	0	0	7	117	5	0	0	0
13	Serine incorporator 1	Q9NRX5	50 kDa	0	2	3	0	0	0	0	0	2	4	0	0	0	0
14	Choline transporter-like protein 1	Q8WWI5	73 kDa	0	0	4	0	0	0	0	0	0	5	0	0	0	0
15	Isoform 2 of Tyrosine-protein kinase Lyn	P07948-2	56 kDa	0	0	3	0	0	0	0	0	0	3	0	0	0	0
16	Flotillin-2	Q14254	53 kDa	0	0	18	0	0	0	0	0	0	42	0	0	0	0
17	Protein Lunapark	Q9C0E8	51 kDa	0	0	6	0	0	0	0	0	0	12	0	0	0	0
18	Brain acid soluble protein 1	P80723	23 kDa	0	0	14	0	0	0	0	0	0	47	0	0	0	0
19	CD82 antigen #	P27701	30 kDa	0	0	3	0	0	0	0	0	0	4	0	0	0	0
20	Protein phosphatase 1B	O75688	33 kDa	0	0	4	0	0	0	0	0	0	5	0	0	0	0
21	Protein-L-isoaspartate O-methyltransferase domain-containing protein 1	Q96MG8	32 kDa	0	0	2	0	0	0	0	0	0	3	0	0	0	0
22	Protein phosphatase 1A	P35813	42 kDa	0	0	11	0	0	0	0	0	0	21	0	0	0	0

23	TLD domain-containing protein KIAA1609	Q6P9B6	21 kDa	0	0	2	0	0	0	0	0	0	2	0	0	0	0
24	cAMP-dependent protein kinase catalytic subunit alpha	P17612	41 kDa	0	0	20	18	0	0	0	0	0	55	39	0	0	0
25	cAMP-dependent protein kinase catalytic subunit beta	C9JK39	41 kDa	0	0	5	4	0	0	0	0	0	9	8	0	0	0
26	Transmembrane protein 106B	Q9NUM4	31 kDa	0	0	3	2	0	0	0	0	0	4	2	0	0	0
27	Elongation factor 1-alpha 1 #	P68104	50 kDa	0	0	6	2	0	0	0	0	0	12	4	0	0	0
28	Golgi reassembly-stacking protein 2	Q9H8Y8	42 kDa	0	0	7	0	3	0	0	0	0	10	0	4	0	0
29	Monocarboxylate transporter 4	O15427	49 kDa	0	0	0	5	0	0	0	0	0	0	9	0	0	0
30	Guanine nucleotide-binding protein G(i) subunit alpha-2	P04899	40 kDa	0	2	7	19	3	0	0	0	3	11	81	4	0	0
31	Guanine nucleotide-binding protein G(k) subunit alpha	P08754	41 kDa	0	0	2	7	0	0	0	0	0	3	21	0	0	0
32	Guanine nucleotide-binding protein G(i) subunit alpha-1	P63096	40 kDa	0	0	0	7	0	0	0	0	0	0	14	0	0	0
33	Isoform Alpha-2 of Guanine nucleotide-binding protein G(o) subunit alpha	P09471-2	40 kDa	0	0	0	7	0	0	0	0	0	0	18	0	0	0
34	Protein XRP2	O75695	40 kDa	0	0	0	10	0	0	0	0	0	0	21	0	0	0
35	MOSC domain-containing protein 1, mitochondrial	Q5VT66	38 kDa	0	0	0	4	0	0	0	0	0	0	5	0	0	0
36	MOSC domain-containing protein 2, mitochondrial	Q969Z3	38 kDa	0	0	0	6	0	0	0	0	0	0	11	0	0	0
37	Sphingolipid delta(4)-desaturase	O15121	38 kDa	0	0	0	5	0	0	0	0	0	0	11	0	0	0
38	Apoptosis-inducing factor 2	Q9BRQ8	37 kDa	0	0	0	2	0	0	0	0	0	0	2	0	0	0
39	Isoform 3 of L-lactate dehydrogenase A chain #	P003383	37 kDa	0	0	0	12	0	0	0	0	0	0	20	0	0	0
40	Protein FAM49B	Q9NUQ9	37 kDa	0	0	0	14	0	0	0	0	0	0	59	0	0	0
41	NADH-cytochrome b5 reductase 3	P00387	34 kDa	0	0	0	18	6	2	0	0	0	0	76	9	3	0
42	Glyceraldehyde-3-phosphate dehydrogenase #	P04406	32 kDa	0	0	0	9	0	0	0	0	0	0	23	0	0	0
43	MARCKS-related protein	P49006	20 kDa	0	0	0	3	0	0	0	0	0	0	6	0	0	0
44	Cytochrome c-type heme lyase	P53701	31 kDa	0	0	0	14	3	0	0	0	0	0	31	3	0	0
45	Nucleolar protein 3	H3BM67	29 kDa	0	0	0	0	5	0	0	0	0	0	0	8	0	0
46	Coiled-coil-helix-coiled-coil-helix domain -containing protein 3, mitochondrial	Q9NX63	27 kDa	0	0	0	0	15	0	0	0	0	0	0	45	0	0

47	Ubiquitin domain-containing protein 2 #	Q8WUN7	26 kDa	0	0	0	0	3	0	0	0	0	0	0	3	0	0
48	E3 ubiquitin-protein ligase ZNRF2	Q8NHG8	24 kDa	0	0	0	0	3	0	0	0	0	0	0	6	0	0
49	Charged multivesicular body protein 6	Q96FZ7	23 kDa	0	0	0	0	5	0	0	0	0	0	0	7	0	0
50	Calcineurin B homologous protein 1	Q99653	22 kDa	0	0	0	0	3	0	0	0	0	0	0	4	0	0
51	Calcineurin B homologous protein 3	Q96BS2	22 kDa	0	0	0	0	6	0	0	0	0	0	0	13	0	0
52	NADH dehydrogenase [ubiquinone] 1 alpha subcomplex assembly factor 4	Q9P032	20 kDa	0	0	0	0	8	0	0	0	0	0	0	15	0	0
53	Neuronal calcium sensor 1	P62166	22 kDa	0	0	0	0	5	0	0	0	0	0	0	9	0	0
54	RING finger protein 141	Q8WVD5	20 kDa	0	0	0	0	2	0	0	0	0	0	0	2	0	0
55	Leucine-rich repeat-containing protein 57	Q8N9N7	16 kDa	0	0	0	0	8	0	0	0	0	0	0	15	0	0
56	CD151 antigen	P48509	15 kDa	0	0	0	0	2	0	0	0	0	0	0	4	0	0
57	Hippocalcin-like protein 1	P37235	22 kDa	0	0	0	0	11	6	0	0	0	0	0	30	11	0
58	CD81 antigen	P60033	30 kDa	0	0	0	0	0	3	2	0	0	0	0	0	10	2
59	ADP-ribosylation factor 1	P84077	21 kDa	2	3	3	4	5	13	6	2	6	4	8	6	211	28
60	ADP-ribosylation factor 4	P18085	21 kDa	0	0	2	2	2	6	3	0	0	2	4	2	52	4
61	ADP-ribosylation factor 5	P84085	21 kDa	0	0	0	0	0	6	0	0	0	0	0	0	25	0
62	Calcineurin subunit B type 1	P63098	21 kDa	0	0	0	0	0	4	0	0	0	0	0	0	8	0
63	ADP-ribosylation factor 6	P62330	20 kDa	0	0	0	0	0	4	0	0	0	0	0	0	20	0
64	ADP-ribosylation factor-like protein 1	P40616	19 kDa	0	0	0	0	0	7	0	0	0	0	0	0	25	0
65	Caveolin-2 #	P51636	18 kDa	0	0	0	0	0	2	0	0	0	0	0	0	4	0
66	Ragulator complex protein LAMTOR1	Q6IAA8	18 kDa	0	0	0	0	0	9	0	0	0	0	0	0	24	0
67	Golgi-associated plant pathogenesis-related protein 1	Q9H4G4	17 kDa	0	0	0	0	0	5	0	0	0	0	0	0	10	0
68	NADH dehydrogenase [ubiquinone] 1 beta subcomplex subunit 7	P17568	16 kDa	0	0	0	0	0	6	0	0	0	0	0	0	13	0
69	Plasminogen receptor (KT)	Q9HBL7	17 kDa	0	0	0	0	0	0	5	0	0	0	0	0	0	14
70	Trafficking protein particle complex 3, isoform CRA_a	A6NDN0	15 kDa	0	0	0	0	0	0	3	0	0	0	0	0	0	4

Table H4: Label-free quantification (LFQ) of proteins enriched in the YnC12 treated samples (four biological replicates) compared to the sample treated with myristic acid (four biological replicates). The LFQ intensity, number of "razor + unique peptides", MS/MS count, sequence coverage are displayed for each replicate (n = 4 biological replicates) for the Myr and YnC12 samples. The enrichment (LFQ) was determined for each protein detected (LFQ = (intensity YnC12)/ (intensity Myr)). Only proteins significantly enriched in the YnC12 experiments (modified t-test FDR = 0.001 and s0 = 1; and with LFQ > 4) are reported. For prediction of *N*-myristoylation, two online bioinformatic tools, the MYR predictor (MP) and Myristoylator (Myrist) were used. The Myr predictor shows three levels of confidence: R= reliable; T= twilight, N= not myristoylated and the Myristoylator has four levels of confidence: H= high probability, M=medium probability, L= low probability, N= not myristoylated. When unique peptides could not be assigned to one unique protein but were assigned instead to a group of 2 or more proteins by MaxQuant, proteins were grouped and had the same number of unique peptides. A column indicates if the protein is palmitoylated (+: found in 1 study, ++: found in 2 studies; +++: found in 3 studies; ++++: found in 4 studies; u: reported as palmitoylated in the UniProtKB/Swiss-Prot database) and a column indicates if the protein is a GPI anchored protein). A column "PR" indicates if the protein was previously experimentally shown to be myristoylated (see Appendix F). Two columns show the results of the t-test (log2 values).

	Gene names	Protein IDs	LFQ	MG	MP	Myrist	GPI	Palm	PR	-Log t-test	t-test diff
1	ARF3;ARF1	P61204	2501	+	T	H	No	+;++	NN	6.74	11.48
2	MARCKS	P29966	1603.6	+	R	H	No		Nat	7.68	10.65
3	PSMC1	P62191	1281.7	+	R	H	No	++	NN	9.85	10.32
4	CHCHD3	Q9NX63	821.73	+	R	H	No	+	NN	10.87	9.68
5	PRKACA	P17612	738.85	+	R	H	No		Nat	7.74	9.50
6	FAM49B	Q9NUQ9	685.68	+	N	M	No	+++	CP	9.21	9.43
7	MARCKSL1	P49006	683.48	+	R	H	No	+		8.92	9.40
8	ARF4	P18085	585.35	+	R	H	No	+	CP	5.61	9.43
9	BASP1	P80723	519.18	+	R	H	No		Nat	4.57	9.75
10	HPCAL1;HPCA	P37235	504.25	+	R	H	No		NN	8.81	8.99
11	ARL1	P40616	499.1	+	R	H	No		CF	9.93	8.96
12	PPM1G	O15355	475.33	+	R	M	No	+	CP	6.18	9.00
13	TESC	Q96BS2	458.36	+	R	H	No			5.57	8.65
14	CYB5R3	P00387	456.54	+	R	H	No	++	NN	4.64	9.47
15	BST2	Q10589	413.73				Pot			9.60	8.70
16	ARF6	P62330	389.49	+	R	H	No		NN	7.72	8.60
17	ARF5	P84085	310.2	+	R	H	No	+	CP	7.38	8.26
18	HCCS	P53701	305.91	+	R	L	No			7.74	8.23
19	GORASP2	Q9H8Y8	265.35	+	R	H	No	u	CP	9.48	8.06
20	TFRC	P02786	260.7				No	++++		6.44	8.14
21	NOL3	O60936	248.48	+	T	L	No			8.04	7.95
22	PTGFRN	Q9P2B2	226.35	+	N	M	No	++		8.45	7.84
23	GNAI3	P08754	221.47	+	R	H	No	u,++++	NN	3.92	8.41
24	LAMTOR1	Q6IAA8	215.27	+	T	H	No			9.68	7.75
25	SCAMP3	O14828	207.68				No	+++		6.91	7.64
26	PLP2	Q04941	205.86				No			9.24	7.68
27	PRKACB	P22694	201.6	+	R	H	No			7.51	7.63
28	FAM129B	Q96TA1	195.94	+	N	H	No			3.74	8.46
29	STOM	P27105	190.15				No	+++		6.98	7.51
30	AIFM2	Q9BRQ8	189.28	+	R	H	No		CF	8.40	7.58
31	CKAP4	Q07065	183.94				No	+++		4.77	7.69
32	DAGLB	Q8NCG7	176.72				No	++		6.46	7.39
33	CD81	P60033	151.79	+	N	N	No	+++	CP	8.77	7.25
34	CD44	P16070	149.09				No	+		6.95	7.20
35	LRRC57	Q8N9N7	143.79	+	N	N	No			9.74	7.17
36	CD9	P21926	127.57				No	+		7.12	6.98
37	CD151	P48509	117.27	+	N	N	No	+		6.06	6.79
38	HADHB	P55084	116.11				No	++		7.68	6.85

39	CD59	P13987	114.87	+	N	N	Yes			6.34	6.76
40	PPM1A	P35813	114.72	+	N	H	No		NN	6.80	6.83
41	SCARB2	Q14108	110.77	+	N	N	No	++		6.78	6.74
42	GNAI1	P63096	102.8	+	R	H	No	u, ++	NN	6.26	6.60
43	CANX	P27824	101.57				No	++++		3.55	7.17
44	DEGS1	O15121	99.003	+	T	H	No		NN	6.22	6.54
45	SLC44A1	Q8WWI5	94.386	+	R	M	No	+		5.62	6.44
46	CHP	Q99653	92.794	+	R	H	No			8.11	6.52
47	CD55	P08174	92.22				Yes			6.39	6.48
48	GLIPR2	Q9H4G4	92.204	+	R	H	No		Nat	4.90	6.29
49	NDUFAF4	Q9P032	90.66	+	N	N	No			8.06	6.51
50	SERINC1	Q9NRX5	85.129	+	N	N	No		CF	9.42	6.42
51	FLOT2	Q14254	83.061	+	N	N	No	+++		3.58	7.05
52	B4GALT1	P15291	82.705				No			7.24	6.38
53	LYN	P07948	79.472	+	R	H	No	u, +	NN	11.3	6.31
54	TMX1	Q9H3N1	78.322				No			7.49	6.32
55	GALNT2	Q10471	77.047				No			4.33	6.53
56	LNP	Q9C0E8	76.456	+	T	H	No		CF	6.98	6.22
57	SRC	P12931	71.615	+	R	H	No	+	Nat	7.40	6.17
58	CACNA2D1	P54289	71.325				No			6.94	6.19
59	PSMC2	P35998	69.677				No			7.08	6.16
60	GNAO1	P09471	67.517	+	R	H	No	u, +++	NN	8.99	6.08
61	CD63	P08962	67.312				No	+		6.34	6.02
62	SERPINB6	P35237	65.566				No			8.75	6.04
63	TMEM106B	Q9NUM4	64.766	+	T	H	No			5.97	5.95
64	SLC16A3	O15427	60.287	+	N	N	No	+		7.42	5.90
65	HLA-C	P30508	59.972				No	+		7.99	5.89
66	SLC1A5	Q15758	59.873				No	+++		6.03	5.83
67	YES1	P07947	59.637	+	R	H	No	u,++	NN	7.38	5.89
68	ZNRF2	Q8NHG8	57.127	+	R	M	No		NN	8.96	5.84
69	IFITM3;IFITM2;IFITM1	Q01628	53.911				No	u		7.10	5.75
70	TSPAN3	O60637	49.346	+	N	N	No			7.27	5.64
71	SPECC1	Q5M775	49.141	+	T	N	No			7.38	5.62
72	TRIM23	P36406	47.786				No			7.67	5.59
73	NPC1	O15118	46.981				No			6.19	5.56
74	BAG5	Q9UL15	45.283				No			7.13	5.50
75	SLC44A2	Q8IWA5	44.272	+	N	N	No			9.16	5.47
76	PI4K2A	Q9BTU6	44.059				No	+++		7.73	5.46
77	MRPS36	P82909	43.587				No			9.06	5.44
78	CHMP6	Q96FZ7	43.551	+	R	H	No		NN	6.31	5.43
79	MARC2	Q969Z3	43.325	+	N	N	No			6.19	5.40
80	NDUFB7	P17568	42.742	+	N	L	No		CF	7.06	5.44
81	PIK3R4	Q99570	41.708	+	T	H	No		CF	5.56	5.30
82	PPM1B	O75688	40.525	+	N	M	No		NN	8.00	5.34
83	PPP3R1	P63098	40.09	+	R	H	No		NN	4.99	5.21
84	UBC;UBB;RPS27A;UBA52	P0CG48	39.625				No	+		3.95	5.60
85	MCAM	P43121	39.458	+	N	N	No	+		7.20	5.29
86	RTN4	Q9NQC3	39.277				No	+		9.05	5.30
87	SLC25A3	Q00325	36.966				No	+		7.57	5.21
88	GNAI2	P04899	35.459	+	R	H	No	u,++++	NN	2.65	7.33
89	CDCA3	Q99618	35.177	+	R	H	No			7.12	5.16

90	PLGRKT	Q9HBL7	35.007	+	N	H	No			7.33	5.14
91	CD276	Q5ZPR3	34.764				No			6.43	5.08
92	SLC30A1	Q9Y6M5	34.261	+	N	N	No			7.60	5.09
93	HLA-B	P30464	33.246				No	+		7.40	5.05
94	CAV1	Q03135	33.014				No	+		1.91	3.73
95	RP2	O75695	31.418	+	R	H	No	u		7.15	5.00
96	TTYH3	Q9C0H2	29.556				No	++		6.32	4.90
97	MARC1	Q5VT66	28.937	+	N	H	No			6.49	4.83
98	RNF141	Q8WVD5	28.772	+	N	H	No			6.81	4.87
99	FMNL1	O95466	28.016	+	T	N	No		NN	5.60	4.73
100	PRKAB2	O43741	27.522	+	N	M	No		NN	7.13	4.78
101	SCARB1	Q8WTV0	26.723	+	N	N	No	+		6.88	4.75
102	SLC7A1	P30825	26.56	+	N	N	No	++		6.10	4.74
103	PLSCR1	O15162	25.97				No	+		8.28	4.69
104	PODXL	O00592	25.747				No			9.61	4.69
105	PPIB	P23284	25.715				No	+		7.41	4.68
106	GOLIM4	O00461	25.293	+	R	H	No	+		7.04	4.64
107	TRAPPC3	O43617	25.221				No	u, ++		5.55	4.59
108	RFTN1	Q14699	24.979	+	N	H	No	u	NN	6.53	4.65
109	LRRC15	Q8TF66	24.217				No			6.49	4.60
110	PRKAB1	Q9Y478	24.185	+	N	N	No		NN	8.94	4.60
111	IMMT	Q16891	23.956				No			1.72	9.07
112	FAM129A	Q9BZQ8	23.466	+	R	H	No			4.54	4.41
113	PRDX6	P30041	23.363				No	+		5.07	4.45
114	RPL22	P35268	22.911				No			7.46	4.51
115	KIAA1609	Q6P9B6	22.851	+	T	H	No		CF	7.37	4.50
116	RHOB	P62745	22.599				No	u, ++		6.19	4.50
117	L1CAM	P32004	22.31				No	+		6.61	4.46
118	SVIP	Q8NHG7	21.587	+	N	N	No			6.74	4.44
119	PRNP	P04156	21.538				Pot			6.52	4.42
120	VAMP3	Q15836	21.275				No	+++		5.32	4.35
121	SLC38A1	Q9H2H9	21.263				No			7.30	4.39
122	DNAJC5	Q9H3Z4	20.957				No	u, ++		5.27	4.30
123	SLC35B2	Q8TB61	20.848				No	+		6.31	4.34
124	GALNT1	Q10472	20.812				No			6.92	4.36
125	SLC38A2	Q96QD8	20.808				No	++		6.67	4.40
126	DIRC2	Q96SL1	20.087	+	R	H	No			5.04	4.28
127	PROCR	Q9UNN8	20.06				No	+		7.18	4.32
128	ACAA2	P42765	19.769				No			6.05	4.33
129	ECE1	P42892	19.706				No	+		5.01	4.22
130	SERINC3	Q13530	19.18	+	N	N	No			7.49	4.25
131	RPL27	P61353	18.794	+	N	N	No			4.94	4.15
132	NCS1	P62166	18.717	+	R	H	No		NN	5.90	4.22
133	SCAMP2	O15127	18.14				No	++		5.79	4.20
134	CXADR	P78310	17.716				No	+		6.10	4.17
135	PCMTD1	Q96MG8	17.647	+	R	H	No			6.48	4.13
136	SNAP23	O00161	17.352				No	u,++++		5.07	4.14
137	PPP3CA;PPP3CB	Q08209	17.211				No			4.03	3.91
138	VASN	Q6EMK4	17.201				No			6.83	4.09
139	LOH12CR1	Q969J3	17.05	+	R	H	No			6.46	4.09
140	MAN1B1	Q9UKM7	16.516				No			6.97	4.04
141	MGRN1	O60291	15.804	+	R	H	No		CF	7.30	4.00

142	AKAP12	Q02952	15.708	+	R	H	No		NN	1.70	5.90
143	VDAC3	Q9Y277	15.665				No	+		1.69	3.30
144	MYOF	Q9NZM1	15.063				No			4.40	3.80
145	CDK1;CDK3;CDK2	P06493	14.845	+	T	N	No			3.90	3.75
146	MDH1	P40925	14.44				No			4.76	3.79
147	RAP2B;RAP2A	P61225	13.863				No	+++		3.71	3.57
148	GLG1	Q92896	13.76				No	+		6.18	3.78
149	SCYL3	Q8IZE3	13.714	+	R	H	No		NN	5.88	3.80
150	VDAC2	P45880	13.701				No	+		3.05	4.08
151	GNB2	P62879	13.586				No			2.81	4.31
152	PTTG1IP	P53801	13.434				No	++		4.12	3.71
153	DYM	Q7RTS9	12.679	+	R	H	No			3.11	3.76
154	TACC1	O75410	12.653	+	R	H	No			4.85	3.59
155	TSPAN4	O14817	12.63				No			6.12	3.63
156	HADHA	P40939	12.613				No	+		6.80	3.66
157	CLN3	Q13286	12.577	+	T	L	No			5.77	3.66
158	CPD	O75976	12.465				No	u, +		4.72	3.57
159	LANCL1	O43813	12.315				No			2.23	3.39
160	OGFRL1	Q5TC84	12.003	+	N	M	No			3.67	3.38
161	RPS25	P62851	11.671				No			6.69	3.53
162	ERGIC3	Q9Y282	11.457				No	++		5.92	3.53
163	RPLP1	P05386	11.248				No			5.78	3.46
164	PRAF2	O60831	10.966				No	+		4.99	3.41
165	DCAF11	Q8TEB1	10.815	+	R	H	No			5.78	3.44
166	PAFAH2	Q99487	10.601	+	N	N	No			3.70	3.27
167	STX12	Q86Y82	10.41				No	++		5.73	3.38
168	PSMD2	Q13200	10.356				No			3.26	3.55
169	PSMA4	P25789	10.275				No			7.46	3.36
170	VAMP7	P51809	10.202				No	+		4.83	3.30
171	C9orf169	A8MQ03	9.8717				No			4.03	3.21
172	TMEM33	P57088	9.7879				No			4.76	3.25
173	MGST3	O14880	9.7201				No	u		6.98	3.29
174	DSG2	Q14126	9.6557				No	+		6.57	3.28
175	TMX3	Q96JJ7	9.5515				No			4.52	3.17
176	AUP1	Q9Y679	9.5354				No	++		4.30	3.15
177	HMGB1;HMGB1P1	P09429	9.3374	+	N	N	No	+	CP	7.49	3.22
178	PSMC3	P17980	9.3372				No			5.41	3.23
179	PRSS21	Q9Y6M0	9.3314	+	N	N	Pot			5.45	3.22
180	CPM	P14384	9.0922				Yes			3.96	3.08
181	NR3C1	P04150	8.961				No			3.53	3.00
182	GPRC5A	Q8NFJ5	8.9461				No	+		5.87	3.16
183	SURF4	O15260	8.8303	+	N	N	No	++		5.91	3.14
184	FMNL2	Q96PY5	8.7937	+	T	H	No		CF	2.16	2.62
185	EFR3A	Q14156	8.6959				No	+		3.54	2.94
186	STBD1	O95210	8.5918	+	R	M	No			5.19	3.08
187	ALPL	P05186	8.5734				Pot			2.11	5.07
188	PCBP1	Q15365	8.4485				No			5.12	3.04
189	BET1	O15155	8.4325				No			4.46	3.04
190	TNFRSF10A	O00220	8.2996				No	+		4.08	2.99
191	TECR	Q9NZ01	8.2742				No			5.87	3.04
192	ABL1	P00519	8.1698	+	T	N	No		NN	6.07	3.03
193	TMEM106C	Q9BVX2	8.1675	+	R	H	No			5.79	3.04

194	TMEM168	Q9H0V1	7.9593				No			3.02	2.83
195	SLC25A6;SLC25A4	P12236	7.8278	+	N	N	No	+;++		2.94	3.18
196	BCAP31	P51572	7.8258	+	R	H	No			3.12	3.05
197	STX7	O15400	7.606				No	+		4.57	2.91
198	SEC61A1;SEC61A2	P61619	7.1242	+	N	N	No			5.54	2.83
199	PVR	P15151	7.1049				No	+		6.31	2.82
200	STEAP3	Q658P3	7.0554				No			5.85	2.80
201	ITFG3	Q9H0X4	6.8538				No			6.83	2.77
202	LNPEP	Q9UIQ6	6.7584				No	+++		5.08	2.75
203	FLOT1	O75955	6.7251				No	+++		1.79	3.32
204	GORASP1	Q9BQQ3	6.6296	+	R	H	No		CF	6.83	2.73
205	TSPAN6	O43657	6.57				No			5.38	2.73
206	TMEM87A	Q8NBN3	6.5601				No			5.10	2.68
207	TRIP13	Q15645	6.555				No			4.25	2.67
208	DDX39B;DDX39A	Q13838	6.2994				No			5.16	2.66
209	ANXA3	P12429	6.2925				No			3.82	2.58
210	RAC2;RAC3;RAC1	P63000	6.2826				No	+		4.55	2.68
211	RPS20	P60866	6.0767				No			5.91	2.61
212	SLCO3A1	Q9UIG8	6.0159				No			2.81	2.44
213	KPNA2	P52292	5.9795				No			5.63	2.58
214	RSPRY1	Q96DX4	5.9041				No	+		4.03	2.51
215	ABCB6	Q9NP58	5.8786				No	+		4.53	2.56
216	MTHFD1	P11586	5.8068				No			5.32	2.53
217	CLPTM1L	Q96KA5	5.7583				No			4.49	2.49
218	TMEM63A	O94886	5.7193				No			7.69	2.52
219	ATP5J2	P56134	5.6876				No			2.57	2.82
220	PSMC5	P62195	5.685				No			1.50	3.20
221	PSMC6	P62333	5.657				No			2.57	2.90
222	PARK7	Q99497	5.6448				No			2.82	2.33
223	RAB1A;RAB1B;RAB1C	P62820	5.5197				No	++		5.10	2.49
224	REEP5	Q00765	5.4723				No	+		5.34	2.47
225	PHB	P35232	5.4565				No	+		4.96	2.43
226	SLC7A5	Q01650	5.4407				No			2.48	2.76
227	UQCRC1	P31930	5.3865				No			7.72	2.43
228	SLC39A10	Q9ULF5	5.2962				No			5.22	2.41
229	MFSD12	Q6NUT3	5.2725	+	N	N	No			4.24	2.37
230	USMG5	Q96IX5	5.0891				No			5.20	2.34
231	TUBA4A	P68366	5.0747				No			2.14	2.90
232	ANXA5	P08758	5.0419				No			3.19	2.25
233	SPAG1	Q07617	5.0051				No			4.69	2.34
234	ANKIB1	Q9P2G1	4.9239	+	R	H	No		CF	4.68	2.26
235	FH	P07954;	4.8268				No			3.32	2.19
236	CLIC1	O0029	4.8073				No	++		2.19	2.84
237	ERGIC2	Q96RQ1	4.7548				No	+		4.04	2.24
238	ELOVL1	Q9BW60	4.64				No	+		4.16	2.22
239	ATP9A	O75110	4.6329				No			4.46	2.22
240	DYNC1I2	Q13409	4.5737				No			4.24	2.16
241	SFT2D3	Q587I9	4.5694				No			3.54	2.15
242	STX6	O43752	4.5311				No	+++		3.54	2.12
243	GOLGA7	Q7Z5G4	4.521				No	u, ++		3.89	2.13
244	PCMTD2	Q9NV79	4.5019	+	R	H	No			4.86	2.14

245	ZDHHC6	Q9H6R6	4.4669	+	N	H	No	+		5.39	2.17
246	YARS	P54577	4.4423	+	N	M	No			3.12	2.05
247	ITGA3	P26006	4.378	+	N	N	No			4.97	2.14
248	PTRH2	Q9Y3E5	4.336				No	++		3.86	2.09
249	OXCT1	P55809	4.3333				No			2.13	2.51
250	TUBB6	Q9BUF5	4.3067				No	+		4.26	2.10
251	USP32	Q8NFA0	4.2938	+	N	H	No			4.50	2.08
252	SLC25A5	P05141	4.2928				No	++		7.05	2.11
253	LMAN2	Q12907	4.2921				No			4.29	2.09
254	VDAC1	P21796	4.2822				No	+		1.87	3.04
255	NEGR1	Q7Z3B1	4.2161				Pot			3.95	2.13
256	MLEC	Q14165	4.1772				No			4.90	2.09
257	MTDH	Q86UE4	4.0372				No	+++		5.87	2.02

Table H5: Double SILAC +/- IMP366 (5 µM). (n= 3 biological replicates). Heavy (R10K8) HeLa cells were treated with DMSO and light (R0K0) HeLa cells were treated with IMP366 (5 µM) (both labelled with YnC12). Samples were mixed in 1:1 ratio. Only proteins significantly depleted in the inhibitor-treated sample (FDR = 0.2; S0=0; side = right) and log2 median H/L ratios higher than 1 were kept. MG = proteins with a N-terminal MG motif. PR = previously reported (Appendix F). For prediction of *N*-myristoylation, two online bioinformatic tools, the MYR predictor (MP) and Myristoylator (Myrist) were used. The Myr predictor shows three levels of confidence: R= reliable; T= twilight, N= not myristoylated and the Myristoylator has four levels of confidence: H= high probability, M=medium probability, L= low probability, N= not myristoylated. When unique peptides could not be assigned to one unique protein but were assigned instead to a group of 2 or more proteins by MaxQuant, proteins were grouped and had the same number of unique peptides. LFQ = LFQ enrichment as determined in Table H4. A column indicates if the protein is palmitoylated (+: found in 1 study, ++: found in 2 studies; +++: found in 3 studies; ++++: found in 4 studies; u: reported as palmitoylated in the UniProtKB/Swiss-Prot database) and a column indicates if the protein is a GPI anchored protein). Two columns show the results of the t-test (log2 values).

Protein names	Gene names	Majority protein IDs	Median	MG	PR	MP	Myrist	LFQ	Palm	GPI	-log t-test p value	t-test difference
NADH dehydrogenase [ubiquinone] 1 alpha subcomplex assembly factor 4	NDUFAF4	Q9P032	5.36	+		N	N	90		No	4.23	5.39
ADP-ribosylation factor-like protein 1	ARL1	P40616	4.84	+	CF	R	H	499		No	2.01	4.84
Calcineurin subunit B type 1	PPP3R1	P63098	4.79	+	NN	R	H	40	-	No	1.36	4.79
cAMP-dependent protein kinase catalytic subunit alpha	PRKACA	P17612;	4.70	+	Nat	R	H	738	-	No	2.20	4.47
Cytochrome c-type heme lyase	HCCS	P53701	4.58	+		R	L	305		No	2.34	4.70
Hippocalcin-like protein 1	HPCAL1	P37235	4.42	+	NN	R	H	504	-	No	2.86	4.60
Protein FAM49B	FAM49B	Q9NUQ9	4.35	+	CP	N	M	685	+++	No	2.77	4.36
NADH-cytochrome b5 reductase 3	CYB5R3	P00387	4.32	+	NN	R	H	456	++	No	2.11	4.74
26S protease regulatory subunit 4	PSMC1	P62191	4.29	+	NN	R	H	128	++	No	3.32	4.29
Coiled-coil-helix-coiled-coil-helix domain-containing protein 3, mitochondrial	CHCHD3	Q9NX63	4.24	+	NN	R	H	821	+	No	3.96	4.22
Brain acid soluble protein 1	BASP1	P80723	4.15	+	Nat	R	H	519		No	3.76	4.09
Proenkephalin-B;Alpha-neoendorphin;Beta-neoendorphin	PDYN	P01213	4.13							No	3.39	4.21
ADP-ribosylation factor 5	ARF5	P84085	4.12	+	CP	R	H	310	+	No	2.81	4.03
MARCKS-related protein	MARCKSL1	P49006	4.05	+		R	H	683	+	No	4.06	4.11
Guanine nucleotide-binding protein G(k) subunit alpha	GNAI3	P08754	3.82	+	NN	R	H	221	u ++++	No	1.93	3.82
Niban-like protein 1	FAM129B	Q96TA1	3.79	+		N	H	195		No	2.14	3.57
Guanine nucleotide-binding protein G(i) subunit alpha-2	GNAI2	P04899	3.75	+	NN	R	H	35	u+++ +	No	2.38	3.77
Ragulator complex protein LAMTOR1	LAMTOR1	Q6IAA8	3.63	+		T	H	215		No	1.50	3.63

Protein phosphatase 1G	PPM1G	O15355	3.57	+	CP	R	M	475	+	No	3.91	3.63
A-kinase anchor protein 12	AKAP12	Q02952	3.46	+	NN	R	H	15		No	1.52	3.05
ADP-ribosylation factor 4	ARF4	P18085	3.44	+	CP	R	H	585	+	No	3.45	3.45
ADP-ribosylation factor 3;ADP-ribosylation factor 1	ARF3;ARF1	P61204	3.38	+	NN	T	H	2501	+;++	No	2.90	3.27
Leucine-rich repeat-containing protein 57	LRRC57	Q8N9N7	3.36	+		N	N	143		No	1.57	3.36
ADP-ribosylation factor 6	ARF6	P62330	3.34	+	NN	R	H	389		No	1.57	3.34
Bromodomain-containing protein 4;Bromodomain-containing protein 3	BRD4;BRD3	O60885	3.30							No	1.71	3.30
Guanine nucleotide-binding protein G(i) subunit alpha-1	GNAI1	P63096	3.29	+	NN	R	H	102	u++	No	1.33	3.29
Golgi reassembly-stacking protein 2	GORASP2	Q9H8Y8	3.23	+	CP	R	H	265	u	No	3.59	3.20
Nucleolar protein 3	NOL3	O60936	3.11	+		T	L	248		No	2.15	3.26
Calcium-binding protein p22	CHP	Q99653	2.94	+		R	H	92	-	No	2.26	3.26
26S protease regulatory subunit 7	PSMC2	P35998	2.90					69	-	No	1.68	2.90
Nesprin-1	SYNE1	Q8NF91	2.88							No	1.47	2.88
Myristoylated alanine-rich C-kinase substrate	MARCKS	P29966	2.63	+	Nat	R	H	160		No	3.41	2.60
E3 ubiquitin-protein ligase MGRN1	MGRN1	O60291	2.51	+	CF	R	H	15		No	1.77	2.51
Cysteine-rich and transmembrane domain-containing protein 1	CYSTM1	Q9H1C7	1.76							No	1.16	1.76
Tyrosine-protein kinase Yes	YES1	P07947	1.71	+	NN	R	H	59	u++	No	1.30	1.71
Calnexin	CANX	P27824	1.66					101	++++	No	2.39	1.55
Transmembrane 4 L6 family member 1	TM4SF1	P30408	1.62							No	2.59	1.59
Polypeptide N-acetylgalactosaminyltransferase 2	GALNT2	Q10471	1.48					77		No	2.28	1.37
Coxsackievirus and adenovirus receptor	CXADR	P78310	1.35					17	u ++	No	1.24	1.58
Podocalyxin	PODXL	O00592	1.34					25		No	1.50	1.34
CD9 antigen	CD9	P21926	1.21					127	+	No	2.45	1.20
CD59 glycoprotein	CD59	P13987	1.20	+		N	N	114		Yes	2.20	1.14
Adenosylhomocysteinase	AHCY	P23526	1.10						-	No	1.18	1.10
Complement decay-accelerating factor	CD55	P08174	1.06					92		Yes	1.44	0.95
Secretory carrier-associated membrane protein 3	SCAMP3	O14828	1.06					207	+++	No	1.65	1.14

Table H6-8: Spike-in SILAC with inhibitor IMP366. Table H6: High confidence NMT substrates. Table H7: Low confidence NMT substrates. Table H8: Protein with no MG motif sensitive to the NMT inhibitor IMP366. (n = 5 replicates). Proteins are ordered by alphabetical order of gene names. The ratios of "lysate treated with inhibitor"/ "spike-in standard" (L/H = light/heavy) were determined for each unique +razor peptide detected. The same spike-in standard was used for each replicate, across the 6 samples with different concentrations of inhibitor. The ratios L/H were normalised to the 0 µM concentration sample for each replicate to allow the comparison between all the samples. When unique peptides could not be assigned to one unique protein but were assigned instead to a group of 2 or more proteins by MaxQuant, proteins were grouped. The number of "razor + unique peptide" and the ratio counts are indicated for each replicate and each concentration of inhibitor. The mean value is indicated for each inhibitor concentration, for each protein. The median, standard deviation, the number of "razor + unique" peptides, spectral counts and sequence coverage can be found in Appendix A (Spike-in inhibitor). The IC_{50} values, errors and slope factors were determined with GraFit 7.0 (back-corrected IC_{50}) using the mean values for each concentration of inhibitor (N=4). Proteins sensitive to NMT inhibition dose dependently are classified as "N-myristoylated-high confidence". When the number of "razor + unique peptide" was low or when the dose-response was ambiguous (more than 30 % residual protein in the sample treated with the highest concentration of inhibitor), the proteins were classified as "*N*-myristoylated-low confidence". For each identified protein, myristoylation prediction (Myr predictor and Myristoylator), palmitoylation, GPI anchor, and LFQ ratio (see Table H4) are shown. When proteins were not sensitive to the NMT inhibitor, they were labelled "not N-myristoylated-high confidence". If the numbers of "razor + unique peptide" were low, the proteins were classified as "not N-myristoylated-low confidence". A column indicates if the protein has been detected before in a chemical proteomics experiments.[173,224]

Table H6: Spike-in SILAC (High confidence NMT substrates)

			Mean Ratio L/H						IC_{50} (µM)										CP		
Protein names	Gene names	Protein IDs	0	0.08	0.2	0.4	1	5	IC_{50}	Error	Slope	MP	Myrist	Pred	PR	Palm	GPI	Hang	Yao SQ	LFQ
Tyrosine-protein kinase ABL1	ABL1	P00519	1	1.19	0.38	0.21	0.31	0.07	0.15	0.25	1.26	T	N	L	CF		No			8
Apoptosis-inducing factor 2	AIFM2	Q9BRQ8	1	0.63	0.35	0.19	0.09	0.23	0.11	0.05	0.96	R	H	H	CF		No			189
A-kinase anchor protein 12	AKAP12	Q02952	1	0.87	0.54	0.29	0.14	0.04	0.23	0.02	1.48	R	H	H	NN		No			16
Ankyrin repeat and IBR domain-containing protein 1	ANKIB1	Q9P2G1	1	0.94	0.81	0.38	0.12	NaN	0.34	0.03	2.3	R	H	H	CF		No			5
ADP-ribosylation factor 1	ARF1	P84077	1	0.70	0.38	0.22	0.11	0.04	0.15	0.01	1.22	T	H	M	NN	++	No	+	+	2501
ADP-ribosylation factor 3	ARF3	P61204	1	0.67	0.36	0.21	0.11	0.04	0.14	0.01	1.2	T	H	M		+	No			2501
ADP-ribosylation factor 4	ARF4	P18085	1	0.95	0.61	0.40	0.21	0.07	0.3	0.05	1.33	R	H	H	CP	+	No	+	+	585
ADP-ribosylation factor 5	ARF5	P84085	1	0.71	0.40	0.23	0.11	0.06	0.15	0.04	1.22	R	H	H	CP	+	No	+	+	310
ADP-ribosylation factor 6	ARF6	P62330	1	0.68	0.42	0.24	0.12	0.06	0.15	0.01	1.11	R	H	H	NN		No			389
ADP-ribosylation factor-like protein 1	ARL1	P40616	1	0.46	0.22	0.14	0.07	0.03	0.07	0.01	1.05	R	H	H	CF		No			499
ADP-ribosylation factor-like protein5B	ARL5B	Q96KC2	1	0.68	0.28	0.22	NaN	0.02	0.12	0.02	1.4	N	M	L	NN		No			
Brain acid soluble protein 1	BASP1	P80723	1	0.79	0.52	0.32	0.16	0.04	0.22	0.01	1.2	R	H	H	Nat		No			519
Cyclin-Y;Cyclin-Y-like protein 1	CCNY;CCNYL1	Q8ND76	1	1.10	1.17	0.74	0.43	0.12	0.76	0.21	1.76	R	H	H	NN	+++	No			
Cell division cycle-associated protein3	CDCA3	Q99618	1	0.56	0.29	0.16	0.08	0.09	0.09	0.02	1.08	R	H	H			No			35
Coiled-coil-helix-coiled-coil-helix domain-containing protein3,mitochondrial	CHCHD3	Q9NX63	1	0.92	0.61	0.34	0.16	0.04	0.27	0.02	1.53	R	H	H	NN	+	No	+	+	822
Charged multivesicular body protein 6	CHMP6	Q96FZ7	1	0.58	0.31	0.14	0.09	0.08	0.1	0.02	1.16	R	H	H	NN		No		+	44
Calcium-binding protein p22	CHP	Q99653	1	1.09	0.75	0.45	0.20	0.07	0.36	0.06	1.72	R	H	H	CF		No			93
Battenin	CLN3	Q13286	1	1.01	0.37	0.27	0.29	0.37	0.23	0.31	0.69	T	L	L			No			13
NADH-cytochrome b5 reductase 3	CYB5R3	P00387	1	0.16	0.08	0.04	0.03	0.03	0.01	0	0.83	R	H	H	NN	++	No		+	457
Sphingolipid delta(4)-desaturaseDES1	DEGS1	O15121	1	0.39	0.17	0.14	0.05	0.04	0.05	0.01	0.96	T	H	M	NN		No			99

Disrupted in renal carcinoma protein 2	DIRC2	Q96SL1	1	0.47	0.31	0.16	0.13	0.18	0.05	0.03	0.57	R	H	H			No			20
Dymeclin	DYM	Q7RTS9	1	0.76	0.40	0.21	0.10	0.05	0.16	0.01	1.43	R	H	H	CF		No			13
Protein Niban	FAM129A	Q9BZQ8	1	0.68	0.42	0.31	0.16	0.14	0.16	0.06	0.83	R	H	H			No			23
Niban-like protein 1	FAM129B	Q96TA1	1	0.49	0.23	0.13	0.06	0.04	0.08	0.01	1.16	N	H	M			No			196
Protein FAM49B	FAM49B	Q9NUQ9	1	0.23	0.10	0.06	0.03	0.03	0.02	0	1	N	M	L	CP	+++	No	+	+	686
Flotillin-2	FLOT2	Q14254	1	0.72	0.42	0.23	0.15	0.28	0.15	0.1	0.74	N	N	N		+++	No			83
Formin-like protein 1	FMNL1	O95466	1	0.46	0.20	0.15	0.10	0.07	0.06	0.01	0.91	T	N	L	NN		No			28
Formin-like protein 2	FMNL2	Q96PY5	1	0.83	0.43	0.47	0.19	NaN	0.25	0.09	0.99	T	H	M	CF		No			9
Golgi-associated plant pathogenesis-related protein 1	GLIPR2	Q9H4G4	1	0.40	0.19	0.10	0.16	0.02	0.04	0.02	0.78	R	H	H	Nat		No			92
Guanine nucleotide-binding protein G(i) subunit alpha-1	GNAI1	P63096	1	0.76	0.46	0.25	0.12	0.05	0.18	0.01	1.28	R	H	H	NN	u, ++	No			103
Guanine nucleotide-binding protein G(i) subunit alpha-2	GNAI2	P04899	1	0.69	0.41	0.22	0.11	0.04	0.15	0.01	1.2	R	H	H	NN	++++	No	+		35
Guanine nucleotide-binding protein G(k) subunit alpha	GNAI3	P08754	1	0.73	0.43	0.23	0.11	0.04	0.17	0.003	1.29	R	H	H	NN	++++	No	+	+	221
Guanine nucleotide-binding protein G(o) subunit alpha	GNAO1	P09471	1	0.63	0.33	0.16	0.08	0.02	0.12	0.01	1.31	R	H	H	NN	u, +++	No	+		68
Golgi reassembly-stacking protein 2	GORASP2	Q9H8Y8	1	0.86	0.57	0.33	0.17	0.07	0.25	0.03	1.32	R	H	H	CP		No		+	265
Cytochrome c-type heme lyase	HCCS	P53701	1	0.45	0.20	0.12	0.06	0.05	0.06	0.01	1.08	R	L	M			No			306
Hippocalcin-like protein 1;Neuron-specific calcium-binding protein hippocalcin	HPCAL1;HPCA	P37235;P84074	1	0.40	0.18	0.09	0.04	0.02	0.06	0	1.15	R	H	H	NN		No			504
TLD domain-containing protein KIAA1609	KIAA1609	Q6P9B6	1	0.52	0.27	0.17	NaN	NaN	0.08	0.01	1.05	T	H	M	CF		No			23
Ragulator complex protein LAMTOR1	LAMTOR1	Q6IAA8	1	0.93	0.55	0.32	0.15	0.07	0.24	0.04	1.54	T	H	M			No	+		215
Protein lunapark	LNP	Q9C0E8	1	0.83	0.44	0.26	0.19	0.14	0.19	0.05	1.2	T	H	M	CF		No			76
Leucine-rich repeat-containing protein 57	LRRC57	Q8N9N7	1	0.43	0.20	0.11	0.05	0.06	0.06	0.01	1.11	N	N	N			No			144
Tyrosine-protein kinase Lyn	LYN	P07948	1	0.56	0.28	0.15	0.08	0.13	0.09	0.02	1.08	R	H	H	NN	u, +	No			79
MOSC domain-containing protein 1, mitochondrial	MARC1	Q5VT66	1	0.36	0.13	0.10	0.05	0.03	0.05	0.01	1.1	N	H	M			No			29
MOSC domain-containing protein 2, mitochondrial	MARC2	Q969Z3	1	0.53	0.18	0.12	0.06	NaN	0.08	0.01	1.47	N	N	N			No			43
Myristoylated alanine-rich C-kinase substrate	MARCKS	P29966	1	1.15	0.96	0.65	0.37	0.11	0.61	0.14	1.52	R	H	H	Nat		No			1604
MARCKS-related protein	MARCKSL1	P49006	1	0.84	0.54	0.30	0.14	0.04	0.23	0.01	1.4	R	H	H		+	No	+	+	683
E3 ubiquitin-protein ligase MGRN1	MGRN1	O60291	1	1.16	0.83	0.62	0.31	0.13	0.53	0.14	1.43	R	H	H	CF		No			16
Neuronal calcium sensor 1	NCS1	P62166	1	0.83	0.52	0.28	0.14	0.04	0.22	0.02	1.4	R	H	H	NN		No			19
NADH dehydrogenase [ubiquinone] 1 alpha subcomplex assembly factor 4	NDUFAF4	Q9P032	1	0.12	0.05	0.06	0.05	0.13	0.002	0.01	0.56	N	N	N			No			91
NADH dehydrogenase [ubiquinone] 1 beta subcomplex subunit 7	NDUFB7	P17568	1	0.69	0.46	0.25	0.10	0.09	0.16	0.02	1.13	N	L	N	CF		No			43

Nucleolar protein 3	NOL3	O60936	1	0.55	0.28	0.14	0.08	0.06	0.09	0.01	1.17	T	L	L			No			248
Protein-L-isoaspartate O-methyl transferase domain-containing protein 1	PCMTD1	Q96MG8	1	0.28	0.16	0.08	0.07	NaN	0.02	0.05	0.79	R	H	H			No			18
Phosphoinositide 3-kinase regulatory subunit 4	PIK3R4	Q99570	1	1.10	0.77	0.56	0.20	0.14	0.42	0.1	1.62	T	H	M	CF		No			42
Protein phosphatase 1A	PPM1A	P35813	1	0.98	0.70	0.44	0.22	0.10	0.35	0.06	1.37	N	H	M	NN		No			115
Protein phosphatase 1B	PPM1B	O75688	1	1.23	0.87	0.47	0.22	0.06	0.37	0.08	1.95	N	M	L	NN		No			41
Protein phosphatase 1G	PPM1G	O15355	1	0.95	0.62	0.37	0.17	0.06	0.29	0.04	1.5	R	M	M	CP	+	No	+	+	475
Calcineurin subunit B type 1	PPP3R1	P63098	1	0.65	0.33	0.17	0.07	0.05	0.12	0.01	1.34	R	H	H	NN		No			40
cAMP-dependent protein kinase catalytic subunit alpha	PRKACA	P17612;	1	0.28	0.13	0.07	0.03	0.02	0.03	0	0.98	R	H	H	Nat		No		+	739
cAMP-dependent protein kinase catalytic subunit beta	PRKACB	P22694	1	0.42	0.20	0.11	0.06	0.05	0.06	0.01	1.05	R	H	H			No			202
5-AMP-activated protein kinase subunit beta-1	PRKAB1	Q9Y478	1	0.33	NaN	NaN	NaN	NaN	0.07	0.01	3.52	N	N	N	NN		No			
26S protease regulatory subunit 4	PSMC1	P62191	1	0.88	0.54	0.31	0.15	0.06	0.24	0.03	1.45	R	H	H	NN	++	No	+	+	1282
Raftlin	RFTN1	Q14699	1	0.45	0.07	0.21	0.16	0.57	0.04	0.03	0.75	N	H	M	NN	u	No			25
RING finger protein 141	RNF141	Q8WVD5	1	0.29	0.14	0.10	NaN	0.24	0.002	0	0.3	N	H	M			No			29
Protein XRP2	RP2	O75695	1	1.06	0.88	0.62	0.28	0.10	0.53	0.07	1.59	R	H	H		u	No			31
Protein-associating with the carboxyl-terminal domain of ezrin	SCYL3	Q8IZE3	1	0.28	0.22	NaN	0.13	0.03	0.01	0.01	0.44	R	H	H	NN		No			
Cytospin-B	SPECC1	Q5M775;	1	0.70	0.21	0.14	0.06	0.05	0.12	0.01	1.94	T	N	L			No			49
Proto-oncogene tyrosine-protein kinase Src	SRC	P12931	1	0.65	0.37	0.17	0.09	0.01	0.13	0.01	1.27	R	H	H	Nat	+	No			72
Tescalcin	TESC	Q96BS2	1	0.78	0.47	0.24	0.12	0.05	0.19	0.02	1.37	R	H	H	CF		No			458
Transmembrane protein 106B	TMEM106B	Q9NUM4	1	0.41	0.20	0.15	0.07	0.07	0.05	0.01	0.83	T	H	M			No			65
Tyrosine-protein kinase Yes	YES1	P07947	1	0.63	0.26	0.15	0.08	NaN	0.11	0.01	1.44	R	H	H	NN	u,++	No			60
E3 ubiquitin-protein ligase ZNRF2	ZNRF2	Q8NHG8	1	0.27	0.13	0.09	0.17	0.15	0.002	0	0.33	R	M	M	NN		No			57

Table H7: Spike-in SILAC (Low confidence NMT substrates).

			Mean Ratio L/H						IC_{50} (μM)									
Protein names	Gene names	Protein IDs	0	0.08	0.2	0.4	1	5	IC_{50}	Error	Slope	MP	Myrist	Pred	PR	Palm	GPI	LFQ
N-myristoylated proteins- Low confidence (low number of razor+unique peptides)																		
ADP-ribosylation factor-like protein 2	ARL2	P36404	1	0.65	0.42	0.27	0.1	NaN	0.15	0.01	1.06	N	N	N			No	21.6
Transmembrane protein C9orf123	C9orf123	Q96GE9	1	0.07	NaN	NaN	0.16	NaN	0	0	0.59	R	H	H			No	
DDB1- and CUL4-associated factor 11	DCAF11	Q8TEB1	1	0.19	NaN	NaN	0.03	NaN	0.01	0	0.84	R	H	H			No	
cAMP-dependent protein kinase catalytic subunit gamma	PRKACG	P22612	1	0.31	0.13	0.07	0.02	0.02	0.04	0	1.15	R	H	H			No	24.2
RING finger protein 11	RNF11	Q9Y3C5	1	NaN	NaN	0.22	0.24	NaN	0.05	0.1	0.53	N	M	L	CF		No	6.63
Small VCP/p97-interacting protein	SVIP	Q8NHG7	1	0.15	0.2	0.12	NaN	NaN	0.01	0	0.32	N	N	N			No	6.63
Ubiquitin carboxyl-terminal hydrolase 32	USP32	Q8NFA0	1	0.58	0.17	0.08	NaN	0.09	0.09	0.01	1.96	N	H	M			No	4.29
N-myristoylated proteins- Low confidence (ambiguous dose response , ratios do not drop below 0.3)																		
Abelson tyrosine-protein kinase 2	ABL2	P42684	1	0.35	NaN	0.4	NaN	NaN	0.03	0.06	0.3	T	M	M			No	13.7
DCN1-like protein 3	DCUN1D3	Q8IWE4	1	1.11	1	0.85	0.51	NaN	N/A	N/A	N/A	R	M	M		+	No	
DDXX46	DDX46	Q7L014	1	0.99	0.82	0.72	0.57	0.6	N/A	N/A	N/A	N	N	N			No	
F-box only protein 17	FBXO17	Q96EF6	1	0.39	0.36	NaN	NaN	NaN	0.99	0.11	1.21	T	H	M			No	
Formin-like protein 3	FMNL3	Q8IVF7	1	0.81	NaN	NaN	NaN	NaN	N/A	N/A	N/A	T	M	M	CF		No	
Guanine nucleotide-binding protein G(I)/G(S)/G(T) subunit beta-3	GNB3	P62873	1	0.71	0.66	0.34	0.37	0.32	N/A	N/A	N/A	N	N	N			No	
Golgi reassembly-stacking protein 1	GORASP1	Q9BQQ3	1	0.12	NaN	NaN	0.51	NaN	N/A	N/A	N/A	R	H	H	CF		No	10.8
L-lactate dehydrogenase A chain	LDHA	P00338	1	0.93	0.77	0.59	0.54	0.55	N/A	N/A	N/A	N	N	N		++	No	
Mitochondrial peptide methionine sulfoxide reductase	MSRA	Q9UJ68	1	1.48	1.13	0.73	NaN	NaN	N/A	N/A	N/A	R	H	H	NN		No	
Monofunctional C1-tetrahydrofolate synthase, mitochondrial	MTHFD1L	Q6UB35	1	0.76	NaN	NaN	NaN	NaN	N/A	N/A	N/A	N	N	N			No	
Opioid growth factor receptor-like protein 1	OGFRL1	Q5TC84	1	0.54	0.74	0.63	NaN	NaN	N/A	N/A	N/A	N	M	L			No	12
Platelet-activating factor acetylhydrolase 2	PAFAH2	Q99487	1	0.6	0.31	NaN	NaN	0.39	N/A	N/A	N/A	N	N	N			No	10.6
Testisin	PRSS21	Q9Y6M0	1	0.74	0.69	0.46	0.45	0.47	N/A	N/A	N/A	N	N	N			Pot	9.33
Inactive tyrosine-protein kinase 7	PTK7	Q13308	1	1.09	0.68	0.62	0.78	0.59	N/A	N/A	N/A	N	N	N		+	No	
Serine incorporator 3	SERINC3	Q13530	1	0.78	0.65	0.54	0.49	0.6	N/A	N/A	N/A	N	N	N			No	19.2
ADP/ATP translocase 3	SLC25A6	P12236	1	0.87	0.7	0.57	0.55	0.57	N/A	N/A	N/A	N	N	N		+;++	No	7.83
Choline transporter-like protein 1	SLC44A1	Q8WWI5	1	0.52	0.51	0.39	0.37	0.41	N/A	N/A	N/A	R	M	M		+	No	94.4
TOM40 homolog	TOMM40	O96008	1	0.69	0.75	0.66	0.41	0.46	N/A	N/A	N/A	T	L	L		+	No	
Probable palmitoyltransferase ZDHHC6	ZDHHC6	Q9H6R6	1	NaN	NaN	0.42	0.53	NaN	0.47	0.55	0.65	N	H	M		+	No	
ZZEF1	ZZEF1	O43149	1	1.45	1.16	0.67	0.44	0.45	N/A	N/A	N/A	R	H	H	CF		No	

Table H8: Spike-in SILAC, protein with no MG motif sensitive to the NMT inhibitor IMP366.

			Mean Ratio L/H								
Protein name	Gene name	Uniprot ID	0	0.1	0.2	0.4	1	5	Palm	GPI	LFQ
BAG family molecular chaperone regulator 5	BAG5	Q9UL15	1	0.55	0.24	0.16	0.06	0.07		No	45
Flotillin-1	FLOT1	O75955	1	0.65	0.42	0.34	0.30	0.17	+++	No	6
Histone H2A.x;Histone H2A type 1-B/E;Histone H2A type 1;Histone H2A type 1-D;Histone H2A type 3;Histone H2A type 1-C;Histone H2A.J;Histone H2A type 1-H;Histone H2A type 1-J;Histone H2A type 1-A;Histone H2A type 2-B	H2AFX;HIST1H2AB;HIST1H2AG;HIST1H2AD;HIST3H2A;HIST1H2AC;H2AFJ;HIST1H2AH;HIST1H2AJ;HIST1H2AA;HIST2H2AB	P16104;P04908;P0C0S8;P20671;Q7L7L0;Q93077;Q9BTM1;Q96KK5;Q99878;Q9BTM1-2;Q96QV6;Q8IUE6	1	0.24	0.14	0.28	0.14	0.11			
LanC-like protein 1	LANCL1	O43813	1	0.86	0.97	0.59	0.41	0.16		No	12
Serine/threonine-protein phosphatase 2B catalytic subunit alpha isoform;Serine/threonine-protein phosphatase 2B catalytic subunit beta isoform	PPP3CA;PPP3CB	Q08209;Q08209-2;Q08209-3;P16298-4;P16298;P16298-3;P16298-2	1	0.69	0.45	0.25	0.17	0.14		No	17
26S protease regulatory subunit 7	PSMC2	P35998	1	0.83	0.47	0.28	0.16	0.09		No	70
26S protease regulatory subunit 6A	PSMC3	P17980	1	0.90	0.60	0.43	0.33	0.28		No	9
26S protease regulatory subunit 6B	PSMC4	P43686;P43686-2	1	0.90	0.65	0.42	0.26	0.17			
26S protease regulatory subunit 8	PSMC5	P62195	1	0.90	0.55	0.40	0.20	0.12		No	6
26S protease regulatory subunit 10B	PSMC6	P62333	1	0.87	0.60	0.36	0.23	0.16		No	6
26S proteasome non-ATPase regulatory subunit 2	PSMD2	Q13200	1	0.83	0.57	0.33	0.26	0.20		No	10
Serpin B6	SERPINB6	P35237	1	1.04	0.83	0.64	0.36	0.19		No	66

Table H9: Base-treatment.
(n= 2 biological replicates). When unique peptides could not be assigned to one unique protein but were assigned instead to a group of 2 or more proteins by MaxQuant, proteins were grouped and had the same number of unique peptides. Heavy (R10K8) YnC12-treated HeLa lysates were not treated and light (grown in the standard media) YnC12-treated HeLa lysates were treated with 0.2M NaOH (both labelled with YnC12). Samples were mixed in 1:1 ratio after the base-treatment. Only proteins significantly depleted in the base-treated sample are shown (FRD 0.01, 250 permutations, S2). Two columns show the results of the t-test (log2 values). MG = proteins with a N-terminal MG motif. PR = previously reported (Appendix F). Pred= combined predictions of MYR predictor and Myristoylator (Section 8.3.9). A column indicates if the protein is palmitoylated (+: found in 1 study, ++: found in 2 studies; +++: found in 3 studies; ++++: found in 4 studies; u: reported as palmitoylated in the UniProtKB/Swiss-Prot database) and a column indicates if the protein is a GPI anchored protein). LFQ = LFQ enrichment as determined in Table H4.

Protein names	Gene names	Protein IDs	ratio base/no base	-Log t-test p value	t-test Difference	MG	PR	Pred	Palm	GPI	LFQ
CD59 glycoprotein	CD59	P13987	17.8	0.7	-22.7	+		N		Yes	
CD44 antigen	CD44	P16070	7.9	0.5	-11.8				+	No	115
Complement decay-accelerating factor	CD55	P08174	8.8	2.6	-11.2					Yes	149
Voltage-dependent anion-selective channel protein 2	VDAC2	P45880	9.0	0.6	-11.1				+	No	92.2
Transferrin receptor protein 1	TFRC	P02786	6.9	2.1	-10.6				++++	No	13.7
Beta-1,4-galactosyltransferase1	B4GALT1	P15291	8.3	1.4	-10.2					No	261
Calnexin	CANX	P27824	3.8	2.8	-9.5				++++	No	82.7
CD276 antigen	CD276	Q5ZPR3	5.9	1.3	-9.0					No	102
Endothelial protein C receptor	PROCR	Q9UNN8	5.7	3.0	-7.8				+	No	34.8
CD151 antigen	CD151	P48509	4.9	3.7	-6.4	+		N	+	No	20.1
Golgi integral membrane protein 4	GOLIM4	O00461	3.3	1.4	-5.8	+		H	+	No	117
Podocalyxin	PODXL	O00592	2.5	1.7	-5.8					No	25.3
Prostaglandin F2 receptor negative regulator	PTGFRN	Q9P2B2	4.4	1.1	-5.5	+		L	++	No	25.7
Lysosome membrane protein 2	SCARB2	Q14108	4.9	4.1	-5.5	+		N	++	No	226
Voltage-dependent calcium channel subunit alpha-2/delta-1	CACNA2D1	P54289	5.3	1.5	-5.3					No	111
Choline transporter-like protein 2	SLC44A2	Q8IWA5	3.2	1.5	-5.3	+		N		No	71.3
Polypeptide N-acetylgalactosaminyltransferase 1	GALNT1	Q10472	3.8	1.3	-5.2					No	44.3
Poliovirus receptor	PVR	P15151	3.4	2.3	-5.1				+	No	20.8
CD81 antigen	CD81	P60033	4.9	1.1	-5.0	+	CP	N	+++	No	7.1
Cysteine-rich and transmembrane domain-containing protein 1	CYSTM1	Q9H1C7	4.3	2.5	-4.9					No	152
Niemann-Pick C1 protein	NPC1	O15118	3.6	1.5	-4.9					No	
CD63 antigen	CD63	P08962	4.3	3.0	-4.7				+	No	47
Cytoskeleton-associated protein 4	CKAP4	Q07065	3.5	1.5	-4.6				+++	No	67.3
Erythrocyte band 7 integral membrane protein	STOM	P27105	4.6	4.8	-4.6				+++	No	184
Serine incorporator 1	SERINC1	Q9NRX5	4.8	2.5	-4.5	+	CF	N		No	190
Bone marrow stromal antigen 2	BST2	Q10589	4.4	2.2	-4.3					Pot	85.1
DnaJ homolog subfamily C member 5	DNAJC5	Q9H3Z4	3.9	2.0	-4.3				++	No	414
CD9 antigen	CD9	P21926	3.0	2.5	-4.2				+	No	21
Neutral amino acid transporter B(0)	SLC1A5	Q15758	3.7	2.5	-4.2				+++	No	128
Transmembrane protein 63B	TMEM63B	Q5T3F8	2.6	0.8	-4.1				++	No	59.9
Adenosine 3-phospho 5-phosphosulfate transporter 1	SLC35B2	Q8TB61	2.8	1.0	-3.8				+	No	
Carboxypeptidase D	CPD	O75976	2.5	0.8	-3.8				+	No	20.8
Caveolin-1	CAV1	Q03135	2.7	2.4	-3.8				+	No	12.5

Leucyl-cystinyl aminopeptidase;Leucyl-cystinyl aminopeptidase, pregnancy serum form	LNPEP	Q9UIQ6	3.8	1.6	-3.8				+++	No	33
Zinc transporter 1	SLC30A1	Q9Y6M5	3.0	1.8	-3.7	+		N	-	No	6.76
Vasorin	VASN	Q6EMK4	1.5	0.5	-3.7					No	34.3
Phosphatidylinositol 4-kinase type 2-alpha	PI4K2A	Q9BTU6	3.2	3.0	-3.6				+++	No	17.2
Neural cell adhesion molecule L1	L1CAM	P32004	3.3	0.8	-3.6				+	No	44.1
Rho-related GTP-binding protein RhoB	RHOB	P62745	2.6	0.8	-3.5				++	No	22.3
Alkaline phosphatase, tissue-nonspecific isozyme	ALPL	P05186	3.5	2.5	-3.5					Prob	22.6
Serine/arginine repetitive matrix protein 2	SRRM2	Q9UQ35	8.4	4.6	-3.3					No	8.57
CD82 antigen	CD82	P27701	4.8	1.9	-3.1	+	CP	N	+	No	
Sn1-specific diacylglycerol lipase beta	DAGLB	Q8NCG7	3.2	1.9	-3.1				++	No	
Leucine-rich repeat-containing protein 15	LRRC15	Q8TF66	3.4	1.6	-2.9					No	177
Secretory carrier-associated membrane protein 3	SCAMP3	O14828	2.2	1.4	-2.8				+++	No	24.2
Myoferlin	MYOF	Q9NZM1	3.5	1.3	-2.7					No	208
Probable phospholipid-transporting ATPase IIA	ATP9A	O75110	1.9	2.2	-2.6					No	15.1
Endothelin-converting enzyme 1	ECE1	P42892	2.2	1.9	-2.4				+	No	4.63
Thioredoxin-related transmembrane protein 1	TMX1	Q9H3N1	1.9	1.7	-2.3					No	19.7
60S ribosomal protein L18	RPL18	Q07020	4.2	2.5	-2.2	+		N		No	78.3
Polypeptide N-acetylgalactosaminyltransferase 2	GALNT2	Q10471	2.1	1.2	-2.2					No	
Serine incorporator 3	SERINC3	Q13530	2.5	1.7	-2.1	+		N		No	77
Endoplasmic reticulum mannosyl-oligosaccharide 1,2-alpha-mannosidase	MAN1B1	Q9UKM7	2.3	1.5	-2.1					No	19.2
Tetraspanin-6	TSPAN6	O43657	2.5	2.1	-1.9					No	16.5
60S ribosomal protein L28	RPL28	P46779	3.7	1.5	-1.8					No	6.57

Table H10: List of NMT substrates identified with high confidence in the current study with GO annotations (localisation, biological process and molecular function). Pred= combined predictions of MYR predictor and Myristoylator (Section 4.8). PR= previously reported to as NMT substrates (Appendix F).

Gene names	Protein IDs	In cell IC_{50} (μM)	Mod pep	Localisation	Biological process	Molecular function	Pred	PR
ABL1	P00519	0.147		Cytoskeleton; Membrane; Mitochondrion; Nucleus; Cytoplasm	DNA repair; Autophagy; Cell adhesion; DNA damage; Endocytosis;Apoptosis	Tyrosine-protein kinase; Transferase;Kinase	L	CF
AIFM2	Q9BRQ8	0.114		Cytoplasm, , Mitochondrion outer membrane	Apoptosis, chromosome condensation	Oxidoreductase, DNA binding	H	CF
AKAP12	Q02952	0.227	+	Cytoplasm, Cytoskeleton	G-protein coupled receptor signaling pathway, positive regulation of cAMP biosynthetic process, positive regulation of protein kinase A signaling cascade, protein targeting	Protein kinase A binding	H	NN
ANKIB1	Q9P2G1	0.344		Unknown	Unknown	Zinc ion binding	H	CF
ARF1	P84077	0.146	+	Cytoplasm, Golgi apparatus	ER-Golgi transport, Protein transport	GTP binding, GTPase activity, receptor signaling protein activity	M	NN
ARF3	P61204	0.135	+				M	
ARF4	P18085	0.301	+				H	CP
ARF5	P84085	0.153	+				H	CP
ARF6	P62330	0.151					H	NN
ARL1	P40616	0.067		Golgi apparatus, Membrane	Golgi organization, Golgi vesicle transport, activation of phospholipase D activity, protein localization to Golgi apparatus, retrograde transport	GTP binding, GTPase activity, enzyme activator activity, metal ion binding	H	CF
ARL5B	Q96KC2	0.123	+	Intracellular	Small GTPase mediated signal transduction	GTP binding	L	NN
BASP1	P80723	0.219		Cell membrane, cell projection	Diaphragm development, glomerular visceral epithelial cell differentiation, gonad development	Transcription corepressor activity, transcription regulatory region DNA binding	H	N
CCNY;CCNYL1	Q8ND76	0.762		Cell membrane, nucleus	Cell division; Wnt signaling pathway;Cell cycle	Cyclin-dependent protein serine/threonine kinase regulator activity	H	NN
CDCA3	Q99618	0.094		Cytoplasm	Cell division; Mitosis; Ubl conjugation pathway;Cell cycle		H	

CHCHD3	Q9NX63	0.273	+	Cytoplasm, Mitochondrion inner membrane, Nucleus	Transcription regulation, inner mitochondrial membrane organization, mitochondrial fusion	negative regulation of transcription, phosphatase binding, protein complex scaffold	H	NN
CHCHD6	Q9NX64	N/A	+	Mitochondrial inner membrane	Cristae formation, response to DNA damage stimulus		H	
CHMP6	Q96FZ7	0.101	+	Endosome, Membrane	Protein transport	Unknown	H	NN
CHP	Q99653	0.361		Cell membrane, Cytoplasm, Cytoskeleton, Endoplasmic reticulum, Nucleus	Protein transport	Protein kinase inhibitor	H	CF
CLN3	Q1328	0.231		Endosome, Lysosome, Membrane	Transport of late endosomes and lysosomes	Unfolded protein binding	L	
CYB5R3	P00387	0.011	+	Cytoplasm, Endoplasmic reticulum, Mitochondrion outer membrane	Cholesterol, lipid, steroid, sterol biosynthesis and metabolism, blood circulation	Oxidoreductase	H	NN
DEGS1	O15121	0.049		Endoplasmic reticulum, Membrane, Mitochondrion	Lipid biosynthesis and metabolism	Oxidoreductase	M	NN
DIRC2	Q96SL1	0.050		Lysosome, membrane	Electrogenic metabolite transporter.	Transport	H	
DYM	Q7RTS9	0.160		Cytoplasm, Golgi apparatus	Golgi organisation, bone development	Unknown	H	CF
FAM129A	Q9BZQ8	0.160		Cytoplasm	Translation regulation;Stress response	Regulates phosphorylation of proteins involved in translation regulation	H	
FAM129B	Q96TA1	0.076	+	Cytoplasm, cell junction	Negative regulation of apoptosis process	phospholipid binding	M	
FAM49B	Q9NUQ9	0.023		Cilium	Unknown	Unknown	L	CP
FLOT2	Q14254	0.150		Cell membrane, endosome	Cell adhesion	Unknown	N	
FMNL1	O95466	0.060		Cell projection; Cytoplasm; Cytoplasmic vesicle; Cell membrane	Cortical actin cytoskeleton organization; regulation of cell shape; substrate-dependent cell migration	Actin filament binding; Rac GTPase binding;GTPase activating protein binding	L	NN
FMNL2	Q96PY5	0.246		Cytoplasm	Regulation of cell morphology and cytoskeletal organization	Unknown	M	CF
GLIPR2	Q9H4G4	0.042		Membrane, Golgi apparatus	Unknown	Unknown	H	N
GNAI1	P63096	0.179	+	Cell membrane, Cytoplasm, Cytoskeleton, Membrane	Cell cycle, cell division	Transducer, GTP binding, GTPase activity, metal ion binding, G-protein beta/gamma-subunit complex binding, G-protein coupled serotonin receptor binding	H	NN
GNAI2	P04899	0.149	+				H	NN
GNAI3	P08754	0.165					H	NN
GNAO1	P09471	0.118		neuron projection;heterotrimeric G-protein complex	Adenylate cyclase-modulating G-protein coupled receptor signaling pathway	Transducer	H	NN
GORASP2	Q9H8Y8	0.248	+	Golgi apparatus, Membrane	Organelle organisation	Unknown	H	CP
HCCS	P53701	0.063	+	Mitochondrion inner membrane	Organ morphogenesis, oxidation-reduction process	Lyase, holocytochrome-c synthase activity	M	

HPCAL1; HPCA	P37235	0.055		Unknown	Inner ear development	Calcium ion binding, actin binding	H	NN
KIAA1609	Q6P9B6	0.085		Unknown	Unknown	Unknown	M	CF
LAMTOR1	Q6IAA8	0.242		Cell membrane, endosome, Lysosome	Cell growth, cellular protein localisation, cellular response to amino acid stimulus, cholesterol homeostasis, endosome localization	Unknown	M	
LNP	Q9C0E8	0.191	+	Cytoplasm	Blood coagulation, embryonic digit morphogenesis, embryonic forelimb morphogenesis, limb development	Developmental protein	M	CF
LRRC57	Q8N9N7	0.060	+	Unknown	Unknown	Unknown	N	
LYN	P07948	0.092		Cell membrane, Cytoplasm, Golgi apparatus, Membrane, Nucleus	Adaptive immunity, Host-virus interaction, Immunity, Inflammatory response, Innate immunity	Tyrosine-protein kinase	H	NN
MARC1	Q5VT66	0.046	+	Mitochondrion outer membrane	nitrate metabolic process;detoxification of nitrogen compound	Oxidoreductase	M	
MARC2	Q969Z3	0.084	+	Miitochondrion outer membrane	nitrate metabolic process	Oxidoreductase	N	
MARCKS	P29966	0.612	+	Cytoplasm, cytoskeleton	Energy reserve metabolic process, regulation of insulin secretion, small molecule metabolic process	Actin filament binding, calmodulin binding	H	N
MARCKS L1	P49006	0.229	+	Cell membrane, cytoplasm	Controls cell movement by regulating actin cytoskeleton homeostasis and filopodium and lamellipodium formation; Positive regulation of cell proliferation	Unknown	H	
MGRN1	O60291	0.527		Cytoplasm; Endosome; Membrane; Nucleus; Cell membrane	Ubl conjugation pathway	Ligase	H	CF
NCS1	P62166	0.216		Cell junction, Cell membrane, Cytoplasm, Golgi apparatus, Membrane, Postsynaptic cell membrane, Synapse	phosphatidylinositol-mediated signaling, positive regulation of exocytosis, regulation of neuron projection development	Calcium ion binding, voltage-gated calcium channel activity	H	NN
NDUFAF4	Q9P032	0.002	+	Mitochondrion	mitochondrial respiratory chain complex I assembly	Involved in the assembly of mitochondrial NADH:ubiquinone oxidoreductase complex (complex I).	N	
NDUFB7	P17568	0.163	+	Membrane, Mitochondrion, Mitochondrion inner membrane	Electron transport, Respiratory chain, Transport	NADH dehydrogenase (ubiquinone) activity	N	CF
NOL3	O60936	0.093	+	Cytoplasm, nucleus	Negative regulation of apoptosis, mRNA processing, mRNA splicing, response to hypoxia	RNA binding	L	
OGFRL1	Q5TC84	N/A	+	Membrane	Unknown	Receptor protein	L	

PCMTD1	Q96MG8	0.024	+	Cytoplasm	Unknown	Protein-L-isoaspartate (D-aspartate) O-methyltransferase activity	H	
PIK3R4	Q99570	0.420		Endosome	Innate immune response, insulin receptor signaling pathway, phosphatidylinositol biosynthetic process, small molecule metabolic process	Serine/threonine-protein kinase, transferase	M	CF
PLGRKT	Q9HBL7	N/A	+	Integral to plasma membrane, mitochondrion	Chemotaxis ,Inflammatory response,Plasminogen activation		M	
PPM1A	P35813	0.354	+	Nucleus	Wnt receptor signaling pathway, cell cycle arrest, insulin receptor signaling pathway, negative regulation of SMAD protein complex assembly, negative regulation of transcription	Hydrolase, Protein phosphatase, metal ion binding	M	NN
PPM1B	O75688	0.373		Cytosoplasm	cytokine-mediated signaling pathway, peptidyl-threonine dephosphorylation	Hydrolase, Protein phosphatase, metal ion binding	L	NN
PPM1G	O15355	0.285	+	Cytoplasm, nucleus	Cell cycle arrest, peptidyl-threonine dephosphorylation	Hydrolase, Protein phosphatase, metal ion binding	M	CP
PPP3R1	P63098	0.123	+	Cytoplasm	Apoptosis	Calcium ion binding protein, calcium-dependent protein serine/threonine phosphatase activity, calmodulin binding protein	H	NN
PRKAB1	Q9Y478	0.066		Cytoplasm, Nucleus	Lipid biosynthesis and metabolism, cell cycle arrest, insulin receptor signaling pathway, positive regulation of gene expression	Protein kinase activity	N	NN
PRKACA	P17612	0.030	+	Cell membrane, Cytoplasm, Membrane, Mitochondrion, Nucleus	Cell proliferation,cell cycle regulation, blood coagulation, transmembrane transport	Serine/threonine-protein kinase, Transferase	H	N
PRKACB	P22694	0.057	+	Cell membrane, Cytoplasm, Nucleus	Cell proliferation,cell cycle regulation, differentiation and regulation of microtubule dynamics, chromatin condensation and decondensation	Serine/threonine-protein kinase, Transferase	H	
PSMC1	P62191	0.236	+	Cytoplasm, Nucleus, Proteasome	Degradation of ubiquitinated proteins	ATP binding, ATPase activity	H	NN
RFTN1	Q14699	0.042		Membrane, cell membrane	Unknown	Unknown	M	NN
RNF141	Q8WVD5	0.002	+	Unknown	Regulation of transcription, DNA-dependent	DNA binding, Zinc ion binding	M	
RP2	O75695	0.535	+	Cell membrane, Cell projection, Cilium, Membrane	Protein transport	GTP binding, GTPase activity, ATP binding, nucleoside diphosphate kinase activity, unfolded protein binding	H	

SCYL3	Q8IZE3	0.010		Cytoplasm; Golgi apparatus;Cell projection	Protein phosphorylation;cell migration	Transferase activity, transferring phosphorus-containing groups;ATP binding	H	NN
SPECC1	Q5M775	0.117	+	Nucleus	Unknown	Unknown	L	
SRC	P12931	0.129		Cell membrane, Mitochondrion inner membrane, Nucleus	Cell adhesion, Cell cycle, Host-virus interaction, Immunity	Transferase, Tyrosine-protein kinase	H	N
TESC	Q96BS2	0.185	+	Cell membrane, Cell projection, Cytoplasm, Membrane, Nucleus	Protein transport, differentiation	Protein kinase inhibitor	H	CF
TMEM106B	Q9NUM4	0.048		Endosome, Lysosome, Membrane	Unknown	Unknown	M	
TOMM40L	Q969M1	N/A	+	Mitochondrial outer membrane, pore complex	Ion transport, protein transport	Porin activity	M	
YES1	P07947	0.108		Cytoplasm; Cytoskeleton; Membrane;Cell membrane	Unknown	Transferase; Tyrosine-protein kinase;Kinase	H	NN
ZNRF2	Q8NHG8	0.002		Cell junction, Cell membrane, Endosome, Lysosome, Membrane, Synapse	Protein ubiquitination	Ligase	M	NN

Appendix I: Turnover experiments

Table I1: Protein half life ($t_{1/2}$) of the 74 NMT substrates identified with high confidence in Chapter 4 (Section 5.3). L/H = chase of the light isotope. T = YnC12 pulse chase and TI = YnC12 pulse chase in the presence of NMT inhibitor IMP366. Two columns indicate the half-lives determined by Cambridge *et al.*[315] and Boisvert *et al.* [314]. A star indicates proteins identified as NMT substrates using AzKTB (identification of the modified peptide). All the other proteins were identified in the spike-in inhibitor experiment described in Section 4.6.

Gene name	L/H $t_{1/2}$ (h)	T t1/2 (h)	TI t1/2 (h)	Turnover (h)_Cambridge *et al.*	Turnover (h)_Boisvert *et al.*
ABL1	N/A	N/A	N/A	N/A	N/A
AIFM2	22.1	15.6	18.5	26.7	N/A
AKAP12	13.9	48.5	65.5	36.2	5.2
ANKIB1	25.1	N/A	N/A	N/A	N/A
ARF1	34.7	63.2	116.3	29.9	18.8
ARF3				N/A	10.8
ARF4	34.5	40.2	68.9	33.3	19.1
ARF5	36.0	63.3	128.9	29.4	20.2
ARF6	31.1	59.6	83.7	35.1	18.6
ARL1	59.2	182.3	256.1	33.1	21.1
ARL5B	6.5	N/A	N/A	N/A	N/A
BASP1	54.1	398.2	2976.6	56.1	20.6
CCNY	18.8	N/A	N/A	N/A	N/A
CCNYL1	32.3	N/A	N/A	N/A	N/A
CDCA3	6.8	N/A	N/A	N/A	N/A
CHCHD3	68.1	134.8	N/A	54.9	32.7
CHCHD6*	20.2	N/A	N/A	N/A	N/A
CHMP6	34.8	71.2	N/A	N/A	21.2
CHP	22.7	14.4	27.3	23.7	N/A
CLN3	N/A	N/A	N/A	18.0	N/A
CYB5R3	49.6	280.3	2520.3	51.7	22.6
DEGS1	26.1	16.5	N/A	24.0	3.9
DIRC2	16.8	N/A	N/A	N/A	N/A
DYM	49.5	56.4	45.9	23.8	N/A
FAM129A	58.5	N/A	N/A	45.5	16.5
FAM129B	38.8	77.2	66.8	36.3	20.8
FAM49B	44.7	599.3	890.2	53.9	25.9
FLOT2	32.6	189.8	N/A	48.8	11.5
FMNL1	30.2	N/A	N/A	26.1	10.1
FMNL2	36.5	N/A	N/A	N/A	16.6
GLIPR2	22.9	N/A	N/A	N/A	N/A
GNAI1	34.2	24.3	40.5	28.2	7.9
GNAI2	27.1	55.2	71.9	33.6	14.7
GNAI3	22.5	36.0	52.9	27.6	13.9
GNAO1	61.7	732.7	N/A	32.2	N/A
GORASP2	53.5	632.8	165.6	53.0	21.2
HCCS	38.5	37.2	33.8	23.6	18.2
HPCAL1;HPCA	42.3	423.3	N/A	50.6	24.2
KIAA1609	21.0	N/A	N/A	N/A	N/A

KIAA1715;LNP	87.1	N/A	N/A	N/A	N/A
LAMTOR1	39.5	25.6	39.7	43.3	N/A
LRRC57	35.9	42.8	53.5	36.6	N/A
LYN	26.7	50.8	N/A	27.4	N/A
MARC1	7.0	N/A	N/A	N/A	N/A
MARC2	48.5	38.1	N/A	N/A	N/A
MARCKS	36.8	60.9	60.3	25.5	15.2
MARCKSL1	31.1	N/A	55.5	N/A	17.9
MGRN1	4.2	N/A	N/A	N/A	N/A
NCS1	19.1	N/A	N/A	28.4	N/A
NDUFAF4	25.9	19.0	N/A	N/A	25.1
NDUFB7	7.6	10.4	67.5	N/A	9.6
NOL3	62.1	182.8	N/A	N/A	24.9
OGFRL1*	21.0	N/A	N/A	N/A	N/A
PCMTD1	29.6	N/A	N/A	16.0	N/A
PIK3R4	26.0	18.5	28.1	22.4	7.9
PLGRKT*	85.8	N/A	N/A	N/A	N/A
PPM1A	63.8	156.0	146.5	33.1	N/A
PPM1B	130.8	N/A	N/A	33.1	N/A
PPM1G	56.9	68.8	79.8	29.8	20.1
PPP3R1	46.6	119.1	154.4	N/A	17.2
PRKAB1	57.2	N/A	N/A	51.8	17.7
PRKACA	31.7	63.7	83.4	35.6	18.0
PRKACB	42.5	59.9	104.1	54.6	N/A
PSMC1	67.1	87.4	93.5	38.4	24.9
RFTN1	24.3	N/A	N/A	N/A	N/A
RNF141	22.0	N/A	N/A	N/A	N/A
RP2	130.8	N/A	N/A	37.7	8.5
SCYL3	35.4	N/A	N/A	N/A	16.7
SPECC1	28.0	28.1	29.2	N/A	N/A
SRC	41.1	117.3	55.0	N/A	16.1
TESC	16.0	12.6	15.5	N/A	N/A
TMEM106B	10.8	6.7	N/A	12.2	N/A
TOMM40L*	N/A	N/A	N/A	N/A	27.7
YES1	33.6	138.6	N/A	27.4	14.5
ZNRF2	56.4	N/A	N/A	N/A	N/A
Average	**38.0**	**126.4**	**263.5**	**34.6**	**17.5**

Appendix J: Membrane-bound peptide sequences prepared using the SPOT™ technology

✓ Membrane A

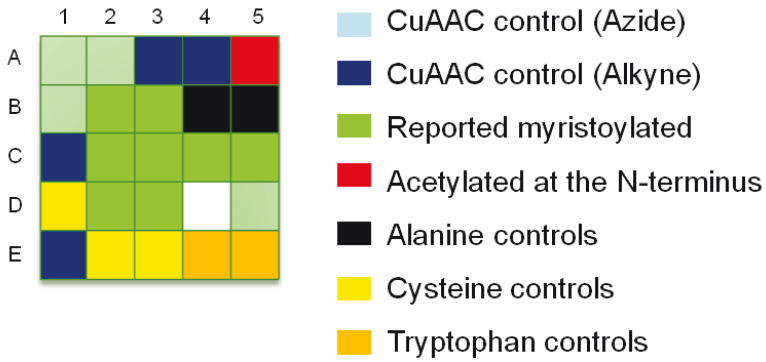

A1	AzGSNKSKPKDASQRRR
A2	AzGLYVSRLFNRLFQKK
A3	YnGSNKSKPKDASQRRR
A4	YnGLYVSRLFNRLFQKK
A5	Capped-GLYVSRLFNRLFQKK
B1	Az
B2	GSNKSKPKDASQRRR
B3	GLYVSRLFNRLFQKK
B4	ASNKSKPKDASQRRR
B5	ALYVSRLFNRLFQKK
C1	Yn
C2	GSNKSKPKDASQRRRPeg
C3	GLYVSRLFNRLFQKKPeg
C4	GSNKSKPKDASQRRr
C5	GLYVSRLFNRLFQKk
D1	GDIEKGKKIFVQKCs
D2	GSNKSKPKDASQRRrPeg
D3	GLYVSRLFNRLFQKkPeg
D4	Space
D5	AzGLYVSRLFNRLFQKk
E1	YnGLYVSRLFNRLFQKk
E2	GDIEKGKKIFVQKCS
E3	GLYVSRLFNRLFQCK
E4	GLSDGEWHLVLNVWG
E5	GLSDGEWHLVLNVWg

-Small letter: low loading (20% Fmoc-AA+ 80% Boc-AA)

-Az: AzC12 incorporated at the N-terminus

-Yn: 5-Hexynoic acid incorporated at the N-terminus

-Peg: Fmoc-NH-PEG_3-COOH incorporated as the first amino acid

✓ Membrane B

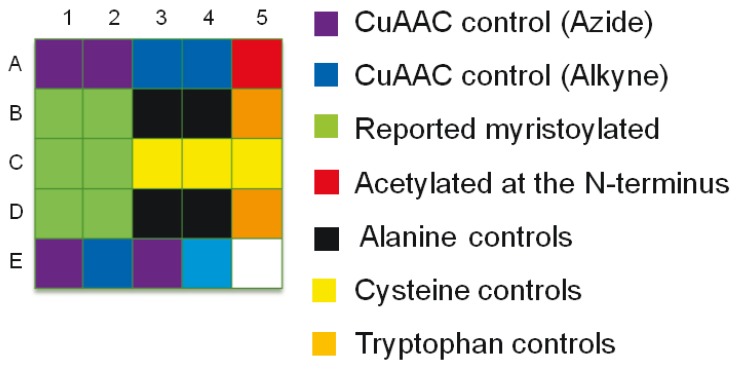

A1	YnGSNKSKPKDASQRRR
A2	YnGLYVSRLFNRLFQKK
A3	AzGLYVSRLFNRLFQKK
A4	AzGSNKSKPKDASQRRR
A5	Capped-GLYVSRLFNRLFQKK
B1	GSNKSKPKDASQRRR
B2	GLYVSRLFNRLFQKK
B3	ASNKSKPKDASQRRR
B4	ALYVSRLFNRLFQKK
B5	GLSDGEWHLVLNVWG
C1	GSNKSKPKDASQRRr
C2	GLYVSRLFNRLFQKk
C3	GDIEKGKKIFVQKCs
C4	GDIEKGKKIFVQKCS
C5	GLYVSRLFNRLFQCK
D1	GSNKSKPK
D2	GLYVSRLF
D3	ASNKSKPK
D4	ALYVSRLF
D5	GLSDGEWHLVLNVWg
E1	YnGLYVSRLFNRLFQKk
E2	AzGLYVSRLFNRLFQKk
E3	Az
E4	Yn
E5	Space

-Small letter: low loading (20% Fmoc-AA+ 80% Boc-AA)

-Az: AzC12 incorporated at the N-terminus

-Yn: 5-Hexynoic acid incorporated at the N-terminus

-Peg: Fmoc-NH-PEG_3-COOH incorporated as the first amino acid

✓ Membrane C

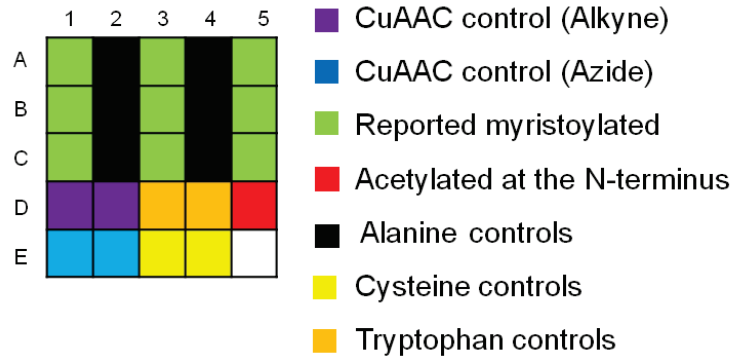

-Small letter: low loading (20% Fmoc-AA+ 80% Boc-AA)

-Az: AzC12 incorporated at the N-terminus

-Yn: 5-Hexynoic acid incorporated at the N-terminus

A1	GSNKSKPKDASQRRR	c SRC
A2	ASNKSKPKDASQRRR	
A3	GSNKSKPK	
A4	ASNKSKPK	
A5	GSNKSKPKDASQRRr	
B1	GNIFEKLFKSLLGKK	Arf 1
B2	ANIFEKLFKSLLGKK	
B3	GNIFEKLF	
B4	ANIFEKLF	
B5	GNIFEKLFKSLLGKk	
C1	GGKLSKKKKGYNVND	BASP1
C2	AGKLSKKKKGYNVND	
C3	GGKLSKKK	
C4	AGKLSKKK	
C5	GGKLSKKKKGYNVNd	
D1	YnGSNKSKPKDASQRRR	CuAAC controls
D2	YnGNIFEKLFKSLLGKK	
D3	GLSDGEWHLVLNVWG	Triptophane controls
D4	GLSDGEWHLVLNVWg	
D5	cappedGSNKSKPKDASQRRR	No terminal Glycine
E1	azGSNKSKPKDASQRRR	Click controls
E2	azGNIFEKLFKSLLGKK	
E3	GDIECGKKIFVQKCS	Cysteine controls
E4	GDIECGKKIFVQKCs	
E5	space	

- ✓ Membrane D

A1	GGGAAAAAGGG
A2	GGGRRRRRGGG
A3	GGGNNNNNGGG
A4	GGGDDDDDGGG
B1	GGGCCCCCGGG
B2	GGGEEEEEGGG
B3	GGGQQQQQGGG
B4	GGGGGGGGGGG
C1	GGGHHHHHGGG
C2	GGGIIIIIGGG
C3	GGGLLLLLGGG
C4	GGGKKKKKGGG
D1	GGGMMMMMGGG
D2	GGGFFFFFGGG
D3	GGGPPPPPGGG
D4	GGGSSSSSGGG
E1	GGGTTTTTGGG
E2	GGGWWWWWGGG
E3	GGGYYYYYGGG
E4	GGGVVVVVGGG

✓ Membrane E

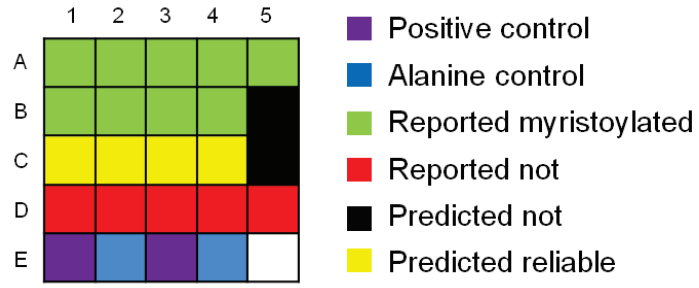

A1	GGQISKGFGKLYRKV	BFSP1	Reported myr
A2	GARASVLSGGKLDAW	HIV-GAG	
A3	GGKWSKSSIVGWPAV	HIV-NEF.(CAA13462)	
A4	GAQFSKTAAKGEAAA	MARCKS	
A5	GCTLSAEDKAAVERS	G protein alpha subunit	
B1	GNSKSGALSKEILEE	Recoverin	
B2	GNEASYPLEMCSHFD	Calcineurin subunit B	
B3	GNRHSQSYTLSEGSQ	Annexin A13b	
B4	GNIFGNLLKSLIGKK	ARF 3	
B5	GDIEKGKKIFVQKCS		Predicted not
C1	GCGCSSHPEDDWMEN	Lck	Predicted reliable
C2	GGRSSCEDPGCPRDE	Hck	
C3	GNSASRNDFEWVYTD	Human sphingolipid delta (4)	
C4	GSLPSRRKSLPSPSL	SRC like adaptor 2	
C5	GLIFAKLWSLFCNQE	ARF like 5b	Predicted not
D1	GDIEKGKKIFVQKCS	Cytochrom C	Reported not
D2	GLSDGEWHLVLNVWG	Myoglobin	
D3	GKITFYEDRNFQGRC	γ crystalline	
D4	GHFTEEDKATITSLW	Hemoglobin γ chain	
D5	GSIGAASMEFCFDVF	Ovalbumin	
E1	GSNKSKPKDASQRRR	c-SRC	Controls
E2	ASNKSKPKDASQRRR		
E3	GGKLSKKKKGYNVND	BASP1	
E4	AGKLSKKKKGYNVND		
E5	Space		

✓ Membrane F

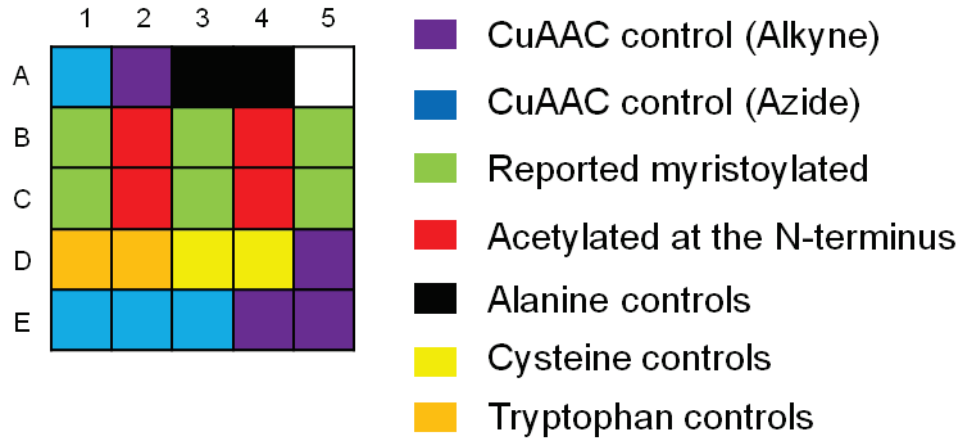

A1	az S G S G S G	
A2	Yn S G S G S G	
A3	A S N K S K P K D A S Q R R R	
A4	A G K L S K K K K G Y N V N D	
A5		
B1	G S N K S K P K D A S Q R R R	c SRC
B2	Capped G S N K S K P K D A S Q R R R	
B3	G S N K S K P K	
B4	Capped G S N K S K P K	
B5	G S N K S K P K D A S Q R R r)	
C1	G G K L S K K K K G Y N V N D	BASP1
C2	A G K L S K K K K G Y N V N D	
C3	G G K L S K K K	
C4	A G K L S K K K	
C5	G G K L S K K K K G Y N V N d	
D1	G L S D G E W H L V L N V W G	Triptophane controls
D2	G L S D G E W H L V L N V W g	
D3	G D I E C G K K I F V Q K C S	Cysteine controls
D4	G D I E C G K K I F V Q K C s	
D5	Yn S G S G S G S G S G S G S G	
E1	Az S G S G S G S G S G S G S G	Click controls
E2	Az G S N K S K P K D A S Q R R R	
E3	Az G N I F E K L F K S L L G K K	Click
E4	Yn G S N K S K P K D A S Q R R R	
E5	Az G N I F E K L F K S L L G K K	

✓ Membrane G

Position	Accession	Uniprot entry name	Sequence
A10	Q6X4W1	NELF_HUMAN	GAAASRRRALRSEAM
A11	Q96BS2	TESC_HUMAN	GAAHSASEEVRELEG
A12	P11488	GNAT1_HUMAN	GAGASAEEKHSRELE
A13	Q6ICN9	Q6ICN9_HUMAN	GAHLVRRYLGDASVE
A14	P17568	NDUB7_HUMAN	GAHLVRRYLGDASVEP
A15	Q8NHG8	ZNRF2_HUMAN	GAKQSGPAAANGRTR
A16	P29966	MARCS_HUMAN	GAQFSKTAAKGEAAA
A17	P00387	NB5R3_HUMAN	GAQLSTLGHMVLFPV
A18	O75896	TUSC2_HUMAN	GASGSKARGLWPFAS
	B2R4Y9	B2R4Y9_HUMAN	
A19	Q9CB01	RABF1_ARATH	GCASSLPDRNSGTLS
A20	P00568	KAD1_HUMAN	GCCSSSDPRREDDLR
A21	O75695	XRP2_HUMAN	GCFFSKRRKADKESR
A22	P06239	LCK_HUMAN	GCGCSSHPEDDWMEN
A23	Q8WXS3	BAALC_HUMAN	GCGGSRADAIEPRYY
A24	Q14699	RFTN1_HUMAN	GCGLNKLEKRDEKRP
A25	Q52LD8	RFTN2_HUMAN	GCGLRKLEDPDDSSP
	Q14DH4	Q14DH4_HUMAN	
A26	P11801	KPSH1_HUMAN	GCGTSKVLPEPPKDV
A27	P07947	YES_HUMAN	GCIKSKENKSPAIKY
A28	P07948	LYN_HUMAN	GCIKSKGKDSLSDDG
A29	P08631-2	HCK_HUMAN	GCMKSKFLQVGGNTF
A30	Q9BSF0	CB088_HUMAN	GCMKSKQTFPFPTIY
B1	A6NI79	CCD69_HUMAN	GCRHSRLSSCKPPKK
B2	B2R6C1	B2R6C1_HUMAN	GCRQSSEEKEAARRS
	P19086	GNAZ_HUMAN	
B3	P63096	GNAI1_HUMAN	GCTLSAEDKAAVERS
	P08754	GNAI3_HUMAN	
	Q5TZX1	Q5TZX1_HUMAN	
	A8KA88	A8KA88_HUMAN	
B4	P09471	GNAO_HUMAN	GCTLSAEERAALERS
B5	A6NGG8	CB071_HUMAN	GCTPSHSDLVNSVAK
B6	P04899	GNAI2_HUMAN	GCTVSAEDKAAAERS
B7	P09769	FGR_HUMAN	GCVFCKKLEPVATAK
B8	P06241	FYN_HUMAN	GCVQCKDKEATKLTE
	B5BU57	B5BU57_HUMAN	
B9	Q9NS86	LANC2_HUMAN	GETMSKRLKLHLGGE
B10	P63117	GFC1_HUMAN	GGAQSKIDPKTPLGC
B11	Q96MG8	PCMD1_HUMAN	GGAVSAGEDNDDLID
B12	Q9NV79	PCMD2_HUMAN	GGAVSAGEDNDELID
B13	P40616	ARL1_HUMAN	GGFFSSIFSSLFGTR
	Q53XB1	Q53XB1_HUMAN	
B14	Q9NZU7	CABP1_HUMAN	GGGDGAAFKRPGDGA
B15	P80723	BASP1_HUMAN	GGKLSKKKKGYNVND
B16	Q8ND25	ZNRF1_HUMAN	GGKQSTAARSRGPFP

Position	Accession	Uniprot entry	Sequence
B19	Q99828	CIB1_HUMAN	GGSGSRLSKELLAEY
	B5BU40	B5BU40_HUMAN	
B20	O75716	STK16_HUMAN	GHALCVCSRGTVIID
B21	Q86XR7	TCAM2_HUMAN	GIGKSKINSCPLSLS
B22	Q9Y689	ARL5A_HUMAN	GILFTRIWRLFNHQE
	Q580I5	Q580I5_HUMAN	
B23	Q17RS7	GEN_HUMAN	GIQGLAKLIADVAPS
B24	B2RC39	B2RC39_HUMAN	GKLHSKPAAVCKRRE
B25	Q969G9	NKD1_HUMAN	
B26	Q969F2	NKD2_HUMAN	GKLQSKHAAAARKRR
B27	P62760	VISL1_HUMAN	GKQNSKLAPEVMEDL
B28	P84074	HPCA_HUMAN	GKQNSKLRPEMLQDL
	B2R9T3	B2R9T3_HUMAN	
B29	Q6FGY1	Q6FGY1_HUMAN	GKQNSKLRPEVLQDL
	P37235	HPCL1_HUMAN	
B30	P61601	NCALD_HUMAN	GKQNSKLRPEVMQDL
	B2RB70	B2RB70_HUMAN	
C1	Q9H4G4	GAPR1_HUMAN	GKSASKQFHNEVLKA
C2	P62166	NCS1_HUMAN	GKSNSKLKPEVVEEL
C3	Q9UM19	HPCL4_HUMAN	GKTNSKLAPEVLEDL
	B2R5U2	B2R5U2_HUMAN	
C4	P62330	ARF6_HUMAN	GKVLSKIFGNKEMRI
	Q6FGZ2	Q6FGZ2_HUMAN	
C5	Q9Y3E7	CHMP3_HUMAN	GLFGKTQEKPPKELV
	Q3ZTS9	Q3ZTS9_HUMAN	
C6	B3KWC8	B3KWC8_HUMAN	GLGVSAEQPAGGAEG
	Q9BQQ3	GORS1_HUMAN	
C7	Q96KC2	ARL5B_HUMAN	GLIFAKLWSLFCNQE
	B0YIW9	B0YIW9_HUMAN	
C8	Q9H0F7	ARL6_HUMAN	GLLDRLSVLLGLKKK
	A8KA93	A8KA93_HUMAN	
C9	P22694-3	KAPCB_HUMAN	GLLKEFLAKAKEDFL
C10	P36405	ARL3_HUMAN	GLLSILRKLKSAPDQ
C11	P36404	ARL2_HUMAN	GLLTILKKMKQKERE
	Q53YD8	Q53YD8_HUMAN	
C12	P22694-7	KAPCB_HUMAN	GLSRKSSDASACSSS
C13	P18085	ARF4_HUMAN	GLTISSLFSRLFGKK
C14	P84085	ARF5_HUMAN	GLTVSALFSRIFGKK
	A4D0Z3	A4D0Z3_HUMAN	
C15	P51451	BLK_HUMAN	GLVSSKKPDKEKPIK
	Q96IN1	Q96IN1_HUMAN	
C16	Q9NR22	ANM8_HUMAN	GMKHSSRCLLLRRKM
C17	P17612	KAPCA_HUMAN	GNAAAAKKGSEQESV
C17	P22694	KAPCB_HUMAN	GNAATAKKGSEVESV
	P22694-8	KAPCB_HUMAN	
	B2RB89	B2RB89_HUMAN	
C18	Q13009	TIAM1_HUMAN	GNAESQHVEHEFYGE
C19	P22612	KAPCG_HUMAN	GNAPAKKDTEQEESV
C20	Q9NPB3	CABP2_HUMAN	GNCAKRPWRRGPKDP

Position	Accession	Uniprot entry name	Sequence
C21	Q9NZU7-2	CABP1_HUMAN	GNCVKYPLRNLSRKD
C22	Q9NZU7-1	CABP1_HUMAN	GNCVKYPLRNLSRKM
C23	Q96LZ3	CANB2_HUMAN	GNEASYPAEMCSHFD
C24	P63098	CANB1_HUMAN	GNEASYPLEMCSHFD
C25	B2RC10	B2RC10_HUMAN	GNEVSLEGGAGDGPL
	Q9UPA5	BSN_HUMAN	
C26	P29728	OAS2_HUMAN	GNGESQLSSVPAQKL
C27	O95843	GUC1C_HUMAN	GNGKSIAGDQKAVPT
C28	P40617	ARL4A_HUMAN	GNGLSDQTSILSNLP
C29	Q13976	KGP1_HUMAN	GNGSVKPKHSKHPDG
C30	P49703	ARL4D_HUMAN	GNHLTEMAPTASSFL
D1	B2RC59	B2RC59_HUMAN	GNIFANLFKGLFGKK
	P84077	ARF1_HUMAN	
D2	Q8IVW1	ARL17_HUMAN	GNIFEKLFKSLLGKK
D3	P61204	ARF3_HUMAN	GNIFGNLLKSLIGKK
D4	A8K6G8	A8K6G8_HUMAN	GNIPPKAKTPLRCIL
	Q9NRZ4	GAW2_HUMAN	
D5	P56559	ARL4C_HUMAN	GNISSNISAFQSLHI
D6	Q53R10	Q53R10_HUMAN	GNLFGRKKQSRVTEQ
	Q4A519	Q4A519_HUMAN	
	Q96FZ7	CHMP6_HUMAN	
D7	Q548C1	Q548C1_HUMAN	GNLKSVAQEPGPPCG
D8	P29474	NOS3_HUMAN	GNLKSVAQEPGPPCG
D9	P63118	GAH2_HUMAN	GNLPPSIPPSSPLAC
D10	Q8N8A4	GAH6_HUMAN	GNQLAGIAPSQILSV
	Q99570	PI3R4_HUMAN	
D11	P42526	HATB_DICDI	GNRAFKAHNGHYLSA
D12	P13231	HATA_DICDI	GNRAFKSHHGHFLSA
D13	P27216	ANX13_HUMAN	GNRHAKASSPQGFDV
D14	P27216-2	ANX13_HUMAN	GNRHSQSYTLSEGSQ
D15	Q6QHC5	DEGS2_HUMAN	GNSASRNDFEWVYTD
D16	Q8IVF5	TIAM2_HUMAN	GNSDSQYTLQGSKNH
D17	P35243	RECO_HUMAN	GNSKSGALSKEILEE
D18	Q53XL0	Q53XL0_HUMAN	GNSMKSTPAPAERPL
	Q13239	SLAP1_HUMAN	
D19	Q6FI01	Q6FI01_HUMAN	GNTSSERAALERHGG
	Q9Y478	AAKB1_HUMAN	
D20	Q8ND76	CCNY_HUMAN	GNTTSCCVSSSPKLR
D21	O43741	AAKB2_HUMAN	GNTTSDRVSGERHGA
D22	P43080	GUC1A_HUMAN	GNVMEGKSVEELSST
D23	B3KWT4	B3KWT4_HUMAN	GQALGIKSCDFQAAR
	P16452	EPB42_HUMAN	
D24	Q4VB97	Q4VB97_HUMAN	GQDQTKQQIEKGLQL
	Q13702	RAPSN_HUMAN	
D25	Q9UMX6	GUC1B_HUMAN	GQEFSWEEAEAAGEI
D26	Q7KYS9	Q7KYS9_HUMAN	GQFLSSTFLEGSPAT
D27	P16452-2	EPB42_HUMAN	GQGEPSQRSTGLAGL
D28	Q6BDI9	REP15_HUMAN	GQKASQQLALKDSKE
D29	O43687	AKA7A_HUMAN	GQLCCFPFSRDEGKI

Position	Accession	Uniprot entry name	Sequence
D30	A6NH57	ARL5C_HUMAN	GQLIAKLMSIFGNQE
E1	P00519	ABL1_HUMAN	GQQPGKVLGDQRRPS
E2	P42684	ABL2_HUMAN	GQQVGRVGEAPGLQQ
E3	Q9BZ96	TTY14_HUMAN	GQSFSCSLHQRRVGE
E4	P62191	PRS4_HUMAN	GQSQSGGHGPGGGKK
	Q53XL8	Q53XL8_HUMAN	
E5	P62690	GAK18_HUMAN	GQTESKYASYLSFIK
	P62691	GAK19_HUMAN	
E6	P62688	GAK15_HUMAN	GQTKSKIKSKYASHL
E7	P62683	GAK1_HUMAN	GQTKSKIKSKYASYL
E8	Q9HDB9	GAK8_HUMAN	GQTKSKTKSKYASYL
E9	Q96PI4	GAK7_HUMAN	GQTKTKSKYASYLSF
E10	Q86UY6	NAA40_HUMAN	GRKSSKAKEKKQKRL
E11	Q59EY7	Q59EY7_HUMAN	GRPIDPREGPGRPPL
E12	O43559	FRS3_HUMAN	GSCCSCLNRDSVPDN
E13	Q8WU20	FRS2_HUMAN	GSCCSCPDKDTVPDN
E14	Q8IZE3	PACE1_HUMAN	GSENSALKSYTLREP
E15	P19087	GNAT2_HUMAN	GSGASAEDKELAKRS
	Q5T697	Q5T697_HUMAN	
E16	A8MTJ3	GNAT3_HUMAN	GSGISSESKESAKRS
	B9EJG5	B9EJG5_HUMAN	
E17	P98073	ENTK_HUMAN	GSKRGISSRHHSLSS
E18	Q8N4G2	ARL14_HUMAN	GSLGSKNPQTKQAQV
E19	Q9H6Q3	SLAP2_HUMAN	GSLPSRRKSLPSPSL
	A8K648	A8K648_HUMAN	
E20	P12931	SRC_HUMAN	GSNKSKPKDASQRRR
E21	Q7RTS9	DYM_HUMAN	GSNSSRIGDLPKNEY
E22	P49006	MRP_HUMAN	GSQSSKAPRGDVTAE
E23	Q99653	CHP1_HUMAN	GSRASTLLRDEELEE
E24	O43745	CHP2_HUMAN	GSRSSHAAVIPDGDS
	A8K2I8	A8K2I8_HUMAN	
E25	Q9H8Y8	GORS2_HUMAN	GSSQSVEIPGGGTEG
	Q53TE3	Q53TE3_HUMAN	
E26	Q96EQ8	RN125_HUMAN	GSVLSTDSGKSAPAS
E27	Q969Q4	ARL11_HUMAN	GSVNSRGHKAEAQVV
E28	Q9Y250	LZTS1_HUMAN	GSVSSLISGHSFHSK
E29	Q9ULE6	PALD_HUMAN	GTTASTAQQTVSAGTP
E30	Q5XKD4	Q5XKD4_HUMAN	GTVLSLSPASSAKGR

Appendix K: Kinetic studies of HIV Gag and HIV Nef

The kinetic parameters of HIV Gag and HIV Nef were determined with the CPM assay, in the presence of saturation amount of MyrCoA (30 or 40 µM) or 4 µM of MyrCoA. The IC_{50s} of IMP366 was also determined in the presence of both peptides at concentration close to K_M.

✓ **HIV Gag** (sequence: G A R A S V L S G G K L D A W)

		HsNMT1	**HsNMT2**
30 µM MyrCoA	K_M (µM)	70.7 ± 3.9	44.8 ± 2.6
	V_{max}	100364 ± 2966	80115 ± 2131
4 µM MyrCoA	K_M (µM)	37.6 ± 10.5	17.7 ± 1.2
	V_{max}	48476 ± 5967	32429 ± 766
10 µM HIV GAG	IC_{50} of IMP366 (nM)	14.1 ± 2.5	12.5 ± 2.2

✓ **HIV Nef** (sequence: G G K W S K S S I V G W P A V)

		HsNMT1	**HsNMT2**
50 µM MyrCoA	K_M (µM)	0.42 ± 0.06	0.34 ± 0.03
	V_{max}	36666 ± 2075	30338 ± 830
30 µM MyrCoA	K_M (µM)	0.31 ± 0.06	0.30 ± 0.08
	V_{max}	45285 ± 2875	32721 ± 3049
4 µM MyrCoA	K_M (µM)	0.34 ± 0.06	0.23 ± 0.03
	V_{max}	21269 ± 1401	19013 ± 813
0.3 µM HIV Nef	IC_{50} of IMP366 (nM)	22.8 ± 1.3	15.2 ± 1.2